THE UNIVERSITY of ADELAIDE

Exploring the bidirectional interface between stress and innate immunity: a focus on glucocorticoid and TLR4-MyD88 signalling

A thesis submitted in fulfilment for the degree of

DOCTOR OF PHILOSOPHY

in

The Discipline of Physiology

Adelaide Medical School

The University of Adelaide

by

JiaJun Liu

September 2017

Table of Contents

Thesis abstract

Multiple bidirectional interactions between stress neuroendocrine and innate immunity have been identified in previous research, but the extent of these interactions remain unresolved. This thesis thus aimed to explore the bidirectional interface between stress and innate immunity, by focusing on glucocorticoid and TLR4-MyD88 signalling. The research was undertaken in a series of 3 studies.

Study 1 investigated the impact of baseline TLR4-MyD88 signalling on the neuroendocrine and behavioural responses to acute stress. Through examining stress responses in mice lacking *Tlr4* or *Myd88,* this study found an intrinsic influence of TLR4-MyD88 signalling on both neuroendocrine and behavioural responses. Aadaptations to the feedforward and feedback pathways of glucocorticoid signalling were also identified.

Studies 2 and 3 explored the effects of glucocorticoid signalling on innate immune function in immunocompetent cells. In these 2 studies, BV2 microglia-like cells, RAW264.7 macrophage-like cells and adult primary microglia were utilised. Study 2 demonstrated a biphasic innate immune response to glucocorticoids, where low concentrations of corticosterone pre-exposure primed, while a high stress-like concentration of corticosterone suppressed TLR4-NF-κB-IL-1β responses. Using pharmacological antagonists, it was further revealed that the priming effect on IL-1β was mediated by mineralocorticoid receptor (MR) signalling, while immunosuppressive actions were mediated by glucocorticoid receptor (GR) signalling.

Study 3 further assessed glucocorticoid actions on non-cytokine innate immune responses via measurements of cell motility, cell death and danger-associated molecular pattern (DAMP)-related protein release. Here, a low concentration of corticosterone increased ATP-induced BV2 cell motility. Signalling via GR, a stress-like concentration of Corticosterone and Dexamethasone caused an increase in cytotoxicity and HMGB1 DAMP protein release.

Collectively, the findings in this thesis provide support for multiple intrinsic connections between the stress neuroendocrine and TLR4 signalling pathway, both *in vivo* and *in vitro.* Further mechanistic insights such as GR and MR signalling were revealed, and the implications of this work to health and disease were also discussed.

Declaration

I certify that this work contains no material which has been accepted for the award of any other degree or diploma in my name, in any university or other tertiary institution and, to the best of my knowledge and belief, contains no material previously published or written by another person, except where due reference has been made in the text. In addition, I certify that no part of this work will, in the future, be used in a submission in my name, for any other degree or diploma in any university or other tertiary institution without the prior approval of the University of Adelaide and where applicable, any partner institution responsible for the joint-award of this degree.

I give consent to this copy of my thesis when deposited in the University Library, being made available for loan and photocopying, subject to the provisions of the Copyright Act 1968.

I acknowledge that copyright of published works contained within this thesis resides with the copyright holder(s) of those works.

I also give permission for the digital version of my thesis to be made available on the web, via the University's digital research repository, the Library Search and also through web search engines, unless permission has been granted by the University to restrict access for a period of time

Acknowledgements

"If your confusion leads you in the right direction, the results can be uncommonly rewarding."

-Haruki Murakami, Hardboiled wonderland, and the end of the world

To my supervisors, Professor Mark Hutchinson, Dr Femke Buisman-Pijlman and Dr Sanam Mustafa, I sincerely thank you for the guidance and all the support throughout the trials and tribulations. To Mark, for being so open and supportive of new ideas; to Femke for the insight and feedback; to Sanam, for all the encouragement and careful consideration.

To the neuroimmunopharmacology lab, thank you all for being so accommodating. It was fun at times, frustrating at times, but an amazing experience being part of the lab.

To everyone in the office, thank you for not saying anything about my loud keyboard, it must have been annoying. Also to Jon, Sam L, Jacob and Sam E, thank you for the banter, without which this PhD would have been rather mundane.

To my family, Ma, Pa, Jiali and Jiayan, thank you for being there for me. Although we were on different continents, knowing that I will always have a safe space somewhere has been, and will always continue to be encouraging.

To Melanie, thank you for putting up with me throughout, your support really helped me through the worst of times.

List of Abbreviations

ACTH	Adrenocorticortropic Hormone
AIM1	Absent in Melanoma 1 Protein
AP-1	Activator Protein 1
ATP	Adenosine Triphosphate
BCL-2	B-cell lymphoma 2
CBG	Corticosteroid Binding Globulin
CD11B	Cluster of Differentiation 11B
CD14	Cluster of Differentiation 14
CORT	Corticosterone
CRF	Corticotropin releasing factor
DAMP	Danger Associated Molecular Pattern
DEX	Dexamethasone
FASLG	Fas Ligand
GC	Glucocorticoid
GR	Glucococrticoid receptor
HMGB1	High Mobility Group Box 1
HPA	Hypothalamus Pituitary Adrenal
IBA-1	Ionised Calcium-binding Adapter 1
IFN-β	Interferon β
IkB	Nuclear Factor of Kappa Light Polypeptide
IKK complex	IkB kinase
IL-18	Interleukin 18
IL-1β	Interleukin 1β
IL-1R1	Interleukin 1 Receptor 1
IL-1RA	Interleukin 1 Receptor Antagonist
IL-6	Interleukin 6
IRAK1	Interleukin 1 Receptor-Associated Kinase 1
IRAK4	Interleukin 1 Receptor-Associated Kinase 4
IRF3	Interferon Regulatory Factor 3
LDH	Lactate Dehydrogenase
LPS	Lipopolysaccharide
MAMP	Microbe-Associated Molecular Pattern
MAP kinases	Mitogen-Activated Protein Kinase
MD2	Myeloid Differentiation Factor 2
MR	Mineralocorticoid Receptor
MyD88	Myeloid Differentiation Primary Response 88
Myd88$^{-/-}$	MyD88 knockout
NF-kB	Nuclear Factor Kappa B
NLRP1	NACHT, LRR and PYD domains-containing protein 1
NLRP3	NACHT, LRR and PYD domains-containing protein 3

P2X7	P2X purinoceptor 7
PAMP	Pathogen-Associated Molecular Pattern
PVN	Paraventricular Nucleus of the Hypothalamus
RAAS	Renin-Angiotensin-Aldosterone System
TAB1	TGF-β activated kinase 1/MAP3K7 binding protein 1
TAB2	TGF-β activated kinase 1/MAP3K7 binding protein 2
TAK1	Transforming growth factor β-activated Kinase 1
TBK1	TANK Binding Kinase 1
TLR	Toll-like Receptor
Tlr4$^{-/-}$	Toll-like Receptor 4 knockout
TNF- α	Tumor Necrosis Factor α
TRAF6	TNF Receptor Associated Factor 6
TRIF	TIR-domain-containing adaptor-inducing interferon-B
XAMP	Xenobiotics-Associated Molecular Pattern

Chapter 1: Stress and innate immunity: Interactions between the neuroendocrine and neuroimmune system, a focus on glucocorticoid and TLR4 signalling

Stress can be broadly defined as an environmental challenge to physiology, originating from physical, psychosocial, chemical and immunological sources. The connection between stress and physiology has been an active area of research since the early 1900s, after the discovery and functional investigation of stress hormones such as glucocorticoids and adrenaline (Selye, 1973). The combination of observational studies and experimental models has demonstrated the physiological effects of stress, and how this can interact with health and disease. Stress can for example, lead to increased drug seeking behaviours and relapse through fundamental change in the reward pathway (Sinha, 2001), and the exacerbation of chronic illnesses (Kemeny and Schedlowski, 2007). Additionally, stress is regarded as an environmental factor that unmasks individual propensity to psychosomatic disorders such as major depressive disorder (Monroe and Simons, 1991). Given the widespread impact to health and disease, the physiological mechanisms behind the maladaptations seen in chronic stress have become a focus of stress research. There is now growing evidence for the involvement of immune and neuroendocrine changes resulting from stress, and this is hypothesised to mediate some of the detrimental health outcomes in high-stressed or chronically-stressed individuals (Chrousos, 2009). This thesis thus aimed to explore the bidirectional interface between neuroendocrine and innate immune function in stress, with focus on the relationship between glucocorticoids and Toll-like receptor 4 (TLR4) pathways.

1.1 An overview of glucocorticoid and innate immune signalling pathways

Given the observed association between stress and sickness, this thesis thus investigated the interactions in overlapping physiological systems: the neuroendocrine stress response and innate immune function. Previous studies have uncovered associations between stress-related disorders and changes to both neuroendocrine and innate immune activity (Chan *et al.*, 2016; Daskalakis *et al.*, 2016). Furthermore, dysregulations in innate immune functioning and neuroendocrine signalling have been uncovered in stress-related disorders (Heiser *et al.*, 2008; Lisi *et al.*, 2013; Horowitz and Zunszain, 2015). However, to resolve the mechanisms underlying how these dysregulations arise, the relationships between these two systems first needs to be established. Interactions between Hypothalamus pituitary adrenal (HPA) axis and toll-like receptor (TLR) functions are best understood, since multiple bidirectional relationships have been uncovered at each stage of these systems (Pace and Miller, 2009; Liu, Buisman-Pijlman and Hutchinson, 2014). The following section contains a brief overview of HPA and TLR signalling pathways.

1.1.1 The neuroendocrine stress response, Hypothalamus Pituitary Adrenal axis, and glucocorticoid signalling

The neuroendocrine stress response

Autonomic stress response

The physiological stress response is mediated by 2 main pathways – the autonomic response and HPA activation, which form rapid and sustained responses respectively.

Discovered in the early 1900s (Cannon, 1915), the autonomic response operates on the seconds to minutes time scale through release of catecholamines noradrenaline and adrenaline, which result in increased sympathetic tone in neuromuscular systems (Ulrich-Lai and Herman, 2009). As a result, this sympathetic response raises heart rate, causes vasoconstriction and mobilises energy stores. Since catecholamines have a brief half-life of 2-3 min in circulation (Dimsdale and Moss, 1980), this sympathetic activation, colloquially termed as the "fight or flight" response, forms the organism's acute responses towards stressors.

The hypothalamus pituitary adrenal stress response

Conversely, HPA activation, through predominantly humoral mechanisms, occurs between minutes and hours after the stress onset (Chrousos, 2009). Initiating in the paraventricular nucleus of hypothalamus (PVN), which receives input from both surrounding vasculature and innervation from deeper brain structures, neurons secrete Corticotrophin Releasing Factor (CRF) neuropeptide into the hypothalamus hypophyseal portal system. This network of blood vessels carries CRF from the PVN to the anterior pituitary, binding to CRF receptors expressed on pituitary cells. In response to CRF, pituitary cells further release adrenocorticotrophic hormone (ACTH) into the general circulation. ACTH binds to melanocortin receptor 2 on cells within the zona fasiculata layer of the adrenal cortex, which secrete glucocorticoids, predominantly cortisol in humans and corticosterone in rodents, as end products in the HPA response (Silverman and Sternberg, 2012).

Blood elevation of glucocorticoids generally occurs within 10 min after stress onset in rodents (Droste *et al.*, 2008), and 10-15 min in humans (King and Liberzon, 2009). Glucocorticoids have a half-life of approximately 8 h in circulation, thus forming the sustained stress response (Chrousos, Pavlaki and Magiakou, 2000). Bioavailability of circulating glucocorticoids is further controlled by binding proteins in blood, mainly corticosteroid binding globulin (CBG; Serpin A6; transcortin) and to a smaller extent Albumin, which concertedly bind up to 95-97% of total circulating glucocorticoids (Richard *et al.*, 2010). When bound to CBG or Albumin, glucocorticoids are unable to cross the cell membrane to activate intracellular steroid receptors. These protein complexes can be disrupted by heat and neutrophil derived elastase, liberating glucocorticoids from binding proteins (Lin, Muller and Hammond, 2010). These mechanisms therefore serve as local tissue-level control of glucocorticoid bioavailability. CBG is further upregulated in response to stress and thus plays an important role in the global distribution of glucocorticoid activity following stress (Kumsta *et al.*, 2007; Minni *et al.*, 2012).

GR and MR intracellular receptors for glucocorticoids

Glucocorticoids signal via intracellular steroid receptors glucocorticoid receptor (GR) and mineralocorticoid receptor (MR).

GR, the classical glucocorticoid signalling receptor:

Ubiquitously expressed, GR serves as the main coordinator of glucocorticoid signalling in each system. GR activation is responsible for mediating stress-induced suppression

of the reproductive system, immunosuppression, and can increase cardiac output. In addition, GR activation in the metabolic system maximise available energy through increased blood glucose by inhibiting storage while mobilising glucose stores (see review Sapolsky, Romero and Munck, 2000). In the central nervous system (CNS), electrophysiological experiments have demonstrated that GR activation can also suppress hippocampal synaptic plasticity and neuronal excitability (Cazakoff and Howland, 2010), while prolonged GR activation can cause increased hippocampal neuronal loss (Sorrells *et al.*, 2014). These general mechanisms serve as links between chronic stress and neurological damage.

GR is basally expressed in the cell cytoplasm, but translocates into the nucleus when bound by glucocorticoids. In the nucleus, GR can either directly cause gene transcription by forming homodimers and binding to glucocorticoid response elements on DNA, or interact with other transcriptional factors to indirectly influence gene transcription (Ratman *et al.*, 2013; Xavier, Kataryna and Anunciato, 2016). In relation to this thesis, the most relevant transcriptional factors that interact with GR are NF-kB and AP-1, which mainly transcribe pro-inflammatory genes in response to immune activation. Through tethering to AP-1 and NF-kB, GR inhibits the transcription of pro-inflammatory genes. This is one main mechanism contributing towards the potent immunosuppressive actions of glucocorticoids (Gupte *et al.*, 2013). Additionally, GR can cause the transcription of anti-inflammatory genes and in high concentrations, trigger apoptosis in immunocompetent cells via upregulation of BCL-2 (Wu *et al.*, 2013; Ferland *et al.*, 2014), therefore performing potent immunosuppressive actions.

MR, the alternative glucocorticoid signalling receptor:

MR binds mineralocorticoids and glucocorticoids at a higher affinity, but is expressed at a lower abundance compared to GR (Reul and de Kloet, 1985). MR is thus implicated in the permissive actions of glucocorticoids, a class of actions that mediate baseline physiological activity (Sapolsky, Romero and Munck, 2000; Harris *et al.*, 2013). Aldosterone, the classical MR agonist, is a mineralocorticoid hormone produced by cells in the zona glomerulosa layer of the adrenal cortex as part of the renin-angiotensin-aldosterone system (RAAS). Functioning as part of the RAAS, MR activation, in response to dehydration or loss of blood volume, is a potent vasoconstrictor, causing increased blood pressure (te Riet *et al.*, 2015). Through these actions, MR activation causes water retention and maintains blood osmolarity in normal physiology. MR therefore represents the cross between two main physiological neuroendocrine systems – osmotic balance and stress.

In contrast to GR actions, MR binding in the brain can facilitate hippocampal glutaminergic excitatory neurotransmission (Karst *et al.*, 2005), and long-term potentiation (Pavlides and McEwen, 1999; Stranahan *et al.*, 2010), which have been proposed as the facilitation of memory formation. MR signalling can also result in immune stimulatory actions (Chantong *et al.*, 2012). Similar to GR actions, upon binding and activation, MR translocates into the nucleus to cause gene transcription and interact with transcriptional factors NF-kB and AP-1 (Fiebeler *et al.*, 2001; Rogerson, Brennan and Fuller, 2004). However, unlike GR, plasma membrane receptors of MR have also been discovered in neurons (Karst *et al.*, 2005). These membrane-bound receptors are regarded as mediators of non-genomic actions of GR,

and can cause rapid changes to neurotransmission (Karst *et al.*, 2005; Groeneweg *et al.*, 2011). The impact of MR surface receptor activation on overall physiology, however, remains poorly characterised.

1.1.2 Toll-like receptors and inflammasome complexes - innate immune factors

The previous section described the neuroendocrine stress system as the endogenous response to exogenous environmental initiators, which have widespread effects on physiological function. The innate immune system, being responsive towards both exogenous and endogenous factors, is therefore a likely candidate for maximal crosstalk between the neuroendocrine stress response and immune function (detailed in 1.1.3). Toll-like receptor 4 (TLR4) and inflammasome innate immune pathways and the HPA axis have been identified as prime focus of the interface between stress and immunity in this thesis.

Toll-like receptors

Toll-like receptors (TLRs) are amongst the best understood innate immune receptors. Initially identified in drosophila flies, TLRs are part of a class of pattern recognition receptors that bind a wide range of agonists broadly classified as endogenous Danger associated molecular patterns (DAMPs) and exogenous pathogen associated molecular patterns (PAMPs or MAMPs) (O'Neill, Golenbock and Bowie, 2013). Certain pharmacological agents, such as morphine (Wang *et al.*, 2012), have also be identified as TLR agonists, forming another class of xenobiotic associated molecular patterns (XAMPs) (Hutchinson *et al.*, 2012).TLRs can be further be classified as membrane-

bound (TLR2, TLR4, TLR5, TLR6, TLR7 and TLR9) and intracellular (TLR3).

When activated, TLRs trigger downstream intracellular signalling via 2 main pathways via separate adaptor proteins: 1) the surface receptor-associated MyD88 pathway, and 2) the intracellular receptor-associated TRIF pathway (Watters, Kenny and O'Neill, 2007). Amongst all TLRs, only TLR4 recruits both adaptor molecules, which gives it the ability to trigger signalling of both TRIF and MyD88, therefore having the most widespread effects when activated.

TLR4 signalling pathway

Membrane-bound TLR4 exists as a receptor complex of two TLR4-MD2 receptor subunits forming homodimers (Kim *et al.*, 2007). The canonical TLR4 PAMP agonist, lipopolysaccharide (LPS), is a constituent of gram-negative bacterial cell wall. Due to the strongly hydrophobic lipid A region and hydrophilic carbohydrate region, LPS molecules for large aggregates in the extracellular space, which have low TLR4 binding affinity (Calabrese, Cighetti and Peri, 2015). LPS binding protein (LBP), an extracellular acute phase protein, recruits LPS aggregates to CD14 co-receptor on the cell membrane, which monomerises LPS aggregates prior to binding to TLR4-MD2 complexes (see review Park and Lee, 2013). DAMPs, such as High mobility group box 1 (HMGB1) and heat shock proteins, have also been identified as TLR4 agonists which bind to the TL4-MD2 complex (Yang *et al.*, 2015). Through potent activation of the TLR4 signalling pathway, HMGB1 has been identified as a key molecule involved in septic shock (Yanai *et al.*, 2013). Also binding to MD2-TLR4, morphine has been shown to induce a pro-inflammatory state via TLR4 (Wang *et al.*, 2012), and through this

mechanism, TLR4 has been implicated in the development of drug reinforcement and pro-inflammatory effects of morphine (Hutchinson *et al.*, 2012).

Signalling via TRIF and MyD88 adaptor molecules, TLR4 activation by PAMPs, DAMPs and XAMPs activates downstream transcriptional factors NF-kB and the IRF3 respectively (Watters, Kenny and O'Neill, 2007). Once bound to the cytoplasmic TIR domain on TLRs, MyD88 recruits IRAK4, which causes IRAK1 phosphorylation, leading to the dissociation of TRAF6 to form an intracellular complex with proteins TAK1, TAB1 and TAB2. Further phosphorylation of this complex leads to the activation of TAK1, which phosphorylates both MAP kinases and the IKK complex, ultimately resulting in the degradation of IκB, allowing translocation of transcriptional factor NF-κB into the nucleus to cause gene transcription (see review Akira and Takeda, 2004). The phosphorylation of TLR4 adapter protein TRIF triggers downstream signalling through cytoplasmic TBK1, causing IKKε activation of IRF3 and IRF7 transcriptional factors (Fitzgerald *et al.*, 2003; Han *et al.*, 2004). Furthermore, via interactions with IκB, TRAF6 phosphorylation resulting from TRIF activation can also cause NF-kB activation (Han *et al.*, 2004). This secondary effect of TRIF is regarded as late-phase TLR4 activation (Akira and Takeda, 2004). Through these MyD88 and TRIF -dependent pathways, TLR4 activation thus coordinates the cellular inflammatory response through transcription of pro-inflammatory cytokines such as TNF-α, IL-1β, IL-6 and IFN-β. Caspase-8 mediated cell apoptosis can also be induced via the TRIF dependent pathway (Weber *et al.*, 2010).

IL-1β and Inflammasome-dependent pathways for cytokine secretion

IL-1β is a pro-inflammatory cytokine, which triggers a strong inflammatory response via interleukin-1 receptor 1 (IL-1R1) expressed on immunocompetent cells. Similar to TLRs, IL-1R1 signals through MyD88-NF-κB intracellular signalling (Brikos *et al.*, 2007). Together with IL-18, IL-1β can have a role in septic shock, since the combined use of IL-1R1 antagonist and IL-18 neutralising antibodies can protect against lethality due to LPS-induced sepsis in mice (Vanden Berghe *et al.*, 2014). Given the potent actions of IL-1β and IL-18, release of these cytokines is tightly regulated through inflammasome signalling, which cleaves pro-IL-1 and pro-IL-18 into mature forms prior to release (Franchi, Muñoz-Planillo and Núñez, 2012).

The currently best understood inflammasome complex consists of proteins NLRP3 ASC and Caspase-1, although AIM2 and NLRP1 inflammasomes are also commonly studied (see review, Martinon, Mayor and Tschopp, 2009). NLRP3 protein is upregulated via NF-κB-induced transcription (Qiao *et al.*, 2012), and can be activated via TRIF-dependent mechanisms TRIF induced Caspase-11 (Rathinam *et al.*, 2012). NLRP3 is therefore produced and regulated downstream of TLR4 signalling. Expression of NLRP3 alone is however insufficient to cause conversion of IL-1β and IL-18. Instead, a second signal is required for the inflammasome activation, which converts pro-caspase-1 into active Caspase-1 (Halle *et al.*, 2008). Various mechanisms have been proposed, but P2X7 purinergic receptor activation is the best understood so far (Gicquel *et al.*, 2014; Franceschini *et al.*, 2015). P2X7 is a membrane-bound, ligand gated, non-specific cation channel that is activated by extracellular adenosine triphosphate (ATP).

Inflammasome activation has been linked to both Ca^{2+} influx (Murakami *et al.*, 2012) and K^{+} efflux (Katsnelson *et al.*, 2015) following purinergic activation. By causing pro-inflammatory signalling through this mechanism, ATP functions as a potent danger signal.

1.1.3 Molecular interactions between glucocorticoid and innate immune signalling

The previous sections described in isolation, the physiological neuroendocrine stress response as well as intracellular innate immune signalling with regards to TLR signalling and inflammasome activation. Given that stress has widespread effects on immune signalling, there are significant overlaps and interactions between the two systems at the molecular level (Figure1).

Expressed in all immunocompetent cells, GR initiates immunosuppression through direct transcription of anti-inflammatory genes, promotion of cell apoptosis, and inhibition of AP-1 and NF-kB signalling through direct association with these transcriptional factors in the nucleus (Gupte *et al.*, 2013; Xavier, Kataryna and Anunciato, 2016). Conversely, while GR predominantly suppresses AP-1 and NF-kB signalling, MR activation instead increases the activity of these transcriptional factors (Fiebeler *et al.*, 2001). Thus, MR signalling has been proposed as a potential mechanism of sometimes paradoxical actions of glucocorticoids across systems. However, the exact roles of GR and MR in these varied glucocorticoid responses during normal physiology is still not well understood, and is therefore explored further in this thesis.

Previous rodent studies suggest that GR may play a role in brain upregulation of NLRP3 inflammasome, through which increasing the potential for conversion and release of IL-1β (Busillo and Cidlowski, 2013; Frank *et al.*, 2014; Sobesky *et al.*, 2016). However, it is still unknown whether GR directly causes NLRP3 gene transcription, or if this occurs via GR interaction with other transcriptional factors. The interaction between GR and the inflammasome complex can also be bidirectional. A recent study has shown NLRP3 inflammasome activated Caspase-1 cleavage of GR, thus inhibiting glucocorticoid signalling in human isolated leukocytes (Paugh *et al.*, 2015). The authors propose that this cleavage of GR is a main mechanism of glucocorticoid resistance, a condition in which immunocompetent cells exhibit decreased GR-dependent immunosuppression and thus result in overshoot of pro-inflammatory responses. The overall physiological significance of this mechanism however, remains to be seen.

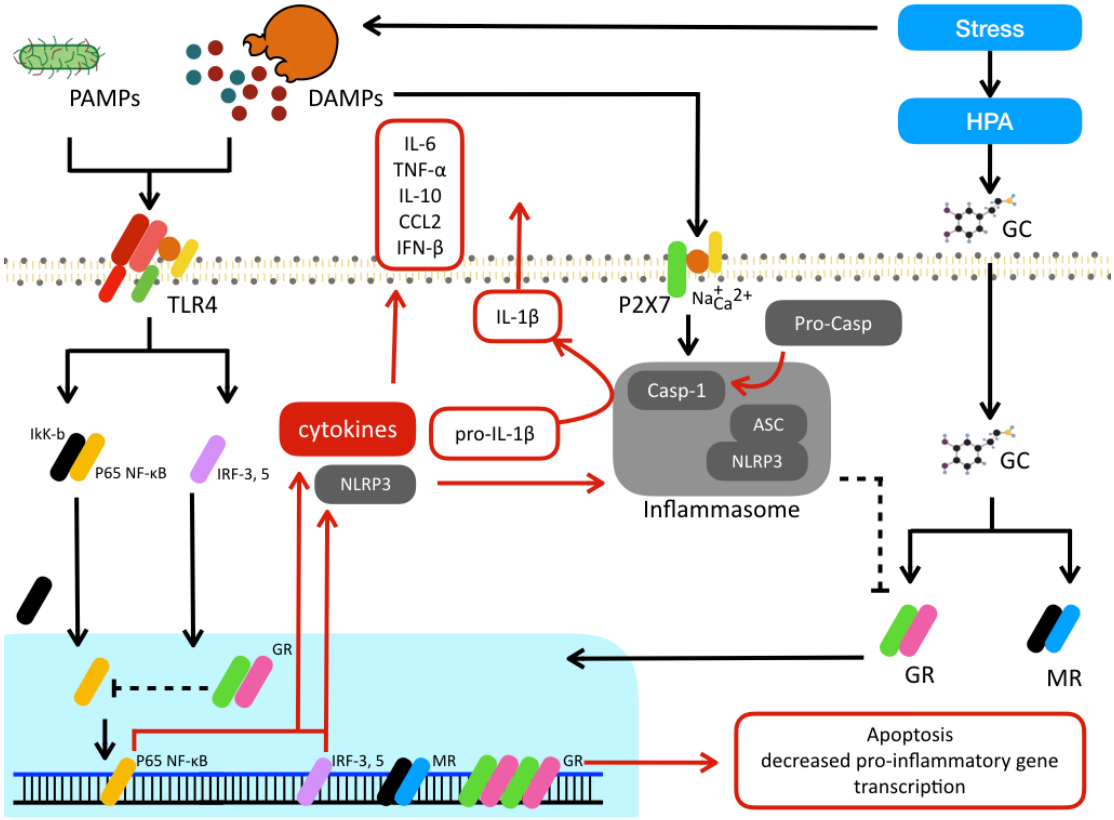

Figure 1. Molecular interactions between glucocorticoid and TLR4 signalling pathways in innate immune cells. Stress causes HPA activation, which results in production of glucocorticoids (GC). GCs passively diffuse across the cell membrane and bind to steroid receptors GR and MR. Upon activation, GR and MR both translocate into the nucleus, resulting in gene transcription. GR-induced actions include cell apoptosis, and decreased pro-inflammatory gene transcription. In response to PAMPs and DAMPs, TLR4 can trigger both TRIF-dependent and MyD88-dependent activation of transcriptional factors, IRF3,5 and p65 NF-κB respectively. These transcriptional factors translocate into the cell nucleus to cause pro- and anti-inflammatory cytokine gene transcription. However, NF-κB-induced pro-inflammatory gene transcription can be inhibited by GR activation. NLRP3 protein is also upregulated by these downstream transcriptional factors, resulting in the assembling of the inflammasome complex. Upon receiving a second signal, in this example P2X7 activation via extracellular ATP, cations including Ca^{2+} diffuse into the cell, triggering inflammasome activation. Pro-caspase-1 becomes converted to active caspase-1, which cleaves pro-IL-1β to active IL-1β prior to release. The inflammasome complex can also cleave GR, thus inhibiting GR signalling. Black arrows represent input, while red arrows indicate output responses. Dotted arrows indicate inhibitory actions.

1.2 A brief examination of research featuring both immune and stress or neuroendocrine components

Given the broad nature of the topics covered in this thesis, summary metrics on research regarding pre-clinical models of stress, neuroendocrine factors and immune function are presented in this section. This analysis aimed to provide an overview of the research areas presently investigated, and the distribution of areas of interest using medline data accessed from the NCBI database. Medline data includes descriptors for each research article, thus providing a systematic approach to preliminary literature review.

1.2.1 Method

All medline data was obtained from pubmed using the Biopython v1.69 (Cock *et al.*, 2009) library via Python 2.7. Medline data containing article summary data including abstracts, titles, MesH terms, author keywords, and Journal names, were extracted from 10586 documents between 1967 to June 2017 using pubmed searchterms:

1) Glucocor* AND (microglia OR immune)
2) ("social defeat" OR "Restraint stress" OR inescapable OR "Forced Swim" OR "Chronic mild" OR "Chronic Unpredictable" OR “Maternal Separation”) AND (immune OR cytokines OR microglia OR inflammation)'

After parsing medline data using Biopython, descriptive metrics were obtained through Pandas 0.19.2 (McKinney, 2010), and graphed using matplotlib 2.0.0 (Hunter, 2007). Further text analysis was applied to the compile corpus of abstracts using NLTK 3.2.4 (Bird, Klein and Loper, 2009) and scikit.learn 0.18.2 (Pedregosa *et al.*, 2011).

Noun frequency within the compiled abstracts was used to access data regarding experimental stress models. Term frequency inverse document frequency (Tfidf) transformation was applied to the full corpus to obtain a transformed word frequency normalised to each document. Full methodological outline and source code used in this analysis is available in Appendix D.

1.2.2 Results

This thesis explores the relationship between stress and physiological adaptations to stress through the interface between the innate immune and neuroendocrine system. A total of 10586 entries were identified from the NCBI database. These entries were most commonly published in immunology-related and behavioural neuroscience related journals (Figure 2). From word frequency analysis in abstracts, 'patient' was found as the second most frequent word used (Figure 3). This result suggests the prevalence of human and clinical studies. Incidentally, the most frequent MesH term was also found to be 'Human' (not shown), thus indicating that human studies are prevalent. Based on word frequency across abstracts, mouse studies appear to be the next most common model, followed by rat. Common terms used in experimental models, such as 'mechanism', 'receptor', 'response', 'function' and 'control' were frequently mentioned. Moreover, cytokine (and interleukin, or 'IL'), and immune function were mentioned frequently across documents, while 'glucocorticoid', the end product of the neuroendocrine stress response, also appears to be common.

Trends in the assigned MesH terms classifying glucocorticoid related studies and cytokine related studies were examined (Figure 4). This analysis revealed that Glucocorticoid MesH terms had an initial growth in interest between 1990 and 2000, but has since plateaued. Conversely, studies featuring cytokines appears to still be in a period of growth in stress and immunity related research. Taken together, interest in the relationship between immune function and stress appears to be growing, but the role of glucocorticoids in this effect has remained constant over the past two decades. Human studies appear to be most prevalent, but use of rodents in stress research is

also common.

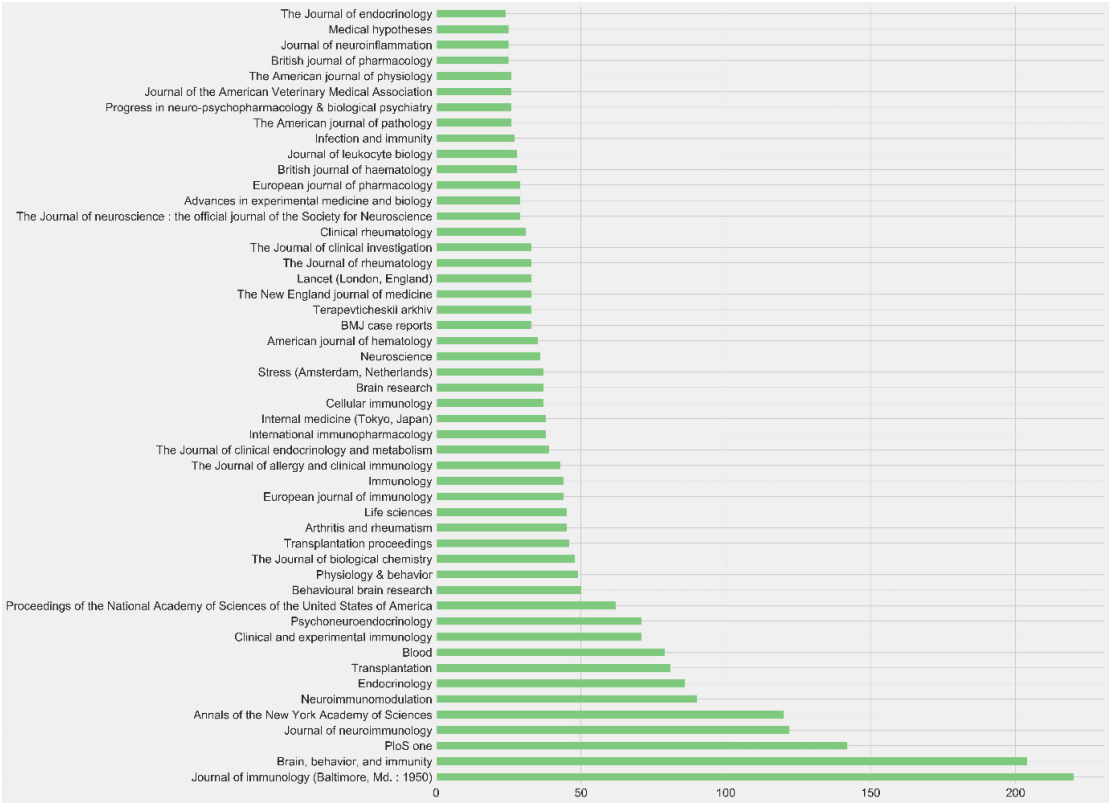

Figure 2. Distribution of publications across 50 most frequent Journals. Research articles are most frequently published in immunology-related journals and general-purpose Journals (PloS one, PNAS) Behavioural neuroscience, neuroendocrinology, neuroimmunology journals followed by general neuroscience journals.

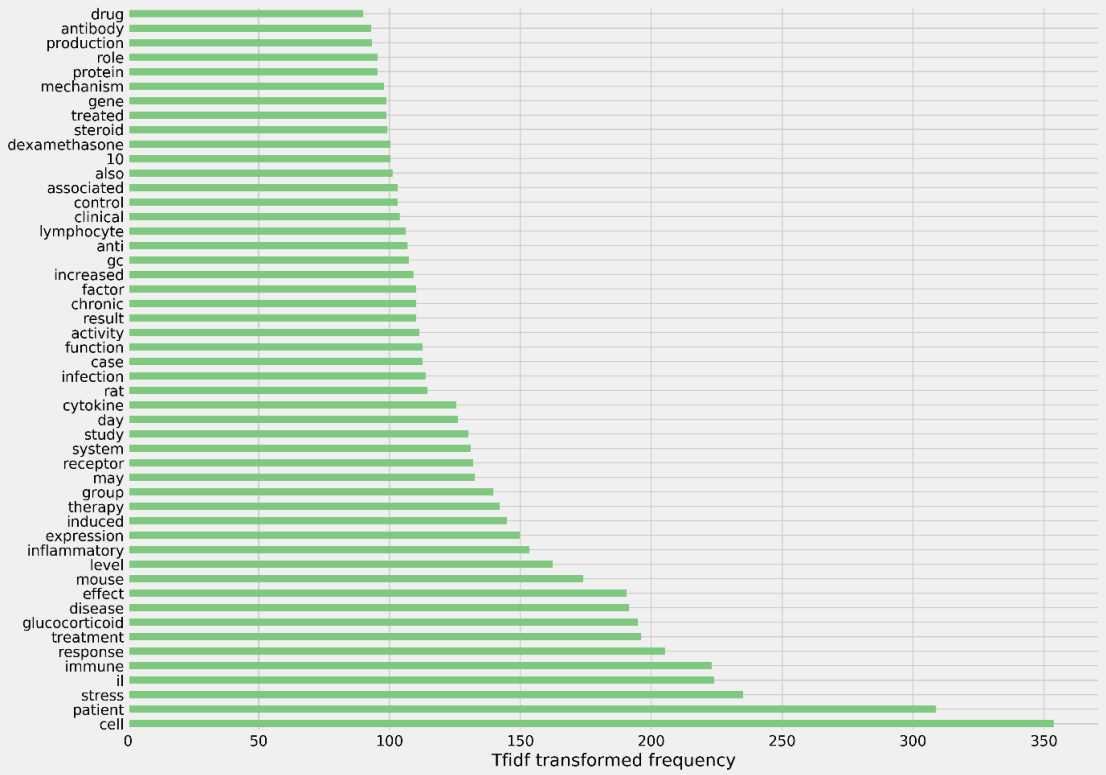

Figure 3. Most frequent terms used across abstracts. Term frequency inverse document frequency analysis on 10510 abstracts.

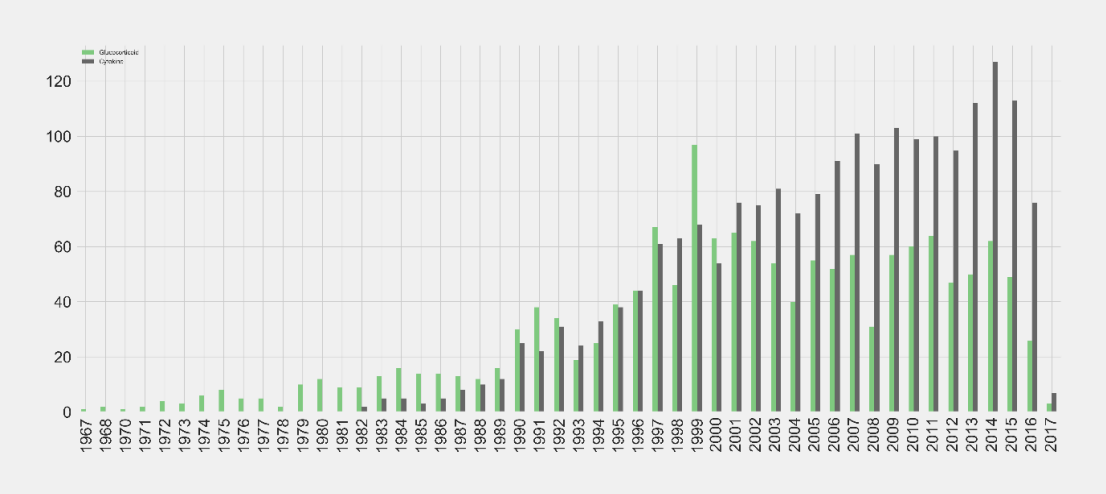

Figure 4. Frequency distribution of Glucocorticoid related and cytokine related MesH terms over time. A general upward interest in cytokine-related studies throughout (Grey), but glucocorticoid related studies (Green) peaked in the late 90s and appears to be relatively stable across the last 10 years. Analysis of MesH terms assigned per year reveal distribution of glucocorticoid (all mentions of Glucocorticoids or dexamethasone) and cytokine (all mentions of cytokine or Interleukin) -related studies.

1.3 An examination of common stress research models (observational and experimental)

1.3.1 Observational studies and common preclinical experimental models in stress research

Important discoveries about stress and physiology have been made from observational work on non-human primates in Africa, mainly exploring the effects of chronic environmental stress on the health of non-human primates (Sapolsky, 2016). Non-human primates, like humans, possess a robust system of social hierarchy. This hierarchy serves as an approximation of socioeconomic differences in humans through similarities in resource inequality and maintenance of dominance of the dominant party (Sapolsky, 2005). Taking advantage of the naturally existing social structure of these primates, work in this area has collectively shown how chronic social stressors can influence health and physiology. Social stress related physiological maladaptations include adverse effects on cardiac health (Shively, Register and Clarkson, 2009), inhibition of reproduction (Altmann, Sapolsky and Licht, 1995), immunosuppression to the point of vulnerability to infectious disease (Cohen *et al.*, 1997), and paradoxically overactivity of the immune system (Snyder-Mackler *et al.*, 2016). Neurological changes such as inhibition of neurogenesis (Wu *et al.*, 2014), and increased apoptotic cell death (Lucassen *et al.*, 2001), have also been identified from this work. Stress can therefore observably cause changes to physiological function, thus having an impact on health and disease.

Observational studies of non-professional caregivers of chronic patients (usually family members), a population undergoing chronic psychosocial stress, has also made

contributions to the associations between stress and adaptations of immune and neuroendocrine systems (Lovell and Wetherell, 2011). Peripheral blood leukocytes obtained from this population group, being convenient samples, have shown functional differences. For example, primary monocytes of caregivers display increased inflammatory activity, as measured by pro-inflammatory gene transcription and cytokine release in response to innate immune stimulation (Miller *et al.*, 2014). Neutrophil phagocytosis can also be impaired in caregivers with highest perceived levels of distress (Vitlic *et al.*, 2016). Taken together, immune dysregulation in a chronically stressed population is therefore evident, but the mechanisms behind cell-type differences amongst immunocompetent cells are still unclear.

1.3.2 Common pre-clinical experimental models of stress in immune-related applications

To experimentally manipulate and understand the mechanistic link between stress and stress adaptations seen in observational models, rodents have been used to develop models of stress that can be controlled in a laboratory setting. These stress models vary greatly in terms of physical presentation and duration, but all stressors have a component of uncontrollability or inescapability. This section briefly describes some common rodent stress models, with associated neurobehavioural and immune adaptations resulting from each stress model.

Inescapable shock

Inescapable shock models of stress involve delivering electrical shocks to the feet or tail that do not cause injury, and usually varied in terms of number of shocks delivered,

duration, and the intensity of each shock (Nguyen *et al.*, 1998; Blandino, Barnum and Deak, 2006). As part of a model of learned helplessness, animals are placed in an inescapable chamber while shocks are delivered. Learned helplessness, a type of depressive-like behaviour, is determined by the lack of active escape behaviours even when put in an escapable situation (Overmier and Seligman, 1967; Chourbaji *et al.*, 2005). The controllability of this stressor can determine the neurobiological responses, since only inescapable shocks cause increased serotonin signalling in the basolateral amygdala, as measured from microdialysis (Amat *et al.*, 1998). Inescapable shock has also been shown to cause loss of neuronal spine synapses in hippocampal CA1 and CA3 regions (Hajszan *et al.*, 2009), and increase in hypothalamus (Blandino, Barnum and Deak, 2006; Hueston and Deak, 2014), thus showing both neuronal and neuroimmune modulation as a result of this physical stressor.

Restraint stress

Restraint stress is another common potent physical stressor, which involves physical restriction of movement without impeding breathing over a time period. Each restraint stress session lasts between 5 min up to 6 h, and can vary from acute administration to repetition over the course of up to 3 weeks (see review for variations Buynitsky and Mostofsky, 2009). The potency of this stressor is demonstrated in the neurological outcomes of repeated administration. For example, previous studies have shown neuronal degradation and atrophy in the basolateral nucleus of the amygdala (Grillo *et al.*, 2015), causing increased neuronal excitability and anxiety behaviours (Hetzel and Rosenkranz, 2014), and hyperalgesia (Gamaro *et al.*, 1998).

The chronicity of restraint stress can influence immune activity. For example, acute restraint stress reduces pro-inflammatory protein expression in plasma but increased pro-inflammatory IL-1β cytokine and iNOS protein in the prefrontal cortex, hippocampus and hypothalamus (Gadek-Michalska *et al.*, 2015). In the same study, 3 – 14 days of repeated restraint stress still elevated pro-inflammatory IL-1β cytokine and iNOS proteins in the hippocampus, hypothalamus, but this increase diminished across time. Taken together, studies using repeated restraint stress thus reveal the neurological, immune and behavioural effects of repeated strong stressors.

Forced swim stress

Other physical stressors include forced swim stress, which can be delivered in an acute setting, or in combination with other stressors in chronic stress models. Forced swim stress involves lowering the rodent into an inescapable body of water, usually between 5 and 15 minutes, with well characterised acute endocrine and neurotransmitter changes (Connor, Kelly and Leonard, 1997; Droste *et al.*, 2008). Water temperature has also been increased or decreased to manipulate the severity of this physical stressor, which also present with different time dynamics of serotonin release (Linthorst, Flachskamm and Reul, 2008). Rodent immobility during forced swim stress is regarded as a depressive-like helplessness behaviour (Porsolt, Le Pichon and Jalfre, 1977), and is thus a common behavioural test used in anti-depressant drug discovery (Yankelevitch-Yahav *et al.*, 2015).

Social defeat stress

Social defeat stress involves the controlled contact between a dominant and non-dominant rodent to induce stress in the non-dominant party (Miczek and O'Donnell, 1978). One important note is that during this period of exposure, there may be varying degrees of physical contact between the parties involved, and thus can be thought of as both a physical and social/psychological stressor. Furthermore, exposure to social defeat can be acute or repeated. Through these models, social defeat has demonstrated deleterious increases in anxiety and depressive-like behaviour, with related neurological and neuroimmune molecular changes in the basolimbic system (see systematic review Vasconcelos, Stein and Almeida, 2015). Social defeat can also cause the migration and infiltration of perivascular monocytes into the brain, which can contribute to pro-inflammatory signalling as a result of stress (Wohleb *et al.*, 2012).

Chronic unpredictable stress or chronic mild stress

Environmental stressors include predator scent, changes to bedding, ambient temperature, food deprivation, white noise, as well as cage rattling. These environmental stressor can be used in isolation, but are normally administered in combination with other physical or social stress models for a duration of days to weeks as part of chronic unpredictable stress or chronic mild stress models (see review, Campos *et al.*, 2013). Chronic unpredictable or chronic mild stress have been developed to better model human stress conditions, in which stressors are less likely to be extreme in severity, but more likely varied over a prolonged period (Willner,

2017). Multiple studies have shown the success in chronic unpredictable stress models in inducing depressive-like and anxiety behaviours (Liu *et al.*, 2013; Chen *et al.*, 2016), and reduction of threshold for substance seeking behaviour in rats (Lin *et al.*, 2002). Apart from behavioural changes, chronic unpredictable stress can reduce serotonergic neuron firing rate in the midbrain raphe (Bambico, Nguyen and Gobbi, 2009). Central immune activation can also increase after chronic mild stress, as measured by an increase in microglia surface area in the hippocampus and midbrain regions (Farooq *et al.*, 2012), and elevated gene transcription of pro-inflammatory cytokines in the hippocampus and hypothalamus (You *et al.*, 2011). Adoption of chronic mild or unpredictable stress has grown substantially over the last decade (Figure 5), supporting the reliability of this stress model in causing neurobehavioural changes (Willner, 2017).

Immune stress

Aside from behavioural stress models, emerging from the field of psychoneuroimmunology, immune stress models have also been developed to understand how behavioural changes can result from immune challenges. These immune challenges can include administration of bacterial infections, aseptic components of bacteria or exogenous cytokines to elicit behavioural and physiological responses (Dantzer, 2004; Lawson, McCusker and Kelley, 2013; Barichello *et al.*, 2014). Early-life models of immune stress exposures have shown long term behavioural, endocrine and immunological adaptations in adulthood have been established (Wohleb *et al.*, 2012; Dinel *et al.*, 2014). Acutely, these immune stressors can also elicit

short-term behavioural change, collectively termed as sickness behaviours, which have become models studying immune, neuroendocrine and neurobehavioural aspects of the adaptations seen in stress (Dantzer and Kelley, 2007).

Maternal separation stress

Maternal separation is a model of early life stress with profound long-term influences on behaviour, immune functioning, and neuroendocrine activity (Ladd *et al.*, 2004; Roque *et al.*, 2014; Hsiao *et al.*, 2016). Maternal separation, as the name implies, induces stress through the removal of the animal's mother for a period. This model is most commonly implemented as a daily separation of 3 h between day 2-12 postpartum in rodents (Vetulani, 2013). Maternal separation has demonstrated an impact on dopaminergic neurotransmission during adolescence, characterised by an increase in tyrosine hydroxylase fibres in the prelimbic cortex and nucleus accumbens, and differential distributions of dopamine receptors across several midbrain structures (Majcher-Maślanka *et al.*, 2017). Neurotransmission can therefore be altered by early life maternal separation.

Interestingly, the delivered stress protocol can have a widely varied impact on long-term measures. As an example, day 2-12, but not day 5-15 maternal separation, caused an increase in depressive like behaviour in adulthood (Roque *et al.*, 2014). In this study, although both maternal separation models resulted in increased glucocorticoid signalling in adulthood, only day 2-12 maternal separation resulted in an elevated CD4/CD8 splenic cell ratio. Additionally, both a decrease in pro-inflammatory

gene expression (Dimatelis *et al.*, 2012), and increase in circulating cytokines IL-1β and IL-6 (Wieck, Andersen and Brenhouse, 2013) resulting from maternal separation stress have been reported. Maternal separation stress models thus reveal the complexity in developmental influence of behavioural, neuroendocrine and immune outcomes.

1.3.3 Frequency distribution of experimental stress models in immune-related research

Behavioural research with regards to stress, glucocorticoids and immunity as a whole appears to be growing rapidly since 2014, approximated using the frequency of 'behavior' term used in abstracts overall. Restraint stress models were most frequently used (571 publications), but both restraint stress and inescapable shock seem to be relatively stable in comparison to total behavioural research. In the context of immunity and glucocorticoid research, forced swim was not commonly used as a stress model on its own (14 publications), while maternal separation (103 publications), chronic mild (121 publications) and unpredictable stress (91 publications) models were more prevalent. Unpredictability in chronic stress appears to be trending after 2014, as opposed to chronic mild stress. Both social defeat and chronic unpredictable stressors seem to be developed at a later date compared to restraint and inescapable shock, but total number of papers featuring social defeat stress was almost equivalent to inescapable shock (137 and 142 respectively) in this dataset. Mention of immune stressors such as LPS in abstracts has been frequent (379 publications) and stable since 1995, but it is difficult to discern whether LPS has been used as a physiological stressor in those studies. For example, LPS could have been used in ex vivo or in vitro applications, and not to elicit behavioural changes.

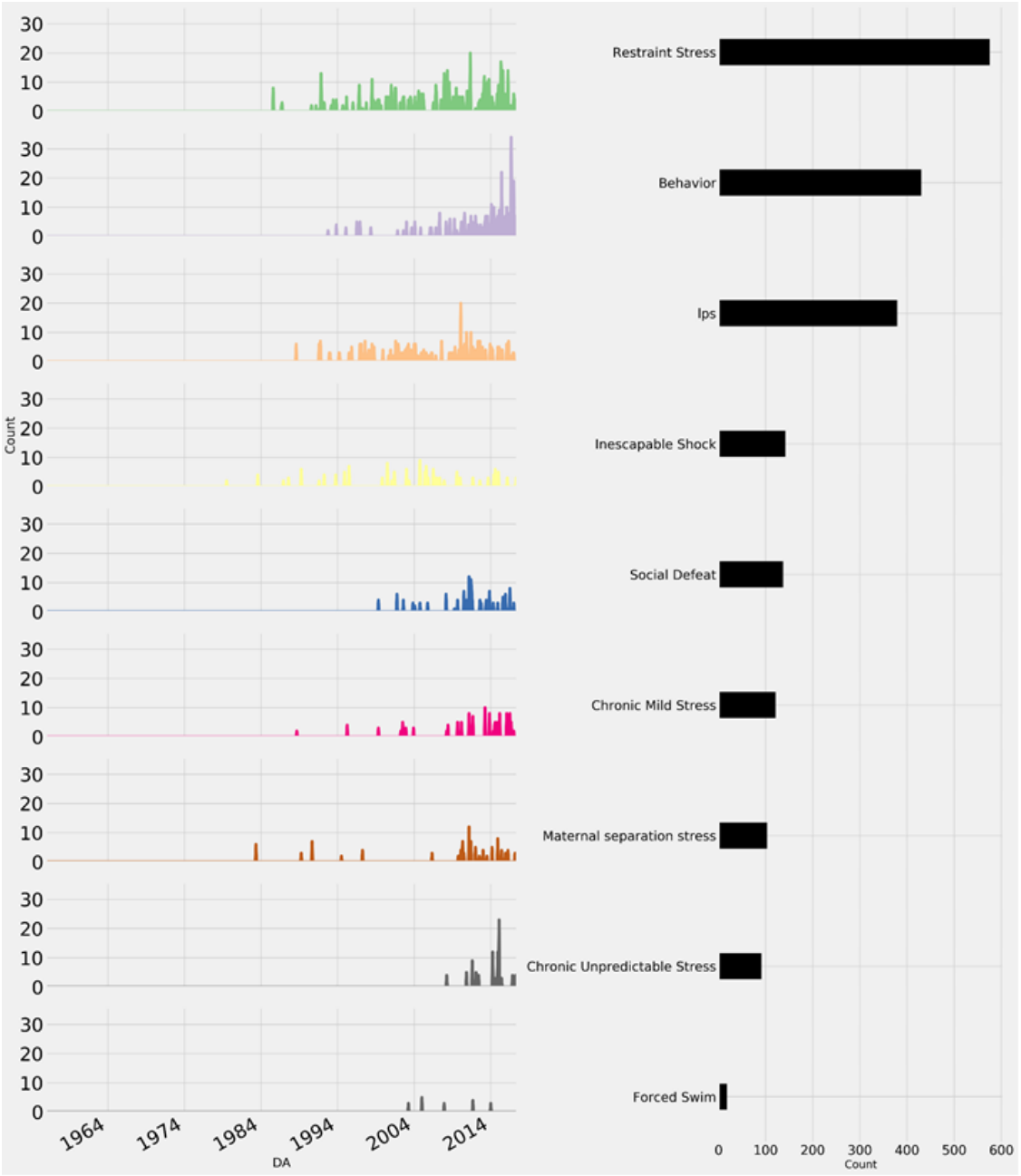

Figure 5. Distribution of stress models approximated from noun phrases in abstracts featuring both stress and immune-related research. Distribution over time of publication, constructed by incidence of defining words or abbreviations for each stress model. Incidence of "Behavior" over time is used as an indication of total trend in behavioural research. Graphs represent distribution over time (A), and Total number of articles using each stress model (B). A total of 1996 publications out of the full 105860 abstracts (18.9%) were identified for this analysis.

Collectively, observational studies and stress models have come to shape important concepts in stress research including the nature of adaptations, and the maladaptations arising from stress. One important concept is the relationship between "dose" and duration of stress in the presentation of outcomes. Stress is understood to have a biphasic and time-dependent nature, where stress is adaptive in the acute and mild setting, while maximal responses occur at mid and extreme levels of stress and in chronic settings (Calabrese *et al.*, 2007; Chrousos, 2009). In addition, characterisation of stress actions also identified complex physiological preparatory, stimulatory, suppressive and permissive actions during the stress responses, which vary according to tissue type, time of measurement, and severity of stress (Sapolsky, Romero and Munck, 2000). The interactions of stress, physiology and disease are therefore a complex area of study, influencing not just behavioural, but endocrine, neurological, reproductive, circulatory and immunological systems. Given the association between stress and health, study of the mechanisms underlying these physiological adaptations will therefore translate to a greater understanding of the detrimental or beneficial health outcomes of stress.

Statement of Authorship

Title of Paper	Toll-like receptor 4: innate immune regulator of neuroimmune and neuroendocrine interactions in stress and major depressive disorder
Publication Status	☑ Published ☐ Accepted for Publication ☐ Submitted for Publication ☐ Unpublished and Unsubmitted work written in manuscript style
Publication Details	Liu, J., Buisman-Pijlman, F. and Hutchinson, M. R. (2014) 'Toll-like receptor 4: innate immune regulator of neuroimmune and neuroendocrine interactions in stress and major depressive disorder.', *Frontiers in neuroscience*, 8(September), p. 309. doi: 10.3389/fnins.2014.00309.

Principal Author

Name of Principal Author (Candidate)	JiaJun Liu
Contribution to the Paper	Planned, prepared and edited the manuscript.
Overall percentage (%)	90 %
Certification:	This paper reports on original research I conducted during the period of my Higher Degree by Research candidature and is not subject to any obligations or contractual agreements with a third party that would constrain its inclusion in this thesis. I am the primary author of this paper.
Signature	Date: **01/09/2017**

Co-Author Contributions

By signing the Statement of Authorship, each author certifies that:

i. the candidate's stated contribution to the publication is accurate (as detailed above);

ii. permission is granted for the candidate in include the publication in the thesis; and

iii. the sum of all co-author contributions is equal to 100% less the candidate's stated contribution.

Name of Co-Author	Dr. Femke Buisman-Pijlman
Contribution to the Paper	Supervised the planning and editing of the manuscript.
Signature	Date: 1/9/17

Name of Co-Author	Prof. Mark R Hutchinson
Contribution to the Paper	Supervised the planning and editing of the manuscript.
Signature	Date: 5.9.17

1.4 Publication- Toll-like receptor 4: innate immune regulator of neuroimmune and neuroendocrine interactions in stress and major depressive disorder

This thesis explores the relationship between stress and physiological adaptations to stress through the interface between the innate immune and neuroendocrine system. In the following review (Liu, Buisman-Pijlman and Hutchinson, 2014), we attempted to understand the bidirectional interactions between the innate immune system and the hypothalamus pituitary and adrenal (HPA) axis, with focus to Toll-like receptor 4 (TLR4) as an innate immune coordinator of these adaptations in the context of major depressive disorder. Concepts such as HPA signalling, glucocorticoid actions and specific examples of neuroimmune components in stress were included in the review.

Toll-like receptor 4: innate immune regulator of neuroimmune and neuroendocrine interactions in stress and major depressive disorder

JiaJun Liu[1], Femke Buisman-Pijlman[2] and Mark R. Hutchinson[1]*

[1] *Neuroimmunopharmacology Group, Discipline of Physiology, School of Medical Sciences, The University of Adelaide, Adelaide, SA, Australia*

[2] *Discipline of Pharmacology, School of Medical Sciences, The University of Adelaide, Adelaide, SA, Australia*

Edited by:
Luba Sominsky, RMIT University, Australia

Reviewed by:
Fulvio D'Acquisto, Queen Mary University of London, UK
Quentin Pittman, University of Calgary, Canada

****Correspondence:***
Mark R. Hutchinson, Discipline of Physiology, School of Medical Sciences, University of Adelaide, L5 Medical School South, Frome Rd., Adelaide, SA 5005, Australia e-mail: mark.hutchinson@adelaide.edu.au

Major depressive disorder (MDD) poses one of the highest disease burdens worldwide. Yet, current treatments targeting serotonergic and noradrenaline reuptake systems are insufficient to provide long-term relief from depressive symptoms in most patients, indicating the need for new treatment targets. Having the ability to influence behavior similar to depressive symptoms, as well as communicate with neuronal and neuroendocrine systems, the innate immune system is a strong candidate for MDD treatments. Given the complex nature of immune signaling, the main question becomes: What is the role of the innate immune system in MDD? The current review presents evidence that toll-like receptor 4 (TLR4), via driving both peripheral and central immune responses, can interact with serotonergic neurotransmission and cause neuroendocrine disturbances, thus integrating with widely observed hallmarks of MDD. Additionally, through describing the multi-directional communication between immune, neural and endocrine systems in stress, TLR4—related mechanisms can mediate stress-induced adaptations, which are necessary for the development of MDD. Therefore, apart from exogenous pathogenic mechanisms, TLR4 is involved in immune changes as a result of endogenous stress signals, playing an integral part in the pathophysiology, and could be a potential target for pharmacological treatments to improve current interventions for MDD.

Keywords: toll-like receptor 4, TLR4, HPA, neuroendocrine, neuroimmunology, stress, depression, MDD

INTRODUCTION

Major depressive disorder (MDD) represents a combination of disturbances to mood, cognition, sleep and appetite, which causes impairment to individual functioning lasting a minimum of 2 weeks (American Psychiatric Association, 2013). MDD consistently ranks within the top 4 highest "years lived with disability" (Vos et al., 2012), and accounts for 7.4% of total disabilityadjusted life years worldwide (Whiteford et al., 2013). In addition, depressive disorders have an estimated 93.5% comorbidity with other diseases, most commonly with chronic pain, anxiety, bipolar disorder, post-traumatic stress disorder, diabetes and neurological disorders (Gadermann et al., 2012). Major depression thus bears one of the highest disease burdens, with matching economic and societal costs. Yet, current pharmacological treatments using serotonin and noradrenaline reuptake inhibitors (SSRI and SNRI, respectively) are inefficient, requiring to treat 7 patients in order to gain one positive outcome (Arroll et al., 2009). This suggests that alterations to the serotonergic pathway are only partly responsible for MDD, and other mechanisms must be involved. Thus, it is sensible to study other systems, in order to improve current treatments for MDD.

Ever since early observations of increased immune markers in psychiatric patients, the immune system has become increasingly associated with various psychosomatic illnesses (Solomon et al., 1969). In the case of MDD, patients exhibit increased circulating peripheral cytokines, which are immune signaling molecules that can be pro or anti-inflammatory (Anisman and Hayley, 2012; Lichtblau et al., 2013). Additionally, a decrease in depressive symptoms is coupled with a normalization of immune signaling levels (Gazal et al., 2013), suggesting that there may be immune involvement in MDD.

NEUROINFLAMMATORY EVENTS: NEUROINFLAMMATION AND NEUROKINE SIGNALING IN MDD

Although immune signaling in the brain is comprised of signals from resident glial cells, peripheral to central immune communications and migration of peripheral cells into central compartments, it is important to note the phenotypic differences between different neuroinflammatory diseases. The term "Neuroinflammation" is commonly used to encompass increased immune activation in the CNS. However, the central nervous system (CNS) can take on different inflammatory states, and there is a distinction between the magnitude of immune responses in the CNS by varied causes. For example, neurodegenerative disorders including Alzheimer's and Parkinson's disease are characterized by widespread immune signaling in the CNS, oxidative stress, and increased immune trafficking into the brain, resulting in systemic inflammation accompanied with progressive damage (Heneka et al., 2014). On the other hand, acute and sub-maximal immune challenges such as that triggered by opioid exposure can also cause increased central immune signaling, but the resulting inflammatory response is of a much lower magnitude (Stevens et al., 2013). This sub-inflammatory state is attributed to the direct actions of opioids on CNS expressed toll-like receptor 4 (TLR4), since opioids readily cross the BBB, rather than the indirect peripheral to central immune response following bacterial infections (Hutchinson and Watkins, 2014; Jacobsen et al., 2014).

Classically, inflammation involves swelling, heat, and pain, coupled with a coordinated infiltration of various immune cells into the affected area. In many neurological conditions, this largescale damage is not seen unless in terminal stages, or in cases of

major BBB compromise. Thus, the use of "neuroinflammation" to refer to central immune activity can become confusing, and a clear distinction between high magnitude and submaximal immune states is required.

Neurokines refer to neurally active cytokines (Nathanson, 2012), which can be upregulated as a result of peripheral infections or innate immune activation without the infectious agent crossing the BBB (McCusker and Kelley, 2013). An important differentiation between increased neurokine signaling and neuroinflammation is the reversibility of the effects. Central cytokine increase resulting from low-grade infections, exercise and stress result in reversible neuronal changes (McCusker and Kelley, 2013). These neuronal changes include the upregulation of AMPA and NMDA receptors, as well as decreased expression of GABA receptors on neurons by cytokines IL-1β and TNF-α, causing reversible increased excitation (see Viviani et al., 2014 for a review). We thus propose the use of the terms "increased neurokine signaling" or "increased central immune signaling" to apply to these sub-inflammatory states, and only when there is large-scale damage as a result of immune cell derived neurotoxicity and inflammation should the term "neuroinflammation" be applied in order to reduce confusion within the literature.

In regards to MDD, current evidence indicates a milder immune signaling phenotype more akin to increased neurokine signaling, rather than neuroinflammation. Compared with the continued accumulated loss of function observed in neurodegenerative disorders such as Alzheimer's and Parkinson's disease, MDD has periods of active disease characterized by depressive episodes followed by remission. During remission, peripheral blood expression of TNF superfamily 12–13 mRNA is lower than in active

disease (Otsuki et al., 2010). This indicates that the immune signaling is influenced by the state of the disorder, but critically, the degree of immune signaling required for the presentation of a disease symptom may be significantly higher than that needed for MDD to be observed, as illustrated by the development of depressive-like behavior prior to the development of significant demyelination in experimental autoimmune encephalitis (Acharjee et al., 2013). Furthermore, structural changes in hippocampal volume measured using MRI appear reversible in patients with MDD (Frodl et al., 2004). Antidepressants (Horikawa et al., 2010; Alboni et al., 2013; Obuchowicz et al., 2014) and cognitive-behavioral therapy (Gazal et al., 2013) are also able to reduce cytokine expression in depressive disorders. Taken together, there is strong evidence for the reversibility of inflammatory markers that closely relates to the state of depressive symptoms. Along with the bidirectional neuroimmune connection, this reversibility and liability of the condition suggests that targeting the central immune system could be a promising treatment option for MDD.

THE ROLE OF TOLL-LIKE RECEPTOR 4 IN MDD Recently, TLR4 has come to the forefront of research linking neuroimmune signaling and MDD, through driving immune to brain communication. TLR4 is an innate immune pattern recognition receptor, which is part of the Interleukin-1 Receptor/TollLike Receptor Superfamily containing a toll-like/IL-1 Receptor (TIR) domain and Leucine-rich repeat motif in the extracellular domain. TLR4 recognizes endogenous danger associated molecular patterns (DAMPs) including heat shock proteins (HSP) and high mobility group box 1 (HMGB1), exogenous pathogen associated molecular patterns (PAMPs) such as lipopolysaccharide (LPS), as well as microbiome/microbe associated molecular patterns (MAMPs) (Akira and Takeda,

2004). Unlike other toll-like receptors, activation of TLR4 triggers pro-inflammatory transcription via 2 adaptor proteins, Myeloid differentiation primary response 88 (MyD88) and TIR domain-containing adapter inducing IFN-β (TRIF), which induces transcription factors NF-κB, AP-1, and IRF3 (Xu et al., 2000; Watters et al., 2007). Activation of these transcription factors causes the production of pro-inflammatory cytokines including IL-1β, TNF-α, IL-6, and CXCL10, along with an upregulation of proteins including cyclooxygenase 2 (COX-2), resulting in pro-inflammatory signaling (Akira and Takeda, 2004).

In the CNS, TLR4 is predominantly expressed on microglia, and is also to a lesser extent expressed on neurons (Zhao et al., 2014). Through modulation of neuroimmune activity, TLR4 is implicated in various neuropathological conditions that afflict the CNS, including neuropathic pain (Lewis et al., 2012) and neurodegenerative diseases (Heneka et al., 2014). Increasingly, these disorders are recognized as existing on a spectrum from altered neuroimmune signaling (e.g., neuropathic pain) through to gross neuroinflammation (e.g., Neurodegenerative diseases).

MDD, being increasingly classified as a neuroimmune disorder, may also have TLR4 involvement (Gárate et al., 2011; Hines et al., 2013). Recent evidence has found that peripheral blood mononuclear cells (PBMC) of patients with MDD express higher levels of TLR4 (Kéri et al., 2014). Importantly, the authors showed that this heightened expression was reduced following treatment, and paralleled improvement in depressive symptoms. This responsiveness toward depressive states indicates that TLR4 activity could directly be involved in the pathophysiology of MDD.

Given the involvement of the immune system in numerous neurological disorders, it is

now accepted that the CNS is not an immune privileged organ that exists in isolation of the immune system. The CNS can no longer be thought of as resistant to immune signals, or protected from immune damage (Ransohoff and Brown, 2012). Rather than separate entities, immune, neuronal and endocrine systems appear to be in constant bidirectional communication and a dysregulation of these systems can result in pathological states within the CNS (see Kelley and McCusker, 2014 for review). The current review thus posits that TLR4, being central to the immune to brain, and immune to neuroendocrine communication, underlies the neuroimmune signaling events observed in the pathophysiology of stress-related disorders including MDD, across systemic and cellular levels.

TLR4 ACTIVITY CAN INFLUENCE BEHAVIOR AND MDD

Using LPS as an agonist, peripheral TLR4 activation is sufficient to cause changes in motivational state and can trigger sickness behavior (Hines et al., 2013). Sickness behavior is characterized by increased anhedonia, lethargy, loss of locomotion and anorexia following immune challenges (Dantzer and Kelley, 2007). Once thought to stem from altered energy balance, it is clear that these immune signaling initiated behavioral adaptations are driven by specific cytokine-dependent signaling cascades (Dantzer, 2004). Thus, an immune stimulus can drive complex higher order behavioral adaptations, providing direct evidence for the link between the immune system and symptoms of depression.

Although the idea of sickness behavior may appear surprising since pathogens themselves are imperceptible by our classic sensory organs, it makes sense that the body needs to know when it encounters pathogens in order to make behavioral

adjustments. Through reduction in locomotion, sickness behavior can promote recovery from the immune challenges. Sickness behavior can therefore be considered as adaptive since it promotes homeostasis within the conditions of the stressor (Dantzer and Kelley, 2007).

The effect of peripheral immune activation on behavior is thought to be mediated by three main mechanisms: (1) peripheral release of pro-inflammatory cytokines can cross the blood brain barrier (BBB) via "leaky" subventricular organs, thus directly increasing neurokine signaling, (2) These activated immune cells can also cross the BBB directly to cause neuroimmune signaling, and (3) peripheral cytokines can also stimulate afferent pathways such as the vagus nerve, causing behavioral changes via neural mechanisms (see McCusker and Kelley, 2013 for review). Besides these mechanisms, emerging evidence have demonstrated that monocytes can adhere and roll along the cerebral vasculature, and can cause increased central immune signaling without crossing the BBB, and this is associated with increases in inducible Nitric Oxide Syntase (D'Mello et al., 2013). The authors further showed that inhibiting this mechanism could improve sickness behavior as a result of peripheral inflammation, thus suggesting another mode of peripheral to central communication with behavioral implications.

Importantly, the trigger for behavioral changes need not originate from pathogenic mechanisms, since cytokine administration is sufficient to elicit sickness behavior similar to bacterial stimulation (Tazi et al., 1988; Dantzer, 2004). This means that other potential sources of immune activation, including endogenous danger signals, or neurogenic activation could trigger this response.

Strong parallels can be drawn between sickness behavior and depressive behavior,

namely reduced locomotion, anhedonia, and dysregulated sleep and food intake (McCusker and Kelley, 2013). Since MDD can be chronic and recurring, the question arises whether patients with MDD are just displaying chronic dysregulation in inflammation or immune signaling? Indeed, patients suffering from MDD display heightened circulating cytokine levels, indicative of increased immune signaling (Anisman and Hayley, 2012; Lichtblau et al., 2013). Furthermore, there is some evidence showing that celecoxib, an NSAID that inhibits COX-2, can improve depression scores as well as increase remission rates in patients receiving anti-depressants (Faridhosseini et al., 2014; Na et al., 2014). In rodent models, NSAID administration can improve depressive-like behavior, measured using the forced swim test and tail suspension tests (Maciel et al., 2013; Guan et al., 2014). Notably however, these studies indicate that the antidepressive effect of NSAID requires a higher dose in order to achieve comparable results to SSRIs, and are more effective in immune stressor induced depressive-like behavior. Additionally, there is some debate about the efficacy of these treatments since NSAIDs can also reduce efficacy of SSRI treatment when given in conjunction, in both animals and patients (Warner-Schmidt et al., 2011). MDD thus appears to have an immune component, but the exact mechanisms behind this interaction require more investigation.

CELL MEDIATED MECHANISMS OF CENTRAL IMMUNE SIGNALING EVENTS ASSOCIATED WITH MDD

It has been confirmed that both peripheral and central administration of LPS can induce sickness behavior, showing that both peripheral and central immune signaling are involved in perpetuating this behavioral change (Huang et al., 2008; Hines et al., 2013). This TLR4 mediated Innate immune signaling in the CNS is mainly undertaken by

2 cell populations, the resident glial cells, and infiltrating peripheral immune cells. Glial cells, consisting of oligodendrocytes, astrocytes and microglia, vastly outnumber neurons by an estimated 10–50fold (Temburni and Jacob, 2001; Banati, 2003). These cells were previously regarded as inert support cells that do not directly influence neurotransmission. However, there is increasing evidence that glial cells are integral to both physiological functions and pathophysiological states in the CNS.

Astrocytes

Astrocytes are the most abundant cell type in the CNS, providing structural and trophic support to neurons. They have star-shaped morphology, with processes that can be in contact with up to 100,000 neurons (Halassa et al., 2007). Although astrocytes are not capable of producing action potentials, neurotransmitter binding to receptors present on astrocytes can induce Ca2+ waves (Sharma and Vijayaraghavan, 2001; Schipke et al., 2011). In addition to forming close appositions with synapses, astrocytes can influence the chemical environment through secretion of various compounds such as ATP, adenosine and acetylcholine, a process known as gliotransmission. Astrocytes can therefore influence neurotransmission on a synaptic level and could play a role in aggregating neural responses. Collectively, astrocyte involvement with synaptic activity is termed the tripartite synapse (Araque et al., 2014).

Across the CNS, astrocytes display different phenotypes and can adopt different states (Sun and Jakobs, 2012). Activated astrocytes display less branching morphological characteristics, and this is associated with glial fribrillary acid protein (GFAP) upregulation (Pekny and Nilsson, 2005). Activated in injury, astrocytes can be both protective by releasing factors facilitating recovery (Gimsa et al., 2013), and disruptive

to neuronal functioning via inhibiting axon growth through formation of glial scars after extended activation (Smith-Thomas et al., 1994; Yuan and He, 2013). Moreover, radial glia located at the subventricular zones also express GFAP, but act as precursor cells capable of differentiating into neurons and astrocytes, which can migrate to several areas including the cortex, displaying ability for adult neurogenesis and cell renewal (Sundholm-Peters et al., 2005). The role of astrocytes is therefore varied and important to normal physiology, but astrocytes can also participate in both neuroimmune signaling and neuroinflammatory disease progression.

In MDD, astrocytes may be involved in the progression of the disease through participating in the reuptake of serotonin. In the presence of TNF-α, serotonin transporters expressed on astrocytes increase reuptake of serotonin in a dose-dependent manner, and this effect is attenuated by administration of SSRIs (Malynn et al., 2013). Interestingly, SSRI are also able to influence astrocytic Ca2+ waves in a similar way to serotonin administration (Schipke et al., 2011). Although unclear whether astrocytes are an integral target for anti-depressant treatment, it appears that astrocytes can play a role in serotonin neurotransmission, and therefore be involved in the pathophysiology of MDD.

Microglia

Microglia are the resident immunocompetent cells in the CNS, and play an active role in neuroinflammatory actions by release of cytokines, chemokines phagocytosis and removal of debris, directly modulating neuroimmune activity. Microglia are thus the main cell type investigated in neuroimmune signaling events and neuroinflammatory/neurodegenerative conditions. Being implicated in synaptic

pruning during CNS development, microglia not only perpetuate damage, but also are integral for normal functioning (Schwartz et al., 2013). Microglia too have different activation states, commonly referred to as M1 and M2, the pro and anti-inflammatory phenotypes, respectively (Olah et al., 2011). When activated to an M1 phenotype, microglia display a more ameboid morphology, and secrete cytokines and chemokines to signal for other immune cells. Microglia can also function as antigen presenting cells through MHC-II expression, therefore possessing the ability to trigger the adaptive immune responses within the CNS (Harms et al., 2013). Expressing pattern recognition receptors such as TLR4, microglia are responsive to DAMPs, MAMPs, and PAMPs. Moreover, TLR4 activation can shift microglia toward a M1 phenotype, inducing pro-inflammatory responses in the CNS (Ajmone-Cat et al., 2013).

Besides functioning as an antigen-presenting cell, microglia can influence neuronal functions through expression of glutamate transporters (Persson et al., 2005), but to a lesser extent as compared to astrocytes (Beschorner et al., 2007). In addition, microglia in the "resting" state actively survey the surrounding area for chemical changes, and can rapidly respond to stimuli (Nimmerjahn et al., 2005). Thus, even during an immunologically dormant state, microglia are able to influence neurotransmission and can rapidly respond to danger signals. Aiding this responsiveness are the toll-like receptors, which can recognize multiple stimuli and modulate the activation states of microglia.

Microglia, through TLR4-dependent signaling (Hines et al., 2013), and production of cytokines (Henry et al., 2009; Dobos et al., 2012), are regarded as mediators of central immune signaling in animal models of sickness behavior. In addition, changes in

microglial reactivity states are also associated with the induction of stress-induced depressive like behavior (Pan et al., 2014). In a recent study, minocycline, an antibiotic that has also shown the ability to suppress central immune signaling by acting on microglia, can prevent the development of depressive-like behavior, tested using sucrose preference and social exploration (Kreisel et al., 2014). This reduction of depressive-like behavior was found in conjunction with changes to microglia morphology and proliferation. On the other hand, the study illustrated that simply inhibiting microglia chronically would not be a viable treatment option, since microglial activation states change from an initial proliferative state to later decline from acute to chronic models, and central immune suppression exacerbates depressivelike behavior in a chronic model. Instead, the authors proposed that depression is related to either an over or under activation of microglia, and treatments should strive toward a balance in activation states. Taken together, microglia appear important in central immune signaling and immune to brain communication in MDD, but this relationship is not is not uni-directional, and appears to be time-dependent.

Peripheral immune cells and their actions on the CNS

Although the CNS is protected from many peripheral factors by the BBB, peripheral immune cells have been found to infiltrate and drive inflammation within the CNS (Schweingruber et al., 2014; Vogel et al., 2014). Perivascular macrophages and circulating monocytes can cross the BBB into the CNS through the expression of adhesion molecules such as ICAM and VCAM on the endothelium of blood vessels surrounding the CNS (Wong et al., 2007). Additionally, peripheral leukocytes can also roll and adhere to the cerebral vasculature, and cause increased central immune

signaling without entering the CNS, thus communicating across the BBB (D'Mello et al., 2013). Glial cells themselves can also release chemokines such as CCL2, which can trigger peripheral immune cell extravasation into CNS tissue (Williams et al., 2013; Shieh et al., 2014). Thus, the central immune system can actively signal for peripheral immune cells to cross the BBB.

Contrary to other models of neuroinflammatory/neurodegenerative disorders Wohleb et al. (2014) have recently shown that peripheral bone marrow-derived cell infiltration is not just evident in models of BBB compromise, but can also occur in sub-inflammatory conditions as well. Interestingly, increased infiltration of peripheral monocytes can influence anxiety-like behavior, once again illustrating the ability for immune signaling to influence higher-order CNS function (Wohleb et al., 2014). This result, however, still needs more investigation, as it is widely held that immune-cell infiltration is a sign of neuroinflammation, and is not evident in sub-maximal levels of central immune signaling.

There is little direct evidence showing peripheral immune cell migration in MDD due to the lack of a representative animal model of MDD. Nevertheless, social defeat and psychological stress can trigger increased trafficking of peripheral cell infiltration (Brevet et al., 2010; Wohleb et al., 2013). Given that MDD is considered a stress disorder (for more information, see Section "what does stress have to do with it?"), this indicates that peripheral cell infiltration could be involved in MDD. However, isolating the exact cause of immune signaling in MDD is challenging, and the extent of peripherally driven immune responses in MDD patients is thus still unknown.

EFFECT OF INCREASED IMMUNE (TLR4) ACTIVITY ON CNS NEUROTRANSMITTER ACTIVITY

So far, the best-characterized neuropathophysiology of MDD within the CNS is the dysregulation in serotonin neurotransmission, but the exact cause of this alteration is still unclear. There is growing evidence that glia are able to influence neurotransmission, and through these mechanisms, glia can contribute to the neuronal adaptations in MDD (Burke et al., 2014; Kreisel et al., 2014). Through close appositions with synapses in tripartite and tetrapartite arrangements, glia have access to the chemical environment of the synapse. Functionally, astrocytes can contribute to glutamate homeostasis by clearing excess glutamate from synapses. During situations of increased neuroimmune signaling, this process is impaired due to the down regulation of astrocyte glutamate transporters (EAAT1 and EAAT2), causing glutamate neurotoxicity and subsequent neuronal death (Tilleux and Hermans, 2008; Persson et al., 2009; Fang et al., 2012).

In relation to MDD, glia express serotonin transporters (Malynn et al., 2013), and can also directly inhibit serotonin production during neuroinflammation through the production of indoleamine-2,3-dioxygenase (IDO). IDO further interferes with the synthesis of serotonin by catalyzing tryptophan, forming quinolinic acid and 3-hydroxy-kynurenine, which can further result in neurotoxicity (O'Connor et al., 2009). Through this pathway, the increase in IDO reduces serotonin signaling as seen in MDD by impairing serotonin production, and can also cause direct damage to serotonergic neurons. Indeed, patients with MDD display and increased circulating kynurenine to tryptophan ratio, suggesting increased IDO activity (Quak et al., 2014). Moreover, this

effect is thought to mediate depressive like behavior as a result of immune activation, as pharmacological inhibition of IDO is able to attenuate the increase in central immune signaling and depressive-like behavior in response to LPS administration in rodant models (Corona et al., 2010; Dobos et al., 2012). The ability of glia to influence serotonergic neurotransmission illustrates that rather than replace earlier notions of what causes depressive symptoms—that is, an impairment in serotonin metabolism—neuroimmune mechanisms instead contribute to and supplement neural mechanisms of disease.

EFFECT OF MDD TREATMENTS ON IMMUNE SIGNALING

The immune to brain communication is not uni-directional, since neuronal functions can also influence the activity of the immune system. This is especially evident in current treatments of MDD using SSRIs or SNRIs that work via alterations to serotonin and noradrenaline, respectively. Anti-depressants have shown to reduce LPS induced peripheral IL-6 and TNF-α production (Manikowska et al., 2014). SSRI administration can also attenuate CRH, TNF-α, and IL-1β mRNA expression in the hypothalamus after chronic treatments (Alboni et al., 2013). Glia are responsive to anti-depressant treatments, since SSRIs can decrease gliotransmission (Dhami et al., 2013), and can partially attenuate microglial secretion of TNF-α in response to LPS. Pharmacologically blocking the reuptake of serotonin can also reduce microglial reactivity and inhibit LPS-induced changes in microglia morphology (Horikawa et al., 2010; Obuchowicz et al., 2014). In addition, there is also evidence that antidepressants are protective against microglial- (Zhang et al., 2012) and MPTP-induced neurotoxicity (Chung et al., 2011). Thus, alterations to serotonergic neurotransmission can also influence glial and central

immune activity, and this may contribute to the anti-depressive effects of SSRI. Together with evidence of immune modulation of neurotransmission, this illustrates the bidirectional communication between the neural and immune systems in both normal and pathophysiology.

WHAT DOES STRESS HAVE TO DO WITH IT?

Stress refers to a challenge to the body's homeostatic state, and can be classified broadly as psychological, physiological and immunological in origin. According to the diathesis-stress model of depression, stress is essential to the development of MDD, as stress is required in order to unmask the underlying individual predisposition to the disorder (Monroe and Simons, 1991). Biological and environmental factors thus interact to produce the physiological and psychological depression phenotype. Stress, regardless of type, activates the hypothalamus pituitary and adrenal (HPA) axis, which forms the neuroendocrine stress response. The HPA axis is therefore the most investigated link between stress and MDD. Furthermore, TLR4 activation is considered an immunological stress, and recent research demonstrates that it is deeply intertwined with the neuroendocrine stress response. Given the innate immune component of MDD as outlined earlier, we propose that the role of TLR4 in MDD is mediated at least in part by its interaction with the HPA axis.

THE CLASSICAL HPA AXIS

When activated, the HPA axis works to restore homeostasis following different stressors (Chrousos, 2009). Activation of the HPA axis begins with neurons in the paraventricular nucleus of the hypothalamus (PVN), which secrete corticotropin releasing hormone (CRH). CRH then stimulates the pituitary gland to release

adrenocorticotropic hormone (ACTH) into the blood circulation. Upon binding to melanocortin 2 receptor (MC2R) expressed on the zona fasciculata layer of the adrenal cortex, ACTH stimulates glucocorticoid (GC) production *de novo*. GC binds to cytoplasmic glucocorticoid receptors (GR) and mineralocorticoid receptors (MR) at a higher affinity (Sapolsky et al., 2000). Due to this higher affinity, the actions of baseline GC are thus associated with MR binding, whereas GR actions are attributed to upregulated GC by stressors.

GR binding causes receptor translocation into the nucleus through the aid of chaperone proteins such as heat shock protein 70 and 90 (HSP70, HSP90, respectively), where it can either dimerise and bind to glucocorticoid response elements (GRE) on DNA to either increase transcription of glucocorticoid responsive genes, or interact with other proteins such as transcription factors NF-κB and AP-1 (see Silverman and Sternberg, 2012 for review). GC actions are therefore extremely complex. Furthermore, most cells express GR, and thus GCs can influence the functions of multiple systems through diverse endocrine actions. GCs are also able to cross the BBB to influence CNS function including feeding back upon its own secretion by signaling via GR in the hippocampus to increase GABAergic tone on the PVN.

HPA ACTIVITY ALTERATIONS IN MDD

The HPA response is markedly changed during depression. Specifically, patients with MDD exhibit heightened cortisol levels in the morning, and possess a flatter diurnal slope throughout the day (Dinan, 1994; Jarcho et al., 2013). This indicates that a dysregulation in HPA activity is involved in the pathophysiology of depression, and further raises important questions as to what causes this HPA dysregulation, as well as

how this fits in with the immune adaptations outlined earlier.

The hypersecretion of cortisol could mean either a problem with the feed-forward secretory pathway, or the negative feedback loop within the HPA axis. The former is unlikely true, as adrenal responsiveness to ACTH is normal in patients with depression (Rubin et al., 2006), showing that adrenal function itself is not altered in depressive disorders. On the other hand, patients exhibit lower responsiveness to the dexamethasone suppression test (DST), which tests GR mediated negative feedback onto HPA activity (Holsboer-Trachsler et al., 1991). Dexamethasone was also found to be less effective in suppressing immune activity in patients with depressive disorders (Maes et al., 1994). Taken together, GR function is modified in MDD, and patients develop what is termed GC resistance. Given that the actions of GR influence multiple systems in the body, GC resistance could serve as a link between MDD and immune dysregulation (Quan et al., 2003; Silverman and Sternberg, 2012).

HPA hyperactivity may be sufficient to cause depressive moods, since patients with Cushing's syndrome, characterized by hypersecretion of cortisol, often exhibit depressive symptoms (Starkman et al., 1981). In rodent models, administration of corticosterone can also elicit depressive-like behavior, and this effect is blocked by spironolactone, an MR antagonist (Wu et al., 2013). Since MR is associated with baseline GC actions, the increased secretion of cortisol in MDD patients may be in part mediating the disorder via MR activation. HPA dysregulation indeed presents itself to be integral to depressive symptoms. However, blocking GC signaling is not feasible due to its widespread effects on cardiovascular, reproductive, metabolic and immune function. Thus, recent attention has been turned toward specific upstream modulators

of HPA activity in stress and MDD. Out of these investigations, the immune component appears to be the most likely target due to the overlaps between immune activation, the monoamine system, and the HPA axis.

ACUTE TLR4 ACTIVATION TRIGGERS THE HPA AXIS

HPA activity is thought to mediate the immune involvement in MDD. Using LPS, previous research has been able to show that TLR4 signaling is able to stimulate the HPA axis (Mohn et al., 2011). Further studies showed that TLR4 activation is sufficient to cause GC release from adrenal cells (Vakharia and Hinson, 2004; Kanczkowski et al., 2013). TLR4 activation can also cause CRH gene upregulation in paraventricular neurons in the hypothalamus (Loum-Ribot et al., 2006), as well as increased CRH in serum (Goebel et al., 2011). Pituitary cells stimulated by LPS also produce ACTH, but there is contrasting data on whether this effect is CRH dependent (Elenkov et al., 1992; Mehet et al., 2012).

Despite clear evidence that innate immune activation via TLR4 can strongly stimulate the HPA axis, the exact mechanism is still unclear, as it is not known if TLR4 can directly modulate neuronal activity, or cause steroidogenesis via intracellular signaling. Part of the problem is, as illustrated earlier, where in the system LPS has the most effect, since it appears that TLR4 is present and can trigger increased secretion of CRH, ACTH, and GC. The other part of the problem lies in the many levels of immune activation that can also influence neuroendocrine activity. The following section reviews how TLR4 signaling can trigger the HPA axis and it's implications for MDD.

Cytokines and HPA activity

Cytokines are secreted by immune competent cells as a result of innate immune

stimulation, including TLR4 activation by various ligands. As previously stated, cytokine administration is sufficient to cause sickness behavior. Cytokines can also upregulate HPA axis signaling on multiple levels through two main ways: (1) through reducing negative feedback on HPA signaling, and (2) by directly stimulating HPA activation. IL-1β, IL-6, and TNF-α are able to reduce the efficacy of GR, thus disinhibiting GR induced negative feedback on HPA activity (Pace et al., 2007; Bogaert et al., 2010). This effect could be due to protein-protein interactions with GR, which enables pro-inflammatory cytokines to influence GR translocation, ligand binding affinity and GR binding to GRE within the nucleus (for review, see Pace and Miller, 2009).

Secondly, cytokines can amplify the feed-forward signaling within the HPA axis. IL-6 has been shown to potentiate CRH activation of ACTH (Mehet et al., 2012), while IL-1β and stress have an additive effect on CRH secretion from the PVN (ChoverGonzalez et al., 1993). Interestingly, peripheral and central IL-1β is upregulated in response to acute stress within 1h, and 3h after stress onset, respectively, and could therefore endogenously prime the HPA response. Moreover, this study also found that the administration of an IL-1β receptor antagonist diminished ACTH responses to restraint stress (Ga˛dek-Michalska et al., 2011), showing that cytokines may partially mediate stress induced HPA activation. Given that an increase in peripheral IL-1β and circulating cortisol is observed in patients with MDD (Maes et al., 1991), this permissive effect on ACTH secretion could be in part driving the dysregulation between the immune and HPA secretion in MDD.

TLR4-related COX-2 production as part of steriodogenesis pathway Besides cytokine interactions, COX-2 has also been shown to mediate TLR4 involvement in modulation of HPA activity. COX-2, an enzyme upregulated by TLR4 activation, catalyzes arachidonic acid into prostaglandin E2, which is part of the steroidogenesis pathway. COX-2 is therefore involved in the synthesis of GC at the level of the adrenal, and is shown to mediate LPS induced steroidogenesis within adrenal cells (Vakharia and Hinson, 2004). Furthermore, pharmacologically blocking COX-2 systemically is able to inhibit restraint stress induced GC both *in vivo* (Mouihate et al., 2010; Ma et al., 2013), and *in vitro* (Martinez Calejman et al., 2011). The effects of COX-2 extend beyond the adrenal gland, as expression of COX-2 in the PVN is important for sympathetic activation in response to restraint stress (Yamaguchi et al., 2010). In addition, COX-2 inhibition can influence higher order functions, buffering the effects of immobilization stress by reduced anxiety behavior and improve locomotor functioning and learning (Kumari et al., 2007).

Long-term effects of TLR4 activity on HPA axis function

Not only can TLR4 activation result in short-term stimulation of the HPA axis, but TLR4 can also influence HPA activity long after the stressor is resolved. For example, a single LPS challenge during early-life is sufficient to hyper-sensitize the CRH and ACTH response to both subsequent LPS and restraint stress when tested in adulthood, without baseline HPA differences when compared to vehicle controls in a rodent model (Mouihate et al., 2010). Early-life TLR4 activation also results in an increase in anxiety behavior during adulthood (Sominsky et al., 2013), thus fundamentally changing the stress response system. This suggests that TLR4 activity during developmentally

sensitive periods may shape the HPA system, priming the system toward hyperreactivity, and may even be changing individual predisposition toward stress-related disorders.

A good way of investigating the developmental consequence of TLR4 is through the use of genetic knockout models. TLR4 knockout mice are observed to have different HPA phenotypes when compared to match wild-type C57Bl/6 counterparts, showing increased adrenal gland volume and correspondingly higher baseline circulating glucocorticoid levels (Zacharowski et al., 2006). The direction of this change is not universally found however, as preliminary findings from our laboratory in Balb/c background TLR4 knockout mice have yielded opposite results. We have found that TLR4 genetic knockout mice have smaller adrenal glands as well as lower circulating GC (unpublished). Additionally, circulating ACTH was also elevated in mice lacking TLR4 when compared to matched controls.

Despite the differences in adrenal size and baseline ACTH levels, we found no difference between wild type and TLR4 knockout mice, in terms of adrenal responsiveness to ACTH administration in the same study (unpublished). Our findings support observations that systemic rather than adrenal MyD88 expression is important in regulating HPA activity (Kanczkowski et al., 2013). Taken together, these results suggest that although the TLR4 pathway can influence HPA activity, the innate immune system has little direct impact on adrenal function, and the observed HPA differences are likely to be driven by mechanisms within the CNS instead.

STRESS AND SYSTEMIC IMMUNITY

It is becoming clear that mood disorders such as depression have both immune and

neuroendocrine components. Through interactions with the neuroendocrine system and central immune signaling, TLR4 is central to the physiological responses to immune stressors as well as baseline HPA activity. Yet at the same time, GCs classically suppress the immune system including the TLR4 pathway. When GCs bind to GR, immune suppression can occur in two main ways. Firstly, GR can directly interact with transcription factors NF-κB and AP-1 through protein-protein interactions, and in the process interfere with the pro-inflammatory transcription (Ratman et al., 2013). Following nuclear translocation, GR can also dimerise and bind to GRE on DNA, upregulating transcription of anti-inflammatory or repressing inflammatory genes such as IL-6 receptor gene (Muzikar et al., 2009). Both mechanisms appear important in driving anti-inflammatory actions of GCs as DNA binding appears important for the resolution of high-dose LPS induced inflammatory and behavioral response (Silverman et al., 2013), while GR can interfere with NF-κB induced transcription of proinflammatory genes (Novac et al., 2006). GR not only functions on the intracellular level, but can also downregulate macrophage expression of TLR4 mRNA in a dose and time dependent manner (Du et al., 2012). Given the varied roles of glucocorticoids in immune suppression, how does stress, which strongly triggers the HPA axis, cause increased immune signaling seen in MDD?

The answer likely lies in stress-induced adaptations, as recent evidence in rodent models has shown that stress itself can be both pro- and anti-inflammatory. Chronic footshock stress can induce bone-marrow derived monocytes infiltration into the hippocampus, thus increasing immune activity (Brevet et al., 2010). Acutely, footshock stress can also result in concurrent neuroendocrine and immune activation,

characterized by increased hypothalamic IL-1β and TNF-α, adrenal IL-6, and COX-2, in addition to circulating ACTH and GC increase (Hueston and Deak, 2014). The authors also showed that injection of ACTH and CRH induced adrenal IL-6 and COX-2 mRNA expression, indicating that HPA activation can be pro-inflammatory. The increase in immune signaling seen in MDD may therefore be driven by stress itself.

The elevation of neurokine signaling appears stressor specific. Illustrating this, a meta-analysis showed that stress-induced IL-1β in the hypothalamus is most reproducible in footshock and immobilization stress models (Deak et al., 2005). On the other hand, social defeat stress increases prefrontal cortex IL1β, IL-6, and TNF-α expression (Audet et al., 2011), in addition to increased monocyte infiltration (Wohleb et al., 2014). These variations in regional cytokine levels thus indicate a complex relationship between stressor type and the innate immune system within the CNS.

To reconcile the biphasic actions of HPA activation, in a recent review, Frank et al. (2013) argued that the timing of immune challenges and measurements is important in determining the direction of glucocorticoid actions. The authors proposed that glucocorticoids are anti- inflammatory during the stressor, but sensitizes the immune response after the stressor has ended, during what the "recovery phase" following the resolution of the stressor (Frank et al., 2013). Thus, timing of the "second-hit" as well as measurements of immune functioning following both stressors is therefore imperative to measuring GC actions on immune function. At this point, it is still unclear what mechanisms drive this biphasic effect, and how long this pro-inflammatory state persists following stress. In the following section, we review potential mechanisms, as well as present the case for TLR4 involvement in mediating the pro-inflammatory

actions of the HPA system.

MECHANISMS OF GLUCOCORTICOID INDUCED PRO-INFLAMMATORY RESPONSES

DIRECT MECHANISMS THROUGH HPA ACTIVATION The HPA axis can directly influence immune signaling in two main ways, by reducing the inhibitory effects of glucocorticoid actions, or by directly stimulating the immune system. As mentioned in the previous section, there appears to be some form of GR adaptation, thus disrupting the actions of GR on the immune system and negative feedback onto the HPA system. This effect termed glucocorticoid resistance. Glucocorticoid resistance is predominantly thought to be due to either a reduced GR expression, or a selective reduction in GRα and a corresponding upregulation of GRβ, the inactive splice variant of the receptor that is unable to bind glucocorticoids (Silverman and Sternberg, 2012). Increased expression of pro-inflammatory cytokines correspond to elevated expression of GRβ, which could drive the disinhibition to immune response (Carvalho et al., 2014). Glucocorticoid resistance not only reduces glucocorticoid mediated immune suppression, but can in itself increase NF-κB responses in PBMC when exposed to glucocorticoids, thus reshaping the response to a previously anti-inflammatory stimulus (Dawson et al., 2012). Contrary to classical actions, HPA activation can also directly trigger the immune response. CRH, which is secreted by PVN cells, may also directly stimulate the innate immune system. When exposed to CRH, mast cells have been shown to undergo degranulation, releasing cytokines into the extracellular space (Theoharides et al., 1995; Alysandratos et al., 2012). This directly implicates CRH in the increased central immune or neurokine signaling in stress-related disorders (Aguirre et al., 2013). On the

other hand, CRH can also induce microglial apoptosis in the nanomolar range (Ock et al., 2006). It is therefore still unclear how the pro and anti-inflammatory effects are balanced in stress induced CRH release.

Pharmacological inhibition of GR reduces VCAM and ICAM expression in the microvasculature (Gregory et al., 2009), indicating the GR specific actions on immune cell migration. Indeed, low doses can be pro-inflammatory by stimulating phagocytosis and chemotaxis of macrophages via a GR mediated mechanism (Zhong et al., 2013). It has been previously established that GCs not only suppress the immune system, but at low doses directly induces production of macrophage migration inhibitory factor (MIF), a pro-inflammatory cytokine (Calandra et al., 1995). MIF can function as a chemokine, and stimulate CCL2 production when administered to the microvasculature, thus promoting migration of inflammatory cells to the site of damage (Gregory et al., 2009). Physiologically, MIF is involved in wound healing through promoting migration of endothelial progenitor cells to wounds (Grieb et al., 2012). Conversely, MIF is also implicated in the development of neuropathic pain (Alexander et al., 2012; Lerch et al., 2014). The exact reason for immune activation following the HPA response is still debated, but one of the more accepted reasons for this effect is that by increasing immune signaling, MIF constrains the HPA response in order to counteract glucocorticoid induced immune cell apoptosis. Through these mechanisms, it is thus possible for heightened HPA activity and immune activation to co-exist in patients with MDD.

TLR4 MEDIATED MECHANISMS OF STRESS-INDUCED PRO-INFLAMMATORY RESPONSE

TLR4 mediates immune priming effects of stress

Given the often-contradictory results on HPA function, the complexity of glucocorticoid signaling is becoming more appreciated. In order to explain the complex actions of glucocorticoids Sapolsky et al. (2000) proposed 4 categories of glucocorticoid action - permissive, inhibitory, excitatory and priming, encapsulating the different receptors activated, timing of response relative to stressors and type of tissue activated. Illustrating this, glucocorticoids are excitatory in terms of heart function but inhibit vascular function, cause the release of glucose aiding energy expenditure, yet also trigger stockpiling of fat in adipose tissue. At the same time, basal glucocorticoid expression can be permissive toward sympathetic activation of the adrenal medulla, thus influencing stress responses even before the HPA activation even occurs. Thus, glucocorticoids have different dose and time response relationships across different tissues, and their actions are dependent on basal or activated HPA states.

Recent studies are beginning to classify the priming or sensitizing effect of stress and HPA activity on immune function. Chronic variable and acute social disruptive stress can sensitize HPA and immune response to subsequent LPS challenge, differentially inducing larger neurokine and peripheral cytokine responses (Gibb et al., 2013). Repeated social defeat stress can also prime immune signaling in peripheral monocytes and dendritic cells in response to LPS, coupled with glucocorticoid resistance during the first 48h after stressor, measured by immune cell expression following GC administration *in vitro* (Powell et al., 2009). Importantly, this immune priming is also seen in microglial populations 24h after glucocorticoid treatment (Frank et al., 2011). Moreover, GC administration *in vivo* has been confirmed to emulate stress induced

immune sensitization (Frank et al., 2010; Dey et al., 2014). This sensitizing effect was further blocked by a GR antagonist, indicating that GR signaling is essential (Frank et al., 2012). TLR2 and TLR4 activity could also be integral to glucocorticoid-induced immune priming in microglia, as administration of their respective antagonists prior to tailshock stress can prevent increased sensitivity in hippocampal tissues collected 24h after the end of the stressor (Weber et al., 2013). Taken together, there appears to be crosstalk between the GR and TLR4 pathways, and both receptors appear to be important in driving immune cell sensitization and increased central immune signaling following stress.

The immune-priming effect of stress is proposed to mediate stress-induced side effects such as allodynia (Loram et al., 2011), and drug abuse (Frank et al., 2011), and could potentially be involved in MDD as well. PBMCs isolated from patients admitted for severe depressive episodes are more responsive to interferon-γ (IFN-γ) stimulation (Schlaak et al., 2012). Along with increased TLR4 mRNA and expression on PBMCs of patients with MDD (Kéri et al., 2014), the increased immune signaling in MDD patients could be indicative of a primed immune system, rather than chronic inflammation.

DAMPs released during stress cause TLR4 activation

DAMPs, or alarmins, are released endogenously from stressed, dead and dying cells as a signal for danger. They include HMGB1, various HSP, ATP, and Uric acid. During normal physiological activation, DAMPS have a non-inflammatory function within the cell. Conversely during situations of tissue damage, when released into the extracellular space, DAMPs alert the immune system to the damage in order to promote repair and direct traffic toward the damaged tissue, thus triggering the

inflammatory response. This inflammatory response is in part driven by TLR4, since DAMPs including HMGB1 and various HSPs can activate the TLR4 pathway (Hutchinson et al., 2009; Laird et al., 2014). Furthermore, ATP can trigger innate immune signaling by activating a protein complex known as the inflammasome, which induces the maturation and release of cytokines IL-1β and IL-18 via a caspase-1 dependent mechanism (Chen et al., 2013). This effect is known to augment the inflammatory response to LPS, therefore amplifying TLR4 signaling (Ghonime et al., 2014). DAMPS including HMGB1, uric acid and HSP72 are also released following tail-shock stress (Faraco et al., 2007; Maslanik et al., 2013), and thus are not limited to situations of tissue damage or cell death. DAMPs could therefore mediate the effect of stress on triggering or sensitizing the immune response, and this increased immune signaling may have wider implications for MDD. It is notable, however, that the mechanisms regulating the secretion of DAMPs in response to stress is not well characterized.

High mobility group box 1. HMGB1 functions as a chaperone protein within the cell by binding to proteins and transporting them between the cytoplasm and nucleus. During damage however, HMGB1 can be released into the extracellular space via an inflammasome mediated mechanism (Lu et al., 2012). Neural tissue is capable of releasing HMGB1 in response to glutamatergic excitotoxicity and glial activation as a result of LPS administration *in vitro* (Faraco et al., 2007). HMGB1 can also activate central immune signaling, as it can trigger TLR4 similar to LPS, via the MD2 and CD14 complex, and requires adaptor protein MyD88 to trigger downstream inflammatory actions (Kim et al., 2013). Moreover, psychological stress itself can induce an increase

in HMGB1. For example, thymocytes are responsive to 15min restraint stress, and release HMGB1 via GR signaling (Billing et al., 2012). There is further evidence showing that HMGB1 and GR can form complexes within the chromatin, increasing the residence time of GR when bound to DNA (Agresti et al., 2005). The functional consequence of this interaction, however, is still unclear. Given that HMGB1 is responsive to stress, interacts with GR, and is able to increase peripheral and central immune signaling, stress-induced immune sensitization through neurokine signaling could therefore be partially mediated by HMGB1.

HMGB1 can also cause an upregulation of Matrix metallopeptidase 9 (MMP9), an enzyme that results in the breakdown of the extracellular matrix (Qiu et al., 2010). Interestingly, increased MMP9 in circulation is associated with mood disorders such as depression and bipolar disorder (Domenici et al., 2010; Rybakowski et al., 2013). Together with evidence that MMP9 can also be upregulated as a consequence of microglial activity (Lively and Schlichter, 2013), MMP9 could be a possible result of stress induced HMGB1 upregulation and immune signaling within the CNS in MDD.

Heat shock proteins. HSPs were first discovered in the drosophila model to be produced in response to hyperthermia, and vary in protein weights ranging up to 110 kDA. HSP regulate the folding and unfolding of other proteins, and are released in response to cellular damage. Signaling danger, extracellular HSP can activate the innate immune system (Colaco et al., 2013). Within the HSP family, HSP70 and HSP90, the 70 and 90kDa variants, are of most relevance to glucocorticoid and TLR4 signaling. HSP70 and HSP90 can bind TLR4, resulting in release of pro-inflammatory cytokines (Gong et

al., 2009; Colaco et al., 2013). Furthermore, HSP90 also serves as a chaperone protein for TLR4, triggering endocytosis in response to ligand binding (Triantafilou and Triantafilou, 2004). Through these mechanisms, HSP90 plays an integral role in TLR4 signaling and in TLR4 related neuropathic pain (Hutchinson et al., 2009). Stress can also induce HSP expression, notably decreasing the ratio between GR and HSP70 and HSP90 expression in the hypothalamus (Simic et al., 2012).

Interestingly, HSP90 is a well-characterized chaperone protein for GR nuclear translocation and permits GC binding to GR (Ricketson et al., 2007). Although important for binding and translocation, Increased HSP90 expression can also impair GR function (Matysiak et al., 2008). This effect increases in chronic stress as compared to acute models of stress, and thus is proposed as one facet of glucocorticoid resistance. Stress induced changes in HSP can therefore either directly activate TLR4, change the trafficking TLR4 and GR, as well alter GR binding capacity. However, to what extent each of these mechanisms is involved, and the magnitude of the change has yet to be investigated in models of depressive-like behavior. Nevertheless, given the involvement in TLR4 and GR signaling, HSP could be an avenue for further research in linking stress and increased immune signaling in MDD.

TLR4 activation as a result of gut translocation of microbes

One way in which TLR4 ligands are upregulated by stress is through intestinal translocation. Recently, the role of gut microbiota in potentiating differences in mood and behavior is gaining traction within the literature (Hsiao et al., 2013). It has been hypothesized that stress can cause a disruption in intestinal tight junctions, which would increase translocation of microbiota into the system, thus inducing

inflammatory responses. Indeed, GR appears to be involved in gut HSP70 upregulation and intestinal permeability in response to restraint stress (Ait-Belgnaoui et al., 2012, 2014).

There is some evidence showing that intestinal decontamination using orally administered antibiotics is able to block the tight junction disruption, as well as inflammatory and HPA responses to psychological stress (Gárate et al., 2011). Furthermore, antibiotic treatment is shown to mirror the ability of TLR4 antagonist in blocking stress induced depressive-like behavior (Gárate et al., 2011). This hypothesis is thus showing promise for developing new medication targeting the gut-brain axis in regulating behavior. On the other hand, the exact mechanisms of this gutbrain communication in respect to stress and MDD are unclear, since both ascending pathways and peripheral immune signaling could potentially be involved. In addition, the extent of intestinal translocation in the acute stress response requires more study, since it is not known if this effect is stressor specific.

CONCLUSIONS

It is evident that the immune, neural and neuroendocrine systems are in constant multi-directional communication, and in the case of stress and MDD, patients exhibit a dysregulation of all three systems. Thus, the difficulty in finding treatment targets lies in untangling the multi-layered relationships. In the current review, we presented evidence centered on immune modulation of CNS and stress-induced adaptations observed in models of MDD. Stress is regarded as a necessary factor for the development of MDD through adaptations to the neuroendocrine and immune responses.

Through use of knockout models as well as pharmacological agonists and antagonists, TLR4 activation has been shown to elicit depression-like symptoms in animal models

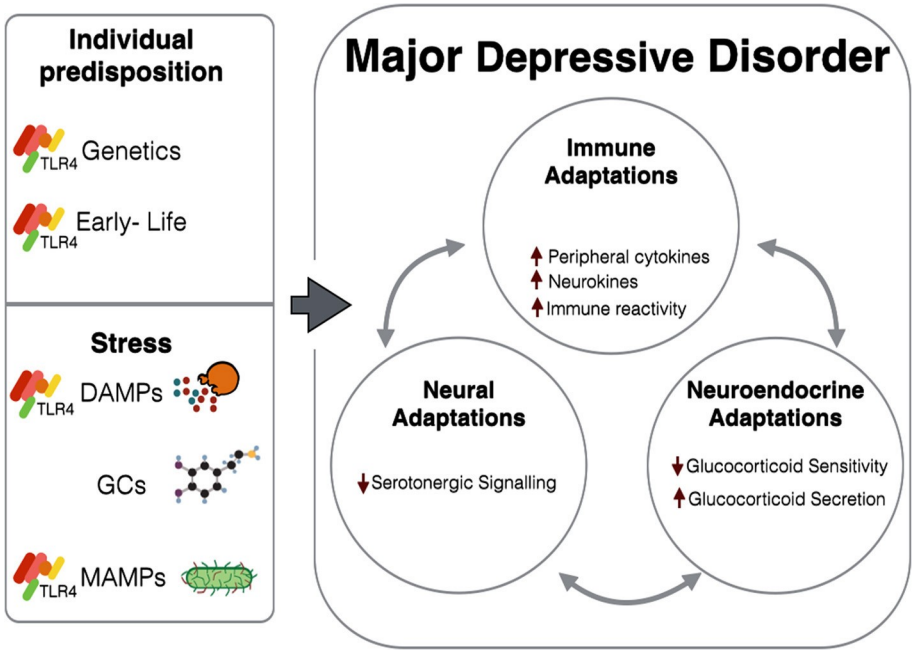

FIGURE 1 | Stress and individual predisposition combine to cause various immune, neuroendocrine, and neural adaptations observed in MDD. Immune adaptations are at least in part attributed to TLR4-related mechanisms, either through direct activation by ligands (DAMPs and MAMPs) released as a result of stress, or by long-term impairment caused by genetics and early-life experiences. GCs can also interact with TLR4-dependent and GR-dependent mechanisms to induce systemic changes. In patients with MDD, these adaptations are not isolated to their respective systems, but instead further augment their deleterious effects through tri-directional communications.

both behaviorally and physiologically. Additionally, TLR4 could potentially mediate stress-induced immune signaling both in the periphery and within the CNS, as well as underlie stress-induced immune activity, through interactions with DAMPs, MAMPs, and GC signaling (**Figure1**). TLR4, an innate immune receptor, could therefore be important in investigating the immune involvement in the pathophysiology of MDD. On the other hand, this direct relationship between TLR4 and depression is still not fully understood, although timing and location of TLR4 activation appears to be important. The mode in which TLR4 influences MDD is not established, even though cytokines appear to be essential to the development of sickness behavior, other mechanisms such as direct interaction between TLR4 signaling pathway and other

receptors (for example, GR) or intracellular signaling molecules could also play a role in the development of the disorder. Furthermore, due to the many compounds that can trigger TLR4 activation, an obvious question would be to identify which of those are most relevant to MDD. Critically, there is a need to move away from the use of LPS in the investigation of MDD, since it constrains the generalizability of conclusions to infectious factors. Although the immune system appears to be involved in the pathophysiology of MDD, it is unlikely that bacterial infections are the main factor, especially given that cytokines themselves can induce behavioral change in the absence of sickness. Instead, individual differences in immune activity could originate from alterations to immune signaling during critical periods during development, genetic disposition, or epigenetic changes that contribute to predispositions (Bilbo and Schwarz, 2009). Moreover, due to the sub-inflammatory and state driven nature of heightened immune signaling in MDD, endogenous mechanisms including DAMPs, neuroendocrine, neurogenic signals, or an increase in gut translocation of microbiomes are more likely involved. Thus, in the search for a more efficacious treatment of MDD, the impact on neural, neuroendocrine and immune systems must be considered within representative models of the disorder.

ACKNOWLEDGMENT

The authors would like to acknowledge Jonathan Henry Webster Jacobsen for the contribution of graphics for **Figure1**.

REFERENCES

Acharjee, S., Nayani, N., Tsutsui, M., Hill, M., Ousman, S., and Pittman, Q. (2013). Altered cognitive-emotional behavior in early experimental autoimmune encephalitis—Cytokine and hormonal correlates. *Brain Behav. Immun.* 33, 164–172. doi: 10.1016/j.bbi.2013.07.003

Agresti, A., Scaffidi, P., Riva, A., Caiolfa, V., and Bianchi, M. (2005). GR and HMGB1 interact only within chromatin and influence each other's residence time. *Mol. Cell* 18, 109–121. doi: 10.1016/j.molcel.2005.03.005

Aguirre, A., Maturana, C., Harcha, P., and Sáez, J. (2013). Possible involvement of TLRs and hemichannels in stress-induced CNS dysfunction via mastocytes, and glia activation. *Mediators Inflamm.* 2013:893521. doi: 10.1155/2013/893521

Ait-Belgnaoui, A., Colom, A., Braniste, V., Ramalho, L., Marrot, A., Cartier, C., et al. (2014). Probiotic gut effect prevents the chronic psychological stress-induced brain activity abnormality in mice. *Neurogastroenterol. Motil.* 26, 510–520. doi: 10.1111/nmo.12295

Ait-Belgnaoui, A., Durand, H., Cartier, C., Chaumaz, G., Eutamene, H., Ferrier, L., et al. (2012). Prevention of gut leakiness by a probiotic treatment leads to attenuated HPA response to an acute psychological stress in rats. *Psychoneuroendocrinology* 37, 1885–1895. doi: 10.1016/j.psyneuen.2012.03.024 Ajmone-Cat, M., Mancini, M., Simone, R., Cilli, P., and Minghetti, L. (2013). Microglial polarization and plasticity: evidence from organotypic hippocampal slice cultures. *Glia* 61, 1698–1711. doi: 10.1002/glia.22550

Akira, S., and Takeda, K. (2004). Toll-like receptor signalling. *Nat. Rev. Immunol.* 4, 499–511. doi: 10.1038/nri1391

Alboni, S., Benatti, C., Montanari, C., Tascedda, F., and Brunello, N. (2013). Chronic antidepressant treatments resulted in altered expression of genes involved in inflammation in the rat hypothalamus. *Eur. J. Pharmacol.* 721, 158–167. doi: 10.1016/j.ejphar.2013.08.046

Alexander, J., Cox, G., Tian, J.-B., Zha, A., Wei, P., Kigerl, K., et al. (2012). Macrophage migration inhibitory factor (MIF) is essential for inflammatory and neuropathic pain and enhances pain in response to stress. *Exp. Neurol.* 236, 351–362. doi: 10.1016/j.expneurol.2012.04.018

Alysandratos, K.-D., Asadi, S., Angelidou, A., Zhang, B., Sismanopoulos, N., Yang, H., et al. (2012). Neurotensin and CRH interactions augment human mast cell activation. *PLoS ONE* 7:e48934. doi: 10.1371/journal.pone.0048934

American Psychiatric Association. (2013). "Depressive disorders," in *Diagnostic and Statistical Manual of Mental Disorders*, 5th Edn., eds J. Fawcett, E. Frank, K. Kendler, J. Angst, M. Maj, W. Coryell, et al. (Arlington, VA: American Psychiatric Publishing), 155. doi: 10.1176/appi.books.9780890425596.807874

Anisman, H., and Hayley, S. (2012). Inflammatory factors contribute to depression and its comorbid conditions. *Sci. Signal.* 5:pe45. doi: 10.1126/scisignal.2003579 Araque, A., Carmignoto, G., Haydon, P., Oliet, S., Robitaille, R., and Volterra, A. (2014). Gliotransmitters travel in time and space. *Neuron* 81, 728–739. doi: 10.1016/j.neuron.2014.02.007

Arroll, B., Elley, C. R., Fishman, T., Goodyear-Smith, F. A., Kenealy, T., Blashki, G., et al. (2009). Antidepressants versus placebo for depression in primary care. *Cochrane Database Syst. Rev.* CD007954. doi: 10.1002/14651858.CD007954

Audet, M.-C., Jacobson-Pick, S., Wann, B., and Anisman, H. (2011). Social defeat promotes specific cytokine variations within the prefrontal cortex upon subsequent aggressive or endotoxin challenges. *Brain Behav. Immun.* 25, 1197–1205. doi: 10.1016/j.bbi.2011.03.010

Banati, R. B. (2003). Neuropathological imaging: *in vivo* detection of glial activation as a measure of disease and adaptive change in the brain. *Br. Med. Bull.* 65, 121–131. doi: 10.1093/bmb/65.1.121

Beschorner, R., Simon, P., Schauer, N., Mittelbronn, M., Schluesener, H., Trautmann, K., et al. (2007). Reactive astrocytes and activated microglial cells express EAAT1, but not EAAT2, reflecting a neuroprotective potential following ischaemia. *Histopathology* 50, 897–910. doi: 10.1111/j.1365-2559.2007.02703.x

Bilbo, S., and Schwarz, J. (2009). Early-life programming of later-life brain and behavior: a critical role for the immune system. *Front. Behav. Neurosci.* 3:14. doi: 10.3389/neuro.08.014.2009

Billing, A., Revets, D., Hoffmann, C., Turner, J., Vernocchi, S., and Muller, C. (2012). Proteomic profiling of rapid non-genomic and concomitant genomic effects of acute restraint stress on rat thymocytes. *J. Proteomics* 75, 2064–2079. doi: 10.1016/j.jprot.2012.01.008

Bogaert, T., Bosscher, K., and Libert, C. (2010). Crosstalk between TNF and glucocorticoid receptor signaling pathways. *Cytokine Growth Factor Rev.* 21, 275–286. doi: 10.1016/j.cytogfr.2010.04.003

Brevet, M., Kojima, H., Asakawa, A., Atsuchi, K., Ushikai, M., Ataka, K., et al. (2010). Chronic foot-shock stress potentiates the influx of bone marrowderived microglia into hippocampus. *J. Neurosci. Res.* 88, 1890–1897. doi: 10.1002/jnr.22362

Burke, N., Kerr, D., Moriarty, O., Finn, D., and Roche, M. (2014). Minocycline modulates neuropathic pain behaviour and cortical M1–M2 microglial gene expression in a rat model of depression. *Brain Behav. Immun.* doi: 10.1016/j.bbi.2014.06.015. [Epub ahead of print].

Calandra, T., Bernhagen, J., Metz, C., Spiegel, L., Bacher, M., Donnelly, T., et al. (1995). MIF as a glucocorticoid-induced modulator of cytokine production. *Nature* 377, 68–71. doi: 10.1038/377068a0

Carvalho, L., Bergink, V., Sumaski, L., Wijkhuijs, J., Hoogendijk, W., Birkenhager, T., et al. (2014). Inflammatory activation is associated with a reduced glucocorticoid receptor alpha/beta expression ratio in monocytes of inpatients with melancholic major depressive disorder. *Transl. Psychiatry* 4:e344. doi: 10.1038/tp.2013.118

Chen, S., Ma, Q., Krafft, P., Hu, Q., Rolland, W., Sherchan, P., et al. (2013). P2X7R/cryopyrin inflammasome axis inhibition reduces neuroinflammation after SAH. *Neurobiol. Dis.* 58, 296–307. doi: 10.1016/j.nbd.2013. 06.011

Chover-Gonzalez, A. J., Harbuz, M. S., and Lightman, S. L. (1993). Effect of adrenalectomy and stress on interleukin-1 beta-mediated activation of hypothalamic corticotropin-releasing factor mRNA. *J. Neuroimmunol.* 42, 155–160. doi: 10.1016/0165-5728(93)90005-J

Chrousos, G. (2009). Stress and disorders of the stress system. *Nat. Rev. Endocrinol.* 5, 374–381. doi: 10.1038/nrendo.2009.106

Chung, Y., Kim, S., Park, J.-Y., Chung, E., Park, K., Won, S., et al. (2011). Fluoxetine prevents MPTP-induced loss of dopaminergic neurons by inhibiting microglial activation. *Neuropharmacology* 60, 963–974. doi: 10.1016/j.neuropharm.2011.01.043

Colaco, C., Bailey, C., Walker, K., and Keeble, J. (2013). Heat shock proteins: stimulators of innate and acquired immunity. *Biomed. Res. Int.* 2013:461230. doi: 10.1155/2013/461230

Corona, A. W., Huang, Y., O'Connor, J. C., Dantzer, R., Kelley, K. W., Popovich, P. G., et al. (2010). Fractalkine receptor (CX3CR1) deficiency sensitizes mice to the behavioral changes induced by lipopolysaccharide. *J. Neuroinflammation* 7:93. doi: 10.1186/1742-2094-7-93

D'Mello, C., Riazi, K., Le, T., Stevens, K., Wang, A., McKay, D., et al. (2013). P-Selectin-mediated monocyte–cerebral endothelium adhesive interactions link peripheral organ inflammation to sickness behaviors. *J. Neurosci.* 33, 14878–14888. doi: 10.1523/JNEUROSCI.1329-13.2013

Dantzer, R. (2004). Cytokine-induced sickness behaviour: a neuroimmune response to activation of innate immunity. *Eur. J. Pharmacol.* 500, 399–411. doi: 10.1016/j.ejphar.2004.07.040

Dantzer, R., and Kelley, K. (2007). Twenty years of research on cytokineinduced sickness behavior. *Brain Behav. Immun.* 21, 153–160. doi: 10.1016/j.bbi.2006.09.006

Dawson, C., Dhanda, A., Conway-Campbell, B., Dimambro, A., Lightman, S., and Dayan, C. (2012). NFκB and glucocorticoid receptor activity in steroid resistance. *J. Recept. Signal Transduct. Res.* 32, 29–35. doi: 10.3109/10799893.2011.641977

Deak, T., Bordner, K., McElderry, N., Barnum, C., Blandino, P., Deak, M., et al. (2005). Stress-induced increases in hypothalamic IL-1: a systematic analysis of multiple stressor paradigms. *Brain Res. Bull.* 64, 541–556. doi: 10.1016/j.brainresbull.2004.11.003

Dey, A., Hao, S., Erion, J., Wosiski-Kuhn, M., and Stranahan, A. (2014). Glucocorticoid sensitization of microglia in a genetic mouse model of obesity and diabetes. *J. Neuroimmunol.* 269, 20–27. doi: 10.1016/j.jneuroim.2014. 01.013

Dhami, K., Churchward, M., Baker, G., and Todd, K. (2013). Fluoxetine and citalopram decrease microglial release of glutamate and d-serine to promote cortical neuronal viability following ischemic insult. *Mol. Cell. Neurosci.* 56, 365–374. doi: 10.1016/j.mcn.2013.07.006

Dinan, T. (1994). Glucocorticoids and the genesis of depressive illness. A psychobiological model. *Br. J. Psychiatry* 164, 365–371. doi: 10.1192/bjp.164.3.365

Dobos, N., Vries, E., Kema, I., Patas, K., Prins, M., Nijholt, I., et al. (2012). The role of indoleamine 2,3-dioxygenase in a mouse model of neuroinflammationinduced depression. *J. Alzheimers Dis.* 28, 905–915. doi: 10.3233/jad-2011111097

Domenici, E., Willé, D., Tozzi, F., Prokopenko, I., Miller, S., McKeown, A., et al. (2010). Plasma protein biomarkers for depression and schizophrenia by multi analyte profiling of case-control collections. *PLoS ONE* 5:e9166. doi: 10.1371/journal.pone.0009166

Du, Q., Min, S., Chen, L.-Y. Y., Ma, Y.-D. D., Guo, X.-L. L., Wang, Z., et al. (2012). Major stress hormones suppress the response of macrophages through downregulation of TLR2 and TLR4. *J. Surg. Res.* 173, 354–361. doi: 10.1016/j.jss.2010. 10.016

Elenkov, I. J., Kovács, K., Kiss, J., Bertók, L., and Vizi, E. S. (1992). Lipopolysaccharide is able to bypass corticotrophin-releasing factor in affecting plasma ACTH and corticosterone levels: evidence from rats with lesions of the paraventricular nucleus. *J. Endocrinol.* 133, 231–236. doi: 10.1677/joe.0.1330231

Fang, J., Han, D., Hong, J., Tan, Q., and Tian, Y. (2012). The chemokine, macrophage inflammatory protein-2γ, reduces the expression of glutamate transporter-1 on astrocytes and increases neuronal sensitivity to glutamate excitotoxicity. *J. Neuroinflammation* 9:267. doi: 10.1186/1742-2094-9-267

Faraco, G., Fossati, S., Bianchi, M., Patrone, M., Pedrazzi, M., Sparatore, B., et al. (2007). High mobility group box 1 protein is released by neural cells upon different stresses and worsens ischemic neurodegeneration *in vitro* and *in vivo*. *J. Neurochem.* 103, 590–603. doi: 10.1111/j.1471-4159.2007.04788.x

Faridhosseini, F., Sadeghi, R., Farid, L., and Pourgholami, M. (2014). Celecoxib: a new augmentation strategy for depressive mood episodes. A systematic review and meta-analysis of randomized placebo-controlled trials. *Hum. Psychopharmacol.* 29, 216–223. doi: 10.1002/hup.2401

Frank, M. G., Miguel, Z. D., Watkins, L. R., and Maier, S. F. (2010). Prior exposure to glucocorticoids sensitizes the neuroinflammatory and peripheral inflammatory responses to E. *coli lipopolysaccharide. Brain Behav. Immun.* 24, 19–30. doi: 10.1016/j.bbi.2009.07.008

Frank, M. G., Thompson, B. M., Watkins, L. R., and Maier, S. F. (2012). Glucocorticoids mediate stress-induced priming of microglial proinflammatory responses. *Brain Behav. Immun.* 26, 337–345. doi: 10.1016/j.bbi.2011.10.005

Frank, M. G., Watkins, L. R., and Maier, S. F. (2011). Stress- and glucocorticoidinduced priming of neuroinflammatory responses: potential mechanisms of stress-induced vulnerability to drugs of abuse. *Brain Behav. Immun.* 25 Suppl. 1, S21–S28. doi: 10.1016/j.bbi.2011.01.005

Frank, M. G., Watkins, L. R., and Maier, S. F. (2013). Stress-induced glucocorticoids as a neuroendocrine alarm signal of danger. *Brain Behav. Immun.* 33, 1–6. doi: 10.1016/j.bbi.2013.02.004

Frodl, T., Meisenzahl, E. M., Zetzsche, T., Höhne, T., Banac, S., Schorr, C., et al. (2004). Hippocampal and amygdala changes in patients with major depressive disorder and healthy controls during a 1-year follow-up. *J. Clin. Psychiatry* 65, 492–499. doi: 10.4088/JCP.v65n0407

Ga˛dek-Michalska, A., Tadeusz, J., Rachwalska, P., Spyrka, J., and Bugajski, J. (2011). Effect of prior stress on interleukin-1β and HPA axis responses to acute stress. *Pharmacol. Rep.* 63, 1393–1403. doi: 10.1016/S1734-1140(11)70703-4 Gadermann, A., Alonso, J., Vilagut, G., Zaslavsky, A., and Kessler, R. (2012). Comorbidity and disease burden in the National Comorbidity Survey Replication (NCS-R). *Depress. Anxiety* 29, 797–806. doi: 10.1002/da.21924 Gárate, I., García-Bueno, B., Madrigal, J., Bravo, L., Berrocoso, E., Caso, J., et al. (2011). Origin and consequences of brain Toll-like receptor 4 pathway stimulation in an experimental model of depression. *J. Neuroinflammation* 8:151. doi: 10.1186/1742-2094-8-151

Gazal, M., Souza, L., Fucolo, B., Wiener, C., Silva, R., Pinheiro, R., et al. (2013). The impact of cognitive behavioral therapy on IL-6 levels in unmedicated women experiencing the first episode of depression: a pilot study. *Psychiatry Res.* 209, 742–745. doi: 10.1016/j.psychres.2013.03.002

Ghonime, M., Shamaa, O., Das, S., Eldomany, R., Fernandes-Alnemri, T., Alnemri, E., et al. (2014). Inflammasome priming by lipopolysaccharide is dependent upon ERK signaling and proteasome function. *J. Immunol.* 192, 3881–3888. doi: 10.4049/jimmunol.1301974

Gibb, J., Al-Yawer, F., and Anisman, H. (2013). Synergistic and antagonistic actions of acute or chronic social stressors and an endotoxin challenge vary over time following the challenge. *Brain Behav. Immun.* 28, 149–158. doi: 10.1016/j.bbi. 2012.11.004

Gimsa, U., Mitchison, N., and Brunner-Weinzierl, M. (2013). Immune privilege as an intrinsic CNS property: astrocytes protect the CNS against T-cellmediated neuroinflammation. *Mediators Inflamm.* 2013:320519. doi: 10.1155/ 2013/320519

Goebel, M., Stengel, A., Wang, L., Reeve, J., and Taché, Y. (2011). Lipopolysaccharide increases plasma levels of corticotropin-releasing hormone in rats. *Neuroendocrinology* 93, 165–173. doi: 10.1159/000322590

Gong, J., Zhu, B., Murshid, A., Adachi, H., Song, B., Lee, A., et al. (2009). T cell activation by heat shock protein 70 vaccine requires TLR signaling and scavenger receptor expressed by endothelial cells-1. *J. Immunol.* 183, 3092–3098. doi: 10.4049/jimmunol.0901235

Gregory, J. L., Hall, P., Leech, M., Morand, E. F., and Hickey, M. J. (2009). Independent roles of macrophage migration inhibitory factor and endogenous, but not exogenous glucocorticoids in regulating leukocyte trafficking. *Microcirculation* 16, 735–748. doi: 10.3109/1073968090 3210421

Grieb, G., Simons, D., Eckert, L., Hemmrich, M., Steffens, G., Bernhagen, J., et al. (2012). Levels of macrophage migration inhibitory factor and glucocorticoids in chronic wound patients and their potential interactions with impaired wound endothelial progenitor cell migration. *Wound Repair Regen.* 20, 707–714. doi: 10.1111/j.1524-475x.2012.00817.x

Guan, X., Shao, F., Xie, X., Chen, L., and Wang, W. (2014). Effects of aspirin on immobile behavior and endocrine and immune changes in the forced swimming test: comparison to fluoxetine and imipramine. *Pharmacol. Biochem. Behav.* 124, 361–366. doi: 10.1016/j.pbb.2014.07.002

Halassa, M., Fellin, T., Takano, H., Dong, J.-H., and Haydon, P. (2007). Synaptic islands defined by the territory of a single astrocyte. *J. Neurosci.* 27, 6473–6477. doi: 10.1523/JNEUROSCI.1419-07.2007

Harms, A., Cao, S., Rowse, A., Thome, A., Li, X., Mangieri, L., et al. (2013). MHCII is required for α-synuclein-induced activation of microglia, CD4 T cell proliferation, and dopaminergic neurodegeneration. *J. Neurosci.* 33, 9592–9600. doi: 10.1523/jneurosci.5610-12.2013

Heneka, M., Kummer, M., and Latz, E. (2014). Innate immune activation in neurodegenerative disease. *Nat. Rev. Immunol.* 14, 463–477. doi: 10.1038/nri3705

Henry, C. J., Huang, Y., Wynne, A. M., and Godbout, J. P. (2009). Peripheral lipopolysaccharide (LPS) challenge promotes microglial hyperactivity in aged mice that is associated with exaggerated induction of both pro-inflammatory IL-1beta and anti-inflammatory IL-10 cytokines. *Brain Behav. Immun.* 23, 309–317. doi: 10.1016/j.bbi.2008.09.002

Hines, D., Choi, H., Hines, R., Phillips, A., and MacVicar, B. (2013). Prevention of LPS-induced microglia activation, cytokine production and sickness behavior with TLR4 receptor interfering peptides. *PLoS ONE* 8:e60388. doi: 10.1371/journal.pone.0060388

Holsboer-Trachsler, E., Stohler, R., and Hatzinger, M. (1991). Repeated administration of the combined dexamethasone-human corticotropin releasing hormone stimulation test during treatment of depression. *Psychiatry Res.* 38, 163–171. doi: 10.1016/0165-1781(91)90041-M

Horikawa, H., Kato, T., Mizoguchi, Y., Monji, A., Seki, Y., Ohkuri, T., et al. (2010). Inhibitory effects of SSRIs on IFN-γ induced microglial activation through the regulation of intracellular calcium. *Prog. Neuropsychopharmacol. Biol. Psychiatry* 34, 1306–1316. doi: 10.1016/j.pnpbp.2010.07.015

Hsiao, E., McBride, S., Hsien, S., Sharon, G., Hyde, E., McCue, T., et al. (2013). Microbiota modulate behavioral and physiological abnormalities associated with neurodevelopmental disorders. *Cell* 155, 1451–1463. doi: 10.1016/j.cell.2013.11.024

Huang, Y., Henry, C., Dantzer, R., Johnson, R., and Godbout, J. (2008). Exaggerated sickness behavior and brain proinflammatory cytokine expression in aged mice in response to intracerebroventricular lipopolysaccharide. *Neurobiol. Aging* 29, 1744–1753. doi: 10.1016/j.neurobiolaging.2007.04.012

Hueston, C., and Deak, T. (2014). The inflamed axis: the interaction between stress, hormones, and the expression of inflammatory-related genes within key structures comprising the hypothalamic–pituitary–adrenal axis. *Physiol. Behav.* 124, 77–91. doi: 10.1016/j.physbeh.2013.10.035

Hutchinson, M., Ramos, K., Loram, L., Wieseler, J., Sholar, P., Kearney, J., et al. (2009). Evidence for a role of heat shock protein-90 in toll like receptor 4 mediated pain enhancement in rats. *Neuroscience* 164, 1821–1832. doi: 10.1016/j.neuroscience.2009.09.046

Hutchinson, M., and Watkins, L. (2014). Why is neuroimmunopharmacology crucial for the future of addiction research? *Neuropharmacology* 76(pt B), 218–227. doi: 10.1016/j.neuropharm.2013.05.039

Jacobsen, J., Watkins, L., and Hutchinson, M. (2014). Discovery of a novel site of opioid action at the innate immune pattern-recognition receptor TLR4 and its role in addiction. *Int. Rev. Neurobiol.* 118, 129–163. doi: 10.1016/b978-0-12801284-0.00006-3

Jarcho, M., Slavich, G., Tylova-Stein, H., Wolkowitz, O., and Burke, H. (2013). Dysregulated diurnal cortisol pattern is associated with glucocorticoid resistance in women with major depressive disorder. *Biol. Psychol.* 93, 150–158. doi: 10.1016/j.biopsycho.2013.01.018

Kanczkowski, W., Alexaki, V.-I., Tran, N., Großklaus, S., Zacharowski, K., Martinez, A., et al. (2013). Hypothalamo-pituitary and immune-dependent adrenal regulation during systemic inflammation. *Proc. Natl. Acad. Sci. U.S.A.* 110, 14801–14806. doi: 10.1073/pnas.1313945110

Kelley, K., and McCusker, R. (2014). Getting nervous about immunity. *Semin. Immunol.* doi: 10.1016/j.smim.2014.01.011. [Epub ahead of print].

Kéri, S., Szabó, C., and Kelemen, O. (2014). Expression of toll-like receptors in peripheral blood mononuclear cells and response to cognitive-behavioral therapy in major depressive disorder. *Brain Behav. Immun.* 40, 235–243. doi: 10.1016/j.bbi.2014.03.020

Kim, S., Kim, S., Pribis, J., Lotze, M., Mollen, K., Shapiro, R., et al. (2013). Signaling of high mobility group box 1 (HMGB1) through toll-like receptor 4 in macrophages requires CD14. *Mol. Med.* 19, 1. doi: 10.2119/molmed.2012.00306

Kreisel, T., Frank, M., Licht, T., Reshef, R., Ben-Menachem-Zidon, O., Baratta, M., et al. (2014). Dynamic microglial alterations underlie stress-induced depressivelike behavior and suppressed neurogenesis. *Mol. Psychiatry* 19, 699–709. doi: 10.1038/mp.2013.155

Kumari, B., Kumar, A., and Dhir, A. (2007). Protective effect of non-selective and selective COX-2-inhibitors in acute immobilization stress-induced behavioral and biochemical alterations. *Pharmacol. Rep.* 59, 699–707.

Laird, M., Shields, J., Sukumari-Ramesh, S., Kimbler, D., Fessler, R., Shakir, B., et al. (2014). High mobility group box protein-1 promotes cerebral edema after traumatic brain injury via activation of toll-like receptor 4. *Glia* 62, 26–38. doi: 10.1002/glia.22581

Lerch, J., Puga, D., Bloom, O., and Popovich, P. (2014). Glucocorticoids and macrophage migration inhibitory factor (MIF) are neuroendocrine modulators of inflammation and neuropathic pain after spinal cord injury. *Semin. Immunol.* doi: 10.1016/j.smim.2014.03.004. [Epub ahead of print].

Lewis, S. S., Loram, L. C., Hutchinson, M. R., Li, C.-M. M., Zhang, Y., Maier, S. F., et al. (2012). (+)-naloxone, an opioid-inactive toll-like receptor 4 signaling inhibitor, reverses multiple models of chronic neuropathic pain in rats. *J. Pain* 13, 498–506. doi: 10.1016/j.jpain.2012.02.005

Lichtblau, N., Schmidt, F., Schumann, R., Kirkby, K., and Himmerich, H. (2013). Cytokines as biomarkers in depressive disorder: current standing and prospects. *Int. Rev. Psychiatry* 25, 592–603. doi: 10.3109/09540261.2013.813442

Lively, S., and Schlichter, L. (2013). The microglial activation state regulates migration and roles of matrix-dissolving enzymes for invasion. *J. Neuroinflammation* 10:75. doi: 10.1186/1742-2094-10-75

Loram, L. C., Taylor, F. R., Strand, K. A., Frank, M. G., Sholar, P., Harrison, J. A., et al. (2011). Prior exposure to glucocorticoids potentiates lipopolysaccharide induced mechanical allodynia and spinal neuroinflammation. *Brain Behav. Immun.* 25, 1408–1415. doi: 10.1016/j.bbi.2011.04.013

Loum-Ribot, E., Lafon, P., Chaigniau, M., Tramu, G., and Corio, M. (2006). Glucocorticoids down-regulate lipopolysaccharide-induced *de novo* production of neurotensin mrna in the rat hypothalamic, paraventricular, corticotrophinreleasing hormone neurons. *Neuroimmunomodulation* 13, 170–178. doi: 10.1159/000098130

Lu, B., Nakamura, T., Inouye, K., Li, J., Tang, Y., Lundbäck, P., et al. (2012). Novel role of PKR in inflammasome activation and HMGB1 release. *Nature* 488, 670–674. doi: 10.1038/nature11290

Ma, Y., Matsuwaki, T., Yamanouchi, K., and Nishihara, M. (2013). Cyclooxygenase-2-related signaling in the hypothalamus plays differential roles in response to various acute stresses. *Brain Res.* 1508, 23–33. doi: 10.1016/j.brainres.2013.02.042

Maciel, I. S., Silva, R. B., Morrone, F. B., Calixto, J. B., and Campos, M. M. (2013). Synergistic effects of celecoxib and bupropion in a model of chronic inflammation-related depression in mice. *PLoS ONE* 8:e77227. doi: 10.1371/journal.pone.0077227

Maes, M., Bosmans, E., Suy, E., Vandervorst, C., DeJonckheere, C., and Raus, J. (1991). Depression-related disturbances in mitogen-induced lymphocyte responses and interleukin-1? and soluble interleukin-2 receptor production. *Acta Psychiatr. Scand.* 84, 379–386. doi: 10.1111/j.1600-0447.1991.tb03163.x

Maes, M., Meltzer, H., Stevens, W., Cosyns, P., and Blockx, P. (1994). Multiple reciprocal relationships between *in vivo* cellular immunity and hypothalamic-pituitary-adrenal axis in depression. *Psychol. Med.* 24, 167–177. doi: 10.1017/S0033291700026933

Malynn, S., Campos-Torres, A., Moynagh, P., and Haase, J. (2013). The proinflammatory cytokine TNF-α regulates the activity and expression of the serotonin transporter (SERT) in astrocytes. *Neurochem. Res.* 38, 694–704. doi: 10.1007/s11064-012-0967-y

Manikowska, K., Mikołajczyk, M., Mikołajczak, P., and Bobkiewicz-Kozłowska, T. (2014). The influence of mianserin on TNF-α, IL-6 and IL-10 serum levels in rats under chronic mild stress. *Pharmacol. Rep.* 66, 22–27. doi: 10.1016/j.pharep.2013.06.003

Martinez Calejman, C., Astort, F., Di Gruccio, J. M., Repetto, E. M., Mercau, M., Giordanino, E., et al. (2011). Lipopolysaccharide stimulates adrenal steroidogenesis in rodent cells by a NFκB-dependent mechanism involving COX-2 activation. *Mol. Cell. Endocrinol.* 337, 1–6. doi: 10.1016/j.mce.2010.12.036

Maslanik, T., Mahaffey, L., Tannura, K., Beninson, L., Greenwood, B., and Fleshner, M. (2013). The inflammasome and danger associated molecular patterns (DAMPs) are implicated in cytokine and chemokine responses following stressor exposure. *Brain Behav. Immun.* 28, 54–62. doi: 10.1016/j.bbi.2012. 10.014

Matysiak, M., Makosa, B., Walczak, A., and Selmaj, K. (2008). Patients with multiple sclerosis resisted to glucocorticoid therapy: abnormal expression of heat-shock protein 90 in glucocorticoid receptor complex. *Mult. Scler.* 14, 919–926. doi: 10.1177/1352458508090666

McCusker, R., and Kelley, K. (2013). Immune-neural connections: how the immune system's response to infectious agents influences behavior. *J. Exp. Biol.* 216, 84–98. doi: 10.1242/jeb.073411

Mehet, D., Philip, J., Solito, E., Buckingham, J., and John, C. (2012). Evidence from *in vitro* and *in vivo* studies showing that nuclear factor-κB within the pituitary folliculostellate cells and corticotrophs regulates adrenocorticotrophic hormone secretion in experimental endotoxaemia. *J. Neuroendocrinol.* 24, 862–873. doi: 10.1111/j.1365-2826.2012.02285.x

Mohn, C., Fernandez-Solari, J., Laurentiis, A., Bornstein, S., Ehrhart-Bornstein, M., and Rettori, V. (2011). Adrenal gland responses to lipopolysaccharide after stress and ethanol administration in male rats. *Stress* 14, 216–226. doi: 10.3109/10253890.2010.532254

Monroe, S. M., and Simons, A. D. (1991). Diathesis-stress theories in the context of life stress research: implications for the depressive disorders. *Psychol. Bull.* 110, 406–425. doi: 10.1037/0033-2909.110.3.406

Mouihate, A., Galic, M. A., Ellis, S. L., Spencer, S. J., Tsutsui, S., and Pittman, Q. J. (2010). Early life activation of toll-like receptor 4 reprograms neural anti-inflammatory pathways. *J. Neurosci.* 30, 7975–7983. doi: 10.1523/JNEUROSCI.6078-09.2010

Muzikar, K. A., Nickols, N. G., and Dervan, P. B. (2009). Repression of DNAbinding dependent glucocorticoid receptor-mediated gene expression. *Proc. Natl. Acad. Sci. U.S.A.* 106, 16598–16603. doi: 10.1073/pnas.0909192106

Na, K.-S., Lee, K., Lee, J., Cho, Y., and Jung, H.-Y. (2014). Efficacy of adjunctive celecoxib treatment for patients with major depressive disorder: a meta-analysis. *Prog. Neuropsychopharmacol. Biol. Psychiatry* 48, 79–85. doi: 10.1016/j.pnpbp.2013.09.006

Nathanson, N. (2012). Regulation of neurokine receptor signaling and trafficking. *Neurochem. Int.* 61, 874–878. doi: 10.1016/j.neuint.2012.01.018

Nimmerjahn, A., Kirchhoff, F., and Helmchen, F. (2005). Resting microglial cells are highly dynamic surveillants of brain parenchyma *in vivo*. *Science* 308, 1314–1318. doi: 10.1126/science.1110647

Novac, N., Baus, D., Dostert, A., and Heinzel, T. (2006). Competition between glucocorticoid receptor and NFκB for control of the human FasL promoter. *FASEB J.* 20, 1074–1081. doi: 10.1096/fj.05-5457com

O'Connor, J., Lawson, M., André, C., Moreau, M., Lestage, J., Castanon, N., et al. (2009). Lipopolysaccharide-induced depressive-like behavior is mediated by indoleamine 2,3-dioxygenase activation in mice. *Mol. Psychiatry* 14, 511–522. doi: 10.1038/sj.mp.4002148

Obuchowicz, E., Bielecka, A., Paul-Samojedny, M., Pudełko, A., and Kowalski, J. (2014). Imipramine and fluoxetine inhibit LPS-induced activation and affect morphology of microglial cells in the rat glial culture. *Pharmacol. Rep.* 66, 34–43. doi: 10.1016/j.pharep.2013.08.002

Ock, J., Lee, H., Kim, S., Lee, W.-H., Choi, D.-K., Park, E., et al. (2006). Induction of microglial apoptosis by corticotropin-releasing hormone. *J. Neurochem.* 98, 962–972. doi: 10.1111/j.1471-4159.2006.03933.x

Olah, M., Biber, K., Vinet, J., and Boddeke, H. (2011). Microglia Phenotype Diversity. *CNS Neurol. Disord. Drug Targets* 10, 108–118. doi: 10.2174/187152711794488575

Otsuki, K., Uchida, S., Wakabayashi, Y., Matsubara, T., Hobara, T., Funato, H., et al. (2010). Aberrant REST-mediated transcriptional regulation in major depressive disorder. *J. Psychiatr. Res.* 44, 378–384. doi: 10.1016/j.jpsychires.2009.09.009

Pace, T., and Miller, A. (2009). Cytokines and glucocorticoid receptor signaling. Relevance to major depression. *Ann. N.Y. Acad. Sci.* 1179, 86–105. doi: 10.1111/j.1749-6632.2009.04984.x

Pace, T. W. W., Hu, F., and Miller, A. H. (2007). Cytokine-effects on glucocorticoid receptor function: relevance to glucocorticoid resistance and the pathophysiology and treatment of major depression. *Brain Behav. Immun.* 21, 9–19. doi: 10.1016/j.bbi.2006.08.009

Pan, Y., Chen, X.-Y., Zhang, Q.-Y., and Kong, L.-D. (2014). Microglial NLRP3 inflammasome activation mediates IL-1β-related inflammation in prefrontal cortex of depressive rats. *Brain Behav. Immun.* 41, 90–100. doi: 10.1016/j.bbi. 2014.04.007

Pekny, M., and Nilsson, M. (2005). Astrocyte activation and reactive gliosis. *Glia* 50, 427–434. doi: 10.1002/glia.20207

Persson, M., Brantefjord, M., Hansson, E., and Rönnbäck, L. (2005). Lipopolysaccharide increases microglial GLT-1 expression and glutamate uptake capacity *in vitro* by a mechanism dependent on TNF-α. *Glia* 51, 111–120. doi: 10.1002/glia.20191

Persson, M., Pekna, M., Hansson, E., and Rönnbäck, L. (2009). The complementderived anaphylatoxin C5a increases microglial GLT-1 expression and glutamate uptake in a TNF-α-independent manner. *Eur. J. Neurosci.* 29, 267–274. doi: 10.1111/j.1460-9568.2008.06575.x

Powell, N., Bailey, M., Mays, J., Stiner-Jones, L., Hanke, M., Padgett, D., et al. (2009). Repeated social defeat activates dendritic cells and enhances Toll-like receptor dependent cytokine secretion. *Brain Behav. Immun.* 23, 225–231. doi: 10.1016/j.bbi.2008.09.010

Qiu, J., Xu, J., Zheng, Y., Wei, Y., Zhu, X., Lo, E., et al. (2010). Highmobility group box 1 promotes metalloproteinase-9 upregulation through Toll-like receptor 4 after cerebral ischemia. *Stroke* 41, 2077–2082. doi: 10.1161/STROKEAHA.110.590463

Quak, J., Doornbos, B., Roest, A., Duivis, H., Vogelzangs, N., Nolen, W., et al. (2014). Does tryptophan degradation along the kynurenine pathway mediate the association between pro-inflammatory immune activity and depressive symptoms? *Psychoneuroendocrinology* 45, 202–210. doi: 10.1016/j.psyneuen.2014.03.013

Quan, N., Avitsur, R., Stark, J., He, L., Lai, W., Dhabhar, F., et al. (2003). Molecular mechanisms of glucocorticoid resistance in splenocytes of socially stressed male mice. *J. Neuroimmunol.* 137, 51–58. doi: 10.1016/S0165-5728(03)00042-0

Ransohoff, R., and Brown, M. (2012). Innate immunity in the central nervous system. *J. Clin. Invest.* 122, 1164–1171. doi: 10.1172/jci58644

Ratman, D., Berghe, W., Dejager, L., Libert, C., Tavernier, J., Beck, I., et al. (2013). How glucocorticoid receptors modulate the activity of other transcription factors: a scope beyond tethering. *Mol. Cell. Endocrinol.* 380, 41–54. doi: 10.1016/j.mce.2012.12.014

Ricketson, D., Hostick, U., Fang, L., Yamamoto, K., and Darimont, B. (2007). A conformational switch in the ligand-binding domain regulates the dependence of the glucocorticoid receptor on Hsp90. *J. Mol. Biol.* 368, 729–741. doi: 10.1016/j.jmb.2007.02.057

Rubin, R., Miller, T., Rhodes, M., and Czambel, R. (2006). Adrenal cortical responses to low- and high-dose ACTH1–24 administration in major depressives vs. matched controls. *Psychiatry Res.* 143, 43–50. doi: 10.1016/j.psychres.2005.10.003

Rybakowski, J., Remlinger-Molenda, A., Czech-Kucharska, A., Wojcicka, M., Michalak, M., and Losy, J. (2013). Increased serum matrix metalloproteinase9 (MMP-9) levels in young patients during bipolar depression. *J. Affect. Disord.* 146, 286–289. doi: 10.1016/j.jad.2012.07.019

Sapolsky, R., Romero, L., and Munck, A. (2000). How do glucocorticoids influence stress responses? integrating permissive, suppressive, stimulatory, and preparative actions1. *Endocr. Rev.* 21, 55–89. doi: 10.1210/edrv.21.1.0389

Schipke, C., Heuser, I., and Peters, O. (2011). Antidepressants act on glial cells: SSRIs and serotonin elicit astrocyte calcium signaling in the mouse prefrontal cortex. *J. Psychiatr. Res.* 45, 242–248. doi: 10.1016/j.jpsychires.2010.06.005

Schlaak, J., Trippler, M., Hoyo-Becerra, C., Erim, Y., Kis, B., Wang, B., et al. (2012). Selective hyper-responsiveness of the interferon system in major depressive disorders and depression induced by interferon therapy. *PLoS ONE* 7:e38668. doi: 10.1371/journal.pone.0038668

Schwartz, M., Kipnis, J., Rivest, S., and Prat, A. (2013). How do immune cells support and shape the brain in health, disease, and aging? *J. Neurosci.* 33, 17587–17596. doi: 10.1523/JNEUROSCI.3241-13.2013

Schweingruber, N., Fischer, H., Fischer, L., Brandt, J., Karabinskaya, A., Labi, V., et al. (2014). Chemokine-mediated redirection of T cells constitutes a critical mechanism of glucocorticoid therapy in autoimmune CNS responses. *Acta Neuropathol.* 127, 713–729. doi: 10.1007/s00401-014-1248-4

Sharma, G., and Vijayaraghavan, S. (2001). Nicotinic cholinergic signaling in hippocampal astrocytes involves calcium-induced calcium release from intracellular stores. *Proc. Natl. Acad. Sci. U.S.A.* 98, 4148–4153. doi: 10.1073/pnas.071540198

Shieh, C.-H., Heinrich, A., Serchov, T., Calker, D., and Biber, K. (2014). P2X7dependent, but differentially regulated release of IL-6, CCL2, and TNF-α in cultured mouse microglia. *Glia* 62, 592–607. doi: 10.1002/glia.22628

Silverman, M. N., Mukhopadhyay, P., Belyavskaya, E., Tonelli, L. H., Revenis, B. D., Doran, J. H., et al. (2013). Glucocorticoid receptor dimerization is required for proper recovery of LPS-induced inflammation, sickness behavior and metabolism in mice. *Mol. Psychiatry* 18, 1006–1017. doi: 10.1038/mp.2012.131

Silverman, M. N., and Sternberg, E. M. (2012). Glucocorticoid regulation of inflammation and its functional correlates: from HPA axis to glucocorticoid receptor dysfunction. *Ann. N.Y. Acad. Sci.* 1261, 55–63. doi: 10.1111/j.17496632.2012.06633.x

Simic, I., Mitic, M., Djordjevic, J., Radojcic, M., and Adzic, M. (2012). Chronic stress decreases availability of heat shock proteins to glucocorticoid receptor in response to novel acute stress in Wistar rat hypothalamus. *Cell. Mol. Neurobiol.* 32, 625–632. doi: 10.1007/s10571-012-9811-9

Smith-Thomas, L., Fok-Seang, J., Stevens, J., Du, J., Muir, E., Faissner, A., et al. (1994). An inhibitor of neurite outgrowth produced by astrocytes. *J. Cell Sci.* 107(pt 6), 1687–1695.

Solomon, G. F., Allansmith, M., McCellan, B., and Amkraut, A. (1969). Immunoglobulins in psychiatric patients. *Arch. Gen. Psychiatry* 20, 272–277. doi: 10.1001/archpsyc.1969.01740150016003

Sominsky, L., Fuller, E. A., Bondarenko, E., Ong, L. K., Averell, L., Nalivaiko, E., et al. (2013). Functional programming of the autonomic nervous system by early life immune exposure: implications for anxiety. *PLoS ONE* 8:e57700. doi: 10.1371/journal.pone.0057700

Starkman, M. N., Schteingart, D. E., and Schork, M. A. (1981). Depressed mood and other psychiatric manifestations of Cushing's syndrome: relationship to hormone levels. *Psychosom. Med.* 43, 3–18. doi: 10.1097/00006842-19810200000002

Stevens, C., Aravind, S., Das, S., and Davis, R. (2013). Pharmacological characterization of LPS and opioid interactions at the toll-like receptor 4. *Br. J. Pharmacol.* 168, 1421–1429. doi: 10.1111/bph.12028

Sun, D., and Jakobs, T. (2012). Structural remodeling of astrocytes in the injured CNS. *Neuroscientist* 18, 567–588. doi: 10.1177/1073858411423441

Sundholm-Peters, N., Yang, H., Goings, G., Walker, A., and Szele, F. (2005). Subventricular zone neuroblasts emigrate toward cortical lesions. *J. Neuropathol. Exp. Neurol.* 64, 1089–1100. doi: 10.1097/01.jnen.0000190066.13312.8f

Tazi, A., Dantzer, R., Crestani, F., and Moal, M. (1988). Interleukin-1 induces conditioned taste aversion in rats: a possible explanation for its pituitaryadrenal stimulating activity. *Brain Res.* 473, 369–371. doi: 10.1016/00068993(88)90868-2

Temburni, M., and Jacob, M. (2001). New functions for glia in the brain. *Proc. Natl. Acad. Sci. U.S.A.* 98, 3631–3632. doi: 10.1073/pnas.081073198

Theoharides, T., Spanos, C., Pang, X., Alferes, L., Ligris, K., Letourneau, R., et al. (1995). Stress-induced intracranial mast cell degranulation: a corticotropinreleasing hormone-mediated effect. *Endocrinology* 136, 5745–5750. doi: 10.1210/endo.136.12.7588332

Tilleux, S., and Hermans, E. (2008). Down-regulation of astrocytic GLAST by microglia-related inflammation is abrogated in dibutyryl cAMP-differentiated cultures. *J. Neurochem.* 105, 2224–2236. doi: 10.1111/j.1471-4159.2008.05305.x

Triantafilou, M., and Triantafilou, K. (2004). Heat-shock protein 70 and heatshock protein 90 associate with Toll-like receptor 4 in response to bacterial lipopolysaccharide. *Biochem. Soc. Trans.* 32, 636–639. doi: 10.1042/BST0320636

Vakharia, K., and Hinson, J. (2004). Lipopolysaccharide directly stimulates cortisol secretion by human adrenal cells by a cyclooxygenase-dependent mechanism. *Endocrinology* 146, 1398–1402. doi: 10.1210/en.2004-0882

Viviani, B., Boraso, M., Marchetti, N., and Marinovich, M. (2014). Perspectives on neuroinflammation and excitotoxicity: a neurotoxic conspiracy? *Neurotoxicology* 43, 10–20. doi: 10.1016/j.neuro.2014.03.004

Vogel, D., Heijnen, P., Breur, M., Vries, H., Tool, A., Amor, S., et al. (2014). Macrophages migrate in an activation-dependent manner to chemokines involved in neuroinflammation. *J. Neuroinflammation* 11:23. doi: 10.1186/17422094-11-23

Vos, T., Flaxman, A. D., Naghavi, M., Lozano, R., Michaud, C., Ezzati, M., et al. (2012). Years lived with disability (YLDs) for 1160 sequelae of 289 diseases and injuries 1990–2010: a systematic analysis for the Global Burden of Disease Study 2010. *Lancet* 380, 2163–2196. doi: 10.1016/S0140-6736(12)61729-2 Warner-Schmidt, J., Vanover, K., Chen, E., Marshall, J., and Greengard, P. (2011). Antidepressant effects of selective serotonin reuptake inhibitors (SSRIs) are attenuated by antiinflammatory drugs in mice and humans. *Proc. Natl. Acad. Sci. U.S.A.* 108, 9262–9267. doi: 10.1073/pnas.1104836108

Watters, T., Kenny, E., and O'Neill, L. (2007). Structure, function and regulation of the Toll/IL-1 receptor adaptor proteins. *Immunol. Cell Biol.* 85, 411–419. doi: 10.1038/sj.icb.7100095

Weber, M., Frank, M., Sobesky, J., Watkins, L., and Maier, S. (2013). Blocking toll-like receptor 2 and 4 signaling during a stressor prevents stress-induced priming of neuroinflammatory responses to a subsequent immune challenge. *Brain Behav. Immun.* 32, 112–121. doi: 10.1016/j.bbi.2013.03.004

Whiteford, H., Degenhardt, L., Rehm, J., Baxter, A., Ferrari, A., Erskine, H., et al. (2013). Global burden of disease attributable to mental and substance use disorders: findings from the Global Burden of Disease Study 2010. *Lancet* 382, 1575–1586. doi: 10.1016/s0140-6736(13)61611-6

Williams, D., Calderon, T., Lopez, L., Carvallo-Torres, L., Gaskill, P., Eugenin, E., et al. (2013). Mechanisms of HIV entry into the CNS: increased sensitivity of HIV infected CD14+CD16+ monocytes to CCL2 and key roles of CCR2, JAM-A, and ALCAM in diapedesis. *PLoS ONE* 8:e69270. doi: 10.1371/journal.pone.0069270

Wohleb, E. S., McKim, D. B., Shea, D. T., Powell, N. D., Tarr, A. J., Sheridan, J. F., et al. (2014). Re-establishment of anxiety in stress-sensitized mice is caused by monocyte trafficking from the spleen to the brain. *Biol. Psychiatry* 75, 970–981. doi: 10.1016/j.biopsych.2013.11.029

Wohleb, E. S., Powell, N. D., Godbout, J. P., and Sheridan, J. F. (2013). Stress-induced recruitment of bone marrow-derived monocytes to the brain promotes anxiety-like behavior. *J. Neurosci.* 33, 13820–13833. doi: 10.1523/JNEUROSCI.1671-13.2013

Wong, D., Prameya, R., and Dorovinizis, K. (2007). Adhesion and migration of polymorphonuclear leukocytes across human brain microvessel endothelial cells are differentially regulated by endothelial cell adhesion molecules and modulate monolayer permeability. *J. Neuroimmunol.* 184, 136–148. doi: 10.1016/j.jneuroim.2006.12.003

Wu, T.-C., Chen, H.-T., Chang, H.-Y., Yang, C.-Y., Hsiao, M.-C., Cheng, M.-L., et al. (2013). Mineralocorticoid receptor antagonist spironolactone prevents chronic corticosterone induced depression-like behavior. *Psychoneuroendocrinology* 38, 871–883. doi: 10.1016/j.psyneuen.2012.09.011

Xu, Y., Tao, X., Shen, B., Horng, T., Medzhitov, R., Manley, J., et al. (2000). Structural basis for signal transduction by the Toll/interleukin-1 receptordomains. *Nature* 408, 111–115. doi: 10.1038/35040600

Yamaguchi, N., Ogawa, S., and Okada, S. (2010). Cyclooxygenase and nitric oxide synthase in the presympathetic neurons in the paraventricular hypothalamic nucleus are involved in restraint stress-induced sympathetic activation in rats. *Neuroscience* 170, 773–781. doi: 10.1016/j.neuroscience.2010. 07.051

Yuan, Y.-M., and He, C. (2013). The glial scar in spinal cord injury and repair. *Neurosci. Bull.* 29, 421–435. doi: 10.1007/s12264-013-1358-3

Zacharowski, K., Zacharowski, P., Koch, A., Baban, A., Tran, N., Berkels, R., et al. (2006). Toll-like receptor 4 plays a crucial role in the immune–adrenal response to systemic inflammatory response syndrome. *Proc. Natl. Acad. Sci. U.S.A.* 103, 6392–6397. doi: 10.1073/pnas.0601527103

Zhang, F., Zhou, H., Wilson, B., Shi, J.-S., Hong, J.-S., and Gao, H.-M. (2012). Fluoxetine protects neurons against microglial activation-mediated neurotoxicity. *Parkinsonism Relat. Disord.* 18, S213–S217. doi: 10.1016/S13538020(11)70066-9

Zhao, M., Zhou, A., Xu, L., and Zhang, X. (2014). The role of TLR4-mediated PTEN/PI3K/AKT/NF-κB signaling pathway in neuroinflammation in hippocampal neurons. *Neuroscience* 269, 93–101. doi: 10.1016/j.neuroscience.2014.03.039

Zhong, H.-J., Wang, H.-Y., Yang, C., Zhou, J.-Y., and Jiang, J.-X. (2013). Low concentrations of corticosterone exert stimulatory effects on macrophage function in a manner dependent on glucocorticoid receptors. *Int. J. Endocrinol.* 2013:19. doi: 10.1155/2013/405127

Conflict of Interest Statement: The authors declare that the research was conducted in the absence of any commercial or financial relationships that could be construed as a potential conflict of interest.

Received: 01 August 2014; accepted: 13 September 2014; published online: 30 September 2014.
*Citation: Liu J, Buisman-Pijlman F and Hutchinson MR (2014) Toll-like receptor 4: innate immune regulator of neuroimmune and neuroendocrine interactions in stress and major depressive disorder. Front. Neurosci. **8**:309. doi: 10.3389/fnins.2014.00309 This article was submitted to Neuroendocrine Science, a section of the journal Frontiers in Neuroscience.*

1.4.2 An addendum: MDD sub-types and dysregulations in Immune neuroendocrine associates

Section 1.4 outlined the association between MDD, neuroendocrine, and innate immune changes, but recent strong evidence have emerged further identifying specific sub-types of MDD that drive this association (Lamers *et al*., 2013). In their longitudinal study including 2329 patients, Lamers et al. (2013) found a stronger positive association between atypical depression and C-reactive protein, IL-6, and TNF-α when compared to melancholic depression. Additionally, atypical depression was found to have a lower association with glucocorticoid dysregulation as compared to melancholic depression (Gold, 2015). Thus, the relationship between neuroendocrine and immune dysregulations in MDD can be further broken down into the different subtypes of MDD, which adds further considerations for future research. Interestingly, a main difference between melancholic depression and atypical depression is the variation in time-of-day in depressive mood. In atypical depression, depressive mood is often strongest in the morning, while it is the reverse in melancholic depression (Gold, 2015). This distinction introduces further consideration of the potential role of circadian rhythm differences in neuroendocrine and immune adaptations.

This consideration of circadian rhythm has also been shown pre-clinical studies. For example, LPS administration during the light-phase has been shown to cause exaggerated sickness behaviour in rats, co-inciding with increased inflammatory gene expression in microglia (Fonken et al., 2015). Furthermore, the administration of inescapable tail shock stress during the light or dark phase, can determine inflammatory priming of microglia harvested 24 h after the onset of stress (Fonken et al., 2016). In this study, only inescapable tail shock stress administered in the light

phase resulted in a primed microglia phenotype to further LPS stimulation. Circadian rhythm difference therefore play an important role in microgilial inflammatory function and stress-induced priming of pro-inflammatory responses.

1.5 An update on key findings in the literature

Since the publication of this review in 2014, additional studies have made important contributions towards the work in this research area. In the following section, I review the relevant recent publications.

1.5.1 Stress and pro-inflammatory priming

Additional findings have strengthened the link between stress and pro-inflammatory priming seen in microglia. A recent systematic review also showed that repeated stress can cause microglia changes in the hippocampus, characterised by increased IBA-1 signalling and morphological change. However, these microglia changes varied widely between stress models, with highest reliability in models of social defeat and inescapable footshock or tailshock stress (Calcia *et al.*, 2016).

Other behavioural implications of primed microglia have also been shown. For example, stress administered prior to foot incision increased post-operative mechanical hyperalgesia and corresponding increased microglia immunofluorescence in the spinal cord (Sun *et al.*, 2016). In this study, hyperalgesia post-operation, and added stress-induced exacerbation of this hyperalgesia was associated with elevated spinal cord IL-1β and TNF-α, concurrent with increased microglia activation. The

increased microglial activation and neurokine elevation was further attenuated by a GR specific antagonist when administered prior to stress administration, suggesting that glucocorticoid signalling via GR plays a role in this neuroimmune priming.

Beyond rodent models of stress, primates have also displayed stress-induced pro-inflammatory priming. In an experimental study lasting two years, rhesus monkeys T cell genes were differentially expressed in association with position within the primate social hierarchy, a natural form of social stress in these primates (Snyder-Mackler *et al.*, 2016). Furthermore, primary T cells obtained from these stressed animals also displayed increased responsiveness toward LPS administration, showing the priming property of chronic stress. Specifically, subordinate females had increased MyD88-NF-κB activity in response to LPS administration while displaying no difference in TRIF pathway-induced gene transcription, thus suggesting that chronic social stress may selectively prime the MyD88-NF-κB pathway.

Taken together, these studies provide compelling evidence for a primed immune system following stress, with behavioural applications to pain research, further extending to the periphery immune system, and this effect has also been demonstrated across species.

1.5.2 HMGB1, an emerging link between stress and pro-inflammatory priming in microglia, further potential mechanisms through TLR4

Further studies investigating the mechanism of stress-induced pro-inflammatory

priming have demonstrated the potential role of DAMPs such as HMGB1. Firstly, HMGB1 protein release was demonstrated from ex vivo hippocampal microglia harvested from rats after inescapable tail shock stress (Weber *et al.*, 2015). The harvested microglia also exhibited increased responsiveness to LPS administration, thus indicating a primed phenotype. In the same study, administration of HMGB1 protein *intra cisterna magna* also caused microglial priming. Furthermore, the microglial priming resulting from inescapable foot shock was attenuated using an administration of HGMB1 antibody. This result identifies a mechanistic role of HMGB1 danger signalling in increased microglial sensitivity to immune stimuli. A notable consideration introduced in the recent focus on HMGB1 release is the specific redox form of HMGB1 required, since it can determine the immune stimulatory properties of the protein (Frank *et al.*, 2015). Disulfide-HMGB1 protein used by Weber and colleagues functions as a TLR4 or RAGE agonist, while the fully reduced form HMGB1 functions as a chemokine instead (Venereau *et al.*, 2012).

The release mechanisms of HMGB1 are another consideration in the priming effect of stress. Monocytes have been shown to release HMGB1 in situations of cell death and Inflammasome activation (Willingham *et al.*, 2009; Vande Walle, Kanneganti and Lamkanfi, 2011), and hyper-acetylation within the cytoplasm (Bonaldi *et al.*, 2003). However, it is unclear if the extracellular elevation of HMGB1 seen after inescapable tail shock is due to cellular damage, or via active mechanisms of release.

The involvement of glucocorticoids may also mediate this stress-related release of

HMGB1. A second study showed that antagonism of glucocorticoid receptor attenuated stress-induced HMGB1 expression in the hippocampus (Sobesky *et al.*, 2016), suggesting the role of glucocorticoid signalling. Taken together, glucocorticoids may mediate stress-induced HMGB1 release, which leads to a priming effect in microglia, and microglia can also release HMGB1 after the animal has been exposed to stress. However, the direct actions of glucocorticoids on microglia in regards to HMGB1 release is still unclear. One consideration is the localisation of HMGB1-related mechanisms, as current evidence of HMGB1 involvement in stress and neuroimmune adaptations is strongest in the hippocampus (Weber et al., 2015; Sobeskey et al., 2016; Ogundele at al., 2017).

1.5.3 Stress actions on immune cell migration

A human study recently demonstrated that pre-treatment with cortisol primed peripheral blood monocyte migration toward sites of injury, modelled by filling blisters with chemokine CCL2 (Yeager *et al.*, 2016). The researchers also showed that exogenous cortisol treatment itself significantly increased chemokine CCL2 and CX3CR1 mRNA 12 h after cortisol treatment, coinciding with a return to baseline in salivary free cortisol levels. This result suggests that the resolution of the endocrine response may be required for the elevation of immune responses. This study thus provides support for the innate immune priming effect of glucocorticoids, while also extending this hypothesis toward cell migration and chemokine involvement in the periphery.

1.6: Aims and hypotheses

The work contained in this thesis aimed to understand the bidirectional relationship between stress and immunity through exploring the interface between innate immune and neuroendocrine systems through 3 studies. Study 1 investigated whether baseline innate immune signalling could influence the acute stress response. Studies 2 and 3 explored mechanisms of glucocorticoid signalling induced priming and immunosuppression on innate immune cells. Study 2 focused on these effects with respect to TLR4-NF-κB pro-inflammatory responses, while Study 3 investigated DAMP secretion as a result of glucocorticoid signalling.

1.6.1 Study 1: Role of baseline TLR4/MyD88 signalling on behavioural and neuroendocrine responses in acute stress

It is now established that both behaviour and HPA activity can be modulated by TLR4 stimulation, since the use of LPS in animal studies has repeatedly shown sickness behaviour and accompanying HPA adaptations (Godbout *et al.*, 2005; Huang *et al.*, 2008; Henry *et al.*, 2009; Martin *et al.*, 2014). Moreover, the lack of *Tlr4* and *Myd88* is protective against LPS-induced behavioural and neuroendocrine changes (Zacharowski *et al.*, 2006; Kanczkowski *et al.*, 2013). However, it is unclear if this deletion of *Tlr4* or *Myd88* has consequences towards these stress responses to non-immunogenic stressors. Study 1 (Chapter 2 and 3) thus focuses on how changes to baseline innate immune functioning can influence behavioural and HPA responses in rodent models of non-immunogenic acute stress.

1) *Impact of TLR4/MyD88 signalling on immobility behaviour and HPA activity after forced swim and tail suspension stressors (Chapter 2)*

To investigate if baseline differences in TLR4/MyD88 signalling can influence behaviour and HPA activity, forced swim and tail suspension stressors were applied, comparing mice that lack either *Tlr4* or *Myd88* (a downstream intracellular adaptor protein involved in TLR and IL-1R1 signalling) with wild type mice. To test if acute signalling deficits can also elicit changes seen in these transgenic animals, acute pharmacological antagonists to TLR4 and IL-1R1 receptors were also administered.

2) *Impact of TLR4/MyD88 signalling on HPA feedforward and feedback mechanisms (Chapter 2)*

Owing to strain differences found in the time response of corticosterone secretion following acute stress, I hypothesised that these changes were a result of long-term adaptations to feedforward and feedback mechanisms. Thus, hypothalamic glucocorticoid receptor and corticosteroid binding globulin were measured at baseline and following forced swim stress to explore hypothalamic feedback mechanisms following stress. Furthermore, to test feed forward mechanisms at the level of the adrenal gland, an *ex vivo* stimulation of adrenal glands using ACTH to induce corticosterone secretion was compared between mouse strains.

3) *Impact of TLR4/MyD88 signalling on the relationship between behavioural immobility and corticosterone levels following stress (Chapter 3)*

Further analysis of the relationship between behavioural immobility and corticosterone responses to forced swim and tail suspension stressors were applied to the data obtained in Chapter 2. This analysis aimed to investigate whether TLR4/MyD88 signalling altered the relationship between neuroendocrine responses, and behaviour.

4) *Effect of LPS administration on ACTH-induced adrenal secretion of corticosterone (Chapter 3)*

Adrenal cells have previously been shown to be responsive toward LPS, causing the secretion of Corticosterone in vitro (Vakharia and Hinson, 2005; Kanczkowski *et al.*, 2013). A co-administration of LPS and ACTH to ex vivo adrenal tissue was used to investigate the potential role of TLR4/MyD88 signalling in adrenal secretion of Corticosterone in wild type controls and mice lacking either *Tlr4* or *Myd88*.

1.6.2 Study 2: Effect of glucocorticoid signalling on cellular priming of innate immune responses in BV-2 microglia-like cells

On the other side of this bidirectional relationship between neuroendocrine and innate immune system, previous *in vivo* findings showed microglia and monocyte priming by stress and glucocorticoids (Yeager, Pioli and Guyre, 2011; Frank *et al.*, 2014; Weber *et al.*, 2015). In these studies, stress elicited an overresponsive innate immune response in microglia and monocytes, characterised by increased NLRP3 and IL-1β

mRNA expression (Frank *et al.*, 2014), and increased IL-6 cytokine release from blood monocytes (Yeager, Pioli and Guyre, 2011). Frank et al. (2014) also showed, using a specific pharmacological antagonist, that GR signalling is essential towards the development of this primed microglia phenotype. However, since these studies were performed on isolated cells after stress or glucocorticoids were administered *in vivo,* it is therefore unknown if this glucocorticoid-dependent action is due to direct effects of glucocorticoid receptor on microglia, or if it requires systemic adaptations to mediate this priming effect. I thus hypothesised that glucocorticoids have direct actions on innate immune signalling in immunocompetent cells *in vitro*. As such, a suitable cell model of microglia was required. A systematic review was therefore conducted in Chapter 3 to verify the suitability of BV2 cells, a microglia-like immortalized cell line for *in vitro* experiments.

Microglia-like BV2 cells were predominantly used for this work to investigate mechanisms of glucocorticoid actions on innate immune priming. Study 2 (Chapters 4 – 7) explores the pro-inflammatory priming effects of corticosterone with focus on IL-1β release in vitro.

1) *Conditions of corticosterone-induced immunosuppression and innate immune sensitization (Chapter 4)*

To test the hypothesis that glucocorticoids only prime the immune system during the "recovery period" following stress, while classical immunosuppressive actions of

glucocorticoids present during ongoing stress, 2 separate models of glucocorticoid pre-treatment were used. The removal prior to (pre-exposure), or persistence of (co-treatment) corticosterone within the system during the immunological challenge was used to model the 'recovery period' and ongoing stress respectively.

Furthermore, to verify reports of the biphasic nature of glucocorticoid actions, a corticosterone concentration-response during pre-treatment was characterised. GR and MR, the two main receptors for corticosterone, have different binding properties and are associated with the effects of high and low concentrations of corticosterone respectively (Tanaka *et al.*, 1997). Thus, direct corticosterone effects on the paradoxical priming and inhibition of LPS-induced IL-1β release was tested using specific glucocorticoid receptor and mineralocorticoid receptor antagonists.

2) *Investigation of corticosterone effects on TLR4-induced IL-1β release pathway (Chapter 4)*

Exploring the effects of corticosterone on TLR4-IL-1β release pathway, specific mechanisms leading to IL-1β release from these immunocompetent cells following TLR4 stimulation were also investigated. NF-κB translocation, conversion of pro-IL-1β, inflammasome-related NLRP3 protein expression, and expressions of inflammasome-related, TLR4-related, and glucocorticoid-related mRNA were investigated as part of this work.

3) *Effect of corticosterone pre-treatment on IL-6 secretion from BV2 microglia cells (Chapter 5)*

Since corticosterone pre-treatments demonstrated differential effects on NF-κB and IL-1β responses from BV2 microglia-like in Chapter 4, further investigation of whether this effect was conserved in IL-6 responses from the same cells. IL-6 is another cytokine downstream of NF-κB activation, and along with IL-1β, has been shown to stimulate HPA activity through increasing CRF secretion from hypothalamic cells (Tilg *et al.*, 1994). Thus, corticosterone pre-treatment actions on IL-6 is another prime target in the immune and neuroendocrine interface.

4) *Effects of corticosterone pre-treatment on IL-1β secretion in a model of peripheral macrophages (Chapter 5)*

Corticosterone also has potent effects on peripheral immune cell signalling, and has demonstrated some priming effects on peripheral immune cells (Smyth *et al.*, 2004; Yeager *et al.*, 2016). Thus, the pre-treatment model established in Chapter 4 was applied to RAW 264.7 macrophage-like cells to investigate the effects of corticosterone pre-treatment on LPS-induced IL-1β responses.

5) *Verification of low-concentration corticosterone pre-exposure model on adult primary microglia (Chapter 6)*

Given the predominant use of BV2 microglia-like cells in Chapters 4-5, the results were verified in experiments utilising primary microglia. Chapter 6 thus aimed to replicate

the corticosterone pre-exposure and LPS treatment model developed using BV2 cells in primary microglia. Pro-inflammatory measures of NF-κB nuclear translocation and cytokine release were assessed in primary microglia to investigate corticosterone priming effects.

6) *Effects of corticosterone and LPS pre-exposure on ATP-induced IL-1β release from BV2 microglia-like cells (Chapter 7)*

The involvement of inflammasome activation and caspase-1 cleavage of pro-IL-1β is required for the release of IL-1β (Willingham et al., 2009). Thus, high concentrations of exogenous ATP, commonly used to induce inflammasome-dependent release of IL-1β (Rada et al., 2014; Franceschini et al., 2015), were used in Chapter 7 to cause inflammasome activation. This experiment investigated the functional significance of inflammasome activity in immune primed cells after corticosterone pre-exposure.

7) *Caspase-1 or 4 dependency of IL-1β release after LPS or ATP from BV2 microglia-like cells (Chapter 7)*

Given the role of caspase-1 in the conversion of pro-IL-1β to mature IL-1β prior to release (Rada *et al.*, 2014), Caspase-1 and 4 dependency of IL-1β in BV2 cells were further investigated using a pharmacological inhibitor, z-YVAD-FMK.

1.6.3 Study 3: Corticosterone actions on cell motility, DAMP-related protein release and cytotoxicity

Apart from pro-inflammatory signalling via cytokine release, immunocompetent cells

also perform other actions such as chemotaxis and phagocytosis. Study 3 (Chapters 8-9) focused on direct corticosterone actions on DAMP-related protein release and cell motility using the models outlined in Study 2.

1) *Effects of high-concentration corticosterone on intracellular localisation of HMGB1 protein in adult primary microglia*

To investigate the potential role of glucocorticoids in stress-induced microglial HMGB1 release, high concentration corticosterone was administered to adult primary microglia *ex vivo*. The effect of corticosterone on cell viability and intracellular localisation of HMGB1 was thus assessed as a measure of releasable HMGB1.

2) *Effects of low and high concentration corticosterone pre-exposure on DAMP-related protein release and cytotoxicity (Chapter 8)*

Given that Study 2 demonstrated pro-inflammatory priming resulting corticosterone pre-exposure applied to BV2 innate immune responses, this cell model was also used to assess corticosterone actions on DAMP release. BV2 cells were therefore challenged with low and high concentrations of corticosterone pre-exposure, followed by LPS treatment, and finally ATP treatment. DAMP-related release of HMGB1, NLRP3, ASC and β actin proteins were measured from cell supernatants after each treatment. Furthermore, since cell death is a common mechanism between corticosterone actions on immunocompetent cells and the release of DAMPS (Yang *et al.*, 2013), corticosterone actions on cell toxicity and loss of cell viability was hypothesised to also associate with DAMP-related protein release.

3) *Role of Glucocorticoid receptor and Mineralocorticoid receptor on DAMP-related protein release and cytotoxicity (Chapter 8)*

The receptor in which corticosterone binds to and signals via to cause changes seen in this study was investigated using specific glucocorticoid receptor and mineralocorticoid receptor antagonists. In addition, a specific agonist to glucocorticoid receptor, dexamethasone, was also used to further test GR specific actions in measures of cell viability, cytotoxicity and DAMP-related protein release.

4) *Effects of low and high concentration corticosterone pre-exposure on ATP-induced cell motility in BV2 cells (Chapter 9)*

Glucocorticoids have been implicated in the regional distribution of immunocompetent cells (Schweingruber *et al.*, 2014). Glucocorticoid pre-exposure has been shown to increase leukocyte migration to areas of injury in humans (Yeager *et al.*, 2016). However, whether this effect is conserved in microglia is largely unknown. I thus hypothesised that this effect is also present in BV2 cells pre-exposed to corticosterone. Using high concentrations of exogenous ATP to induce cell motility, a compound shown in primary microglia to induce migration ex vivo, differences in cell motility was tested in the pre-exposure model.

5) *Effects of low and high concentration corticosterone and LPS pre-exposure on DAMP-related protein release following exogenous ATP administration (Chapter 9)*

Exogenous ATP induces microvesicle shedding, and this mechanism is implicated in the release of cytokines and DAMPS following inflammasome activation and pyroptosis (Vande Walle, Kanneganti and Lamkanfi, 2011). Given that corticosterone pre-exposure increased cell motility and rate of cell membrane blebbing, the extracellular supernatant was assessed for expression of DAMP-related proteins. Furthermore, cytotoxicity and cell viability were also assessed following exogenous ATP administration to approximate the rate of cell death resulting from these treatment conditions.

Collectively, Studies 1-3 aimed to understand the bidirectional relationship between the stress neuroendocrine and innate immune signalling system through use of *in vivo* and *in vitro* experimental models. Investigating the effect of glucocorticoids on innate immune function, immunocompetent cells were pre-treated with glucocorticoids *in vitro*, and changes in innate-immune function were quantified. Conversely, the role of innate immune signalling on behavioural and neuroendocrine responses to stress was tested using acute stress exposure in TLR4-MyD88 knockout mice and acute pharmacological antagonists.

1.7 References

Akira, S. and Takeda, K. (2004) 'Toll-like receptor signalling', *Nature Reviews Immunology*, 4(July), pp. 499–511. doi: 10.1038/nri1391.

Altmann, J., Sapolsky, R. and Licht, P. (1995) 'Baboon fertility and social status', *Nature*, 377(6551), pp. 688–689. doi: 10.1038/377688a0.

Amat, J., Matus-Amat, P., Watkins, L. R. and Maier, S. F. (1998) 'Escapable and inescapable stress differentially alter extracellular levels of 5-HT in the basolateral amygdala of the rat', *Brain Research*, 812(1–2), pp. 113–120. doi: 10.1016/S0006-8993(98)00960-3.

Bambico, F. R., Nguyen, N. T. and Gobbi, G. (2009) 'Decline in serotonergic firing activity and desensitization of 5-HT1A autoreceptors after chronic unpredictable stress', *European Neuropsychopharmacology*. Elsevier B.V., 19(3), pp. 215–228. doi: 10.1016/j.euroneuro.2008.11.005.

Barichello, T., Dagostim, V. S., Generoso, J. S., Simões, L. R., Dominguini, D., Silvestre, C., Michels, M., Carvalho, M., Jornada, L. K., Comim, C. M., Dal-pizzol, F., Lucio, A. and Quevedo, J. (2014) 'Neonatal Escherichia coli K1 meningitis causes learning and memory impairments in adulthood', *Journal of Neuroimmunology*. Elsevier B.V., 272(1–2), pp. 35–41. doi: 10.1016/j.jneuroim.2014.05.003.

Vanden Berghe, T., Demon, D., Bogaert, P., Vandendriessche, B., Goethals, A., Depuydt, B., Vuylsteke, M., Roelandt, R., Van Wonterghem, E., Vandenbroecke, J., Choi, S. M., Meyer, E., Krautwald, S., Declercq, W., Takahashi, N., Cauwels, A. and Vandenabeele, P. (2014) 'Simultaneous targeting of IL-1 and IL-18 is required for protection against inflammatory and septic shock', *American Journal of*

Respiratory and Critical Care Medicine, 189(3), pp. 282–291. doi: 10.1164/rccm.201308-1535OC.

Bird, S., Klein, E. and Loper, E. (2009) *Natural Language Processing with Python*, *O'Reilly Media*. doi: 10.1097/00004770-200204000-00018.

Blandino, P., Barnum, C. J. and Deak, T. (2006) 'The involvement of norepinephrine and microglia in hypothalamic and splenic IL-1β responses to stress', *Journal of Neuroimmunology*, 173(1–2), pp. 87–95. doi: 10.1016/j.jneuroim.2005.11.021.

Bonaldi, T., Talamo, F., Scaffidi, P., Ferrera, D., Porto, A., Bachi, A., Rubartelli, A., Agresti, A. and Bianchi, M. E. (2003) 'Monocytic cells hyperacetylate chromatin protein HMGB1 to redirect it towards secretion', *EMBO Journal*, 22(20), pp. 5551–5560. doi: 10.1093/emboj/cdg516.

Brikos, C., Wait, R., Begum, S., O'Neill, L. a J. and Saklatvala, J. (2007) 'Mass spectrometric analysis of the endogenous type I interleukin-1 (IL-1) receptor signaling complex formed after IL-1 binding identifies IL-1RAcP, MyD88, and IRAK-4 as the stable components.', *Molecular & cellular proteomics : MCP*, 6(9), pp. 1551–1559. doi: 10.1074/mcp.M600455-MCP200.

Busillo, J. M. and Cidlowski, J. a. (2013) 'The five Rs of glucocorticoid action during inflammation: ready, reinforce, repress, resolve, and restore.', *Trends in endocrinology and metabolism: TEM*. Elsevier Ltd, 24(3), pp. 109–19. doi: 10.1016/j.tem.2012.11.005.

Buynitsky, T. and Mostofsky, D. I. (2009) 'Restraint stress in biobehavioral research: Recent developments', *Neuroscience and Biobehavioral Reviews*, 33(7), pp.

1089–1098. doi: 10.1016/j.neubiorev.2009.05.004.

Calabrese, E. J., Bachmann, K. A., Bailer, A. J., Bolger, P. M., Borak, J., Cai, L., Cedergreen, N., Cherian, M. G., Chiueh, C. C., Clarkson, T. W., Cook, R. R., Diamond, D. M., Doolittle, D. J., Dorato, M. A., Duke, S. O., Feinendegen, L., Gardner, D. E., Hart, R. W., Hastings, K. L., Hayes, A. W., Hoffmann, G. R., Ives, J. A., Jaworowski, Z., Johnson, T. E., Jonas, W. B., Kaminski, N. E., Keller, J. G., Klaunig, J. E., Knudsen, T. B., Kozumbo, W. J., Lettieri, T., Liu, S. Z., Maisseu, A., Maynard, K. I., Masoro, E. J., McClellan, R. O., Mehendale, H. M., Mothersill, C., Newlin, D. B., Nigg, H. N., Oehme, F. W., Phalen, R. F., Philbert, M. A., Rattan, S. I. S., Riviere, J. E., Rodricks, J., Sapolsky, R. M., Scott, B. R., Seymour, C., Sinclair, D. A., Smith-Sonneborn, J., Snow, E. T., Spear, L., Stevenson, D. E., Thomas, Y., Tubiana, M., Williams, G. M. and Mattson, M. P. (2007) 'Biological stress response terminology: Integrating the concepts of adaptive response and preconditioning stress within a hormetic dose-response framework', *Toxicology and Applied Pharmacology*, 222(1), pp. 122–128. doi: 10.1016/j.taap.2007.02.015.

Calabrese, V., Cighetti, R. and Peri, F. (2015) 'Molecular simplification of lipid A structure: TLR4-modulating cationic and anionic amphiphiles', *Molecular Immunology*. Elsevier Ltd, 63(2), pp. 153–161. doi: 10.1016/j.molimm.2014.05.011.

Calcia, M. A., Bonsall, D. R., Bloomfield, P. S., Selvaraj, S., Barichello, T. and Howes, O. D. (2016) 'Stress and neuroinflammation: A systematic review of the effects of stress on microglia and the implications for mental illness', *Psychopharmacology*,

233(9), pp. 1637–1650. doi: 10.1007/s00213-016-4218-9.

Campos, A. C., Fogaça, M. V., Aguiar, D. C. and Guimarães, F. S. (2013) 'Animal models of anxiety disorders and stress', *Revista Brasileira de Psiquiatria*, 35(SUPPL.2), pp. 101–111. doi: 10.1590/1516-4446-2013-1139.

Cannon, W. B. (1915) 'Bodily Changes in Pain, Hunger, Fear and Rage; An Account of Recent Researches into the Function of Emotional Excitement', *Science*, 42(1089), pp. 696–700.

Cazakoff, B. N. and Howland, J. G. (2010) 'Acute stress disrupts paired pulse facilitation and long-term potentiation in rat dorsal hippocampus through activation of glucocorticoid receptors', *Hippocampus*, 20(12), pp. 1327–1331. doi: 10.1002/hipo.20738.

Chan, M. K., Cooper, J. D., Bot, M., Steiner, J., Penninx, B. W. J. H. and Bahn, S. (2016) 'Identification of an Immune-Neuroendocrine Biomarker Panel for Detection of Depression: A Joint Effects Statistical Approach', *Neuroendocrinology*, 103(6), pp. 693–710. doi: 10.1159/000442208.

Chantong, B., Kratschmar, D. V, Nashev, L. G., Balazs, Z. and Odermatt, A. (2012) 'Mineralocorticoid and glucocorticoid receptors differentially regulate NF-kappaB activity and pro-inflammatory cytokine production in murine BV-2 microglial cells', *Journal of Neuroinflammation*. Journal of Neuroinflammation, 9(1), p. 1. doi: 10.1186/1742-2094-9-260.

Chen, J., Wang, Z. zhen, Zuo, W., Zhang, S., Chu, S. feng and Chen, N. hong (2016) 'Effects of chronic mild stress on behavioral and neurobiological parameters -

Role of glucocorticoid', *Hormones and Behavior*. Elsevier Inc., 78, pp. 150–159. doi: 10.1016/j.yhbeh.2015.11.006.

Chourbaji, S., Zacher, C., Sanchis-Segura, C., Dormann, C., Vollmayr, B. and Gass, P. (2005) 'Learned helplessness: Validity and reliability of depressive-like states in mice', *Brain Research Protocols*, 16(1–3), pp. 70–78. doi: 10.1016/j.brainresprot.2005.09.002.

Chrousos, G. P. (2009) 'Stress and disorders of the stress system.', *Nature reviews. Endocrinology*. Nature Publishing Group, 5(7), pp. 374–381. doi: 10.1038/nrendo.2009.106.

Chrousos, G., Pavlaki, A. N. and Magiakou, M. A. (2000) 'Glucocorticoid Therapy and Adrenal Suppression', *Endotext*, (2), pp. 1–27. Available at: http://www.ncbi.nlm.nih.gov/pubmed/25905379.

Cock, P. J. A., Antao, T., Chang, J. T., Chapman, B. A., Cox, C. J., Dalke, A., Friedberg, I., Hamelryck, T., Kauff, F., Wilczynski, B. and De Hoon, M. J. L. (2009) 'Biopython: Freely available Python tools for computational molecular biology and bioinformatics', *Bioinformatics*, 25(11), pp. 1422–1423. doi: 10.1093/bioinformatics/btp163.

Cohen, S., Line, S., Manuck, S. B., Rabin, B. S., Heise, E. R. and Kaplan, J. R. (1997) 'Chronic social stress, social status, and susceptibility to upper respiratory infections in nonhuman primates.', *Psychosomatic medicine*, 59(3), pp. 213–221. doi: 10.1097/00006842-199705000-00001.

Connor, T. J., Kelly, J. P. and Leonard, B. E. (1997) 'Forced swim test-induced

neurochemical, endocrine, and immune changes in the rat', *Pharmacology Biochemistry and Behavior*, 58(4), pp. 961–967. doi: 10.1016/S0091-3057(97)00028-2.

Dantzer, R. (2004) 'Cytokine-induced sickness behaviour: a neuroimmune response to activation of innate immunity.', *European journal of pharmacology*, 500(1–3), pp. 399–411. doi: 10.1016/j.ejphar.2004.07.040.

Dantzer, R. and Kelley, K. W. (2007) 'Twenty years of research on cytokine-induced sickness behavior.', *Brain, behavior, and immunity*, 21(2), pp. 153–60. doi: 10.1016/j.bbi.2006.09.006.

Daskalakis, N. P., Cohen, H., Nievergelt, C. M., Baker, D. G., Buxbaum, J. D., Russo, S. J. and Yehuda, R. (2016) 'New translational perspectives for blood-based biomarkers of PTSD: From glucocorticoid to immune mediators of stress susceptibility', *Experimental Neurology*. Elsevier Inc., 284, pp. 133–140. doi: 10.1016/j.expneurol.2016.07.024.

Dimatelis, J. J., Pillay, N. S., Mutyaba, A. K., Russell, V. A., Daniels, W. M. U. and Stein, D. J. (2012) 'Early maternal separation leads to down-regulation of cytokine gene expression', *Metabolic Brain Disease*, 27(3), pp. 393–397. doi: 10.1007/s11011-012-9304-z.

Dimsdale, J. E. and Moss, J. (1980) 'Short-term catecholamine response to psychological stress.', *Psychosomatic medicine*, 42(5), pp. 493–497. doi: 10.1097/00006842-198009000-00003.

Dinel, A.-L., Joffre, C., Trifilieff, P., Aubert, A., Foury, A., Le Ruyet, P. and Layé, S. (2014)

'Inflammation early in life is a vulnerability factor for emotional behavior at adolescence and for lipopolysaccharide-induced spatial memory and neurogenesis alteration at adulthood.', *Journal of neuroinflammation*, 11(1), p. 155. doi: 10.1186/s12974-014-0155-x.

Droste, S. K., de Groote, L., Atkinson, H. C., Lightman, S. L., Reul, J. M. H. M. and Linthorst, A. C. E. (2008) 'Corticosterone levels in the brain show a distinct ultradian rhythm but a delayed response to forced swim stress.', *Endocrinology*, 149(7), pp. 3244–53. doi: 10.1210/en.2008-0103.

Farooq, R. K., Isingrini, E., Tanti, A., Le Guisquet, A. M., Arlicot, N., Minier, F., Leman, S., Chalon, S., Belzung, C. and Camus, V. (2012) 'Is unpredictable chronic mild stress (UCMS) a reliable model to study depression-induced neuroinflammation?', *Behavioural Brain Research*. Elsevier B.V., 231(1), pp. 130–137. doi: 10.1016/j.bbr.2012.03.020.

Ferland, C. L., Harris, E. P., Lam, M. and Schrader, L. A. (2014) 'Facilitation of the HPA axis to a novel acute stress following chronic stress exposure modulates histone acetylation and the ERK/MAPK pathway in the dentate gyrus of male rats.', *Endocrinology*, 155(8), pp. 2942–52. doi: 10.1210/en.2013-1918.

Fiebeler, A., Schmidt, F., Muller, D. N., Park, J. K., Dechend, R., Bieringer, M., Shagdarsuren, E., Breu, V., Haller, H. and Luft, F. C. (2001) 'Mineralocorticoid receptor affects AP-1 and nuclear factor-kappab activation in angiotensin II-induced cardiac injury.', *Hypertension*, 37(2 Pt 2), pp. 787–793. doi: 10.1161/01.HYP.37.2.787.

Fitzgerald, K. a, McWhirter, S. M., Faia, K. L., Rowe, D. C., Latz, E., Golenbock, D. T.,

Coyle, A. J., Liao, S.-M. and Maniatis, T. (2003) 'IKKepsilon and TBK1 are essential components of the IRF3 signaling pathway.', *Nature immunology*, 4(5), pp. 491–6. doi: 10.1038/ni921.

Franceschini, A., Capece, M., Chiozzi, P., Falzoni, S., Sanz, J. M., Sarti, A. C., Bonora, M., Pinton, P. and Di Virgilio, F. (2015) 'The P2X7 receptor directly interacts with the NLRP3 inflammasome scaffold protein', *The FASEB Journal*, 29(6), pp. 2450–2461. doi: 10.1096/fj.14-268714.

Fonken, L. K., Frank, M. G., Kitt, M. M., Barrientos, R. M., Watkins, L. R. and Maier, S. F. (2015) 'Microglia inflammatory responses are controlled by an intrinsic circadian clock', *Brain, Behavior, and Immunity*, 45, pp. 171–179. doi: 10.1016/j.bbi.2014.11.009.

Fonken, L. K., Weber, M. D., Daut, R. a., Kitt, M. M., Frank, M. G., Watkins, L. R. and Maier, S. F. (2016) 'Stress-induced neuroinflammatory priming is time of day dependent', *Psychoneuroendocrinology*. Elsevier Ltd, 66, pp. 82–90. doi: 10.1016/j.psyneuen.2016.01.006.

Franchi, L., Muñoz-Planillo, R. and Núñez, G. (2012) 'Sensing and reacting to microbes through the inflammasomes.', *Nature immunology*, 13(4), pp. 325–32. doi: 10.1038/ni.2231.

Frank, M. G., Hershman, S. A., Weber, M. D., Watkins, L. R. and Maier, S. F. (2014) 'Chronic exposure to exogenous glucocorticoids primes microglia to pro-inflammatory stimuli and induces NLRP3 mRNA in the hippocampus', *Psychoneuroendocrinology*. Elsevier Ltd, 40, pp. 191–200. doi: 10.1016/j.psyneuen.2013.11.006.

Frank, M. G., Weber, M. D., Fonken, L. K., Hershman, S. A., Watkins, L. R. and Maier, S. F. (2015) 'The redox state of the alarmin HMGB1 is a pivotal factor in neuroinflammatory and microglial priming: a role for the NLRP3 inflammasome', *Brain, Behavior, and Immunity*. Elsevier Inc., pp. 1–10. doi: 10.1016/j.bbi.2015.10.009.

Gadek-Michalska, A., Tadeusz, J., Rachwalska, P. and Bugajski, J. (2015) 'Chronic stress adaptation of the nitric oxide synthases and IL-1β levels in brain structures and hypothalamic-pituitary-adrenal axis activity induced by homotypic stress', *Journal of Physiology and Pharmacology*, 66(3), pp. 427–440.

Gamaro, G. ., Xavier, M. ., Denardin, J. ., Pilger, J. ., Ely, D. ., Ferreira, M. B. . and Dalmaz, C. (1998) 'The Effects of Acute and Repeated Restraint Stress on the Nociceptive Response in Rats', *Physiology & Behavior*, 63(4), pp. 693–697. doi: 10.1016/S0031-9384(97)00520-9.

Gicquel, T., Victoni, T., Fautrel, A., Robert, S., Gleonnec, F., Guezingar, M., Couillin, I., Catros, V., Boichot, E. and Lagente, V. (2014) 'Involvement of purinergic receptors and NOD-like receptor-family protein 3-inflammasome pathway in the adenosine triphosphate-induced cytokine release from macrophages.', *Clinical and experimental pharmacology & physiology*, 41(4), pp. 279–86. doi: 10.1111/1440-1681.12214.

Godbout, J. P., Chen, J., Abraham, J., Richwine, A. F., Berg, B. M., Kelley, K. W. and Johnson, R. W. (2005) 'Exaggerated neuroinflammation and sickness behavior in aged mice following activation of the peripheral innate immune system.', *The FASEB journal : official publication of the Federation of American Societies for*

Experimental Biology, 19(10), pp. 1329–1331. doi: 10.1096/fj.05-3776fje.

Gold, P. W. (2015) 'The organization of the stress system and its dysregulation in depressive illness', *Molecular Psychiatry*. Nature Publishing Group, 20(1), pp. 32–47. doi: 10.1038/mp.2014.163.

Grillo, C. A., Risher, M., Macht, V. A., Bumgardner, A. L., Hang, A., Gabriel, C., Mocaër, E., Piroli, G. G., Fadel, J. R. and Reagan, L. P. (2015) 'Repeated restraint stress-induced atrophy of glutamatergic pyramidal neurons and decreases in glutamatergic efflux in the rat amygdala are prevented by the antidepressant agomelatine', *Neuroscience*, 284, pp. 430–443. doi: 10.1016/j.neuroscience.2014.09.047.

Groeneweg, F. L., Karst, H., de Kloet, E. R. and Joëls, M. (2011) 'Rapid non-genomic effects of corticosteroids and their role in the central stress response.', *The Journal of endocrinology*, 209(2), pp. 153–67. doi: 10.1530/JOE-10-0472.

Gupte, R., Muse, G. W., Chinenov, Y., Adelman, K. and Rogatsky, I. (2013) 'Glucocorticoid receptor represses proinflammatory genes at distinct steps of the transcription cycle.', *Proceedings of the National Academy of Sciences of the United States of America*, 110(36), pp. 14616–21. doi: 10.1073/pnas.1309898110.

Hajszan, T., Dow, A., Warner-Schmidt, J. L., Szigeti-Buck, K., Sallam, N. L., Parducz, A., Leranth, C. and Duman, R. S. (2009) 'Remodeling of Hippocampal Spine Synapses in the Rat Learned Helplessness Model of Depression', *Biological Psychiatry*, 65(5), pp. 392–400. doi: 10.1016/j.biopsych.2008.09.031.

Halle, A., Hornung, V., Petzold, G. C., Stewart, C. R., Monks, B. G., Reinheckel, T., Fitzgerald, K. A., Latz, E., Moore, K. J. and Golenbock, D. T. (2008) 'The NALP3 inflammasome is involved in the innate immune response to amyloid-beta', *Nat Immunol*, 9(8), pp. 857–865. doi: 10.1038/ni.1636.

Han, K. J., Su, X., Xu, L. G., Bin, L. H., Zhang, J. and Shu, H. B. (2004) 'Mechanisms of the TRIF-induced Interferon-stimulated Response Element and NF-κB Activation and Apoptosis Pathways', *Journal of Biological Chemistry*, 279(15), pp. 15652–15661. doi: 10.1074/jbc.M311629200.

Harris, a P., Holmes, M. C., de Kloet, E. R., Chapman, K. E. and Seckl, J. R. (2013) 'Mineralocorticoid and glucocorticoid receptor balance in control of HPA axis and behaviour.', *Psychoneuroendocrinology*. Elsevier Ltd, 38(5), pp. 648–58. doi: 10.1016/j.psyneuen.2012.08.007.

Heiser, P., Lanquillon, S., Krieg, J. C. and Vedder, H. (2008) 'Differential modulation of cytokine production in major depressive disorder by cortisol and dexamethasone', *European Neuropsychopharmacology*. Elsevier B.V. and ECNP, 18(12), pp. 860–870. doi: 10.1016/j.euroneuro.2008.07.003.

Henry, C. J., Huang, Y., Wynne, A. M. and Godbout, J. P. (2009) 'Peripheral lipopolysaccharide (LPS) challenge promotes microglial hyperactivity in aged mice that is associated with exaggerated induction of both pro-inflammatory IL-1β and anti-inflammatory IL-10 cytokines', *Brain, Behavior, and Immunity*. Elsevier Inc., 23(3), pp. 309–317. doi: 10.1016/j.bbi.2008.09.002.

Hetzel, A. and Rosenkranz, J. A. (2014) 'Distinct effects of repeated restraint stress on basolateral amygdala neuronal membrane properties in resilient adolescent and

adult rats.', *Neuropsychopharmacology : official publication of the American College of Neuropsychopharmacology*. Nature Publishing Group, 39(9), pp. 2114–30. doi: 10.1038/npp.2014.60.

Horowitz, M. A. and Zunszain, P. A. (2015) 'Neuroimmune and neuroendocrine abnormalities in depression: Two sides of the same coin', *Annals of the New York Academy of Sciences*, 1351(1), pp. 68–79. doi: 10.1111/nyas.12781.

Hsiao, Y. M., Tsai, T. C., Lin, Y. T., Chen, C. C., Huang, C. C. and Hsu, K. Sen (2016) 'Early life stress dampens stress responsiveness in adolescence: Evaluation of neuroendocrine reactivity and coping behavior', *Psychoneuroendocrinology*. Elsevier Ltd, 67, pp. 86–99. doi: 10.1016/j.psyneuen.2016.02.004.

Huang, Y., Henry, C. J., Dantzer, R., Johnson, R. W. and Godbout, J. P. (2008) 'Exaggerated sickness behavior and brain proinflammatory cytokine expression in aged mice in response to intracerebroventricular lipopolysaccharide', *Neurobiology of Aging*, 29(11), pp. 1744–1753. doi: 10.1016/j.neurobiolaging.2007.04.012.

Hueston, C. M. and Deak, T. (2014) 'The inflamed axis: the interaction between stress, hormones, and the expression of inflammatory-related genes within key structures comprising the hypothalamic-pituitary-adrenal axis.', *Physiology & behavior*. Elsevier Inc., 124, pp. 77–91. doi: 10.1016/j.physbeh.2013.10.035.

Hunter, J. D. (2007) 'Matplotlib: A 2D graphics environment', *Computing in Science and Engineering*, 9(3), pp. 99–104. doi: 10.1109/MCSE.2007.55.

Hutchinson, M. R., Northcutt, a L., Hiranita, T., Wang, X., Lewis, S. S., Thomas, J., van

Steeg, K., Kopajtic, T. A., Loram, L. C., Sfregola, C., Galer, E., Miles, N. E., Bland, S. T., Amat, J., Rozeske, R. R., Maslanik, T., Chapman, T. R., Strand, K. A., Fleshner, M., Bachtell, R. K., Somogyi, A. A., Yin, H., Katz, J. L., Rice, K. C., Maier, S. F. and Watkins, L. R. (2012) 'Opioid activation of toll-like receptor 4 contributes to drug reinforcement.', *The Journal of neuroscience : the official journal of the Society for Neuroscience*, 32(33), pp. 11187–200. doi: 10.1523/JNEUROSCI.0684-12.2012.

Kanczkowski, W., Alexaki, V., Tran, N., Großklaus, S., Zacharowski, K., Martinez, A., Popovics, P., Block, N. L., Chavakis, T., Schally, A. V and Bornstein, S. R. (2013) 'Hypothalamo-pituitary and immune-dependent adrenal regulation during systemic inflammation.', *Proceedings of the National Academy of Sciences of the United States of America*, 110(36), pp. 14801–6. doi: 10.1073/pnas.1313945110.

Karst, H., Berger, S., Turiault, M., Tronche, F., Schütz, G. and Joëls, M. (2005) 'Mineralocorticoid receptors are indispensable for nongenomic modulation of hippocampal glutamate transmission by corticosterone.', *Proceedings of the National Academy of Sciences of the United States of America*, 102(52), pp. 19204–19207. doi: 10.1073/pnas.0507572102.

Katsnelson, M. a., Rucker, L. G., Russo, H. M. and Dubyak, G. R. (2015) 'K+ Efflux Agonists Induce NLRP3 Inflammasome Activation Independently of Ca2+ Signaling', *The Journal of Immunology*. doi: 10.4049/jimmunol.1402658.

Kemeny, M. E. and Schedlowski, M. (2007) 'Understanding the interaction between psychosocial stress and immune-related diseases: A stepwise progression', *Brain, Behavior, and Immunity*, 21(8), pp. 1009–1018. doi: 10.1016/j.bbi.2007.07.010.

Kim, H. M., Park, B. S., Kim, J. I., Kim, S. E., Lee, J., Oh, S. C., Enkhbayar, P., Matsushima,

N., Lee, H., Yoo, O. J. and Lee, J. O. (2007) 'Crystal Structure of the TLR4-MD-2 Complex with Bound Endotoxin Antagonist Eritoran', *Cell*, 130(5), pp. 906–917. doi: 10.1016/j.cell.2007.08.002.

King, A. P. and Liberzon, I. (2009) 'Assessing the neuroendocrine stress response in the functional neuroimaging context', *NeuroImage*, 47(3), pp. 1116–1124. doi: 10.1016/j.neuroimage.2009.05.055.

Kumsta, R., Entringer, S., Hellhammer, D. H. and Wüst, S. (2007) 'Cortisol and ACTH responses to psychosocial stress are modulated by corticosteroid binding globulin levels.', *Psychoneuroendocrinology*, 32(8–10), pp. 1153–7. doi: 10.1016/j.psyneuen.2007.08.007.

Ladd, C. O., Huot, R. L., Thrivikraman, K. V, Nemeroff, C. B. and Plotsky, P. M. (2004) 'Long-term adaptations in glucocorticoid receptor and mineralocorticoid receptor mRNA and negative feedback on the hypothalamo-pituitary-adrenal axis following neonatal maternal separation.', *Biological psychiatry*, 55(4), pp. 367–75. doi: 10.1016/j.biopsych.2003.10.007.

Lamers, F., Vogelzangs, N., Merikangas, K. R., de Jonge, P., Beekman, a T. F. and Penninx, B. W. J. H. (2013) 'Evidence for a differential role of HPA-axis function, inflammation and metabolic syndrome in melancholic versus atypical depression.', *Molecular psychiatry*. Nature Publishing Group, 18(6), pp. 692–9. doi: 10.1038/mp.2012.144.

Lawson, M. A., McCusker, R. H. and Kelley, K. W. (2013) 'Interleukin-1 beta converting enzyme is necessary for development of depression-like behavior following intracerebroventricular administration of lipopolysaccharide to mice', *Journal of*

Neuroinflammation. Journal of Neuroinflammation, 10(1), p. 1. doi: 10.1186/1742-2094-10-54.

Lin, D., Bruijnzeel, A. W., Schmidt, P. and Markou, A. (2002) 'Exposure to chronic mild stress alters thresholds for lateral hypothalamic stimulation reward and subsequent responsiveness to amphetamine', *Neuroscience*, 114(4), pp. 925–933. doi: 10.1016/S0306-4522(02)00366-4.

Lin, H. Y., Muller, Y. A. and Hammond, G. L. (2010) 'Molecular and structural basis of steroid hormone binding and release from corticosteroid-binding globulin', *Molecular and Cellular Endocrinology*, 316(1), pp. 3–12. doi: 10.1016/j.mce.2009.06.015.

Linthorst, A. C. E., Flachskamm, C. and Reul, J. M. H. M. (2008) 'Water temperature determines neurochemical and behavioural responses to forced swim stress: an in vivo microdialysis and biotelemetry study in rats.', *Stress (Amsterdam, Netherlands)*, 11(2), pp. 88–100. doi: 10.1080/10253890701533231.

Lisi, L., Camardese, G., Treglia, M., Tringali, G., Carrozza, C., Janiri, L., Russo, C. Dello and Navarra, P. (2013) 'Monocytes from Depressed Patients Display an Altered Pattern of Response to Endotoxin Challenge', *PLoS ONE*, 8(1), p. e52585. doi: 10.1371/journal.pone.0052585.

Liu, J., Buisman-Pijlman, F. and Hutchinson, M. R. (2014) 'Toll-like receptor 4: innate immune regulator of neuroimmune and neuroendocrine interactions in stress and major depressive disorder.', *Frontiers in neuroscience*, 8(September), p. 309. doi: 10.3389/fnins.2014.00309.

Liu, W., Sheng, H., Xu, Y., Liu, Y., Lu, J. and Ni, X. (2013) 'Swimming exercise ameliorates depression-like behavior in chronically stressed rats: relevant to proinflammatory cytokines and IDO activation.', *Behavioural brain research*. Elsevier B.V., 242, pp. 110–6. doi: 10.1016/j.bbr.2012.12.041.

Lovell, B. and Wetherell, M. A. (2011) 'The cost of caregiving: Endocrine and immune implications in elderly and non elderly caregivers', *Neuroscience and Biobehavioral Reviews*. Elsevier Ltd, 35(6), pp. 1342–1352. doi: 10.1016/j.neubiorev.2011.02.007.

Lucassen, P. J., Vollmann-Honsdorf, G. K., Gleisberg, M., Czéh, B., De Kloet, E. R. and Fuchs, E. (2001) 'Chronic psychosocial stress differentially affects apoptosis in hippocampal subregions and cortex of the adult tree shrew', *European Journal of Neuroscience*, 14(1), pp. 161–166. doi: 10.1046/j.0953-816X.2001.01629.x.

Majcher-Maślanka, I., Solarz, A., Wędzony, K. and Chocyk, A. (2017) 'The effects of early-life stress on dopamine system function in adolescent female rats', *International Journal of Developmental Neuroscience*, 57, pp. 24–33. doi: 10.1016/j.ijdevneu.2017.01.001.

Martin, S. A., Dantzer, R., Kelley, K. W. and Woods, J. A. (2014) 'Voluntary wheel running does not affect lipopolysaccharide-induced depressive-like behavior in young adult and aged mice.', *Neuroimmunomodulation*, 21(1), pp. 52–63. doi: 10.1159/000356144.

Martinon, F., Mayor, A. and Tschopp, J. (2009) 'The Inflammasomes: Guardians of the Body', *Annual Review of Immunology*, 27(1), pp. 229–265. doi: 10.1146/annurev.immunol.021908.132715.

McKinney, W. (2010) 'Data Structures for Statistical Computing in Python', *Proceedings of the 9th Python in Science Conference*, 1697900(Scipy), pp. 51–56. Available at: http://conference.scipy.org/proceedings/scipy2010/mckinney.html.

Miczek, K. A. and O'Donnell, J. M. (1978) 'Intruder-evoked aggression in isolated and nonisolated mice: Effects of psychomotor stimulants and l-Dopa', *Psychopharmacology*, 57(1), pp. 47–55. doi: 10.1007/BF00426957.

Miller, G. E., Murphy, M. L. M., Cashman, R., Ma, R., Ma, J., Arevalo, J. M. G., Kobor, M. S. and Cole, S. W. (2014) 'Greater inflammatory activity and blunted glucocorticoid signaling in monocytes of chronically stressed caregivers', *Brain, Behavior, and Immunity*. Elsevier Inc., 41, pp. 191–199. doi: 10.1016/j.bbi.2014.05.016.

Minni, A. M., Dorey, R., Piérard, C., Dominguez, G., Helbling, J.-C., Foury, A., Béracochéa, D. and Moisan, M.-P. (2012) 'Critical role of plasma corticosteroid-binding-globulin during stress to promote glucocorticoid delivery to the brain: impact on memory retrieval.', *Endocrinology*, 153(10), pp. 4766–74. doi: 10.1210/en.2012-1485.

Monroe, S. M. and Simons, a D. (1991) 'Diathesis-stress theories in the context of life stress research: implications for the depressive disorders.', *Psychological bulletin*, 110(3), pp. 406–425.

Murakami, T., Ockinger, J., Yu, J., Byles, V., McColl, a., Hofer, a. M. and Horng, T. (2012) 'Critical role for calcium mobilization in activation of the NLRP3 inflammasome', *Proceedings of the National Academy of Sciences*, 109(28), pp. 11282–11287. doi: 10.1073/pnas.1117765109.

Nguyen, K. T., Deak, T., Owens, S. M., Kohno, T., Fleshner, M., Watkins, L. R. and Maier, S. F. (1998) 'Exposure to acute stress induces brain interleukin-1β protein in the rat', *Journal of Neuroscience*, 18(6), pp. 2239–2246. Available at: http://www.scopus.com/inward/record.url?eid=2-s2.0-0032521115&partnerID=40&md5=a46c72b11bd551b9de9cde4cda986c0a.

O'Neill, L. a J., Golenbock, D. and Bowie, A. G. (2013) 'The history of Toll-like receptors - redefining innate immunity.', *Nature reviews. Immunology*, 13(6), pp. 453–60. doi: 10.1038/nri3446.

Ogundele, O. M., Ebenezer, P. J., Lee, C. C. and Francis, J. (2017) 'Stress-altered synaptic plasticity and DAMP signaling in the hippocampus-PFC axis; elucidating the significance of IGF-1/IGF-1R/CaMKIIα expression in neural changes associated with a prolonged exposure therapy', *Neuroscience*. IBRO, 353(April), pp. 147–165. doi: 10.1016/j.neuroscience.2017.04.008.

Overmier, J. B. and Seligman, M. E. (1967) 'Effects of inescapable shock upon subsequent escape and avoidance responding', *Journal of Comparative and Physiological Psychology*, 63(1), pp. 28–33. doi: 10.1037/h0024166.

Pace, T. W. W. and Miller, A. H. (2009) 'Cytokines and glucocorticoid receptor signaling: Relevance to major depression', *Annals of the New York Academy of Sciences*, 1179, pp. 86–105. doi: 10.1111/j.1749-6632.2009.04984.x.

Park, B. S. and Lee, J.-O. (2013) 'Recognition of lipopolysaccharide pattern by TLR4 complexes', *Experimental & Molecular Medicine*. Nature Publishing Group, 45(12), p. e66. doi: 10.1038/emm.2013.97.

Paugh, S. W., Bonten, E. J., Savic, D., Ramsey, L. B., Thierfelder, W. E., Gurung, P., Malireddi, R. K. S., Actis, M., Mayasundari, A., Min, J., Coss, D. R., Laudermilk, L. T., Panetta, J. C., McCorkle, J. R., Fan, Y., Crews, K. R., Stocco, G., Wilkinson, M. R., Ferreira, A. M., Cheng, C., Yang, W., Karol, S. E., Fernandez, C. a, Diouf, B., Smith, C., Hicks, J. K., Zanut, A., Giordanengo, A., Crona, D., Bianchi, J. J., Holmfeldt, L., Mullighan, C. G., den Boer, M. L., Pieters, R., Jeha, S., Dunwell, T. L., Latif, F., Bhojwani, D., Carroll, W. L., Pui, C.-H., Myers, R. M., Guy, R. K., Kanneganti, T.-D., Relling, M. V and Evans, W. E. (2015) 'NALP3 inflammasome upregulation and CASP1 cleavage of the glucocorticoid receptor cause glucocorticoid resistance in leukemia cells', *Nature Genetics*. Nature Publishing Group, 47(6), pp. 607–614. doi: 10.1038/ng.3283.

Pavlides, C. and McEwen, B. S. (1999) 'Effects of mineralocorticoid and glucocorticoid receptors on long-term potentiation in the CA3 hippocampal field', *Brain Research*, 851(1–2), pp. 204–214. doi: 10.1016/S0006-8993(99)02188-5.

Pedregosa, F., Varoquaux, G., Gramfort, A., Michel, V., Thirion, B., Grisel, O., Blondel, M., Louppe, G., Prettenhofer, P., Weiss, R., Dubourg, V., Vanderplas, J., Passos, A., Cournapeau, D., Brucher, M., Perrot, M. and Duchesnay, É. (2011) 'Scikit-learn: Machine Learning in Python', *Journal of Machine Learning Research*, 12, pp. 2825–2830. doi: 10.1007/s13398-014-0173-7.2.

Porsolt, R. D., Le Pichon, M. and Jalfre, M. (1977) 'Depression: a new animal model sensitive to antidepressant treatments', *Nature*, 266(5604), pp. 730–732. doi: 10.1038/266730a0.

Qiao, Y., Wang, P., Qi, J., Zhang, L. and Gao, C. (2012) 'TLR-induced NF-κB activation

regulates NLRP3 expression in murine macrophages', *FEBS Letters*. Federation of European Biochemical Societies, 586(7), pp. 1022–1026. doi: 10.1016/j.febslet.2012.02.045.

Rada, B., Park, J. J., Sil, P., Geiszt, M. and Leto, T. L. (2014) 'NLRP3 inflammasome activation and interleukin-1β release in macrophages require calcium but are independent of calcium-activated NADPH oxidases', *Inflammation Research*, pp. 821–830. doi: 10.1007/s00011-014-0756-y.

Rathinam, V. A. K., Vanaja, S. K., Waggoner, L., Sokolovska, A., Becker, C., Stuart, L. M., Leong, J. M. and Fitzgerald, K. A. (2012) 'TRIF Licenses Caspase-11-Dependent NLRP3 Inflammasome Activation by Gram-Negative Bacteria', *Cell*, 150(3), pp. 606–619. doi: 10.1016/j.cell.2012.07.007.

Ratman, D., Vanden, W., Dejager, L., Libert, C., Tavernier, J., Beck, I. M. and Bosscher, K. De (2013) 'Molecular and Cellular Endocrinology How glucocorticoid receptors modulate the activity of other transcription factors : A scope beyond tethering', *Molecular and Cellular Endocrinology*. Elsevier Ireland Ltd, 380(1–2), pp. 41–54. doi: 10.1016/j.mce.2012.12.014.

Reul, J. M. and de Kloet, E. R. (1985) 'Two receptor systems for corticosterone in rat brain: microdistribution and differential occupation.', *Endocrinology*, 117(6), pp. 2505–11. doi: 10.1210/endo-117-6-2505.

Richard, E. M., Helbling, J., Tridon, C., Desmedt, A., Minni, A. M., Cador, M., Pourtau, L., Konsman, J.-P., Mormède, P. and Moisan, M.-P. (2010) 'Plasma transcortin influences endocrine and behavioral stress responses in mice.', *Endocrinology*, 151(2), pp. 649–59. doi: 10.1210/en.2009-0862.

te Riet, L., van Esch, J. H. M., Roks, A. J. M., van den Meiracker, A. H. and Danser, A. H. J. (2015) 'Hypertension: Renin-Angiotensin-Aldosterone System Alterations', *Circulation Research*, 116(6), pp. 960–975. doi: 10.1161/CIRCRESAHA.116.303587.

Rogerson, F. M., Brennan, F. E. and Fuller, P. J. (2004) 'Mineralocorticoid receptor binding, structure and function', *Molecular and Cellular Endocrinology*, 217(1–2), pp. 203–212. doi: 10.1016/j.mce.2003.10.021.

Roque, S., Mesquita, A. R., Palha, J. A., Sousa, N. and Correia-Neves, M. (2014) 'The Behavioral and Immunological Impact of Maternal Separation: A Matter of Timing', *Frontiers in Behavioral Neuroscience*, 8(May), pp. 1–10. doi: 10.3389/fnbeh.2014.00192.

Sapolsky, R. M. (2005) 'The Influence of Social Hierarchy on Primate Health', *Science*, 308(5722), pp. 648–652. doi: 10.1126/science.1106477.

Sapolsky, R. M. (2016) 'Proinflammatory primates', *Science*, 354(6315), pp. 967–968. doi: 10.1126/science.aal3170.

Sapolsky, R. M., Romero, L. M. and Munck, A. U. (2000) 'How Do Glucocorticoids Influence Stress Responses ? Integrating Permissive, Suppressive, Stimulatory and Preparative Actions *', *Endocrine Reviews*, 21(April), pp. 55–89.

Schweingruber, N., Fischer, H. J., Fischer, L., van den Brandt, J., Karabinskaya, A., Labi, V., Villunger, A., Kretzschmar, B., Huppke, P., Simons, M., Tuckermann, J. P., Flügel, A., Lühder, F. and Reichardt, H. M. (2014) 'Chemokine-mediated redirection of T cells constitutes a critical mechanism of glucocorticoid therapy in

autoimmune CNS responses.', *Acta neuropathologica*, 127(5), pp. 713–29. doi: 10.1007/s00401-014-1248-4.

Selye, H. (1973) 'The Evolution of the Stress Concept: The originator of the concept traces its development from the discovery in 1936 of the alarm reaction to modern therapeutic applications of syntoxic and catatoxic hormones', *American Scientist*, 61(6), pp. 692–699. Available at: http://www.jstor.org/stable/27844072.

Shively, C. a, Register, T. C. and Clarkson, T. B. (2009) 'Social stress, visceral obesity, and coronary artery atherosclerosis in female primates.', *Obesity (Silver Spring, Md.)*. Nature Publishing Group, 17(8), pp. 1513–1520. doi: 10.1038/oby.2009.74.

Silverman, M. N. and Sternberg, E. M. (2012) 'Glucocorticoid regulation of inflammation and its functional correlates: from HPA axis to glucocorticoid receptor dysfunction.', *Annals of the New York Academy of Sciences*, 1261, pp. 55–63. doi: 10.1111/j.1749-6632.2012.06633.x.

Sinha, R. (2001) 'How does stress increase risk of drug abuse and relapse?', *Psychopharmacology*, 158(4), pp. 343–59. doi: 10.1007/s002130100917.

Smyth, G. P., Stapleton, P. P., Freeman, T. A., Concannon, E. M., Mestre, J. R., Duff, M., Maddali, S. and Daly, J. M. (2004) 'Glucocorticoid pretreatment induces cytokine overexpression and nuclear factor-κB activation in macrophages', *Journal of Surgical Research*, 116(2), pp. 253–261. doi: 10.1016/S0022-4804(03)00300-7.

Snyder-Mackler, N., Sanz, J., Kohn, J. N., Brinkworth, J. F., Morrow, S., Shaver, A. O., Grenier, J.-C., Pique-Regi, R., Johnson, Z. P., Wilson, M. E., Barreiro, L. B. and

Tung, J. (2016) 'Social status alters immune regulation and response to infection in macaques', *Science*, 354(6315), pp. 1041–1045. doi: 10.1126/science.aah3580.

Sobesky, J. L., Angelo, H. M. D., Watkins, L. R., Maier, S. F., Weber, M. D., Anderson, N. D., Barrientos, R. M. and Frank, M. G. (2016) 'Glucocorticoids Mediate Short-Term High-Fat Diet Induction of Neuroinflammatory Priming , the NLRP3 Inflammasome , and the Danger Signal', 3(August).

Sorrells, S. F., Munhoz, C. D., Manley, N. C., Yen, S. and Sapolsky, R. M. (2014) 'Glucocorticoids increase excitotoxic injury and inflammation in the hippocampus of adult male rats', *Neuroendocrinology*, 100, pp. 129–140. doi: 10.1159/000367849.

Stranahan, A. M., Arumugam, T. V., Lee, K. and Mattson, M. P. (2010) 'Mineralocorticoid receptor activation restores medial perforant path LTP in diabetic rats', *Synapse*, 64(7), pp. 528–532. doi: 10.1002/syn.20758.

Sun, R., Zhao, Z., Feng, J., Bo, J., Rong, H., Lei, Y., Lu, C., Zhang, X., Hou, B., Sun, Y., Liu, Y., Ma, Z. and Gu, X. (2016) 'Glucocorticoid-Potentiated Spinal Microglia Activation Contributes to Preoperative Anxiety-Induced Postoperative Hyperalgesia', *Molecular Neurobiology*. Molecular Neurobiology. doi: 10.1007/s12035-016-9976-1.

Tanaka, J., Fujita, H., Seiji, M., Kazuko, T., Sashiro, S. and Nubuji, M. (1997) 'Glucocorticoid and Mineralocorticoid Receotors in Microglial Cells: The Two Receptors Mediate Differential Effects of Corticosterone', *Glia*, 20, pp. 23–37.

Tilg, H., Trehu, E., Atkins, M., Dinarello, C. and Mier, J. (1994) 'Interleukin-6 (IL-6) as an

anti-inflammatory cytokine: induction of circulating IL-1 receptor antagonist and soluble tumor necrosis factor receptor p55', *Blood*, 83(1), pp. 113–18.

Ulrich-Lai, Y. M. and Herman, J. P. (2009) 'Neural regulation of endocrine and autonomic stress responses.', *Nature reviews. Neuroscience*, 10(6), pp. 397–409. doi: 10.1038/nrn2647.

Vakharia, K. and Hinson, J. P. (2005) 'Lipopolysaccharide directly stimulates cortisol secretion by human adrenal cells by a cyclooxygenase-dependent mechanism.', *Endocrinology*, 146(3), pp. 1398–1402. doi: 10.1210/en.2004-0882.

Vasconcelos, M., Stein, D. J. and Almeida, R. M. M. de (2015) 'Social defeat protocol and relevant biomarkers, implications for stress response physiology, drug abuse, mood disorders and individual stress vulnerability: a systematic review of the last decade', *Trends in Psychiatry and Psychotherapy*, 37(2), pp. 51–66. doi: 10.1590/2237-6089-2014-0034.

Venereau, E., Casalgrandi, M., Schiraldi, M., Antoine, D. J., Cattaneo, A., De Marchis, F., Liu, J., Antonelli, A., Preti, A., Raeli, L., Shams, S. S., Yang, H., Varani, L., Andersson, U., Tracey, K. J., Bachi, A., Uguccioni, M. and Bianchi, M. E. (2012) 'Mutually exclusive redox forms of HMGB1 promote cell recruitment or proinflammatory cytokine release.', *The Journal of experimental medicine*, 209(9), pp. 1519–28. doi: 10.1084/jem.20120189.

Vetulani, J. (2013) 'Early maternal separation: a rodent model of depression and a prevailing human condition.', *Pharmacological reports : PR*, 65(6), pp. 1451–61. doi: 10.1016/S1734-1140(13)71505-6.

Vitlic, A., Lord, J. M., Taylor, A. E., Arlt, W., Bartlett, D. B., Rossi, A., Arora-Duggal, N., Welham, A., Heald, M., Oliver, C., Carroll, D. and Phillips, A. C. (2016) 'Neutrophil function in young and old caregivers', *British Journal of Health Psychology*, 21(1), pp. 173–189. doi: 10.1111/bjhp.12156.

Vande Walle, L., Kanneganti, T.-D. and Lamkanfi, M. (2011) 'HMGB1 release by inflammasomes.', *Virulence*, 2(2), pp. 162–165. doi: 10.4161/viru.2.2.15480.

Wang, X., Loram, L. C., Ramos, K., de Jesus, A. J., Thomas, J., Cheng, K., Reddy, A., Somogyi, A. a, Hutchinson, M. R., Watkins, L. R. and Yin, H. (2012) 'Morphine activates neuroinflammation in a manner parallel to endotoxin.', *Proceedings of the National Academy of Sciences of the United States of America*, 109(16), pp. 6325–30. doi: 10.1073/pnas.1200130109.

Watters, T. M., Kenny, E. F. and O'Neill, L. A. J. (2007) 'Structure, function and regulation of the Toll/IL-1 receptor adaptor proteins.', *Immunology and cell biology*, 85(6), pp. 411–9. doi: 10.1038/sj.icb.7100095.

Weber, a, Kirejczyk, Z., Besch, R., Potthoff, S., Leverkus, M. and Häcker, G. (2010) 'Proapoptotic signalling through Toll-like receptor-3 involves TRIF-dependent activation of caspase-8 and is under the control of inhibitor of apoptosis proteins in melanoma cells.', *Cell death and differentiation*, 17(6), pp. 942–51. doi: 10.1038/cdd.2009.190.

Weber, M. D., Frank, M. G., Tracey, K. J., Watkins, L. R. and Maier, S. F. (2015) 'Stress Induces the Danger-Associated Molecular Pattern HMGB-1 in the Hippocampus of Male Sprague Dawley Rats: A Priming Stimulus of Microglia and the NLRP3 Inflammasome.', *The Journal of neuroscience : the official journal of the Society*

for Neuroscience, 35(1), pp. 316–24. doi: 10.1523/JNEUROSCI.3561-14.2015.

Wieck, A., Andersen, S. L. and Brenhouse, H. C. (2013) 'Evidence for a neuroinflammatory mechanism in delayed effects of early life adversity in rats: Relationship to cortical NMDA receptor expression', *Brain, Behavior, and Immunity*. Elsevier Inc., 28, pp. 218–226. doi: 10.1016/j.bbi.2012.11.012.

Willingham, S. B., Allen, I. C., Bergstralh, D. T., Brickey, W. J., Huang, M. T.-H., Taxman, D. J., Duncan, J. A. and Ting, J. P.-Y. (2009) 'NLRP3 (NALP3, Cryopyrin) facilitates in vivo caspase-1 activation, necrosis, and HMGB1 release via inflammasome-dependent and -independent pathways.', *Journal of immunology (Baltimore, Md. : 1950)*, 183(3), pp. 2008–15. doi: 10.4049/jimmunol.0900138.

Willner, P. (2017) 'The chronic mild stress (CMS) model of depression: History, evaluation and usage', *Neurobiology of Stress*. Elsevier Inc, 6, pp. 78–93. doi: 10.1016/j.ynstr.2016.08.002.

Wohleb, E. S., Fenn, A. M., Pacenta, A. M., Powell, N. D., Sheridan, J. F. and Godbout, J. P. (2012) 'Peripheral innate immune challenge exaggerated microglia activation, increased the number of inflammatory CNS macrophages, and prolonged social withdrawal in socially defeated mice.', *Psychoneuroendocrinology*. Elsevier Ltd, 37(9), pp. 1491–505. doi: 10.1016/j.psyneuen.2012.02.003.

Wu, I., Shin, S. C., Cao, Y., Bender, I. K., Jafari, N., Feng, G., Lin, S., Cidlowski, J. A., Schleimer, R. P. and Lu, N. Z. (2013) 'Selective glucocorticoid receptor translational isoforms reveal glucocorticoid-induced apoptotic transcriptomes', *Cell Death and Disease*, 4(1), p. e453. doi: 10.1038/cddis.2012.193.

Wu, M. V, Shamy, J. L., Bedi, G., Choi, C.-W. J., Wall, M. M., Arango, V., Boldrini, M., Foltin, R. W. and Hen, R. (2014) 'Impact of Social Status and Antidepressant Treatment on Neurogenesis in the Baboon Hippocampus', *Neuropsychopharmacology*, 39(8), pp. 1861–1871. doi: 10.1038/npp.2014.33.

Xavier, A. M., Kataryna, A. and Anunciato, O. (2016) 'Gene expression Control by Glucocorticoid Receptors during innate immune Responses', 7(April), pp. 1–8. doi: 10.3389/fendo.2016.00031.

Yanai, H., Matsuda, A., An, J., Koshiba, R., Nishio, J., Negishi, H., Ikushima, H., Onoe, T., Ohdan, H., Yoshida, N. and Taniguchi, T. (2013) 'Conditional ablation of HMGB1 in mice reveals its protective function against endotoxemia and bacterial infection', *Proceedings of the National Academy of Sciences*, 110(51), pp. 20699–20704. doi: 10.1073/pnas.1320808110.

Yang, H., Antoine, D. J., Andersson, U. and Tracey, K. J. (2013) 'The many faces of HMGB1: molecular structure-functional activity in inflammation, apoptosis, and chemotaxis.', *Journal of leukocyte biology*, 93(6), pp. 865–73. doi: 10.1189/jlb.1212662.

Yang, H., Wang, H., Ju, Z., Ragab, A. a, Lundbäck, P., Long, W., Valdes-ferrer, S. I., He, M., Pribis, J. P., Li, J., Lu, B., Gero, D., Szabo, C., Antoine, D. J., Harris, H. E., Golenbock, D. T., Meng, J., Roth, J., Chavan, S. S., Andersson, U., Billiar, T. R., Tracey, K. J. and Al-abed, Y. (2015) 'MD-2 is required for disulfide HMGB1 – dependent TLR4 signaling', 212(1), pp. 0–9. doi: 10.1084/jem.20141318.

Yankelevitch-Yahav, R., Franko, M., Huly, A. and Doron, R. (2015) 'The Forced Swim Test as a Model of Depressive-like Behavior', *Journal of Visualized Experiments*,

(97), pp. 1–7. doi: 10.3791/52587.

Yeager, M. P., Pioli, P. A., Collins, J., Barr, F., Metzler, S., Sites, B. D. and Guyre, P. M. (2016) 'Glucocorticoids enhance the in vivo migratory response of human monocytes', *Brain, Behavior, and Immunity*. Elsevier Inc., 54, pp. 86–94. doi: 10.1016/j.bbi.2016.01.004.

Yeager, M. P., Pioli, P. A. and Guyre, P. M. (2011) 'Cortisol Exerts Bi-Phasic Regulation of Inflammation in Humans', *Dose-Response*, 9(3), pp. 332–347. doi: 10.2203/dose-response.10-013.Yeager.

You, Z., Luo, C., Zhang, W., Chen, Y., He, J., Zhao, Q., Zuo, R. and Wu, Y. (2011) 'Pro- and anti-inflammatory cytokines expression in rat's brain and spleen exposed to chronic mild stress: Involvement in depression', *Behavioural Brain Research*. Elsevier B.V., 225(1), pp. 135–141. doi: 10.1016/j.bbr.2011.07.006.

Zacharowski, K., Zacharowski, P. A., Koch, A., Baban, A., Tran, N., Berkels, R., Papewalis, C., Schulze-Osthoff, K., Knuefermann, P., Zähringer, U., Schumann, R. R., Rettori, V., McCann, S. M. and Bornstein, S. R. (2006) 'Toll-like receptor 4 plays a crucial role in the immune-adrenal response to systemic inflammatory response syndrome.', *Proceedings of the National Academy of Sciences of the United States of America*, 103(16), pp. 6392–7. doi: 10.1073/pnas.0601527103.

Study 1: Effects of Baseline TLR4-MyD88 signalling on Behavioural and Neuroendocrine Responses to acute non-immunogenic stressors

- **Chapter 2 – Manuscript:** *Tlr4* and *Myd88* genetic knockout mice exhibit differences in behavioural and neuroendocrine stress responses to acute non-immunogenic stressors.

- **Chapter 3 – Linking Chapter:** From stress to innate immune signalling

- **Tables:** Summary tables for systematic review

Statement of Authorship

Title of Paper	*Tlr4* and *Myd88* genetic knockout mice exhibit differences in behavioural and neuroendocrine stress responses to acute non-immunogenic stressors.
Publication Status	☐ Published ☐ Accepted for Publication ☒ Submitted for Publication ☐ Unpublished and Unsubmitted work written in manuscript style
Publication Details	Submitted for review in *Psychoneuroendocrinology*

Principal Author

Name of Principal Author (Candidate)	JiaJun Liu
Contribution to the Paper	Planned and conducted the study, supervised experimental procedures, performed data analysis, interpreted results, prepared and edited the manuscript
Overall percentage (%)	85%
Certification:	This paper reports on original research I conducted during the period of my Higher Degree by Research candidature and is not subject to any obligations or contractual agreements with a third party that would constrain its inclusion in this thesis. I am the primary author of this paper.
Signature	Date: 01/09/2017

Co-Author Contributions

By signing the Statement of Authorship, each author certifies that:

i. the candidate's stated contribution to the publication is accurate (as detailed above);

ii. permission is granted for the candidate in include the publication in the thesis; and

iii. the sum of all co-author contributions is equal to 100% less the candidate's stated contribution.

Name of Co-Author	Mr. James Firth
Contribution to the Paper	Assisted in performing tail suspension experiments for figures 2(D) and 3(B) and 4, and preparation of written work.
Signature	Date: 3/9/2017

Name of Co-Author	Dr. Femke Buisman-Pijlman
Contribution to the Paper	Supervised the study design, preparation and editing of manuscript
Signature	Date: 1/9/17

Please cut and paste additional co-author panels here as required.

Name of Co-Author	Dr. Kenner C. Rice
Contribution to the Paper	Provided (+)- Naltrexone used in figure 4 and supplementary figure 4, and assisted in the preparation of written work.
Signature	Date September 5, 2017

Name of Co-Author	Prof. Mark Hutchinson
Contribution to the Paper	Supervised the study design, interpretation of results, planning and editing of manuscript.
Signature	Date 5.9.17

Chapter 2 – manuscript: Tlr4 and *Myd88* genetic knockout mice exhibit differences in behavioural and neuroendocrine stress responses to acute non-immunogenic stressors.

JiaJun Liu [a,b] James Firth[a], Femke Buisman-Pijlman[c,d], Kenner C. Rice[e],

and Mark R. Hutchinson[a,b]

a. Adelaide Medical School, Discipline of Physiology, University of Adelaide, Level 5 Medical School South, Frome Rd, Adelaide, 5005, Australia
b. Australian Research Council Centre of Excellence for Nanoscale BioPhotonics, Adelaide, Australia
c. Adelaide Medical School, Discipline of Pharmacology, University of Adelaide, Level 5 Medical School North, Frome Road, Adelaide, 5005, Australia
d. Robinson Research Institute, University of Adelaide
e. Drug Design and Synthesis Section, Molecular Targets and Medications Discovery Branch, Intramural Research Program, National Institute on Drug Abuse and the National Institute on Alcohol Abuse and Alcoholism, National Institutes of Health, Department of Health and Human Services, 9800 Medical Center Drive, Bethesda, Maryland 20892-3373, United State

Corresponding Author: JiaJun Liu

Email: jiajun.liu@adelaide.edu.au

Address: S516 Medical School South, Frome Rd, Adelaide, South Australia 5005, Australia

Phone Number: +61425067445

Keywords:

Innate Immunity, TLR4, MyD88, Knockout, Stress, Hypothalamus Pituitary Adrenal Axis, Behaviour, Corticosterone

Abstract:

Innate immune Toll-like receptor 4 (TLR4) agonists, such as lipopolysaccharide (LPS), induce acute sickness behaviours, and cause long-term maladaptive stress behaviours when administered during development. Yet, the impact of TLR4-MyD88 signalling on the behavioural and neuroendocrine acute stress response is not well characterised. The current paper thus investigated these stress responses in *Tlr4* (*Tlr4*$^{-/-}$) and *Myd88* (*Myd88*$^{-/-}$) null mutant mice. The importance of TLR4-MyD88 signalling at the time of stress was also assessed using acute pharmacological antagonists IL-1RA and (+)-Naltrexone. Using these manipulations of TLR4 and MyD88 signalling, we examined their effects on behavioural immobility during forced swim stress and tail suspension stress, followed by corticosterone (CORT) release resulting from these non-immunogenic stressors.

Strain differences in glucocorticoid receptor (GR), corticosteroid binding globulin (CBG) expression, and adrenal sensitivity to adrenocorticotropic hormone (ACTH) via *ex vivo* cultures were also explored. Mice lacking *Myd88* exhibited increased immobility and circulating CORT following forced swim stress, while both *Myd88*$^{-/-}$ and *TLR4*$^{-/-}$ mice displayed decreased immobility during tail suspension stress. *TLR4*$^{-/-}$ mice further exhibited an increased duration of CORT elevation following the tail suspension stressor. Additionally, Hypothalamic CBG was elevated in *Tlr4*$^{-/-}$ compared to *Myd88*$^{-/-}$ mice, while both strains exhibited differences in forced swim stress induced hypothalamic GR expression changes. Moreover, *Myd88*$^{-/-}$ and *TLR4*$^{-/-}$ adrenals displayed elevated CORT release in response to ACTH (100 nM) for 6h. IL-1RA did not alter forced swim or tail suspension stressors or CORT release. (+)-Naltrexone did not

modify behaviour in forced swim and tail suspension stress, but elevated CORT levels overall. Baseline innate immune signalling therefore shapes both behavioural and neuroendocrine stress responses, but acute antagonism of TLR4-MyD88 signalling at the time of stress does not significantly impact these stress responses.

Introduction

Stress is a risk factor for the development and outcome of various conditions, ranging from major depressive disorder to chronic inflammatory diseases and cancer progression (Kemeny and Schedlowski, 2007; Liu, Buisman-Pijlman and Hutchinson, 2014). Although the exact mechanisms are unclear, stress-related disorders often present with dysregulation in behavioural and physiological stress responses, as well as systemic imbalances in innate immune system function. Understanding the associational or causal relationships between immune function and the stress response is therefore imperative towards investigating the aetiology of stress-related disorders. The current study thus investigates whether the innate immune system can influence the physiological and behavioural stress response triggered by non-immunological challenges.

1.1 The hypothalamus pituitary adrenal axis neuroendocrine stress response:

Psychological and physical stresses trigger a neuroendocrine response, which consists of two main systems, namely the noradrenergic and the hypothalamus pituitary adrenal (HPA) axis. The noradrenergic system is often associated with acute actions of stress, as part of the sympathetic drive, while the HPA axis is associated with longer lasting actions, due to the involvement of multiple endocrine factors (Sapolsky, Romero and Munck, 2000). HPA signalling initiates in the paraventricular nucleus of the hypothalamus, secreting corticosteroid releasing factor (CRF), which binds to receptors in the anterior pituitary gland, resulting in the release of adrenocorticotropic hormone (ACTH). ACTH further enters they systemic circulation to stimulate cells expressing melanocortin receptor 2 (MC2) in the zona fasciculata layer in the adrenal

cortex to synthesise and release glucocorticoids (Tsigos and Chrousos, 2002). Glucocorticoids, mainly cortisol in humans and corticosterone (CORT) in rodents, is a major stress steroid hormone that binds to cytosolic glucocorticoid (GR) and mineralocorticoid (MR) receptors, via which, glucocorticoids exert stress-related actions on various systems in the minutes – to hours timeframe.

CBG and GR

GR, the highly abundant receptor for CORT is known to exert the classical CORT actions in various tissues. For example, CORT binding to GR is immune suppressive when acting on peripheral immune cells. These actions via GR are due to 2 main mechanisms, in which GR translocates into the nucleus, resulting in 1) direct actions on gene transcription through binding to Glucocorticoid Response Elements on DNA, or 2) protein-protein interactions with other transcription factors in the nucleus (Silverman and Sternberg, 2012; De Bosscher *et al.*, 2014). When in circulation, 97% of CORT is bound to Corticosteroid Binding Globulin (CBG) or Albumin, and is therefore unable to diffuse across the cell membrane to reach intracellular receptors (Richard *et al.*, 2010). CBG is therefore an important regulator of CORT bioavailability, and changes in CBG expression reflect inverse availability of CORT for physiological actions.

1.2 Innate immune signalling can trigger the HPA axis and alter behaviour:

Experimental innate immune challenges, most commonly via administration of lipopolysaccharide (LPS), an agonist at Toll-like receptor 4 (TLR4), can result in both behavioural and neuroendocrine changes related to both stress and the HPA system. Behaviourally, LPS administration causes increased anhedonia, lethargy, anorexia and

loss of locomotion, a cluster of changes classified as sickness behaviour (Dantzer and Kelley, 2007; Hines *et al.*, 2013). Parallels can be drawn between sickness behaviour, a behavioural state that aids recovery from immune challenges, and depressive-like behaviour. Characterised by increased helplessness as measured by immobility in forced-swim and tail-suspension stressors, as well as increased anhedonia, measured by loss of preference to sweet-tasting solutions in two-bottle choice tests in rodents, depressive-like behaviour is also evident in the later stages of sickness behaviour following LPS administration (Dantzer *et al.*, 2008; McCusker and Kelley, 2013).

Unsurprisingly, behavioural changes as a result of LPS administration is accompanied by neuroendocrine activation in mice, triggering HPA activation as measured by increased circulating CORT levels and hypothalamic CRF mRNA (Adzic *et al.*, 2015). Innate immune stimulation also triggers HPA signalling events at each level of the system, independent of top down triggers. LPS administration directly induces CORT production and release from adrenal cells *in vitro* (Vakharia and Hinson, 2005), while pituitary cells stimulated with LPS can also directly produce ACTH without the presence of CRF (Elenkov *et al.*, 1992). At the level of the hypothalamus, there is emerging evidence for associations between CRF expressing neurons and TLR4 signalling (June *et al.*, 2015; Zhang *et al.*, 2016). In addition to LPS induced effects, pro-inflammatory factors interleukin-1β (IL-1β) and nitric oxide released as a result of innate immune stimulation, can also cause CRF secretion from the PVN via involvement of neuronal signalling from noradrenaline inputs (Hsieh, Li and Chen, 2010). Taken together, targeted agonists to the innate immune system, such as LPS, or downstream cytokine receptor signals, like IL-1β, provide strong evidence that the

innate immune system interacts with the HPA axis on multiple levels. Consequently, immune challenges can be considered a unique stressor.

Although there is emerging evidence that *Tlr4* genetic deletion confers some resistance against learned-helplessness in mice (Cheng *et al.*, 2016), little is known about how basal or aseptic TLR4- MyD88 signalling modifies the acute neuroendocrine and behavioural responses to non-immunogenic stressors. The current study thus aims to 1) characterise the neuroendocrine and behavioural stress response through measuring signalling events following forced swim and tail suspension stress models in transgenic mice lacking *Tlr4* or *Myd88*. MyD88 is an important adaptor molecule that is part of the TLR and IL-1R1 signalling pathway, 2) to further verify if differences in HPA activity is related to adrenal sensitivity to ACTH via use of an *ex vivo* model of adrenal stimulation in mice lacking *Tlr4* or *Myd88*, and 3) to investigate the impact of innate immune TLR4 or MyD88 signalling at the time of stress through use of acute pharmacological antagonism of innate immune signalling.

Methods

2.1 Animals

All animal experiments were approved by the University of Adelaide animal ethics committee. Experiments were conducted on male, 8-11 weeks old Balb/c wildtype, Balb/c background *Tlr4* knockout (*Tlr4*$^{-/-}$), and Balb/c background *Myd88* knockout (*Myd88*$^{-/-}$) mice. Mice were kept in a 12-hr light/dark cycle, with food and water provided *ad libitum*. To reduce variability due to handling and environmental stress, all animals were acclimatised to the facility for 1 week, and handled for 5 days before experimentation.

Given that body weight can be influenced by neuroendocrine function (Akana *et al.*, 1985; Scherer, Holmes and Harris, 2012), it could potentially explain any baseline neuroendocrine differences. Each mouse was thus weighed prior to tissue collection. *Tlr4*$^{-/-}$ mice exhibited a significantly higher body weight compared to both Balb/c control mice (mean difference = 2.01 g, $p<0.0001$) and *Myd88*$^{-/-}$ mice (mean difference = 1.15 g, $p<0.05$), while there was no significant difference between *Myd88*$^{-/-}$ and Balb/c body weights (mean difference = 0.86 g, $p=0.16$) (Figure 1).

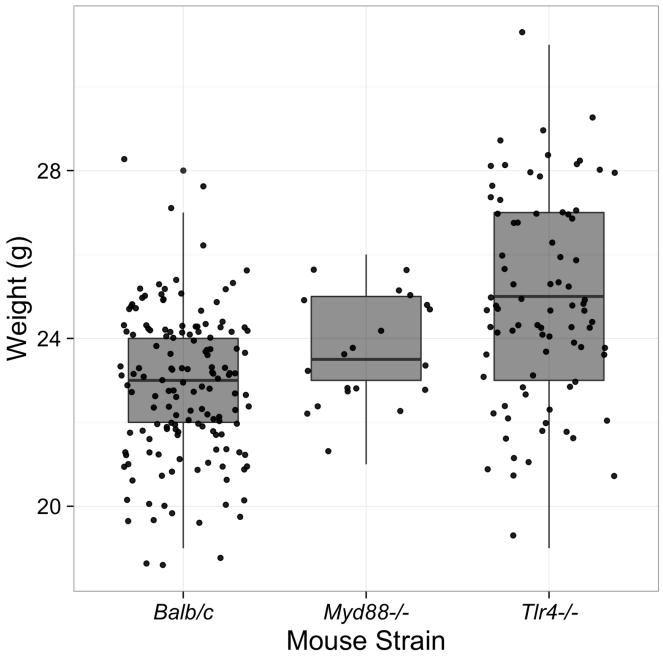

Figure 1. Tlr4-/- mice have higher total body weights compared to Balb/c and Myd88-/- mice. Boxplot of total body weights of Balb/c (N = 194), *Myd88*$^{-/-}$ (N = 41), and *Tlr4*$^{-/-}$ (N= 90) mice, aged between 8-11 weeks old. Significance levels for individual group differences using pairwise post-hoc comparisons with Tukey correction indicated by * (p<0.05) ** (p<0.01), ***(p<0.001), **** (p<0.0001).

2.2 Forced swim stress and Tail suspension stress

To investigate if TLR4 and MyD88 signalling influence the behavioural and neuroendocrine stress response, Forced Swim Stress and Tail suspension stress were utilised on Balb/c, *Myd88*$^{-/-}$ and *Tlr4*$^{-/-}$ mice separately. Acute activity of TLR4 and IL-1R1 was further tested using pharmacological antagonists, (+)- Naltrexone (60 mg/kg) and IL-1RA (100 mg/kg, PharmaLink, USA), or saline as vehicle controls. Animals were intraperitoneally injected with vehicle control, (+)- Naltrexone, or IL-1RA 20 min before administration of stress paradigms according to previously determined effective dose (Wu *et al.*, 2011, 2012). This dose of IL-1RA has also previously shown blood brain barrier permeability within 30 min of intraperitoneal administration (Shavit *et al.*,

2005). (+)-Naltrexone was employed in this fashion owing to its established TLR4 inhibitory effects (Wu *et al.*, 2012) and beneficial CNS pharmacokinetic profile (Northcutt *et al.*, 2015).

Forced swim stress:

Each mouse was lowered into a clear acrylic cylinder measuring 20cm x 46cm (diameter x height) half-filled with 22-25 °C water for 6 min, and allowed to swim freely. Mice were recorded from top-view using a Logitech web camera, and videos were manually analysed using ANY-maze software (Version 5.1, ANY-maze, UK). Immobility, defined as the lack of active swimming movements apart from keeping the head oriented above water, was measured as a marker of depressive-like behaviour (Linthorst, Flachskamm and Reul, 2008). Each animal's strain and treatment was blinded to the assessor during measurement of immobility to eliminate bias in data collection. Serum circulating CORT was measured 15, 30, and 45 min after the start of the stressor, as 30 min was shown to be the peak CORT following forced swim stress (Qian *et al.*, 2011).

Tail suspension stress:

Tail suspension has also been used as an alternative measure for depressive-like behaviour in rodents (Steru *et al.*, 1985). This stressor was thus employed to verify differences observed in forced swim stress. Briefly, mice were suspended on their tails for 6 min. Mice were recorded from the front view using a Logitech web camera, and videos were manually analysed using ANY-maze software. Immobility, defined as the lack of climbing behaviour, was also measured as an indication of depressive-like

behaviour. Each animal's strain and treatment was blinded to the assessor. Serum circulating CORT was measured 21, 36 and 51 min after the start of the stressor.

2.3 Strain comparisons of Adrenal size and function

As a potential explanation for strain differences between CORT responses following stress, adrenal cortex size, total adrenal weight and adrenal function were compared.

Histological adrenal cortex size measurement

Naïve animals were deeply anesthetised via overdose of sodium pentobarbitone (600 mg/kg, Virbac, Australia) and fixed via cardiac perfusion of 4% paraformaldehyde. Adrenals were harvested, post-fixed in 4% PFA overnight, and dehydrated over 3 days in 30% sucrose. Tissues were flash frozen in liquid nitrogen, and sectioned into 10um slices on a cryostat. Adrenals were stained with Haemotoxylin and Eosin (H&E). Slides were imaged and analysed using Image J (64-bit) software (1.48v, National Institute of Health, USA). Adrenal gland and cortex sizes were compared by measuring the respective areas of the 4 largest sections per adrenal (Zacharowski *et al.*, 2006). For each image, an intensity threshold was set to exclude the adrenal medulla and background in ImageJ (64-bit) software, creating a mask over the area occupied by the adrenal cortex.

Ex vivo adrenal stimulation

In order to discern if strain differences in stress-induced circulating CORT were due to sensitivity of adrenals to ACTH, *ex vivo* stimulation of adrenals with ACTH (Phoenix Pharmaceuticals 001-06, USA) was performed based on previously reported methods

(Richter *et al.*, 2008). Briefly, adrenals were harvested with the attached surrounding adipose tissue, washed briefly in ice-cold PBS, and kept in serum free DMEM + L-glutamine (Life Technologies, 25030081, Australia) until further processing. Under a dissecting microscope, adrenals from each animal were stripped from the surrounding adipose tissue and cut into halves. Each half adrenal was subsequently weighed, before incubating in DMEM +L-glutamine for 4 h in individual wells in 24-well plates. Following incubation, the media was replaced with vehicle, 1 nM, or 100 nM ACTH (Phoenix Pharmaceuticals 001-06, USA). At 1hr and 2 h post administration, 100 μl of supernatant was removed from each well, and replenished with the appropriate treatments. After a total of 6 h of ACTH stimulation, total supernatant was harvested. CORT was measured from each sample, and controlled for weight of adrenal tissue in each well (Enzo Life Sciences, 900-097, USA).

2.4 Protein quantification of GR and CBG

Western blots were used to quantify Corticosteroid Binding Globulin (CBG) and glucocorticoid receptor (GR) protein expression in hypothalamus tissues. Hypothalamus tissues were either harvested 30 min after the onset of stress (during peak CORT secretion), or from control home cage animals, homogenised in TBS-triton (0.05%) with protease inhibitor cocktail (Sigma Aldrich, P8340, Germany), and normalised to 1 μg/ul in laemmli buffer. 20 μg of protein from blood serum and hypothalamus tissues were loaded and separated by molecular weight via electrophoresis onto 8% and 4-10% gradient polyacrylamide gels respectively. Following electrophoresis, proteins were transferred onto nitrocellulose membranes and blocked using 3% Skim milk for 1hr at room temperature. Each membrane was

incubated in primary antibodies for CBG (R&D systems AF4065, 1:500, USA), GR (Santa-Cruz M-20, 1:50, USA), and Actin (Sigma Aldrich, 1:500, Germany) as loading control, overnight at 4 °C. After washes in PBSTween20, membranes were incubated with the respective IR fluorescent conjugated secondary antibodies (Donkey anti-goat 800nm: 925-32214, Donkey anti-rabbit 680nm: 924-68021, Li-cor, USA) for 1 h at room temperature, and imaged using the Odyssey infrared scanner (Li-cor, USA). Ratio-metric quantification of band intensity was performed using ImageJ (64-bit). All band intensities were measured relative to a standard control sample to constrain inter-gel variability.

2.5 Quantifying circulating and adrenal secreted CORT

To determine adrenal gland activity, stress and ACTH-induced CORT were measured (see *ex vivo adrenal stimulation* section 2.3). Blood samples were collected via cardiac puncture, and centrifuged at 5500 xg to separate blood serum and stored at -20 °C. CORT from serum and adrenal supernatant samples was measured using an ELISA kit (Enzo Life Sciences, 900-097, USA) according to the manufacturer's protocol.

2.6 Statistics

Strain differences in forced swim immobility was analysed using a one-way ANOVA. As the Shapiro-Wilk test revealed that tail suspension immobility was significantly not normally distributed, a non-parametric Kruskal-Wallis test was used to examine strain differences in tail suspension immobility instead. Two-way ANOVAs were used to analyse strain and time effects on forced swim and tail suspension stress-induced

CORT release. All post-hoc multiple pairwise comparisons were adjusted using Tukey's correction to control for the number of comparisons made.

For *ex vivo* adrenal tissue stimulations with ACTH, since each animal's adrenals were halved, providing 4 halves in total, multiple and repeated measures were made per animal. Thus, linear mixed effects model using the nlme package in R was utilised, assigning each animal as a random effect to control for inter-animal variability. All statistical analysis were performed on R (version 3.3.1)(64-bit) statistical software (R Core Team, 2015).

Results

3.1 Genetic knockout of *Myd88* increases forced swim, but decreases tail suspension immobility, while knockout of *Tlr4* only decreases tail suspension immobility.

Baseline behavioural differences during tail suspension stress and forced swim stress was assessed between each mouse strain to test if genetic knockouts of *Tlr4* or one of its key signalling pathways, *Myd88*, impact baseline immobility behaviours in the same way. Immobility during the forced swim test was significantly influenced by strain ($F(2,55) = 24.25$, $p < 0.0001$) (Figure 2A,C). Post-hoc pairwise multiple comparisons between individual strains using Tukey's correction revealed that *Myd88*$^{-/-}$ mice had increased immobility during forced swim stress as compared to both Balb/c (mean difference = 67.5 s, $p<0.0001$), and *Tlr4*$^{-/-}$ (mean difference = 78.9 s, $p<0.0001$) mice. However, there was no significant difference between Balb/c and mice lacking *Tlr4* (mean difference = 11.4 s, $p = 0.55$). In addition, latency to first immobile episode during forced swim stress significantly differed between mouse strains ($F(2,55) = 4.71$, $p<0.05$) (Figure 2E). Post-hoc analysis showed that *Myd88*$^{-/-}$ animals had decreased immobility latency compared to *Tlr4*$^{-/-}$ mice (mean difference = 17.1 s, $p<0.05$), but neither transgenic strain significantly differed from Balb/c wild type mice ($p>0.05$).

Due to the significantly non-normal distribution of tail suspension behavioural immobility data, as assessed by the Shapiro-Wilk Normality test ($p< 0.05$; Figure 2B), the non-parametric Kruskal-Wallis rank sum test was used instead of parametric 1-way ANOVA, revealing that mouse strain significantly influenced immobility during the tail suspension test ($\chi^2(2)= 17.14$, $p<0.001$)(Figure 2D). Further post-hoc non-parametric

multiple comparisons using Fisher's approximation method and Tukey's correction showed that *Tlr4*$^{-/-}$ ($p<0.0001$), and *Myd88*$^{-/-}$ ($p<0.01$) mice had lower immobility when compared to Balb/c controls, but were not significantly different from each other ($p = 0.30$).

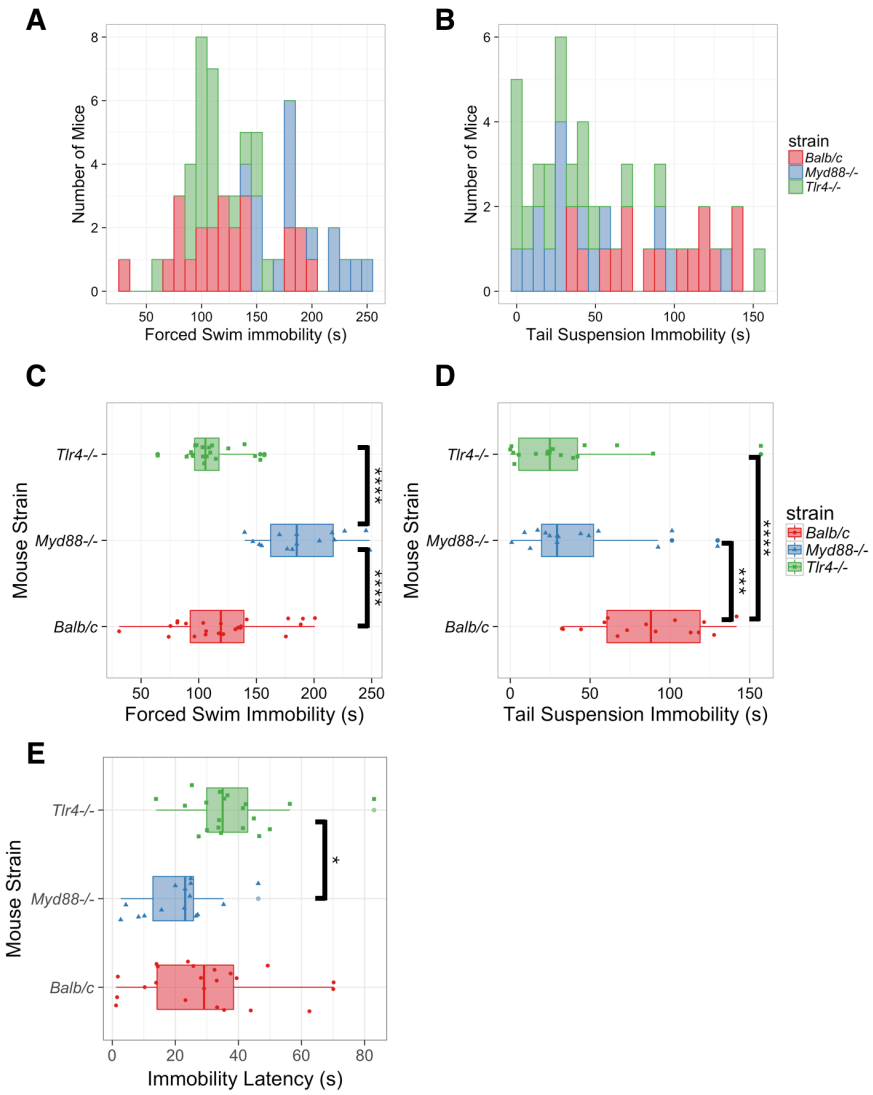

Figure 2. Tlr4-/- mice exhibit decreased behavioural immobility during tail-suspension stress Myd88-/- mice display increased immobility during forced swim stress, but decreased immobility during tail suspension stress. A-B) Histogram showing normal distribution of immobility (s) during forced swim stress (A) and skewed distribution of immobility during tail suspension stress (B) according to mouse strain. C-D) box and whisker plots summarising median, full range, 25th, and 75th percentile values for immobility during forced swim (C) and tail suspension (D) stress. Latency to first immobile episode during forced swim stress (E). Significance levels for individual group differences using pairwise post-hoc comparisons with Tukey correction indicated by * ($p<0.05$) ** ($p<0.01$), ***($p<0.001$), **** ($p<0.0001$).

3.2 Lack of *MyD88*, but not *Tlr4* results in both an accelerated, and an extended CORT elevation following acute forced swim stress.

Owing to the differences in the behavioural outcomes between strains and between tests, we explored the HPA consequences of these stressors in the search for a molecular mediator of this effect that may lie downstream from the TLR4 and MyD88 signalling events engaged by the FST and TST challenges.

A two-way ANOVA was utilised to examine the effects of strain and time after onset of forced swim stress on serum measured CORT concentrations. The analysis revealed main effects of strain ($F(2,69)= 3.30$, $p <0.05$), and time after onset of stress ($F(3,69) = 42.43$, $p<0.0001$). The interaction between strain and time did not significantly account for overall variability in the dataset ($F(6,69)=2.06$, $p=0.069$) (Figure 3A).

Further multiple comparisons applied using Tukey's correction showed that neither *Myd88*$^{-/-}$ mice (mean difference = 64.0 ng/ml, $p = 0.07$), nor *Tlr4*$^{-/-}$ mice (mean difference = -4.7 ng/ml, $p = 0.98$) had significantly different overall circulating CORT concentrations when compared to Balb/c wild type mice overall. *Tlr4*$^{-/-}$ and *Myd88*$^{-/-}$ mice did not significantly differ in overall circulating CORT concentrations (mean difference = 68.7 ng/ml, $p = 0.06$).

The baseline CORT concentration in *Myd88*$^{-/-}$ (mean difference = -57.7 ng/ml, p= 0.99), and *Tlr4*$^{-/-}$ mice (mean difference = -52.3 ng/ml, p = 0.99) were not significantly different to Balb/c controls. Following forced swim stress, Balb/c wild-type mice did

not have a significant elevation in CORT concentration from baseline at 15 min post stress onset (mean difference = 165.9 ng/ml, p = 0.75), but had significantly increased circulating CORT concentration 30 min post stress onset (mean difference = 282.7 ng/ml, p< 0.0001), but is again no different from baseline 45 min following forced swim stress (mean difference = -118.33 ng/ml, p = 0.99). Peak CORT concentrations at 30 min post stress were significantly higher than both 15 min (mean difference = 185.3 ng/ml, p<0.05) and 45 min post stress onset (mean difference = -300.6 ng/ml, p<0.0001) in Balb/c mice.

Similarly, CORT concentrations from *Tlr4*$^{-/-}$ mice were not significantly elevated 15 min post stress onset (mean difference = 145.2 ng/ml, p = 0.36), but was significantly increased from baseline at 30 min post stress onset (mean difference = 283.0 ng/ml, p<0.0001), while it was no different from baseline at 45 min post stress onset (mean difference = 112.8 ng/ml, p<0.74). CORT concentrations were not significantly different between 30 min and 15 min post stress onset in *Tlr4*$^{-/-}$ mice (mean difference = 130.8 ng/ml, p= 0.36), but had significantly decreased between 30 min and 45 min (mean difference = -221.8 ng/ml, p<0.01).

In mice lacking MyD88 however, there was already a significant increase in circulating CORT at 15 min post onset of forced swim stress (mean difference = 223.6 ng/ml, p<0.05), peaking at 30min (mean difference = 446.1 ng/ml, p<0.0001) and persisting through 45 min (mean difference = 237.9 ng/ml, p<0.05) compared to baseline concentrations. Moreover, circulating CORT levels in *Myd88*$^{-/-}$ mice at 30 min is significantly higher than 15 min post stress onset (mean difference = 222.5 ng/ml,

p<0.05), but not significantly different from 45 min post stress onset (mean difference = 208.2 ng/ml, *p* = 0.06).

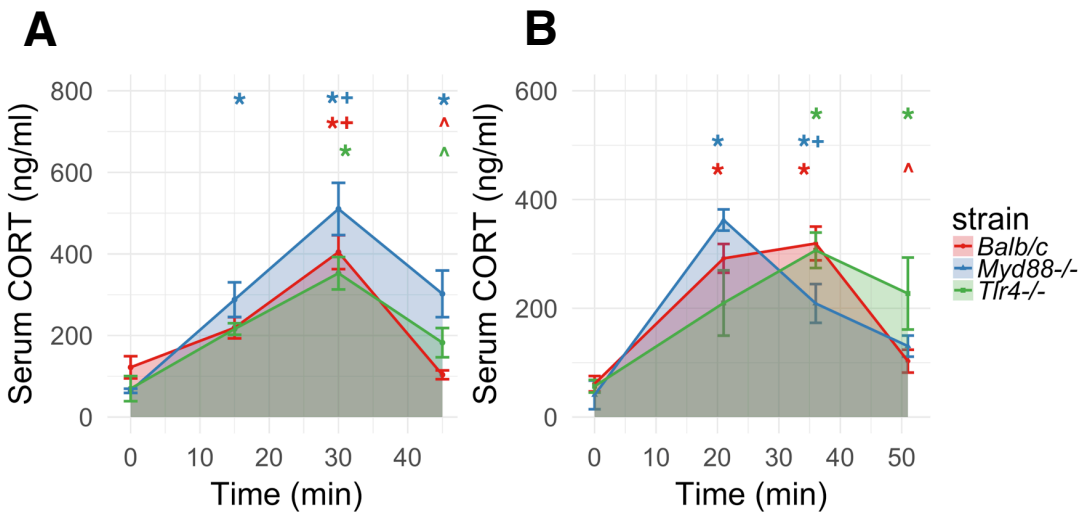

Figure 3. Myd88-/- mice exhibit sustained elevation of circulating CORT over time after forced swim stress, while Tlr4-/- mice show sustained elevation of circulatiang cort after tail suspension stress. A) Serum CORT levels at baseline, 15min, 30min and 45min post onset of forced swim stress. B) Serum CORT levels at baseline, 21min, 36min and 51min post onset off tail suspension stress. Error bars reprersent SEM values around mean levels. Colours indicatae mouse strain (N=5 each group). Significant comparisons (p<0.05) for individual group differences using pairwise post-hoc comparisons with Tukey correction indicated by * Compared to baseline; + Compared to either 15 min [Forced swim stress], or 21 min [Tail suspension stress]; ^ Compared to either 30 min [Forced swim stress], or 36 min [Tail suspension stress].

3.3 Tlr4$^{-/-}$ mice display delayed CORT secretion, while *Myd88*$^{-/-}$ mice exhibit increased rate of change in CORT levels following tail suspension stress.

The 2-way ANOVA applied to CORT results following tail suspension stress showed a significant t ime ($F(3,49)= 39.25$ $p<0.0001$) and interaction effect between stress and time ($F(6,49) = 4.42$, $p<0.01$), but no significant strain effect was observed ($F(2,49)= 1.03$, $p=0.36$)(Figure 3B).

Tukey post-hoc pairwise comparisons further showed that neither *Myd88*$^{-/-}$ mice, nor *Tlr4*$^{-/-}$ mice differed significantly from Balb/c mice in baseline (*Myd88*$^{-/-}$: mean difference = -20.6 ng/ml, $p= 0.99$; *Tlr4*$^{-/-}$: mean difference = -4.6 ng/ml, $p= 0.99$), 21 min post stress (*Myd88*$^{-/-}$: mean difference = 70.6 ng/ml, $p=0.90$; *Tlr4*$^{-/-}$: mean difference = -83.0 ng/ml, $p= 0.84$), 36 min post stress (*Myd88*$^{-/-}$: mean difference = -110.3 ng/ml, $p= 0.31$; *Tlr4*$^{-/-}$: mean difference = -12.5 ng/ml, $p= 0.99$), and 51 min post tail suspension stress (*Myd88*$^{-/-}$: mean difference = 27.7 ng/ml, $p= 0.99$; *Tlr4*$^{-/-}$: mean difference = 124.4 ng/ml, $p=0.21$).

In Balb/c animals, CORT was significantly elevated by 21 min after tail suspension stress (mean difference = 230.6 ng/ml, $p<0.001$), reached peak at 36 min post onset of stress (mean difference = 258.0 ng/ml, $p<0.0001$), and was not different from baseline at 51 min post stress onset (mean difference = 41.5 ng/ml, $p=0.99$). However, there was no significant difference between 21 min and 36 min post stress onset (mean difference = 27.3 ng/ml, $p = 0.99$), but a significant decrease in CORT levels was

observed between 51 min and 36 min post tail suspension stress in Balb/c mice (mean difference = -216.5 ng/ml, $p<0.001$).

Mice lacking *MyD88* also displayed elevated CORT at 21 min post stress onset (mean difference = 321.7 ng/ml, p<0.0001), and 36 min post stress onset (mean difference = 168.3 ng/ml, $p<0.05$), but did not significantly differ from baseline 51 min after tail suspension stress (mean difference = 89.8 ng/ml p = 0.68). Unlike Balb/c mice, *Myd88*$^{-/-}$ mice displayed lower circulating CORT in 36min when compared to 21 min post stress onset (mean difference = -153.5 ng/ml, $p<0.05$), but did not significantly differ between 36 min and 51 min (mean difference = -78.5 ng/ml, $p = 0.83$).

In *Tlr4*$^{-/-}$ mice, there was no significant CORT elevation from baseline 21 min after stress onset (mean difference = 153.2 ng/ml, $p = 0.12$), but had significantly increased CORT concentrations 36 min post stress onset (mean difference = 250.1 ng/ml, $p<0.0001$), persisting through 51 min after tail suspension stress (mean difference = 170.6 ng/ml, $p<0.05$). Moreover, there was no significant difference in CORT levels between 21 min and 36 min post stress onset (mean difference = 96.9 ng/ml, $p = 0.56$), and between 51 min and 36 min post stress onset (mean difference = -79.5, $p = 0.73$).

3.4 Acute administration of TLR4 and IL-1R1 pharmacological antagonists do not alter behavioural stress responses, but do modify peak stress-induced CORT elevation.

IL-1RA and (+)- Naltrexone, respective inhibitors of IL-1R1 and TLR4 innate immune receptors, were used to investigate if acute pharmacological antagonism is sufficient

to induce behavioural and neuroendocrine changes seen in genetic knockout animals. Behaviourally, neither IL-1RA, nor (+)-Naltrexone influenced immobility during forced swim stress ($F(2,22)= 0.208$, $p = 0.81$), as assessed by a one-way ANOVA. Due to sufficiently non-normal distribution of tail suspension immobility, the Kruskal-Wallis rank sum test was used to analyse tail suspension data, revealing that neither drug significantly influenced behavioural immobility as well ($\chi^2(2)= 2.07$, $p = 0.35$) (Figure 4A).

Despite the lack of behavioural differences, a 2-way ANOVA revealed significant effects of drug ($F(2,71)= 3.32$, $p<0.05$), and stress ($F(2,71)= 13.74$, $p<0.0001$) on circulating CORT measured in the same animals (Figure 4B). There was, no significant interaction effect found between drug and stress on CORT concentration ($F(4,71)= 0.56$, $p = 0.69$). All CORT values were log transformed due to differences in scaling between forced swim stress, tail suspension stress and home cage control CORT levels. Post-hoc multiple pairwise comparisons using Tukey's correction found that (+)-Naltrexone itself significantly elevated CORT concentrations when compared to saline controls (mean difference = 62.42 ng/ml, $p<0.05$). Both forced swim stress (mean difference = 135.27 ng/ml, $p<0.0001$) and tail suspension stress (mean difference = 438.80 ng/ml, $p<0.0001$) significantly increased circulating CORT when compared to home cage controls. Furthermore, tail suspension stress elicited significantly higher CORT in circulation than forced swim stress (mean difference = 303.53 ng/ml, $p<0.0001$).

When separating out each condition however, neither IL-1RA, nor (+)-Naltrexone significantly altered circulating CORT measures in home caged (IL-1RA: mean

difference = 19.92 ng/ml, p = 0.87; (+)-Naltrexone: mean difference = 45.83 ng/ml, p = 0.99), force swim stress (IL-1RA: mean difference = 26.58 ng/ml, p = 0.99; (+)-Naltrexone: mean difference = 86.6 ng/ml, p = 0.76), and tail suspension stress (IL-1RA: mean difference = 101.41 ng/ml, p = 0.99; (+)-Naltrexone: mean difference = 66.87 ng/ml, p = 0.99) conditions.

Saline-treated animals displayed increased CORT in response to both forced swim stress (mean difference = 131.34 ng/ml, $p<0.0001$) and tail suspension stress (mean difference = 337.85 ng/ml, $p<0.0001$). Similarly, (+)-Naltrexone treatment also increased circulating CORT following forced swim (mean difference = 172.11 ng/ml, $p<0.01$), and tail suspension (mean difference = 490.23 ng/ml, $p<0.0001$) stress conditions when compared to home caged controls receiving the same drug at matched timings. In IL-1RA-treated animals however, only tail-suspension stress increased CORT (mean difference = 347.85 ng/ml $p<0.0001$), while forced swim stress did not significantly elevate serum CORT when compared to home cage controls receiving the same drug (mean difference = 84.84 ng/ml, $p=0.31$).

Finally, tail suspension stress significantly elevated serum CORT levels in both (+)-Naltrexone-treated animals (mean difference = 318.11 ng/ml, $p<0.05$) and IL-1RA-treated animals (mean difference = 263.01 ng/ml, $p<0.05$) when compared to forced swim stress.

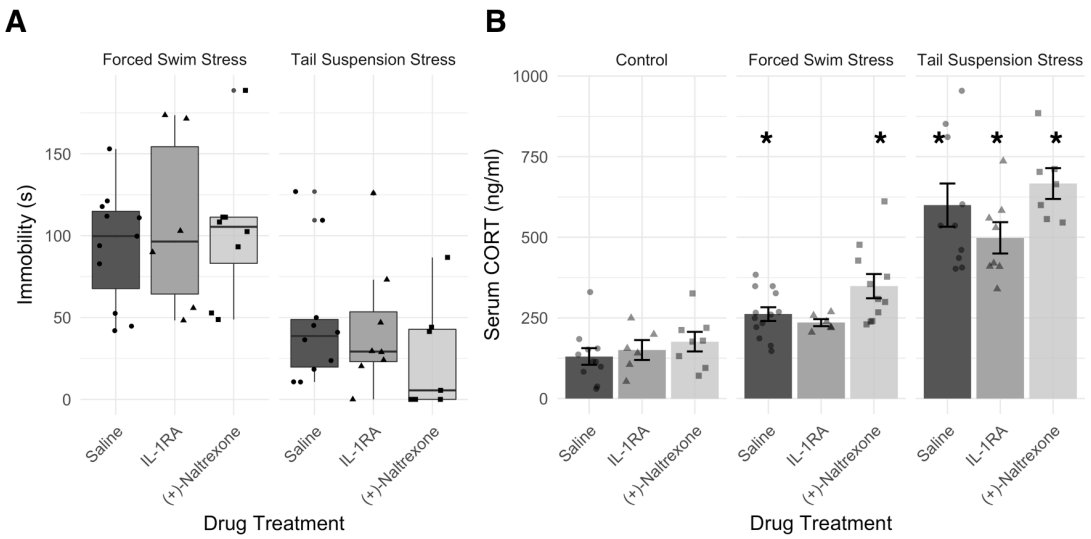

Figure 4. Acute pharmacological antagonists to TLR4 and IL-1R1 do not alter immobility during Forced swim and Tail suspension stress. TLR4 antagonism using (+)-Naltrexone significantly elevates circulating CORT levels. A) Box and whisker plot showing median, full range, 25th and 75th percentile of Immobility during forced swim and tail suspenion stress after administration of acute TLR4 and IL-1R1 antagonists, (+)-Naltrexone (60 mg/kg) and IL-1RA (100 mg/kg), respectively. Pharmacological antagonists were administered 20 min prior to onset of stress. B) Bar plot showing mean and sem of peak serum CORT levels following administration of (+)-Naltrexone (60 mg/kg) or IL-1RA (100 mg/kg)(N= 6-8). CORT levels were measured 30 min post Forced swim stress and 36 min post tail suspension stress. * indicates significant elevations in serum CORT concentrations compared to Home cage control animals administered with each corresponding drug ($p<0.05$).

3.5 Absence of *MyD88* or *Tlr4* alters hypothalamus CBG and GR expression.

To investigate if MyD88 and TLR4 signalling influenced the overall capacity of CORT to elicit its effect in the animals, hypothalamic CBG (impacting CORT bioavailability) and GR protein expression (impacting CORT's pharmacodynamic actions) were measured using western blots. A two-way ANOVA applied to hypothalamic CBG expression levels revealed statistically significant main effects of mouse strain ($F(2,29) = 5.20$, $p<0.05$), and forced swim stress ($F(1,29) = 6.65$, $p<0.05$), but no significant interaction between strain and stress ($F(2,29)= 0.62$, $p=0.55$) (Figure 5B). Tukey post-hoc analysis further revealed that the *Tlr4*$^{-/-}$ hypothalamus displayed a significantly higher level, of CBG expression than the *Myd88*$^{-/-}$ hypothalamus (mean difference = 0.36 units, $p<0.01$). Neither knockout strains significantly differed in hypothalamic CBG expression from Balb/c wild type mice. However, there was an overall increase in CBG expression following stress (mean difference = 0.22 units, $p<0.05$).

On the other hand, hypothalamic GR expression was not significantly different between mouse strains ($F(2,23)= 0.87$, $p=0.43$), nor forced swim stress ($F(1,23)=0.05$, $p=0.83$) overall. However, the interaction between mouse strain and stress significantly influenced GR expression ($F(2,23)=4.18$, $p<0.05$), indicating that lack of *Tlr4* or *MyD88* changes GR expression after stress. Tukey post hoc test did not reveal any individual group differences due to a large variability in the data (Figure 5A).

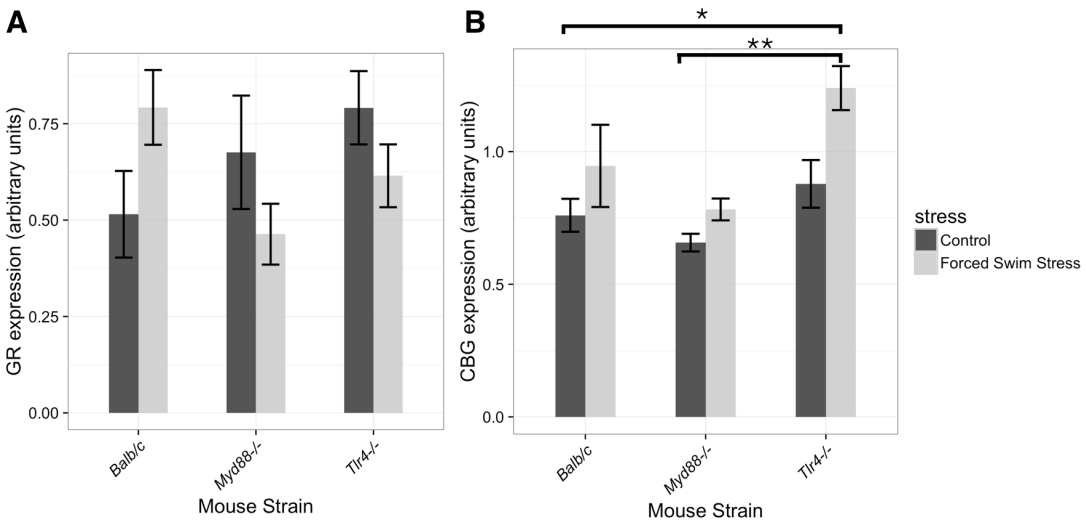

Figure 5. Tlr4-/- mice exhibit higher hypothalamic CBG expression compared to Myd88-/-. Forced swim stress causes changes in hypothalamic GR expression amongst the different mouse strains. A) Hypothalamic GR expression measured in home cage controls and 30 min post forced swim stress (N = 5). B) Hypothalamic CBG expression measured in home cage controls and 30 min post forced swim stress (N = 5). Error bars represent SEM around the mean for each group. Significance levels for individual group differences using pairwise post-hoc comparisons with Tukey correction indicated by * ($p<0.05$) ** ($p<0.01$), ***($p<0.001$), **** ($p<0.0001$).

3.6 Ex Vivo stimulation of adrenals with ACTH elicits increased CORT in *Myd88*$^{-/-}$ adrenals without differences in adrenal sizes.

Analysis of adrenal cortex area as a ratio of total adrenal size from H&E stained histological adrenal cross-sections revealed no significant main effect of strain in comparing the ratios of adrenal cortex area:total adrenal area ($F(2,13)= 0.70$, $p=0.51$) (Figure 6A). Furthermore, neither *Myd88*$^{-/-}$ (B = 0.01 mg, $t(12) = -0.01$, $p = 0.99$), nor *Tlr4*$^{-/-}$ (B = 0.59 mg, $t(12) = 0.82$, $p = 0.43$) animals had significantly different adrenal weights when compared to Balb/c animals (Figure 6B).

To further investigate if strain differences in circulating CORT following stress were due to changes in adrenal sensitivity to ACTH, adrenal tissues from each strain were treated with vehicle, 1 nM, or 100 nM ACTH peptide, and CORT secretion was analysed over the course of 6 h stimulation period. A linear mixed effects regression model was constructed to investigate the effects of ACTH concentration, duration of administration and mouse strain, on CORT secretion per mg of adrenal tissue, controlled for inter-animal variability. The model revealed that administration of 100 nM ACTH was able to significantly increase CORT secretion in Balb/c (B = 6.4 ng/mg/h, $t(105)= 3.82$,$p< 0.001$), *Tlr4*$^{-/-}$ (B = 9.0 ng/mg/hr, $t(105) = 5.44$, $p < 0.0001$), and *Myd88*$^{-/-}$ (B = 10.8 ng/mg/h, $t(105) = 6.48$, $p <0.0001$), over the period of 6 hours (Figure 6C). In addition, comparison of least squares means between the variables using Tukey's adjustment revealed that both *Myd88*$^{-/-}$ (mean difference = 16.4 ng/mg, $p < 0.05$), and *Tlr4*$^{-/-}$ (mean difference = 14.0 ng/mg, $p <0.05$) adrenals secreted more CORT per mg tissue in response to 100 nM ACTH after 6 h.

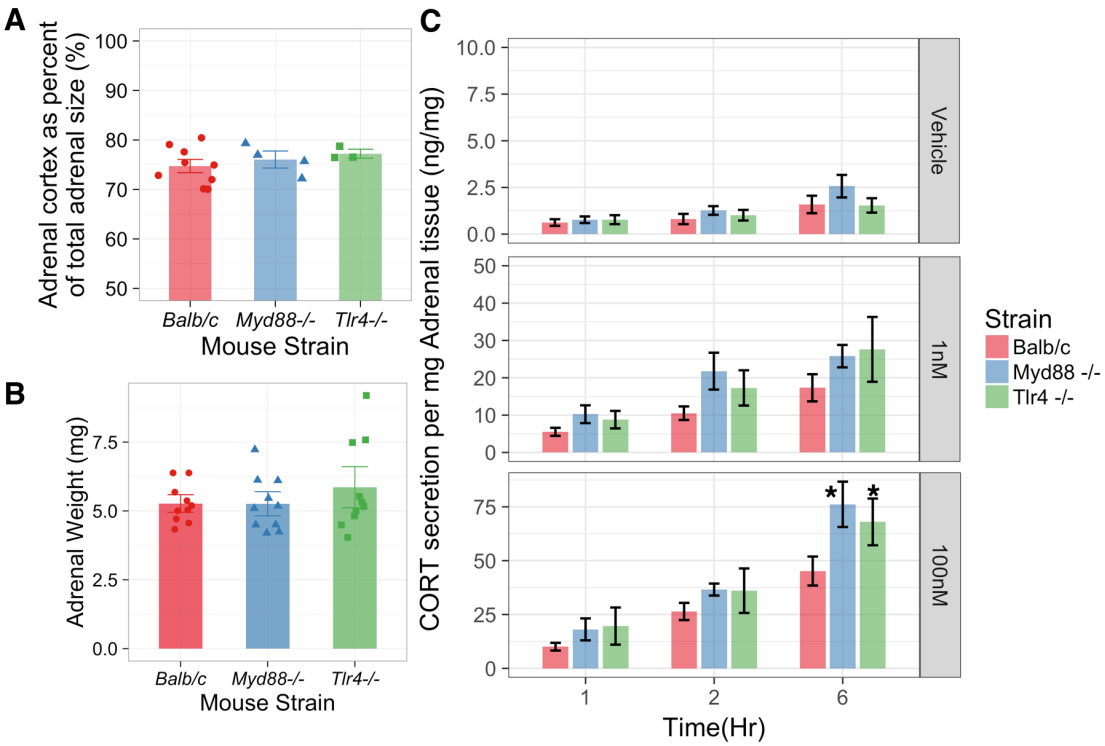

Figure 6. Myd88-/- and Tlr4-/- mouse adrenals secrete higher CORT in response to 6 h stimulation with 100nM ACTH despite no differences in adrenal size or ratio of adrenal cortex: total adrenal. A) Percent of adrenal cortex to total adrenal area calculated from H&E stained adrenal sections (N= 3-9). B) Total adrenal weight (N = 5). C) CORT concentration measured from medium following vehicle, 1 nM and 100 nM ACTH stimulation for 1, 2 and 6 h (N = 5). Error bars represent SEM around group means. * Represent significant elevations in CORT concentrations compared to Balb/c adrenals administered the same concentration of ACTH at the indicated time ($p<0.05$).

Discussion

The data accumulated in the current study suggest that the genetic absence of innate immune signalling molecules, MyD88 and TLR4 can alter behavioural and CORT responses to acute non-immunogenic stressors in mice, as measured by behavioural immobility during forced swim and tail suspension stressors. The observed effects are stressor dependent, and require genetic deletion, while pharmacological antagonists did not influence the acute stress response. Investigating the potential role of measures of adrenal sensitivity to ACTH further showed that *Myd88*$^{-/-}$ and *Tlr4*$^{-/-}$ adrenals both secreted increased CORT compared to wild type adrenals. Furthermore, hypothalamic CBG and GR expression revealed potential strain differences in CORT bioavailability and receptor negative feedback.

4.1 Strain differences in behavioural and CORT responses

Despite displaying significant differences in overall body weights, transgenic mice did not differ in total adrenal weight and adrenal cortex size. Moreover, baseline CORT was also no different between mouse strains, suggesting that baseline neuroendocrine activity is unchanged. This result is inconsistent with a previous study, which reported that mice lacking *Tlr4* had increased baseline CORT secretion (Zacharowski et al., 2006). This conflict is likely due to different background mouse strains used. Here, the transgenic mice were of Balb/c background, as opposed to C57/bl6 mice in the earlier study.

During forced swim stress, *Myd88*$^{-/-}$ mice displayed increased behavioural immobility compared to wild type mice, and decreased immobility latency compared to *Tlr4*$^{-/-}$

mice. These differences were concurrent with elevated CORT concentrations after the stressor. On the other hand, although there was a decrease in tail suspension immobility in both *Tlr4*$^{-/-}$ and *Myd88*$^{-/-}$ mice, this behavioural result was not mirrored by CORT responses; *Myd88*$^{-/-}$ mice had faster resolution of CORT response, while *Tlr4*$^{-/-}$ mice had a delayed CORT response following tail suspension stress. The results from transgenic mice thus show that TLR4 and MyD88 signalling shapes the neuroendocrine and behavioural acute stress response, but in different ways depending on the stressor used.

4.2 Neuroendocrine responses do not necessarily mirror immobility behaviour

An interesting observation made in this study is the relationship between behavioural immobility and subsequent CORT concentrations. Further analysis into relationships between CORT at either time points and behavioural immobility (See supplementary S1 – S3) revealed that behavioural immobility during forced swim stress can be adequately explained by variation in CORT concentrations across time amongst mouse strains (see supplementary S1), whereas variability in immobility during tail suspension stress could not be explained by a similar model (See supplementary S2). Additionally, TLR4 and IL-1R1 targeted pharmacological antagonists appeared to unmask a significant positive relationship between forced swim immobility and CORT, while there was no significant relationship in the case of tail suspension stress (See supplementary S3). These findings imply that behavioural immobility performance does not necessarily relate to the level of physiological stress that the animal experiences, and warrants further investigation.

4.3 Inequivalence between tail suspension and forced swim stressors

Although immobility during forced swim stress and tail suspension stress serve as measures of depressive-like behaviour, we report differences in performance between both tests in our mouse strains. Initially proposed as a more pharmacologically sensitive approach when compared to forced swim (Steru *et al.*, 1985), tail suspension results should not conflict with forced swim immobility. Yet, consistent with our findings here, response differences between both stressors have previously been reported. In one study, phenylephrine and leptin were unable to influence tail suspension immobility in CD1 mice, but significantly increased forced swim immobility (Kurosawa, Shimizu and Seki, 2015). Imipramine, a selective serotonin reuptake inhibitor, also appears to differentially influence forced swim and tail suspension immobility in C57Bl/6 mice, but displayed the same dose-dependent trends in Swiss mice (Bai *et al.*, 2001). Like our current findings of much lower baseline immobility during tail suspension stress in *Tlr4*$^{-/-}$ and *Myd88*$^{-/-}$ mice, but not Balb/c mice, Bai et al (2001) also report the same difference in NIH-Swiss mice but not C57Bl/6 mice.

While multiple anti-depressants have been able to decrease tail suspension and forced swim immobility (Cryan, Mombereau and Vassout, 2005), it is important to note that genetic manipulations may also cause long term adaptations in selective systems which, in the case of *Myd88*$^{-/-}$ mice, may have resulted in differential performances in forced swim and tail suspension stressors. This difference contradicts the usefulness of both tests in determining depressive-like behaviour. Taken together, the behavioural and neuroendocrine inconsistencies seen in tail suspension and forced swim stress warrant further investigation.

4.4 Acute TLR4 and IL-1R1 pharmacological antagonists do not influence behavioural and CORT responsiveness following acute stress

Whilst *Tlr4*$^{-/-}$ and *Myd88*$^{-/-}$ mice exhibit differences in behavioural immobility and circulating CORT levels following stress, acute pharmacological antagonism of TLR4 by administering (+)-Naltrexone to Balb/c mice did not yield the same changes. This finding is in agreement with the lack of acute LPS and anti-inflammatory drug-induced changes in neuroendocrine and behaviour short term (Deak *et al.*, 2005). Consistent with the current results with IL-1RA and (+)-Naltrexone, the authors also demonstrated that acute anti-inflammatory treatment indomethacin, α-MSH and minocycline did not have any effect on forced swim immobility. Thus, genetic deletion of these innate immune signalling molecules fundamentally changes the behavioural and neuroendocrine responses, but acute TLR4-MyD88 signalling has little impact on stress, suggesting that TLR4 and IL-1R1 signalling at the time of acute stress does not determine behavioural and neuroendocrine responses. Taken together, these results suggest that the connection between innate immune signalling and the HPA axis, though intrinsic, is not direct, and likely requires downstream adaptations.

Rather than replicate the CORT responses found in transgenic mice, (+)- Naltrexone instead elevated circulating CORT, regardless of stress. Interestingly, (+)-Naltrexone can also elevate circulating CORT in mice lacking *Tlr4* (see supplementary S4). This finding suggests that the drug itself may have some biological effects independent of TLR4, or can act directly on the HPA axis, but the exact mechanisms are unknown at this time. Further studies would be required to investigate the exact mechanism of this

effect on the HPA axis. Previous experiments in our lab have shown that (+)-Naltrexone causes a decrease in core body temperature, indicating that this drug may have some non-specific effects on the physiological temperature system, possibly acting at the level of the hypothalamus (data not published). These non-specific actions are unlikely to be due to off-target actions on 64 common neuronal receptors, ion channels and enzymes including serotonin, norepinephrine and dopamine transporters, as demonstrated by NovaScreen assays (Hutchinson *et al.*, 2012; Northcutt *et al.*, 2015). Therefore, without altering behavioural immobility during forced swim and tail-suspension stress, (+)-Naltrexone can influence HPA activity, and result in increased CORT concentration in circulation.

These results thus indicate the complex relationship between innate immune signalling and stress, and further show that acute pharmacological antagonists are largely ineffective in altering the neuroendocrine and behavioural response. Rather, differences in stress responses likely stem from either the developmental or long-term lack of TLR4 and MyD88 signalling.

4.5 Tlr4$^{-/-}$ and *Myd88*$^{-/-}$ mice exhibit altered adrenal and hypothalamic function to neuroendocrine stimulation

Given the diminished role of acute innate immune signalling, the observed strain differences in CORT responses following stress could be due to fundamental differences in the neuroendocrine system related to increased compensatory mechanisms as a result of a chronic lack of MyD88 or TLR4. To further investigate whether strain differences in CORT levels following stress was related to innate

differences in HPA functioning, an *ex vivo* model of ACTH administration directly onto adrenal tissue was implemented to test strain differences in adrenal sensitivity of ACTH. Indeed, without significant difference in total adrenal size, *Myd88*$^{-/-}$ and *Tlr4*$^{-/-}$ adrenals had significantly increased CORT secretion per mass of tissue following a maximal pharmacological dose of ACTH. This result suggests that the lack of TLR4 and MyD88 could increase adrenal sensitivity to ACTH. However, previous findings have shown that a conditional knockout of adrenal MyD88 did not significantly change CORT secretion in response to LPS-induced CORT secretion *in vivo*, while a general knockout of *Myd88* gene from all tissues was able to attenuate LPS-induced CORT secretion (Kanczkowski *et al.*, 2013). This effect could have been due to the stressor of choice, as we have similarly found LPS did not modify adrenal CORT secretion in response to ACTH in Balb/c, *Tlr4*$^{-/-}$, nor *Myd88*$^{-/-}$ adrenals (see supplementary S5).

Adrenal ACTH sensitivity differences do not fully explain differences seen *in vivo*, as there was no significant difference in the 1 nM concentration of ACTH, which represents the concentrations achieved at physiological relevant stress levels. Furthermore, the time taken in order to show significant differences in adrenal sensitivity does not mirror *in vivo* data obtained, as the adrenals were still producing CORT after 6 h of ACTH stimulation, while CORT levels generally returned to baseline within 45 min after forced swim and tail suspension stress in Balb/c mice. Measurements of CBG and GR expression, associated with the negative feedback and bioavailability of CORT respectively, provide more information on CORT signalling in these animals.

Stress induced an increase in CBG expression within the hypothalamus, agreeing with previously found increases in circulation (Qian *et al.*, 2011). Although we found strain differences in CBG expression, this difference was most pronounced between *Tlr4*$^{-/-}$ and *Myd88*$^{-/-}$ mice, indicating that the relationship between innate immune signalling and neuroendocrine signalling is more complex than initially anticipated. Moreover, there was a significant interaction effect between mouse strain and forced swim stress in hypothalamus GR expression, demonstrating strain differences in hypothalamic GR expression in response to stress. Taken together, the innate immune system influences the HPA response on multiple levels, in both CORT secretion and regulation.

The results in the study collectively highlight that transgenic mice display baseline HPA adaptations that likely contribute towards the stress response. However, the exact mechanisms underpinning these changes are currently unresolved. Given the current findings of adaptations at the level of the hypothalamus and adrenals in transgenic lacking *Tlr4* or *Myd88*, future studies are required to address the importance of these adaptations through specific experimental manipulations at each point in the HPA axis. In addition, previous studies have shown that mice lacking *Tlr4* or *Myd88* display altered microbiome, although this effect was accounted by isolated breeding colonies (Ubeda *et al.*, 2012). Given the increasing evidence of gut bacteria in neuroendocrine and behavioural adaptations (Rea, Dinan and Cryan, 2016; Reber *et al.*, 2016), these documented adaptations may explain some of the differences seen in this study, providing a potential basis for further research.

Furthermore, the neuronal aspect of stress, such as neurotransmission in stress-related brain regions was not investigated here. Given that immobility during forced swim and tail suspension stressors are linked to serotonergic and noradrenaline neurotransmission (Connor, Kelly and Leonard, 1997), neural adaptations may mediate the neuroendocrine and behavioural differences in *Tlr4*$^{-/-}$ and *Myd88*$^{-/-}$ animals. Future studies including measures and manipulation of serotonergic signalling in these animals may be warranted. Relatedly, the potential impact of differences in hypothalamic CORT signalling and bioavailability, via differential CBG and GR expressions between strains remains unknown, and presents as another avenue for further exploration.

Conclusion

To our knowledge, this is the first study to investigate neuroendocrine and behavioural responses to both forced swim and tail suspension acute stressors in mice lacking *Tlr4* or *Myd88*. The current study demonstrates that these mice differ in behavioural and HPA stress response to acute, non-immunogenic stressors. While baseline TLR4 and MyD88 signalling causes multiple differences in the stress response, TLR4-MyD88 signalling activity during an acute stressor does not display the same actions. These stress response differences are unlikely influenced by innate immune signalling at the time of stress, but a result of adaptations following chronic deletion of TLR4 or MyD88. Given the growing evidence of the bidirectional relationship between the innate immune system and the stress response (see Liu et al. 2014 for a review), these results further substantiate the fundamental connection between both systems.

Acknowledgements

A portion of this work was supported by the NIH Intramural Research Programs of the National Institute on Drug Abuse (NIDA) and the National Institute of Alcohol Abuse and Alcoholism**.** JL is the recipient of an Adelaide Graduate Research Scholarship. This work was supported by the Australian Research Council Centre of Excellence for Nanoscale BioPhotonics [CE140100003]. The authors declare no conflict of interests.

References

Azic, M., Djordjevic, J., Mitic, M., Brkic, Z., Lukic, I., & Radojcic, M. (2015). The contribution of hypothalamic neuroendocrine, neuroplastic and neuroinflammatory processes to lipopolysaccharide-induced depressive-like behaviour in female and male rats: Involvement of glucocorticoid receptor and C/EBP-β. *Behavioural Brain Research*, *291*, 130–139. http://doi.org/10.1016/j.bbr.2015.05.029

Akana, S. F., Cascio, C. S., Shinsako, J., & Dallman, M. F. (1985). Corticosterone: narrow range required for normal body and thymus weight and ACTH. *American Journal of Physiology*, *249*(5 Pt 2), R527–R532.

Bai, F., Li, X., Clay, M., Lindstrom, T., & Skolnick, P. (2001). Intra- and interstrain differences in models of "behavioral despair." *Pharmacology Biochemistry and Behavior*, *70*(2–3), 187–192. http://doi.org/10.1016/S0091-3057(01)00599-8

Cheng, Y., Pardo, M., Armini, R. de S., Martinez, A., Mouhsine, H., Zagury, J.-F., … Beurel, E. (2016). *Stress-induced neuroinflammation is mediated by GSK3-dependent TLR4 signaling that promotes susceptibility to depression-like behavior*. *Brain, Behavior, and Immunity*. Elsevier Inc. http://doi.org/10.1016/j.bbi.2015.12.012

Cryan, J. F., Mombereau, C., & Vassout, A. (2005). The tail suspension test as a model for assessing antidepressant activity: Review of pharmacological and genetic studies in mice. *Neuroscience and Biobehavioral Reviews*, *29*(4–5), 571–625. http://doi.org/10.1016/j.neubiorev.2005.03.009

Dantzer, R., & Kelley, K. W. (2007). Twenty years of research on cytokine-induced sickness behavior. *Brain, Behavior, and Immunity*, *21*(2), 153–60.

http://doi.org/10.1016/j.bbi.2006.09.006

Dantzer, R., O'Connor, J. C., Freund, G. G., Johnson, R. W., & Kelley, K. W. (2008). From inflammation to sickness and depression: when the immune system subjugates the brain. *Nature Reviews. Neuroscience*, *9*(1), 46–56. http://doi.org/10.1038/nrn2297

De Bosscher, K., Beck, I. M., Dejager, L., Bougarne, N., Gaigneaux, A., Chateauvieux, S., … Haegeman, G. (2014). Selective modulation of the glucocorticoid receptor can distinguish between transrepression of NF-κB and AP-1. *Cellular and Molecular Life Sciences : CMLS*, *71*(1), 143–63. http://doi.org/10.1007/s00018-013-1367-4

Deak, T., Bellamy, C., D'Agostino, L. G., Rosanoff, M., McElderry, N. K., & Bordner, K. A. (2005). Behavioral responses during the forced swim test are not affected by anti-inflammatory agents or acute illness induced by lipopolysaccharide. *Behavioural Brain Research*, *160*(1), 125–134. http://doi.org/10.1016/j.bbr.2004.11.024

Elenkov, I. J., Kovács, K., Kiss, J., Bertók, L., & Vizi, E. S. (1992). Lipopolysaccharide is able to bypass corticotrophin-releasing factor in affecting plasma ACTH and corticosterone levels: evidence from rats with lesions of the paraventricular nucleus. *The Journal of Endocrinology*, *133*(2), 231–236.

Hines, D. J., Choi, H. B., Hines, R. M., Phillips, A. G., & MacVicar, B. a. (2013). Prevention of LPS-Induced Microglia Activation, Cytokine Production and Sickness Behavior with TLR4 Receptor Interfering Peptides. *PLoS ONE*, *8*(3), e60388. http://doi.org/10.1371/journal.pone.0060388

Hsieh, C. H., Li, H. Y., & Chen, J. C. (2010). Nitric oxide and interleukin-1β mediate noradrenergic induced corticotrophin-releasing hormone release in organotypic cultures of rat paraventricular nucleus. *Neuroscience*, *165*(4), 1191–1202.

http://doi.org/10.1016/j.neuroscience.2009.12.003

Hutchinson, M. R., Northcutt, A. L., Hiranita, T., Wang, X., Lewis, S. S., Thomas, J., … Watkins, L. R. (2012). Opioid activation of toll-like receptor 4 contributes to drug reinforcement. *The Journal of Neuroscience : The Official Journal of the Society for Neuroscience*, *32*(33), 11187–200. http://doi.org/10.1523/JNEUROSCI.0684-12.2012

June, H. L., Liu, J., Warnock, K. T., Bell, K. a, Balan, I., Bollino, D., … Aurelian, L. (2015). CRF-Amplified Neuronal TLR4/MCP-1 Signaling Regulates Alcohol Self-Administration. *Neuropsychopharmacology : Official Publication of the American College of Neuropsychopharmacology*, *40*(6), 1549–59. http://doi.org/10.1038/npp.2015.4

Kanczkowski, W., Alexaki, V., Tran, N., Großklaus, S., Zacharowski, K., Martinez, A., … Bornstein, S. R. (2013). Hypothalamo-pituitary and immune-dependent adrenal regulation during systemic inflammation. *Proceedings of the National Academy of Sciences of the United States of America*, *110*(36), 14801–6. http://doi.org/10.1073/pnas.1313945110

Kemeny, M. E., & Schedlowski, M. (2007). Understanding the interaction between psychosocial stress and immune-related diseases: A stepwise progression. *Brain, Behavior, and Immunity*, *21*(8), 1009–1018. http://doi.org/10.1016/j.bbi.2007.07.010

Kurosawa, N., Shimizu, K., & Seki, K. (2015). The development of depression-like behavior is consolidated by IL-6-induced activation of locus coeruleus neurons and IL-1β-induced elevated leptin levels in mice. *Psychopharmacology*. http://doi.org/10.1007/s00213-015-4084-x

Linthorst, A. C. E., Flachskamm, C., & Reul, J. M. H. M. (2008). Water temperature determines neurochemical and behavioural responses to forced swim stress: an in vivo microdialysis and biotelemetry study in rats. *Stress (Amsterdam, Netherlands)*, *11*(2), 88–100. http://doi.org/10.1080/10253890701533231

Liu, J., Buisman-Pijlman, F., & Hutchinson, M. R. (2014). Toll-like receptor 4: innate immune regulator of neuroimmune and neuroendocrine interactions in stress and major depressive disorder. *Frontiers in Neuroscience*, *8*(September), 309. http://doi.org/10.3389/fnins.2014.00309

McCusker, R. H., & Kelley, K. W. (2013). Immune-neural connections: how the immune system's response to infectious agents influences behavior. *The Journal of Experimental Biology*, *216*(Pt 1), 84–98. http://doi.org/10.1242/jeb.073411

Northcutt, A. L., Hutchinson, M. R., Wang, X., Baratta, M. V, Hiranita, T., Cochran, T. A., … Watkins, L. R. (2015). DAT isn't all that: cocaine reward and reinforcement require Toll-like receptor 4 signaling. *Molecular Psychiatry*, *20*(12), 1525–37. http://doi.org/10.1038/mp.2014.177

Qian, X., Droste, S. K., Gutièrrez-Mecinas, M., Collins, A., Kersanté, F., Reul, J. M. H. M., & Linthorst, A. C. E. (2011). A rapid release of corticosteroid-binding globulin from the liver restrains the glucocorticoid hormone response to acute stress. *Endocrinology*, *152*(10), 3738–48. http://doi.org/10.1210/en.2011-1008

R Core Team. (2015). R: A language and environment for statistical computing. Vienna, Austria: R Foundation for Statistical Computing.

Rea, K., Dinan, T. G., & Cryan, J. F. (2016). The microbiome: A key regulator of stress and neuroinflammation. *Neurobiology of Stress*, *4*, 23–33. http://doi.org/10.1016/j.ynstr.2016.03.001

Reber, S. O., Siebler, P. H., Donner, N. C., Morton, J. T., Smith, D. G., Kopelman, J. M., … Lowry, C. A. (2016). Immunization with a heat-killed preparation of the environmental bacterium Mycobacterium vaccae promotes stress resilience in mice. *Proceedings of the National Academy of Sciences*, *113*(22), E3130–E3139. http://doi.org/10.1073/pnas.1600324113

Richard, E. M., Helbling, J.-C., Tridon, C., Desmedt, A., Minni, A. M., Cador, M., … Moisan, M.-P. (2010). Plasma transcortin influences endocrine and behavioral stress responses in mice. *Endocrinology*, *151*(2), 649–59. http://doi.org/10.1210/en.2009-0862

Richter, H. G., Torres-Farfan, C., Garcia-Sesnich, J., Abarzua-Catalan, L., Henriquez, M. G., Alvarez-Felmer, M., … Seron-Ferre, M. (2008). Rhythmic expression of functional MT1 melatonin receptors in the rat adrenal gland. *Endocrinology*, *149*(3), 995–1003. http://doi.org/10.1210/en.2007-1009

Sapolsky, R. M., Romero, M., & Munck, A. U. (2000). How Do Glucocorticoids Influence Stress Responses? Integrating Permissive, Suppressive, Stimulatory, and Preparative Actions. *Endocrine Reviews*, *21*(1), 55–89. http://doi.org/10.1210/er.21.1.55

Scherer, I. J., Holmes, P. V, & Harris, R. B. S. (2012). The importance of corticosterone in mediating restraint-induced.pdf, *102*(2), 225–233. http://doi.org/10.1016/j.physbeh.2010.11.014.The

Shavit, Y., Wolf, G., Goshen, I., Livshits, D., & Yirmiya, R. (2005). Interleukin-1 antagonizes morphine analgesia and underlies morphine tolerance. *Pain*, *115*(1–2), 50–59. http://doi.org/10.1016/j.pain.2005.02.003

Silverman, M. N., & Sternberg, E. M. (2012). Glucocorticoid regulation of inflammation

and its functional correlates: from HPA axis to glucocorticoid receptor dysfunction. *Annals of the New York Academy of Sciences*, *1261*, 55–63. http://doi.org/10.1111/j.1749-6632.2012.06633.x

Steru, L., Chermat, R., Thierry, B., & Simon, P. (1985). The tail suspension test: A new method for screening antidepressants in mice. *Psychopharmacology*, *85*, 367–370. http://doi.org/10.1007/BF00428203

Tsigos, C., & Chrousos, G. P. (2002). Hypothalamic – pituitary – adrenal axis , neuroendocrine factors and stress, *53*, 865–871.

Ubeda, C., Lipuma, L., Gobourne, A., Viale, A., Leiner, I., Equinda, M., … Pamer, E. G. (2012). Familial transmission rather than defective innate immunity shapes the distinct intestinal microbiota of TLR-deficient mice. *The Journal of Experimental Medicine*, *209*(8), 1445–56. http://doi.org/10.1084/jem.20120504

Vakharia, K., & Hinson, J. P. (2005). Lipopolysaccharide directly stimulates cortisol secretion by human adrenal cells by a cyclooxygenase-dependent mechanism. *Endocrinology*, *146*(3), 1398–1402. http://doi.org/10.1210/en.2004-0882

Wu, Y., Lousberg, E. L., Moldenhauer, L. M., Hayball, J. D., Coller, J. K., Rice, K. C., … Hutchinson, M. R. (2012). Inhibiting the TLR4-MyD88 signalling cascade by genetic or pharmacological strategies reduces acute alcohol-induced sedation and motor impairment in mice. *British Journal of Pharmacology*, *165*(5), 1319–29. http://doi.org/10.1111/j.1476-5381.2011.01572.x

Wu, Y., Lousberg, E. L., Moldenhauer, L. M., Hayball, J. D., Robertson, S. A., Coller, J. K., … Hutchinson, M. R. (2011). Attenuation of microglial and IL-1 signaling protects mice from acute alcohol-induced sedation and/or motor impairment. *Brain, Behavior, and Immunity*, *25*(SUPPL. 1), S155–S164.

http://doi.org/10.1016/j.bbi.2011.01.012

Zacharowski, K., Zacharowski, P. A., Koch, A., Baban, A., Tran, N., Berkels, R., … Bornstein, S. R. (2006). Toll-like receptor 4 plays a crucial role in the immune-adrenal response to systemic inflammatory response syndrome. *Proceedings of the National Academy of Sciences of the United States of America*, *103*(16), 6392–7. http://doi.org/10.1073/pnas.0601527103

Zhang, G., Yu, L., Chen, Z., Zhu, J., Hua, R., Qin, X., … Zhang, Y. (2016). Activation of corticotropin-releasing factor neurons and microglia in paraventricular nucleus precipitates visceral hypersensitivity induced by colorectal distension in rats. *Brain, Behavior, and Immunity*, *55*, 93–104. http://doi.org/10.1016/j.bbi.2015.12.02

Chapter 3: From stress to innate immune signalling

3.1 Additional effects of TLR4-MyD88 signalling on stress responses: Relationships between behavioural immobility and CORT elevations resulting from stress

Chapter 2 presented the results of chronic and acute inhibition of TLR4-MyD88 signalling on the behavioural and neuroendocrine stress response. The results showed that stress responses were modified in forced swim stress and tail suspension stress, but these adaptations differ between *Tlr4* deficient and *Myd88* deficient mice depending on the stressor administered. Conversely, acute pharmacological antagonists to TLR4 and IL-1R1 did not replicate differences seen in the knockout models, thus suggesting that these behavioural and neuroendocrine differences only emerged after long-term innate immune signalling changes. The data presented in this section were included in the supplementary material accompanying the Chapter 2 manuscript.

Despite significant strain differences in both circulating corticosterone concentrations and immobility behaviour during these stressors, how these adaptations relate to each other is unclear. Thus, linear regression was applied to further investigate the relationship between these behavioural and neuroendocrine changes. The involvement of TLR4 signalling in the induction of CORT signalling seen in Balb/c mice administered with (+)- Naltrexone was also examined using $Tlr4^{-/-}$ mice. Since the deletion of *Tlr4* and *Myd88* both caused an increase in ex vivo CORT secretion from adrenal tissues (Chapter 2, figure 5), immune signalling may either have a direct influence on CORT secretion, or cause an indirect adaptation to adrenal tissue

sensitivity. To test this, LPS was administered in conjunction with ACTH to adrenal tissues, to examine if acute immune stimulation can influence CORT secretion.

3.1.1 CORT response has little relationship with forced swim and tail suspension immobility

Forced swim stress

A linear regression model demonstrated that CORT secretion at 15, 30 and 45 min following the stressor between the mouse strains significantly accounted for variation in behavioural immobility following forced swim stress ($R^2 = 0.36$, $p < 0.001$) (Figure 1). The model output revealed a small positive relationship between CORT levels in *Myd88*$^{-/-}$ animals 45min post forced swim stress ($B = 0.15$, $p<0.02$). There was no significant relationship between circulating CORT concentration after stress and immobility during forced swim stress in all other strains ($p>0.05$).

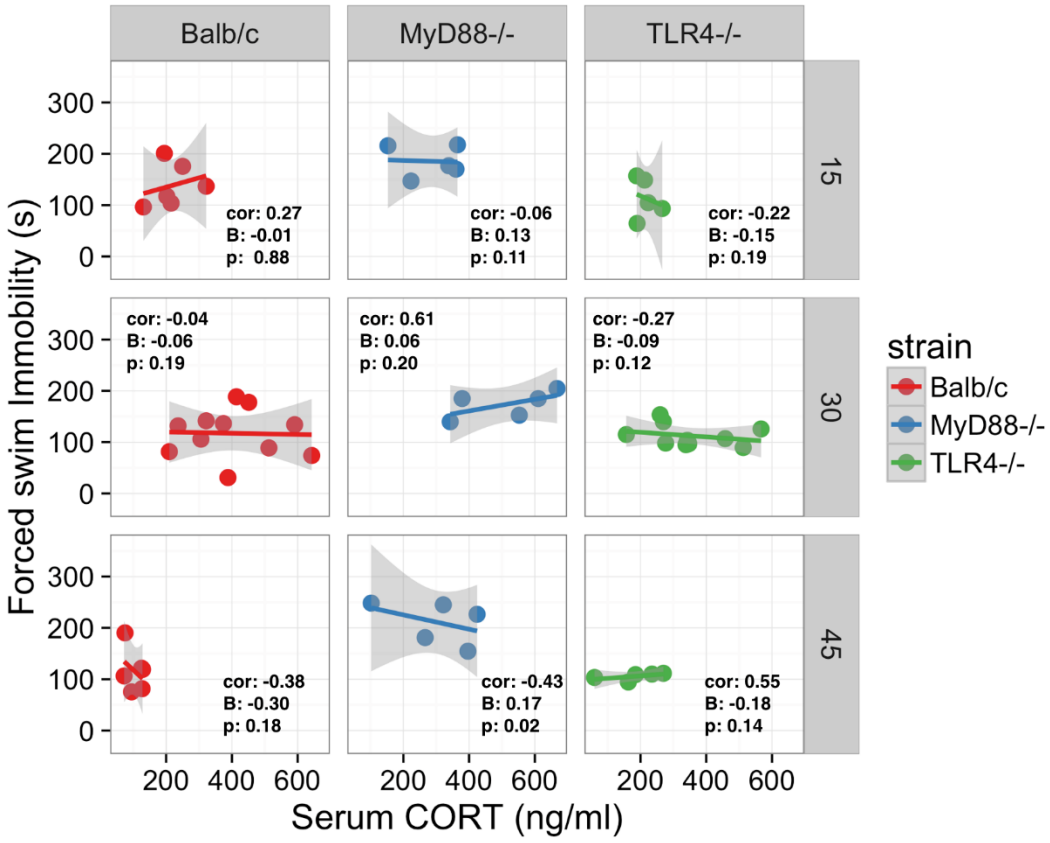

Figure 1. Behavioural immobility during forced swim has little relationship with circulating CORT. Scatter plots describing the relationship between Serum CORT (x-axis) across 15, 30 and 45 min post Forced swim stress, and forced swim immobility (y-axis) in Balb/c, *Myd88*$^{-/-}$ and *Tlr4*$^{-/-}$ mice. Error bands represent 95% confidence intervals.

Tail-suspension stress

A linear model was constructed to investigate if behavioural immobility during tail suspension stress is related to CORT secretion 21, 36 and 51 min following the stressor. The linear model was unable to significantly account for variation in tail suspension immobility ($R^2 = 0.14$, $p = 0.099$) (Figure 2). Furthermore, there was no significant relationship between CORT and behavioural immobility regardless of time or mouse strain ($p>0.05$).

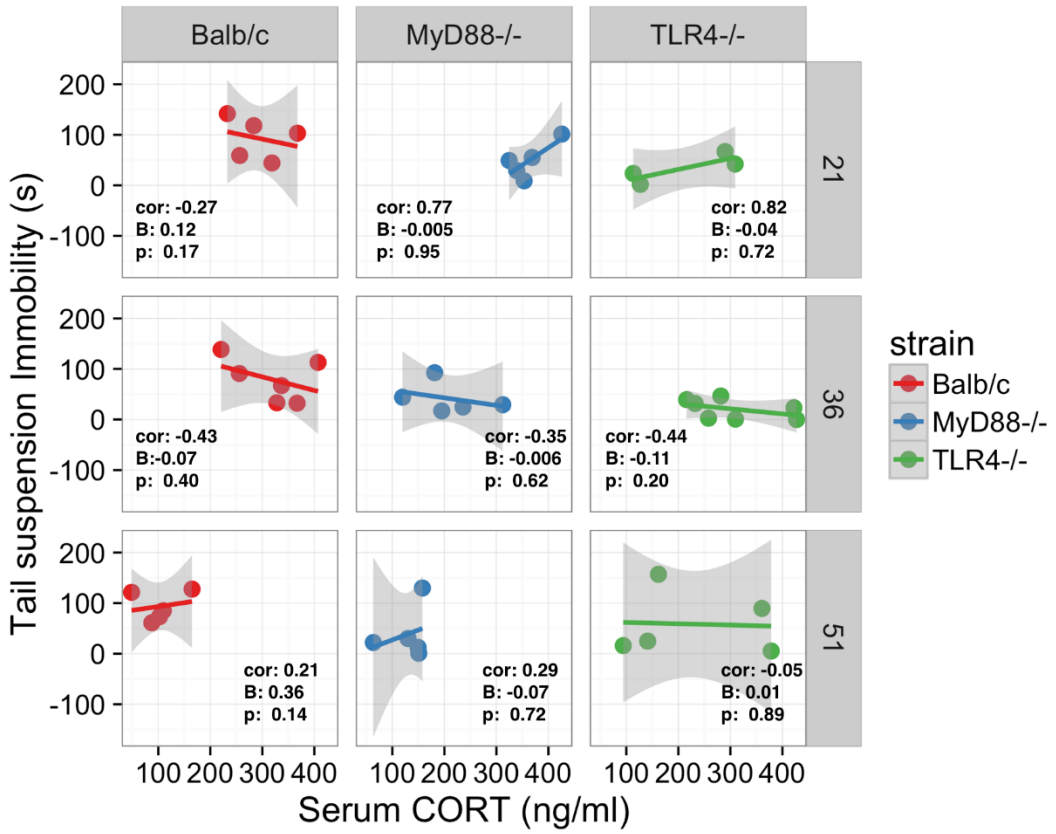

Figure 2. Behavioural Immobility during Tail Suspension stress is not related to circulating CORT in all mouse strains assessed. Scatter plots describing the relationship between Serum CORT (x-axis) across 21, 36 and 51 min post Tail suspension stress, and Tail suspension immobility (y-axis) in Balb/c, *Myd88*$^{-/-}$ and *Tlr4*$^{-/-}$ mice. Error bands represent 95% confidence intervals.

3.1.2 Peak CORT response is related to forced swim stress immobility following IL-1RA and (+)- Naltrexone.

Although there was little relationship between CORT levels and behavioural immobility in naïve mice (Figure 1 and 2), a small positive linear relationship between CORT levels 30 min post stress and forced swim immobility was observed in Balb/c mice treated with IL-1RA ($B = 0.24$, $p<0.05$) or (+)-Naltrexone ($B = 0.13$, $p < 0.05$) (Figure 3). Similar to naïve mice, there was no significant relationship between circulating CORT and forced swim immobility following saline treatment ($B = 0.15$, $p = 0.095$), and no significant relationship between CORT and tail suspension stress regardless of drug treatment ($p>0.05$).

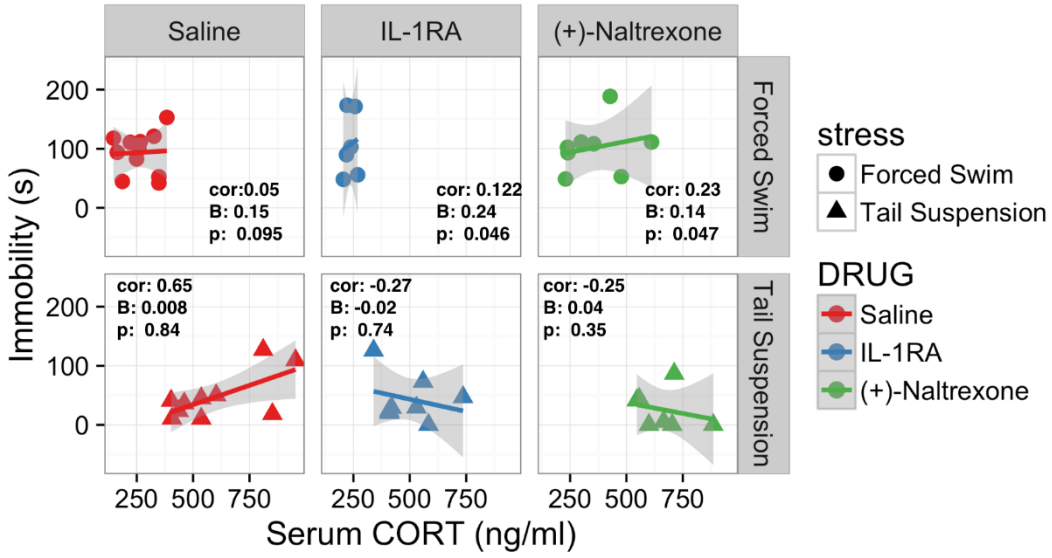

Figure 3. Behavioural Immobility during Forced swim stress has a positive linear relationship with circulating CORT after stress, following IL-1RA and (+)-Naltrexone administration. Tail Suspension immobility is not related to circulating CORT under all drug conditions. Scatter plots describing the relationship between peak Serum CORT (x-axis), and behavioural immobility (y-axis) during either forced swim or tail suspension stress in Balb/c mice. Error bands represent 95% confidence intervals.

3.1.3 (+)- Naltrexone administration elevates serum CORT levels in *Tlr4*$^{-/-}$ mice

Behavioural immobility was not significantly influenced by acute treatment of (+)-Naltrexone or IL-1RA ($F(2,13) = 0.44$, $P = 0.65$) (Figure 4). However, a 2-way ANOVA analysing the effect of forced swim stress and drug treatment on serum CORT in *Tlr4*$^{-/-}$ mice demonstrated significant main effects of forced swim stress ($F(1,28)= 20.0$, $p<0.001$) and drug treatment ($F(2,28) = 7.56$, $p<0.01$), but no significant interaction effect ($F(2,28)= 1.76$, $p=0.19$)(Figure 4B). Further post hoc pairwise multiple comparisons using Tukey corrections revealed that circulating CORT levels was significantly higher in *Tlr4*$^{-/-}$ mice after (+)-Naltrexone when compared to Saline administration (mean difference = 166.8 ng/ml, $p<0.01$) and IL-1RA (mean difference = 124.2 ng/ml, $p<0.05$). Forced swim stress on its own resulted in an average of 150.1 ng/ml increase in circulating CORT ($p<0.001$).

Additionally, forced swim stress significantly increased CORT 30 min after the onset of stress in saline-treated (mean difference = 216.0, $p<0.01$), but not in IL-1RA (mean difference = 114.8 ng/ml, $p=0.35$), and (+)- Naltrexone-treated (mean difference = 62.8 ng/ml, $p= 0.94$) *Tlr4*$^{-/-}$ mice compared to respective drug-treated home cage controls. Interestingly, (+)-Naltrexone itself increased CORT in home cage control *Tlr4*$^{-/-}$ mice compared to saline treated animals (mean difference = 238.7 ng/ml, $p<0.01$).

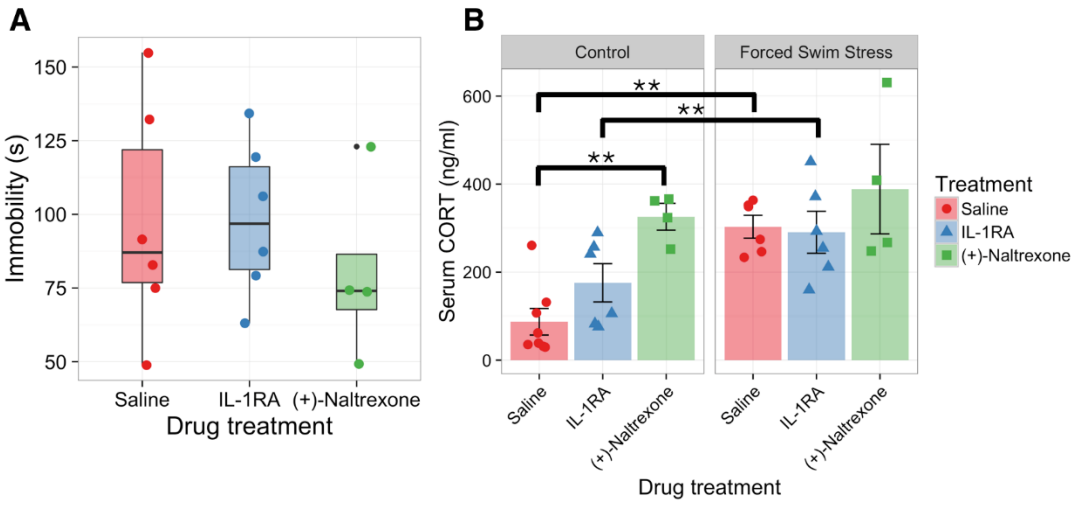

Figure 4. (+)-Naltrexone elevates circulating CORT in Tlr4-/- mice. A) Boxplot of forced swim immobility in *Tlr4*$^{-/-}$ mice administered with either Saline vehicle, IL-1RA (100mg/kg) or (+)-Naltrexone (N = 4 – 5). B) Circulating CORT in TLR4-/- mice administered with either saline vehicle, IL-1RA or (+)- Naltrexone either in home cage controls or 30min after forced swim stress. Error bars represent SEM, p-values represented by * < 0.05, **< 0.01, ***<0.001, ****<0.0001.

3.1.4 LPS does not influence CORT release from adrenals when co-administered with 1 nM ACTH

A linear mixed effects model controlling for repeated measures for each mouse revealed no significant main effect of LPS in modifying 1 nM ACTH-induced CORT release from adrenal tissue isolated from mice (B = 0.83 ng/ml, p = 0.88). When compared to 1 h stimulation, only 6 h of ACTH stimulation significantly elevated CORT concentrations measured (B = 11.79 ng/ml, $p<0.05$). Furthermore, there was no difference in CORT secretion between *Myd88*$^{-/-}$ mice (B = 4.71ng/ml, p = 0.53), or *Tlr4*$^{-/-}$ mice (B = 3.26 ng/ml, p=0.66) and Balb/c mice.

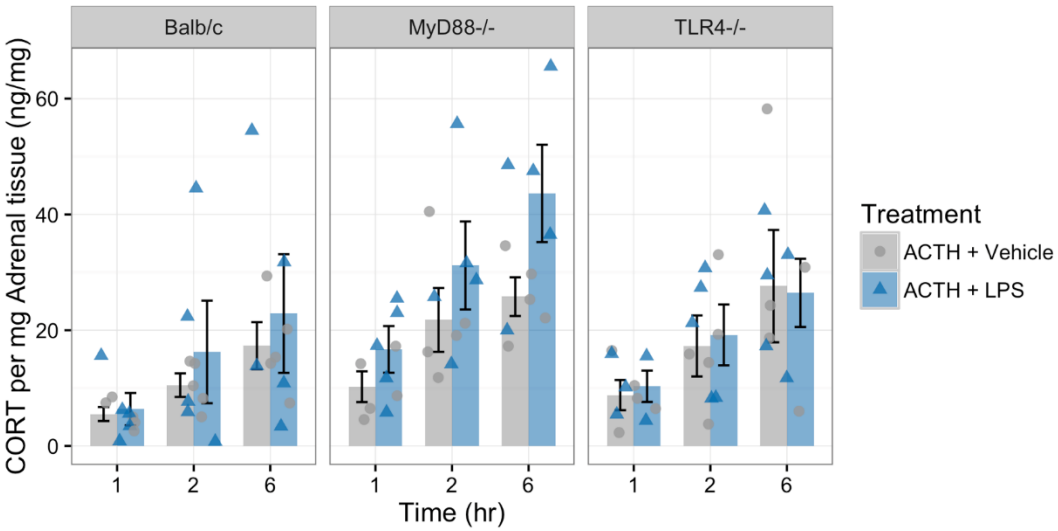

Figure 5. LPS co-administration does not influence adrenal secretion of CORT in response to 1 nM ACTH. Bar graphs representing mean ± SEM of CORT secretion 1 h, 2 h and 6hr following ACTH secretion with either LPS (100 ng/ml) or vehicle co-treatment.

3.1.6 Discussion

Chronic administration of CORT has previously been shown to decrease locomotor activity and increase forced swim immobility anhedonia behaviour (Sturm *et al.*, 2015). The results presented here however, show that immobility performance during forced swim and tail suspension stressors is not indicative of CORT output in response to stressors, since immobility performance was not significantly associated with CORT levels measured after the stressor. Thus, although immobility behaviour can change based on CORT exposure, immobility behaviour may not be an indication of intensity of neuroendocrine responses, and this relationship does not appear to be bidirectional.

The results here show that (+)-Naltrexone, a putative TLR4 inhibitor, demonstrated TLR4-independent actions, since a similar increase in CORT was observed in *Tlr4*$^{-/-}$ mice and Balb/c controls (Chapter 2). The exact mechanism of this increase is unknown, but one possible mechanism may be related to changes in body temperature following drug administration previously observed in other experiments from this group (data not shown). Cold stress is an acute stressor which causes both a decrease in body temperature and increase in circulating ACTH (Van Den Beukel *et al.*, 2015). This decrease in body temperature dynamically interacts with further stressors, in one study causing hyper secretion of CORT and increased body temp in response to restraint stress, but can also decrease the CORT release in response to LPS (Tomoyoshi Miyamoto *et al.*, 2017). Thus, a more in-depth investigation regarding body temperature changes after (+)-Naltrexone treatment is required in future experiments.

Despite increased sensitivity to ACTH in *Myd88*$^{-/-}$ and *Tlr4*$^{-/-}$ adrenals, the lack of LPS-induced CORT secretion from *ex vivo* stimulation of adrenal tissues here suggests that acute TLR4-MyD88 activity in adrenal tissues does not influence ACTH sensitivity of the tissue. This result is consistent with previous findings showing that a conditional knockout of adrenal MyD88 does not influence LPS-induced CORT secretion (Kanczkowski *et al.*, 2013). Furthermore, in combination with the inability of IL-1RA and (+)-Naltrexone to cause changes to the stress response (Chapter 2), acute innate immune signalling thus appears to have little effect on HPA activity. Taken together, these results indicate that deletion of TLR4-MyD88 pathway causes intrinsic differences to HPA secretion, but acute TLR4-MyD88 signalling does not modify adrenal sensitivity to ACTH.

3.2 Bidirectionality: The effects of stress on immune function

Thus far, the results have shown that innate immune signalling can modify HPA responses and behaviour in the whole animal, demonstrating the relationship between the two systems *in vivo*. In the opposite direction, there is growing evidence that acute (Frank *et al.*, 2007) and repeated stressors (Sawicki *et al.*, 2015) can prime the central immune system to over-respond towards an immune stimulus. This effect can be replicated using chronic glucocorticoid treatments, abolished by adrenalectomy, and attenuated by GR pharmacological antagonism (Frank *et al.*, 2012). NLRP3 inflammasome has also been implicated in this priming effect (Zhang *et al.*, 2015), potentially mediating the increased IL-1β responses in this stress-induced priming (Frank *et al.*, 2015; Sobesky *et al.*, 2016). However other groups have shown stress-induced peripheral monocyte migration into the brain, and thus hypothesised that

these recruited monocytes mediate the immune over-responsiveness seen in stress (Wohleb *et al.*, 2014; McKim *et al.*, 2017). The role of resident microglia is therefore difficult to discern, since these effects were tested *in vivo*, and can be mediated by systemic factors.

Given that infiltrating monocytes can eventually differentiate into microglia, and there is currently no clear way to isolate infiltrating monocytes from resident microglia (Ransohoff and Perry, 2009), the increased reactivity of the microglia seen in *ex vivo* models may therefore be influenced by monocyte recruitment. So far, there is no clear understanding that glucocorticoids act on resident microglia to induce this primed state, or if this process is mediated by systemic actions. The direct actions of glucocorticoids in the priming of microglia is therefore currently unresolved.

Furthermore, glucocorticoids can bind to two main receptors, the high abundance but low affinity glucocorticoid receptor (GR) and low abundance but high affinity mineralocorticoid receptor (MR) (Lu *et al.*, 2006). Previous research suggest that GR and MR may mediate different actions of glucocorticoids, and in the immune system, GR actions are immunosuppressive (Dawson *et al.*, 2012), while MR actions are immune stimulatory (Chantong *et al.*, 2012). Using aldosterone as the specific MR agonist, the authors demonstrated that MR activation can increase pro-inflammatory signalling, measured by IL-6, TNF-α protein and gene expression, as well as upstream NF-κB translocation. Since actions of GR and MR in stress-induced priming of microglia is still unclear, the next study therefore aims to test the immunosuppressive and priming actions of glucocorticoids in an in-vitro system modelling microglia.

3.3 Functional differences between BV2 and primary microglia

BV2 cells were chosen as an immunocompetent cell line originating from microglia (Blasi, Barluzzi and Bocchini, 1990). This cell line has previously shown functional signalling from the two main glucocorticoid binding receptors, GR and MR (Chantong *et al.*, 2012; Nakatani *et al.*, 2012). However, due to the immortalization process, some differences from primary microglia are expected. Recent transcriptome and RNAseq analysis show significant differences in gene expression responses to TLR4 and TLR3 signalling (Das *et al.*, 2015, 2016). In these two studies, the authors compared gene expression between BV2 and CD11B positive primary microglia isolated via magnetic separation from neonatal mice. LPS or poly-IC were administered as TLR4 and TLR3 agonists respectively. In their 2015 study, the authors found that BV2 cells were deficient in Interferon regulatory factor 3 (IRF3) -related gene transcription. IRF3 is a transcriptional factor downstream of TRIF-dependent pathway following TLR3 and TLR4 binding, and is an important part of innate immune antiviral responses (Yang *et al.*, 2016). Thus, a lack of IRF3 signalling may thus reduce BV2 cell responsiveness to viral challenges.

Das and colleagues (2016) further investigated differences in LPS-induced gene transcription, comparing BV2 and primary microglial responses 2 and 4 h post LPS treatment. In this study, the researchers found that the gene expression profile 4 h after LPS treatment was markedly different between BV2 cells and microglia, with 35 upregulated genes unique to BV2 cells (out of a total of 399 total genes), 692 upregulated genes unique to primary microglia (out of a total of 946 total upregulated genes). In this analysis, 264 genes were shared between BV2 cells and primary

microglia. Using network analysis, the authors classified these unique genes under transcriptional families in microglia, which included BATF, BATF3, FOXP4, IRF2, IRF5, IRF8, KLR3, NFXL1 and STAT5A. Conversely, shared transcriptional families included NF-κB-dependent genes, IRF1, IRF3, IRF7 IRF9, REL, RELB, STAT1-6 and ATF3. Interestingly, IRF3 was found as a common transcriptional factor, unlike their 2015 study. These results therefore suggest that gene transcription resulting from IRF3 activity may be impaired but not missing, and may be dependent on timing or differences in agonists used. In relation to pro-inflammatory cytokines resulting from LPS treatment, BV2 cells exhibited a lower magnitude of TNF-α gene expression, illustrated by a relative downregulation 4 h post treatment in BV2 cells compared to primary microglia. IL-1β mRNA however, showed a similar scale and relationship between treatments at 2 and 4h post LPS treatment. Thus, the differences between the cell lines in MyD88 – NF-κB dependent signalling may be different in scale, but this is also subject to treatment times and individual gene transcripts.

Another study has also shown overlap and differences between the gene expression profiles after LPS treatment in BV2 cells and primary microglia using a transcriptome approach (Henn *et al.*, 2009). Similar to Das and colleagues 2016, this study found a 90% overlap in BV2 genes, but only a 17% overlap in primary microglia genes 4 h after LPS treatment. Furthermore, CCL3, CCL4, IL-1β, SOCS3, Caspase 9, Caspase 4, BclA1a, Ifit1, Ifit3, IRF1 and TDKi mRNA expression were reduced in BV2 cells 4 and 16 h after LPS treatment. Conversely, similarities in transcription of ICAM, NFKBia, NFKB1-P50/105, TLR2, GP49a and SAAT genes were also found. Taken together, these studies suggest that gene expression profile differs between BV2 cells and primary microglia,

but these appear to be dependent on differential activity of transcriptional factors and timing. Moreover, NF-κB transcriptional factor dependent gene expression were reported as most conserved, while IRF dependent genes vary more between BV2 cells and primary microglia.

Henn et al, (2009) demonstrated that BV2 conditioned media can cause NF-κB translocation, a pro-inflammatory measure, in primary astrocytes. Thus, BV2 cells are able to release pro-inflammatory factors that have paracrine effects. However, the functional differences between BV2 cells and primary microglia are still not well understood. A brief systematic review was therefore conducted to make comparisons between BV2 and primary microglia function.

3.3.1 Method

Articles featuring both BV2 cells and primary microglia were accessed via NCBI's database via search term "(BV2 OR "BV-2") AND "Primary Microglia"", which yielded 153 articles (Figure 6). Inclusion criteria was the following: 1) Articles required to feature both primary microglia and BV2 cells; 2) Both cell types required to undergo the same treatment conditions, and 3) the same measures were performed at the end of the treatment conditions. Of the 153 studies, 121 met the criteria and were included in this review. Performance on each common measure between BV2 cells and primary microglia was assessed, comparing the scale of values and the overall pattern of results.

In addition, the method of primary microglia isolation, treatments and measures were recorded and contrasted. Treatment conditions were further classified as immune-stimulatory, or immune regulatory/inhibitory. Descriptive metrics were processed and graphed in Python 3.5 programming language using Pandas 0.20.2 (McKinney, 2010) and Matplotlib 2.0.2 (Hunter, 2007) libraries.

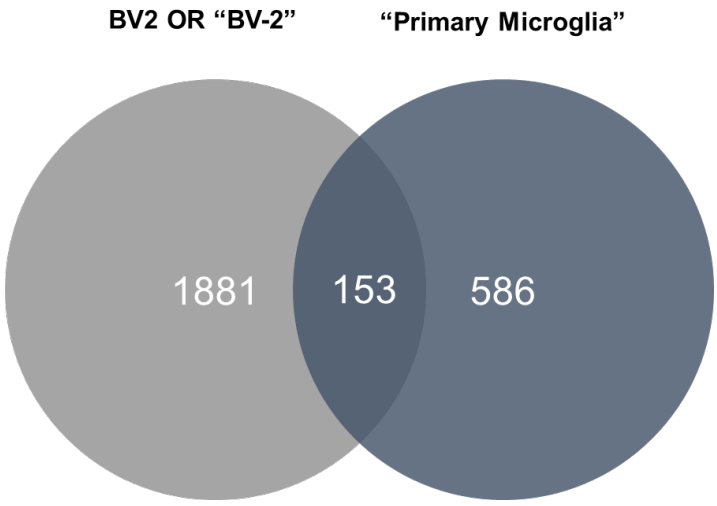

Figure 6. NCBI entries for articles featuring BV2 or Primary microglia.

3.3.2 Results and Discussion

The results of this systematic review are summarised in Table 1. Of the 121 studies sampled, 7 different methods of microglia isolation were used on rat and mouse brain tissue (Figure 7). The most common method was the “shake off’ isolation of neonatal rodents (52 mouse and 40 rat studies), which involves culturing mixed glia in T75 flasks for between 10-21 days before dislodging microglia from adherent astrocytes prior to experimentation (Joseph, Venero and Walker, 2013). These primary microglia appear to have high similarity to BV2 cells across different measures (Figure 7). Notably, primary microglia obtained via CD11b+ magnetic selection appear to be most different from BV2 cells. Specific differences were found in only one study, which showed a lower baseline expression of IL-6, Nos2, ARG1 and IGF1 protein in conjunction with increased Marco and TNF-α mRNA in BV2 cells compared to magnetically selected primary microglia (Flowers *et al.*, 2017). The same study also showed that gene expression was similar in response to IL-4 anti-inflammatory cytokine treatment, but TNF-α elicited lower TNF-α mRNA expression in BV2 cells.

The studies overwhelmingly administered TLR4 agonist, LPS, as the main immune stimulant to elicit response outcomes (76 studies total) (Figure 8A). The distribution of outcome similarities across immune stimulants varied widely, but BV2 cells mostly showed similar outcome patterns compared to primary microglia, except for CX3CR1 protein expression (Figure 8B). After LPS administration, 195 of 205 measures achieved similar outcome patterns between BV2 cells and primary microglia. Of those with similar patterns in results, 37 measures exhibited reduced response magnitude in BV2 cells and 24 showed increased BV2 magnitude of responses. The most frequent

outcome measure applied to LPS treated cells (Figure 9) was NO (20 studies), and most frequent cytokine measures were TNF-α (protein: 16 studies, mRNA: 14 studies), IL-1β (protein: 6 studies, mRNA: 11 studies) and IL-6 (protein: 6 studies, mRNA: 8 studies). Comparatively, anti-inflammatory measures only represented a small proportion of outcomes measured. IL-10 was the only anti-inflammatory cytokine assessed in 4 out of 76 studies using LPS as the immune stimulant.

Most BV2 cell differences after LPS administration were assessed in conjunction with immune regulatory or anti-inflammatory treatments. In one study, primary microglia exhibited more processes per cell overall, and were less sensitive to the immune regulatory conditioned media from mesenchymal stem cells after TLR4 activation (Ooi, Dheen and Sam Wah Tay, 2015). BV2 cells also demonstrated increased sensitivity to LPS treatment, requiring a shorter duration to induce upregulation of IBA-1 protein expression (Horvath *et al.*, 2008). Furthermore, another study showed that while the LPS treatment elicited similar upregulation of IL-1β mRNA in BV2 cells, they were not responsive to CDDO-ME immune regulatory treatment, a synthetic analog of olenolic acid (Tran *et al.*, 2008). Similarly, Bachstetter et al. 2010 showed that BV2 cells displayed a smaller reduction in TNF-α protein after inhibition of p38MAPK after LPS treatment, but a greater reduction in IL-1β protein under the same conditions. This study thus demonstrates a potential differential dependency on p38MAPK for cytokine secretion from BV2 cells. Only one study demonstrated differential BV2 responses to LPS, where BV2 cells exhibited increased CD23 expression, but secreted less IL-10 (Zhang *et al.*, 2013). This study therefore suggests that anti-inflammatory cytokine responses resulting from LPS may be impaired in BV2 cells. Notably, besides TLR4

stimulation, BV2 cells also display similar responses to ischemia and hypoxia (Yao, Kan, Kaur, *et al.*, 2013; Yao, Kan, Lu, *et al.*, 2013; Lallier *et al.*, 2016), and IFN-gamma stimulation. Primary microglia and BV2 cells therefore display some similarity across physiological function, but the sample size for these comparisons are much smaller than canonical TLR4 stimulation using LPS.

Conversely, immune regulatory pathways examined by the studies are not well characterised, since a large proportion of studies administered natural extracts of unconfirmed mechanism (20 of 121 studies), out of 47 total types of immune regulatory agents (Figure 10). The next most used immune regulatory compound is IL-4 cytokine featured in four studies, and cell conditioned media as an immune regulator in three other studies. Given that the functional mechanisms of natural compounds are not well understood, and vary widely between each different compound, few representative studies for each immune inhibitory pathway was investigated. Thus, more studies are required to assess the comparative efficacy of BV2 cell use in the assessment of anti-inflammatory treatments.

Across the studies sampled, 208 total outcome measures were utilised, representing the most diverse set of metrics. Amongst all the outcome measures in the sample, NO is the most frequently employed inflammatory marker across BV2 and primary microglia (31 studies out of 121). From the results across studies, BV2 cells appear to have a similar or higher magnitude of NO release, and largely follow a similar pattern to primary microglia (Figure 11). TNF-α protein and mRNA are the most common pro-inflammatory cytokine measure, followed by IL-1β. Although the pattern between

TNF-α protein and mRNA are similar, the pattern in IL-1β protein (0 uncommon out of 12 measures) secretion appear to be more conserved between primary microglia and BV2 cells as compared to IL-1β mRNA (5 uncommon out of 17 measures). Moreover, BV2 cells exhibit either similar or lower IL-1β mRNA and protein release, suggesting that the magnitude of responses is more likely lower than primary microglia. Intracellular signalling molecules such as Heat shock factor 1 and IKKβ-α, and surface proteins such as CD45, CD80 and CD11b also show similar expressions. Additionally, innate immune functions such as phagocytosis (6 similar out of 8 total measures) and cell motility (1 out of 3 total measures) are also similar between BV2 and microglia.

Similar to studies investigating TLR4 stimulation, assessment of pro-inflammatory measures greatly outnumbers anti-inflammatory measures overall. Again, IL-10 is the only anti-inflammatory measure in the top 14 most frequently assessed outcome, and only reported in five studies, indicating a lack of understanding about anti-inflammatory signalling in these cells. Thus, anti-inflammatory signalling is largely ignored in most studies, and require more investigation.

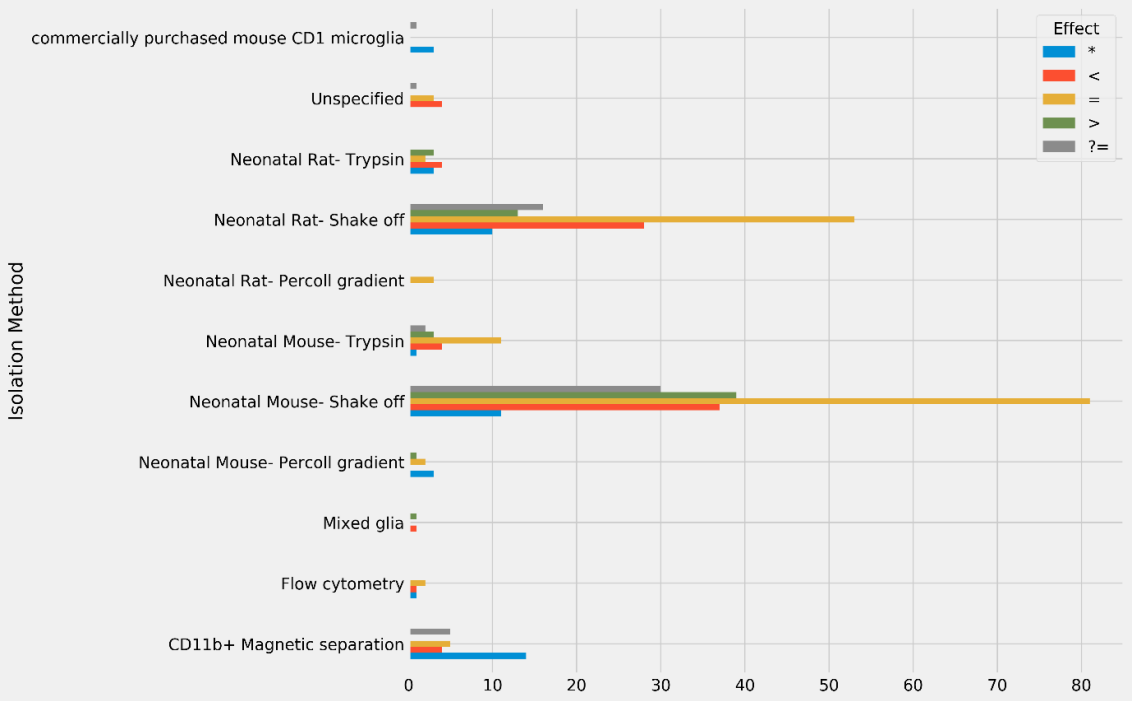

Figure 7. Distribution of outcome similarity between BV2 and primary microglia, grouped according to different primary cell isolation methods. The 'shake off' method was most frequently used to isolate primary microglia from neonatal mice and rats. BV2 cells displayed large similarities across measures with both neonatal mouse and rat derived microglia, with the exception of magnetic separation derived neonatal mouse microglia. Different pattern in outcomes (*; blue), outcome measures lower in magnitude in BV2 cells (<; red), similar scale and pattern of results (=; yellow), outcome measures larger in magnitude in BV2 cells compared to primary microglia (>; green), and magnitude difference unclear, but pattern in outcome measures similar between BV2 cells and primary microglia.

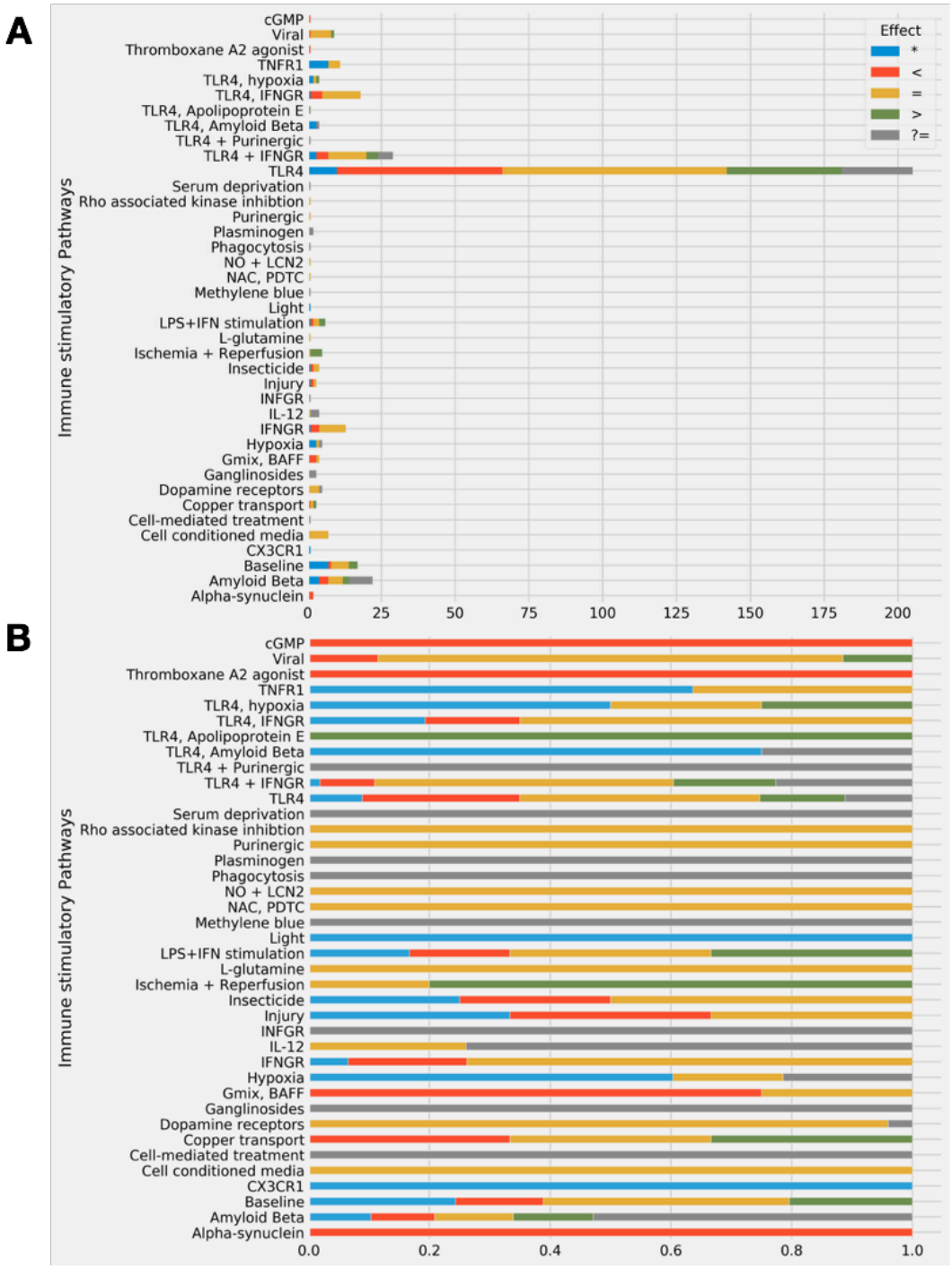

Figure 8. Distribution of outcome similarity resulting from different immune stimulatory treatments. Stacked bar graphs represent total counts (A) and normalised distribution of outcome similarity (B). TLR4 agonist, LPS was used as the primary immune stimulant across studies. Most outcome results compared between BV2 cells and primary microglia were similar, but the scale of these outcomes ranged between studies and outcomes. Different pattern in outcomes (*; blue), outcome measures lower in magnitude in BV2 cells (<; red), similar scale and pattern of results (=; yellow), outcome measures larger in magnitude in BV2 cells compared to primary microglia (>; green), and magnitude difference unclear, but pattern in outcome measures similar between BV2 cells and primary microglia.

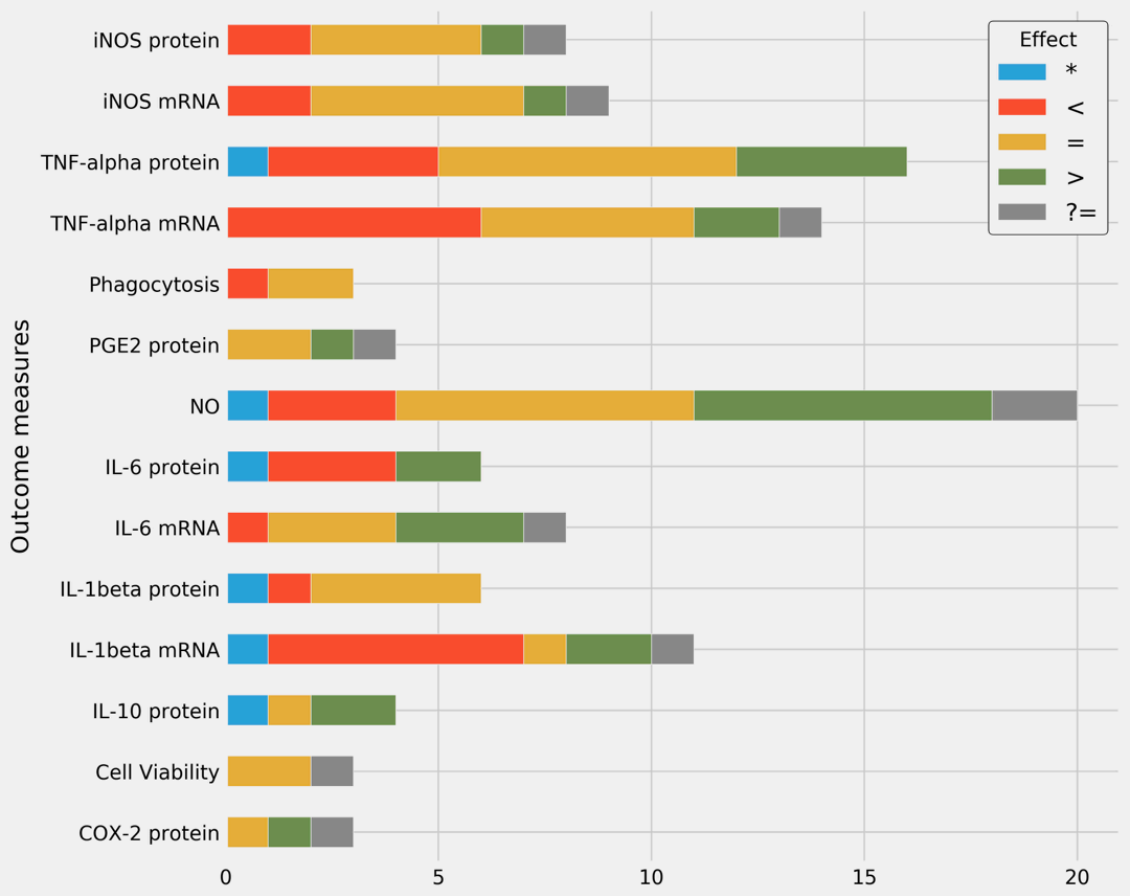

Figure 9. Distribution of outcome similarity across measures applied to LPS-treated cells. Only measures applied more than twice across the whole dataset are displayed. Different pattern in outcomes (*; blue), outcome measures lower in magnitude in BV2 cells (<; red), similar scale and pattern of results (=; yellow), outcome measures larger in magnitude in BV2 cells compared to primary microglia (>; green), and magnitude difference

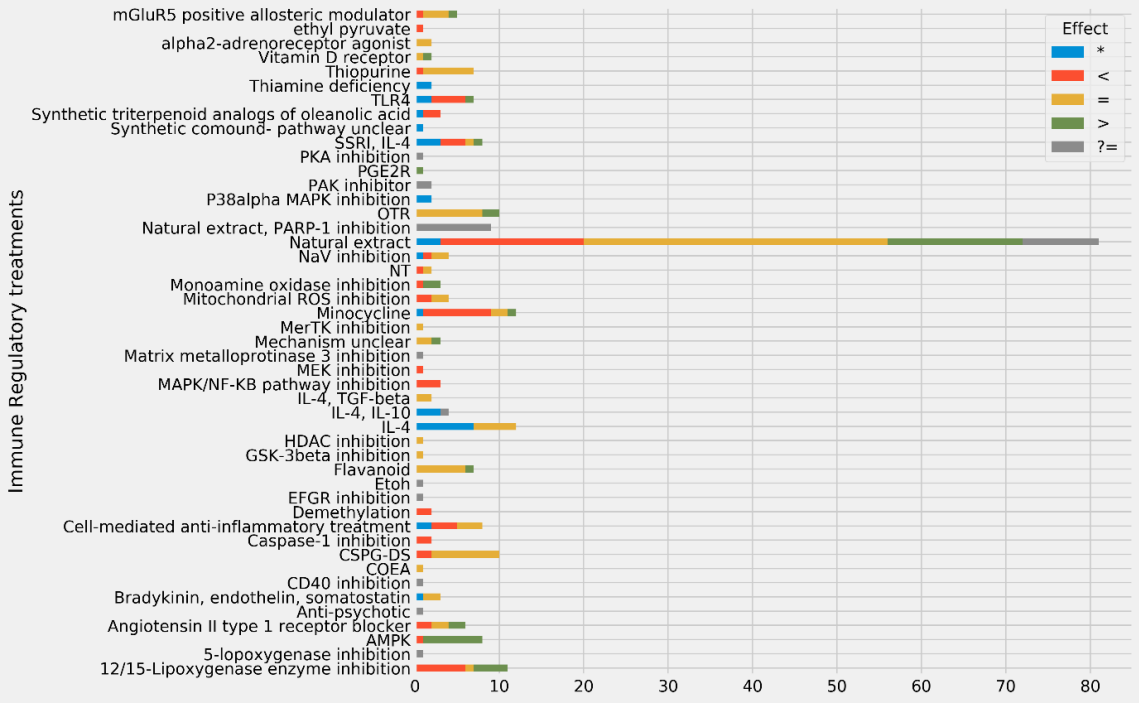

Figure 10. Distribution of outcome similarity resulting from different immune regulatory treatments. Studies that investigated the effects of immune regulatory compounds in both BV2 cells and primary microglia disproportionately used natural extracts or flavonoids. Response patterns appear similar in BV2 and primary microglia across measures following most anti-inflammatory treatments. BV2 responses to IL-4 and IL-10 anti-inflammatory cytokines appear to be most different to primary microglia. Different pattern in outcomes (*; blue), outcome measures lower in magnitude in BV2 cells (<; red), similar scale and pattern of results (=; yellow), outcome measures larger in magnitude in BV2 cells compared to primary microglia (>; green), and magnitude difference unclear, but pattern in outcome measures similar between BV2 cells and primary microglia.

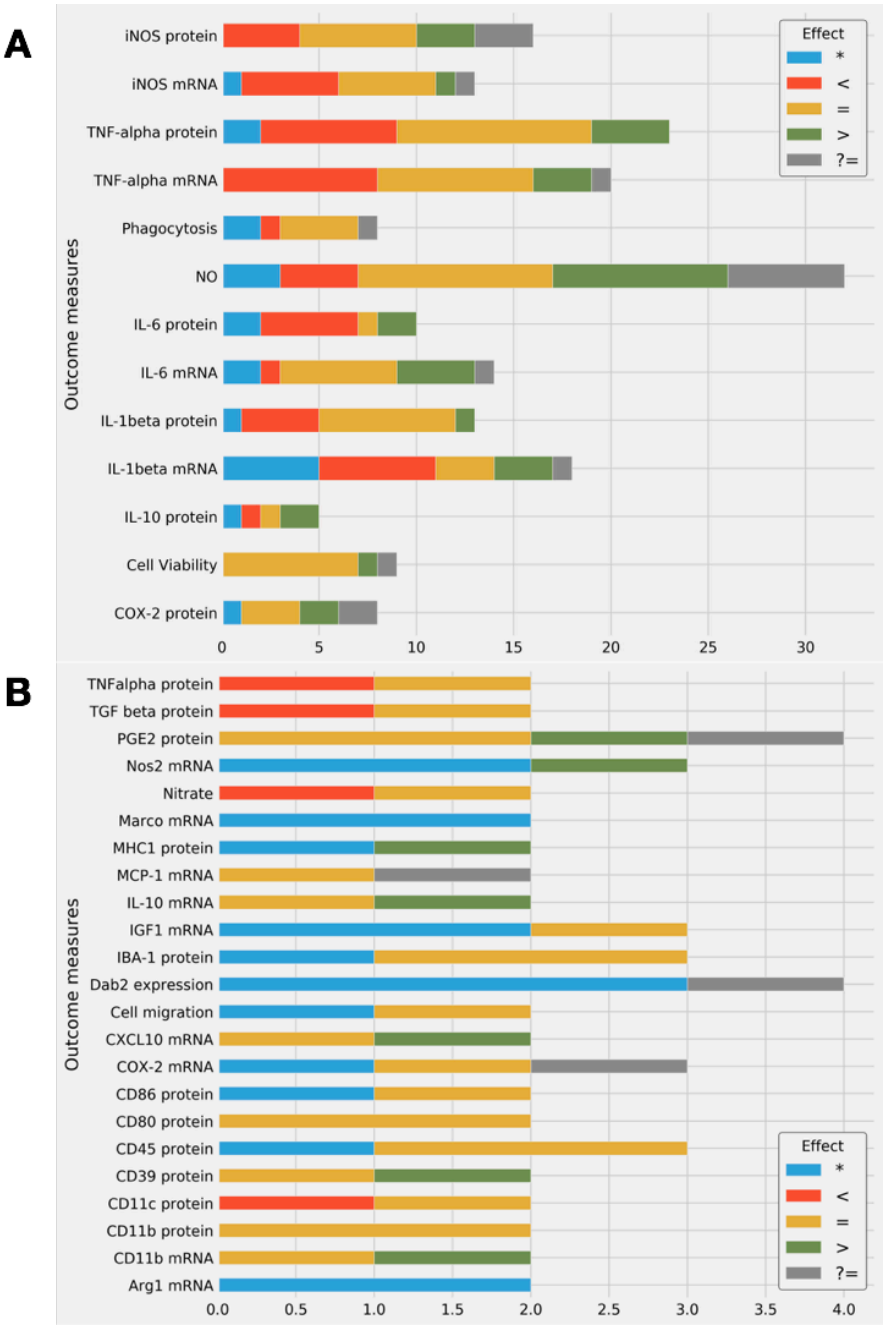

Figure 11. Distribution of outcome similarity across measures. Stacked bar graphs represent distribution of outcome comparisons between BV2 cells and primary microglia across measures repeated at least 5 times (A), and between 2 and 4 times (B). NO is the most measured outcome measure across studies, with most results following similar patterns in BV2 cells and primary microglia. TNF-α and IL-1β are the most commonly measured cytokines. Non-immune signalling molecule measures such as cell viability and phagocytosis are also similar between BV2 and primary microglia. Different pattern in outcomes (*; blue), outcome measures lower in magnitude in BV2 cells (<; red), similar scale and pattern of results (=; yellow), outcome measures larger in magnitude in BV2 cells compared to primary microglia (>; green), and magnitude difference unclear, but pattern in outcome measures similar between BV2 cells and primary microglia.

3.3.3 Conclusion

BV2 cells display a large overlap in the pattern of functional responses when compared directly with primary microglia, while microglia display a larger range of responses at the gene transcription level (Henn *et al.*, 2009; Das *et al.*, 2016). Some differences were seen in TRIF-dependent pathways (Das *et al.*, 2015), but such differences were not well represented by the measures assessed in the current systematic review. In NF-κB related signalling however, BV2 cells exhibit more response similarities with primary microglia, although the scale of these responses is frequently different between the two cell types. Across the studies sampled here, BV2 cells exhibited increased and decreased responses in NF-κB signaling when compared to primary microglia, both in gene and protein expression. Furthermore, IL-1β and TNF-α cytokine responses are largely similar between BV2 cells and primary microglia, while other responses such as NO, iNOS expression, morphological change and phagocytic ability are also conserved to some degree in BV2 cells.

One important consideration in this systematic analysis is the lack of direct comparisons between primary microglia types, namely between adult and neonatal microglia, as well as between cultured and freshly isolated microglia. In a study comparing the phenotypes of adult, neonatal, cultured and cell-line derived microglia, transcriptomic differences were evident between each of these microglia models (Butovsky *et al.*, 2013). Most notably, freshly isolated adult microglia displayed elevated gene expression across multiple genes including Tlr3, Tlr7, chemokine Ccl2, anti-inflammatory cytokine Tgfb, and transcriptional factor Sall1. In this study, the addition of TGF-β and MCSF to culture media in long-term cultures of adult microglia

reversed the relative down regulation of some of these genes measured, suggesting that TGF-β may be able to normalise microglial phenotype in culture. Despite the predominant use of cultured primary microglia, TGF-β was not used to enhance the microglial phenotype in the studies sampled for the current analysis. Thus, it is unknown if the overall significance of these studies can be extrapolated beyond each microglial model used in each of these studies.

Furthermore, LPS was most frequently used as the immune stimulant throughout the studies investigated here, but some evidence also suggests that BV2 cells have also displayed similar responsiveness to Amyloid β, ischemia responses, and cytokine treatments compared to primary microglia. Taken together, BV2 cells are immunocompetent, and can model some pro-inflammatory microglial responses reliably. Despite transcriptional differences seen in recent RNAseq studies, the most well conserved responses seen across studies are TNF-α, NO and IL-1β responses to TLR4 stimulation using LPS. However, the magnitude of these responses can vary frequently, and can be either larger or smaller than, or equivalent to levels seen from primary microglia. Thus, BV2 cells appear adequate for primary mechanistic investigations in LPS- induced responses, but translatability of results from BV2 responses would require further verification in vivo or using primary microglia.

References

Van Den Beukel, J. C., Boon, M. R., Steenbergen, J., Rensen, P. C. N., Meijer, O. C., Themmen, A. P. N. and Grefhorst, A. (2015) 'Cold exposure partially corrects disturbances in lipid metabolism in a male mouse model of glucocorticoid excess', Endocrinology, 156(11), pp. 4115–4128. doi: 10.1210/en.2015-1092.

Blasi, E., Barluzzi, R. and Bocchini, V. (1990) 'Immortalization of murine microglial cells by a v- raf/v- myc carrying retrovirus', Journal of neuroimmunology, 27, pp. 229–237. Available at: http://www.sciencedirect.com/science/article/pii/016557289090073V (Accessed: 26 December 2014).

Butovsky, O., Jedrychowski, M. P., Moore, C. S., Cialic, R., Lanser, A. J., Gabriely, G., Koeglsperger, T., Dake, B., Wu, P. M., Doykan, C. E., Fanek, Z., Liu, L., Chen, Z., Rothstein, J. D., Ransohoff, R. M., Gygi, S. P., Antel, J. P. and Weiner, H. L. (2013) 'Identification of a unique TGF-β–dependent molecular and functional signature in microglia', Nature Neuroscience, 17(1), pp. 131–143. doi: 10.1038/nn.3599.

Chantong, B., Kratschmar, D. V, Nashev, L. G., Balazs, Z. and Odermatt, A. (2012) 'Mineralocorticoid and glucocorticoid receptors differentially regulate NF-kappaB activity and pro-inflammatory cytokine production in murine BV-2 microglial cells', Journal of Neuroinflammation. Journal of Neuroinflammation, 9(1), p. 1. doi: 10.1186/1742-2094-9-260.

Das, A., Chai, J. C., Kim, S. H., Lee, Y. S., Park, K. S., Jung, K. H. and Chai, Y. G. (2015) 'Transcriptome sequencing of microglial cells stimulated with TLR3 and TLR4 ligands', BMC Genomics. BMC Genomics, 16(1), p. 517. doi: 10.1186/s12864-015-1728-5.

Das, A., Kim, S. H., Arifuzzaman, S., Yoon, T., Chai, J. C., Lee, Y. S., Park, K. S., Jung, K. H. and Chai, Y. G. (2016) 'Transcriptome sequencing reveals that LPS-triggered transcriptional responses in established microglia BV2 cell lines are poorly representative of primary microglia', Journal of Neuroinflammation. Journal of Neuroinflammation, pp. 1–18. doi: 10.1186/s12974-016-0644-1.

Dawson, C., Dhanda, A., Conway-Campbell, B., Dimambro, A., Lightman, S. and Dayan, C. (2012) 'NFκB and glucocorticoid receptor activity in steroid resistance.', Journal of receptor and signal transduction research, 32(1), pp. 29–35. doi: 10.3109/10799893.2011.641977.

Flowers, A., Bell-Temin, H., Jalloh, A., Stevens, S. M. and Bickford, P. C. (2017) 'Proteomic anaysis of aged microglia: shifts in transcription, bioenergetics, and nutrient response', Journal of Neuroinflammation. Journal of Neuroinflammation, 14(1), p. 96. doi: 10.1186/s12974-017-0840-7.

Frank, M. G., Baratta, M. V, Sprunger, D. B., Watkins, L. R. and Maier, S. F. (2007) 'Microglia serve as a neuroimmune substrate for stress-induced potentiation of CNS pro-inflammatory cytokine responses.', Brain, behavior, and immunity, 21(1), pp. 47–59. doi: 10.1016/j.bbi.2006.03.005.

Frank, M. G., Thompson, B. M., Watkins, L. R. and Maier, S. F. (2012) 'Glucocorticoids mediate stress-induced priming of microglial pro-inflammatory responses', Brain, Behavior, and Immunity. Elsevier Inc., 26(2), pp. 337–345. doi: 10.1016/j.bbi.2011.10.005.

Frank, M. G., Weber, M. D., Watkins, L. R. and Maier, S. F. (2015) 'Stress sounds the alarmin: The role of the danger-associated molecular pattern HMGB1 in stress-

induced neuroinflammatory priming', Brain, Behavior, and Immunity. Elsevier Inc., pp. 1–7. doi: 10.1016/j.bbi.2015.03.010.

Henn, A., Lund, S., Hedtjärn, M., Schrattenholz, A., Pörzgen, P. and Leist, M. (2009) 'The suitability of BV2 cells as alternative model system for primary microglia cultures or for animal experiments examining brain inflammation.', ALTEX : Alternativen zu Tierexperimenten, 26(2), pp. 83–94.

Horvath, R. J., Nutile-McMenemy, N., Alkaitis, M. S. and DeLeo, J. A. (2008) 'Differential migration, LPS-induced cytokine, chemokine, and NO expression in immortalized BV-2 and HAPI cell lines and primary microglial cultures', Journal of Neurochemistry, 107(2), pp. 557–569. doi: 10.1111/j.1471-4159.2008.05633.x.

Hunter, J. D. (2007) 'Matplotlib: A 2D graphics environment', Computing in Science and Engineering, 9(3), pp. 99–104. doi: 10.1109/MCSE.2007.55.

Joseph, B., Venero, J. L. and Walker, J. M. (2013) Methods in Molecular Biology, vol. 1041. Microglia: Methods and Protocols.

Kanczkowski, W., Alexaki, V., Tran, N., Großklaus, S., Zacharowski, K., Martinez, A., Popovics, P., Block, N. L., Chavakis, T., Schally, A. V and Bornstein, S. R. (2013) 'Hypothalamo-pituitary and immune-dependent adrenal regulation during systemic inflammation.', Proceedings of the National Academy of Sciences of the United States of America, 110(36), pp. 14801–6. doi: 10.1073/pnas.1313945110.

Lallier, S. W., Graf, A. E., Waidyarante, G. R. and Rogers, L. K. (2016) 'Nurr1 expression is modified by inflammation in microglia', NeuroReport, 27(15), pp. 1120–1127. doi: 10.1097/WNR.0000000000000665.

Lu, N. Z., Wardell, S. E., Burnstein, K. L., Defranco, D., Fuller, P. J. and Giguere, V. (2006) 'The Pharmacology and Classification of the Nuclear Receptor Superfamily:

Glucocorticoid, Mineralocorticoid, Progesterone, and Androgen Receptors', Journal of Biological Chemistry, 58(4), pp. 782–797. doi: 10.1124/pr.58.4.9.Multiple.

McKim, D. B., Weber, M. D., Niraula, A., Sawicki, C. M., Liu, X., Jarrett, B. L., Ramirez-Chan, K., Wang, Y., Roeth, R. M., Sucaldito, A. D., Sobol, C. G., Quan, N., Sheridan, J. F. and Godbout, J. P. (2017) 'Microglial recruitment of IL-1β-producing monocytes to brain endothelium causes stress-induced anxiety', Molecular Psychiatry. Nature Publishing Group, (January), pp. 1–11. doi: 10.1038/mp.2017.64.

McKinney, W. (2010) 'Data Structures for Statistical Computing in Python', Proceedings of the 9th Python in Science Conference, 1697900(Scipy), pp. 51–56. Available at: http://conference.scipy.org/proceedings/scipy2010/mckinney.html.

Miyamoto, T., Funakami, Y., Kawashita, E., Nomura, A., Sugimoto, N., Saeki, H., Tsubota, M., Ichida, S. and Kawabata, A. (2017) 'Repeated cold stress enhances the acute restraint stress-induced hyperthermia in mice', Biological and Pharmaceutical Bulletin, 40(1), pp. 11–16. doi: 10.1248/bpb.b16-00343.

Miyamoto, T., Funakami, Y., Kawashita, E., Tomita, S., Nomura, A., Sugimoto, N., Saeki, H., Miyazakia, T., Tsubota, M., Ichida, S. and Kawabata, A. (2017) 'Enhanced Hyperthermic Responses to Lipopolysaccharide in Mice Exposed to Repeated Cold Stress', Pharmacology, 99(3–4), pp. 172–178. doi: 10.1159/000454815.

Nakatani, Y., Amano, T., Tsuji, M. and Takeda, H. (2012) 'Corticosterone suppresses the proliferation of BV2 microglia cells via glucocorticoid, but not mineralocorticoid receptor.', Life sciences. Elsevier Inc., 91(15–16), pp. 761–70. doi: 10.1016/j.lfs.2012.08.019.

Ooi, Y. Y., Dheen, S. T. and Sam Wah Tay, S. (2015) 'Paracrine effects of mesenchymal stem cells-conditioned medium on microglial cytokines expression and nitric oxide production', NeuroImmunoModulation, 22(4), pp. 233–242. doi: 10.1159/000365483.

Ransohoff, R. M. and Perry, V. H. (2009) 'Microglial physiology: unique stimuli, specialized responses.', Annual review of immunology, 27, pp. 119–45. doi: 10.1146/annurev.immunol.021908.132528.

Sawicki, C. M. M., McKim, D. B. B., Wohleb, E. S. S., Jarrett, B. L. L., Reader, B. F. F., Norden, D. M. M., Godbout, J. P. P. and Sheridan, J. F. F. (2015) 'Social defeat promotes a reactive endothelium in a brain region-dependent manner with increased expression of key adhesion molecules, selectins and chemokines associated with the recruitment of myeloid cells to the brain', Neuroscience. IBRO, 302, pp. 151–164. doi: 10.1016/j.neuroscience.2014.10.004.

Sobesky, J. L., D'Angelo, H. M., Weber, M. D., Anderson, N. D., Frank, M. G., Watkins, L. R., Maier, S. F. and Barrientos, R. M. (2016) 'Glucocorticoids Mediate Short-Term High-Fat Diet Induction of Neuroinflammatory Priming, the NLRP3 Inflammasome, and the Danger Signal HMGB1', eNeuro, 3(4), pp. 1–17. doi: 10.1523/ENEURO.0113-16.2016.

Sturm, M., Becker, A., Schroeder, A., Bilkei-Gorzo, A. and Zimmer, A. (2015) 'Effect of chronic corticosterone application on depression-like behavior in C57BL/6N and C57BL/6J mice', Genes, Brain and Behavior, 14(3), pp. 292–300. doi: 10.1111/gbb.12208.

Tran, T. A., McCoy, M. K., Sporn, M. B. and Tansey, M. G. (2008) 'The synthetic triterpenoid CDDO-methyl ester modulates microglial activities, inhibits TNF

production, and provides dopaminergic neuroprotection', Journal of Neuroinflammation, 5(1), p. 14. doi: 10.1186/1742-2094-5-14.

Wohleb, E., McKim, D., Shea, D. and Powell, N. (2014) 'Re-establishment of anxiety in stress-sensitized mice is caused by monocyte trafficking from the spleen to the brain', Biological psychiatry. Elsevier, pp. 1–12. doi: 10.1016/j.biopsych.2013.11.029.

Yang, S., Zhan, Y., Zhou, Y., Jiang, Y., Zheng, X., Yu, L., Tong, W., Gao, F., Li, L., Huang, Q., Ma, Z. and Tong, G. (2016) 'Interferon regulatory factor 3 is a key regulation factor for inducing the expression of SAMHD1 in antiviral innate immunity', Scientific Reports, 6(1), p. 29665. doi: 10.1038/srep29665.

Yao, L., Kan, E. M., Kaur, C., Dheen, S. T., Hao, A., Lu, J. and Ling, E. A. (2013) 'Notch-1 signaling regulates microglia activation via NF-κB pathway after hypoxic exposure in vivo and in vitro', PLoS ONE, 8(11), pp. 1–15. doi: 10.1371/journal.pone.0078439.

Yao, L., Kan, E. M., Lu, J., Hao, A., Dheen, S. T., Kaur, C. and Ling, E. (2013) 'Toll-like receptor 4 mediates microglial activation and production of inflammatory mediators in neonatal rat brain following hypoxia: role of TLR4 in hypoxic microglia', Journal of Neuroinflammation, 10(1), p. 785. doi: 10.1186/1742-2094-10-23.

Zhang, H., Li, Y., Yu, J., Guo, M., Meng, J., Liu, C., Xie, Y., Feng, L., Xiao, B. and Ma, C. (2013) 'Rho kinase inhibitor fasudil regulates microglia polarization and function', NeuroImmunoModulation, 20(6), pp. 313–322. doi: 10.1159/000351221.

Zhang, Y., Liu, L., Liu, Y. Z., Shen, X. L., Wu, T. Y., Zhang, T., Wang, W., Wang, Y. X. and Jiang, C. L. (2015) 'NLRP3 inflammasome mediates chronic mild stress-induced

depression in mice via neuroinflammation', International Journal of Neuropsychopharmacology, 18(8), pp. 1–8. doi: 10.1093/ijnp/pyv006.

Chapter 3: Table

Table 1. Summary table of 121 studies comparing outcome measures between BV2 cells and primary microglia isolated using different methods. Isolation method key: A: Neonatal mouse "shake off", B: Neonatal rat "shake off", At: Neonatal mouse trypsin, Bt: Neonatal rat trypsin, C: Mouse CD11b+ magnetic isolation, E: Neonatal mouse Percoll gradient. BV2 vs PM comparison key: =: Similar scale and relationship between treatments. > Higher magnitude of response in BV2 cells, but similar relationships between treatments. <: Lower magnitude of response in BV2 cells, but similar relationships between treatments. ?=: Scale unclear, but similar relationships between treatments. * Different relationship between treatments in BV2 cells, see notes column for more details.

Study	Author date	Isolation Method	Immune stimulatory treatment	Immune stimulatory pathway	Immune regulatory treatment	Immune regulatory pathway	Measures	BV2 vs PM	Notes
1	Xu et al. 2015[1]	A	LPS 100ng/ml	TLR4	Telmisartan	Angiotensin II type 1 receptor blocker	TNF-α mRNA, IL-1β mRNA	<	
							AMPK phosphorylation, CD206 protein	=	
							IL-10 protein, CD206 YM1/2 mRNA	>	
2	Weng et al. 2017[2]	A	LPS 500ng/ml 6h	TLR4	Ampelopsin (Natural extract) anti-inflammatory treatment	Natural extract	PGE2 protein COX-2 mRNA, IL-1β mRNA and Protein	<	
							NO, iNOS mRNA, TNF-α mRNA, IL-6 mRNA	=	
							TNF-α protein, IL-6 protein	>	

3	Townsend et al. 2016 [3]	E	LPS 100ng/ml 8h	TLR4	Sulforaphane (natural extract) anti-inflamamtory treatment	Natural extract	IL-1β, IL-6, iNOS mRNA	<	
							IL-6 protein	>	
4	Lee et al. 2015[4]	B	LPS 10 ng/ml for primary microglia, 100ng/ml for BV2 cells 16h	TLR4	B-Lapachone (natural extract) anti-inflammatory treatment	Natural extract	ROS, MMP-8 protein	<	
							IL-1β protein, iNOS mRNA, TNF- α mRNA, IL-10 mRNA, MMP3, MMP9 , TIMP-2 protein	=	examined pathways: PKA/CREP, Nrf2/ARE
							NO, TNF-α protein, IL-6 protein, IL-10 protein, IL-1β mRNA, IL-6 mRNA	>	

5	Ni et al., 2015 [5]	A	Oxygen-glucose deprivation + reperfusion	Ischemia + Reperfusion		let-7c-5p microRNA	=	
						iNOS protein, COX-2 protein, TNF-α mRNA, IL-6 mRNA	>	Brain tissue v BV2
6	Gresa-Arribas et al., 2012 [6]	A	TLR4 + IFNGR	LPS+IFN stimulation		MAP2 immunoreactivity	*	Both primary microglia and BV2 cell co-cultures with neurons mediated decrease in neuronal viability (MPA2) in response to LPS+IFN (48 h treatment). Only BV2 cells were sensitive towards extracellular KCl concentrations - higher concentrations induced decreased neuronal cell viability.
						IL-6	<	
						TNF-α protein, COX-2 protein	=	
						iNOS, NO production	>	Neuron- BV2 vs Neuron-primary Microglia co-culture

7	Su et al., 2015 [7]	Bt	LPS+ IFNgamma stimulation	TLR4 + IFNGR	Fluoxetine & S-citalopram (SSRI), IL-4 anti-inflammatory treatment	SSRI, IL-4	IL-6 mRNA		Absolute gene expression fold change after treatment is higher in primary microglia, BV2 cells also less responsive to anti-inflammatory effects of S-citalopram
							TNF-α protein	*	BV2 more sensitive to LPS+IFN-gamma treatment
							IL-1β mRNA	*	Similar in scale of measurements, but BV2 cells are less responsive to anti-inflammatory effects of S-citalopram
							CD-69 protein	*	Similar resposnes to LPS+LFN-gamma, but anti-inflammatory properties of SSRI are different (Inverse dose-relationship of SSRI in primary microglia, but postiive

								relationship in BV2 cells)
							TNF-α mRNA, iNOS mRNA, IL-10mRNA	<
							CD206 protein	=
							IL-1β protein	>
8	Costa et al., 2013 [8]	Unspecified	Cocaine	Dopamine receptors			Cell Viability	=
							CHOP protein	?=
9	Jung et al., 2013 [9]	B	LPS 100ng/ml 24 h	TLR4	short chain ceramides anti-inflamamatory treatments	Mechanism unclear	TNF-α mRNA, IL-10 protein	=
							NO	>
10	Xu et al., 2013 [10]	A	LPS 100ng/ml	TLR4	Baicalein (12/15-Lipoxygenase enzyme inhibitor) anti-inflammatory treatment	12/15-Lipoxygenase enzyme inhibition	TNF-α mRNA, IL-1β mRNA, IL-6 mRANA, IL-12p40 mRNA, CCL20mRNA, LTB4 protein	<
							13-HODE	=
							CXCL10 mRNA, CCL2 mRNA, 12-HETE protein, 15-HETE protein	>

11	Von Leden et al. 2013 [11]	B	808nm Wavelength light	Light			ROS production 24 h after treatment	*	Similar scale of ROS production, but BV2 cells more sensitive to lower Laser power (Joules)
12	Han et al., 2013 [12]	A	24 h LPS (100ng/ml for BV2 and 1 ug/ml for primary microglia)	TLR4	Dalesconols B (natural extract), PJ34	Natural extract, PARP-1 inhibition	NO release, iNOS mRNA, PGE2 protein, COX-2 mRNA, TNF-α mRNA, IL-1β mRNA, IL-6 mRNA, MCP-1 mRNA, MIP-1 α mRNA	?=	
13	Stoica et al., 2014 [13]	B	LPS 100ng/ml	TLR4			Nitrate, TNF-α protein	<	
14	Cizkova et al., 2014 [14]	B	Conditioned media from injured spinal cord tissue	Injury	Bone marrow stromal cell conditioned media(immune modulation)	Cell-mediated anti-inflammatory treatment	NO	*	Similar scale of expression after inflammatory treatment, but BV2 cells less sensistive to Bone marrow stromal cell media exposure-induced recovery
							Ramified cell morphology	<	
							Trans-well Chemotaxis (stimulated by conditioned media or ATP); Cell	=	

							necrosis and apoptosis		
15	Zhang et al., 2014 [15]	B	LPS 1uM 24 h	TLR4	Dexmedotomidine (α2-adrenoreceptor agonist) anti-inflammatory treatment	α2-adrenoreceptor agonist	NO, iNOS protein	=	
16	Hur et al., 2014 [16]	Bt	LPS	TLR4	25-hydroxyvitamin D3 anti-inflammatory treatment	Vitamin D receptor	NO	=	
							1-α hydoxylase	>	
17	Bell-Temin et al., 2015 [17]	commercially purchased mouse CD1 microglia	LPS (5ng/ml, 30ng/ml)	TLR4, Amyloid B	IL4/IL13 , aB immune complex, IL-10	IL-4, IL-10	Dab2 expression	*	Decreased in response to IL-10 treatment in BV2, but increased in primary microglia
							Dab2 expression	*	Decreased in response to aB-IC in BV2 but increased in primary microglia
							Dab2 expression	*	Decresed in response to LPS in

									BV2, but increased in microglia
							Dab2 expression	?=	Increased in response to IL4 + IL-13 in both BV2 and Primary Microglia
18	Ooi et al., 2015 [18]	At	LPS 1ug/ml	TLR4	Mesenchymal Stem cell conditioned medium	Cell-mediated anti-inflammatory treatment	Process number (morphology)	*	Primary microglia exhibit more processes per cell, less sensitive to MSC-CM alone
							IL-6 TNF-α protein	=	
19	Loane et al., 2014 [19]	A	IFNgamma treatment	IFNGR	V70360172 (mGluR5 positive allosteric modulators) anti-inflammatory treatment	mGluR5 positive allosteric modulator	TNF-α protein	<	
							NO	=	
							TNF-α protein,	=	
							NO	>	
20	Zhou et al., 2014 [20]	A	LPS 100ng/ml 6h	TLR4	1,2-dithiocyclopentene-3-thione (hydrogen sulfide donor, caused increase in AMPK activity)	AMPK	Arginase protein	<	

							pAMPK/total AMPK protein ratio, iNOS mRNA, TNF-α mRNA, IL-1β mRNA, IL-6 mRNA, YM1/w mRNA, IL-10 mRNA	>	
21	Duan et al., 2014 [21]	B	HIV-1 Tat protein	Viral			CX3CR1 mRNA, CX3CR1 protein	=	
							TNF-α mRNA, IL-1β mRNA, IL-6 mRNA, CXCL10 mRNA	=	More similar to Rat microglia than Human microglia
22	Flowers et al., 2017 [22]	C	Baseline, TNFα 20ng/ml 24 h, IL4 20ng/ml 24 h	Baseline			Baseline: TNF, IL-1β mRNA, IL6 mRNA, Nos2 mRNA, Marco mRNA, Arg1 mRNA, IGF1 mRNA	*	Baseline: Blunted IL6, nos2,ARG1 and IGF1, increased Marco and TNF mRNA expression in BV2 cells compared to primary microglia
				TNFR1	IL4	IL-4	TNF mRNA, IL-1β mRNA, IL-6 mRNA, Nos2 mRNA, Marco mRNA, Arg1 mRNA, IGF1 mRNA	*	Apart from TNF-α induced TNF-α mRNA, which showed downregulation in BV2 cells compared to upregulation in primary microglia, gene expression was imilar
							ARG1 mRNA, IGF1 mRNA, FIZZ1 mRNA, YM-1 mRNA	=	

23	Wang et al., 2016 [23]	B	LPS 500ng/ml 24 h	TLR4	Forsythiaside A (natural extract) anti-inflammatory treatment	Natural extract	Cell Viability, TNF-α protein, PGE2 protein, IL-1β protein, Nitrate	=	
24	Fu et al., 2016 [24]	B	Y27632 or fasudil (Rho-associated Kinase Inhibitors)	Rho associated kinase inhibtion			Uptake rate (endocytosis)	=	
25	Matt et al., 2016 [25]	C	LPS 100ng/ml 4h	TLR4	5-azacytidine (demethylating agent)	Demethylation	IL-1β promotor methylation, mRNA	<	
26	Kim et al., 2016 [26]	A	LPS 50ng/ml for Primary microglia, 100ng/ml for BV2 24 h	TLR4			Nitric oxide, Cell Viability	?=	
27	Lallier et al., 2016 [27]	E	Maternal LPS+ neonatal hyperoxia for primary microglia, LPS (50ng/ml) + hyperoxia (48h) for BV2	TLR4, hypoxia			IL-1β mRNA, iNOS mRNA	*	BV2 cells increased IL-1β and inos mRNA after LPS+hyperoxia, but no effect was seen in primary microglia
							TGF-β mRNA	=	
							Nurr1 mRNA	>	
28	Zhou et al., 2016 [28]	E	LPS	TLR4			IKKB mRNA	=	
29	Hossain et al., 2017 [29]	Flow cytometry	Permethrin or δmethrin (insecticide compound)	Insecticide	TTX (NAV blocker)	NaV inhibition	Sodium channel protein	*	BV2 missing NAV1.1, 1.5, 1.8

							TNF-α protein	<
							Cell Viability, Intracellular Sodium	=
30	Moidunny et al., 2016 [30]	A	EcoHIV 35ng	Viral			HIV-LTR mRNA	<
							OSM protein	>
31	Yang et al., 2016 [31]	B	U46619 (Thromboxane A2 agonist) U0126 (MEK inhibitor)	Thromboxane A2 agonist	MEK inhibition	MEK inhibition	IL-1β protein	<
32	Wang et al, 2016 [32]	A	LPS 100ng/ml + IFN 10ng/ml 12 h OR IL-4 10ng/ml for 36h	TLR4 + IFNGR	IL-4	IL-4	TRAM1 protein mRNA	=
33	Zhou et al 2016 [33]	Unspecified	α-syn	A-synuclein	zYVAD (caspase-1 inhibitor) for BV2, Caspase-1 knockout for primary microglia	Caspase-1 inhibition	miR-7/US, IL-1β protein	<
34	Gong et al., 2016 [34]	A	LPS 100ng/ml + IFNgamma 10ng/ml 12 h	TLR4, IFNGR			TIRAP mRNA TIRAP protein	=
35	Brandenburg et al., 2010 [35]	B	LPS 100ng/ml 6h/	TLR4	Sulforaphane (natural extract) anti-inflammatory treatment	Natural extract	NF-kB translocation	<
36	Majerova et al 2014 [36]	B	LPS 250ng/ml 24 h	TLR4			Phagocytosis, Intracellular	<

							degredation of Tau protein		
							Phagocytosis	=	
37	Horvath et al. 2008 [37]	B	LPS 1, 5ug/ml 24 or 48 h	TLR4	Minocycline anti-inflammatory treatment	Minocycline	IBA-1 protein	*	BV2 cells requre a shorter duration of LPS treatment to upregulate IBA1 protein expression
							Nitrate production, TNF-α protein, IL-1β protein, pro-IL-1β protein, IL-6 protein, MCP-1 release, pERK 44 protein, pERK 42 protein	<	
							Cell migration, TNF-α protein	=	
							Intracellular IL-1β protein	>	
38	Zhou et al., 2012 [38]	A			IL-4 10ng/ml, TGFβ (1ng/ml) 24 h	IL-4, TGF-β	Morphology, Arg1 Ym1 protein	=	
39	Jia et al., 2012 [39]	A	Amylopid β (20uM) protein	Amyloid B	Berberine (natural extract) anti-inflammatory treatment	Natural extract	IL-6 protein	*	BV2 cells do not show sensitivity to Berberine alone, but respond similarly in Berberine + Aβ
							COX-2 protein, COX-2 mRNA	*	BV2 cells more responsive toward Aβ treatment,

									similar response in Berberine + Aβ
							iNOS protein, iNOS mRNA	<	
							IL-6 mRNA, MCP-1 mRNA, MCP-1 protein	=	
40	Qu et al., 2012 [40]	B	LPS 1ug/ml 30min	TLR4	C225, AG1478 (EGFR inhibitors)	EGFR inhibition	CD11b protein pEGFR protein	?=	
41	Berkovich et al, 2010 [41]	B	FAM-AmyloidB	Amyloid B	Bradykinin, endothelin, somatostatin immune modulators	Bradykinin, endothelin, somatostatin	Phagocytosis	*	BV2 more sensistive to Endothelin treatment
							Phagocytosis, Somatostatin	=	
42	Gresa-Arribas et al, 2010 [42]	At	LPS 100ng/ml + IFN gamma 30ng/ml	TLR4 + IFNGR	Chrysin (flavonoid) anti-inflammatory treatment	Flavanoid	TNF-α protein, iNOS protein, COX-2 protein, Neuronal viability in co-culture, NO production in co-culture, TNFα potein in co-culture	=	
							*	>	
43	Napoli et al., 2009 [43]	A	CX3CL1	CX3CR1			Cell migration	*	BV2 less sensitive to treatment

			LPS 500ng/ml OR IFN-gamma 500U/ml	Baseline			cKIT protein, CD11b protein, CD45 protein, CD34 protein, MHC class II protein, B1 integrin protein	=	
							α4 integrin protein, B7.2, F4/80	>	
				TLR4, IFNGR			Phagocytosis	*	BV2 cells more sensitive to treatment
							iNOS, TNFα protein, TGF β protein, IL-1β protein	<	
							iNOS protein, TNFα protein, TGF β protein, IL-1β protein	=	
44	Pocivavsek et al., 2009 [44]	B	LPS 100ng/ml 24 h	TLR4, Apolipoprotein E			NO	>	
45	Lee et al., 2008 [45]	A	LPS 10ng/ml	TLR4			RGS10 protein	?=	
46	Tran et al., 2008 [46]	A	LPS 10ng/ml 4hr	TLR4	CDDO-ME (Synthetic triterpenoid analogs of oleanolic acid) anti-inflamamtory treatment	Synthetic triterpenoid analogs of oleanolic acid	IL-1β mRNA	*	Absoulute expression is lower in BV2 cells, relationships between LPS treatment similar in BV2, but not responsive to anti-

								inflammatory treatment
							TNF-α mRNA, Mip1α mRNA	<
47	Paradasi et al., 2008 [47]	B	Fluorescent beads	Phagocytosis			Phagocytosis	?=
48	Lee et al., 2007 [48]	B	Ceruloplasmin (copper transport protein)	Copper transport			iNOS mRNA	<
							TNF-α mRNA	=
							IL-1β mRNA	>
49	Jutana et al., 2006 [49]	B	LPS 1ug/ml 4h	TLR4	BW-N 70C (5-lopoxygenase inhibitor) anti-inflammatory treatment	5-lopoxygenase inhibition	NF-kB activity	?=
50	Tzeng et al., 2005 [50]	B	LPS 10ng/ml	TLR4	Neurotropin 3	NT	Phagocytosis	<
							iNos protein	=
51	kim et al., 2005 [51]	A	Serum Deprived Media	Serum deprivation	cMMP-3 (Matrix metalloprotinase 3 inhibitor)	Matrix metalloprotinase 3 inhibition	TNF-α protein	?=
52	Min et al., 2004 [52]	B	Plasminogen	Plasminogen	PAK inhibitor	PAK inhibitor	TNF-α mRNA, IL-1β mRNA	?=
53	Kim et al., 2002 [53]	B	Ganglinosides 50ug/ml	Ganglinosides			STAT 1 phosphorylation	?=

54	Kim et al., 2003 [54]	B	Ganglinosides 50ug/ml, IFN-gamma, LPS	Ganglinosides	Curcumin anti-inflammatory treatment	Natural extract	iNOS, COX-2	?=	
55	Nomura et al., 2017 [55]	B	LPS	TLR4	UNC569 (MerTK inhibitor) anti-inflammatory treatment	MerTK inhibition	Phagocytosis	=	
56	Yu et al., 2017 [56]	A	Baseline				CD39 protein, MHC1 protein	>	
			LPS	TLR4			TNF-α protein		
							IL-10 protein, IL-6 protein		Different expression responses compared to primary microglia
							CD39 protein, CD50 protein, CD80 protein, CCL2	=	
			LPS, IFN gamma	TLR4, IFNGR			MHC1 protein, CD86 protein, CD45 protein		Different expression responses compared to primary microglia
							CD45 protein, CD11b protein, CD11c protein, MHCII protein, CD40 protein, CD80 protein, CD86 protein	=	
57	Huang et al., 2017 [57]	A	Methylene blue	Methylene blue	PKA inhibition	PKA inhibition	Heat shock factor 1 protein	?=	

58	Alqinyah et al., 2017	A	LPS 10ng/ml	TLR4	Trichostatin A (HDAC inhibitor)	HDAC inhibition	RGS10 mRNA	=
59	Lan et al.m 2017 [58]	A	LPS 50ng/ml	TLR4	Pinocembrin (natural extract) anti-inflmmatory treatment	Natural extract	NF-kB protein	?=
60	Jaimes et al., 2017 [59]	C	LPS	TLR4	Mesenchymal stem cell microvesicles	Cell-mediated anti-inflammatory treatment	TNF-α mRNA, IL-1β mRNA	<
							IL-6 mRNA	=
61	Guo et al., 2017 [60]	F	Cocaine	Dopamine receptors			Mir-124 microRNA, DNMT1 (DNA methyltransferase), pri-miR-124-2 and pri-miR-124-2 promoter methylation rate	=
62	Chen et al., 2016 [61]	A	LPS	TLR4	LLDT-8 (natural extract)	Natural extract	Nitrate mRNA, iNOS mRNA, IL-1β mRNA, TNF-α mRNA	<
							Cell Viability	=
63	Gordon et al., 2016 [62]	A	LPS	TLR4			PKCδ mRNA	?=
64	Huang et al. 2016 [63]	B	LPS	TLR4	6-MP (thiopurine) anti-inflammatory treatment	Thiopurine	Nur66 mRNA	<

							TNF-α secretion and mRNA, Nur66/HDAC ratio, pAkt/Akt protein, p-S6K/S6K protein, p-4E-P1 protein, 4E-BP1 protein	=
65	Yuan et al., 2016 [64]	A	LPS	TLR4	Oxytocin anti-inflamamtory treatment	OTR	Oxytocin receptor protein, IBA-1 protein, TNF-α mRNA, TNF-α protein, IL-1β mRNA, IL-1β protein, COX-2 mRNA, iNOS mRNA	=
							COX-2 protein, iNOS protein	>
66	Song et al., 2016 [65]	A	LPS	TLR4	Schizandrin A (Natural extract)	Natural extract	NO, IL-6 mRNA, TNF-α mRNA	>
67	Huang et al., 2016 [66]	A	LPS	TLR4	Z-guggulsterone (natural extract)	Natural extract	iNOS protein	<
							IkBα protein	=
							NO	>
68	Chuang et al., 2015 [67]	C	LPS + IFN-gamma	TLR4 + IFNGR			p-ERK1/2 protein, t-ERK 1/2 protein, p-cPLA2 protein, t-cPLA2, iNOS	?=
69	Zhang et al., 2015 [68]	A	Hypoxia	Hypoxia	resveratrol (natural extract) anti-inflammatory treatment	Natural extract	IBA-1 protein	=

70	Kouchi 2015 [69]	A	LPS	TLR4			MAGL mRNA	?=	
71	Miranda et al., 2015 [70]	Mixed glia	LPS	TLR4			IL-1β mRNA	<	
							Nos2 mRNA	>	
72	Park et al., 2015 [71]	Unspecified	LPS	TLR4	Mito-TEMPO (mitochondrial ROS inhibitor)	Mitochondrial ROS inhibition	TNF-α mRNA, IL-1β mRNA	<	
							IL-6 mRNA, iNOS mRNA	=	
73	Lee et al., 2015 [72]	At			HX10LN (natural extract)	Natural extract	HO-1 protein	?=	
74	Min et al., 2014 [73]	B	LPS	TLR4	EOP (ethyl pyruvate derivative)	ethyl pyruvate	NO	<	
75	Thounaojam et al., 2014 [74]	A	Japanese encphalitis virus	Viral			MIR-155 microRNA	=	
76	Yao et al., 2013 [75]	B	Hypoxia	Hypoxia			Δ-1 mRNA, Notch-1 mRNA, Hes-1 mRNA	*	BV2 cells more sensitive to hypoxia
77	Song et al., 2013 [76]	E	IFN-gamma	IFNGR			NO	*	BV2 cells more sensitive to IFN-gamma
78	Huang et al., 2013 [77]	A	LPS	TLR4	TSG (natural extract) anti-inflammatory treatment	Natural extract	iNOS protein, Apoptosis, NF-kB binding activity	=	
							NO	>	
79	Zhang et al., 2013 [78]	A	LPS	TLR4	LPS	TLR4	IL-10, CD23	*	BV2 more sensitive to LPS in CD23 expression less sensitive in IL-10 expression

							IL-12 protein, CD11c protein, iNOS protein, NO	<	
							Arg-1 protein	>	
80	Kim et al., 2013 [79]	B	LPS	TLR4	GLA (natural extract) anti-inflammatory treatment	Natural extract	NO, iNOS protein, COX-2 protein, p-IKBα/IKBα, p-p38/p38	?=	
81	Yao et al., 2013 [80]	B	Hypoxia	Hypoxia			TLR4 protein	?=	
82	Chung et al., 2013 [81]	At	LPS	TLR4	1H,8H-Pyrano[3,4-c]pyran-1,8-dione anti-inflammatory treatment	MAPK/NF-KB pathway inhibition	NO, TNF-α protein, IL-6 protein	<	
83	Paranjape et al., 2012 [82]	A	Amyloid B protofibrils	Amyloid B			TNF-α mRNA	<	
84	Chung et al., 2012 [83]	At	LPS	TLR4	Phenelzine (monoamine oxidase inhibitor)	Monoamine oxidase inhibition	IL-6 protein	<	
							NO, TNF-α protein	>	
85	Sheng et al., 2011 [84]	A	LPS+LFNgamma	TLR4 + IFNGR			NO	=	
86	Bachstetter et al., 2011 [85]	B	LPS	TLR4	069A (P38α MAPK)	P38α MAPK inhibition	IL-1β protein, TNF-α protein	*	BV2 cells more sensitive to anti-inflammatory treatment
87	Wang et al., 2011 [86]	B	LPS	TLR4	Scutellarin (natural extract) anti-inflammatory treatment	Natural extract	TNF-α protein, iNOS mRNA, TNF-α mRNA, IL-1β mRNA	<	

88	Yeh et al., 2011 [87]	B	C6-derived ECM	Cell conditioned media			IL-1β protein, IL-1β mRNA, IL-18 mRNA, IL-18 protein, IL-6 protein, IL-6 mRNA, Cell Migration	=
89	Wang et al., 2010 [88]	B	LPS	TLR4	GSK-3β inhibitors	GSK-3β inhibition	TNF-α mRNA	=
90	Kao et al., 2011 [89]	B	LPS+ IFN gamma	TLR4 + IFNGR	Luteolin	Natural extract	IL-1β protein, TNF-α protein	=
							NO	>
91	Jiang et al., 2010 [90]	At	ATP	Purinergic			Calcium concentration	=
92	McHugh et al., 2010 [91]	A	Baseline	Baseline			GPR18 mRNA	<
93	Hwang et al., 2010 [92]	At	LPS + IFN-gamma	TLR4 + IFNGR			GITR mRNA, GITRL mRNA	=
94	Nimmervoll et al., 2009 [93]	A	8-Br-cGMP	cGMP			Chomatin condensation	<
95	Svoboda et al., 2009 [94]	A	L-glutamine	L-glutamine			Chromatin condensation	=
96	Pietr et al., 2009 [95]	A	LPS	TLR4			CB2 mRNA, GPR55 mRNA	=
97	Kim et al., 2009 [96]	B	Gmix, BAFF	Gmix, BAFF			IL-6 protein, TNF-α protein, IL-10 protein	<
							BAFF protein	=
98	Son et al., 2008 [97]	B	LPS	TLR4	PN (natural extract) anti-inflammatory treatment	Natural extract	NO, iNOS protein, COX-2 protein	=

							PGE2 protein	>	
99	Jana et al., 2009 [98]	A	IL-12 p40 homodimer	IL-12			IL-16 mRNA	?=	
100	Jana et al., 2009 [99]	A	IL-12 p40 homodimer	IL-12			lymphotoxin-α	?=	
101	Jana et al., 2008 [100]	A	Amyloid B	Amyloid B			TLR3 mRNA, TLR8 mRNA	>	
101	Jana et al., 2008 [101]	A	Amyloid B	Amyloid B			TLR1 mRNA, TLR2 , RNA, TLR4 mRNA, TLR6 mRNA, TLR5 mRNA, TLR7 mRNA, TLR9 mRNA	?=	
102	Zheng et al., 2008 [102]	At	LPS + ATP	TLR4 + Purinergic	Spiperone	Anti-psychotic	NO	?=	
103	Pan et al., 2008 [103]	A	LPS	TLR4	Tripchloride (natural extract) anti-inflammatory treatment	Natural extract	TNF-α protein, IL-1β protein, PGE2 protein, Nitrate	=	
104	Roy et al., 2008 [104]	A	NAC, PDTC	NAC, PDTC			CD11b mRNA	=	
105	Chang et al., 2008 [105]	B	LPS	TLR4	LCY-2-CHO (synthetic compound) anti-inflammatory treatment	Synthetic comound-pathway unclear	NO	*	BV2 more responsive to anti-inflammatory treatment
106	Ebert et al., 2008 [106]	A	IFN-gamma	IFNGR	CSPG-DS	CSPG-DS	Cbr2 mRNA, Irf7 mRNA	<	

							CD28 mRNA, Gas6 mRNA, IFi44 mRNA, Cxcl10 mRNA, Phagocytosis, NO, Cell Viability, Casp3/7 activity	=
107	Zheng et al., 2008 [107]	A	LPS	TLR4	Fisetin (Flavanoid) anti-inflammatory treatment	Natural extract	NO, TNF-α protein	=
108	Jana et al., 2007 [108]	A	LPS	TLR4			IL-6 mRNA	<
							iNOS mRNA, TNF-α mRNA	=
109	Lee et al., 2007 [109]	At	NO + LCN2	NO + LCN2			Cell Viability	=
110	Roy et al., 2006 [110]	A	LPS	TLR4			NO	=
							CD11b mRNA	>
111	Lee et al., 2004 [111]	B	LPS	TLR4	Etoh	Etoh	NO	?=
112	Jana et al., 2003 [112]	A	IL-12p40 OR IL-12p402 OR IL-12p70	IL-12			TNF-α mRNA	=
113	Lee et al., 2003 [113]	A	LPS +/- IFN gamma	TLR4, IFNGR			Cell Viability	=
114	Kim et al., 2003 [114]	B	LPS	TLR4	COEA	COEA	NO	=
115	Suk et al., 2003 [115]	Bt	LPS + IFN	TLR4 + IFNGR	Baicalein	Natural extract	NO	<
							Cell Viability	>

116	Dasgupta et al., 2002 [116]	A	MBP-primed T cells	Cell-mediated treatment			NO	?=	
117	kim et al. 2002 [117]	B	LPS, VIP	TLR4			CD40 mRNA	?=	
118	Jana et al., 2001 [118]	A	IFN-gamma	INFGR	CD40 antibody	CD40 inhibition	NO	?=	
119	Pahan et al., 2001 [119]	A	IL-12p40	IL-12			NO	?=	
120	Park et al., 2000 [120]	A	LPS	TLR4	Thiamine deficiency	Thiamine deficiency	KGDHC activity	*	BV2 more sensitive to treatments
							MTT	*	BV2 less sensitive to treatments
121	Petrova et al., 1999 [121]	B	LPS	TLR4	PGE2	PGE2R	TNF-α protein	>	

Refences

1. Xu, Y. *et al.* Telmisartan prevention of LPS-induced microglia activation involves M2 microglia polarization via CaMKKβ-dependent AMPK activation. *Brain. Behav. Immun.* **50,** 298–313 (2015).
2. Weng, L. *et al.* Ampelopsin attenuates lipopolysaccharide-induced inflammatory response through the inhibition of the NF-κB and JAK2/STAT3 signaling pathways in microglia. *Int. Immunopharmacol.* **44,** 1–8 (2017).
3. Townsend, B. E. & Johnson, R. W. Sulforaphane induces Nrf2 target genes and attenuates inflammatory gene expression in microglia from brain of young adult and aged mice. *Exp. Gerontol.* **73,** 42–48 (2016).
4. Lee, E.-J., Ko, H.-M., Jeong, Y.-H., Park, E.-M. & Kim, H.-S. β-Lapachone suppresses neuroinflammation by modulating the expression of cytokines and matrix metalloproteinases in activated microglia. *J. Neuroinflammation* **12,** 133 (2015).
5. Ni, J. *et al.* MicroRNA let-7c-5p protects against cerebral ischemia injury via mechanisms involving the inhibition of microglia activation. *Brain. Behav. Immun.* **49,** 75–85 (2015).
6. Gresa-Arribas, N. *et al.* Modelling Neuroinflammation In Vitro: A Tool to Test the Potential Neuroprotective Effect of Anti-Inflammatory Agents. *PLoS One* **7,** e45227 (2012).
7. Su, F., Yi, H., Xu, L. & Zhang, Z. Fluoxetine and S-citalopram inhibit M1 activation and promote M2 activation of microglia in vitro. *Neuroscience* **294,** 60–68 (2015).
8. Costa, B. M., Yao, H., Yang, L. & Buch, S. Role of endoplasmic reticulum (ER) stress in cocaine-induced microglial cell death. *J. Neuroimmune Pharmacol.* **8,** 705–714 (2013).
9. Jung, J. *et al.* Biochimica et Biophysica Acta Anti-in fl ammatory mechanism of exogenous C2 ceramide in lipopolysaccharide-stimulated microglia. *BBA - Mol. Cell Biol. Lipids* **1831,** 1016–1026 (2013).
10. Xu, J. *et al.* Inhibition of 12/15-lipoxygenase by baicalein induces microglia PPARβ/δ: a potential therapeutic role for CNS autoimmune disease. *Cell Death Dis.* **4,** e569 (2013).

11. Leden, R. E. Von *et al.* 808 nm Wavelength Light Induces a Dose-Dependent Alteration in Microglial Polarization and Resultant Microglial Induced Neurite Growth. **263,** 253–263 (2013).

12. Han, L. *et al.* Dalesconols B inhibits lipopolysaccharide induced inflammation and suppresses NF-κB and p38/JNK activation in microglial cells. *Neurochem. Int.* **62,** 913–921 (2013).

13. Stoica, B. A. *et al.* PARP-1 Inhibition Attenuates Neuronal Loss, Microglia Activation and Neurological Deficits after Traumatic Brain Injury. *J. Neurotrauma* **31,** 758–772 (2014).

14. Cizkova, D. *et al.* Modulation properties of factors released by bone marrow stromal cells on activated microglia: an in vitro study. *Sci. Rep.* **4,** 7514 (2014).

15. Zhang, X. *et al.* Dexmedetomidine inhibits inducible nitric oxide synthase in lipopolysaccharide-stimulated microglia by suppression of extracellular signal-regulated kinase. *Neurol Res* **37,** 238–245 (2015).

16. Hur, J., Lee, P., Kim, M. J. & Cho, Y.-W. Regulatory Effect of 25-hydroxyvitamin D3 on Nitric Oxide Production in Activated Microglia. *Korean J. Physiol. Pharmacol.* **18,** 397–402 (2014).

17. Bell-Temin, H. *et al.* Novel molecular insights into classical and alternative activation states of microglia as revealed by SILAC-based proteomics. *Mol. Cell. Proteomics* **14,** 1–36 (2015).

18. Ooi, Y. Y., Dheen, S. T. & Sam Wah Tay, S. Paracrine effects of mesenchymal stem cells-conditioned medium on microglial cytokines expression and nitric oxide production. *Neuroimmunomodulation* **22,** 233–242 (2015).

19. Loane, D. J. *et al.* Novel mGluR5 Positive Allosteric Modulator Improves Functional Recovery , Attenuates Neurodegeneration , and Alters Microglial Polarization after Experimental Traumatic Brain Injury. 857–869 (2014). doi:10.1007/s13311-014-0298-6

20. Zhou, X. *et al.* CaMKKβ-Dependent Activation of AMP-Activated Protein Kinase Is Critical to Suppressive Effects of Hydrogen Sulfide on Neuroinflammation. *Antioxid. Redox Signal.* **21,** 1741–1758 (2014).

21. Duan, M. *et al.* HIV-1 Tat disrupts CX3CL1-CX3CR1 axis in microglia via the NF-κBYY1 pathway. *Curr. HIV Res.* **12,** 189–200 (2014).

22. Flowers, A., Bell-temin, H., Jalloh, A., Jr, S. M. S. & Bickford, P. C. Proteomic analysis of aged microglia : shifts in transcription , bioenergetics , and nutrient response. 1–15 (2017). doi:10.1186/s12974-017-0840-7

23. Wang, Y., Zhao, H., Lin, C., Ren, J. & Zhang, S. Forsythiaside A Exhibits Anti-inflammatory Effects in LPS-Stimulated BV2 Microglia Cells Through Activation of Nrf2 / HO-1 Signaling Pathway. *Neurochem. Res.* **41,** 659–665 (2016).

24. Fu, P. *et al.* Rho-Associated Kinase Inhibitors Promote Microglial Uptake Via the ERK Signaling Pathway. *Neurosci. Bull.* **32,** 83–91 (2016).

25. Matt, S. M. *et al.* Aging and peripheral lipopolysaccharide can modulate epigenetic regulators and decrease IL-1β promoter DNA methylation in microglia. *Neurobiol. Aging* **47,** 1–9 (2016).

26. Kim, B.-W. *et al.* A novel synthetic compound MCAP suppresses LPS-induced murine microglial activation in vitro via inhibiting NF-kB and p38 MAPK pathways. *Acta Pharmacol. Sin.* **37,** 334–343 (2016).

27. Lallier, S. W., Graf, A. E., Waidyarante, G. R. & Rogers, L. K. Nurr1 expression is modified by inflammation in microglia. *Neuroreport* **27,** 1120–1127 (2016).

28. Zhou, H. J. *et al.* Downregulation of miR-199b promotes the acute spinal cord injury through IKK??-NF-??B signaling pathway activating microglial cells. *Exp. Cell Res.* **349,** 60–67 (2016).

29. Hossain, M. M., Liu, J. & Richardson, J. R. Pyrethroid Insecticides Directly Activate Microglia Through Interaction With Voltage-Gated Sodium Channels. **155,** 112–123 (2017).

30. Moidunny, S. *et al.* Oncostatin M promotes excitotoxicity by inhibiting glutamate uptake in astrocytes : implications in HIV-associated neurotoxicity. *J. Neuroinflammation* 1–18 (2016). doi:10.1186/s12974-016-0613-8

31. Yang, W. *et al.* Thromboxane A2 receptor stimulation enhances microglial interleukin-1β and NO biosynthesis mediated by the activation of ERK pathway. *Front. Aging Neurosci.* **8,** 1–13 (2016).

32. Wang, H., Liu, C., Han, M., Cheng, C. & Zhang, D. TRAM1 Promotes Microglia M1 Polarization. 287–296 (2016). doi:10.1007/s12031-

015-0678-3

33. Zhou, Y. *et al.* MicroRNA-7 targets Nod-like receptor protein 3 inflammasome to modulate neuroinflammation in the pathogenesis of Parkinson's disease. *Mol. Neurodegener.* **11,** 28 (2016).

34. Gong, L. *et al.* Toll-Interleukin 1 Receptor domain-containing adaptor protein positively regulates BV2 cell M1 polarization. *Eur. J. Neurosci.* **43,** 1674–1682 (2016).

35. Brandenburg, L. O., Kipp, M., Lucius, R., Pufe, T. & Wruck, C. J. Sulforaphane suppresses LPS-induced inflammation in primary rat microglia. *Inflamm. Res.* **59,** 443–450 (2010).

36. Majerova, P. *et al.* Microglia display modest phagocytic capacity for extracellular tau oligomers. *J. Neuroinflammation* **11,** 161 (2014).

37. Horvath, R. J., Nutile-McMenemy, N., Alkaitis, M. S. & DeLeo, J. A. Differential migration, LPS-induced cytokine, chemokine, and NO expression in immortalized BV-2 and HAPI cell lines and primary microglial cultures. *J. Neurochem.* **107,** 557–569 (2008).

38. Zhou, X., Spittau, B. & Krieglstein, K. TGF β signalling plays an important role in IL4-induced alternative activation of microglia. 1–14 (2012).

39. Jia, L. *et al.* Berberine suppresses amyloid-beta-induced inflammatory response in microglia by inhibiting nuclear factor-kappaB and mitogen-activated protein kinase signalling pathways. 1510–1521 (2012). doi:10.1111/j.2042-7158.2012.01529.x

40. Qu, W. *et al.* Inhibition of EGFR / MAPK signaling reduces microglial inflammatory response and the associated secondary damage in rats after spinal cord injury. 1–14 (2012).

41. Fleisher-Berkovich, S. *et al.* Distinct modulation of microglial amyloid beta phagocytosis and migration by neuropeptides. *J. Neuroinflammation* **7,** 61 (2010).

42. Gresa-Arribas, N., Serratosa, J., Saura, J. & Solà, C. Inhibition of CCAAT/enhancer binding protein δ expression by chrysin in microglial cells results in anti-inflammatory and neuroprotective effects. *J. Neurochem.* **115,** 526–536 (2010).

43. Napoli, I., Kierdorf, K. & Neumann, H. Microglial precursors derived from mouse embryonic stem cells. *Glia* **57,** 1660–1671 (2009).

44. Pocivavsek, A., Burns, M. P. & Rebeck, G. W. Low-density lipoprotein receptors regulate microglial inflammation through c-Jun N-terminal kinase. *Glia* **57,** 444–453 (2009).

45. Lee, J.-K. *et al.* Regulator of G-Protein Signaling 10 Promotes Dopaminergic Neuron Survival via Regulation of the Microglial Inflammatory Response. *J. Neurosci.* **28,** 8517–8528 (2008).

46. Tran, T. A., McCoy, M. K., Sporn, M. B. & Tansey, M. G. The synthetic triterpenoid CDDO-methyl ester modulates microglial activities, inhibits TNF production, and provides dopaminergic neuroprotection. *J. Neuroinflammation* **5,** 14 (2008).

47. Paradisi, S. *et al.* Blockade of chloride intracellular ion channel 1 stimulates Aβ phagocytosis. *J. Neurosci. Res.* **86,** 2488–2498 (2008).

48. Lee, K., Yun, S., Nyon, K., Song, Y. & Lee, E. H. Activation of microglial cells by ceruloplasmin. **1,** 1–8 (2007).

49. Jatana, M. *et al.* Inhibition of NF-kappaB activation by 5-lipoxygenase inhibitors protects brain against injury in a rat model of focal cerebral ischemia. *J. Neuroinflammation* **3,** 12 (2006).

50. Tzeng, S. F., Huang, H. Y., Lee, T. I. & Jwo, J. K. Inhibition of lipopolysaccharide-induced microglial activation by preexposure to neurotrophin-3. *J. Neurosci. Res.* **81,** 666–676 (2005).

51. Kim, Y. S. *et al.* Matrix Metalloproteinase-3 : A Novel Signaling Proteinase from Apoptotic Neuronal Cells That Activates Microglia. **25,** 3701–3711 (2005).

52. Min, K.-J., Yang, M.-S., Jou, I. & Joe, E. Protein kinase A mediates microglial activation induced by plasminogen and gangliosides. *Exp. Mol. Med.* **36,** 461–7 (2004).

53. Kim, O. S., Park, E. J., Joe, E. & Jou, I. JAK-STAT Signaling Mediates Gangliosides-induced Inflammatory Responses in Brain Microglial Cells *. **277,** 40594–40601 (2002).

54. Kim, H. Y., Park, E. J., Joe, E. -h. & Jou, I. Curcumin Suppresses Janus Kinase-STAT Inflammatory Signaling through Activation of Src Homology 2 Domain-Containing Tyrosine Phosphatase 2 in Brain Microglia. *J. Immunol.* **171,** 6072–6079 (2003).

55. Nomura, K., Vilalta, A., Allendorf, D. H., Hornik, T. C. & Brown, G. C. Activated Microglia Desialylate and Phagocytose Cells via

Neuraminidase, Galectin-3, and Mer Tyrosine Kinase. *J. Immunol.* 1502532 (2017). doi:10.4049/jimmunol.1502532

56. Yu, A. C., Neil, S. E. & Quandt, J. A. High yield primary microglial cultures using granulocyte macrophage-colony stimulating factor from embryonic murine cerebral cortical tissue. *J. Neuroimmunol.* **307,** 53–62 (2017).

57. Huang, C. *et al.* Methylene blue increases the amount of HSF1 through promotion of PKA-mediated increase in HSF1-p300 interaction. *Int. J. Biochem. Cell Biol.* **84,** 75–88 (2017).

58. Lan, X. *et al.* Pinocembrin protects hemorrhagic brain primarily by inhibiting toll-like receptor 4 and reducing M1 phenotype microglia. *Brain. Behav. Immun.* **61,** 326–339 (2017).

59. Jaimes, Y., Naaldijk, Y., Wenk, K., Leovsky, C. & Emmrich, F. Mesenchymal Stem Cell-Derived Microvesicles Modulate Lipopolysaccharides-Induced Inflammatory Responses to Microglia Cells. *Stem Cells* **35,** 812–823 (2017).

60. Guo, M. L. *et al.* Cocaine-mediated downregulation of microglial miR-124 expression involves promoter DNA methylation. *Epigenetics* **11,** 819–830 (2016).

61. Chen, Y. *et al.* LLDT-8 protects against cerebral ischemia / reperfusion injury by suppressing post-stroke in fl ammation. *J. Pharmacol. Sci.* **131,** 131–137 (2016).

62. Gordon, R. *et al.* Protein kinase C?? upregulation in microglia drives neuroinflammatory responses and dopaminergic neurodegeneration in experimental models of Parkinson's disease. *Neurobiol. Dis.* **93,** 96–114 (2016).

63. Huang, H., Chang, H., Tsai, M., Chen, J. & Wang, M. 6-Mercaptopurine attenuates tumor necrosis factor- α production in microglia through Nur77-mediated transrepression and PI3K / Akt / mTOR signaling-mediated translational regulation. *J. Neuroinflammation* 1–20 (2016). doi:10.1186/s12974-016-0543-5

64. Yuan, L. *et al.* Oxytocin inhibits lipopolysaccharide-induced inflammation in microglial cells and attenuates microglial activation in lipopolysaccharide-treated mice. *J. Neuroinflammation* **13,** 77 (2016).

65. Song, F. *et al.* Schizandrin A Inhibits Microglia-Mediated Neuroninflammation through Inhibiting TRAF6-NF- κ B and Jak2-Stat3

Signaling Pathways. 1–16 (2016). doi:10.1371/journal.pone.0149991

66. Huang, C. *et al.* Z-guggulsterone negatively controls microglia-mediated neuroinflammation via blocking I??B-??-NF-??B signals. *Neurosci. Lett.* **619,** 34–42 (2016).

67. Chuang, D. Y., Simonyi, A., Kotzbauer, P. T., Gu, Z. & Sun, G. Y. Cytosolic phospholipase A2 plays a crucial role in ROS/NO signaling during microglial activation through the lipoxygenase pathway. *J. Neuroinflammation* **12,** 199 (2015).

68. Zhang, L., Li, Y.-J., Wu, X.-Y., Hong, Z. & Wei, W.-S. MicroRNA-181c negatively regulates the inflammatory response in oxygen-glucose-deprived microglia by targeting Toll-like receptor 4. *J. Neurochem.* **132,** 713–723 (2015).

69. Kouchi, Z. Biochemical and Biophysical Research Communications Monoacylglycerol lipase promotes Fc g receptor-mediated phagocytosis in microglia but does not regulate LPS-induced upregulation of in fl ammatory cytokines. *Biochem. Biophys. Res. Commun.* **464,** 603–610 (2015).

70. De Miranda, B. R. *et al.* The Nurr1 Activator 1,1-Bis(3'-Indolyl)-1-(p-Chlorophenyl)Methane Blocks Inflammatory Gene Expression in BV-2 Microglial Cells by Inhibiting Nuclear Factor κB. *Mol. Pharmacol.* **87,** 1021–34 (2015).

71. Park, J. *et al.* Mitochondrial ROS govern the LPS-induced pro-inflammatory response in microglia cells by regulating MAPK and NF-κB pathways. *Neurosci. Lett.* **584,** 191–196 (2015).

72. Suk Lee, D. *et al.* Effective suppression of nitric oxide production by HX106N through transcriptional control of heme oxygenase-1. *Exp. Biol. Med.* **240,** 1136–1146 (2015).

73. Min, S. *et al.* EOP, a newly synthesized ethyl pyruvate derivative, attenuates the production of inflammatory mediators via p38, ERK and NF-??B pathways in lipopolysaccharide-activated BV-2 microglial cells. *Molecules* **19,** 19361–19375 (2014).

74. Thounaojam, M. C. *et al.* MicroRNA 155 Regulates Japanese Encephalitis Virus-Induced Inflammatory Response by Targeting Src Homology 2-Containing Inositol Phosphatase 1. *J. Virol.* **88,** 4798–4810 (2014).

75. Yao, L. *et al.* Notch-1 signaling regulates microglia activation via NF-κB pathway after hypoxic exposure in vivo and in vitro. *PLoS One*

8, 1–15 (2013).

76. Song, D. *et al.* The anti-inflammatory property of human bone marrow-derived mesenchymal stem/stromal cells is preserved in late-passage cultures. *J. Neuroimmunol.* **263,** 55–63 (2013).

77. Huang, C. *et al.* TSG (2,3,4' ,5-tetrahydroxystilbene 2-O-β-D-glucoside) suppresses induction of pro-inflammatory factors by attenuating the binding activity of nuclear factor-κB in microglia. *J. Neuroinflammation* **10,** 129 (2013).

78. Zhang, H. *et al.* Rho kinase inhibitor fasudil regulates microglia polarization and function. *Neuroimmunomodulation* **20,** 313–322 (2013).

79. Kim, B. W. *et al.* Regulation of Microglia Activity by Glaucocalyxin-A: Attenuation of Lipopolysaccharide-Stimulated Neuroinflammation through NF-??B and p38 MAPK Signaling Pathways. *PLoS One* **8,** (2013).

80. Yao, L. *et al.* Toll-like receptor 4 mediates microglial activation and production of inflammatory mediators in neonatal rat brain following hypoxia : role of TLR4 in hypoxic microglia. 1–21 (2013).

81. Chung, H.-S., Kim, S.-N., Jeong, J.-H. & Bae, H. A Novel Synthetic Compound 4-Acetyl-3-methyl-6-(2-bromophenyl)pyrano[3,4-c]pyran-1,8-dione Inhibits the Production of Nitric Oxide and Proinflammatory Cytokines Via the NF-?B Pathway in Lipopolysaccharide-Activated Microglia Cells. *Neurochem. Res.* **38,** 807–814 (2013).

82. Paranjape, G. S., Terrill, S. E., Gouwens, L. K., Ruck, B. M. & Nichols, M. R. Amyloid- β (1 – 42) Protofibrils Formed in Modified Artificial Cerebrospinal Fluid Bind and Activate Microglia. 312–322 (2013). doi:10.1007/s11481-012-9424-6

83. Chung, H. S., Kim, H. & Bae, H. Phenelzine (monoamine oxidase inhibitor) increases production of nitric oxide and proinflammatory cytokines via the NF-κB pathway in lipopolysaccharide-activated microglia cells. *Neurochem. Res.* **37,** 2117–2124 (2012).

84. Sheng, W. *et al.* Pro-inflammatory cytokines and lipopolysaccharide induce changes in cell morphology, and upregulation of ERK1/2, iNOS and sPLA2-IIA expression in astrocytes and microglia. *J. Neuroinflammation* **8,** 121 (2011).

85. Bachstetter, A. D. *et al.* Microglial p38a MAPK is a key regulator of proinflammatory cytokine up-regulation induced by toll-like receptor (TLR) ligands or beta-amyloid (Ab). *J. Neuroinflammation* **8,** 43–53 (2010).

86. Wang, S. *et al.* Neuroprotection of Scutellarin is mediated by inhibition of microglial inflammatory activation. *Neuroscience* **185,** 150–160 (2011).

87. Yeh, W.-L., Lu, D.-Y., Liou, H.-C. & Fu, W.-M. A forward loop between glioma and microglia: glioma-derived extracellular matrix-activated microglia secrete IL-18 to enhance the migration of glioma cells. *J. Cell. Physiol.* **227,** 558–68 (2012).

88. Wang, M., Huang, H., Chen, W., Chang, H. & Kuo, J. Glycogen synthase kinase-3β inactivation inhibits tumor necrosis factor-α production in microglia by modulating nuclear factor κB and MLK3/JNK signaling cascades. *J. Neuroinflammation* **7,** 99 (2010).

89. Kao, T. K. *et al.* Luteolin inhibits cytokine expression in endotoxin/cytokine-stimulated microglia. *J. Nutr. Biochem.* **22,** 612–624 (2011).

90. Jiang, S. X., Benson, C. L., Zaharia, L. I., Abrams, S. R. & Hou, S. T. Abscisic acid does not evoke calcium influx in murine primary microglia and immortalised murine microglial BV-2 and N9 cells. *Biochem. Biophys. Res. Commun.* **401,** 435–439 (2010).

91. McHugh, D. *et al.* N-arachidonoyl glycine, an abundant endogenous lipid, potently drives directed cellular migration through GPR18, the putative abnormal cannabidiol receptor. *BMC Neurosci.* **11,** 44 (2010).

92. Hwang, H., Lee, S., Lee, W. H., Lee, H. J. & Suk, K. Stimulation of glucocorticoid-induced tumor necrosis factor receptor family-related protein ligand (GITRL) induces inflammatory activation of microglia in culture. *J. Neurosci. Res.* **88,** 2188–2196 (2010).

93. Nimmervoll, B., Svoboda, N., Sacha, B. & Kerschbaum, H. H. Sustained elevation of cyclic guanosine monophosphate induces apoptosis in microglia. *Brain Res. Bull.* **80,** 428–432 (2009).

94. Svoboda, N. & Kerschbaum, H. H. L-Glutamine-induced apoptosis in microglia is mediated by mitochondrial dysfunction. *Eur. J. Neurosci.* **30,** 196–206 (2009).

95. Pietr, M. *et al.* Differential changes in GPR55 during microglial cell activation. *FEBS Lett.* **583,** 2071–2076 (2009).

96. Kim, K. S., Park, J.-Y., Jou, I. & Park, S. M. Functional implication of BAFF synthesis and release in gangliosides-stimulated microglia. *J. Leukoc. Biol.* **86,** 349–359 (2009).

97. Son, Y.-H. *et al.* Roles of MAPK and NF-kappaB in interleukin-6 induction by lipopolysaccharide in vascular smooth muscle cells. *J.*

Cardiovasc. Pharmacol. **51,** 71–77 (2008).

98. Jana, M. & Pahan, K. IL-12 p40 homodimer, but not IL-12 p70, induces the expression of IL-16 in microglia and macrophages. *Mol. Immunol.* **46,** 773–783 (2009).

99. Jana, M. & Pahan, K. Induction of lymphotoxin-?? by interleukin-12 p40 homodimer, the so-called biologically inactive molecule, but not IL-12 p70. *Immunology* **127,** 312–325 (2009).

100. Jana, M., Palencia, C. A. & Pahan, K. Fibrillar Amyloid- Peptides Activate Microglia via TLR2: Implications for Alzheimer's Disease. *J. Immunol.* **181,** 7254–7262 (2008).

101. Jana, M. Induction of lymphotoxin- a by interleukin- 12 p 40 homodimer , the so-called biologically inactive molecule , but not IL- 12 p 70. 312–325 (2008). doi:10.1111/j.1365-2567.2008.02985.x

102. Zheng, L. T. *et al.* The antipsychotic spiperone attenuates inflammatory response in cultured microglia via the reduction of proinflammatory cytokine expression and nitric oxide production. *J. Neurochem.* **107,** 1225–1235 (2008).

103. Pan, X. dong *et al.* Neuroprotective role of tripchlorolide on inflammatory neurotoxicity induced by lipopolysaccharide-activated microglia. *Biochem. Pharmacol.* **76,** 362–372 (2008).

104. Roy, A. *et al.* Reactive oxygen species up-regulate CD11b in microglia via nitric oxide: Implications for neurodegenerative diseases. *Free Radic. Biol. Med.* **45,** 686–699 (2008).

105. Chang, L. *et al.* Inhibition of nitric oxide production by the carbazole compound LCY-2-CHO via blockade of activator protein-1 and CCAAT / enhancer-binding protein activation in microglia. **76,** 507–519 (2008).

106. Ebert, S. *et al.* Chondroitin sulfate disaccharide stimulates microglia to adopt a novel regulatory phenotype. *J. Leukoc. Biol.* **84,** 736–740 (2008).

107. Zheng, L. T., Ock, J., Kwon, B. M. & Suk, K. Suppressive effects of flavonoid fisetin on lipopolysaccharide-induced microglial activation and neurotoxicity. *Int. Immunopharmacol.* **8,** 484–494 (2008).

108. Jana, M., Jana, A., Liu, X., Ghosh, S. & Pahan, K. Involvement of Phosphatidylinositol 3-Kinase-Mediated Up-Regulation of I B in Anti-Inflammatory Effect of Gemfibrozil in Microglia. *J. Immunol.* **179,** 4142–4152 (2007).

109. Lee, S. *et al.* A Dual Role of Lipocalin 2 in the Apoptosis and Deramification of Activated Microglia. *J. Immunol.* **179,** 3231–3241 (2007).

110. Roy, A., Fung, Y. K., Liu, X. & Pahan, K. Up-regulation of microglial CD11b expression by nitric oxide. *J. Biol. Chem.* **281,** 14971–14980 (2006).

111. Lee, H. *et al.* Ethanol selectively modulates inflammatory activation signaling of brain microglia. *J. Neuroimmunol.* **156,** 88–95 (2004).

112. Jana, M., Dasgupta, S., Saha, R. N., Liu, X. & Pahan, K. Induction of tumor necrosis factor- a (TNF- a) by interleukin-12 p40 monomer and homodimer in microglia and macrophages. 519–528 (2003). doi:10.1046/j.1471-4159.2003.01864.x

113. Lee, H. *et al.* Role of antiproliferative B cell translocation gene-1 as an apoptotic sensitizer in activation-induced cell death of brain microglia. *J. Immunol.* **171,** 5802–5811 (2003).

114. Kim, J. M. *et al.* Ethyl acetate soluble fraction of Cnidium officinale MAKINO inhibits neuronal cell death by reduction of excessive nitric oxide production in lipopolysaccharide-treated rat hippocampal slice cultures and microglia cells. *J. Pharmacol. Sci.* **92,** 74–78 (2003).

115. Suk, K., Lee, H., Kang, S. S., Cho, G. J. & Choi, W. S. Flavonoid baicalein attenuates activation-induced cell death of brain microglia. *J. Pharmacol. Exp. Ther.* **305,** 638–645 (2003).

116. Dasgupta, S., Jana, M., Liu, X. & Pahan, K. Myelin Basic Protein-primed T Cells Induce Nitric Oxide Synthase in Microglial Cells: IMPLICATIONS FOR MULTIPLE SCLEROSIS. *J. Biol. Chem.* **277,** 39327–39333 (2002).

117. Kim, W. K., Ganea, D. & Jonakait, G. M. Inhibition of microglial CD40 expression by pituitary adenylate cyclase-activating polypeptide is mediated by interleukin-10. *J. Neuroimmunol.* **126,** 16–24 (2002).

118. Jana, M. *et al.* Ligation of CD40 Stimulates the Induction of Nitric-oxide Synthase in Microglial Cells. *J. Biol. Chem.* **276,** 44527–44533

(2001).

119. Pahan, K. *et al.* Induction of Nitric-oxide Synthase and Activation of NF-?? B by Interleukin-12 p40 in Microglial Cells. *J. Biol. Chem.* **276,** 7899–7905 (2001).

120. Park, L. C. H., Calingasan, N. Y., Uchida, K., Zhang, H. & Gibson, G. E. Metabolic impairment elicits brain cell type-selective changes in oxidative stress and cell death in culture. *J. Neurochem.* **74,** 114–124 (2000).

121. Petrova, T. V, Akama, K. T. & Eldik, L. J. Van. Selective Modulation of BV-2 Microglial Activation by Prostaglandin E 2. **274,** 28823–28827 (1999).

Study 2: Effects of corticosterone pre-treatment on TLR4-NF-κB pro-inflammatory responses

- **Chapter 4 – Manuscript:** Corticosterone pre-exposure increases NF-κB translocation and sensitizes IL-1β responses in BV2 microglia-like cells

- **Chapter 5 – Addendum:** CORT pre-treatment inhibits LPS-induced IL-6 production from BV2 cells and IL-1β release from RAW264.7 macrophage-like cells. (pages 41-61)

- **Chapter 6 – Addendum:** Low concentration CORT pre-exposure primes TLR4 mediated NFκB-TNF-α responses in adult primary mouse microglia. (pages 62-76)

- **Chapter 7 – Linking Chapter:** Extracellular ATP and caspase-1 independent IL-1β release; assessing immune activity beyond cytokine release (pages 77-95)

Statement of Authorship

Title of Paper	Corticosterone pre-exposure increases NF-κB translocation and sensitizes IL-1β responses in BV2 microglia-like cells
Publication Status	☐ Published ☐ Accepted for Publication ☒ Submitted for Publication ☐ Unpublished and Unsubmitted work written in manuscript style
Publication Details	Submitted for publication in *Frontiers in Immunology – Molecular Innate Immunity,* and is currently under review

Principal Author

Name of Principal Author (Candidate)	JiaJun Liu
Contribution to the Paper	Designed and condeucted the study, performed data analsyis, interpreted results, prepared and edited the manuscript
Overall percentage (%)	85%
Certification:	This paper reports on original research I conducted during the period of my Higher Degree by Research candidature and is not subject to any obligations or contractual agreements with a third party that would constrain its inclusion in this thesis. I am the primary author of this paper.
Signature	Date **05/09/2017**

Co-Author Contributions

By signing the Statement of Authorship, each author certifies that:

i. the candidate's stated contribution to the publication is accurate (as detailed above);
ii. permission is granted for the candidate in include the publication in the thesis; and
iii. the sum of all co-author contributions is equal to 100% less the candidate's stated contribution.

Name of Co-Author	Dr. Sanam Mustafa
Contribution to the Paper	Supervised the experimental design, results interpretation, planning and editing of the manuscript.
Signature	Date 05/09/2017

Name of Co-Author	Dr. Daniel Barratt		
Contribution to the Paper	Assisted in molecular techniques and analysis methods used in preparing figure 6 of the manuscript, and preparation of written work.		
Signature		Date	05/09/2017

Name of Co-Author	Prof. Mark Hutchinson		
Contribution to the Paper	Supervised the study design, results interpretation, planning and editing of the manuscript.		
Signature		Date	5.9.17

Chapter 4- Manuscript: Corticosterone pre-exposure increases NF-κB translocation and sensitizes IL-1β responses in BV2 microglia-like cells

JiaJun Liu[a,c] , Sanam Mustafa[a,c], Daniel Thomas Barratt[b]

and Mark Rowland Hutchinson[a,c]

a. Adelaide Medical School, Discipline of Physiology, The University of Adelaide, Level 5 Medical School South, Frome Rd, Adelaide, 5005, Australia

b. Adelaide Medical School, Discipline of Pharmacology, The University of Adelaide, Level 5 Medical School North, Frome Road, Adelaide, 5005, Australia

c. Australian Research Council Centre of Excellence for Nanoscale BioPhotonics, University of Adelaide, Australia

Abstract

Corticosterone (CORT), a critical mediator of the hypothalamus pituitary adrenal axis in rodents, is a stress hormone that is classically viewed as possessing immune suppressive properties. CORT is now appreciated to also mediate the neuroimmune priming effect of stress to innate immune stimulation, and hence serves as a mechanistic link to the neuroimmune involvement in stress-related disorders. However, these dichotomous actions of CORT remain poorly defined. This study investigated the conditions and concentration dependency of CORT's actions required to prime the innate immune system. Here we measured the effect of CORT pre-treatment on the downstream pro-inflammatory responses of BV2 mouse microglia-like cells stimulated by lipopolysaccharide (LPS) and TNF-α.

We quantified the concentration dependent CORT-mediated attenuation and enhancement of LPS stimulated inflammatory response. A high physiological concentration (500 nM) of CORT attenuated LPS-induced inflammatory IL-1β cytokine production in a glucocorticoid receptor dependent manner. However, a low concentration (50 nM) of CORT increased expression and release of IL-1β in a mineralocorticoid receptor dependent manner, with accompanied increases in NF-κB translocation and changes to related gene transcription. This was however, not associated with a corresponding increase in total cell expression of NLRP3 protein. These results suggest that a mild elevation in CORT may cause selective adaptations in microglia-like cells to over-respond to a second immune challenge in a non-classical manner, thus partially explaining both pro- and anti-inflammatory effects of CORT reported in the literature.

1. Introduction

1.1Chronic stress can be pro-inflammatory:

Chronic psychological stress is associated with the development of psychosomatic disorders such as post-traumatic stress disorder and major depressive disorder (Liu, Buisman-Pijlman and Hutchinson, 2014; Groer *et al.*, 2015), as well as the exacerbation and persistence of neurological damage (Sorrells *et al.*, 2014; Jones *et al.*, 2015). Yet, while the neuroendocrine responses to stress are well established, the inflammatory nature of the conditions suggests that immune dysregulation plays an integral role in chronic stress.

Chronic stress itself can result in increased pro-inflammatory innate immune responses. For example, blood monocytes of non-professional patient caregivers were found to produce more IL-6 in response to LPS stimulation (Miller *et al.*, 2014). Moreover, physically healthy soldiers with combat experience also exhibited increased plasma C-Reactive-Protein (CRP), an acute-phase protein produced during inflammation, which further correlated with depressive and post-traumatic stress disorder assessment scores (Groer *et al.*, 2015). Meta-analyses have further uncovered a link between physiological stress-related depression and increases in pro-inflammatory factors such as CRP, IL-1 and IL-6, thus implicating an immune consequence of the physiological stress response (Howren, Lamkin and Suls, 2009; Valkanova, Ebmeier and Allan, 2013).

In animal studies, increased pro-inflammatory markers have been observed across several stress paradigms. For example, concurrent neuroendocrine and immune

activation can be observed in the peripheral circulation of animals that have received foot shock stress, illustrating the inter-connected nature between the neuroendocrine and immune system in stress responses (Hueston and Deak, 2014). This study also demonstrated that the administration of neuroendocrine hormones, Adrenocorticotropic hormone (ACTH) and corticosteroid releasing hormone (CRH) is sufficient to stimulate increased inflammatory markers, *Il6* and *COX2* mRNA expression, in the adrenals of the same animals. Social defeat stress models have also elicited increased monocyte infiltration across the blood brain barrier to specific brain sites, and this is associated with increased microglial *Ccl2* and *Il1b* mRNA expression (Sawicki *et al.*, 2015). Additionally, pre-natal restraint stress (Diz-Chaves *et al.*, 2012), and chronic mild stress both induced increased microglial reactivity (Pan *et al.*, 2014). Taken together, stress can result in an inflammatory event *in vivo*.

1.2 Microglia as a key stress sensitive cell type:

Microglia, resident immune-like cells of the CNS, have become central to the investigation of stress effects on inflammation. An increase in hypothalamic IL-1β cytokine as a result of foot shock stress can be blocked by minocycline, a glial attenuator (Blandino, Barnum and Deak, 2006). More recently, stress has been shown to sensitise hippocampal microglial reactivity to LPS stimulation, resulting in increased *Il1b* mRNA (Frank *et al.*, 2012). This effect was attenuated using a glucocorticoid receptor antagonist, thus demonstrating that glucocorticoids (CORT) (the end product of the neuroendocrine stress response) can modify microglial function, causing a 'primed' state to further immune challenges. Their studies have also highlighted the role of the NLRP3 inflammasome in the inflammatory actions of stress. The NLRP3

inflammasome acts to cleave pro-IL-1β into the mature form prior to its release (Frank *et al.*, 2014a). The increased sensitivity of microglia to inflammatory signals could have detrimental consequences for various neurodegenerative diseases (de Pablos *et al.*, 2014; Jones *et al.*, 2015).

1.3 Neuroendocrine stress response and innate immune function:

The implication of glucocorticoids in the immune-priming effect is paradoxical, since CORT is classically regarded as strongly immune suppressive (Muzikar, Nickols and Dervan, 2009; Du *et al.*, 2012; Silverman *et al.*, 2012). However, there is some evidence that the timing of the immune challenge is important. It has been hypothesised that CORT is anti-inflammatory in the acute phase during stressor onset, but can sensitize the immune system during the "recuperation-phase" after the stressor has been resolved (Frank, Watkins and Maier, 2013). This effect could also be in conjunction with alterations to the innate immune system, most notably the TLR4 pathway which is capable of responding to endogenous and exogenous factors, or the inflammasome pathway which is necessary for the production and release of IL-1β and IL18 (Liu, Buisman-Pijlman and Hutchinson, 2014). However, direct actions of CORT in this priming effect on microglia are not well understood.

To test the hypothesis that CORT can be anti-inflammatory during ongoing exposure, but can leave the immune system sensitized after its removal, the current study aimed to investigate the pro- and anti-inflammatory actions of CORT in microglia-like BV2 cells, focusing on the IL-1β release pathway following NF-κB activation through administration of LPS and TNF-α as innate immune stimulants. Given the importance of

the inflammasome in the conversion and release of IL-1β, the role of the NLRP3 inflammasome in those effects was also investigated.

2. Materials and Methods

2.1 Cell Culture

BV2 microglia-like cell lines were maintained in Dulbecco's modified Eagle's medium (DMEM) supplemented with 10 % (v/v) foetal bovine serum (FBS) and 2 mM L-glutamine + 50 U/ml Penicillin + 50 ug/ml Streptomycin + 100 μg/ml Normocin. Cells were grown in a humidified incubator of 95%air/5%CO2 at 37°C. BV2 cells were seeded at a density of 7.5 x 10^4 cells/ well in 24-well plates for cytokine experiments, 5 x 10^4 cells/well in 12-well plates for fluorescent immunocytochemistry analysis, and 2 x 10^5 cells/well in 6-well plates for gene expression studies.

2.2 Experimental design and *in vitro* cell treatment timing

A concentration response was characterised using BV2 cells pre-treated with 50 nM – 1 μM corticosterone (CORT) or volume-matched ethanol vehicle for 24 h prior to LPS (100 ng/ml) or vehicle treatment conditions. Pre-treatment was either left present during immune stimulation (co-treatment model), or removed prior to immune stimulation (pre-exposure model) and supernatant IL-1β was measured. The selection of the 24 h time point for CORT pre-treatment at the concentration of 50 nM was further verified in a time response (0.5h – 24 h). A 24 h administration of 50 nM and 500 nM of CORT pre-treatment was selected for further experiments measuring 100 ng/ml TNF-α (R&D systems, 410-MT/CF, USA) -induced supernatant IL-1β release, as well as LPS- induced NF-kB translocation. Concurrent IL-1β release with intracellular protein expression was also measured after 24 h LPS treatment, while gene transcription was measured after 6 and 24 h of LPS administration (Figure 1). Collected supernatants were centrifuged at 500 g for 10 min at 4 °C, and cells were harvested to prepare cell lysates for further western blot or qPCR analysis. All treatments were

paired with respective concentration-matched vehicle controls within each biological replicate.

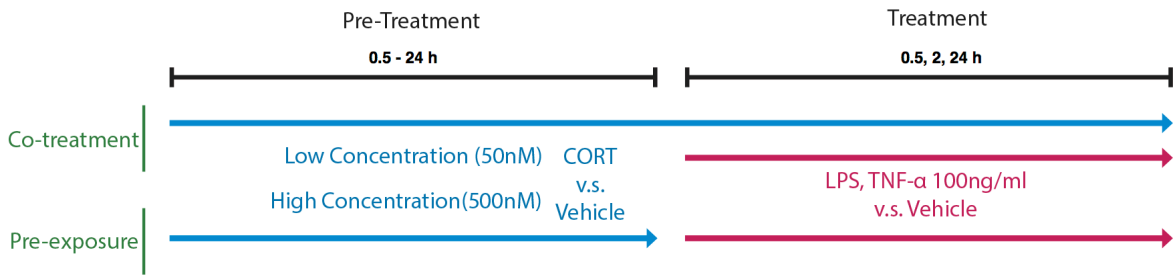

Figure 1. A schematic of the in vitro cell treatment timing of pre-exposure and co-treatment paradigms.

2.3 Protein and released cytokine quantification

Intracellular NLRP3 and pro-IL-1β were quantified using western blot analysis. Following treatment, adherent cells were washed 3 times in 1 ml ice-cold PBS, then incubated on ice with 100 µl RIPA buffer for 5 min. Cell lysates were transferred to 1.5 ml tubes and rotated on a tube rotator at 4°C for 1 h. Cell lysates were centrifuged at 20,000 g at 4°C for 10 min to remove cellular debris. Protein concentration was determined (BCA assay [Thermo Fisher]) and normalised to 1 µg/µl in laemmli buffer and stored at -80°C before analysis by SDS-PAGE and western blotting. Twenty-five micrograms of total protein was resolved on a 4-12% bis-tris gel at a constant 200 V, and transferred onto nitrocellulose membranes at 20 V. Membranes were blocked for 2 hours at room temperature in 5% skim milk in TBS-tween20 and incubated overnight at 4°C in primary antibodies for HMGB1 (Abcam 19256 1:2000), NLRP3 (adipogen AG-20B-0014, 1:2000), pro-IL-1β (Abcam 9722, 1:1000), and loading control B Actin (Sigma-Aldrich A2066, 1: 2000). Appropriate secondary antibodies (1:10000 dilution) conjugated to either 700 nm or 800 nm infrared fluorophores were applied for 1 h at

room temperature, and blots were developed using the Odyssey scanner. Western blot image analysis was performed using imageJ (64-bit) software.

Released cytokines were measured using ELISA for IL-1β (BD bioscience 559603) in half-area 96 well plates according to manufacturer's specifications. Absorbance wavelengths (405 nm signal - 560 nm signal correction), indicating IL-1β levels, were measured using a Synergy MX plate reader (Biotek). IL-1β levels were quantified against known concentrations of IL-1β standards between 15.625 pg/ml – 2000 pg/ml. Assay acceptance criteria were determined by an R^2 value larger than 0.95 for standard curve fit.

2.4 Nuclear Translocation of NF-κB and changes in cell morphology

NF-κB is a transcription factor downstream of innate immune receptor activation, and is usually bound to Ikkb in the cytoplasm. The p65 subunit translocation to the nucleus is indicative of increased transcription of pro-inflammatory genes, and therefore is a measure of the innate immune response (see Medzhitov & Horng 2009 for a review). BV-2 cells display NF-κB/p65 nuclear translocation in response to LPS exposure (Cao *et al.*, 2010).

Intracellular localisation of NF-κB was quantified using fluorescent immunocytochemistry. Briefly, BV2 cells were plated onto poly-D-lysine coated coverslips. BV2 cells underwent either low (50 nM) or high (500 nM) concentration CORT or vehicle pre-exposure for 24 h prior to replacement with 1 ug/ml LPS or vehicle for a further 30 min or 2 h. Cells were fixed in 4% PFA with 5% sucrose for 10 min and

stained with the respective antibodies (Rabbit anti- NF-κB, 1:500, Abcam ab 16502) for 2 hours. Secondary antibodies (Donkey anti-Rabbit 488, 1:1000 dilution, Life Technologies A21206; 488 nm excitation), DAPI (405 nm excitation, 1:10 000; nuclear stain) and Wheat Germ Agglutin (633 nm excitation, 1:200; membrane stain) were then added for a further 1 h. Following staining, coverslips were inverted and mounted onto slides and imaged under the confocal microscope (Leica SP-5).

Nuclear translocation of NF-κB was quantified via measuring the intensity values of DAPI (nucleus), NF-κB and WGA (cell membrane) across the longest diameter of the cell, yielding an intensity profile plot for each cell. This was applied to 15 cells per image using FIJI's distribution of ImageJ-64 bit (Schindelin *et al.*, 2012). NF-κB expression was measured by integrating the area under curve using the trapezoid method between the bounds of the nucleus, and between the bounds of the cell membrane. The proportion of NF-κB expression in the nucleus vs total was further normalised to the proportion of nucleus diameter to total cell diameter, thus describing the distribution of NF-κB within the cell:

$$Nuclear\ Translocation = \frac{NF-\kappa B\ expression\ within\ nucleus}{Total\ cell\ NF-\kappa B} \div \frac{Nucleus\ Diameter}{Cell\ Diameter}$$

Where:

Nuclear translocation degree = 1 would indicate an even distribution of NF-κB between nucleus and cytoplasm, <1 would indicate distribution of NF-κB favouring the cytoplasm, and >1 indicates NF-κB distribution favouring the nucleus.

BV2 cells can present with morphological changes, which can be associated with phagocytic capacity (Laurenzi *et al.*, 2001). Furthermore, since microglia retract their processes and become amoeboid shaped in response to LPS (Kloss *et al.*, 2001), we thus measured the morphological change in BV2 cells in response to LPS following 50 nM CORT pre-exposure. Due to the rod-shaped morphology of BV2 cells, cell shape was inferred by measuring the change in proportion of nucleus diameter to cell diameter across the widest width of each cell. For example, a retraction of cell processes, reflected by a reduction in total cell diameter, and an increase in proportion of nucleus to cell diameter, implies an amoeboid shape associated with a pro-inflammatory phenotype (Kloss *et al.*, 2001; Kongsui *et al.*, 2015).

2.5 Polymerase Chain Reaction

To investigate steroid receptor, TLR4 pathway, and inflammasome-related gene transcription following a 6 h and 24 h inflammatory challenge (100 ng/ml LPS), real time quantitative PCR was conducted according to manufacturer's specifications (Biorad 175271). RNA was extracted from BV2 cell samples using a Maxwell 16 LEV simplyRNA Cells kit (Promega A208B) according to manufacturer's recommendations. RNA concentration and purity were determined by UV absorbance at 260 and 280 nm. cDNA templates were obtained via reverse transcription (High Capacity cDNA reverse transcription kit [Applied Biosystems 4638814]) of 900ng of RNA according to manufacturer standard protocol. Triplicate PCR reactions (40 cycles [95 °C for 5 s -> 62°C for 30 s]) containing 10 uL of cDNA, 300 nM primers (Table 1.) and 10 uL SYBRgreen iTaq Supermix (Biorad 1725120) in a final volume of 20 uL detected Gapdh,

Nr3C1, Nr3c2, Trif, Md2, Cd14, Tlr4, MyD88, Nlrp3, Pycard and Casp1. SYBRgreen fluorescence signal was measured using the Biorad CFX96 thermocycler. Reaction efficiencies between 90-105% were confirmed, and linear dynamic ranges determined, for each gene using 5 serial dilutions of cDNA from LPS and vehicle-treated BV2 cells.

Fold change was quantified as $2^{-\Delta\Delta ct}$ from Gapdh and a standard un-treated control sample. Product specificity was confirmed by post-PCR melt-curve analysis. Absence of dsDNA amplification was confirmed by a No Reverse Transcription control, and no template (water) controls were included in every gene assay run to control for non-specific PCR amplification.

Table 1. Primer sequences and gene grouping used.

Primer	Group	Forward	Reverse
GAPDH	CONTROL	AGG TCG GTG TGA ACG GAT TTG	TGT AGA CCA TGT AGT TGA GGT CA
NR3C1	STEROID RECEPTOR	AGC TCC CCC TGG TAG AGA C	GGT GAA GAC GCA GAA ACC TTG
NR3C2	STEROID RECEPTOR	GAA GAG CCC CTC TGT TTG CAG	TCC TTG AGT GAT GGG ACT GTG
TRIF	TLR PATHWAY	AAC CTC CAC ATC CCC TGT TTT	GCC CTG GCA TGG ATA ACC A
MD2	TLR PATHWAY	CGC TGC TTT CTC CCA TAT TGA	CCT CAG TCT TAT GCA GGG TTC A
CD14	TLR PATHWAY	CTC TGT CCT TAA AGGC GGC TTA C	GTT GCG GAG GTT CAA GAT GTT
TLR4	TLR PATHWAY	GCC TTT CAG GGA ATT AAG CTC C	GAT CAA CCG ATG GAC GTG TAA A
MYD88	TLR PATHWAY	TCA GTG TCT TAC CCT TGG T	AAA CTG CGA GTG GGG TCA G
NLRP3	INFLAMMASOME	ATT ACC CGC CCG AGA AAG G	TCG CAG TCA AAG ATC CAC ACA G
Pycard	INFLAMMASOME	CTT GTC AGG GGA TGA ACT CAA AA	GCC ATA CGA CTC CAG ATA GTA GC
CASP1	INFLAMMASOME	ACA AGG CAC GGG ACC TAT G	TCC CAG TCA GTC CTG GAA ATG

2.6 Statistical Analysis

To assess CORT pre-treatment concentration and time effects, IL-1β concentration, measured from supernatant samples, were converted to a percent change from volume and time-matched vehicle pre-treated controls. Subsequently, each CORT pre-

treated group varying in concentration, pre-treatment model or time, was compared to baseline value using a linear model with the intercept set at 1x fold.

To quantify effects of treatment (LPS vs vehicle), pre-treatment drug (CORT vs vehicle), pre-treatment concentration (50 nM vs 500 nM) and pre-treatment model (pre-exposure vs co-treatment), a 4-way ANOVA followed by post-hoc pairwise comparisons using Tukey's correction were applied to evaluate total intracellular NLRP3 expression.

To investigate the possible relationship between pro- and released IL-1β, a linear-mixed effects (LME) model was fit to [LPS - vehicle] supernatant IL-1β (sIL1resp) and log([LPS / vehicle] pro-IL-1β) expression (proIL1fold) using the following formula in the nlme package for R:

lme(sIL1resp ~ log(proIL1fold)* Pre-treatment* Pre-treatment Concentration, random = (~1|N))

Where each biological replicate (N) was denoted as a random effect to statistically control for repeated measures within each biological replicate. Linear mixed effects models were also used to assess pre-treatment effects in TNF-a induced IL-1β release, as well as GR and MR antagonist effects on CORT pre-treatment in respect to IL-1β secretion after LPS treatment.

Effects of pre-exposure conditions on gene transcription fold change of LPS-treated/ vehicle-treated cells were analysed by multiple linear regression, with variable

selection and regularisation via LASSO regression and cross-validation analysis using the glmnet statistical package. Further analysis on individual gene contribution towards the resultant linear regression model after regularisation was obtained via relaimpo statistical package. All analysis was done using R (64-bit) statistical program (version 3.3.1) (R Core Team, 2016).

3 Results

3.1 Concentration and time dependency of CORT pre-treatment models on LPS-induced IL-β responses

CORT pre-exposure exhibited a biphasic concentration response on LPS-induced supernatant IL-1β (Figure 2A). Low concentration (50 nM) pre-exposure requires > 16 h duration to achieve significant priming of released IL-1β response (Figure 2B).

A linear model significantly accounted for variation in percentage change of IL-1β release between CORT pre-treatment and volume matched vehicles across the concentration response (R^2 = 0.52, p<0.0001). In addition, the pre-exposure model and co-treatment models elicited significantly different LPS-induced IL-1β release (Mean difference = 1.40 fold, t(36)= 3.91, p<0.001). Comparisons to vehicle reference group found that the co-treatment of CORT and LPS was significantly inhibited IL-1β release at 50nM (Mean difference = -0.60 fold, t(36)= -2.37, *p*<0.05), 300 nM (Mean difference = -0.69 fold, t(36)= -2.72, *p*<0.05), 1 μM (Mean difference = -0.70 fold, t(36)= -2.76, *p*<0.01). Conversely, CORT pre-exposure significantly elevation of LPS-induced extracellular IL-1β at 50nM (Mean difference =0.80 fold, t(36)= 3.16, *p*<0.01), 100 nM (Mean difference = 1.15 fold, t(36)= 4.52, *p*<0.001) and 150 nM (Mean difference = 0.55 fold, t(36)= 2.18, *p*<0.05).

A linear model was constructed, assessing the time-dependency of IL-1β release, represented as percentage change between 50nM CORT pre-exposure and time-matched vehicles (R^2 = 0.69, p<0.001). When comparing 24h LPS-induced IL-1β in each pre-exposure duration to vehicle, CORT only caused significant elevation in IL-1β after 16 h (Mean difference = 1.66 fold, t(13) = 2.96, p<0.05), 20 h (Mean difference = 1.63

fold, $t(13) = 2.91$, $p<0.05$), and 24 h (Mean difference = 1.87 fold, $t(13) = 5.27$, $p<0.001$).

Previous rodent experiments conducted in the lab have found approximately 500 nM – 1 μM CORT concentrations measured from mouse serum following acute stress. Together with the concentration and time responses, further analysis focused on investigation of a low (50 nM) and physiological high (500 nM) concentration.

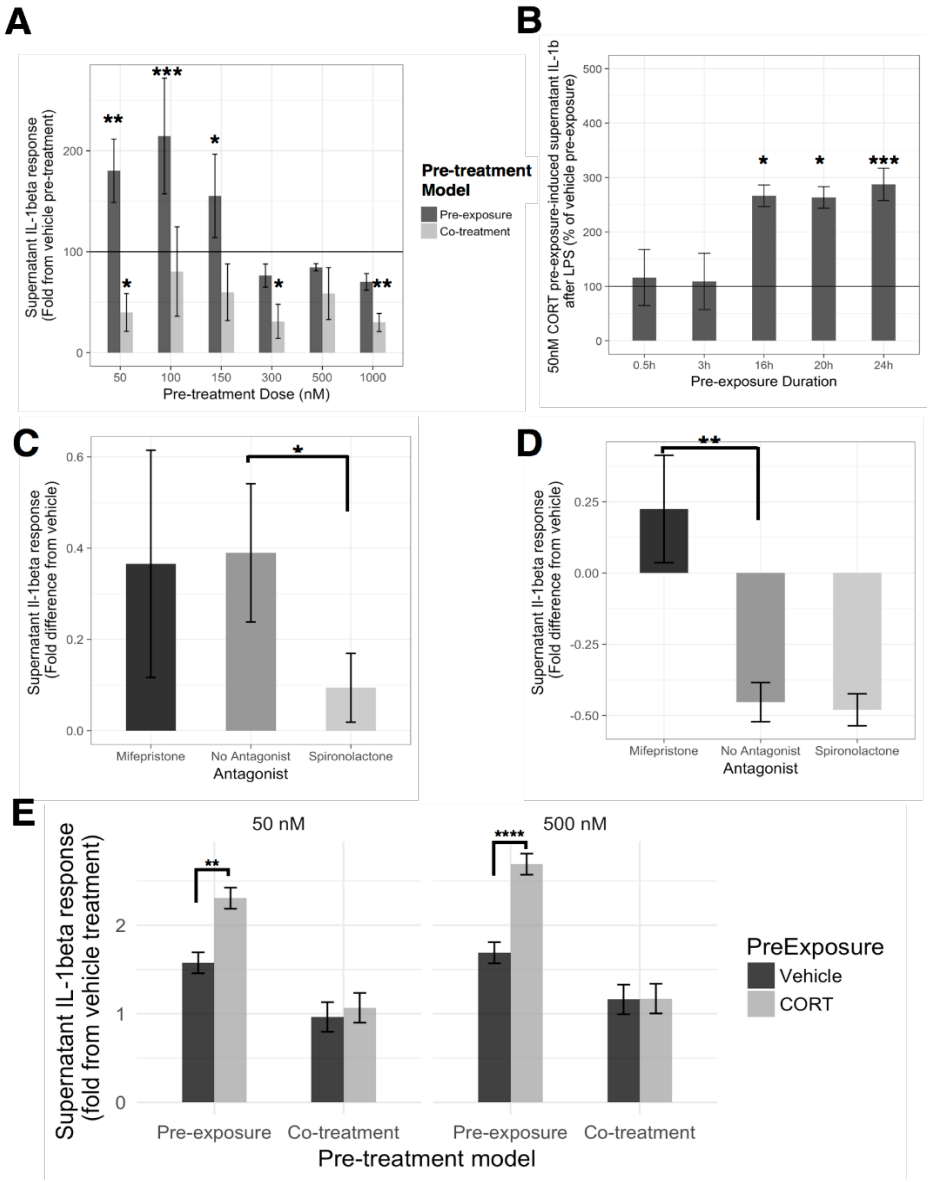

Figure 2. CORT pre-exposure exhibits concentration and time dependent inhibition and priming of LPS- and TNF-α induced IL-1β release in BV2 cells. Low concentration pre-exposure priming of IL-1β release is attenuated by a MR antagonist, while co-treatment inhibition of IL-1β is reversed by a GR antagonist. A) IL-1β Concentration response in 24h CORT pre-exposure/ co-treatment models measured after 24 h LPS-vehicle treatment (N=6). B) 24 h LPS-induced IL-1β response after 50 nM CORT pre-exposure varying in length of time (N=4). Stars represent p-values comparing each individual CORT + LPS IL-1β response to vehicle + LPS controls. C,D) Role of GR and MR using specific antagonists, Mifepristone and Spironolactone respectively, on low concentration CORT pre-exposure effects on IL-1β release from BV2 cells (A; N = 9), and with co-treatment (B; N = 5). All supernatant IL-1β values represented as fold difference in LPS-induced IL-1β from vehicle pre-treated controls. E) Fold change in IL-1β following 24 h pre-treatment + 24 h 100 ng/ml TNF-α. CORT pre-exposure increased IL-1β responses, while the co-treatment model resulted in no significant difference from vehicle pre-treated cells (N = 3). Error bars represent mean +- SEM. * <0.05, **<0.01, ***<0.001, ****<0.0001.

3.2 Pharmacological MR antagonism attenuated low-concentration CORT pre-exposure priming of IL-1β release, while GR antagonism abolished CORT co-treatment inhibition of LPS -induced IL-1β release

To further investigate the mechanism by which low concentration CORT pre-treatment models act to sensitize, or inhibit, the IL-1β response to LPS, specific antagonists to MR and GR, Spironolactone (1 uM) and Mifepristone (1 uM) respectively, were co-administered with CORT pre-treatment conditions (Figure 2 C,D). In this experiment, low concentration CORT pre-exposure and LPS treatment significantly elevated IL-1β measured in the supernatant compared to vehicle controls ($b = 6.95$, $t(16) = 3.06$, $p<0.01$) (Figure 2C). Spironolactone abolished the priming effect of low concentration CORT pre-exposure ($b = -6.06$, $t(16) = -2.14$, $p<0.05$), whereas Mifepristone did not significantly modify CORT-induced priming ($b = -2.43$, $t(16) = -0.86$, $p = 0.40$). On the other hand, LPS-induced IL-1β secretion was significantly inhibited when CORT was co-incubated with LPS treatment ($b = -11.97$, $t(8) = -4.14$, $p<0.01$). This CORT co-treatment resultant inhibition effect was abolished by Mifepristone ($b = 14.74$, $t(8)=3.60$, $p<0.01$), but was not significantly influenced by Spironolactone co-administration ($b = -1.05$, $t(8) = -0.26$, $p = 0.80$) (Figure 2D).

3.3 CORT pre-exposure sensitized TNF-α-induced IL-1β release from BV2 cells

LPS is a compound that exists on gram negative bacterial cell walls, which do not readily cross the blood brain barrier under normal circumstance (see review Coureuil et al., 2017). Instead, humoral mechanisms, via cytokine responses in the periphery have been proposed as main communicators between the peripheral immune system and microglia in the CNS (McCusker and Kelley, 2013). Thus, TNF-α (100ng/ml) was

used in place of LPS during the treatment stage. TNF-α was selected as the immune stimulant since it is an early phase pro-inflammatory cytokine which stimulates IL-1β release from innate immune cells (Franchi, Eigenbrod and Núñez, 2009).

Since all treatments and controls were applied to each individual biological replicate, a linear mixed effects model was used to account for repeated measures for each biological replicate. In this experiment, CORT pre-treatment significantly increased the TNF-α induced change in IL-1β release (B = 0.17 fold, $t(26)=4.35$, $p<0.001$), while co-treatment in general decreased TNF-α induced IL-1β release (B=-0.61 fold, $t(26)=-2.98$, $p<0.01$) (Figure 2E). CORT pre-treatment significantly interacted with co-treatment model to cause an even greater decrease in IL-1β (B=-0.63 fold, $t(26)=-2.15$, $p<0.05$). Post hoc pairwise group comparisons with Tukey's correction further showed that 50nM CORT pre-exposure (mean difference = 0.73 fold, $p<0.01$) and 500 nM CORT pre-exposure (mean difference = 1.0 fold, $p<0.0001$) both significantly elevated TNF-α induced IL-1β release compared to volume-matched vehicle pre-exposure. CORT co-treatment at both concentrations did not significantly inhibit TNF-α induced IL-1β release when compared to volume matched vehicle co-treatments ($p>0.05$).

3.4 CORT (50 nM) pre-exposure causes more IL-1β release when controlling for intracellular pro-IL-1β expression.

As IL-1β requires conversion from pro-IL-1β to mature IL-1β within the cell before release (Duitman, Orinska and Bulfone-Paus, 2011), the relationship between intracellular pro-IL-1β and supernatant IL-1β levels was investigated to determine if CORT had disrupted this process. A linear mixed effects model

was used to control for repeated measures from the same passage of cells, assessing the relationship between extracellular IL-1β and intracellular pro-IL-1β expression measured in pre-treatment models (Figure 3A).

CORT co-treatment with LPS inhibited IL-1β release (mean difference and 95% CI for CORT present - not present during LPS treatment = -11.36 ± 7.06 pg/ml). CORT therefore attenuates LPS-induced IL-1β secretion when present during LPS treatment.

While there was no significant overall relationship between pro-IL-1β and supernatant IL-1β in vehicle pre-exposure (b = 4.14, t(27) = 1.22, p = 0.23), CORT pre-exposure caused a significantly more positive relationship between pro-IL-1β and released IL-1β (b = 19.56, t-value (27) = -4.47, p<0.001). Importantly, there was also a significant interaction between CORT pre-exposure, pre-exposure concentration, and pro-IL-1β (b = 26.78, t-value (27) = 4.01, p< 0.001), indicating that low concentration CORT pre-exposure significantly potentiates the conversion and release of IL-1β in response to LPS, with no influence on the total pro-IL-1β expression levels (mean difference and 95% CI for LPS-treated vehicle pre-exposed – LPS-treated CORT pre-exposed cells = 0.34 ± 0.18). In CORT co-treated BV2 cells, there was an overall positive relationship between pro-IL-1β expression levels and supernatant IL-1β levels (b = 18.57, t-value (26) = 5.36, p<0.01), but CORT co-treatment did not significantly modify this relationship (b = -8.40, t-value (26) = 0.82, p=0.42) (Figure 3B).

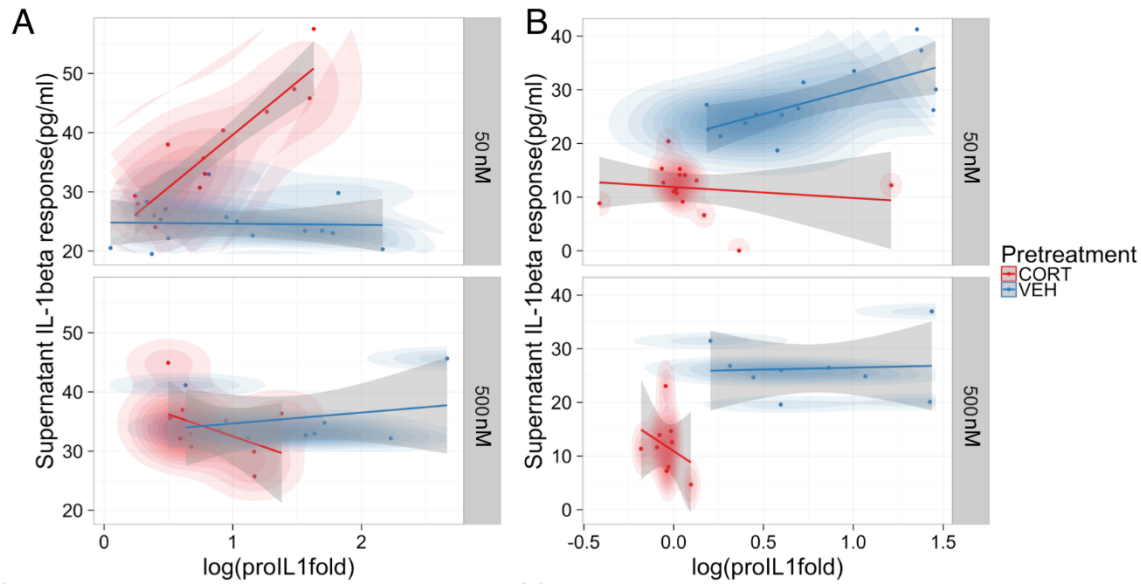

Figure 3. Low concentration CORT pre-exposure increases release of supernatant IL-1β, but high concentration CORT pre-exposure and CORT co-treatment decrease release of supernatant IL-1β and cell expression of pro-IL-1β protein in LPS-stimulated BV2 cells. A-B) Scatter plot with probability density describing linear mixed effects model constructed between intracellular pro-IL-1β protein expression and supernatant IL-1β levels after 100 ng/ml LPS treatment following Low (50 nM; n = 16) and High (500 nM; n = 8) concentration CORT vs. vehicle pre-exposed cells. Pre-exposure model (A), and CORT co-treatment model (B). All supernatant IL-1β values reported subtracted vehicle (no LPS)-treated baseline levels as control.

3.5 CORT pre-exposure in BV2 cells does not alter total NLRP3 protein expression

NLRP3 constitutes part of the inflammasome complex which cleaves pro-IL-1β into mature IL-1β before release from microglia (Hanamsagar, Torres and Kielian, 2011). To investigate the mechanism behind the increased conversion and release of IL-1β by BV2 cells pre-treated with 50 nM CORT, expression levels of NLRP3 were measured. NLRP3 staining using fluorescent immunocytochemistry confirmed the presence of NLRP3 in the cytosol of BV2 cells following LPS treatment (Figure. 4A, 4B).

Western blot quantification of NLRP3 expression showed that LPS treatment ($F(1, 191)= 55.41$, $p < 0.0001$) significantly increased NLRP3 expression (Figure 4C). High concentration pre-exposure, regardless of volume-matched ethanol vehicle or CORT, exhibited a significantly lower NLRP3 expression versus low concentration pre-treatments overall ($F(1,191) = 14.11$, $p< 0.001$), whereas co-treatment of LPS and CORT or vehicle resulted in more NLRP3 protein expression compared to pre-treated cells ($F(1,191) = 4.36$, $p< 0.05$). However, CORT pre-treatment in itself did not significantly influence total NLRP3 expression ($F(1,191) = 0.036$, $p = 0.85$; Fig. 4A). These data suggest that the CORT-mediated increased conversion and subsequent release of IL-1β with LPS is not due to increases in total NLRP3 expression within the cytoplasm.

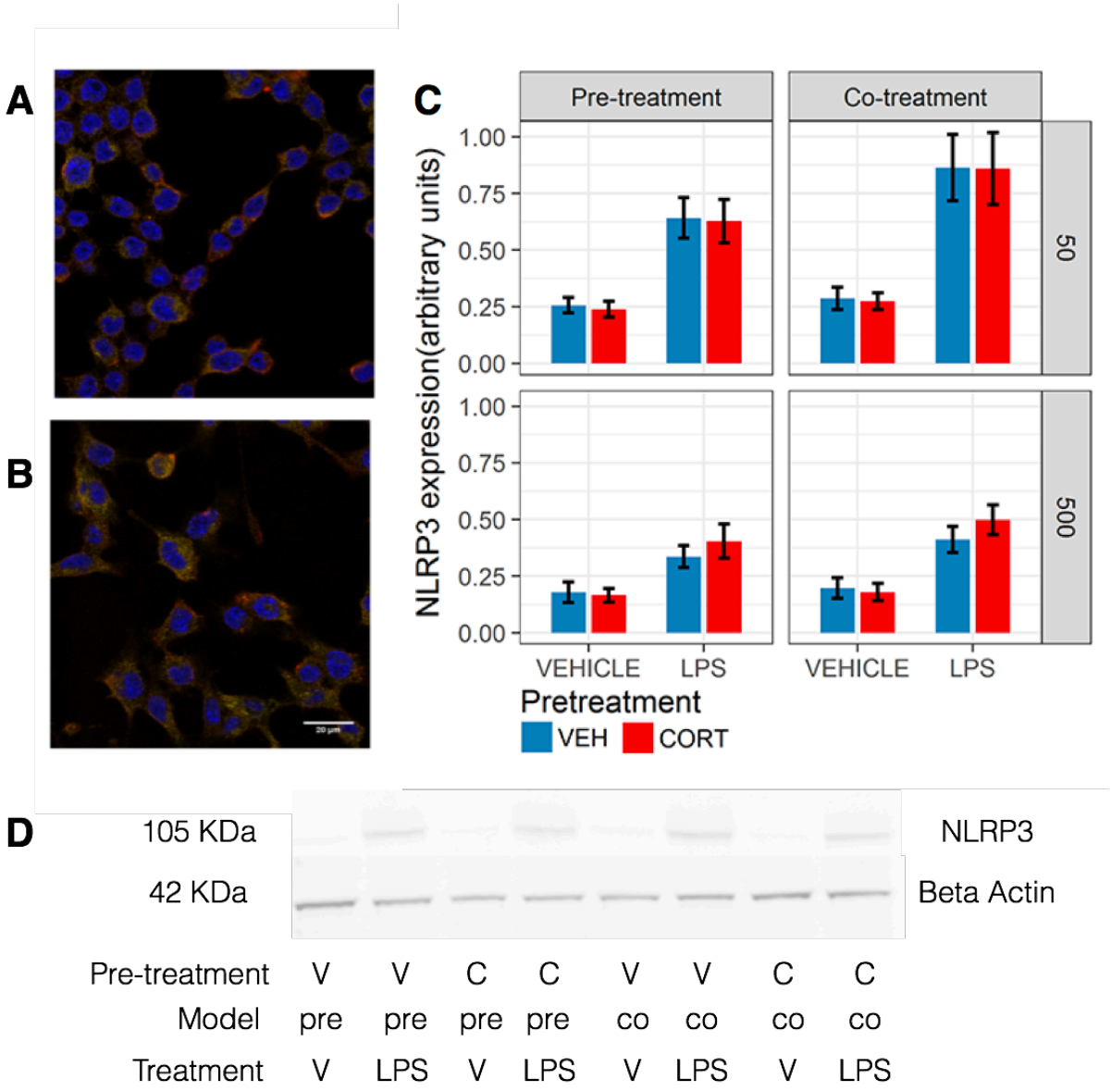

Figure 4. CORT pre-exposure and co-treatment do not alter NLRP3 expression following LPS. A,B) Fluorescent Immunocytochemistry showing NLRP3 expression (yellow) in the cytoplasm, between nucleus (Blue) and cell membrane (Red) in CORT (B) and vehicle (C) pre-exposed cells and LPS treatment. C) Western blot measurements of NLRP3 expression measured from BV2 cells that received either Low (50 nM; n = 16) or High (500 nM; n =8) concentration CORT or vehicle exposure, followed by LPS (100 ng/ml) or vehicle treatment. CORT pre-treatment included pre-exposure and co-treatment conditions. D) Representative western blot displaying NLRP3 and B Actin protein expression for lysates of low concentration pre-treatment + treatment conditions.

3.6 Low but not high concentration CORT pre-exposure enhances NF-κB translocation in BV2 cells

Given that low concentration CORT pre-exposure primed both LPS and TNF-α -induced IL-1β responses, increased NF-κB translocation may a potential mechanism of this effect. The effect of CORT pre-exposure on LPS -induced NF-κB translocation was thus investigated (Figure 5).

As expected, LPS treatment significantly upregulated BV2 cell NF-κB p65 translocation in both low ($F(1,13) = 59.33$, $p < 0.0001$) and high CORT concentration pre-exposure conditions ($F(1,13) = 62.02$, $p < 0.0001$) (Figure 5A, 5B). Low concentration CORT pre-exposure in BV2 cells significantly increases NF-κB translocation ($F(1,13) = 4.89$, $p<0.05$). However, no significant interaction between low concentration CORT pre-exposure and LPS treatment was observed on NF-κB translocation ($F(1,13) = 1.13$, $p = 0.31$). No significant pre-exposure ($F(1,13) = 0.58$, $p = 0.46$), nor pre-exposure x treatment interactions ($F(1,13) = 0.35$, $p = 0.56$) were observed in high concentration pre-exposure conditions in BV2 cells (Figure 5C). Tukey post hoc test did not show any significant difference between individual groups ($p>0.05$).

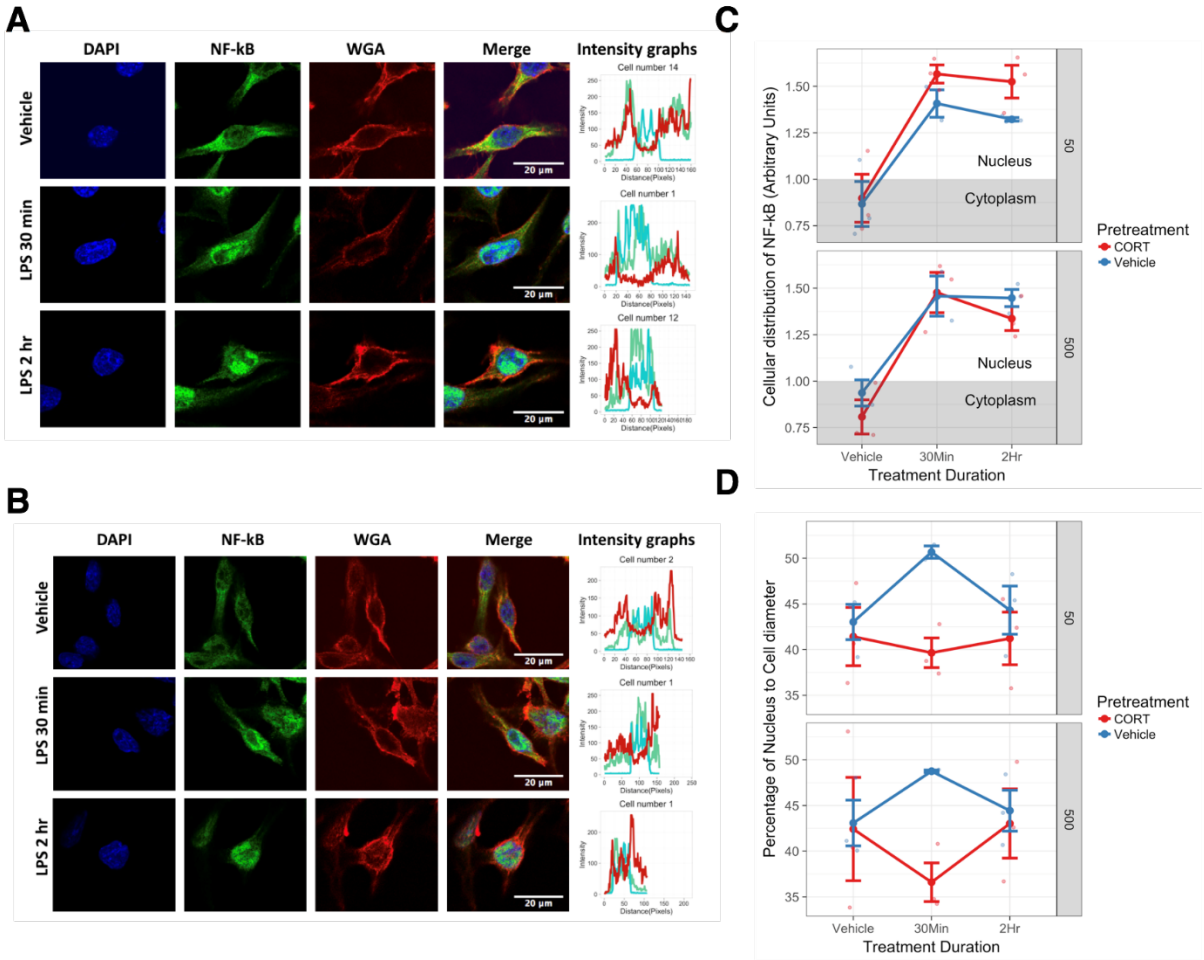

Figure 5. CORT pre-exposure (50 nM) induces increased NF-κB translocation while both 50 nM and 500 nM prevent increased nucleus:cell diameter 30 min after LPS treatment. A, B) Fluorescent Immunocytochemistry for NF-κB (Green), nucleus (Blue), cell membrane (Red), and profile intensity plots across cell diameter shown for one sample cell in vehicle vs 30 min vs 2 h LPS following: A) vehicle , B) low concentration (50 nM) CORT pre-exposure. C) Summary values representing nuclear expression of NF-κB proportional to total expression of NF-κB across the cell diameter, further normalised to the proportion of nucleus to cell diameter. Value <1: expression distribution favours cytoplasm, value >1: expression distribution favours nucleus. D) Summary values for nucleus:cell diameter at baseline, 30 min and 2 h following LPS treatment. A lower value reflects decreased nucleus proportion of cell diAmeter, a measure of increased process length. All measures were made after pre-exposure + treatment. Error bars represent mean ± SEM values.

3.7 CORT pre-exposure induced a significantly more ramified morphology in response to LPS treatment.

Measuring the length of the widest BV2 cell diameter and the proportion of nucleus to total cell diameter provides a measure of cell morphology. In this case a higher value indicates an ameboid BV2 cell shape, and a lower value indicates a ramified BV2 cell morphology.

At both low and high concentrations, CORT pre-exposure induced a significantly more ramified morphology in BV2 cells overall ($F(1,27)= 7.84$, $p<0.01$) (Figure 5D). In addition, the 2-way ANOVA analysis revealed a significant interaction effect between LPS treatment duration and pre-exposure ($F(1,27) = 5.33$, $p<0.05$). Post-hoc analysis conducted using Tukey's correction further revealed a significantly lower nucleus:cell diameter in CORT + LPS conditions compared to vehicle pre-exposure+ LPS conditions overall (mean difference = 6.39, $p< 0.05$), and CORT + LPS 30 min conditions compared to vehicle + LPS 30 min conditions (mean difference = 9.68, $p< 0.05$).

3.8 Inflammasome-related and steroid receptor-related gene expression in CORT pre-exposed BV2 cells following 6 h and 24 h LPS administration:

The increase in NF-kB translocation in cells pre-exposed to low concentration CORT suggests that gene transcription may be altered. To identify possible pathways involved in eliciting IL-1β release following low- concentration CORT pre-exposure, gene expression correlates with secreted IL-1β protein were investigated in BV2 cells. Thus, concurrent TLR-related, inflammasome-related and steroid receptor-related gene expressions were measured via qPCR to investigate gene expression contribution towards CORT-induced priming of IL-1β protein secretion in BV2 cells (Figure 6A).

Due to a relatively large number of gene expression measures, there was redundancy within the model. Lasso regularisation was therefore utilised to identify key genes contributing to the variation in IL-1β release in response to LPS, and yielded different sets of contributing genes for vehicle (R^2 = 0.61; Tlr4, Cd14, Nr3c2 and Nlrp3), and CORT (R^2 = 0.94, Pycard, Nlrp3 and Cd14) pre-exposed BV2 cells (Figure 6A). Furthermore, relative importance analysis applied to each model revealed varying contributions for each gene in both pre-exposure conditions (Figure 6B). In vehicle pre-exposed cells, Nlrp3 accounted for 61.1% of 61.4% total variation explained in the linear model. In CORT pre-exposed cells however, Nlrp3 mRNA expression only accounted for 37.1% of 93.9% variation in IL-1β, whereas Pycard and Cd14 mRNA expression contributed 31.1% and 29.3% respectively, thus indicating that CORT pre-exposure has an impact on LPS-induced gene transcription in relation to IL-1β release from BV2 cells.

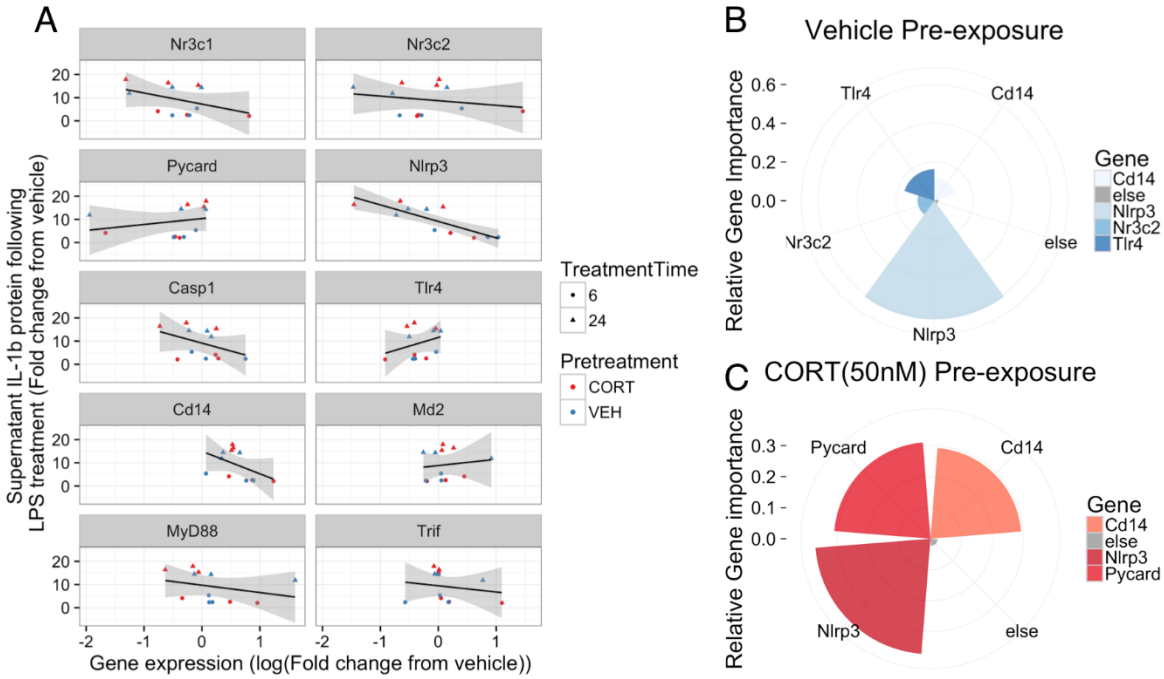

Figure 6. Changes in IL-1β release in BV2 cells receiving CORT 50 nM pre-exposure is associated with increased involvement of Pycard and Cd14 gene expression profiles 6 h and 24 h post LPS administration. A) Individual gene expression correlates with LPS-induced IL-1β protein secretion measured in supernatant from BV2 cells, following either 50 nM CORT or volume-matched vehicle pre-exposure (N = 3). Gene expression is represented as fold change from vehicle/vehicle treated controls. B-C) Relative contribution of each lasso regularisation-selected gene in multiple linear regression models, explaining variation in LPS-induced IL-1β protein release in vehicle pre-exposed (B) and 50 nM CORT pre-exposed (C) BV2 cells.

4 Discussion

The current results have provided evidence that CORT can cause a non-classical change in innate immune responses in BV2 microglia-like cells. Low concentration (50 nM) 24 h CORT pre-exposure resulted in increased NF-κB p65 translocation while preventing amoeboid cell morphology in response to LPS exposure. Furthermore, low concentration CORT pre-exposure preferentially sensitized the IL-1β response to LPS in a MR-dependent manner. To our knowledge, this is the first study to show the mechanisms underpinning direct CORT priming and immunosuppressive actions on BV2 microglia-like cells in vitro, providing a basis to further investigate the neuroimmune system as a potential mediator of stress-induced maladaptations.

4.2 Low concentration CORT causes increased IL-1β conversion and release, NF-κB nuclear translocation but prevented change in morphology in response to LPS:

The current study found that low concentrations of CORT in BV2 cells induces an inflammatory profile that is characterised by increased NF-κB nuclear translocation and IL-1β release while retaining ramified morphology during LPS challenges as compared to vehicle pre-exposed cells. This is consistent with previous findings showing that stress can induce increased ramified morphology in prefrontal microglia (Hinwood *et al.*, 2012).

Furthermore, a low concentration of CORT may alter the pathways involved in IL-1β conversion and secretion, specifically via Pycard and CD14 gene transcription, in addition to NLRP3 that predominated in vehicle treated cells. We thus propose that CORT pre-exposure can prime BV2 cells towards a distinct secretory and gene expression profile while retaining a ramified cell morphology, which is indicative of

'resting' state (Kloss *et al.*, 2001). These results suggest that CORT pre-exposure may prime a pro-inflammatory state, while protecting BV2 cells from over-responding to immune stimuli.

4.2 Low concentration CORT pre-exposure increases, while high concentration CORT pre-treatment and CORT co-treatment inhibit, pro-IL-1β protein conversion and release in response to LPS:

CORT, being a predominantly anti-inflammatory steroid hormone, was shown to suppress IL-1β secretion from LPS-treated cells when present during the subsequent immune challenge without significant change to cell viability after LPS treatment (data not shown). This is consistent with the classical research (Chrousos, 2009; Muzikar, Nickols and Dervan, 2009), and indicates the robustness of the anti-inflammatory effects of CORT. However, concentration response results indicate that low concentration CORT pre-exposure primed IL-1β release following LPS stimulation.

Interestingly, this CORT pre-exposure priming effect was conserved in TNF- α induced IL-1β release as well. Together with the increased NF-kB translocation in BV2 cells pre-exposed to low concentration CORT, these results suggest that CORT may cause IL-1β release via adaptations to NF-kB signalling. IL-1β is a potent pro-inflammatory cytokine, which is implicated in various neurological disease states from neuronal hyper-excitability in epilepsy (Vezzani *et al.*, 2011), to impairments in learning and memory, as well as perpetuation of sickness and depressive behaviours (Huang *et al.*, 2008). This CORT-induced priming of IL-1β secretion could therefore contribute to the maladaptive outcomes of stress.

Although the elevation of IL-1β only occurs in lower concentrations of CORT pre-exposure, this effect is supported by previous studies (Smyth *et al.*, 2004; Busillo, Azzam and Cidlowski, 2011). Smyth et al. established that 100 nM CORT could prime future immune responses in RAW264.7 macrophage-like cells after removal of CORT. This low concentration effect was further explored by Yeager et al. 2011. Similar to the findings here, the researchers described a biphasic concentration response to cortisol in humans, where patients who received cortisol pre-exposure exhibited exaggerated responses to LPS challenge in a concentration and time dependent manner. CORT has also been shown to exhibit permissive effects towards inflammation at low concentrations, inhibitory at higher concentrations, and mediate the priming effects in inflammation following stress (Sapolsky, Romero and Munck, 2000; Frank *et al.*, 2012; Sapolsky, 2015).

Using specific antagonists to GR and MR, the two CORT binding receptors, the current study has further demonstrated that this low concentration CORT priming of IL-1β release is MR dependent, while high concentration CORT-induced suppression of IL-1β relies on GR binding. This result is consistent with the binding properties of the receptors implicated in the immune-priming and immune-suppressive actions of CORT; as MR is a high-affinity and low abundance receptor for CORT, while GR is a low-affinity and high abundance receptor (Tanaka *et al.*, 1997). Moreover, previous findings showing that both CORT and aldosterone, a MR specific agonist, was also able to increase NF-kB translocation and downstream pro-inflammatory gene transcription in BV2 cells (Chantong *et al.*, 2012). The authors were also able to inhibit this increase in NF-kB translocation using a MR antagonist, thus consistent with the MR-dependent

CORT priming of IL-1β release seen here. The removal-dependent pre-exposure of CORT demonstrated here therefore fits into the paradigm of priming innate immune responses following small increases in CORT concentration, and further provided evidence that this effect may be related to MR rather than GR actions.

The specific circumstances which allow CORT to cause a switch from anti- to pro-inflammatory actions after removal from the system is consistent with the hypothesis that stress can cause immune sensitisation during the "recuperation phase" (Frank *et al.*, 2015). Although inconsistent with previous evidence showing increased microglia NLRP3 mRNA expression from animals chronically administered with CORT (Frank *et al.*, 2014b), the results here indicate that either: 1) gross intracellular expression levels are not sensitive enough to elicit IL1β interactions with the inflammasome, or 2) other mechanisms may be contributing to the increased IL-1β conversion and response observed. For example, emerging evidence shows that extracellular inflammasome complexes may contribute to inflammatory signalling (Baroja-Mazo *et al.*, 2014). Future studies would thus be required to address this. Moreover, Pycard, which encodes ASC protein as part of the inflammasome, appears to be associated with IL-1β release in CORT pre-exposed cells, unlike vehicle pre-exposed cells. This suggests that the NLRP3 inflammasome is unlikely to be the only inflammasome complex involved in CORT pre-exposure priming of the innate immune response since ASC forms a common part in multiple inflammasomes, including NLRP1, NR3C4, and AIM2 inflammasomes (Guo, Callaway and Ting, 2015). Further investigation into other inflammasome complexes and their interactions with pro-IL-1β is therefore required.

An important consideration is the use of BV2 cells in this study, an immortalised cell line developed from mouse microglia using retroviral infection (Blasi, Barluzzi and Bocchini, 1990). BV2 cells have impaired IRF3-dependent gene transcription following LPS treatment when compared to primary microglia harvested from neonatal mice, indicating altered TRIF signalling (Das *et al.*, 2015). Despite these differences, morphological change (Laurenzi *et al.*, 2001), NLRP3 inflammasome activation (Zhou *et al.*, 2016), TLR4-MyD88 signalling (Gong *et al.*, 2016), and NF-kB translocation (Brandenburg *et al.*, 2010), have all been shown similarly in BV2 cells and primary microglia. BV2 cells are therefore immunocompetent and bear functional similarities to primary microglia. However, primary microglial cell culture should still be pursued in future studies for translation of these findings to age- and sex- related differences in stress models.

5 Conclusions

The current study found that CORT, a predominantly anti-inflammatory steroid hormone, is also able to produce non-classical sensitization ofpro-inflammatory responses in BV2 microglia-like cells. The MR- dependent, pro-inflammatory effect of CORT is apparent after low concentration 24 h pre-exposure, after which increases in NF-κB p65 nuclear translocation, and ultimately IL-1β conversion and release, can be detected following LPS treatment. Thus, low concentration CORT potentially primes responses in BV2 microglia-like cells to a subsequent innate immune challenge.

IL-1β may further provide a direct link between the neuroendocrine stress response and depressive behaviours. For example, chronically stressed mice with small elevations in circulating CORT also have increased circulating and brain IL-1β expression, concurrent with increased anhedonia and decreased social exploration, all measures of rodent depressive-like behaviours (Goshen *et al.*, 2008). In the same study, IL-1 receptor knockout mice and adrenalectomised wild type mice exhibit similar protection from behavioural effects of chronic stress, providing some evidence that IL-1β and CORT signalling may both be involved. The current findings provide evidence that, under the right conditions, CORT can directly influence microglia-like cells to favour secretion of IL-1β in the event of TLR4 activation, thus identifying a link between the two systems in innate-immune function.

Acknowledgments

The authors would like to thank Professor Guillemin for his kind provision of BV2 cells used in this study. JL is the recipient of an Adelaide Graduate Research Scholarship. This work was supported by the Australian Research Council Centre of Excellence for Nanoscale BioPhotonics [CE140100003]. The authors declare no conflict of interests.

References

Baroja-Mazo A, Martín-Sánchez F, Gomez AI, Martínez CM, Amores-Iniesta J, Compan V, Barberà-Cremades M, Yagüe J, Ruiz-Ortiz E, Antón J, Buján S, Couillin I, Brough D, Arostegui JI, Pelegrín P. 2014. The NLRP3 inflammasome is released as a particulate danger signal that amplifies the inflammatory response. Nat Immunol:1–5.

Blandino P, Barnum CJ, Deak T. 2006. The involvement of norepinephrine and microglia in hypothalamic and splenic IL-1β responses to stress. J Neuroimmunol 173:87–95.

Blasi E, Barluzzi R, Bocchini V. 1990. Immortalization of murine microglial cells by a v-raf/v- myc carrying retrovirus. J Neuroimmunol 27:229–237.

Brandenburg LO, Kipp M, Lucius R, Pufe T, Wruck CJ. 2010. Sulforaphane suppresses LPS-induced inflammation in primary rat microglia. Inflamm Res 59:443–450.

Busillo JM, Azzam KM, Cidlowski JA. 2011. Glucocorticoids sensitize the innate immune system through regulation of the NLRP3 inflammasome. J Biol Chem 286:38703–13.

Cao Q, Li P, Lu J, Dheen ST, Kaur C, Ling E-A. 2010. Nuclear factor-κB/p65 responds to changes in the Notch signaling pathway in murine BV-2 cells and in amoeboid microglia in postnatal rats treated with the γ-secretase complex blocker DAPT. J Neurosci Res 88:n/a-n/a.

Chantong B, Kratschmar D V, Nashev LG, Balazs Z, Odermatt A. 2012. Mineralocorticoid and glucocorticoid receptors differentially regulate NF-kappaB activity and pro-inflammatory cytokine production in murine BV-2 microglial cells. J Neuroinflammation 9:1.

Chrousos GP. 2009. Stress and disorders of the stress system. Nat Rev Endocrinol 5:374–381.

Coureuil M, Lécuyer H, Bourdoulous S, Nassif X. 2017. A journey into the brain: insight into how bacterial pathogens cross blood–brain barriers. Nat Rev Microbiol 15:149–159.

Das A, Chai JC, Kim SH, Lee YS, Park KS, Jung KH, Chai YG. 2015. Transcriptome sequencing of microglial cells stimulated with TLR3 and TLR4 ligands. BMC Genomics 16:517.

Diz-Chaves Y, Pernía O, Carrero P, Garcia-Segura LM. 2012. Prenatal stress causes alterations in the morphology of microglia and the inflammatory response of the hippocampus of adult female mice. J Neuroinflammation 9:71.

Du Q, Min S, Chen LY, Ma Y Da, Guo XL, Wang ZG, Wang ZG. 2012. Major stress hormones suppress the response of macrophages through down-regulation of TLR2 and TLR4. J Surg Res 173:354–361.

Duitman EH, Orinska Z, Bulfone-Paus S. 2011. Mechanisms of cytokine secretion: A portfolio of distinct pathways allows flexibility in cytokine activity. Eur J Cell Biol 90:476–483.

Franchi L, Eigenbrod T, Núñez G. 2009. Cutting edge: TNF-alpha mediates sensitization to ATP and silica via the NLRP3 inflammasome in the absence of microbial stimulation. J Immunol 183:792–6.

Frank MG, Hershman SA, Weber MD, Watkins LR, Maier SF. 2014. Chronic exposure to exogenous glucocorticoids primes microglia to pro-inflammatory stimuli and induces NLRP3 mRNA in the hippocampus. Psychoneuroendocrinology 40:191–200.

Frank MG, Thompson BM, Watkins LR, Maier SF. 2012. Glucocorticoids mediate stress-induced priming of microglial pro-inflammatory responses. Brain Behav Immun 26:337–345.

Frank MG, Watkins LR, Maier SF. 2013. Stress-induced glucocorticoids as a neuroendocrine alarm signal of danger. Brain Behav Immun 33:1–6.

Frank MG, Weber MD, Watkins LR, Maier SF. 2015. Stress sounds the alarmin: The role of the danger-associated molecular pattern HMGB1 in stress-induced neuroinflammatory priming. Brain Behav Immun:1–7.

Gong L, Zhu S, Gong L, Target MD, Province J. 2016. TIRAP positively regulates BV2 cells M1 polarization.

Goshen I, Kreisel T, Ben-Menachem-Zidon O, Licht T, Weidenfeld J, Ben-Hur T, Yirmiya R. 2008. Brain interleukin-1 mediates chronic stress-induced depression in mice via adrenocortical activation and hippocampal neurogenesis suppression. Mol Psychiatry 13:717–28.

Groer MW, Kane B, Williams SN, Duffy A. 2015. Relationship of PTSD Symptoms With Combat Exposure, Stress, and Inflammation in American Soldiers. Biol Res Nurs 17:303–10.

Guo H, Callaway JB, Ting JP. 2015. Inflammasomes : mechanism of action , role in disease , and therapeutics. Nat Med 21:677–687.

Hanamsagar R, Torres V, Kielian T. 2011. Inflammasome activation and IL-1β/IL-18 processing are influenced by distinct pathways in microglia. J Neurochem 119:736–48.

Hinwood M, Morandini J, Day TA, Walker FR. 2012. Evidence that microglia mediate the neurobiological effects of chronic psychological stress on the medial

prefrontal cortex. Cereb Cortex 22:1442–54.

Howren MB, Lamkin DM, Suls J. 2009. Associations of depression with C-reactive protein, IL-1, and IL-6: a meta-analysis. Psychosom Med 71:171–186.

Huang Y, Henry CJ, Dantzer R, Johnson RW, Godbout JP. 2008. Exaggerated sickness behavior and brain proinflammatory cytokine expression in aged mice in response to intracerebroventricular lipopolysaccharide. Neurobiol Aging 29:1744–1753.

Hueston CM, Deak T. 2014. The inflamed axis: the interaction between stress, hormones, and the expression of inflammatory-related genes within key structures comprising the hypothalamic-pituitary-adrenal axis. Physiol Behav 124:77–91.

Jones KA, Zouikr I, Patience M, Clarkson AN, Isgaard J, Johnson SJ, Spratt N, Nilsson M, Walker FR. 2015. Chronic stress exacerbates neuronal loss associated with secondary neurodegeneration and suppresses microglial-like cells following focal motor cortex ischemia in the mouse. Brain Behav Immun 48:57–67.

Kloss CU, Bohatschek M, Kreutzberg GW, Raivich G. 2001. Effect of lipopolysaccharide on the morphology and integrin immunoreactivity of ramified microglia in the mouse brain and in cell culture. Exp Neurol 168:32–46.

Kongsui R, Johnson SJ, Graham BA, Nilsson M, Walker FR. 2015. A combined cumulative threshold spectra and digital reconstruction analysis reveal structural alterations of microglia within the prefrontal cortex following low-dose LPS administration. Neuroscience 310:629–640.

Laurenzi MA, Arcuri C, Rossi R, Marconi P, Bocchini V. 2001. Effects of microenvironment on morphology and function of the microglial cell line BV-2. Neurochem Res 26:1209–1216.

Liu J, Buisman-Pijlman F, Hutchinson MR. 2014. Toll-like receptor 4: innate immune regulator of neuroimmune and neuroendocrine interactions in stress and major depressive disorder. Front Neurosci 8:309.

McCusker RH, Kelley KW. 2013. Immune-neural connections: how the immune system's response to infectious agents influences behavior. J Exp Biol 216:84–98.

Medzhitov R, Horng T. 2009. Transcriptional control of the inflammatory response. Nat Rev Immunol 9:692–703.

Miller GE, Murphy MLM, Cashman R, Ma R, Ma J, Arevalo JMG, Kobor MS, Cole SW. 2014. Greater inflammatory activity and blunted glucocorticoid signaling in monocytes of chronically stressed caregivers. Brain Behav Immun 41:191–199.

Muzikar K a, Nickols NG, Dervan PB. 2009. Repression of DNA-binding dependent glucocorticoid receptor-mediated gene expression. Proc Natl Acad Sci U S A 106:16598–16603.

de Pablos RM, Herrera AJ, Espinosa-Oliva AM, Sarmiento M, Muñoz MF, Machado A, Venero JL. 2014. Chronic stress enhances microglia activation and exacerbates death of nigral dopaminergic neurons under conditions of inflammation. J Neuroinflammation 11:34.

Pan Y, Chen XY, Zhang QY, Kong LD. 2014. Microglial NLRP3 inflammasome activation mediates IL-1β-related inflammation in prefrontal cortex of depressive rats. Brain Behav Immun:1–11.

R Core Team. 2016. R: A language and environment for statistical computing. R Found Stat Comput.

Sapolsky RM. 2015. Stress and the brain: individual variability and the inverted-U. Nat Neurosci 18:1344–1346.

Sapolsky RM, Romero LM, Munck AU. 2000. How Do Glucocorticoids Influence Stress Responses ? Integrating Permissive, Suppressive, Stimulatory and Preparative Actions *. Endocr Rev 21:55–89.

Sawicki CM, McKim DB, Wohleb ES, Jarrett BL, Reader BF, Norden DM, Godbout JP, Sheridan JF. 2015. Social defeat promotes a reactive endothelium in a brain region-dependent manner with increased expression of key adhesion molecules, selectins and chemokines associated with the recruitment of myeloid cells to the brain. Neuroscience 302:151–164.

Schindelin J, Arganda-Carreras I, Frise E, Kaynig V, Longair M, Pietzsch T, Preibisch S, Rueden C, Saalfeld S, Schmid B, Tinevez J-Y, White DJ, Hartenstein V, Eliceiri K, Tomancak P, Cardona A. 2012. Fiji: an open-source platform for biological-image analysis. Nat Methods 9:676–682.

Silverman MN, Mukhopadhyay P, Belyavskaya E, Tonelli LH, Revenis BD, Doran JH, Ballard BE, Tam J, Pacher P. 2012. Glucocorticoid receptor dimerization is required for proper recovery of LPS-induced inflammation , sickness behavior and metabolism in mice. Mol Psychiatry 18:1006–1017.

Smyth GP, Stapleton PP, Freeman TA, Concannon EM, Mestre JR, Duff M, Maddali S, Daly JM. 2004. Glucocorticoid pretreatment induces cytokine overexpression and nuclear factor-κB activation in macrophages. J Surg Res 116:253–261.

Sorrells SF, Munhoz CD, Manley NC, Yen S, Sapolsky RM. 2014. Glucocorticoids increase excitotoxic injury and inflammation in the hippocampus of adult male rats. Neuroendocrinology 100:129–140.

Tanaka J, Fujita H, Seiji M, Kazuko T, Sashiro S, Nubuji M. 1997. Glucocorticoid and Mineralocorticoid Receotors in MIcroglial Cells: The Two Receptors Mediate

Differential Effects of Corticosterone. Glia 20:23–37.

Valkanova V, Ebmeier KP, Allan CL. 2013. CRP , IL-6 and depression : A systematic review and meta-analysis of longitudinal studies. J Affect Disord 150:736–744.

Vezzani A, Maroso M, Balosso S, Sanchez M, Bartfai T. 2011. IL-1 receptor/Toll-like receptor signaling in infection, inflammation, stress and neurodegeneration couples hyperexcitability and seizures. Brain Behav Immun 25:1281–1289.

Yeager MP, Pioli PA, Guyre PM. 2011. Cortisol exerts bi-phasic regulation of inflammation in humans. Dose-Response 9:332–347.

Zhou Y, Lu M, Du R-H, Qiao C, Jiang C-Y, Zhang K-Z, Ding J-H, Hu G. 2016. MicroRNA-7 targets Nod-like receptor protein 3 inflammasome to modulate neuroinflammation in the pathogenesis of Parkinson's disease. Mol Neurodegener 11:28.

Chapter 5: CORT pre-treatment inhibits LPS-induced IL-6 production from BV2 cells, and IL-1β release from RAW 264.7 macrophage-like cells.

5.1 Introduction

Chapter 4 focused on innate-immune priming via TLR4 activation using LPS, with IL-1β as the main pro-inflammatory endpoint. However, the effects of CORT pre-exposure on other cytokines were not investigated. Since NF-κB translocation was increased in low concentration CORT pre-exposure, further exploration another cytokine downstream of NF-κB activation, IL-6, was investigated here.

NF-κB/p65 coordinates the transcription of various pro-inflammatory cytokines and chemokines (Pahl, 1999). IL-6 is another NF-κB pathway dependent cytokine (Son *et al.*, 2008), which is readily released from both BV2 cells and primary microglia in a similar manner (see systematic review from Chapter 3). Released IL-6 has both pro-inflammatory and anti-inflammatory actions. Physiologically, together with IL-1β, IL-6 induces production of hypothalamic PGE2 (Navarra *et al.*, 1992) and Substance P (Brito *et al.*, 2016), thereby increasing body temperature during pathogenic infections. Interestingly, IL-6 signalling in the hypothalamus can induce CRF release, thus causing HPA activation (Tilders *et al.*, 1994). Through binding to membrane bound gp130 and IL-6R, IL-6 inhibits epithelial cell apoptosis (Scheller *et al.*, 2011), and triggers the production of anti-inflammatory cytokines IL-1RA and IL-10 (Tilg *et al.*, 1994; Steensberg *et al.*, 2003), thus acting in an anti-inflammatory manner. IL-6 therefore coordinates both pro-and anti-inflammatory signalling actions. Given that CORT was shown to increase NF-κB translocation and IL-1β release in Chapter 4, IL-6 may also be

altered. This change would have consequences towards the coordination of inflammatory signalling, and was therefore investigated using the CORT pre-treatment model in the current chapter.

Chapter 4, in primarily focusing on microglia-like BV2 cells, did not consider the potential role of peripheral immune cells. Stress and CORT have demonstrated potent effects on peripheral immunocompetent cells. For example, social defeat stress has been shown to cause increased migration and brain infiltration of peripheral monocytes, thus influencing cell motility (Sawicki *et al.*, 2015; Wohleb *et al.*, 2016). Furthermore, pre-exposure to glucocorticoids also induced increased leukocyte migration toward peripheral sites of injury (Yeager *et al.*, 2016). Biphasic actions of CORT have also been demonstrated by peripheral immunocompetent cells. For example, low concentration CORT was previously shown to increase IL-6 responses from RAW 264.7 cells (Smyth *et al.*, 2004), and in isolated human monocytes (Yeager, Pioli and Guyre, 2011). Conversely, glucocorticoids are also clinically administered to manage systemic inflammatory disorders including auto-immune diseases and other chronic inflammation conditions (Sacre *et al.*, 2013). Thus, there is evidence for both immunosuppressive and immune stimulatory actions of glucocorticoids in the periphery. The current chapter therefore investigated this potential biphasic effect on peripheral immune cells, using the same treatment model established in Chapter 4.

This Chapter thus aimed to better characterise the effect of CORT pre-treatment on peripheral immune cells, as well as on BV2 NF-κB signalling. This was accomplished

through use of RAW264.7 cells a model of peripheral macrophages, and production of IL-6 cytokine from BV2 cells following CORT pre-exposure.

5.2 Methods

The general methods were based on those mentioned in chapter 4 with minor modifications.

5.2.1 Cell culture (RAW 264.7)

RAW267.4 cells were maintained in Dulbecco's modified Eagle's medium (DMEM) supplemented with 10 % (v/v) foetal bovine serum (FBS) and 2 mM L-glutamine + 50 U/ml Penicillin + 50 µg/ml Streptomycin + 100 µg/ml Normocin. Cells were grown in a humidified incubator of 95%air/5%CO2 at 37°C. Prior to experimental treatments, RAW264.7 cells were seeded at a density of $3.5x10^4$ cells per well in poly-D-lysine coated 96-well plates.

RAW264.7 cells were first pre-treated with varying concentrations of corticosterone (50nM - 1µM) or corresponding volume-matched vehicle for 24 h, followed by a further 24 h stimulation of LPS (100 ng/ml) to establish a concentration response (Figure 3A). CORT was either removed from the system (pre-exposure), or remained in the system during LPS treatment (co-treatment). A concentration of 50nM and 500nM was selected in further measurements of intracellular protein expression to maintain consistency with BV2 cell experiments in Chapter 4.

A time response was characterised between 0.5 h and 24 h pre-treatment + LPS treatment (Figure 3B). Supernatant expression of IL-1β was measured using an ELISA

kit (BD Bioscience, 559603, USA) after pre-treatment+treatment. Through Western blot analysis (as described in Chapter 4), Intracellular HMGB1, pro-IL-1β, and NLRP3 expression was measured after LPS treatment for both 50 nM and 500 nM CORT pre-treatment models.

5.2.2 BV2 Supernatant IL-6 measurements

IL-6 was measured from BV2 cell supernatants following 24 h pre-treatment concentration response of CORT (50nM – 1 μM), as described in Chapter 4. An IL-6 ELISA Kit (BD-Bioscience, 550950, USA) was used in accordance to manufacturer's specifications. A standard curve was used between 7.8 pg/ml to 1 ng/ml. Due to the high concentration of IL-6 found in the supernatants that exceeded the detection range of ELISA, supernatant samples were diluted (1:10) in assay diluent.

5.3 Results and Discussion

5.3.1 CORT pre-exposure and co-treatment attenuates LPS-induced IL-6 release from BV2 cells in a concentration-dependent manner.

CORT, at concentrations equal to and above 150nM exhibits inhibitory effects on IL-6 regardless of pre-exposure or co-treatment with LPS (Figure 1). A linear model constructed significantly explained variability in LPS-induced (LPS-vehicle treatment) supernatant IL-6 measured from BV2 cells after 24h CORT pre-exposure or co-treatment, represented as a percentage of each corresponding vehicle pre-treatment condition (R^2=0.74, p<0.0001). The model revealed significant CORT pre-treatment inhibition of LPS-induced IL-6 at 150nM (Pre-exposure: B= -24.41%, t(19)=-2.10, p<0.05; Co-treatment: B=-37.57%, t(19)=-2.64, p<0.05), 300nM(Pre-exposure: B= -25.28%, t(19)=-2.17, p<0.05; Co-treatment: B=-48.73%, t(19)=-3.42, p<0.01), 500nM (Pre-exposure: B= -56.46%, t(19)=-4.86, p<0.001; Co-treatment: B=-48.20%, t(19)=-3.39, p<0.01) and 1µM (Pre-exposure: B= -35.53%, t(19)=-3.06, p<0.01; Co-treatment: B=-57.01%, t(19)=-4.00, p<0.001) concentrations. Pairwise comparisons between least squares means for each group using Tukey's adjustment did not show any significant group differences between each concentration regardless of pre-exposure or co-treatment models (p>0.05). There was no significant independent effect of pre-treatment model (B = 5.64%, t(19)=0.34, p=0.74).

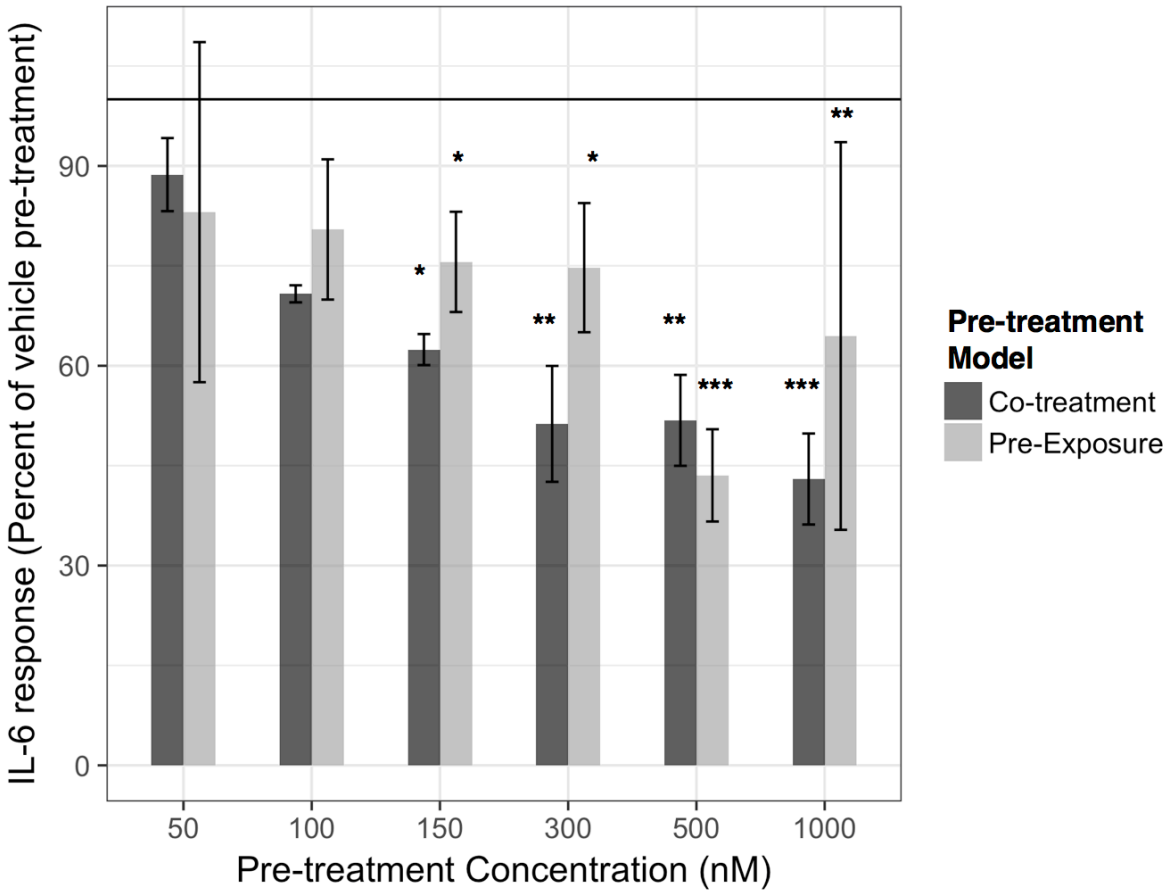

Figure 1. CORT pre-treatment is inhibitory towards IL-6 release from BV2 cells in a concentration-dependent manner. Bars represent mean ± SEM IL-6 response after CORT+LPS as percentage of vehicle+LPS in both pre-exposure and co-treatment models (N=3). Stars denote p-values comparing each individual CORT + LPS IL-6 response to each corresponding volume matched vehicle + LPS control (100% reference value). * <0.05, **<0.01, ***<0.001, ****<0.0001.

5.3.2 GR antagonist Mifepristone reversed 50 nM CORT pre-treatment inhibition of IL-6.

Linear mixed effects model showed that the GR antagonist, mifepristone, abolished CORT pre-treatment induced inhibition of IL-6 ($B = 9.6$ ng/ml, $t(20) = 3.34$, $p < 0.01$) (Figure 2). Co-treatment model also exhibited increased IL-6 inhibition overall ($B = -16.5$ ng/ml, $t(20) = -5.73$, $p < 0.0001$). Post hoc pairwise comparisons further revealed that mifepristone significantly reversed CORT pre-exposure (mean difference = 9.6 ng/ml, $p < 0.01$) and co-treatment (mean difference = 26.1 ng/ml, $p < 0.0001$) –induced inhibition. A MR antagonist did not modify CORT pre-exposure (mean difference = 3.2 ng/ml, $p = 0.52$), but significantly attenuated CORT co-treatment (mean difference = 7.7 ng/ml, $p < 0.05$) inhibition of IL-6 release from BV2 cells.

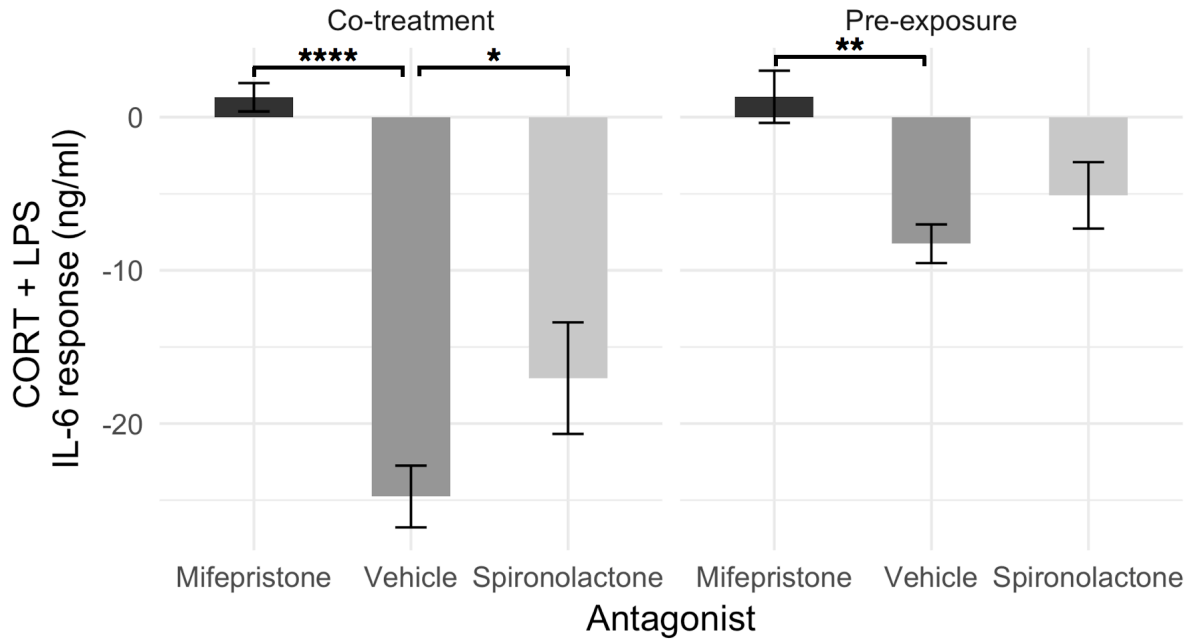

Figure 2. Mifepristone reverses 50 nM CORT pre-exposure and co-treatment -induced IL-6 inhibition, while Spironolactone only reduces CORT co-treatment inhibition of IL-6 release from BV2 cells. Bar graphs representing [CORT + antagonist] + LPS induced IL-6 responses when compared to respective [vehicle + antagonist]+vehicle controls (N=5). Error bars represent mean +- sem.* <0.05, **<0.01, ***<0.001, ****<0.0001.

5.3.3 Inequivalence in CORT pre-exposure effects on IL-1β and IL-6 cytokine release from BV2 cells

As demonstrated in Chapter 4, 50nM CORT pre-exposure primes the LPS-induced IL-1β response and NF-κB translocation. The priming effect does not appear to extend towards all transcriptional or translational events downstream of NF-κB. This is demonstrated here in regards to IL-6 release, and the lack of CORT pre-exposure effects on intracellular NLRP3 expression measured at the same time point in Chapter 4. Moreover, an interesting contrast between IL-6 results presented here, and the concentration-response of IL-1β reported in Chapter 4, is the dose required to cause inhibition. It appears that 150nM is sufficient to cause inhibition in IL-6 while concurrently priming IL-1β responses in BV2 cells (Chapter 4).

The results here indicate that inhibition of GR signalling reversed 50 nM CORT pre-treatment inhibition of LPS-induced IL-6 release, therefore further substantiating the finding that CORT signals via GR to act in an immunosuppressive manner. Conversely, MR inhibition was unable to influence pre-exposure model levels of IL-6 release, but significantly reduced CORT co-treatment inhibition of IL-6 release. This result demonstrates that MR may also contribute towards IL-6 inhibition, which is inconsistent with previous studies showing pro-inflammatory properties of aldosterone, a specific MR agonist (Bay-Richter *et al.*, 2012; Zhu *et al.*, 2012). Further exploration of the mechanisms underlying the actions of MR in IL-6 release are therefore required to reconcile these differences.

The lack of IL-6 priming presented implies that CORT may selectively modify events downstream from NF-κB translocation, and the same concentration of CORT can elicit opposite effects on IL-1β and IL-6 release. Further experiments are required to understand this dichotomous relationship between CORT and cytokine release across the concentration response. A secretome analysis can be used to network the protein release at each concentration, while interrogation of the intracellular signalling pathways that mediate these changes should be further investigated.

5.3.4 Concentration, time and pre-treatment model-dependent CORT inhibition of IL-1β release from RAW 264.7 cells

Concentration response

Variability in LPS-induced IL-1β in the supernatant following CORT pre-treatment at different concentrations was significantly explained by a linear model (R^2=0.57, p<0.0001). Each value is represented as a % of each corresponding volume-match vehicle for every biological replicate (100% would indicate no change from vehicle). CORT co-treatment caused a significant decrease in IL-1β compared to vehicle co-treatment (B=-45.52, t(36)= 2.34, p>0.05). With the exception of 300nM (B=-18.09%, t(36)=-1.32, p=0.20), all other concentrations significantly inhibited IL-1β release into the supernatant (50 nM: B=-33.40%, t(36)=-2.43, p<0.05; 100 nM: B=-57.00%, t(36)=-4.14, p<0.001; 150 nM: B=-37.94%, t(36)=-2.76, p<0.01; 500 nM: B=-61.61%, t(36)=-4.48, p<0.0001; 1 µM: B=-54.53%, t(36)=-3.97, p<0.0001). Conversely, only 1 µM CORT pre-exposure caused a significant reduction in IL-1β response compared to volume matched vehicles (B=-28.93%, t(36)=-2.11, p<0.05). Thus, increasing concentrations of CORT cause a greater reduction in IL-1β release from macrophage-like RAW264.7 cells.

Time response

When compared to vehicle pre-treatment, only 0.5 h CORT pre-exposure significantly inhibited IL-1β release (B = -35.09%, t(16)=-3.16, p<0.01). Conversely, CORT co-treatment significantly inhibited LPS-induced IL-1β for all time points measured (0.5 h: B = -56.00%, t(16)=-5.04, p<0.001; 1 h: B = -46.46%, t(16)=-4.18, p<0.001; 3 h: B = -46.33%, t(16)=-4.17, p<0.001; 24 h: B = -51.44%, t(16)=-4.63, p<0.001). The linear

model was significant in accounting for variability in LPS-induced supernatant IL-1β following 50 nM CORT pre-treatment in RAW264.7 cells differing in length of pre-exposure duration (R^2=0.78, p<0.0001). Each value was represented as a % of each corresponding vehicle pre-treatment within every biological replicate.

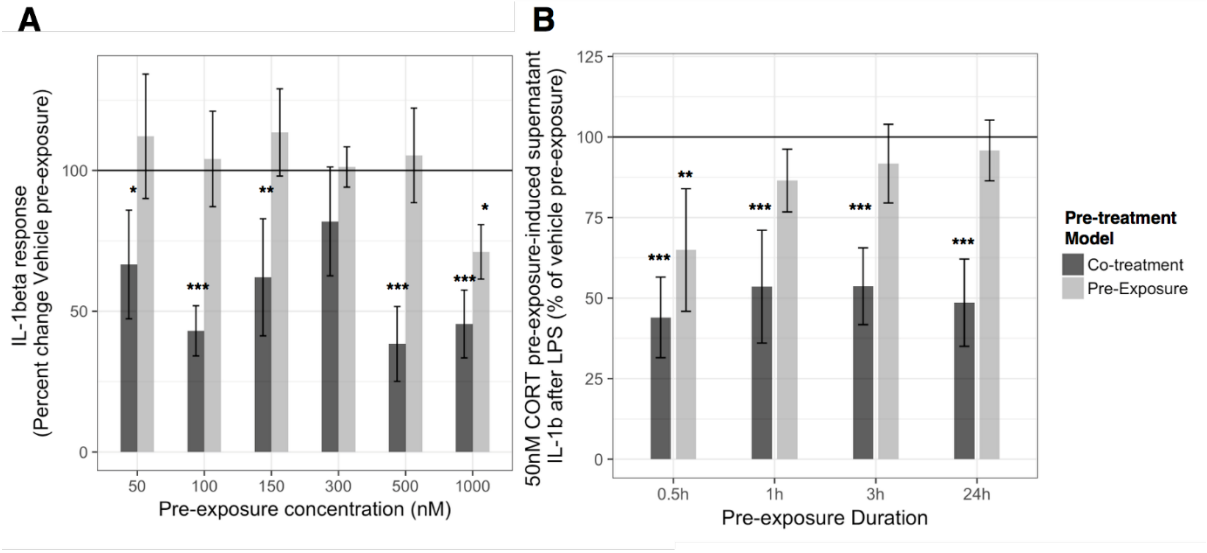

Figure 3. CORT co-treatment is inhibitory towards LPS-induced IL-1β responses in RAW264.7 cells regardless of concentration. A) IL-1β Concentration response in 24h CORT pre-exposure/ co-treatment models measured after 24h LPS-vehicle treatment (N=4). B) 24h LPS-induced IL-1β response after 50nM CORT pre-exposure varying in length of time. All values are represented as % of vehicle pre-treatment+ LPS response (N=4). Stars represent p-values comparing each individual CORT + LPS IL-6 response to each corresponding volume and time matched vehicle + LPS control (100% reference value). * <0.05, **<0.01, ***<0.001, ****<0.0001.

5.3.5 CORT pre-treatment does not significantly influence HMGB1 or pro-IL-1 expression, but increases NLRP3 expression in RAW264.7 cells.

Western blot measurements (Figure 4A) of intracellular protein measures were statistically analysed using ANOVAs for each protein measure, and subsequent pairwise group comparisons using Tukey's post hoc test was implemented.

HMGB1 expression

RAW264.7 cells were administered pre-treatment + treatment conditions, where pre-treatment model (pre-exposure vs co-treatment) and pre-treatment concentration (50nM vs 500nM) were varied. CORT pre-treatment failed to significantly account for variability in HMGB1 expression overall ($F(1,39)=1.83$, $p=0.18$). Pre-treatment model ($F(1,39)=9.91$, $p<0.01$) and concentration of pre-treatment ($F(1,39)=7.59$, $p<0.01$) significantly accounted from variability in intracellular HMGB1 expression (Figure 4B). No significant interaction between each term was present ($p>0.05$). Post hoc pairwise comparisons using Tukey's correction showed that co-treatment models elicited a higher HMGB1 expression compared to pre-exposure models regardless of CORT or vehicle pre-treatment, 50nM or 500nM pre-treatment concentration (mean difference = 0.24, $p<0.01$), while 500nM pre-treatment concentration significantly elevated HMGB1 expression regardless of pre-treatment model, CORT or vehicle pre-treatment (mean difference = 0.21, $p<0.01$).

Pro-IL-1β expression

A 3-way ANOVA showed that only the pre-treatment model significantly modified fold change in Pro-IL-1β expression in response to LPS measured from RAW264.7 cells

(F(1,16)= 4.93, p<0.05) (Figure 4C). Pre-treatment of CORT (F(1,16)=0.17, p=0.69) and dose of pre-treatment (F(1,16)=0.65, p=0.43) did not significantly account for variability in the Pro-IL-1β response from LPS treatment. Additionally, no significant interaction effect was found (p>0.05). Tukey's Post hoc pairwise test further revealed that co-treatment model elicited a significantly lower Pro-IL-1β response compared to the pre-exposure model (mean difference =14.3 fold, p<0.05).

NLRP3 expression

Fold change in RAW264.7 NLRP3 protein expression (Figure 4D) after LPS response was significantly modified by CORT pre-treatment (F(1,16)= 4.92, p<0.05) independent of pre-treatment model or concentration. No significant pre-treatment concentration (F(1,16)=3.03, p=0.10), or pre-treatment model (F(1,16)=0.00, p=0.99) effects were found. In addition, no significant interaction was evident (p>0.05). Tukey's post hoc pairwise comparisons showed that CORT pre-treatment significantly elevated NLRP3 response to LPS in RAW264.7 cells overall (mean difference = 0.75 fold, p<0.05).

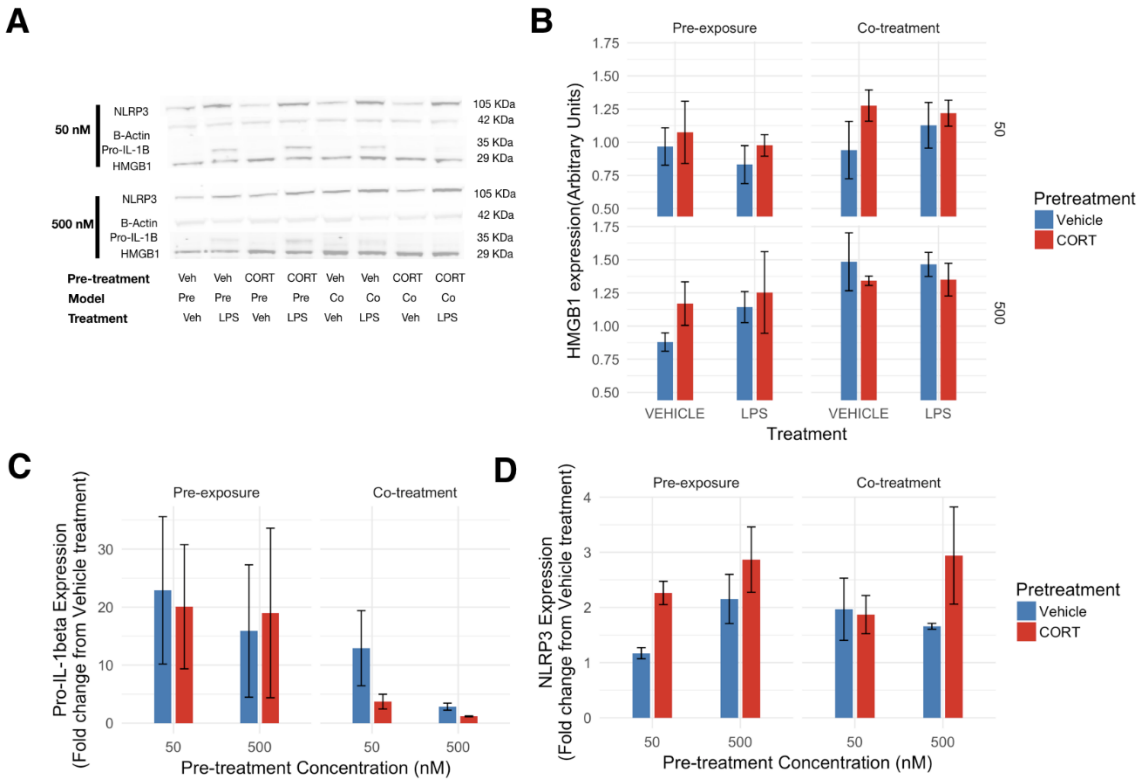

Figure 4. HMGB1, Pro-IL-1β, and NLRP3 expression in RAW264.7 cells were differentially modified by CORT pre-treatment. A) Representative western blots and mean intensity values for HMGB1 (B), LPS-induced fold change in Pro-IL-1β (C) and LPS-induced fold change in NLRP3 (D) expression measured after pre-treatment + treatment conditions (N=6). All bars represent mean+- SEM values.

5.3.6 Inequivalence in CORT pre-treatment effects between macrophage-like RAW264.7 cells and microglia-like BV2 cells

Macrophage-like RAW264.7 cells exhibit no CORT pre-exposure priming of the IL-1β response to LPS seen in BV2 cells, but showed increased NLRP3 expression after LPS treatment. Although 100 nM CORT pre-exposure was previously shown to increase LPS-induced IL-6 release from RAW264.7 cells (Smyth *et al.*, 2004), there are important differences between the methods adopted; the previous study measured IL-6 instead of IL-1β investigated here, and the experimental model of pre-exposure was different. The authors also found that CORT priming effect was most effective after a recovery period of 12-24 h before addition of LPS to the system, and only exposed the cells to CORT for 1 h as opposed to 24 h pre-treatment model used in this study.

Furthermore, unlike BV2 cells in chapter 4, RAW264.7 cells exhibited increased LPS-induced NLRP3 expression after 50nM CORT pre-exposure. This increase in NLRP3 expression was previously noted in hippocampal tissue and primary microglia after inescapable tail shock (Weber *et al.*, 2015). In the periphery, glucocorticoid administration also elevated LPS-induced NLRP3 mRNA expression in THP- 1 monocyte-like cells (Busillo, Azzam and Cidlowski, 2011). However, the lack of concurrent IL-1β increase further reinforces the lack of correlation between total expression of NLRP3 and actual IL-1β release seen in Chapter 4. The relationship between inflammasome expression and activity is thus more complex than initially anticipated. The results here suggest that these CORT pre-exposed RAW264.7 cells may require a second signal to trigger the inflammasome response and IL-1β release.

The differences between RAW264.7 cells and BV2 cells indicate differential sensitivities towards CORT. However, the role of GR and MR in mediating these effects was not investigated here. Since Chapter 4 demonstrated that GR binding caused inhibition, while MR binding mediated the priming effects of CORT on IL-1β, differential receptor activity or expression may thus contribute towards this variance in effects of CORT pre-exposure. Additional experiments are therefore required to ascertain the extent and mechanism of these potential peripheral-central innate immune cell differences.

5.4 Conclusion

The current chapter uncovered further complexity of CORT pre-treatment actions. Firstly, although a biphasic IL-1β response to CORT pre-exposure was characterised in Chapter 4, this effect was not seen in IL-6 release. Instead, CORT pre-exposure caused a monotonic concentration-dependent inhibition of LPS-induced IL-6 production. Secondly, unlike the opposing actions of GR and MR on IL-1β release, CORT-induced inhibition of IL-6 was abolished by both GR and MR antagonists. This result suggests that both receptors are involved in inhibitory actions on IL-6 production.

The priming effect of CORT pre-exposure on IL-1β release in BV2 cells was not replicated in macrophage-like RAW264.7 cells. Furthermore, intracellular NLRP3 protein expression was also increased by CORT pre-treatment in RAW264.7, while no change was evident in BV2 cells. These preliminary results suggest potential differences between microglia and macrophages, but additional studies in more physiologically relevant models are required to confirm such differences.

Collectively, the findings here demonstrate that the concentration, time and pre-treatment model effects of CORT shown in Chapter 4 do not cause a global priming of the NF-κB-dependent innate immune response. Instead, cytokine-dependent and cell type-dependent differences are evident. Thus, CORT pre-exposure priming of innate immune responses are more complex than previously thought, and require more study to establish a physiological role of these effects.

References

Bay-Richter, C., Hallberg, L., Ventorp, F., Janelidze, S. and Brundin, L. (2012) 'Aldosterone synergizes with peripheral inflammation to induce brain IL-1β expression and depressive-like effects', *Cytokine*. Elsevier Ltd, 60(3), pp. 749–754. doi: 10.1016/j.cyto.2012.08.016.

Brito, H. O., Barbosa, F. L., Reis, R. C. dos, Fraga, D., Borges, B. S., Franco, C. R. C. C. and Zampronio, A. R. (2016) 'Evidence of substance P autocrine circuitry that involves TNF-α, IL-6, and PGE2 in endogenous pyrogen-induced fever', *Journal of Neuroimmunology*. Elsevier B.V., 293, pp. 1–7. doi: 10.1016/j.jneuroim.2016.01.016.

Busillo, J. M., Azzam, K. M. and Cidlowski, J. A. (2011) 'Glucocorticoids sensitize the innate immune system through regulation of the NLRP3 inflammasome.', *The Journal of biological chemistry*, 286(44), pp. 38703–13. doi: 10.1074/jbc.M111.275370.

Navarra, P., Pozzoli, G., Brunetti, L., Ragazzoni, E., Besser, M. and Grossman, A. (1992) 'Interleukin-1 beta and interleukin-6 specifically increase the release of prostaglandin E2 from rat hypothalamic explants in vitro.', *Neuroendocrinology*, 56, pp. 61–68.

Pahl, H. L. (1999) 'Activators and target genes of Rel/NF-kappaB transcription factors.', *Oncogene*, 18(49), pp. 6853–66. doi: 10.1038/sj.onc.1203239.

Sacre, K., Dehoux, M., Chauveheid, M. P., Chauchard, M., Lidove, O., Roussel, R. and Papo, T. (2013) 'Pituitary-adrenal function after prolonged glucocorticoid therapy for systemic inflammatory disorders: an observational study.', *The Journal of*

clinical endocrinology and metabolism, 98(8), pp. 3199–205. doi: 10.1210/jc.2013-1394.

Sawicki, C. M. M., McKim, D. B. B., Wohleb, E. S. S., Jarrett, B. L. L., Reader, B. F. F., Norden, D. M. M., Godbout, J. P. P. and Sheridan, J. F. F. (2015) 'Social defeat promotes a reactive endothelium in a brain region-dependent manner with increased expression of key adhesion molecules, selectins and chemokines associated with the recruitment of myeloid cells to the brain', *Neuroscience*. IBRO, 302, pp. 151–164. doi: 10.1016/j.neuroscience.2014.10.004.

Scheller, J., Chalaris, A., Schmidt-Arras, D. and Rose-John, S. (2011) 'The pro- and anti-inflammatory properties of the cytokine interleukin-6', *Biochimica et Biophysica Acta - Molecular Cell Research*, 1813(5), pp. 878–888. doi: 10.1016/j.bbamcr.2011.01.034.

Smyth, G. P., Stapleton, P. P., Freeman, T. A., Concannon, E. M., Mestre, J. R., Duff, M., Maddali, S. and Daly, J. M. (2004) 'Glucocorticoid pretreatment induces cytokine overexpression and nuclear factor-κB activation in macrophages', *Journal of Surgical Research*, 116(2), pp. 253–261. doi: 10.1016/S0022-4804(03)00300-7.

Son, Y.-H., Jeong, Y.-T., Lee, K.-A., Choi, K.-H., Kim, S.-M., Rhim, B.-Y. and Kim, K. (2008) 'Roles of MAPK and NF-kappaB in interleukin-6 induction by lipopolysaccharide in vascular smooth muscle cells.', *Journal of cardiovascular pharmacology*, 51(1), pp. 71–77. doi: 10.1097/FJC.0b013e31815bd23d.

Steensberg, A., Fischer, C. P., Keller, C., Møller, K. and Pedersen, B. K. (2003) 'IL-6 enhances plasma IL-1ra, IL-10, and cortisol in humans.', *American journal of physiology. Endocrinology and metabolism*, 285(2), pp. E433–E437. doi:

10.1152/ajpendo.00074.2003.

Tilders, F. J. H., DeRuk, R. H., Van Dam, A. M., Vincent, V. A. M., Schotanus, K. and Persoons, J. H. A. (1994) 'Activation of the hypothalamus-pituitary-adrenal axis by bacterial endotoxins: Routes and intermediate signals', *Psychoneuroendocrinology*, 19(2), pp. 209–232. doi: 10.1016/0306-4530(94)90010-8.

Tilg, H., Trehu, E., Atkins, M., Dinarello, C. and Mier, J. (1994) 'Interleukin-6 (IL-6) as an anti-inflammatory cytokine: induction of circulating IL-1 receptor antagonist and soluble tumor necrosis factor receptor p55', *Blood*, 83(1), pp. 113–18.

Weber, M. D., Frank, M. G., Tracey, K. J., Watkins, L. R. and Maier, S. F. (2015) 'Stress Induces the Danger-Associated Molecular Pattern HMGB-1 in the Hippocampus of Male Sprague Dawley Rats: A Priming Stimulus of Microglia and the NLRP3 Inflammasome.', *The Journal of neuroscience : the official journal of the Society for Neuroscience*, 35(1), pp. 316–24. doi: 10.1523/JNEUROSCI.3561-14.2015.

Wohleb, E. S., Franklin, T., Iwata, M. and Duman, R. S. (2016) 'Integrating neuroimmune systems in the neurobiology of depression', *Nature Reviews Neuroscience*. Nature Publishing Group, 17(8), pp. 497–511. doi: 10.1038/nrn.2016.69.

Yeager, M. P., Pioli, P. A., Collins, J., Barr, F., Metzler, S., Sites, B. D. and Guyre, P. M. (2016) 'Glucocorticoids enhance the in vivo migratory response of human monocytes', *Brain, Behavior, and Immunity*. Elsevier Inc., 54, pp. 86–94. doi: 10.1016/j.bbi.2016.01.004.

Yeager, M. P., Pioli, P. A. and Guyre, P. M. (2011) 'Cortisol Exerts Bi-Phasic Regulation of Inflammation in Humans', *Dose-Response*, 9(3), pp. 332–347. doi: 10.2203/dose-response.10-013.Yeager.

Zhu, C., Wang, Q., Zhou, J., Liu, H., Hua, F., Yang, H. and Hu, Z. (2012) 'The mineralocorticoid receptor-p38MAPK-NFκB or ERK-Sp1 signal pathways mediate aldosterone-stimulated inflammatory and profibrotic responses in rat vascular smooth muscle cells.', *Acta pharmacologica Sinica*. Nature Publishing Group, 33(7), pp. 873–8. doi: 10.1038/aps.2012.36

Chapter 6: Low concentration CORT pre-exposure primes TLR4 mediated NF-κB and TNF-α responses in adult primary mouse microglia

6.1 Introduction

Chapter 4 demonstrated the priming effect of low concentration CORT on LPS-induced IL-1β conversion and release. Further upstream of IL-1β responses, pro-inflammatory transcriptional factor NF-κB translocation was also increased in BV2 cells pre-exposed to low concentration CORT, thus indicating that CORT pre-exposure primes the TLR4 mediated NF-κB-IL-1β pathway. However, one main limitation of this result is the use of the BV2 immortalised cell-line, which constrains the translatability of these results. As demonstrated by the systematic review in Chapter 3, LPS-related response patterns in BV2 cells exhibit high similarity to primary microglia, but the scale of BV2 responses are often higher or lower than those of primary microglia. Although IL-1β and TNF-α cytokine responses were most similar between BV2 cells and primary microglia, there is limited support in regards to comparable NF-κB transcriptional factor nuclear translocation. Therefore, although CORT-induced priming has been shown in BV2 cells, replication of these results in primary microglia is imperative towards verification of these actions.

The differences between neonatal and adult microglia is a methodological concern when undertaking a study using primary microglia. As shown in Chapter 3, the most common method of obtaining neonatal primary microglia requires long-term (approximately 2 – 3 weeks) co-culture with astrocytes *in vitro* prior to experimental treatments. This culture period almost equalling the whole 21-day *in utero* mouse

development is devoid of physiological growth factors that would normally be present. Moreover, neonatal microglia lack morphologically complex processes when compared to adult microglia, as measured by fractal dimension from imaging data (Floden and Combs, 2011). In addition, assessed via flow-cytometry of multiple surface markers, lower expression levels of CD39 and MHCII were evident in neonatal primary cultured microglia compared to adult mouse microglia (Yu, Neil and Quandt, 2017). Functionally, adult primary rat microglia have exhibited elevated LPS-induced IL-1β and IL-6 protein responses, but decreased TNF-α and NO release under the same conditions (Schell *et al.*, 2007). Besides LPS responses, adult primary microglia also demonstrated a decreased ability to phagocytose both synthetic Amyloid β protein and those derived from brain tissue of patients with Alzheimer's Disease, an effect associated with CD36 expression and CD47 function (Floden and Combs, 2011). Collectively, these reported functional differences suggest that the variation between adult and neonatal primary microglia are not simply due to overall sensitivity, but are a result of multiple adaptations of the innate immune response.

Given that previous studies have shown stress-induced priming of adult primary microglia (Kreisel *et al.*, 2014), the current chapter thus aimed to verify low concentration CORT priming results found in BV2 cells using the adult primary mouse microglia model. To that end, LPS-induced cytokine release, morphological change, and NF-κB translocation responses were thus investigated in adult primary microglia pre-exposed to low concentration CORT.

6.2 Methods

6.2.1 Percoll gradient isolation of adult primary mouse microglia

Adult primary microglia were used to verify NF-κB translocation cell morphology and cytokine results obtained from BV2 cells in Chapter 4. Primary microglia were isolated according to previously published methods, which yielded > 90% microglial purity (Frank *et al.*, 2006; Wohleb *et al.*, 2014). Briefly, 5-6 week old Balb/c mice were culled via pentobarbitone overdose (60 mg/ml). Cardiac perfusion of ice-cold saline was used to remove blood and from the vasculature. The whole mouse brain was quickly removed and placed ice-cold HBSS (without Ca^{2+}, Mg^{2+}). Each brain was hemisected aseptically, and meninges were removed under a dissecting microscope. The resultant brain tissue was subsequently chopped with a sterile blade to approximately 1 mm^3 size prior to papain enzymatic dissociation (130-092-628, Miltenyi, Germany) in the gentleMac system (Miltenyi, Germany) according to manufacturer's recommendations.

Dissociated cell suspensions and 10 ml PBS were passed through a 70 µm cell strainer into a 50 ml centrifuge tube, and centrifuged at 600 g for 6 min at 10 °C. The cell pallet was resupended in 3 ml 70% isotonic Percoll solution (17-0891-02, GE Helathcare Life Sciences, USA) and transferred into a 15 ml centrifuge tube. The percoll gradient was subsequently constructed by gently layering 3 ml of 50% , 3 ml of 35%, then 2 ml of 0% (PBS) isotonic Percoll. Each tube was then centrifuged at 2000 g for 20 min at 10 °C with minimal acceleration and brake. Using a sterile pasteur pipette, the debris containing layer between 0% and 35% was aspirated. Microglia between the 70% and

50% layers were collected and transferred to a fresh 15 ml centrifuge tube. All collected cells were re-suspended in DMEM containing 10% FBS + 2 mM L-glutamine + 50 U/ml Penicillin + 50 ug/ml Streptomycin + 100 ug/ml Normocin prior to trypan-blue cell counts. Each mouse brain typically yielded between 3 x 10^5 and 6 x 10^5 total microglia, which had 70-90% cell viability.

Using fluorescent immunocytochemistry for microglia markers IBA-1 (1:500) and CD11B (1:500), and GFAP (1:1000) as an astrocyte marker, microglia purity was determined. Each cell was counter-stained with DAPI to identify nuclei. All cells imaged were positive for IBA-1 and CD-11B, but GFAP negative (See Figure 4 in Appendix A).

6.2.2 Experimental procedure

Following isolation and cell counts, primary microglia were seeded at a density of 4 x 10^4 cells/ well onto poly-D-lysine coated 96-well plates for cytokine and cell viability quantification, and 1 x 10^5 cells/well in 8-well Ibidi glass-bottom slides (80827, Ibidi, Germany) for fluorescent immunocytochemistry experiments. Microglia were left to adhere to each surface overnight prior to experimental treatment.

Based on methods described in Chapter 4, microglia were first pre-exposed to 50 nM CORT or volume-matched vehicle for 24 h. Following pre-exposure, all media was aspirated, and cells were briefly washed using PBS prior to application of LPS or vehicle treatment. For cytokine and cell viability analysis, microglia were treated with 100 ng/ml LPS for 24 h. At the end of all drug treatments, each plate was centrifuged at 600 g for 5 min in order to pallet cellular debris prior to collection of supernatant.

For analysis of NF-κB translocation, primary microglia were treated with either vehicle, or 1 μg/ml LPS for a duration of 30 min, 2 h or 4 h before fixation using PFA and staining with respective antibodies (see Chapter 4, section 2.4 for details). Due to use of the 8-well slides preventing coverslip application, confocal imaging was performed with PBS in each well at 63x magnification (Leica SP5).

6.2.3 Quantification of cytokine release from adult primary mouse microglia

Supernatant TNF-α and IL-1β protein expression was measured using the appropriate ELISA kits according to manufacturer's specifications. The TNF-α ELISA (Biolegend, 430902, USA) was calibrated to standards between 7.8 pg/ml – 500 pg/ml concentration, while IL-1β ELISA (Biolegend, 432602, USA) had a detectable rage between 15.6 pg/ml and 2000 pg/ml.

6.2.4 Measurement of cell viability

Microglial cell viability was measured using the neutral red dye uptake assay according to previously published methods (Repetto, del Peso and Zurita, 2008). Neutral red dye is passively cell membrane permeable, and accumulates in lysosomes of viable cells. Following removal of supernatants after pre-exposure and treatment, neutral red dye diluted in serum free media was added to each well and incubated at 37 °C 5% CO_2 for 2 h to allow the dye to accumulate. Following incubation, supernatants were removed and each well was washed twice using PBS to remove excess dye. A destaining solution containing 48% ethanol + 1% glacial acetic acid was added to each well to leech the intracellularly accumulated dye out of each cell. Finally, fluorescence intensity at 530

nm excitation and 645 nm emission was measured using a microplate reader (Biotek, USA). An increase in fluorescence intensity indicated increased cell viability.

6.2.5 Quantification of morphological changes and NF-κB translocation in adult primary mouse microglia

Primary microglia exhibited a more diverse morphological phenotype when compared to BV2 cells, in which overall cell morphology and nuclei were not of a uniform shape (Figure 1A). Given the non-bipolar morphology in most primary microglia, the longest diameter across each cell is an inaccurate measure of morphology. Thus, a separate image analysis method was utilised to more accurately quantify NF-κB nuclear translocation and morphological changes in primary microglia. Details and source code used in this method are detailed in Appendix C (Translocator 0.0.2).

Using the threshold function in imageJ, the nucleus and NF-κB channels were thresholded to the respective signal prior to application of the "analyse particles" function. This function was configured to identify every particle above 10 μm^2 in size, and save each particle as a separate region of interest (ROI). Thus, a unique ROI was obtained for each nucleus and NF-κB signal per identified cell. At least 10 cells per experimental replicate were used for further analysis. On the original NF-κB signal containing channel, the identified nucleus and NF-κB ROI was applied to each cell in focus. By further applying conditional operations to each pair of ROI, measures for the overlap between nucleus and total NF-κB signal (Nucleus NF-κB), and the combination of nucleus and total NF-κB signal (Total cell NF-κB) was further computed. Measures of area and integrated density were thus obtained for every nucleus and total NF-κB

signal. Integrated density of signal intensity is a measure of mean pixel intensity * area of signal, thus quantifying the density of NF-κB signal over each area. The degree of NF-κB translocation per identified cell was calculated as:

$$\left(\frac{Nucleus\ NF-\kappa B\ integrated\ density}{Total\ cell\ NF-\kappa B\ integrated\ density}\right) \div \left(\frac{Nucleus\ area}{Total\ area}\right)$$

Similar to measures of NF-κB translocation in BV2 cells (Chapter 4, section 2.4), a value larger than 1 indicates NF-κB expression favouring the nucleus, a value less than 1 indicates NF-κB expression favouring the cytoplasm, while a value of 1 indicates an overall uniform NF-κB expression in both the nucleus and cytoplasm.

6.2.6 Statistical analysis

Statistical methods here are similar to those used in Chapter 4. Briefly, linear mixed effects models were used to control for repeated measures on cells isolated from the same animal. For NF-κB, each cell was treated as a repeated measure within each biological replicate (different isolations). A total of 10 biological replicates were used for TNF-α measurements, while 5 biological replicates were used for NF-κB translocation analysis.

6.3 Results

6.3.1 Low concentration CORT pre-exposure prevents LPS-induced morphological change in adult primary microglia

To verify the effects of low concentration CORT pre-exposure on cell morphology and NF-κB translocation seen in BV2 cells, isolated adult primary microglia were pre-exposed to 50 nM CORT for 24 h prior to either vehicle, 30 min, 2 h or 4 h 1 μg/ml LPS treatment (Figure 1A).

LPS treatment did not significantly influence nucleus size measured after 30 min (B = 1.2 μm^2, t(399) = 0.53, p=0.60), and 2 h (B = 1.2 μm^2, t(399) = 0.58, p=0.56) treatment (Supplementary S1). However, total nucleus size was significantly increased after 4 h LPS treatment (B = 7.5 μm^2, t(399) = 2.57, p<0.05). Post-hoc pairwise comparisons did not show any individual group difference (p>0.05).

A retraction of cell processes leads to an overall decrease in overall cell area, and an ameboid morphology. Ameboid cell morphology was thus measured by an elevation in percentage of nucleus area : total area per identified cell (figure 1B). LPS treatment significantly induced a more ameboid morphology after 30 min (B=19.8 %, t(399) = 4.13, p<0.0001) and 2 h (B=16.9 %, t(399)=3.92, p<0.001) treatment. No significant difference in percentage of nucleus: total area was found when measured after 4 h LPS treatment (B=-1.27 %, t(399)=-0.21, p=0.83). Post-hoc comparisons further showed that CORT pre-exposed microglia significantly lower percentage of nucleus: total area compared to vehicle pre-exposed microglia when measured after 30 min LPS (mean difference = 16.8 %, p<0.001), and 2 h LPS (mean difference = 10.0 %, p<0.05). CORT

pre-exposure did not significantly influence cell morphology after vehicle treatment (mean difference = 1.0 %, p=0.80) or 4 h after LPS (mean difference = 8.1 %, p=0.32).

6.3.2 Low concentration CORT pre-exposure increases LPS-induced p65 NF-κB translocation in adult primary microglia

NF-κB translocation, measured by an increase in nucleus integrated density of intensity of p65 NF-κB signal normalised to the proportion of nucleus: total area (Figure 1C), was significantly increased in response to 4 h LPS treatment ($B = 0.16$, $t(399)= 2.28$, $p<0.05$) in vehicle pre-exposed cells. Conversely, CORT pre-exposed microglia exhibited significant NF-κB translocation after 2 h ($B = 0.12$, $t(399)= 2.60$, $p<0.01$) and 4 h ($B = 0.24$, $t(399)= 2.82$, $p<0.01$) LPS treatment. Post-hoc pairwise comparisons further showed that CORT pre-exposed microglia displayed significantly higher NF-κB translocation after 30 min (mean difference = 0.12, $p<0.05$) and 2 h (mean difference =0.13, $p<0.01$) LPS, compared to respective vehicle pre-exposed cells. No significant effect of CORT pre-exposure was evident in vehicle treated (mean difference =0.03, p=0.48), and 4 h LPS-treated microglia (mean difference = 0.11, p=0.24).

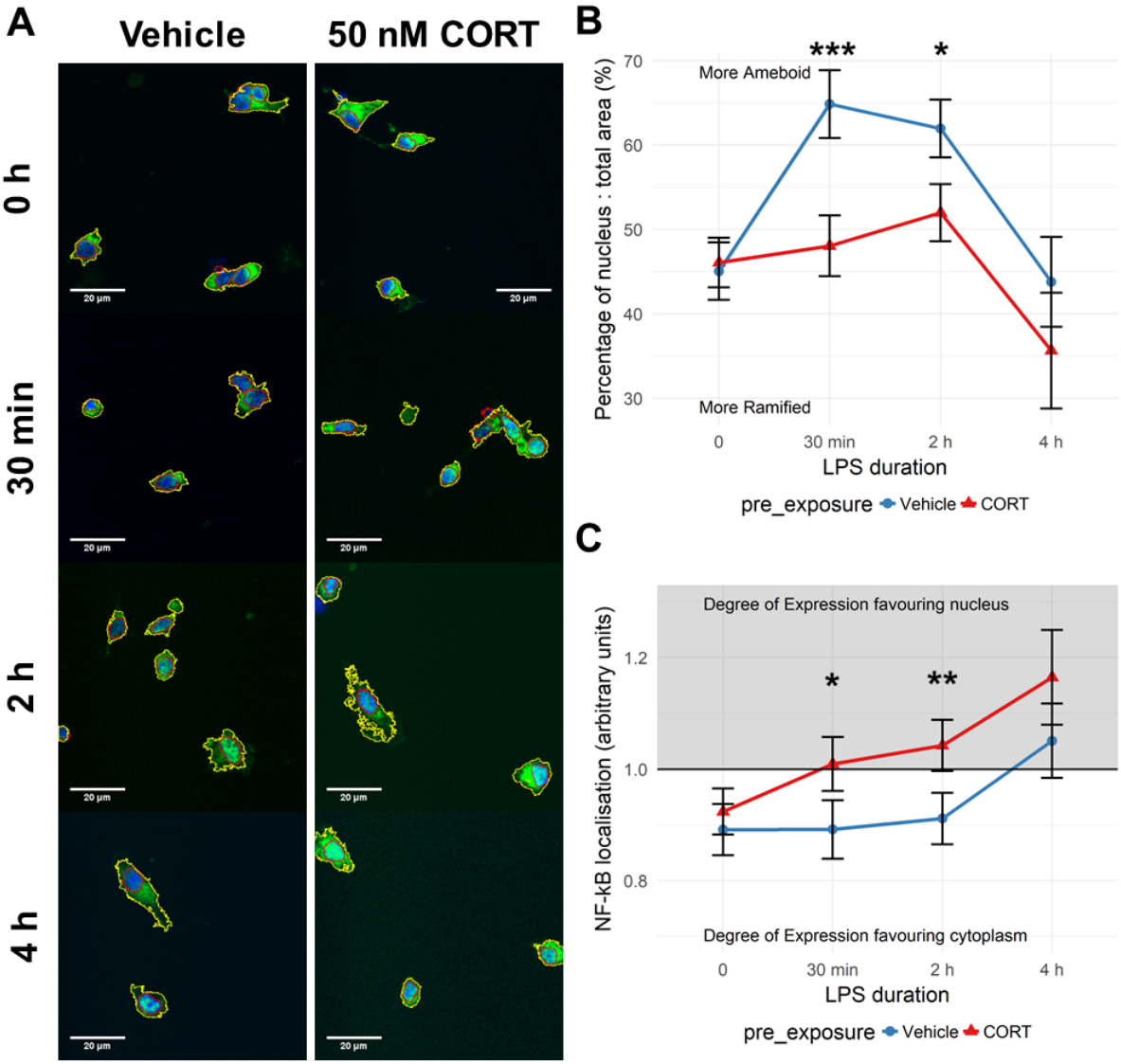

Figure 1. Primary microglia pre-exposed to 50 nM CORT display increased LPS-induced p65 NF-κB nuclear translocation, while retaining a more ramified morphology. (A) Representative fluorescent immunocytochemistry images of microglia p65 NF-κB protein expression following 24 h vehicle or 50 nM CORT pre-exposure and either 0 h, 30 min, 2 h or 4 h 1 µg/ml LPS treatment. Blue channel with red bounds represents cell nucleus (DAPI), while green channel with yellow bounds represents p65 NF-κB expression. The scale bar indicates 20 µm actual size. (B) Percentage of nucleus area occupying the total cell area per cell was calculated from the area of identified nucleus (red bounds) and identified total area (yellow bounds) (N = 5). (C) Intracellular NF-κB localisation calculated from the integrated density of signal intensity (intensity * area) normalised to the ratio of nucleus: total area. A value > 1 indicates expression favouring the cell nucleus, while a value < 1 indicates expression favouring the cell cytoplasm (N = 5). Statistically significant post-hoc pairwise comparisons between CORT and vehicle pre-exposure using Tukey's adjustment are denoted by: * <0.05, ** <0.01, *** <0.001.

6.3.3 CORT (50 nM) pre-exposure increases LPS-induced TNF-α release from adult primary microglia without influencing cell viability

Primary microglia were also used to verify the effects of low-concentration CORT pre-exposure on 24 h 100 ng/ml LPS-induced cytokine production. Both IL-1β and TNF-α were measured in cell supernatant, but IL-1β release from primary microglia was below the detection range of the ELISA assay (<5 pg/ml). IL-1β concentrations were thus excluded from further analysis.

Conversely, LPS significantly increased TNF-α release from primary microglia (B = 14.1 pg/ml, $t(94) = 6.3$, $p<0.0001$) (Figurer 2A). CORT pre-exposure alone did not modify TNF-α concentration (B = -0.3 pg/ml, $t(94)= -0.14$, $p =0.89$), but a significantly interacted with LPS treatment to cause a further TNF-α elevation (B = 6.76 pg/ml, $t(94)= 2.13$, $p<0.05$). Post-hoc pairwise comparisons using Tukey's adjustment further revealed that CORT pre-exposed, LPS treated microglia released significantly more TNF-α compared to vehicle pre-exposed cells (mean difference = 6.4 pg/ml, $p<0.01$).

Cell viability, measured by neutral red uptake from cells following 24 h CORT pre-exposure and 24 h LPS treatment, was not significantly influenced by CORT pre-exposure (B= -85, $t(94) = -0.95$, $p =0.34$) (Figure 2B). LPS treatment significantly decreased cell viability (B= -272, $t(94)= -3.08$, $p<0.01$), but there was no significant interaction between pre-exposure and treatment conditions (B = 234, $t(94)= 1.97$, $p =0.06$). Post-hoc comparisons did not show any significant difference between individual groups ($p>0.05$).

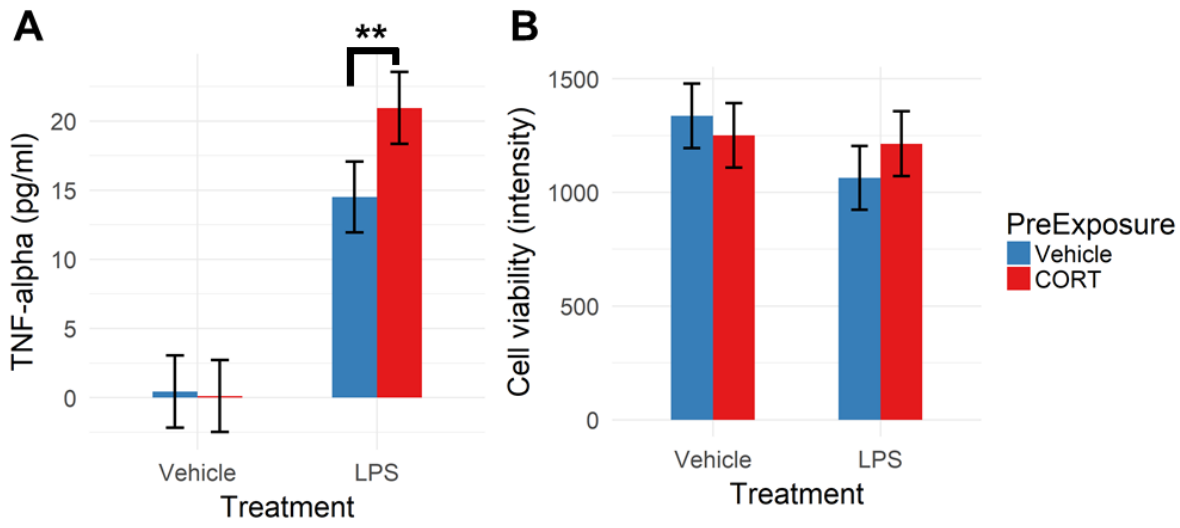

Figure 2. CORT pre-exposure primes further LPS-induced TNF-α release from primary microglia. (A) supernatant TNF-α concentration measured after 24 h CORT (50 nM) or vehicle pre-exposure followed by 24 h LPS (100 ng/ml) treatment. (B) Cell viability measured by neutral red uptake from microglia measured after pre-exposure and treatment. All experiments were performed on N = 10 biological replicates. Statistically significant post-hoc pairwise comparisons between CORT and vehicle pre-exposure using Tukey's adjustment are denoted by: * <0.05, ** <0.01, *** <0.001.

6.4 Discussion

CORT pre-exposure in adult primary microglia demonstrated partial replication of the BV2 study (Chapter 4). Consistent with findings in BV2 cells, CORT pre-exposure primed both NF-κB nuclear translocation in adult primary microglia and LPS-induced TNF-α release. Due to low overall concentrations of IL-1β however, priming of IL-1β release was unable to be accurately measured here. Collectively, these findings provide support for the TLR4-NF-κB priming effect of low concentration CORT in microglia.

When comparing results here to findings in Chapter 4, primary microglia exhibited a lower sensitivity to LPS when compared to BV2 cell responses to the same conditions. Overall, BV2 cells exhibited significant NF-κB translocation after 30 min of LPS treatment, whereas primary microglia only showed significant NF-κB translocation after 4 h in vehicle pre-exposed cells. Furthermore, despite a lower seeding density (2.5×10^4 cells/cm^2 for BV2 cells and 1.5×10^5 cells/cm^2 for primary microglia), BV2 cells exhibited increased IL-1β responses. This result could potentially be attributable to 1) significant cell loss during drug administration, or 2) a requirement for a second signal to induce inflammasome activation and IL-1β release in primary microglia. Given that classical release of IL-1β requires inflammasome activation, LPS alone may be insufficient to induce a significant IL-1β response in microglia. However, multiple studies have previously found IL-1β release from primary microglia stimulated with LPS alone (Horvath *et al.*, 2008; Pan *et al.*, 2008; Xu *et al.*, 2013; Wang *et al.*, 2016; Yuan *et al.*, 2016), suggesting that the lack of IL-1β seen here is more likely due to low cell numbers, or a result of the isolation protocol used. Nevertheless, the current findings

show that relative cell viability was not significantly different between pre-exposure groups, but decreased by LPS treatment. This cell viability result thus indicates that pre-exposure differences in TNF-α is unlikely attributable to cell death-related mechanisms.

Consistent with morphological analysis of BV2 cells, low concentration CORT pre-exposure also prevented LPS-induced ameboid morphological changes in primary microglia. Despite this lack of morphological adaptation, CORT pre-exposure also caused an increase in NF-κB translocation, thus replicating the responses seen *in vitro* from BV2 cells (Chapter 4). Downstream of NF-κB nuclear translocation, CORT pre-exposure also potentiated TNF-α release, therefore sensitising the TLR4-TNF-α pathway as well. Collectively, these results confirm that CORT induces a surveillance state in microglia, priming the innate immune response toward further stimulation. These results also provide further evidence that CORT may play a direct role in stress-induced priming of microglia seen from previous *in vivo* studies (Frank, Watkins and Maier, 2011; Wohleb *et al.*, 2014; Frank *et al.*, 2015; Fonken *et al.*, 2016).

Although direct effects of CORT pre-exposure were verified here, the role of GR and MR in mediating CORT effects is still unknown in these primary microglia. Chapter 4 demonstrated that the priming effects of low concentration CORT on IL-1β release was abolished by a MR specific antagonist, while high concentration CORT-induced inhibition of IL-1β release was reversed by a GR specific antagonist. Conversely, previous *in vivo* studies have shown that stress and CORT induced microglia priming were GR-dependent (Frank *et al.*, 2012; Sobesky *et al.*, 2016). The specific antagonists

have not been utilised in the experiments here, but is an important consideration for future experiments to resolve the exact mechanisms of CORT actions on primary microglia. Additionally, the biphasic concentration-response relationship of CORT pre-exposure has yet to be confirmed in primary microglia, and further experiments are therefore required.

6.5 Conclusion

CORT exhibits direct effects on primary microglia *ex vivo* to induce a primed phenotype. After a pre-exposure to low concentration CORT, these microglia over-respond to a subsequent TLR4 stimulation, characterised by increased NF-κB nuclear translocation and downstream TNF-α release. Taken together with previous findings that GR antagonism can prevent stress-induced priming of microglia (Frank *et al.*, 2012; Sobesky *et al.*, 2016), direct actions of CORT on microglia may therefore mediate this effect. However, further studies, such as GR and MR pharmacological antagonists, are required to ascertain the exact mechanisms underlying these direct CORT actions.

References

Floden, A. M. and Combs, C. K. (2011) 'Microglia demonstrate age-dependent interaction with amyloid-β fibrils.', *Journal of Alzheimer's disease : JAD*, 25(2), pp. 279–93. doi: 10.3233/JAD-2011-101014.

Fonken, L. K., Weber, M. D., Daut, R. a., Kitt, M. M., Frank, M. G., Watkins, L. R. and Maier, S. F. (2016) 'Stress-induced neuroinflammatory priming is time of day dependent', *Psychoneuroendocrinology*. Elsevier Ltd, 66, pp. 82–90. doi: 10.1016/j.psyneuen.2016.01.006.

Frank, M. G., Thompson, B. M., Watkins, L. R. and Maier, S. F. (2012) 'Glucocorticoids mediate stress-induced priming of microglial pro-inflammatory responses', *Brain, Behavior, and Immunity*. Elsevier Inc., 26(2), pp. 337–345. doi: 10.1016/j.bbi.2011.10.005.

Frank, M. G., Watkins, L. R. and Maier, S. F. (2011) 'Stress- and glucocorticoid-induced priming of neuroinflammatory responses: Potential mechanisms of stress-induced vulnerability to drugs of abuse', *Brain, Behavior, and Immunity*. Elsevier Inc., 25(SUPPL. 1), pp. S21-8. doi: 10.1016/j.bbi.2011.01.005.

Frank, M. G., Weber, M. D., Watkins, L. R. and Maier, S. F. (2015) 'Stress sounds the alarmin: The role of the danger-associated molecular pattern HMGB1 in stress-induced neuroinflammatory priming', *Brain, Behavior, and Immunity*. Elsevier Inc., pp. 1–7. doi: 10.1016/j.bbi.2015.03.010.

Frank, M. G., Wieseler-Frank, J. L., Watkins, L. R. and Maier, S. F. (2006) 'Rapid isolation of highly enriched and quiescent microglia from adult rat hippocampus: Immunophenotypic and functional characteristics', *Journal of Neuroscience*

Methods, 151, pp. 121–130. doi: 10.1016/j.jneumeth.2005.06.026.

Horvath, R. J., Nutile-McMenemy, N., Alkaitis, M. S. and DeLeo, J. A. (2008) 'Differential migration, LPS-induced cytokine, chemokine, and NO expression in immortalized BV-2 and HAPI cell lines and primary microglial cultures', *Journal of Neurochemistry*, 107(2), pp. 557–569. doi: 10.1111/j.1471-4159.2008.05633.x.

Kreisel, T., Frank, M. G., Licht, T., Reshef, R., Ben-Menachem-Zidon, O., Baratta, M. V, Maier, S. F. and Yirmiya, R. (2014) 'Dynamic microglial alterations underlie stress-induced depressive-like behavior and suppressed neurogenesis.', *Molecular psychiatry*. Nature Publishing Group, 19(6), pp. 699–709. doi: 10.1038/mp.2013.155.

Pan, X. dong, Chen, X. chun, Zhu, Y. g., Zhang, J., Huang, T. w., Chen, L. m., Ye, Q. yong and Huang, H. p. (2008) 'Neuroprotective role of tripchlorolide on inflammatory neurotoxicity induced by lipopolysaccharide-activated microglia', *Biochemical Pharmacology*, 76(3), pp. 362–372. doi: 10.1016/j.bcp.2008.05.018.

Repetto, G., del Peso, A. and Zurita, J. L. (2008) 'Neutral red uptake assay for the estimation of cell viability/cytotoxicity.', *Nature protocols*, 3(7), pp. 1125–31. doi: 10.1038/nprot.2008.75.

Schell, J. B., Crane, C. A., Smith, M. F. and Roberts, M. R. (2007) 'Differential ex vivo nitric oxide production by acutely isolated neonatal and adult microglia', *Journal of Neuroimmunology*, 189(1–2), pp. 75–87. doi: 10.1016/j.jneuroim.2007.07.004.

Sobesky, J. L., D'Angelo, H. M., Weber, M. D., Anderson, N. D., Frank, M. G., Watkins, L. R., Maier, S. F. and Barrientos, R. M. (2016) 'Glucocorticoids Mediate Short-Term

High-Fat Diet Induction of Neuroinflammatory Priming, the NLRP3 Inflammasome, and the Danger Signal HMGB1', *eNeuro*, 3(4), pp. 1–17. doi: 10.1523/ENEURO.0113-16.2016.

Wang, Y., Zhao, H., Lin, C., Ren, J. and Zhang, S. (2016) 'Forsythiaside A Exhibits Anti-inflammatory Effects in LPS-Stimulated BV2 Microglia Cells Through Activation of Nrf2/HO-1 Signaling Pathway', *Neurochemical Research*. Springer US, 41(4), pp. 659–665. doi: 10.1007/s11064-015-1731-x.

Wohleb, E. S., McKim, D. B., Shea, D. T., Powell, N. D., Tarr, A. J., Sheridan, J. F. and Godbout, J. P. (2014) 'Re-establishment of anxiety in stress-sensitized mice is caused by monocyte trafficking from the spleen to the brain', *Biological Psychiatry*, 75(12), pp. 970–981. doi: 10.1016/j.biopsych.2013.11.029.

Xu, J., Zhang, Y., Xiao, Y., Ma, S., Liu, Q., Dang, S., Jin, M., Shi, Y., Wan, B. and Zhang, Y. (2013) 'Inhibition of 12/15-lipoxygenase by baicalein induces microglia PPARβ/δ: a potential therapeutic role for CNS autoimmune disease', *Cell Death and Disease*, 4(4), p. e569. doi: 10.1038/cddis.2013.86.

Yu, A. C., Neil, S. E. and Quandt, J. A. (2017) 'High yield primary microglial cultures using granulocyte macrophage-colony stimulating factor from embryonic murine cerebral cortical tissue', *Journal of Neuroimmunology*. Elsevier, 307(February), pp. 53–62. doi: 10.1016/j.jneuroim.2017.03.018.

Yuan, L., Liu, S., Bai, X., Gao, Y., Liu, G., Wang, X., Liu, D., Li, T., Hao, A. and Wang, Z. (2016) 'Oxytocin inhibits lipopolysaccharide-induced inflammation in microglial cells and attenuates microglial activation in lipopolysaccharide-treated mice', *Journal of Neuroinflammation*. Journal of Neuroinflammation, 13(1), p. 77. doi:

10.1186/s12974-016-0541-7.

Chapter 7: Extracellular ATP and caspase-1 independent IL-1β release; assessing immune activity beyond cytokine release.

7.1 Introduction

Chapter 4 reported an increase in extracellular IL-1β with concurrent decrease in intracellular pro-IL-1β expression from BV2 cells pre-exposed to 50nM CORT for 24 h, followed by a further 24 h treatment with 100 ng/ml LPS. The CORT pre-exposure model did not influence NLRP3 expression in BV2 cells. However, IL-1β classically requires activation of inflammasomes, best characterised by caspase-1 dependent conversion and release via the NLRP3 inflammasome complex formation (see review Latz et al., 2013). Experimentally, NLRP3 inflammasome activation in immunocompetent cells generally requires two steps. First, individual proteins, NLRP3, ASC and pro-caspase-1 are upregulated during a priming phase, and in a second activation phase, pro-caspase-1 conversion to active caspase-1 occurs after the cell receives a danger signal (Broz and Dixit, 2016). The first priming step usually follows a NF-κB transcriptional event via LPS or TNF-α administration, while the second danger signal can range from a high concentration of ATP (Rada *et al.*, 2014; Gustin *et al.*, 2015; Monif *et al.*, 2016) to uric acid and silica nanoparticles (Sandberg *et al.*, 2012; Hari *et al.*, 2014). The mechanism of ATP-induced inflammasome activation further involves Ca^{2+} influx via purinergic P2X7 receptors (Monif *et al.*, 2016) or K^{+} efflux (Katsnelson *et al.*, 2015).

This chapter thus further investigated if low-concentration CORT pre-exposure functionally primes the NLRP3 inflammasome complex. Administration of 1mM ATP was selected as the inflammasome activator (Sigma-Aldrich, A2383, Germany) following pre-exposure + treatment to prime the system (Figure 1). Further

inflammasome dependency of IL-1β release was investigated through use of a caspase -1 and caspase-4 inhibitor, z-YVAD-FMK (R&D Bioscience, FMK005, USA). The methods used in this chapter are similar to Chapter 4, with slight modifications to drugs administered.

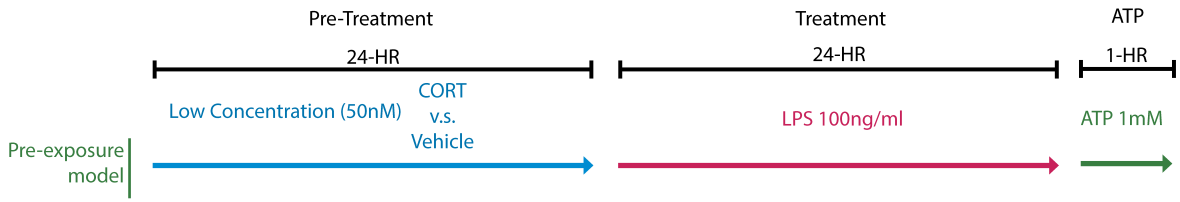

Figure 1. Study design. CORT pre-exposure (50nM) was applied for 24 h and removed prior to a second 24 h of LPS(100ng/ml) treatment. Finally, LPS was removed from BV2 cells while ATP (1mM) or vehicle (HBSS) was applied to the cells. IL-1β was measured from the supernatant at the end of all drug treatments.

7.2 Results

7.2.1 CORT pre-exposed cells are not responsive to further ATP-induced IL-1β.

Support vector machine (SVM) was implemented here to distinguish between CORT or vehicle pre-exposure from intracellular pro-IL-1β and extracellular IL-1β expression following pre-exposure+LPS (before ATP treatment) or pre-exposure+LPS+ATP (after 1 h ATP/ vehicle treatment) (Figure 2).

Support vector machine (SVM) is an algorithm to resolve boundaries which best distinguish between classes on a vector space through selecting a hyperplane which maximises distances between the classes, and can be adapted in a linear or non-linear manner through selection of different kernels (see review Noble, 2006). Common implementations of SVM to biological data include classification of imaging data (Larroza *et al.*, 2015), and drug design (Han *et al.*, 2007). SVM has also been successful in classifying psychiatric patient groups through analysis of neuroimaging and proteomics data (Orrù *et al.*, 2012). An important consideration is the descriptive nature of this analysis due to the small sample size, thus lacking cross-validation to assess over-fitting of the dataset. Nevertheless, SVM successfully classified treatment groups above chance, before ATP treatment (accuracy = 0.84, $p < 0.0001$), after 1 h vehicle treatment (accuracy = 0.84, $p<0.0001$), and after 1 h ATP treatment (accuracy = 0.90, $p<0.0001$).

Moreover, an evident shift in the decision boundaries between CORT and vehicle pre-exposed cells is observed before and after ATP or vehicle treatments. Before ATP was

added to the system, CORT pre-exposure elicited increased IL-1β levels in the supernatant, as compared to vehicle while having a decreased intracellular pro-IL-1β expression (top-left corner). After ATP or vehicle was introduced to the system however, CORT pre-exposure caused a decrease in both supernatant IL-1β and intracellular pro-IL-1β, thus predominantly occupying the lower-left corner relative to vehicle pre-exposed cells.

Given that NLRP3 remained unchanged in CORT pre-exposed cells (see Chapter 4), this result suggests that the inflammasome may no longer be active by the time ATP was introduced to the system in low concentration pre-exposed cells. A second possibility could be that the CORT pre-exposure-dependent increase in conversion and release of IL-1β measured after LPS may be inflammasome-independent.

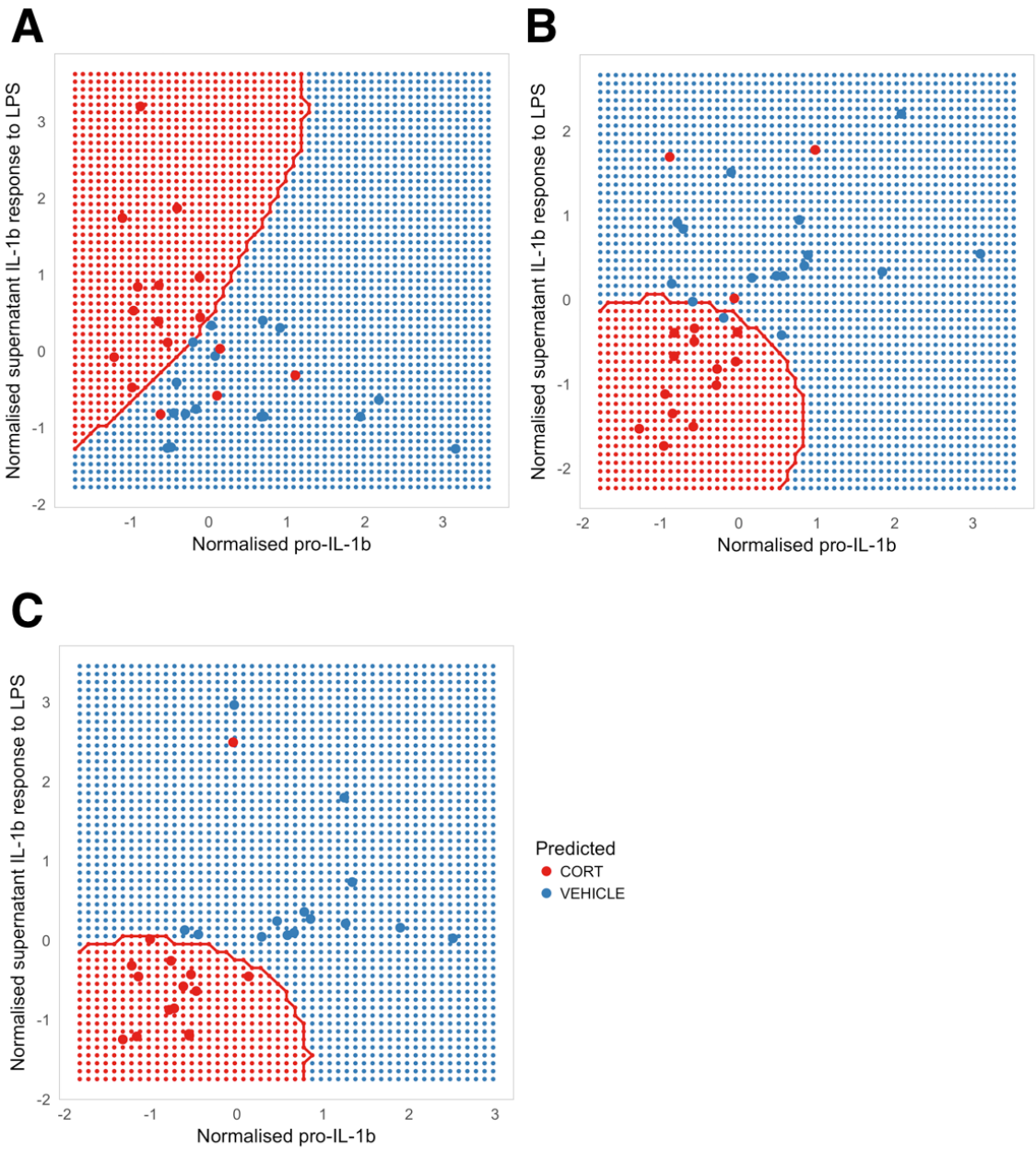

Figure 2 Support vector machine analysis illustrate ATP-insensitivity in CORT pre-exposed BV2 cells. Scatter plots of IL-1β measured from the supernatant (y-axis) and pro-IL-1β expression from cell lysates (x-axis) in the same cells (N= 16). Resolved SVM boundaries between CORT pre-exposed and vehicle pre-exposed cells are shifted when IL-1β is measured before ATP administration (pre-exposure + LPS) (A), after pre-exposure + LPS + ATP (B), and after pre-exposure + LPS + vehicle (C) conditions. Large points represent data measured from experiments. All values are z-score normalized to remove scaling differences between measures.

7.2.2 Caspase inhibition fails to prevent IL-1β release from BV2 cells.

To test caspase-dependence of IL-1β release from BV2 cells, a cell permanent caspase-1 and caspase-4 inhibitor, z-YVAD-FMK (0, 100 nM, 1 µM, and 10 µM) was incubated in the presence or absence of LPS (100 ng/ml) for 24 h. Administration of z-YVAD-FMK *in vitro* was previously shown to inhibit IL-1β release (Halle *et al.*, 2008; Kaushik *et al.*, 2012), and Fas-mediated apoptosis (Choi, Jeong and Benveniste, 2004). In this experiment, extracellular IL-1β was measured after LPS treatment, and after LPS treatment + 1 h ATP. This pilot experiment was done without CORT pre-exposure to characterise the concentrations required to achieve inhibition of IL-1β release (Figure 3).

As assessed by a linear mixed effects model controlling for repeated measures, YVAD-FMK did not significantly influence IL-1β release from BV2 cells at any concentration (100 nM: B= 0.32 fold, t(21)= 0.65, p=0.52; 1000 nM: B=0.32 fold, t(21)= 0.65, p=0.52, 10 uM: B=-0.15 fold, t(21)=-0.30, p=0.76). No z-YVAD-FMK concentration significantly interacted with 1mM ATP treatment either (100 nM: B= -0.26 fold, t(21)= -0.37, p=0.72; 1000 nM: B=-0.71fold, t(21)= -1.01., p=0.33, 10 uM: B=0.05 fold, t(21)=0.07, p=0.94). Thus, IL-1β release appears to be caspase-1 and caspase-4 independent in BV2 cells.

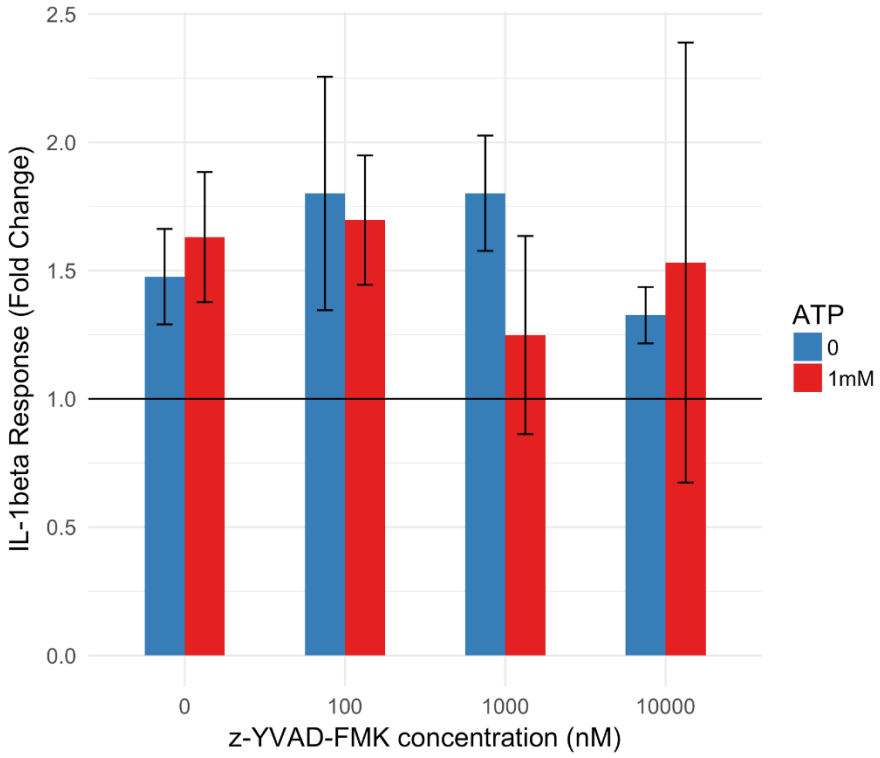

Figure 3. IL-1β release from BV2 cells is not influenced by caspase-1 and caspase-4 inhibition. Bar graphs representing mean± SEM of IL-1β response to LPS or LPS+ATP when LPS was co-incubated with varying concentrations of z-YVAD-FMK (N=4). Fold change was calculated from samples treated with vehicle + corresponding z-YVAD-FMK concentrations within each biological replicate.

7.3 Discussion

Investigating the role of inflammasome activation, the current chapter reports a decrease in ATP-induced IL-1β conversion and release from low concentration CORT pre-exposed cells when compared to vehicle pre-exposed controls. Furthermore, using a pharmacological inhibitor, a lack of caspase-1 or -4 dependency in the release of IL-1β from BV2 cells was also demonstrated. Thus, the role of inflammasome activation in IL-1β release from BV2 microglia-like cells is unclear.

This insensitivity to z-YVAD-FMK treatment contradicts previous findings demonstrating a successful inhibition of IL-1β release from BV2 cells using the same caspase antagonist (Kaushik *et al.*, 2012). However, one notable difference from our experiment is the use of Japanese Encephalitis virus in the previous study, which could induce a stronger caspase-dependency in BV2 cells as compared to the LPS+ATP treatment here. Furthermore, LPS+ATP-induced IL-1β release in primary microglia is only partially dependent on caspases (Burm *et al.*, 2015). In agreement with the results seen here, this study also showed that 10 μM YVAD-FMK is unable to modify LPS+inflammasome activation-induced IL-1β release from microglia. Thus, similar to primary microglia, BV2 cells appear to have decreased dependency on caspase-1 in the release of IL-1β. Further investigations into the exact release mechanisms involved are therefore required.

The potential inflammasome-independent CORT-priming as suggested here is inconsistent with previous findings associating microglia inflammasome activation with glucocorticoid-induced neuroimmune priming (see review Frank et al., 2015).

However, an important distinction is that while inescapable tail shock has been shown to increase hippocampal NLRP3 (Weber *et al.*, 2015), most glucocorticoid-related elevation of microglia NLRP3 are shown at the mRNA level (Frank *et al.*, 2014).

Consistent with our results showing that CORT pre-exposure does not influence intracellular NLRP3 expression, chronic dexamethasone, a synthetic GR specific agonist, did not change overall NLRP3 expression in the frontal cortex and hippocampus, despite an increase in caspase-1 activity and neurodegeneration (Hu *et al.*, 2016). A limitation of chapter 4 is the sole measurement of intracellular NLRP3. Emerging evidence shows that extracellular inflammasomes can act in a DAMP-like manner and amplify pro-inflammation (Baroja-Mazo *et al.*, 2014), potentially via paracrine exosomal transport (Wang *et al.*, 2016). The existence of extracellular inflammasome in the brain is still unclear, and requires further study. Together with results in Chapter 4 showing an increased role of *Pycard* gene expression in the release of IL-1β from CORT pre-exposed BV2 cells, a study of both intracellular and extracellular inflammasome components following CORT pre-exposure is therefore pursued in Study 3.

DAMP signalling through HMGB1 has been implicated in the priming of microglia following stress (see review Frank et al., 2015). *In vivo* inescapable tail shock stress-induced microglia priming can be prevented by an *intracisterna magna* injection of a HMGB1 antibody, and further replicated by administration of a TLR4 agonist, disulfide-HMGB1 (Weber *et al.*, 2015). This study demonstrates the dependency of microglia priming on HMGB1 signalling, but the exact role of glucocorticoids on this HMGB1

signalling has not been established. Furthermore, it is unclear if glucocorticoids can directly act on microglia to cause the increase of HMGB1, or if this effect arises from a systemic adaptation to physiological stress.

Apart from priming the cytokine and DAMP responses in microglia, stress and CORT can also cause increased immune cell migration. Social defeat stress increases monocyte infiltration in rodent studies, and this is related to increased chemokine CCL2 expression (Wohleb *et al.*, 2012). Moreover, glucocorticoids can induce increased chemokine CXCR4 expression, and this is associated with the regulation and redistribution of T-Cells in the periphery (Okutsu *et al.*, 2005), while CORT can prime peripheral leukocyte cell migration to sites of injury in humans (Yeager *et al.*, 2016). In the CNS however, it is unclear if CORT and stress have any effect on microglia motility. Microglia are extremely motile, and have been shown to migrate towards sites of injury (Zhang *et al.*, 2016). One such signal is ATP, released as DAMP, as microglia and BV2 cells have been shown to move towards a high concentration of extracellular ATP (Choi *et al.*, 2010; Persson *et al.*, 2014).

7.4 Conclusion

The current study found a priming effect of low concentration CORT pre-exposure in BV2 cells and adult primary microglia. This was characterised by the increase in TLR4 mediated NF-κB translocation and some downstream pro-inflammatory cytokine. BV2 microglia-like cells exhibited an exacerbated IL-1β but not IL-6 response, while adult primary microglia showed priming of TNF-α release. The effects of CORT pre-exposure on inflammasome activation in BV2 cells were unclear, since overall expression was

unchanged, and ATP-induced IL-1β responses were supressed by the pre-exposure. However, pro-inflammatory cytokine release only represents part of the innate immune response. Given the actions of glucocorticoids on the motility of peripheral immunocompetent cells, together with knowledge of release of DAMPs such as HMGB1 after stress models, the next study thus shifts the focus towards DAMPs, cellular damage and ATP-induced cell motility as other assessments of CORT effects on immune activity outside of cytokine signalling pathways in BV2 cells.

References

Baroja-Mazo, A., Martín-Sánchez, F., Gomez, A. I., Martínez, C. M., Amores-Iniesta, J., Compan, V., Barberà-Cremades, M., Yagüe, J., Ruiz-Ortiz, E., Antón, J., Buján, S., Couillin, I., Brough, D., Arostegui, J. I. and Pelegrín, P. (2014) 'The NLRP3 inflammasome is released as a particulate danger signal that amplifies the inflammatory response.', *Nature immunology*, (5 mM), pp. 1–5. doi: 10.1038/ni.2919.

Broz, P. and Dixit, V. M. (2016) 'Inflammasomes: mechanism of assembly, regulation and signalling', *Nature Reviews Immunology*, 16(7), pp. 407–420. doi: 10.1038/nri.2016.58.

Burm, S. M., Zuiderwijk-Sick, E. a, 't Jong, A. E. J., van der Putten, C., Veth, J., Kondova, I. and Bajramovic, J. J. (2015) 'Inflammasome-Induced IL-1β Secretion in Microglia Is Characterized by Delayed Kinetics and Is Only Partially Dependent on Inflammatory Caspases.', *The Journal of neuroscience : the official journal of the Society for Neuroscience*, 35(2), pp. 678–87. doi: 10.1523/JNEUROSCI.2510-14.2015.

Choi, C., Jeong, E. and Benveniste, E. N. (2004) 'Caspase-1 Mediates Fas-Induced Apoptosis and is Up-Regulated by Interferon- in Human Astrocytoma Cells', *Journal of Neuro-Oncology*, 67(1/2), pp. 167–176. doi: 10.1023/B:NEON.0000021896.52664.9e.

Choi, M. S., Cho, K. S., Shin, S. M., Ko, H. M., Kwon, K. J., Shin, C. Y. and Ko, K. H. (2010) 'ATP induced microglial cell migration through non-transcriptional activation of matrix metalloproteinase-9', *Archives of Pharmacal Research*, 33(2), pp. 257–

265. doi: 10.1007/s12272-010-0211-8.

Frank, M. G., Hershman, S. A., Weber, M. D., Watkins, L. R. and Maier, S. F. (2014) 'Chronic exposure to exogenous glucocorticoids primes microglia to pro-inflammatory stimuli and induces NLRP3 mRNA in the hippocampus', *Psychoneuroendocrinology*. Elsevier Ltd, 40, pp. 191–200. doi: 10.1016/j.psyneuen.2013.11.006.

Frank, M. G., Weber, M. D., Watkins, L. R. and Maier, S. F. (2015) 'Stress sounds the alarmin: The role of the danger-associated molecular pattern HMGB1 in stress-induced neuroinflammatory priming', *Brain, Behavior, and Immunity*. Elsevier Inc., pp. 1–7. doi: 10.1016/j.bbi.2015.03.010.

Gustin, A., Kirchmeyer, M., Koncina, E., Felten, P., Losciuto, S., Heurtaux, T., Tardivel, A., Heuschling, P. and Dostert, C. (2015) 'NLRP3 Inflammasome Is Expressed and Functional in Mouse Brain Microglia but Not in Astrocytes', *PLOS ONE*. Edited by T. A. Kufer, 10(6), p. e0130624. doi: 10.1371/journal.pone.0130624.

Halle, A., Hornung, V., Petzold, G. C., Stewart, C. R., Monks, B. G., Reinheckel, T., Fitzgerald, K. A., Latz, E., Moore, K. J. and Golenbock, D. T. (2008) 'The NALP3 inflammasome is involved in the innate immune response to amyloid-beta', *Nat Immunol*, 9(8), pp. 857–865. doi: 10.1038/ni.1636.

Han, L. Y., Zheng, C. J., Xie, B., Jia, J., Ma, X. H., Zhu, F., Lin, H. H., Chen, X. and Chen, Y. Z. (2007) 'Support vector machines approach for predicting druggable proteins: recent progress in its exploration and investigation of its usefulness', *Drug Discovery Today*, 12(7–8), pp. 304–313. doi: 10.1016/j.drudis.2007.02.015.

Hari, A., Zhang, Y., Tu, Z., Detampel, P., Stenner, M., Ganguly, A. and Shi, Y. (2014) 'Activation of NLRP3 inflammasome by crystalline structures via cell surface contact.', *Scientific reports*, 4(DECEMBER), p. 7281. doi: 10.1038/srep07281.

Hu, W., Zhang, Y., Wu, W., Yin, Y., Huang, D., Wang, Y., Li, W. and Li, W. (2016) 'Chronic glucocorticoids exposure enhances neurodegeneration in the frontal cortex and hippocampus via NLRP-1 inflammasome activation in male mice', *Brain, Behavior, and Immunity*. Elsevier Inc., 52, pp. 58–70. doi: 10.1016/j.bbi.2015.09.019.

Katsnelson, M. a., Rucker, L. G., Russo, H. M. and Dubyak, G. R. (2015) 'K+ Efflux Agonists Induce NLRP3 Inflammasome Activation Independently of Ca2+ Signaling', *The Journal of Immunology*. doi: 10.4049/jimmunol.1402658.

Kaushik, D. K., Gupta, M., Kumawat, K. L. and Basu, A. (2012) 'Nlrp3 inflammasome: Key mediator of neuroinflammation in murine japanese encephalitis', *PLoS ONE*, 7(2). doi: 10.1371/journal.pone.0032270.

Larroza, A., Moratal, D., Paredes-Sánchez, A., Soria-Olivas, E., Chust, M. L., Arribas, L. A. and Arana, E. (2015) 'Support vector machine classification of brain metastasis and radiation necrosis based on texture analysis in MRI', *Journal of Magnetic Resonance Imaging*, 42(5), pp. 1362–1368. doi: 10.1002/jmri.24913.

Latz, E., Xiao, T. S. and Stutz, A. (2013) 'Activation and regulation of the inflammasomes', *Nature Reviews Immunology*, 13(6), pp. 397–411. doi: 10.1038/nri3452.

Monif, M., Reid, C. A., Powell, K. L., Drummond, K. J., O'Brien, T. J. and Williams, D. A.

(2016) ‘Interleukin-1β has trophic effects in microglia and its release is mediated by P2X7R pore’, *Journal of Neuroinflammation*. Journal of Neuroinflammation, 13(1), p. 173. doi: 10.1186/s12974-016-0621-8.

Noble, W. S. (2006) ‘What is a support vector machine?’, *Nature Biotechnology*, 24(12), pp. 1565–1567. doi: 10.1038/nbt1206-1565.

Okutsu, M., Ishii, K., Niu, K. J. and Nagatomi, R. (2005) ‘Cortisol-induced CXCR4 augmentation mobilizes T lymphocytes after acute physical stress.’, *American journal of physiology. Regulatory, integrative and comparative physiology*, 288(3), pp. R591-9. doi: 10.1152/ajpregu.00438.2004.

Orrù, G., Pettersson-Yeo, W., Marquand, A. F., Sartori, G. and Mechelli, A. (2012) ‘Using Support Vector Machine to identify imaging biomarkers of neurological and psychiatric disease: A critical review’, *Neuroscience & Biobehavioral Reviews*. Elsevier Ltd, 36(4), pp. 1140–1152. doi: 10.1016/j.neubiorev.2012.01.004.

Persson, A.-K., Estacion, M., Ahn, H., Liu, S., Stamboulian-Platel, S., Waxman, S. G. and Black, J. a. (2014) ‘Contribution of sodium channels to lamellipodial protrusion and Rac1 and ERK1/2 activation in ATP-stimulated microglia’, *Glia*, 62(12), pp. 2080–2095. doi: 10.1002/glia.22728.

Rada, B., Park, J. J., Sil, P., Geiszt, M. and Leto, T. L. (2014) ‘NLRP3 inflammasome activation and interleukin-1β release in macrophages require calcium but are independent of calcium-activated NADPH oxidases’, *Inflammation Research*, pp. 821–830. doi: 10.1007/s00011-014-0756-y.

Sandberg, W. J., Låg, M., Holme, J. A., Friede, B., Gualtieri, M., Kruszewski, M., Schwarze, P. E., Skuland, T. and Refsnes, M. (2012) 'Comparison of non-crystalline silica nanoparticles in IL-1β release from macrophages.', *Particle and fibre toxicology*, 9(1), p. 32. doi: 10.1186/1743-8977-9-32.

Sawicki, C. M. M., McKim, D. B. B., Wohleb, E. S. S., Jarrett, B. L. L., Reader, B. F. F., Norden, D. M. M., Godbout, J. P. P. and Sheridan, J. F. F. (2015) 'Social defeat promotes a reactive endothelium in a brain region-dependent manner with increased expression of key adhesion molecules, selectins and chemokines associated with the recruitment of myeloid cells to the brain', *Neuroscience*. IBRO, 302, pp. 151–164. doi: 10.1016/j.neuroscience.2014.10.004.

Wang, L., Fu, H., Nanayakkara, G., Li, Y., Shao, Y., Johnson, C., Cheng, J., Yang, W. Y., Yang, F., Lavallee, M., Xu, Y., Cheng, X., Xi, H., Yi, J., Yu, J., Choi, E. T., Wang, H. and Yang, X. (2016) 'Novel extracellular and nuclear caspase-1 and inflammasomes propagate inflammation and regulate gene expression: a comprehensive database mining study', *Journal of Hematology & Oncology*. Journal of Hematology & Oncology, 9(1), p. 122. doi: 10.1186/s13045-016-0351-5.

Weber, M. D., Frank, M. G., Tracey, K. J., Watkins, L. R. and Maier, S. F. (2015) 'Stress Induces the Danger-Associated Molecular Pattern HMGB-1 in the Hippocampus of Male Sprague Dawley Rats: A Priming Stimulus of Microglia and the NLRP3 Inflammasome.', *The Journal of neuroscience : the official journal of the Society for Neuroscience*, 35(1), pp. 316–24. doi: 10.1523/JNEUROSCI.3561-14.2015.

Wohleb, E. S., Fenn, A. M., Pacenta, A. M., Powell, N. D., Sheridan, J. F. and Godbout, J.

P. (2012) ‘Peripheral innate immune challenge exaggerated microglia activation, increased the number of inflammatory CNS macrophages, and prolonged social withdrawal in socially defeated mice.’, *Psychoneuroendocrinology*. Elsevier Ltd, 37(9), pp. 1491–505. doi: 10.1016/j.psyneuen.2012.02.003.

Yeager, M. P., Pioli, P. A., Collins, J., Barr, F., Metzler, S., Sites, B. D. and Guyre, P. M. (2016) ‘Glucocorticoids enhance the in vivo migratory response of human monocytes’, *Brain, Behavior, and Immunity*. Elsevier Inc., 54, pp. 86–94. doi: 10.1016/j.bbi.2016.01.004.

Zhang, F., Nance, E., Alnasser, Y., Kannan, R. and Kannan, S. (2016) ‘Microglial migration and interactions with dendrimer nanoparticles are altered in the presence of neuroinflammation’, *Journal of Neuroinflammation*. Journal of Neuroinflammation, pp. 1–11. doi: 10.1186/s12974-016-0529-3.

Study 3: Effects of corticosterone on DAMP-related protein release, cytotoxicity and cell viability

- **Chapter 8 – Manuscript:** Glucocorticoid receptor signalling influences cytotoxicity and DAMP-related protein release in BV2 and microglia

- **Chapter 9 – Supplement:** Additional effects of corticosterone using a pre-exposure + treatment + ATP model

Statement of Authorship

Title of Paper	Glucocorticoid receptor signalling influences cytotoxicity and DAMP-related protein release in BV2 and microglia
Publication Status	☐ Published ☐ Accepted for Publication ☒ Submitted for Publication ☐ Unpublished and Unsubmitted w ork w ritten in manuscript style
Publication Details	Submitted for review in *Psychoneuroendocrinology*

Principal Author

Name of Principal Author (Candidate)	JiaJun Liu
Contribution to the Paper	Designed and condeucted the study, performed data analysis and interpretation, prepared and edited the manuscript
Overall percentage (%)	90%
Certification:	This paper reports on original research I conducted during the period of my Higher Degree by Research candidature and is not subject to any obligations or contractual agreements with a third party that would constrain its inclusion in this thesis. I am the primary author of this paper.
Signature	Date

Co-Author Contributions

By signing the Statement of Authorship, each author certifies that:

i. the candidate's stated contribution to the publication is accurate (as detailed above);

ii. permission is granted for the candidate in include the publication in the thesis; and

iii. the sum of all co-author contributions is equal to 100% less the candidate's stated contribution.

Name of Co-Author	Dr. Sanam Mustafa
Contribution to the Paper	Supervised the study design, interpretation of results, planning and editing of the manuscript
Signature	Date 05/09/2017

Name of Co-Author	Prof. Mark Hutchinson
Contribution to the Paper	Supervised the study design, interpretation of results, planning and editing of the manuscript.
Signature	Date

Please cut and paste additional co-author panels here as required.

Chapter 8 – Manuscript: Glucocorticoid receptor signalling influences cytotoxicity and DAMP-related protein release in BV2 and microglia

JiaJun Liu[1,2], Sanam Mustafa[1,2] and Mark R Hutchinson[1,2]

1. Discipline of Physiology, Adelaide Medical School, University of Adelaide, Adelaide, South Australia, Australia 5005

2. Australian Research Council Centre of Excellence for Nanoscale BioPhotonics, University of Adelaide, Adelaide, South Australia, Australia 5005

Abstract

Emerging evidence demonstrates that glucocorticoid release can increase peripheral immune cell migration, increase HMGB1 release (a danger associated molecular pattern; DAMP), and upregulate inflammasome activity. However, the mechanisms underpinning the glucocorticoid impact on DAMP signalling within neuroimmune-like cells remains poorly defined. The current study thus explored the integrated impact of corticosterone (CORT) pre-exposure, combined with innate immune activation using lipopolysaccharide (LPS), on DAMP-related protein release and migration. This was tested on microglia-like BV2 cells and adult primary microglia. Cytotoxicity, cell viability and extracellular DAMP protein expression of HMGB1, ASC and NLRP3 were measured in BV2 cells, while cell viability and intracellular HMGB1 localisation was measured in primary microglia. Glucocorticoid receptor (GR) and Mineralocorticoid receptor (MR) dependency was assessed using specific pharmacological antagonists.

In this study, CORT pre-exposed primary microglia exhibited cytoplasmic localisation of HMGB1 expression, indicating a larger probability for release. In BV2 microglia-cells, CORT increased measures of cytotoxicity and extracellular HMGB1 expression, while significantly decreasing cell viability directly after 24 h pre-exposure in a GR dependent manner. After a further 24 h treatment with either LPS or vehicle, CORT pre-exposure increased extracellular NLRP3 and ASC expression, while still causing a persistent increase in extracellular HMGB1. These effects were not reversed by either GR or MR antagonists. Taken together, CORT exposure coordinates complex and persistent actions on immunocompetent BV2 cells and microglia, influencing the immune

response through increased cell motility, release of DAMPs and cytotoxicity, in part via GR signalling.

Introduction

Glucocorticoids, primarily corticosterone (CORT) in rodents, and cortisol in humans, are a class of steroid hormones most associated with the neuroendocrine stress response. With receptors expressed ubiquitously in different tissues, glucocorticoid actions are varied and complex. Glucocorticoids appear to have paradoxical actions on the immune system, exhibiting both immunosuppressive and immune 'priming' actions (Sapolsky, Romero and Munck, 2000; Bellavance and Rivest, 2014). Since chronic stress and glucocorticoid signalling have become increasingly associated with stress-related neuropsychiatric disorders such as depression, anxiety and cognitive decline (Chiba *et al.*, 2012; Hu *et al.*, 2016), resolving these seemingly different actions in the neuroimmune system would contribute to an understanding of the mechanisms and aetiology of these disorders.

1.1 Stress and glucocorticoids cause immunosuppression

Glucocorticoids are classically regarded as immunosuppressive through glucocorticoid receptor (GR) signalling. After glucocorticoids bind to cytoplasmic GR in immunocompetent cells, the receptors translocate into the nucleus, and either interact with pro-inflammatory and anti-inflammatory transcriptional factors, or form homodimers and bind to Glucocorticoid Response Elements on DNA, ultimately resulting in increased anti-inflammatory gene transcription, or repression of pro-inflammatory genes (see review Xavier et al., 2016). Moreover, glucocorticoids also cause apoptosis of immunocompetent cells through regulation of BCL-2 and REDD1 (Viegas *et al.*, 2008; Molitoris *et al.*, 2011; Wu *et al.*, 2013), thus contributing towards immunosuppression.

1.2 Immune 'priming' effects of glucocorticoids

Conversely, emerging evidence has demonstrated that stress and glucocorticoids can cause a 'primed' neuroimmune response in microglia, a predominant immunocompetent cell type in the brain, during the recovery period after stress (see review Frank et al., 2016). This effect has been shown to last up to 4 days after resolution of inescapable tail shock stress (Johnson *et al.*, 2002). Stress induced priming is characterised by pro-inflammatory gene upregulation in microglia responding to innate immune stimuli such as lipopolysaccharide (LPS) following chronic stress or administration of CORT, and this effect requires GR signalling in vivo (Frank *et al.*, 2012, 2014).

At present, the mechanisms of CORT induced immune priming are unclear, but prior evidence displayed the involvement of HMGB1 protein, as this priming effect was abolished by an administered HMGB1 neutralising antibody to inhibit receptor binding (Weber *et al.*, 2015). Nucleic HMGB1 functions as a chaperone protein and facilitates binding of transcriptional factors to DNA to enable gene transcription during normal physiology (Klune *et al.*, 2008). Extracellular HMGB1, however, can function as a potent endogenous Danger Associated Molecular Pattern (DAMP or alarmin), which have pro-inflammatory actions via TLR4 and RAGE innate immune receptors (Yang *et al.*, 2013). The immune-active forms of HMGB1 are related to the redox state of the protein; the disulfide bonds on C23 and C45 are integral for cytokine activity and the fully reduced form of the protein has chemokine activity (Venereau *et al.*, 2012). Evidence from monocytes indicate that hyperacetylation of HMGB1 in the cytoplasm

may be involved in the release of HMGB1 (Bonaldi *et al.*, 2003). Additionally, cell death and injury through inflammasome activation (Vande Walle, Kanneganti and Lamkanfi, 2011) can cause the release of disulfide-HMGB1 from monocytes (Willingham *et al.*, 2009). Lipopolysaccharide (LPS), a potent innate immune agonist, has also been shown to induce HMGB1 release (Schierbeck *et al.*, 2010). However, the exact mechanisms involved in stress-specific HMGB1 release are currently unresolved.

Taken together, apart from the potential differences in timing and order of CORT exposure, the mechanisms underlying paradoxical immunosuppressive and immune priming effects of CORT in central immune cells are not well established. The current study thus aimed to investigate the role of CORT-induced cell damage and release of DAMPs, such as HMGB1 in microglia. Microglia-like BV2 cells were further used to explore potential mechanisms of CORT effects. We used a CORT pre-exposure model followed by an LPS immune stimulation in these cells, which produced a 'priming' phenotype in these BV2 cells from previous lab experiments (Chapters 4-6). Further study of the dependency on CORT receptors GR and mineralocorticoid receptor (MR) was tested using specific pharmacological agonists and antagonists to these receptors.

2 Methods

2.1 Animals

Male Balb/c mice (5-6 weeks old) were maintained under conditions of 12 h light/dark cycle, with food and water provided *ad libitum*. All experimental procedures were conducted in accordance to the University of Adelaide animal ethics committee.

2.2 Adult primary microglia isolation using Percoll gradient

Microglia were isolated according to previously published methods with minor modifications (Wohleb *et al.*, 2014). This method was previously shown to obtain >90% purity of primary microglia samples. Briefly, Balb/c mice were culled via pentobarbitone overdose (60 mg/ml) prior to cardiac perfusion using ice-cold saline. Working aseptically, brains were hemisected, and meninges were removed under a dissecting microscope. Brain tissue was subsequently chopped into approximately 1 mm^3 size prior to papain enzymatic dissociation (130-092-628, Miltenyi, Germany) using the gentleMac system (Miltenyi, Germany) according to the manufacturer's recommendations.

Dissociated cell suspensions and 10 ml PBS were passed through a 70 µm cell strainer to remove large debris, and centrifuged at 600 g for 6 min at 10 °C to form a cell pallet. After aspirating the supernatant, the cell palette was resupended in 3 ml 70% isotonic Percoll solution (17-0891-02, GE Healthcare Life Sciences, USA) and transferred into a fresh 15 ml centrifuge tube. Careful not to mix each layer, 3 ml 50% , 3 ml 35%, then 2 ml 0% (PBS) isotonic Percoll were gently layered on top to construct an ordinal density gradient. Samples were subsequently centrifuged at 2000 g for 20 min at 10 °C with minimal acceleration and brake. After centrifugation, the top layer containing myelin

and debris between 0% and 35% was discarded using a sterile pasteur pipette. Using a fresh pasteur pipette, microglia between the 70% and 50% layers were collected and transferred to a fresh 15 ml centrifuge tube. After addition of 10 ml PBS, each cell suspension was centrifuged at 600 g for 6 min at 10 °C to obtain a microglial cell pallet. Finally, all cells were re-suspended in DMEM containing 10% FBS +2 mM L-glutamine + 50 U/ml Penicillin + 50 ug/ml Streptomycin + 100 ug/ml Normocin, prior to trypan-blue cell counts. Each mouse brain typically yielded between 3 x 10^5 and 6 x 10^5 total microglia.

Microglia purity was determined via fluorescent immunocytochemistry for microglial markers IBA-1 (1:500) and CD11B (1:500), and GFAP (1:1000) as an astrocyte marker. Each sample was counterstained with DAPI to identify nuclei. All cells imaged were positive for IBA-1 and CD-11B, but GFAP negative (Supplementary material).

2.3 HMGB1 Immunocytochemistry of primary microglia

Due to low cell numbers, HMGB1 expression and LDH activity was not detectable in supernatants of the isolated primary microglia (Supplementary material). Thus, total and localised intracellular HMGB1 protein expression was measured via fluorescent immunocytochemistry instead. For this experiment, 1 x 10^5 primary microglial cells were seeded per well in 8-well glass-bottom slides (80827, Ibidi, Germany), and maintained at 37 °C with 5% CO2 in a cell incubator to attach overnight. Media was then removed, and microglia were treated with either 500 nM CORT or volume-matched ethanol vehicle for a further 24 h. Following drug treatment, cells were fixed using 4% PFA + 5% sucrose solution for 10 min. Non-specific binding sites were blocked

using 5% normal donkey serum in PBS triton 0.15% for a further 10 min. Primary antibody to HMGB1 (1:500) was applied overnight at 4 °C. Secondary antibody (Donkey anti-Rabbit 488 nM, 1:1000, Life Technologies A21206) and nucleus counterstain (DAPI, 1:10,000) were applied for 1 h, at room temperature. Cells were imaged under a confocal microscope (Leica SP5, Germany) at 63x magnification.

2.4 Image analysis technique for HMGB1 localisation

All fluorescent immunocytochemistry image analysis was performed using Fiji's distribution of ImageJ (64-bit) software (Schindelin *et al.*, 2012). An intensity threshold was first applied to both the 405 nm (DAPI) and 488 nm (HMGB1) channels, to identify the nucleus and HMGB1 signal per image. Using the "Analyse Particles" algorithm, each signal above 10 μm diameter was identified for each channel, creating a mask per identified particle. Each mask for nucleus and per cell HMGB1 signal was then saved as individual regions of interest (ROI). On the original (no threshold) HMGB1 containing channel, all ROI for nuclei and HMGB1 signal areas were loaded into ROI manager. Each nucleus and HMGB1 signal was paired, and conditional ROI were obtained using "AND" (HMGB1 signal overlapping with nucleus ROI) and "OR" (sum of HMGB1 and nucleus ROI) for each pair of ROI. Mean intensity, integrated density and area values were measured for each ROI. A graphical representation of how the degree of HMGB1 cytoplasmic translocation was calculated is detailed in the Supplementary material.

2.5 BV2 Cell Culture

BV2 microglia-like cell lines were maintained in Dulbecco's modified Eagle's medium (DMEM) supplemented with 10 % (v/v) foetal bovine serum (FBS) and 2 mM L-

glutamine + 50 U/ml Penicillin + 50 ug/ml Streptomycin + 100 ug/ml Normocin. Cells were grown in a humidified incubator of 95%air/5%CO2 at 37°C. Cells were plated at a density of $7.5x10^4$ cells per well in 12-well plates for live-cell imaging, and $4x10^5$ cells per well in 6-well plates for protein release experiments.

2.6 Experimental design

BV2 cells were pre-exposed to 50 or 500 nM CORT (± antagonists), or DEX, or volume-matched ethanol vehicle diluted in serum-free DMEM + L-glutamine for 24 h. This pre-exposure was followed by a second 24h treatment with either LPS or vehicle (N = 6 for each group). After each drug exposure, cell supernatants were harvested.

2.7 Measuring cytotoxicity and viability

As CORT (Wu *et al.*, 2013) can induce apoptosis in immune-competent cells, changes in cell viability and cytotoxicity were monitored throughout the treatment period. Cytotoxicity was measured from cell supernatants using a lactate-dehydrogenase (LDH) activity measurement kit (Thermo Fisher Scientific 88954, USA) according to manufacturer's specifications. LDH is an essential intracellular enzyme, and is released from damaged cells. An accumulation of extracellular LDH therefore a marker of cell damage and cytotoxicity.

To measure cell viability, Neutral red dye (Sigma-Aldrich N7005, Germany) was used to label live cells according to published protocols with minor modifications (Repetto, del Peso and Zurita, 2008). Briefly, after all drug treatments were completed, cell supernatants were removed, and samples were centrifuged at 1000 x g for 10 min to

pellet all cellular debris. The supernatant was then removed for further protein quantification and LDH measurements. Since a decrease in adhered cell viability may result from the detachment of viable cells into the supernatant, viability of the detached cells as a result of treatments were also measured. Thus, both the cell pellet after centrifugation of supernatant samples (detached cells), and cells left attached to the plates were then incubated with DMEM containing neutral red dye for 1hr to stain viable cells. All cells were then washed trice using PBS, and a de-staining solution containing 48% ethanol and 1% glacial acetic acid was added to samples for 10 min and shaken at 100 rpm at room temperature to leech all dye taken up by viable cells into the solution. Finally, absorbance level at 540 nm was measured using a plate reader (BioTek, USA), where a larger absorbance reading represents increased cell viability.

2.8 Protein quantification of extracellular HMGB1, ASC and NLRP3

Western blots were used to measure levels of extracellular HMGB1, ASC and NLRP3. Following treatment, supernatants were harvested and centrifuged (1000 x g, 10 min) to remove cellular debris. 5x Laemmli buffer was combined with the supernatant portion for storage at -80°C until further use. Final supernatant samples used in western blot measurement thus contained 80% cell solution and 20% Laemmli buffer.

Supernatant samples (60 ul) were resolved on a 4-12% bis-tris gel (Life Technologies Bolt gels, USA) at a constant 200 V, and transferred onto nitrocellulose membranes at 20 V. Membranes were blocked using 5% skim milk in TBS-tween20 and incubated overnight at 4°C in primary antibodies for HMGB1 (1:5000 dilution, Abcam 19256,

USA), NLRP3 (1:2000 dilution, Adipogen AG-20B-0014, USA), and ASC (1:1000 dilution, Adipogen AL177, USA). Appropriate secondary antibodies (1:10000 dilution; Donky anti-mouse 800 nm: 925-32212; Donkey anti-rabbit 680 nm: 924-68021, Li-cor, USA) were applied for 1h at room temperature, and blots were developed using the Odyssey scanner (Li-cor, USA). Western blot image analysis was performed using ImageJ (64-bit) software.

HMGB1 was reliably detected from cell supernatants directly after 24 h pre-exposure, while ASC and NLRP3 proteins were only reliably present after 24 h pre-exposure + 24 h treatment with either LPS or vehicle.

2.9 Data analysis and statistics

All statistical analyses were performed using R (64-bit, version 3.3.1) software (R Core Team, 2016). HMGB1 translocation immunocytochemistry data was analysed using linear mixed modelling via the nlme package, with each biological replicate used as the random-effect. Each cell was thus regarded as repeated measures within each biological replicate. Linear mixed effects modelling was also used for supernatant protein measures of HMGB1, NLRP3 and ASC, as well as cytotoxicity and Neutral red uptake in both attached and detached cells, controlling for repeated measures within each biological replicate. Post hoc comparisons were made using the lsmeans package, which computes group differences based off least squares means using Tukey's adjustment for multiple comparisons.

Principal Component Analysis (PCA) using the prcomp function from the stats package in R was utilised to visualise the group differences across cell damage and supernatant

protein measures. PCA reduces dimensionality by projecting variability across each measure onto a lower dimensional space while retaining as much variability as possible, thus allowing for the visualisation of multiple measures across the same axes. All measures were normalised to reduce uneven weights due to scaling differences

Support vector machines (SVM) analysis using the 'radial' kernel was performed using the e1071 package in R to classify the combined values from all measures into different receptor signalling groups. This analysis determines if receptor signalling is a distinguishing factor in measures of cell damage and protein expression. Model performance was assessed using the confusionMatrix function from the caret package. This analysis assesses the SVM model accuracy in classifying the data points according to the grouping variables, as well as individual classification performance for each class label.

3 Results

3.1 CORT induces microglial HMGB1 cytoplasmic translocation

Total cell viability, measured by neutral red uptake, was not significantly different between CORT exposed and vehicle exposed primary microglia ($t(3)= 0.25$, $p = 0.82$) (Supplementary material). At basal conditions, HMGB1 is predominantly expressed in the cell nucleus. During cellular stress or immune activation however, HMGB1 translocates into the cytoplasm prior to exocytosis release in macrophages and microglia (Bonaldi *et al.*, 2003; Kim *et al.*, 2008). An elevation in cytoplasmic HMGB1 is therefore indicative of increased potential for DAMP signaling. Since western blot analysis revealed no detectable level of HMGB1 protein from microglia supernatant

(Supplementary material), single cell localisation of HMGB1 expression via fluorescent immunocytochemistry was performed (Figure 1).

After exposure to 500 nM CORT for 24 h, there was no change in the integrated density of HMGB1 signal (mean difference = 917, $t(275) = 0.85$, $p = 0.39$; Figure 1B), indicating that overall HMGB1 expression is unchanged. However, compared to vehicle, total area of HMGB1 expression per cell (Figure 1C) was significantly higher in CORT exposed microglia (mean difference = 33.4 µm2, $t(275) = 2.12$, $p<0.05$). Additionally, significant HMGB1 cytoplasmic translocation (Figure 1D) was evident in CORT exposed cells ($B = 0.62$, $t(202) = 2.31$, $p<0.05$), but not vehicle exposed cells ($B = 0.42$, $t(202)=1.51$, $p = 0.13$). Due to low effect size however, there was no significant difference in cytoplasmic translocation between CORT and vehicle (mean difference = 0.21, $p= 0.31$). This result suggests that the culture conditions may not be ideal for these cells, and this method may require further refinement. Nevertheless, given the increased HMGB1 expression area and significant cytoplasmic translocation, the results provide some support for the potential role of CORT-induced HMGB1 release.

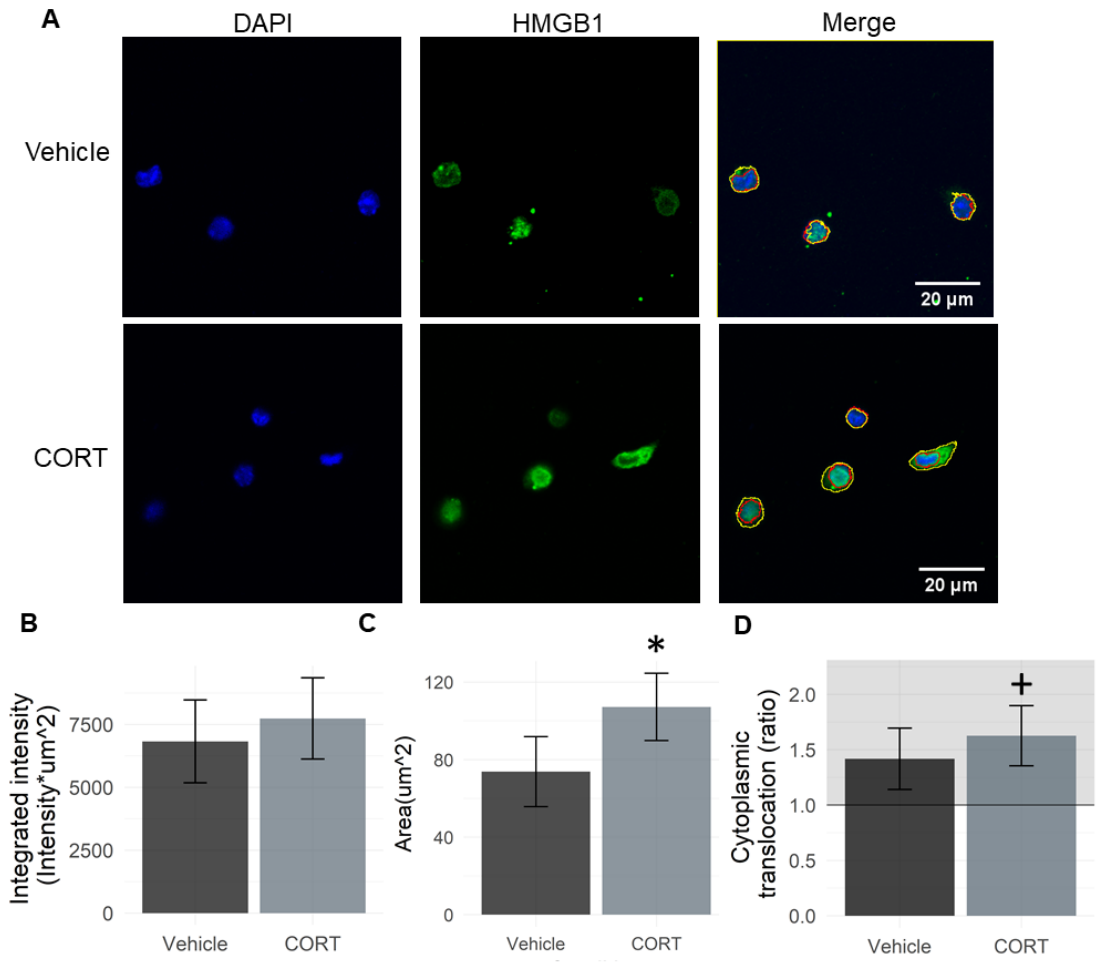

Figure 1. CORT pre-exposed primary microglia exhibited HMGB1 cytoplasmic translocation while total HMGB1 expression remained unchanged. Representative images illustrating nucleus (DAPI; 405 nm blue), HMGB1 expression (488 nm green) and merged channels (A). Red borders indicate DAPI expression, while yellow borders indicate total HMGB1 expression + nucleus area per identified cell (N=5 animals). Bar graphs indicate mean +- SE of total area (B) and integrated intensity (C) of HMGB1 expression in cells exposed to either vehicle or 500 nM CORT for 24 h. Calculated degree of cytoplasmic translocation (F). Significant pairwise comparisons denoted by * ($p<0.05$), + ($p<0.05$ compared to value = 1).

3.2 CORT and DEX pre-exposure increases BV2 extracellular HMGB1, NLRP3 and ASC protein expression

Intracellular HMGB1 was basally localised to the nuclei in in BV2 cells (Supplementary material). However, unlike primary microglia, HMGB1 is measurable by western blot after 24 h CORT or vehicle exposure (Figure 2A). Additionally, NLRP3 and ASC protein expression was detectable in supernatant samples after a further 24 h LPS treatment.

3.2.1 HMGB1

The linear mixed effects model showed that 500 nM CORT ($B = 0.17$, $t(18)= 5.05$, $p<0.0001$) and DEX ($B = 0.24$, $t(18)= 5.28$, $p< 0.0001$) both increased HMGB1 expression in the supernatant (Figure 2B), but are no different from each other (Mean difference = 0.08, $p=0.25$).

When HMGB1 was measured in supernatant following pre-exposure + treatment (Figure 2C), only CORT ($B = 0.08$, $t(49)=3.31$, $p<0.01$), but not DEX ($B = 0.04$, $t(49)= 1.19$, $p=0.24$) had an overall effect in increasing HMGB1 expression. LPS treatment did not significantly influence supernatant HMGB1 expression ($B = 0.04$, $t(49)=1.70$, $p=0.10$). Pairwise comparisons further revealed that CORT pre-exposure elevated HMGB1 regardless of vehicle (mean difference = 0.08, $p<0.05$) or LPS treatment (mean difference = 0.09, $p<0.01$), when compared to vehicle pre-exposure controls.

3.2.2 ASC

Extracellular ASC expression after pre-exposure + treatment was significantly increased by CORT overall ($B = 0.16$, $t(49)= 2.21$, $p<0.05$), but was not influenced by DEX pre-

exposure or LPS treatment ($p>0.05$). Post-hoc pairwise comparisons did not show any significant group difference after Tukey's adjustment ($p>0.05$) (Figure 2D).

3.2.3 NLRP3

Measured after pre-exposure + treatment, CORT pre-exposure ($B = 0.07$, $t(49)= 2.69$, $p<0.01$) and LPS treatment ($B = 0.07$, $t(49)= 2.76$, $p<0.01$) significantly elevated supernatant expression of NLRP3 overall (Figure 2E), while there was no main effect of DEX pre-exposure ($B = 0.03$, $t(49)= 0.88$, $p=0.39$). Post-hoc tests further showed that LPS significantly increase NLRP3 expression from CORT pre-exposed cells (mean difference = 0.08, $p<0.05$). CORT + LPS also elevated NLRP3 expression compared to vehicle pre-exposed cells (mean difference = 0.08, $p<0.05$).

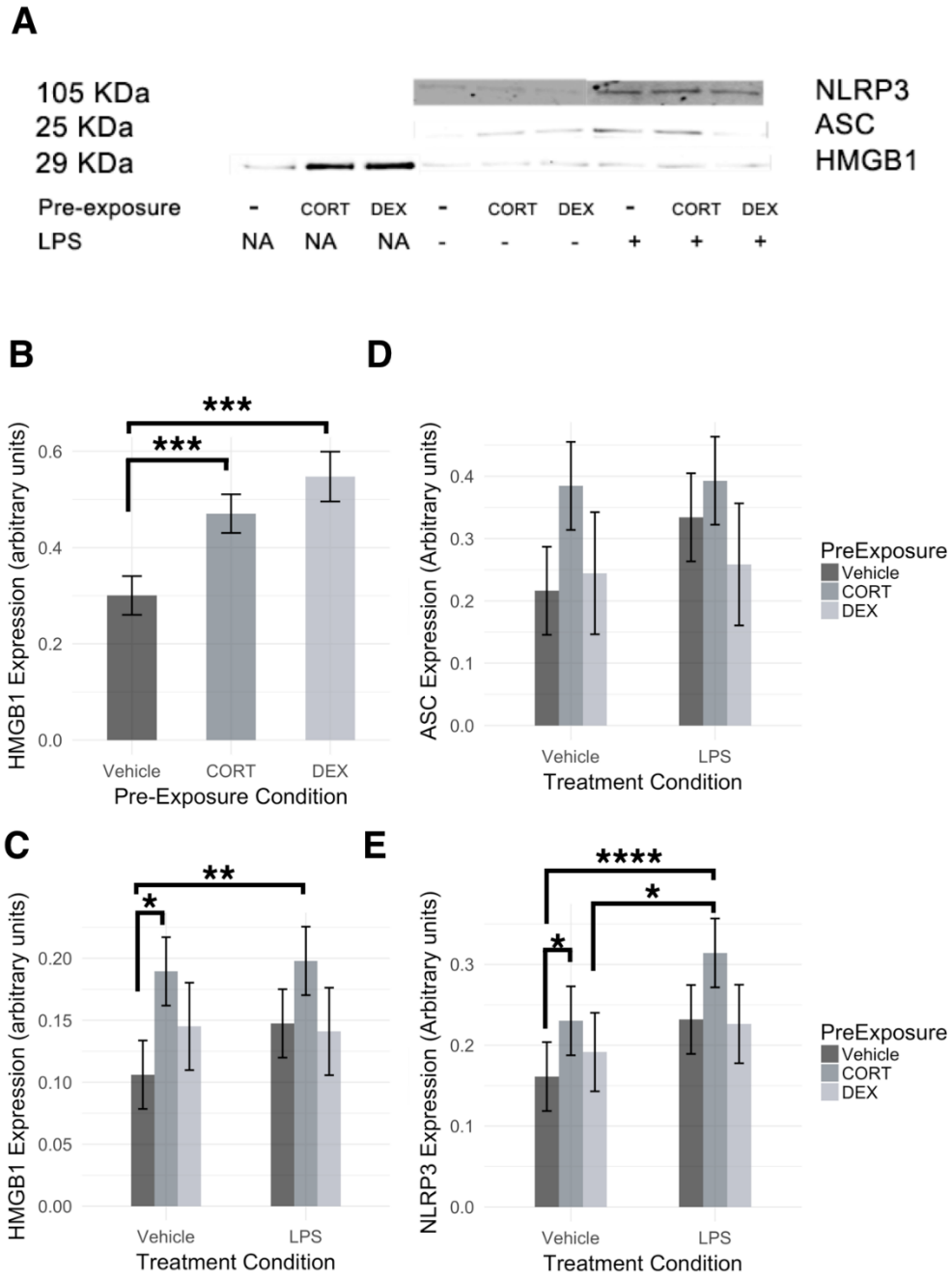

Figure 2. Exposure to 24 h CORT and DEX increases HMGB1 protein measures from cell supernatant. HMGB1 and NLRP3 expression are elevated after a further 24 h treatment with vehicle or LPS in CORT pre-exposed cells. A) Representative western blots for 500 nM pre-exposure conditions. All pre-exposure conditions are removed from system prior to application of 24 h vehicle or LPS treatment. Bar graphs showing B-C) HMGB1 expression D) ASC expression and E) NLRP3 expression in cell supernatant after B,D) CORT vehicle or DEX 24h exposure (500 nM) and C,E) after a further 24 h of vehicle or LPS treatment. Significance levels for individual group differences using pairwise post-hoc comparisons with Tukey correction indicate by * ($p<0.05$) ** ($p<0.01$), ***($p<0.001$), **** ($p<0.0001$).

3.3 GR but not MR antagonist attenuates CORT pre-exposure elevation of extracellular HMGB1, no effect on NLRP3 and ASC expression.

Since CORT and DEX caused increased HMGB1 release, while only CORT increased extracellular NLRP3 expression, specific GR and MR antagonists, Mifepristone and Spironolactone respectively, were used to confirm GR dependency of these effects (Figure 3A).

3.3.1 HMGB1

Consistent with 3.5.1, supernatant HMGB1 expression (Figure 3B) was elevated by CORT exposure ($B = 0.34$, $t(25)= 5.30$, $p<0.0001$). GR and MR antagonists, Mifepristone ($B = 0.08$, $t(25)= 1.31$, $p=0.20$) and Spironolactone ($B = 0.03$, $t(25)= 0.52$, $p = 0.61$) did not cause an overall change in HMGB1 expression independently, but CORT induced elevations of HMGB1 expression was significantly inhibited by Mifepristone ($B = -0.22$, $t(25)= -2.41$, $p<0.05$). Post-hoc comparisons further revealed a significantly higher supernatant HMGB1 expression in *[CORT + vehicle]* (mean difference = 0.34, $p<0.001$), as well as *[CORT + Spironolactone]* (mean difference = 0.22, $p<0.05$), but not in *[CORT+ Mifepristone]* (mean difference = 0.12, $p= 0.42$) when compared to respective *[vehicle + antagonist]* conditions. Spironolactone and Mifepristone did not significantly modify HMGB1 expression from vehicle-exposed cells ($p>0.05$).

In the *[pre-exposure + antagonist] + treatment* model (Figure 3B), only LPS treatment caused an overall increase in HMGB1 expression in the supernatant ($B = 0.12$, $t(55)= 2.75$, $p<0.01$), while CORT pre-exposure did not independently alter HMGB1 expression in this model ($B = 0.06$, $t(55)= 1.32$, $p= 0.19$). Neither GR nor MR

antagonists caused a change in HMGB1 expression overall, and did not interact with either LPS treatment or CORT pre-exposure ($p>0.05$).

3.3.2 ASC and NLRP3

After *[pre-exposure + antagonist] + treatment*, there was no significant effects of CORT, antagonists or treatment on ASC (Figure 3C) or NLRP3 (Figure 3D) expression as shown by the linear mixed effects model ($p>0.05$).

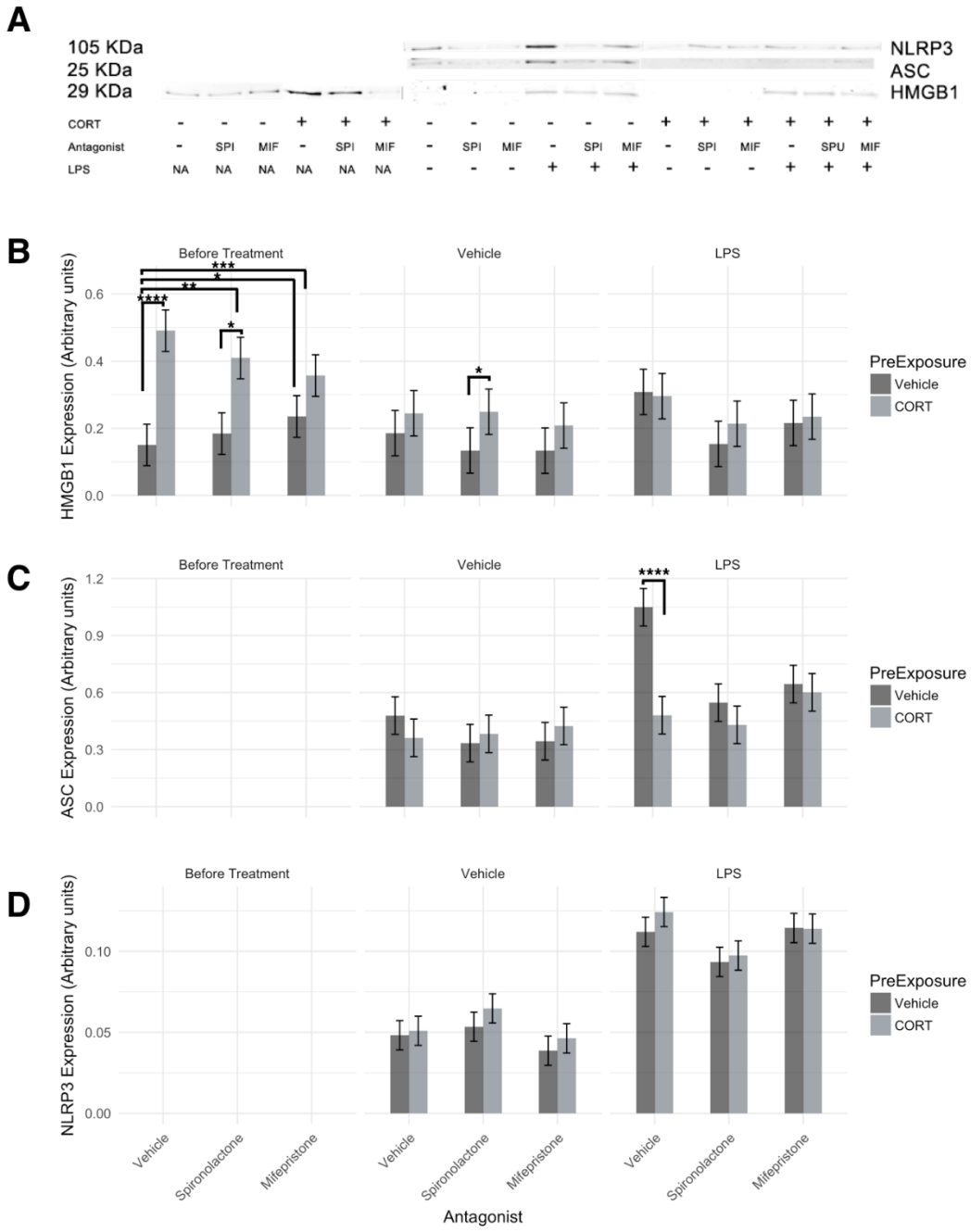

Figure 3. CORT effects on released HMGB1 expression were reduced by mifepristone co-treatment, while measures of ASC and NLRP3 were insensitive to both antagonists. A) Representative western blots for all conditions. Bar graphs showing western blot measures of B) HMGB1 expression C) ASC expression and D) NLRP3 expression in cell supernatant after 24h CORT (500nM) exposure in conjunction with Spironolactone (1uM) and Mifepristone (1uM) (Before treatment) and after either vehicle or LPS treatment Significance levels for individual group differences using pairwise post-hoc comparisons with Tukey correction indicate by * ($p<0.05$) ** ($p<0.01$), ***($p<0.001$), **** ($p<0.0001$).

3.4 CORT and DEX pre-exposure increases supernatant LDH activity, decreases cell viability of attached cells, but increases cell viability in suspended cells harvested from BV2 cell supernatant.

Glucocorticoids, signalling through GR, are cytotoxic to peripheral immune cells (Wu *et al.*, 2013). Given previous findings of GR dependent priming of microglia DAMP and cytokine signalling (Sobesky *et al.*, 2016), we investigated if cell damage and loss of cell viability could potentially explain the increase in DAMP related protein release from BV2 cells (Figure 4).

3.4.1 Cytotoxicity

Cytotoxicity was assessed by measuring LDH activity from cell supernatants after 24 h CORT or DEX pre-exposure, and also after a further 24 h LPS treatment (Figure 4A). DEX significantly increased LDH activity before LPS administration ($B = 0.13$, $t(25) = 3.07$, $p<0.01$). In contrast, there was no overall effect of CORT ($B = 0.03$, $t(25) = 0.83$, $p=0.41$), or pre-exposure concentration ($B= 0.067$, $t(25) = -1.58$, $p =0.13$). Further analysis revealed that at 50 nM, only DEX significantly increased LDH activity compared to vehicle (mean difference = 0.13, $p<0.05$). At 500 nM, both CORT (mean difference = 0.11, $p<0.05$) and DEX (mean difference = 0.21, $p<0.001$) significantly elevated LDH activity when compared to volume matched vehicle controls.

After a further 24 h of treatment with either LPS or vehicle (Figure 4B), LPS significantly elevated LDH activity in the supernatant ($B= 0.03$, $t(25)= 2.22$, $p<0.05$). Neither 500 nM CORT ($B=0.03$, $t(25)=1.67$, $p=0.11$) nor 500 nM DEX ($B=-0.02$, $t(25)=-1.07$, $p =0.30$) altered LDH activity independently, but a significant interaction effect between DEX pre-exposure and LPS treatment on LDH activity was found ($B=-0.06$, $t(25)=-2.88$,

p<0.01). Pairwise comparisons showed significant reductions in LDH activity between *DEX+LPS* and *vehicle+LPS* (mean difference =0.08, p<0.001), as well as *DEX+LPS* and *CORT+LPS* (mean difference = 0.07, p<0.01).

3.4.2 Cell Viability

Cell viability, as measured by neutral red dye uptake by cells adhered to the plate (Figure 4C, D), was significantly reduced after 24h DEX (B= -0.21, t(25)=-4.55, p<0.001), but not CORT (B=-0.08, t(25)= -1.78, p=0.09) overall. Concentration did not significantly influence cell viability (B=0.05, t(25)= 1.11, p= 0.27). Pairwise comparisons further revealed a significant decrease in cell viability after 50 nM DEX (mean difference = 0.21, p<0.001) and CORT (mean difference = -0.13, p<0.05). At a concentration of 500 nM, both CORT (mean difference = 0.13, p<0.05) and DEX (mean difference = 0.25, p<0.0001) decreased cell viability when compared to vehicle. DEX further decreased cell viability compared to 500 nM CORT (mean difference = 0.12, p<0.05), indicating more potent effects on cell viability.

In attached cell viability measured after *pre-exposure (500 nM) + treatment* conditions (Figure 4D), LPS treatment following all pre-exposure treatments did not significantly influence cell viability (B = 0.06, t(25) = -1.92, p=0.066), but DEX pre-exposure significantly decreased cell viability (B = -0.10, t(25)= -3.19, p<0.01). Pairwise comparisons further revealed that in *pre-exposure + vehicle* conditions, only DEX pre-exposed cells exhibited decreased viability (mean difference = 0.10, p<0.05). Neither CORT or DEX pre-exposures caused a persistent decrease in cell viability under *pre-exposure + LPS* conditions (p>0.05). However, *both CORT + LPS* (mean difference =

0.13, p<0.01) and *DEX + LPS* (mean difference = 0.12, p<0.05) treated cells displayed significantly decreased viability compared to *vehicle + vehicle* control.

Cell viability in detached cells harvested from the supernatant (Figure 4E) was not significantly modified by CORT (B= 0.02, t(25)=1.84, p=0.078), nor DEX (B=1.92, t(25)= 1.92, p =0.066).

When measured following pre-exposure+treatment (Figure 4F), detached cell viability was significantly increased in response to LPS treatment (B = 0.26, t(25)= 3.04, p<0.01). There was no independent effect of CORT (B = 0.01, t(25)= 0.14, p =0.89), or DEX (B=0.09, t(25)= 1.03, p = 0.31) pre-exposure, but a trending interaction between DEX pre-exposure and LPS treatment was present (B= -0.24, t(25)= -2.02, p =0.054). No significant group difference was found after Tukey adjustment (p>0.05).

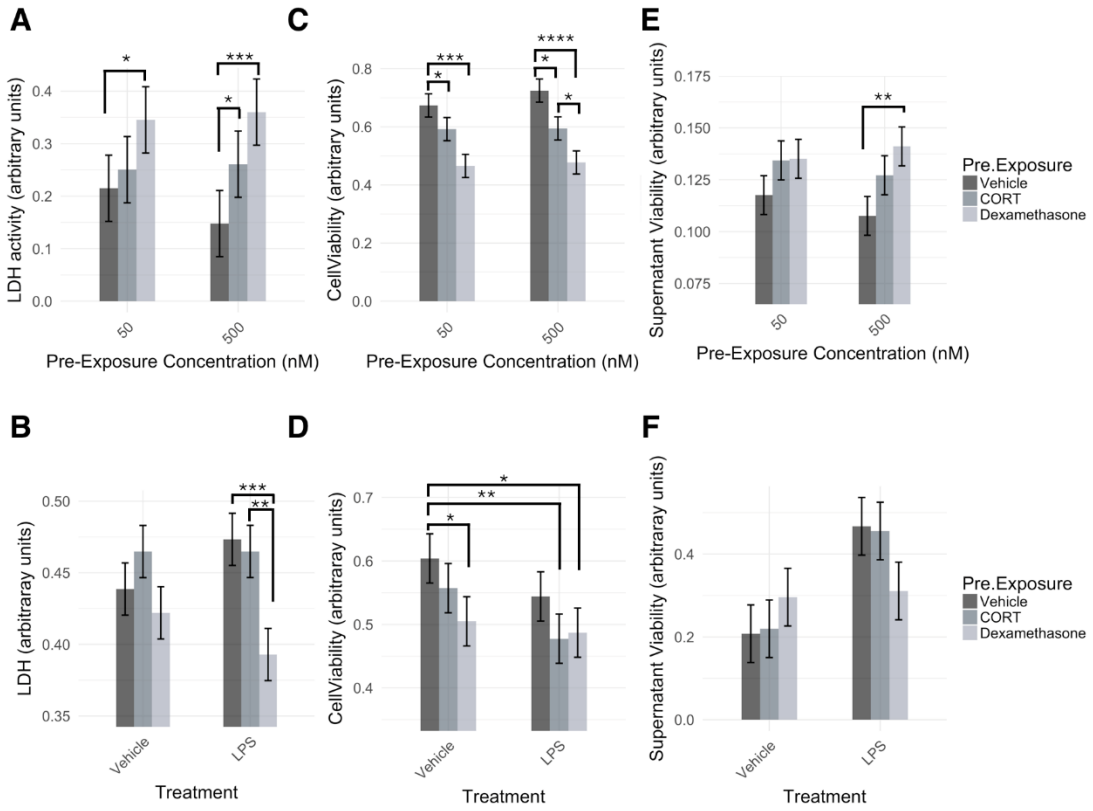

Figure 4. CORT and DEX exposure increases LDH activity and detached cell viability, while decreasing attached cell viability. Only Pre-exposure to DEX decreases measures of cell viability and LDH activity measured after a further 24h vehicle and LPS treatment. Bar graphs showing A-B) LDH measures C-D) Attached cell viability E-F) Detached cell viability after A,C,E) 24h Exposure to either vehicle, CORT or DEX, and B,D,F) following a further 24h of vehicle or LPS treatment. All pre-exposure conditions are removed from the culture system prior to application of 24h vehicle or LPS treatment (N=6). Significance levels for individual group differences using pairwise post-hoc comparisons with Tukey correction indicate by * ($p<0.05$) ** ($p<0.01$), ***($p<0.001$), **** ($p<0.0001$).

3.5 CORT effects on measures of cell viability and cytotoxicity are influenced by co-administration with a GR but not a MR antagonist.

To further investigate the role of GR and MR signalling in CORT actions, specific antagonists, Mifepristone and Spironolactone respectively, were co-administered during pre-exposure conditions ([pre-exposure+antagonist]) (Figure 5).

3.5.1 Cytotoxicity

The effects of *[CORT pre-exposure + GR or MR antagonists]* on LDH activity in supernatants were analysed (Figure 5A). In agreement with section 3.4.1, CORT significantly increased cytotoxicity ($B = 0.12$, $t(55) = 2.66$, $p<0.05$). There was no significant independent effect of GR antagonist Mifepristone ($B = 0.01$, $t(55)= 0.13$, $p =0.89$), MR antagonist, Spironolactone ($B = -0.01$, $t(55)= -0.09$, $p = 0.93$), nor any interaction between CORT and antagonists ($p>0.05$). Pairwise comparisons showed that 500 nM CORT increased LDH activity in both *[CORT + vehicle]* (mean difference = 0.12, $p<0.05$) and *[CORT + Spironolactone]* (mean difference = 0.10, $p<0.05$) conditions. Cytotoxicity was not significantly increased in mifepristone co-treated cells (mean difference = 0.01, $p= 0.83$). Low concentration CORT did not significantly influence LDH when co-treated with vehicle, Mifepristone or Spironolactone ($p>0.05$).

When measured after a further 24 hour treatment with either vehicle or LPS (Figure 5B), cytotoxicity was not significantly influenced by LPS ($B = 0.04$, $t(55)=1.72$, $p=0.09$), or CORT ($B = -0.01$, $t(55) = -0.5$, $p= 0.62$). No main or interaction effect of antagonists alone was found ($p>0.05$).

3.5.2 Cell viability

Similar to 3.4.2, adherent cell viability (Figure 5C) was significantly reduced by CORT (B = -0.12, t(55)= -3.88, p<0.001). There was no significant effect of pre-exposure concentration (B = -0.01, t(55)=-0.22, p=0.83), and neither antagonists influenced cell viability independently (p>0.05). Mifepristone abolished the CORT effect on viability (B = 0.14, t(55)= 2.94, p<0.01), but Spironolactone did not significantly interact with CORT (B = 0.05, t(55)=1.04, p=0.30). Further pairwise comparison revealed that 500 nM CORT significantly decreased cell viability when co-treated with vehicle (mean difference = 0.13, p<0.001) and Spironolactone (mean difference = 0.08, p<0.05). *[CORT + Mifepristone]* was no different from *[vehicle+Mifepristone]* treated cells (mean difference = 0.01, p=0.78). Low concentration CORT did not modify cell viability when co-treated with any antagonist or vehicle (p>0.05).

Attached cell viability measured after a further 24 h treatment with either LPS or vehicle (Figure 5D) was significantly decreased by both LPS treatment (B=-0.15, t(55)=-4.89, p<0.0001), and CORT pre-exposure (B=-0.08, t(55)=-2.16, p<0.05). Neither antagonists influenced cell viability alone (p>0.05), but GR antagonist Mifepristone significantly interacted with CORT pre-exposure to increase attached cell viability (B = 0.09, t(55)= 2.06, p<0.05). Pairwise comparisons revealed significant cell viability reductions in *[CORT+vehicle]* (mean difference = 0.08, p<0.05) and [CORT+ Spironolactone] (mean difference = 0.04, p<0.05), but not *[CORT + Mifepristone]* (mean difference = 0.01, p = 0.77). *[CORT + antagonist]* did not modify attached cell viability in LPS-treated cells (p>0.05).

Detached cell viability (Figure 5E) was not independently influenced by Mifepristone (B = -0.01, t(55)= -0.60, p=0.55) or Spironolactone (B = -0.01, t(55)=-0.20, p=0.84), but 500 nM CORT caused a significant increase in viable detached cells (B = 0.03, t(55)=3.05, p<0.01). Pairwise comparisons further reveled significant elevations in viable detached cells after *[500nM CORT+vehicle]* (mean difference = 0.03, p<0.001) and *[500nM CORT+Spironolactone]* (mean difference = 0.03, p<0.001), but this difference was not present in *[500nM CORT+Mifepristone]* conditions (mean difference = 0.01, p=0.16). Low concentration CORT did not influence detached cell viability (p>0.05).

Detached cell viability measured after *[pre-exposure + antagonist] + treatment* (Figure 5F), was not independently influenced by CORT pre-exposure, GR or MR antagonists (p>0.05). LPS treatment strongly increased viable detached cells (B =0.71, t(55)= 6.78, p<0.0001), but CORT pre-exposure prior to LPS treatment decreased this effect overall (B = -0.32, t(55)=-2.18, p<0.05). Spironolactone also significantly interacted with pre-exposure to decrease detached cell viability (B = -0.37, t(55)= -2.51, p<0.05). Pairwise comparisons showed a decrease in supernatant cell viability after [*CORT + vehicle] + LPS* (mean difference = 0.35, p<0.01) and *[CORT + Mifepristone] + LPS* (mean difference =0.25, p<0.05), but not in *[CORT + Spironolactone] + LPS* conditions (mean difference =0.12, p=0.25) relative to vehicle pre-exposure controls.

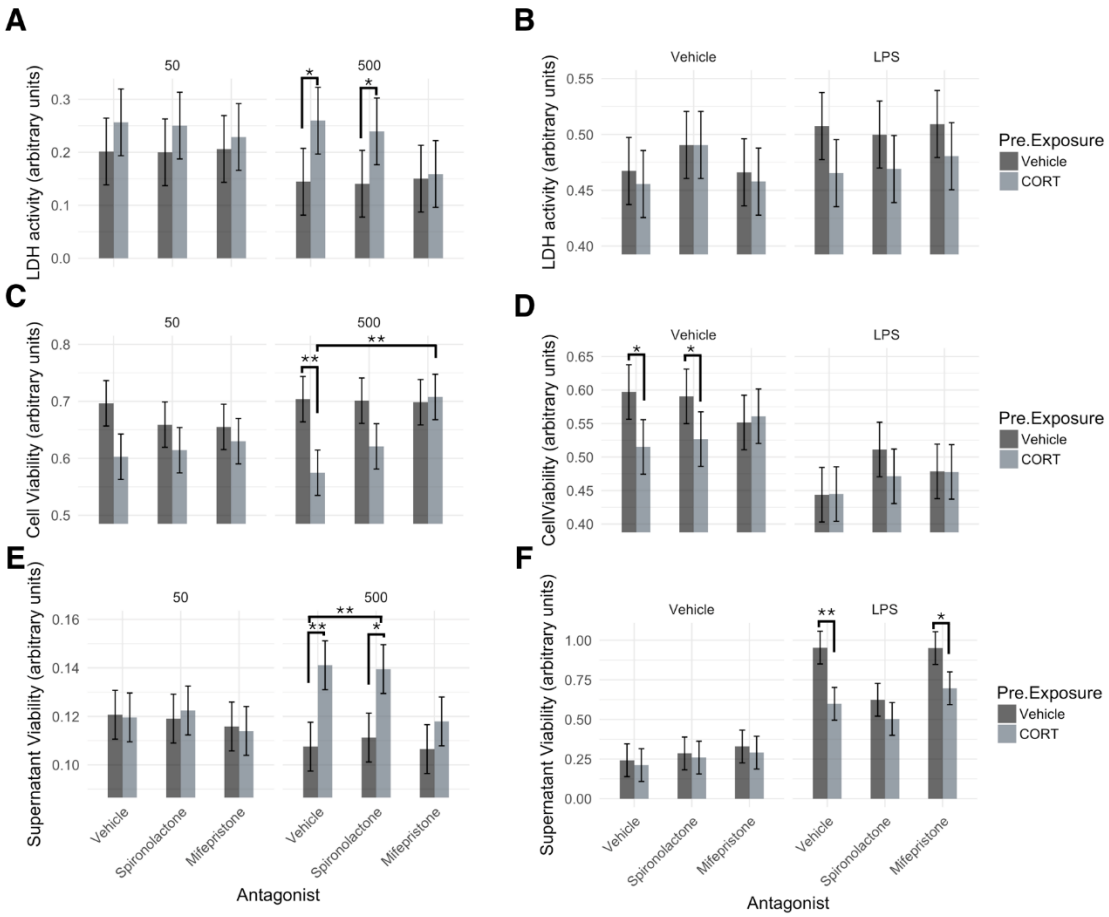

Figure 5. Mifepristone but not spironolactone normalises 24 h CORT effects on LDH activity and measures of cell viability. Bar graphs showing A-B) LDH measures C-D) Attached cell viability E-F) Detached cell viability after A,C,E) 24 h Exposure to Pre-exposure+antagonist, and B,D,F) following a further 24 h of vehicle or LPS treatment. All pre-exposure conditions are removed from system prior to application of 24 h vehicle or LPS treatment (N = 6). Significance levels for individual group differences using pairwise post-hoc comparisons with Tukey correction indicate by * ($p<0.05$) ** ($p<0.01$), ***($p<0.001$), **** ($p<0.0001$).

3.6 GR and GR + MR signalling effects can be distinguished from no GR and no MR signalling using measures of extracellular HMGB1, cell viability and LDH.

Through individual analyses, we have shown that CORT and DEX can alter cell viability, cytotoxicity and extracellular HMGB1, NLRP3 and ASC expression. These measures were further influenced by GR signalling, as identified by GR and MR antagonists and GR specific agonist DEX. To visualise the relationship between these measures, as well as evaluate the importance of GR and MR signalling, PCA analysis and SVM classification was applied to the results here.

Two-dimension principal components preserved 60% (PC1: 33.5%; PC2: 26.5%) of variability within the dataset, while a third principal component (PC3) contributed an additional 15.4% of variance (Figure 6A). Groups were then encoded according to GR or MR receptor activity, where: vehicle pre-exposed cells (*no GR or MR*), [CORT without antagonist] pre-exposure (*GR+MR*), DEX or [CORT + Spironolactone] pre-exposure (*GR only*), and [CORT + Mifepristone] pre-exposure (*MR only*). As expected from previous linear model analysis, influence of GR and MR activity appear diminished when each variable was measured after pre-exposure + treatment, illustrated by the overlap between each group and vehicle controls on the 2-dimensional principal component space. When measured directly after 24 h [pre-exposure ± antagonist], there appears to be increased separation between *GR only* and GR+MR groups with the *no GR or MR* control group.

SVM classification analysis between receptor signalling groups was applied using extracellular HMGB1 protein expression, LDH activity and both detached and attached

cell viability measured directly after 24h [pre-exposure ± antagonist] conditions (Figure 6B). SVM classification significantly distinguished between receptor signalling classes (accuracy = 0.72, $p<0.0001$). Individually, *No GR or MR* (balanced accuracy: 0.85), *GR+MR* (balanced accuracy: 0.82), *GR only* (balanced accuracy: 0.74) groups performed above chance, while *MR only* classification (balanced accuracy: 0.5) was no different to chance. The confusion matrix (supplementary material) shows that *MR only* signalling is indistinguishable from *No GR or MR* signalling groups. *GR only* signalling appears to be distinguishable from *no GR or MR* and *MR only* groups, suggesting that GR actions have the most impact on measures of supernatant protein expression, LDH activity and cell viability measured in this study.

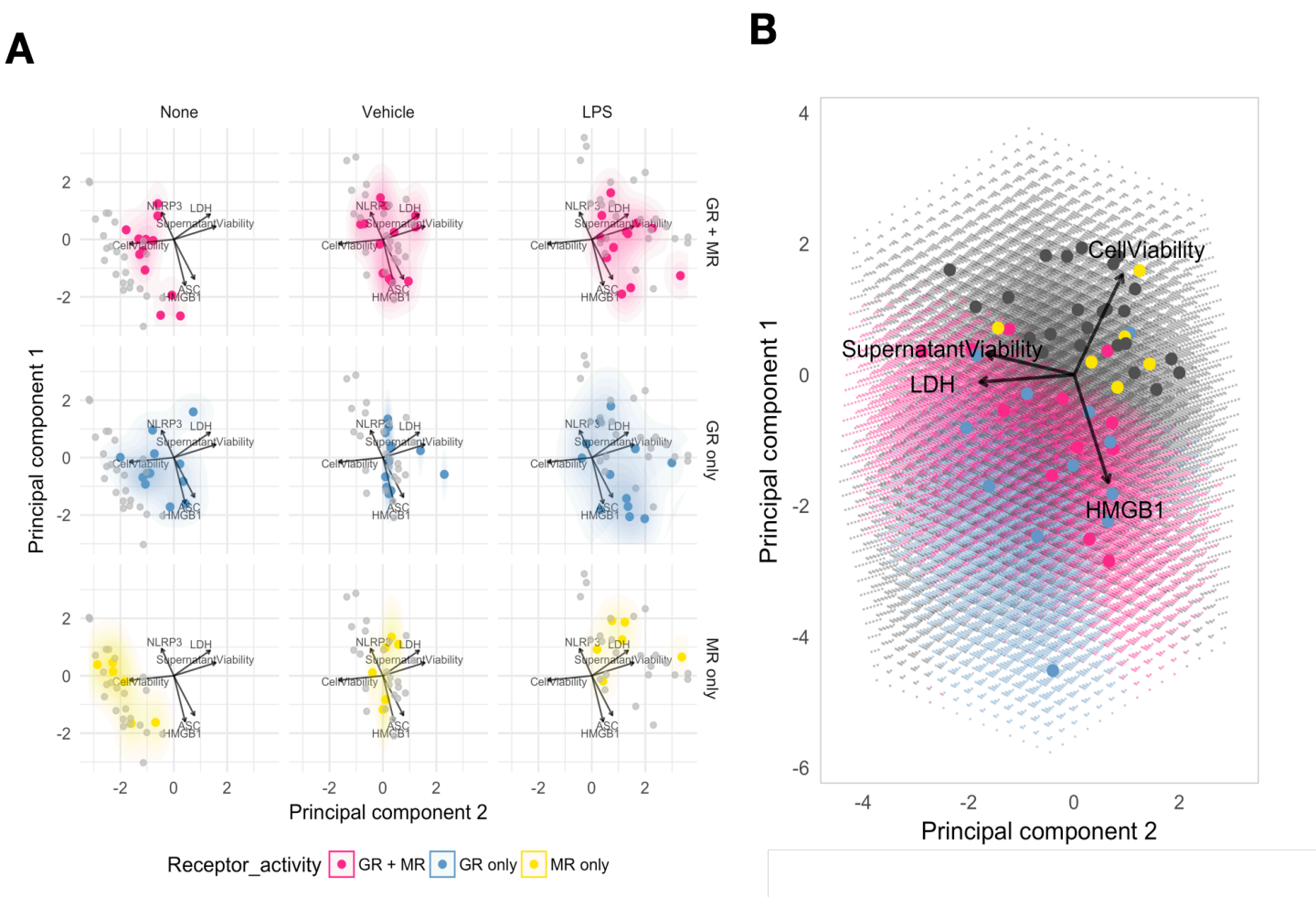

Figure 6. PCA visualisation of extracellular protein, cytotoxicity and cell viability measures according to MR or GR receptor activity. A) Scatter plots show PCA-transformed values on a 2 dimensional-axis grouped across treatment conditions and GR or MR receptor activity. Arrows represent directional variability across the listed measures. Each individual point is a separate experiment. B) PCA-transformed values on a 2-dimensional axis showing actual data (large points) and SVM-predicted distribution (coloured background). Successful classification of GR activity represented by separation between boundaries identified (Blue vs Grey).

4 Discussion

The current study explored CORT exposure in the presence or absence of specific pharmacological antagonists to GR and MR, in models of microglia. Here, intracellular HMGB1 localisation analysis in adult primary microglia displayed significant HMGB1 cytoplasmic translocation in microglia exposed to 500 nM CORT for 24 h. This result provides partial support for CORT-induced HMGB1 release in microglia. We thus further assessed DAMP related protein release directly after 24 h exposure, after a further 24 h vehicle or LPS treatment in BV2 microglia-like cells. Measures of cell viability and cytotoxicity were also analysed as potential pathways for DAMP release. The results suggest that CORT, signalling through GR can cause increased cell damage, persisting through a second immune challenge 24 h after removal of glucocorticoids from the system. In BV2 cells, the increase in HMGB1 was also found concurrently with these measures of cell damage, and were not present when GR was blocked. Meanwhile, the innate immune activity of the system was also modified, as demonstrated by the elevation of the inflammasome-related NLRP3 and ASC measured after pre-exposure + treatment in response to CORT pre-exposure. This increase was not influenced by either antagonist treatment. CORT actions are thus strongest when measured directly after pre-exposure, and appear to signal via GR rather than MR to decrease cell viability, increase cytotoxicity and elevate extracellular HMGB1 protein expression. Collectively, these data provide novel insights into the mechanisms via CORT may impact microglial functions during and after a stress induced neuroendocrine event.

4.1 CORT exposure induces cytoplasmic localisation of HMGB1 expression in adult primary microglia

As measured by integrated density of fluorescent intensity, CORT treatment resulted in no overall difference in total, cytoplasmic and nucleus HMGB1 expression in primary microglia. Additionally, CORT exposed cells exhibited significant HMGB1 cytoplasmic translocation. This result indicates that although total expression is not influenced by CORT exposure, HMGB1 expression is localised to cytoplasmic portion of microglia. Given that cytoplasmic translocation of HMGB1 is part of the release pathway (Bonaldi *et al.*, 2003), our findings suggest that CORT may increase the probability for HMGB1 release. However, due to the lack of clear difference from vehicle, and undetectable extracellular HMGB1 signal (Supplementary S6), more investigation is required to verify this result in primary microglia under more suitable cell culture conditions, or *in vivo*. Nevertheless, given that previous findings of HMGB1 release from isolated rat microglia pre-exposed to inescapable tail shock stress (Weber et al., 2015), the collective results in BV2 and adult primary microglia here lend support towards direct actions of stress hormone CORT, signalling via GR, in microglial HMGB1 release.

4.2 Through GR signalling, CORT and DEX exposure increase cytotoxicity and extracellular protein measures while decreasing cell viability

BV2 cells were used to investigate potential mechanisms of CORT actions on DAMP-related protein release. In these cells, CORT and DEX treatment increased HMGB1 protein expression measured from the supernatant, but this elevation was reduced by a GR antagonist, indicating GR specific signalling. Considering individual measures, CORT-induced cytotoxicity increase, and decrease in adherent cell viability were abolished by a GR antagonist. In contrast, none of these effects were influenced by a

MR antagonist. Furthermore, administration of GR-specific agonist, DEX, confirmed the GR-dependency of these actions. Agreeing with these direct comparisons, a SVM classifier applied to the combined measures in this study distinguished between receptor signalling. GR only signalling and GR + MR signalling exerted the most change, while MR only signalling was no different from vehicle groups across all measures. These findings are consistent with animal studies demonstrating the involvement of GR in HMGB1-related microglial priming (Sobesky *et al.*, 2016). Taken together, the results suggest that GR, rather than MR signalling, is important for the CORT exposure changes seen here in extracellular protein expression, cytotoxicity and cell viability. Overall, these effects are consistent with the classical immunosuppressive actions of high concentrations of CORT, characterised by the induction of cell death of immunocompetent cells (Wu *et al.*, 2013).

4.3 Extracellular HMGB1 elevation and decrease in cell viability persists 24 h after pre-exposure to CORT and DEX

LPS has been shown to induce HMGB1 release RAW264.7 macrophage-like cells and primary macrophages (Kim *et al.*, 2016; Lee *et al.*, 2017). However, it is still unknown if LPS induces HMGB1 release from BV2 cells, and if CORT can modify that response. Potential interactions between CORT pre-exposure and LPS treatment were thus examined in BV2 cells. After an exposure period of 24 h to CORT, DEX or vehicle, BV2 cells were further incubated with either LPS or vehicle for a further 24 h. After the immune challenge, however, CORT-induced elevation in LDH was lost, while attached cell viability remained decreased, suggesting that CORT effects on cytotoxicity is not persistent.

Following the 24 h DEX pre-exposure however, a 24 h LPS treatment produced a reduction in LDH and supernatant cell viability. This may be an effect of significantly lower cell numbers, as indicated by low cell viability in the system carried on from the DEX pre-exposure. Furthermore, both LDH and supernatant cell viability are more influenced by LPS treatment at this time-point, showing that CORT effects on cytotoxicity and cell health resolve once it is removed from the culture system. Attached cell viability remained decreased in both DEX and CORT pre-exposed cells, and the CORT effect was abolished in Mifepristone co-treated cells, further substantiating the GR specificity of CORT-induced cytotoxicity.

Measures of protein release show that CORT, not DEX, caused persistent elevation in HMGB1, NLRP3 and ASC overall after a second 24 h treatment period, regardless of vehicle or LPS administration. Both Mifepristone and Spironolactone were unable to counteract these changes. Taken together, persistent CORT actions are not fully explained by classical GR and MR binding, and an unknown secondary mechanism likely mediates these effects.

An important consideration is the predominant use of immortalised BV2 microglia-like cells in this study, which have previously shown differences from primary microglia isolated from neonatal mice at the transcriptional level. The most notable difference is the impaired IRF3 activation as a result of TLR3 and TLR4 stimulation in BV2 cells, suggesting compromised TRIF-dependent signalling (Das *et al.*, 2015). Despite these transcriptional differences, active purinergic signalling (Mead *et al.*, 2012), NLRP3

inflammasome activation (Zhou *et al.*, 2016), TLR-MyD88 signalling (Gong *et al.*, 2016) and NF-kB translocation (Brandenburg *et al.*, 2010), have been demonstrated similarly in both BV2 and primary microglia. BV2 cells also possess comparable phagocytic (Majerova *et al.*, 2014) and motility functions to primary microglia (Horvath *et al.*, 2008), thus showing innate immune competency of these cells.

The current work further identified some association between primary microglia and BV2 cells. Given that CORT increased extracellular HMGB1 in BV2 cells and caused cytoplasmic translocation of HMGB1 in primary microglia, there is partial agreement between the two cell types in CORT actions. However, the same result was not evident in measures of cell viability, since, unlike BV2 cells, there was not significant effect of CORT on cell viability in primary microglia. A notable consideration here, is that cell viability in general was much lower in primary microglia as compared to BV2 cells, while LDH activity measured here was below the detectable range of the assay (data not shown). There may be insufficient cells sampled here to show any significant difference between treatments. Single cell analysis with fluorescent immunocytochemistry was thus used to circumvent low cell numbers. Nevertheless, although beyond the scope of this study, further primary microglial cell culture work should be pursued to further test the mechanisms underlying CORT actions.

5 Conclusion

The current study demonstrates preliminary findings in primary microglia and BV2 cells that CORT, in part through GR signalling, can cause complex changes to cell health and proteins in the extracellular space lasting beyond the presence of CORT in the system. Consistent with the classical understanding of CORT actions on immune cells, we found a reduction in cell viability and increase in cytotoxicity in a microglia-like cell line. Moreover, at this stress-like concentration, glucocorticoids are immunosuppressive towards cytokine release (Yeager, Pioli and Guyre, 2011). Yet, this stress level concentration of CORT increases danger signals such as HMGB1, and inflammasome-related proteins in the extracellular space, which may have implications for immune signalling. The current study has thus demonstrated potential concurrent immune-priming and immunosuppressive actions of CORT, through GR receptor action.

References

Bellavance M, Rivest S. 2014. The HPA - Immune Axis and the Immunomodulatory Actions of Glucocorticoids in the Brain. Front Immunol 5:136.

Bonaldi T, Talamo F, Scaffidi P, Ferrera D, Porto A, Bachi A, Rubartelli A, Agresti A, Bianchi ME. 2003. Monocytic cells hyperacetylate chromatin protein HMGB1 to redirect it towards secretion. EMBO J 22:5551–5560.

Brandenburg LO, Kipp M, Lucius R, Pufe T, Wruck CJ. 2010. Sulforaphane suppresses LPS-induced inflammation in primary rat microglia. Inflamm Res 59:443–450.

Chiba S, Numakawa T, Ninomiya M, Richards MC, Wakabayashi C, Kunugi H. 2012. Chronic restraint stress causes anxiety- and depression-like behaviors, downregulates glucocorticoid receptor expression, and attenuates glutamate release induced by brain-derived neurotrophic factor in the prefrontal cortex. Prog Neuro-Psychopharmacology Biol Psychiatry 39:112–119.

Das A, Chai JC, Kim SH, Lee YS, Park KS, Jung KH, Chai YG. 2015. Transcriptome sequencing of microglial cells stimulated with TLR3 and TLR4 ligands. BMC Genomics 16:517.

Frank MG, Hershman SA, Weber MD, Watkins LR, Maier SF. 2014. Chronic exposure to exogenous glucocorticoids primes microglia to pro-inflammatory stimuli and induces NLRP3 mRNA in the hippocampus. Psychoneuroendocrinology 40:191–200.

Frank MG, Thompson BM, Watkins LR, Maier SF. 2012. Glucocorticoids mediate stress-induced priming of microglial pro-inflammatory responses. Brain Behav Immun 26:337–345.

Frank MG, Weber MD, Watkins LR, Maier SF. 2016. Stress-induced neuroinflammatory priming: A liability factor in the etiology of psychiatric disorders. Neurobiol Stress 4:62–70.

Gong L, Wang H, Sun X, Liu C, Duan C, Cai R, Gu X, Zhu S. 2016. Toll-Interleukin 1 Receptor domain-containing adaptor protein positively regulates BV2 cell M1 polarization. Eur J Neurosci 43:1674–1682.

Horvath RJ, Nutile-McMenemy N, Alkaitis MS, DeLeo JA. 2008. Differential migration, LPS-induced cytokine, chemokine, and NO expression in immortalized BV-2 and HAPI cell lines and primary microglial cultures. J Neurochem 107:557–569.

Hu W, Zhang Y, Wu W, Yin Y, Huang D, Wang Y, Li W, Li W. 2016. Chronic glucocorticoids exposure enhances neurodegeneration in the frontal cortex and hippocampus via NLRP-1 inflammasome activation in male mice. Brain Behav Immun 52:58–70.

Johnson JD, O'Connor K a, Deak T, Stark M, Watkins LR, Maier SF. 2002. Prior stressor exposure sensitizes LPS-induced cytokine production. Brain Behav Immun 16:461–476.

Kim J Bin, Lim CM, Yu YM, Lee JK. 2008. Induction and subcellular localization of high-mobility group box-1 (HMGB1) in the postischemic rat brain. J Neurosci Res 86:1125–1131.

Kim YM, Park EJ, Kim JH, Park SW, Kim HJ, Chang KC. 2016. Ethyl pyruvate inhibits the acetylation and release of HMGB1 via effects on SIRT1/STAT signaling in LPS-activated RAW264.7 cells and peritoneal macrophages. Int Immunopharmacol

41:98–105.

Klune J, Dhupar R, Carninal J, Billar TR, Tsung A. 2008. HMGB1: Endogenous Danger Signaling. Mol Med 14:1.

Lee DU, Ko YS, Kim HJ, Chang KC. 2017. 13-Ethylberberine reduces HMGB1 release through AMPK activation in LPS-activated RAW264.7 cells and protects endotoxemic mice from organ damage. Biomed Pharmacother 86:48–56.

Majerova P, Zilkova M, Kazmerova Z, Kovac A, Paholikova K, Kovacech B, Zilka N, Novak M. 2014. Microglia display modest phagocytic capacity for extracellular tau oligomers. J Neuroinflammation 11:161.

Mead EL, Mosley A, Eaton S, Dobson L, Heales SJ, Pocock JM. 2012. Microglial neurotransmitter receptors trigger superoxide production in microglia; consequences for microglial-neuronal interactions. J Neurochem 121:287–301.

Molitoris JK, McColl KS, Swerdlow S, Matsuyama M, Lam M, Finkel TH, Matsuyama S, Distelhorst CW. 2011. Glucocorticoid elevation of dexamethasone-induced gene 2 (Dig2/RTP801/REDD1) protein mediates autophagy in lymphocytes. J Biol Chem 286:30181–30189.

Nakatani Y, Amano T, Tsuji M, Takeda H. 2012. Corticosterone suppresses the proliferation of BV2 microglia cells via glucocorticoid, but not mineralocorticoid receptor. Life Sci 91:761–70.

R Core Team. 2016. R: A language and environment for statistical computing. R Found Stat Comput.

Repetto G, del Peso A, Zurita JL. 2008. Neutral red uptake assay for the estimation of

cell viability/cytotoxicity. Nat Protoc 3:1125–31.

Sapolsky RM, Romero M, Munck AU. 2000. How Do Glucocorticoids Influence Stress Responses? Integrating Permissive, Suppressive, Stimulatory, and Preparative Actions. Endocr Rev 21:55–89.

Schierbeck H, Wähämaa H, Andersson U, Harris HE. 2010. Immunomodulatory drugs regulate HMGB1 release from activated human monocytes. Mol Med 16:343–51.

Schindelin J, Arganda-Carreras I, Frise E, Kaynig V, Longair M, Pietzsch T, Preibisch S, Rueden C, Saalfeld S, Schmid B, Tinevez J-Y, White DJ, Hartenstein V, Eliceiri K, Tomancak P, Cardona A. 2012. Fiji: an open-source platform for biological-image analysis. Nat Methods 9:676–682.

Sobesky JL, D'Angelo HM, Weber MD, Anderson ND, Frank MG, Watkins LR, Maier SF, Barrientos RM. 2016. Glucocorticoids Mediate Short-Term High-Fat Diet Induction of Neuroinflammatory Priming, the NLRP3 Inflammasome, and the Danger Signal HMGB1. eNeuro 3:1–17.

Venereau E, Casalgrandi M, Schiraldi M, Antoine DJ, Cattaneo a., De Marchis F, Liu J, Antonelli a., Preti a., Raeli L, Shams SS, Yang H, Varani L, Andersson U, Tracey KJ, Bachi a., Uguccioni M, Bianchi ME. 2012. Mutually exclusive redox forms of HMGB1 promote cell recruitment or proinflammatory cytokine release. J Gen Physiol 140:i6–i6.

Viegas LR, Hoijman E, Beato M, Pecci A. 2008. Mechanisms involved in tissue-specific apopotosis regulated by glucocorticoids. J Steroid Biochem Mol Biol 109:273–278.

Vande Walle L, Kanneganti T-D, Lamkanfi M. 2011. HMGB1 release by inflammasomes.

Virulence 2:162–165.

Weber MD, Frank MG, Tracey KJ, Watkins LR, Maier SF. 2015. Stress Induces the Danger-Associated Molecular Pattern HMGB-1 in the Hippocampus of Male Sprague Dawley Rats: A Priming Stimulus of Microglia and the NLRP3 Inflammasome. J Neurosci 35:316–24.

Willingham SB, Allen IC, Bergstralh DT, Brickey WJ, Huang MT-H, Taxman DJ, Duncan JA, Ting JP-Y. 2009. NLRP3 (NALP3, Cryopyrin) facilitates in vivo caspase-1 activation, necrosis, and HMGB1 release via inflammasome-dependent and -independent pathways. J Immunol 183:2008–15.

Wohleb ES, McKim DB, Shea DT, Powell ND, Tarr AJ, Sheridan JF, Godbout JP. 2014. Re-establishment of anxiety in stress-sensitized mice is caused by monocyte trafficking from the spleen to the brain. Biol Psychiatry 75:970–981.

Wu I, Shin SC, Cao Y, Bender IK, Jafari N, Feng G, Lin S, Cidlowski JA, Schleimer RP, Lu NZ. 2013. Selective glucocorticoid receptor translational isoforms reveal glucocorticoid-induced apoptotic transcriptomes. Cell Death Dis 4:e453.

Xavier AM, Anunciato AKO, Rosenstock TR, Glezer I. 2016. Gene Expression Control by Glucocorticoid Receptors during Innate Immune Responses. Front Endocrinol (Lausanne) 7:1–8.

Yang H, Antoine DJ, Andersson U, Tracey KJ. 2013. The many faces of HMGB1: molecular structure-functional activity in inflammation, apoptosis, and chemotaxis. J Leukoc Biol 93:865–73.

Yeager MP, Pioli PA, Guyre PM. 2011. Cortisol Exerts Bi-Phasic Regulation of

Inflammation in Humans. Dose-Response 9:332–347.

Zhou Y, Lu M, Du R-H, Qiao C, Jiang C-Y, Zhang K-Z, Ding J-H, Hu G. 2016. MicroRNA-7 targets Nod-like receptor protein 3 inflammasome to modulate neuroinflammation in the pathogenesis of Parkinson's disease. Mol Neurodegener 11:28.

Supplementary material

S1 Fluorescent immunocytochemistry characterisation of microglia purity

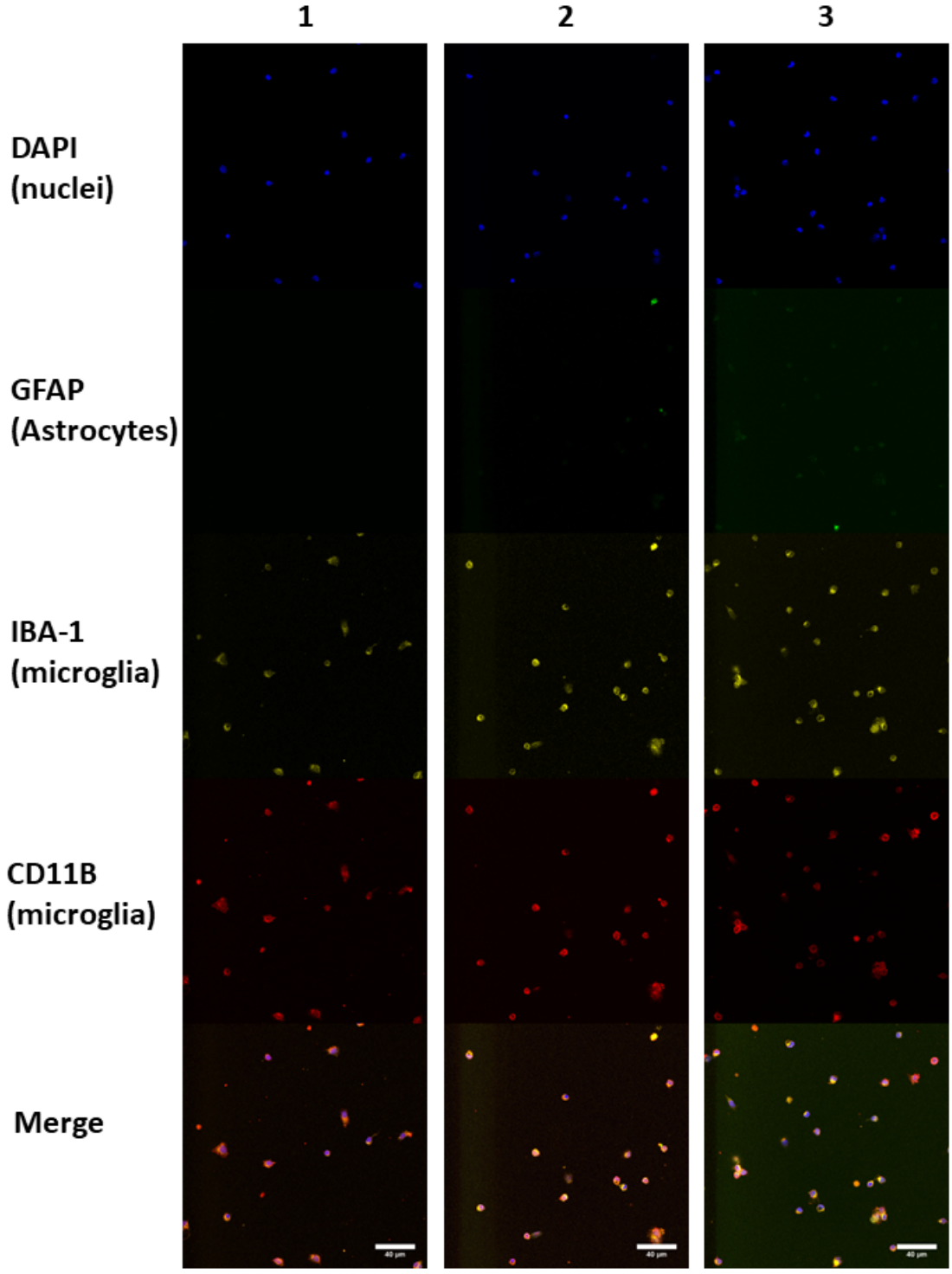

Figure S1. Immunocytochemistry characterisation of Percoll microglia isolation. Panels display representative individual channels and merged image (from top to bottom), from 3 separate isolations (left to right).

S2 Calculating the degree of HMGB1 cytoplasmic translocation from primary microglia

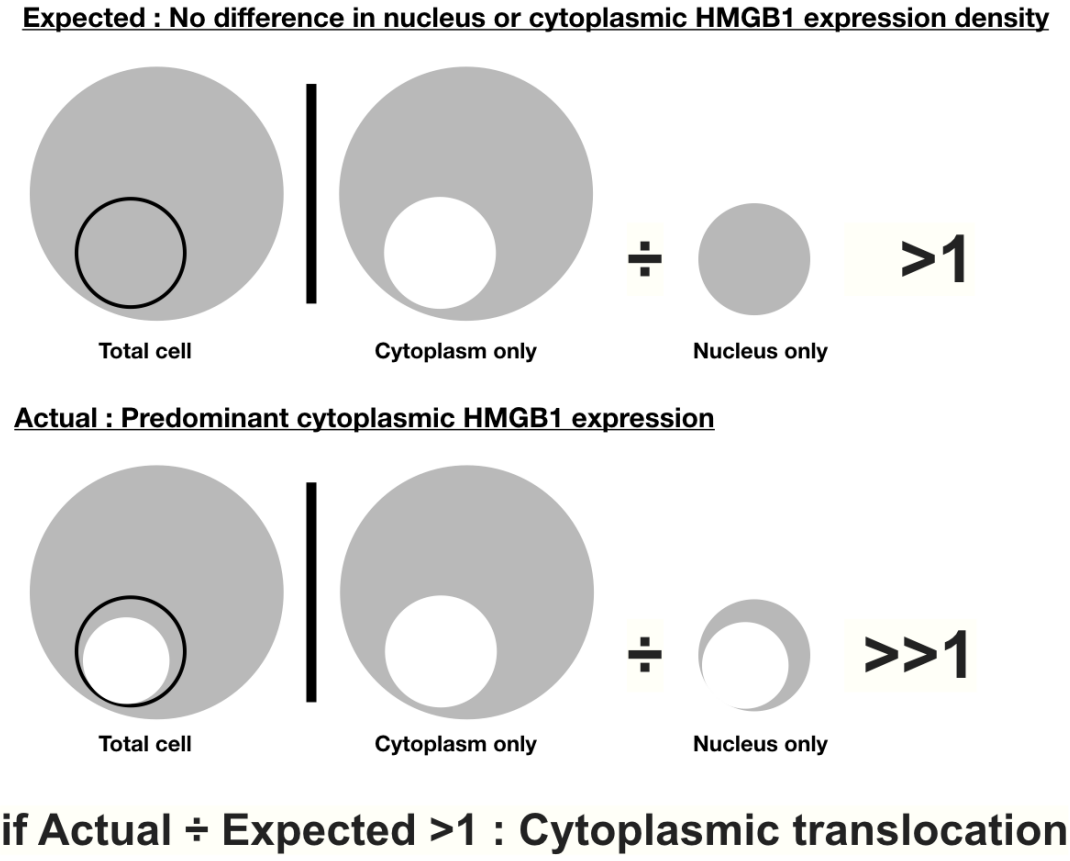

Figure S2. Calculating the degree of HMGB1 cytoplasmic translocation. Each cell was segmented into nucleus and cytoplasmic portion of using DAPI occupied area (top) and HMGB1 signal (bottom), giving respective expected and actual HMGB1 values overlapping with the nucleus. If there is predominant Cytoplasmic HMGB1 expression, the ratio of cytoplasmic:nucleus HMGB1 expression would exceed that of total nucleus to cytoplasmic area. Thus, cytoplasmic translocation of signal, calculated as a ratio of Actual:Expected would exceed the value of 1. Conversely, if there was no difference in nucleus or cytoplasmic distribution of HMGB1, the translocation value would be equal to 1.

S3 CORT does not significantly influence microglial viability (Neutral red measurement); No detectable extracellular HMGB1

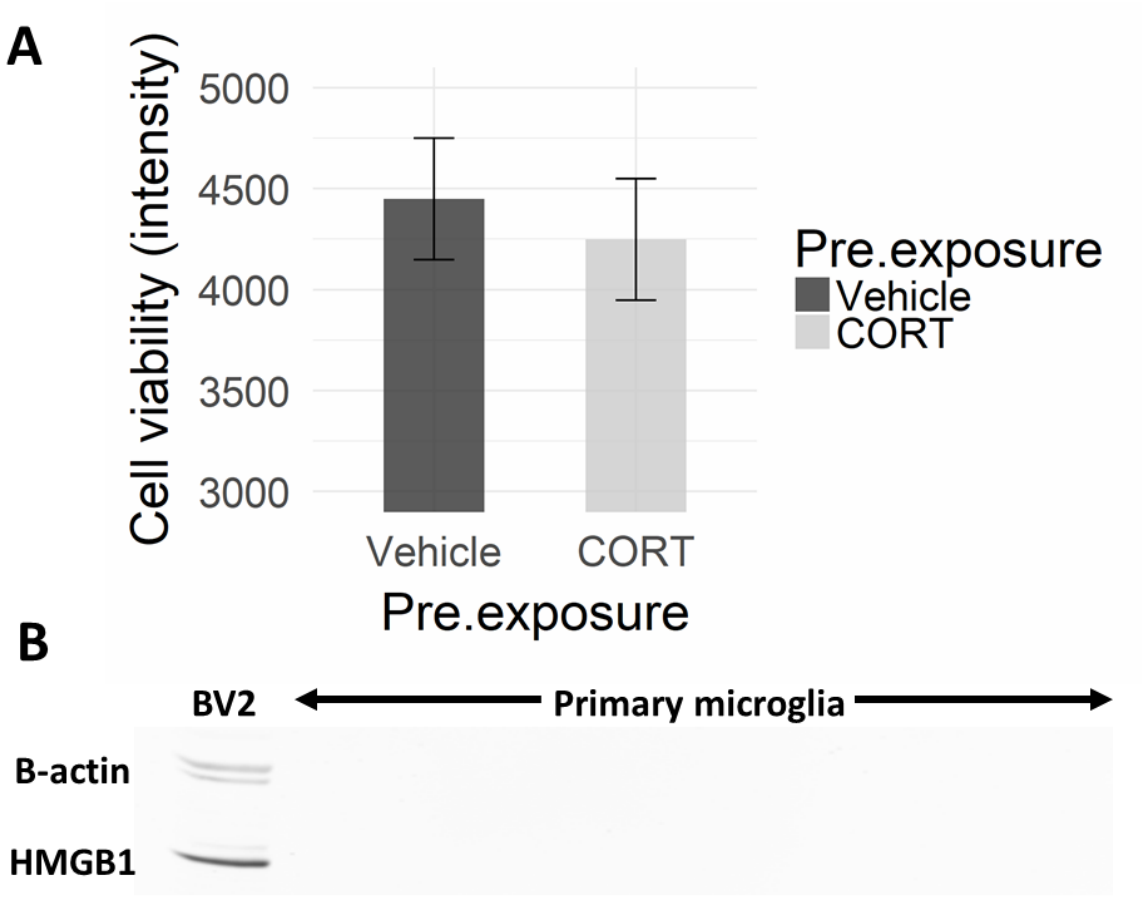

Figure S3 CORT exposure does not influence microglial cell viability. A) bar graph representing mean ± SEM of cell viability follow 24 h 500 nM CORT administration. B) Representative western blot showing no HMGB1 or β-actin expression in supernatants from primary microglia.

S4 Nuclear localisation of baseline BV2 signal

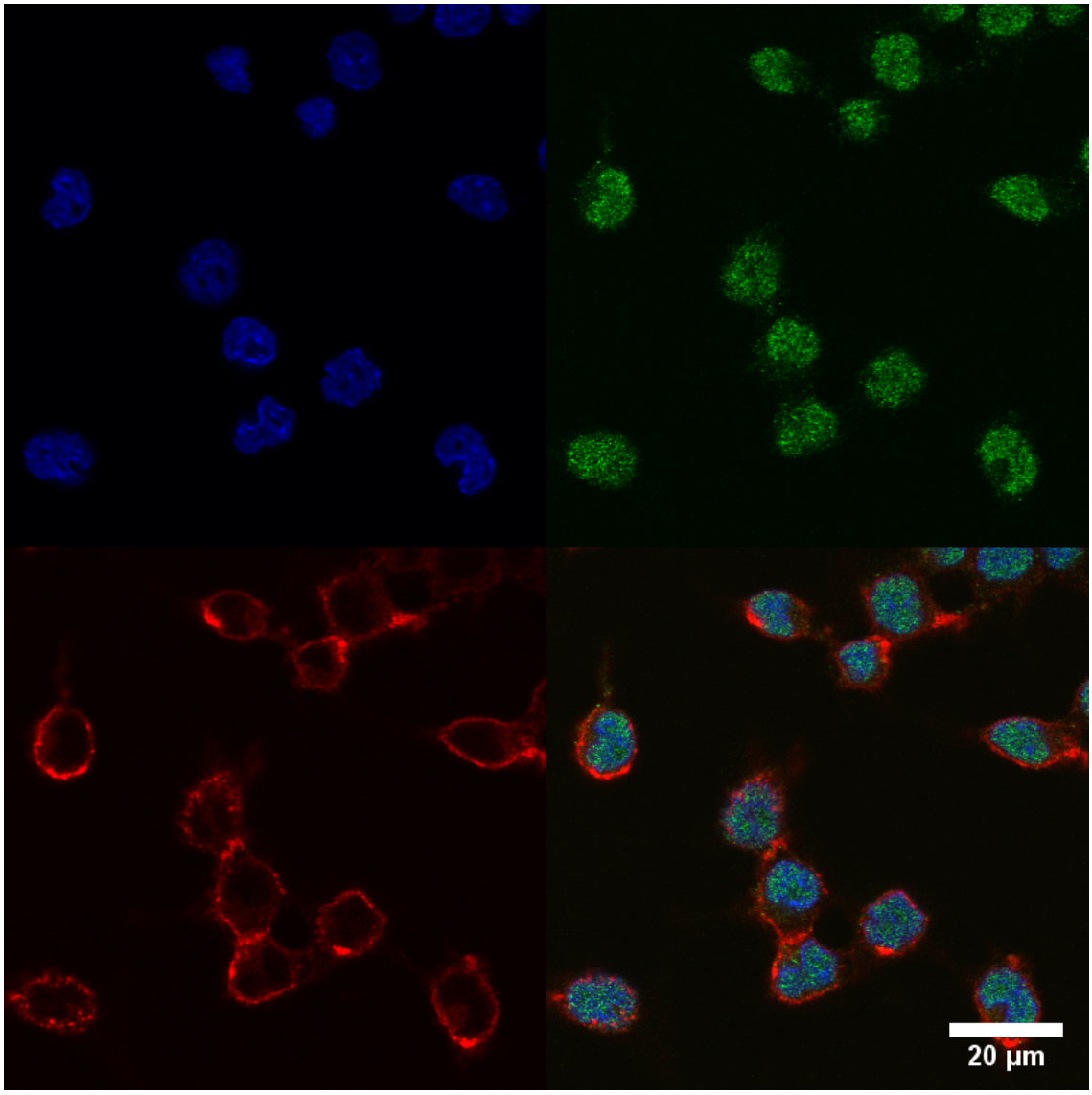

Figure S4. HMGB1 is predominantly localised to the cell nucleus in BV2 microglia-like cells. Immunocytochemistry images displaying DAPI (blue), HMGB1 (green) and cell membrane (red) signals in BV2 cells under 63x magnification.

S5 Confusion matrix for SVM analysis

Predicted values	Actual Values: No GR No MR	GR + MR	GR only	MR only
No GR No MR	24	2	1	6
GR + MR	0	9	5	0
GR only	0	1	6	0
MR only	0	0	0	0

Table S1. Confusion matrix for SVM analysis. Correctly classified values are underlined, while the numbers in all other cells represent misclassifications in the corresponding classes.

S5 SVM model performance

Overall Statistics

Accuracy : 0.7222
95% CI : (0.5836, 0.8354)
No Information Rate : 0.4444
P-Value [Acc > NIR] : 3.323e-05

	No GR No MR	GR + MR	GR only	MR only
Sensitivity	1.00	0.75	0.50	0.00
Specificity	0.70	0.88	0.98	1.00
Pos Pred Value	0.73	0.64	0.86	NaN
Neg Pred Value	1.00	0.93	0.87	0.89
Prevalence	0.44	0.22	0.22	0.11
Detection Rate	0.44	0.17	0.10	0.00
Detection Prevalence	0.61	0.26	0.13	0.00
Balanced Accuracy	0.85	0.82	0.74	0.50

Table S2. SVM model performance

Chapter 9: Corticosterone primes ATP-induced cell motility and DAMP-related protein release from BV2 microglia-like cells

9.1 Introduction

Studies 2 and 3 have mainly examined innate immune responses through measuring activity of pro-inflammatory pathways resulting in cytokine (Chapter 4-7) or DAMP (Chapter 8) production. However, besides these pro-inflammatory actions, microglia perform varied functions as part of the body's defence system. Other microglial innate immune actions include phagocytosis, cell migration and antigen presentation (Prinz and Priller, 2014). Interestingly, stress and CORT have also been shown to modify these functions, stimulating phagocytosis (Liu *et al.*, 1999), reducing the antigen presentation in dendritic cells (Elftman *et al.*, 2007), and increasing T-cell migration (Okutsu *et al.*, 2005).

Previous studies have demonstrated that stress can result in increased brain monocyte infiltration, and this phenomenon is associated with chemokine signalling via CCL2 and CXCL2 (Wohleb et al., 2012). CORT may also mediate some of the stress-related effects on peripheral innate immune cell motility. For example, with the exception of blood monocytes, restraint stress acutely increases leukocytes in plasma 6 min after stress onset in Sprague Dawley rats (Dhabhar *et al.*, 2012). However, the authors showed that unlike upregulations seen following norepinephrine and epinephrine administration, CORT administration in adrenalectomized animals decreased total white blood cell, monocyte, lymphocyte, helper T cells, and B cells in blood plasma after 2 h. Additionally, CORT administration can cause CXCR4 elevation, ultimately resulting in T-cell motility and redistribution (Okutsu *et al.*, 2005; Besedovsky, Born

and Lange, 2014). Using a CORT pre-exposure model, a human study found CORT-induced increase in monocyte migration to sites of injury, thus indicating that this mobilising effect is conserved in humans (Yeager *et al.*, 2016). Low concentrations of CORT (30-150 nM) can increase adherence, chemotaxis and phagocytosis in murine peritoneal macrophages, and these actions are further blocked by Mifepristone, a GR antagonist (Zhou *et al.*, 2010). Evidence for CORT-induced immune cell motility is thus strongest in peripheral immune cells, while the effects of CORT on central immune cell motility remain unclear.

Additionally, some indirect support for CORT-induced cell motility was shown in Chapter 8, as CORT concurrently decreased adhered cell viability and increased viable cells measured from the supernatant. These results suggest that the movement of viable cells to the supernatant may account for the loss in attached cell viability. Thus, CORT may not necessarily cause cytotoxicity in all immunocompetent cells, but also mobilise a portion of the cell population. BV2 microglia-like cells therefore appear to be suitable for further testing of these actions on cell motility.

Apart from exogenous PAMPs such as LPS, innate immune cells are also responsive towards endogenous danger signals such as ATP, which do not directly signal via TLRs. Instead, ATP activates purinergic receptors including P2X4 and P2X7, causing varied functions such as cell migration (Dou *et al.*, 2012), pyroptotic cell death (Fink and Cookson, 2006), and the release of IL-1β, and HMGB1 via inflammasome activation (Willingham *et al.*, 2009). Moreover, ATP can also cause permeabilisation and formation of membrane pores, allowing extracellular proteins to enter the cell during

inflammasome activation (Russo *et al.*, 2016). Given the varied actions of ATP, and the potential for CORT to modify these cell responses, the current chapter thus aimed to investigate the effect of pre-exposure + treatment + ATP on BV2 microglia-like cells (Figure 1). Cells were monitored under live-cell microscopy during ATP treatment to test if CORT pre-exposure can influence innate immune cell motility. Since high concentrations of ATP can induce pyroptosis, measures of cytotoxicity and cell viability in attached and detached cells were conducted. Both intracellular and extracellular expressions of HMGB1, NLRP3 and ASC proteins are reported for each condition to investigate the potential impact of ATP on DAMP-related protein release. Additionally, the effects of GR and MR antagonism on cell motility during ATP administration in CORT pre-exposed+LPS treated BV2 were also measured.

9.2 Methods

Methods for BV2 cell culture, cell viability measurements and western blot procedure were outlined in Chapter 8.

9.2.1 Experimental design

BV2 cells were pre-exposed to CORT (50/500 nM)(± antagonists), or volume-matched ethanol vehicle diluted in serum-free DMEM + L-glutamine for 24 h, followed by a second 24h treatment with either LPS or vehicle (N = 6 for each group) (Figure 1). Concentrations and times are based on previous data from Chapter 4. Finally, ATP or vehicle was added to each well, and cells were imaged under a live-cell microscope. After the drug exposure, cell supernatants were harvested and centrifuged to pellet cellular debris. The supernatant was used for measurements of extracellular LDH activity and protein expression and cell viability was measured in the pellet (supernatant cell viability). Cell viability of adherent cells was also measured.

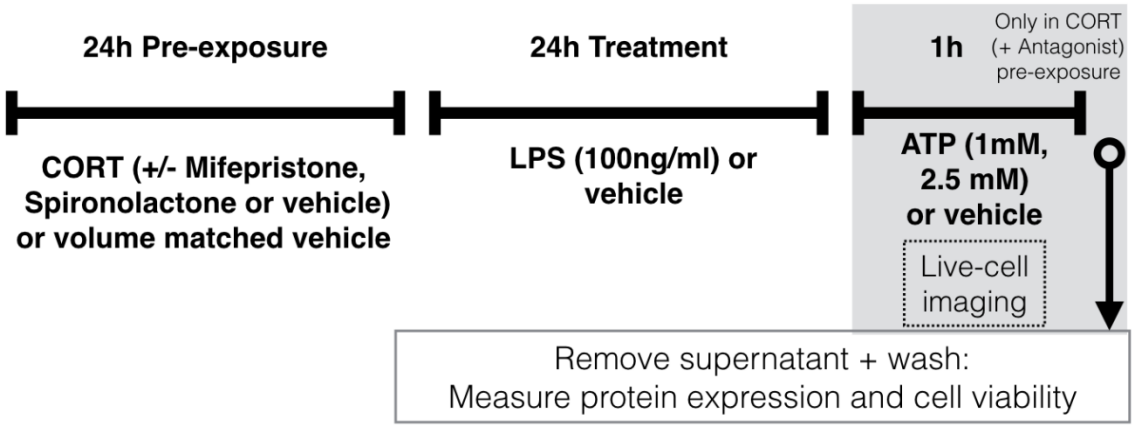

Figure 1. Experimental design. Measures of cell viability, cytotoxicity, extracellular and intracellular protein expression were performed after 24 h pre-exposure, 24 h treatment and 1 h ATP treatment. Supernatants were collected after ATP administration for analysis. Exact methods for quantifying cell viability, cytotoxicity and protein expression was detailed in Chapter 8.

9.2.2 ATP-induced Cell motility measurements

Live cell microscopy was used instead of trans-well migration assay due to the ability to image rale-time rate of migration, and retain concurrent information on cell morphology. Since CORT has previously demonstrated effects on BV2 cell morphology (Chapter 4), this measure may be important towards understanding CORT effects in cell responses to ATP. To image cell motility, live-cell microscopy was conducted under 20x magnification using a Nikon Ti E Live Cell Microscope equipped with a humidified incubator attachment held (95% air / 5% CO2, 37°C). Cell media was switched to either HBSS with Ca^{2+} and Mg^{2+} ions (vehicle) or HBSS + 1 mM ATP (ATP) conditions during live-cell imaging over a total period of 1 h. Cells were imaged at the same position every minute for the 50 min of the 1 h incubation, resulting in 50 frames per well.

Cell motility measurements were performed on .tif image stacks comprised of 50 images obtained from live-cell microscopy. A semi-automated cell tracking from CellTracker software (Piccinini, Kiss and Horvath, 2016) developed in Matlab, on the 2016b distribution of the software (MathWorks, USA) was used for image analysis. For each image stack, more than 30 cells were selected and tracked over each frame. Each tracked cell was monitored, and inconsistent tracks (ie. tracking of the wrong cell between frames) were removed. Cell motility is measured by total distance travelled per cell during the imaging period.

9.2.3 Data analysis and statistics

All statistical analyses were performed using R (64-bit, version 3.3.1) software (R Core Team, 2016). Cell motility data was analysed using linear mixed modelling via the nlme

package, with each biological replicate used as the random-effect. Each cell was thus sampled, and regarded as repeated measures within each biological replicate. Linear mixed effects models were utilised for analysis of cell viability, cytotoxicity and protein measures. Each measure was assigned as the dependent variable, while pre-exposure, antagonists, treatment and ATP concentrations were assigned as fixed independent variables. Each biological replicate was set as the random-effect, and each condition was therefore regarded as repeated measures for each N.

9.2 Results

9.2.1 Low concentration CORT pre-exposure increases cell motility and changes in cell morphology in response to LPS and ATP

Binding to purinergic receptors, extracellular ATP functions as a DAMP to cause microglia migration towards sites of damage (Ohsawa and Kohsaka, 2011; Koizumi *et al.*, 2013), and have been demonstrated to increase BV2 cell motility (Choi *et al.*, 2010). Given that glucocorticoid pre-exposure similarly cause peripheral immune cell migration to sites of injury (Yeager *et al.*, 2016), we investigated whether CORT pre-exposure can also influence BV2 cell motility in response to exogenous ATP (1 mM) (Figure 2A, B).

As expected, there was a significant main effect of LPS ($B = 54.85$, $t(2693)= 3.98$, $p<0.001$) and LPS+ATP ($B = 29.14$, $t(2693)= 2.13$, $p< 0.05$) on increasing cell motility as measured by total distance travelled by the cells across 50 min of imaging. CORT pre-exposure+LPS ($B = 56.22$, $t(2693)= 2.97$, $p<0.01$) and CORT pre-exposure+LPS+ATP ($B = 78.30$, $t(2693)= 4.16$, $p< 0.0001$) conditions caused a further increase in cell motility.

Post hoc analysis showed no significant differences between CORT or vehicle pre-exposed cells in the absence of LPS or ATP ($p>0.05$) . A 50 nM CORT pre-exposure significantly increased cell motility in LPS+ATP treated cells (mean difference = 56.95, $p<0.01$). This effect was not present in 500 nM pre-exposed BV2 cells (mean difference = 15.63, $p=0.99$).

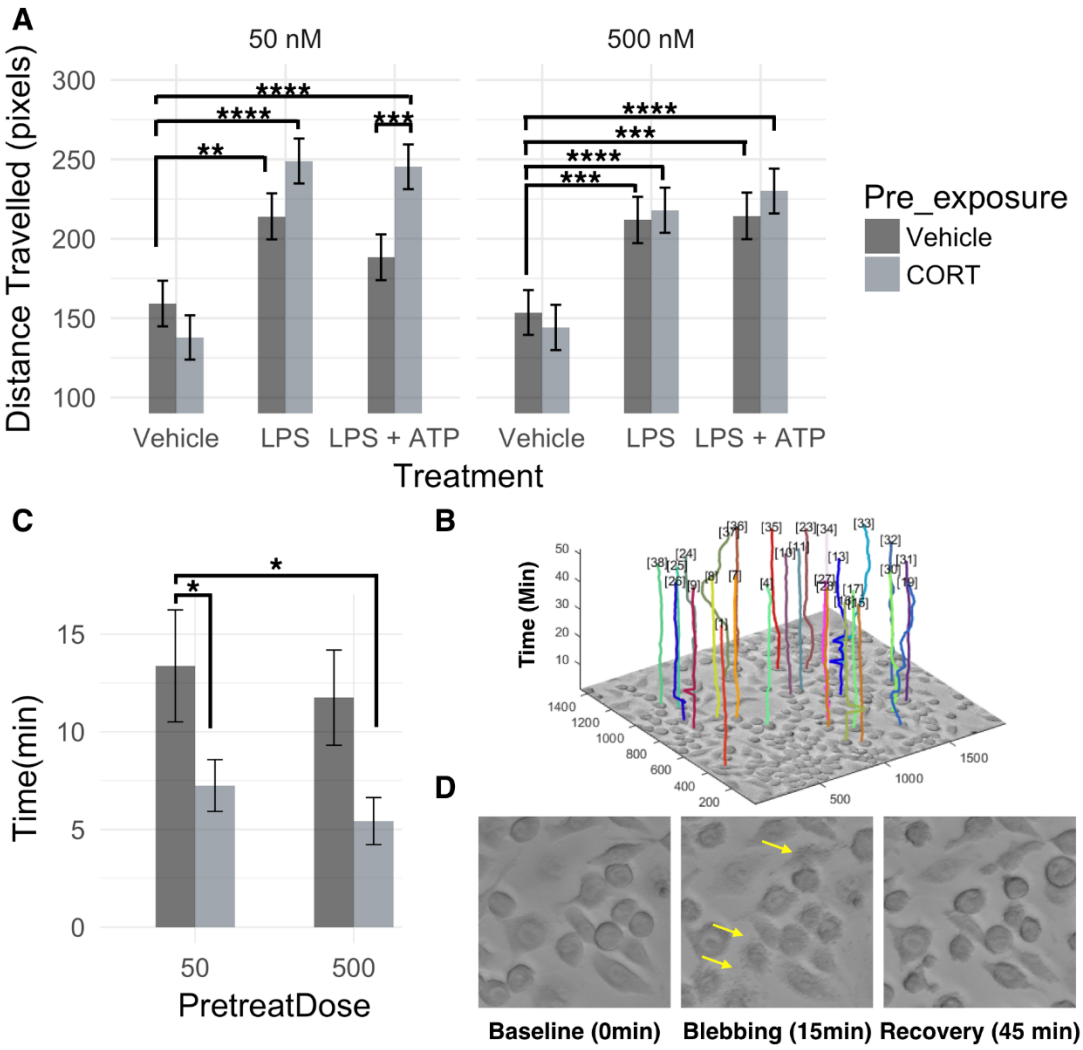

Figure 2. CORT pre-exposure increases cell motility and rate of cellular 'blebbing' morphological change in response to 1 mM ATP. A) Total distance travelled by BV2 cells after 24 h LPS (100 ng/ml) or vehicle, measured during 1h treatment of either vehicle (HBSS) or ATP (1 mM) (N = 6). CORT pre-exposure (light grey) further increases LPS+ATP-induced cell motility (N = 6). B) Representative image of distance travelled. Lines indicate positioning of tracked cells across time. C) Effect of CORT pre-exposure on time taken to show 'blebbing' morphology in cells (N = 6). D). Example images demonstrating transient cellular 'blebbing' and recovery during 1h ATP (1 mM) treatment. Significance levels for individual group differences using pairwise post-hoc comparisons with Tukey correction indicate by * ($p<0.05$) ** ($p<0.01$), ***($p<0.001$), **** ($p<0.0001$).

9.3.2 CORT pre-exposure reduces time to 'blebbing' in response to ATP

CORT pre-exposure, independent of concentration, significantly decreased time taken to achieve 'blebbing' morphology (Figure 2 C, D) under ATP treatment ($B = -6.13$, $t(20) = -2.83$, $p<0.05$). There was no independent concentration effect ($B = -1.63$, $t(20) = -0.75$, $p = 0.46$), or interaction effect between CORT pre-exposure and concentration of pre-exposure ($B = 0.06$, $t(20) = 0.02$, $p = 0.98$). Post hoc analysis further showed that CORT reduced time taken for 'blebbing' to occur in both 50 nM (mean difference = 6.1 min, $p<0.05$) and 500 nM (mean difference =7.7 min, $p < 0.05$) pre-exposure when compared to volume matched vehicle pre-exposure control.

9.3.3 GR and MR antagonists do not influence CORT pre-exposure priming of ATP-induced increased cell motility

Measured from *[pre-exposure + antagonist] + Treatment + ATP* treated BV2 cells, cell motility (Figure 3) was significantly increased by CORT pre-exposure ($B=21$ pixels, $t(3090)=2.05$, $p<0.05$), and decreased by LPS treatment ($B=-39$ pixels, $t(3090) = -3.42$, $p<0.001$) overall. CORT pre-exposure significantly interacted with LPS treatment to increase cell motility ($B=34$ pixels, $t(3090) = 2.24$, $p<0.05$). Neither GR ($B=-9$ pixels, $t(3090) = -0.84$, $p=0.40$) or MR ($B=-14.63$ pixels, $t(3090) = -1.38$, $p=0.17$) antagonists independently modified cell motility. GR and MR antagonists significantly interacted in combination with CORT (GR: $B=-33$ pixels, $t(3090) = -2.22$, $p<0.05$; MR: $B=-32$ pixels, $t(3090) = -2.17$, $p<0.05$) and LPS (GR: $B=33$ pixels, $t(3090) = -2.13$, $p<0.05$; MR: $B=42$ pixels, $t(3090) = 2.73$, $p<0.01$) to modify cell motility. Post hoc pairwise comparisons of least squares means using Tukey's adjustment further showed significant increases in cell motility in *[CORT+vehicle]+vehicle* compared to *[vehicle+vehicle]+vehicle* (mean difference = 21 pixels, $p<0.05$), *[CORT+vehicle]+LPS* compared to *[vehicle+vehicle]+LPS*

(mean difference = 56 pixels, p<0.0001), *[CORT+Mifepristone]+LPS* compared to

[vehicle+Mifepristone]+LPS (mean difference = 42 pixels, p<0.0001) treated cells.

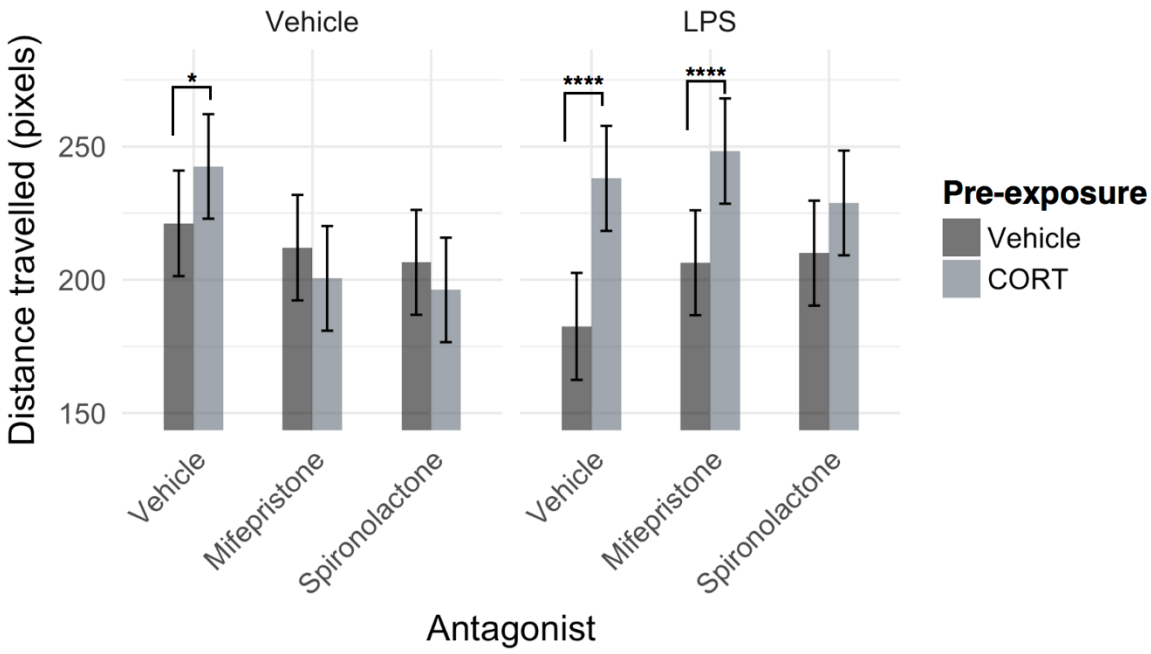

Figure 3. GR or MR antagonists fail to modify CORT pre-exposure + ATP -induced increases in cell motility. Bar plots show total distance travelled by cells under live-cell microscopy during 1 h ATP treatment (N=6). All values represent least squares means ± standard errors. Asterisks represent pairwise comparisons using Tukey's correction. * <0.005, **<0.01, ***<0.001, ****<0.0001.

9.3.4 Pre-exposure + Treatment + ATP effects on measures of cytotoxicity and cell viability

Cell viability

Cell viability was measured by neutral red uptake from viable cells after *pre-exposure+treatment+ATP* conditions (Figure 4A). A linear mixed effects model accounting for repeated measures within each biological replicate revealed a significant decrease in attached cell viability following 1 mM ATP administration (B = -0.09, t(88)= -2.4, p<0.05). Increasing the concentration of pre-exposure from 50 nM to 500 nM further decreased this 1 mM ATP-induced decrease of cell viability regardless of vehicle or CORT administration (B=-0.13, t(88)=-2.20, p<0.05), while LPS treatment significantly interacted with 2.5 mM ATP to cause a decrease in cell viability overall (B=-0.13, t(88)=-2.49, p<0.05). At this time point, CORT pre-exposure did not have a significant overall effect on cell viability (B=0.03, t(88)=0.72, p=0.47). Tukey post hoc pairwise comparisons of least squares means further revealed significantly lower attached cell viability in *500 nM CORT+vehicle+2.5 mM ATP* treated cells (mean difference = 0.12, p<0.01), and *500 nM CORT+LPS+2.5 mM ATP* treated cells (mean difference =0.14, p<0.01) with vehicle pre-exposed cells.

Detached cell viability (Figure 4B), measured from cells in the supernatants harvested at the end of all drug treatments, was increased by both 1 mM (B = 0.39, t(88)=7.06, p<0.0001) and 2.5 mM (B=0.29, t(88)=5.23, p<0.0001) ATP treatments. This result is expected, since ATP increases cell motility in BV2 cells, thus causing increased detachment from the well surfaces. LPS significantly interacted with ATP treatment,

paradoxically decreased detached cell viability after 1 mM ATP treatment (B=-0.22, t(88)=-2.86, p<0.01), but increased detached cell viability after 2.5 mM ATP treatment (B = 0.24, t(88)=3.13, p<0.01). 500 nM pre-exposure also significantly interacting with 1 mM ATP treatment to cause an increase in detached cell viability (B = 0.21, t(88)=2.48, p<0.05). CORT pre-exposure did not independently influence detached cell viability measured after ATP (B = 0.05, t(88)=0.92, p=0.36) independently. Post hoc tests further revealed that *500 nM CORT+LPS+1 mM ATP* (mean difference =0.14, p<0.05), and *500 nM CORT+LPS+2.5 mM ATP* (mean difference = 0.15, p<0.05) significantly decreased cell viability in the supernatant.

Cytotoxicity

Cytotoxicity (Figure 4C), as measured by LDH activity in cell supernatants harvested at the end of all drug treatments, was increased by 1 mM ATP (B = 0.08, t(88)=2.53, p<0.05) independent of all other conditions. ATP 1 mM further interacted with 500 nM pre-exposure conditions (B = 0.15, t(88)=2.96, p<0.01), causing further increases to LDH. Administration of 2.5 mM ATP significantly interacted with LPS to cause an increase in LDH (B = 0.16, t(88)=3.63, p<0.001). Independent of ATP treatment, 500 nM pre-exposure interacted with LPS to cause elevated LDH activity (B = 0.17, t(88)=3.46, p<0.001). Post hoc pairwise comparisons showed a significant LDH increase in 50 nM CORT +LPS+2.5 mM ATP treated cells compared to vehicle pre-exposure controls (mean difference = 0.09, p<0.01). No other CORT-vehicle pre-exposure comparisons reached statistical significance (p>0.05).

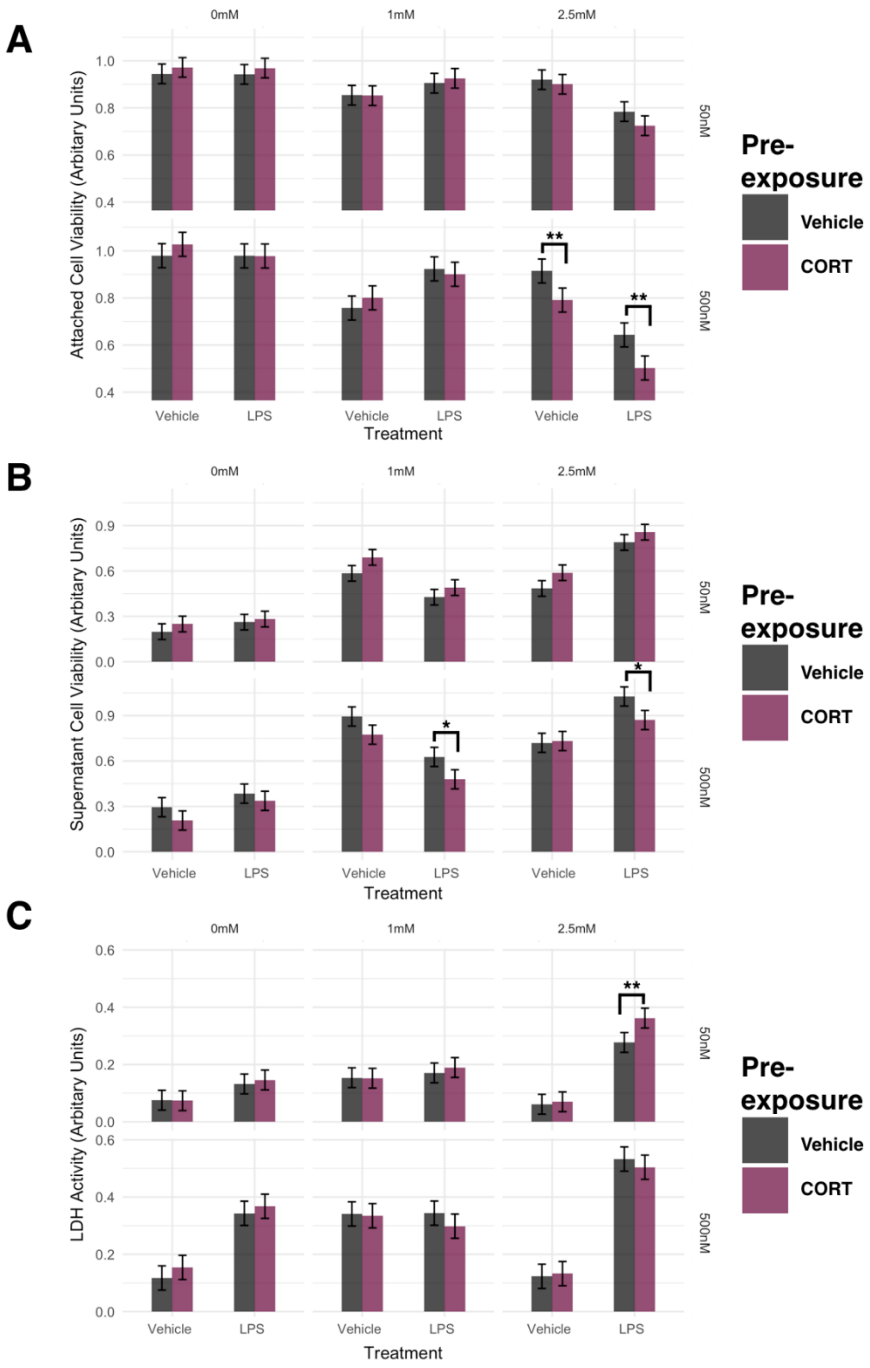

Figure 4. CORT pre-exposure (50 nM) increases cytotoxicity after CORT+LPS+2.5 mM ATP, while CORT (500 nM) pre-exposure decreases cell viability measured after Pre-exposure+Treatment+ATP conditions. A) Viability of cells left attached after all treatments, B) Viability of cells detached after 1 h ATP treatment, C) LDH activity measured from cell supernatants after all treatments (N=6). All values represent least squares means +/- standard errors. Asterisks represent pairwise comparisons using Tukey's correction. * <0.005, **<0.01, ***<0.001, ****<0.0001.

9.3.5 Extracellular NLRP3 and ASC, but not HMGB1 is influenced by CORT pre-exposure, measured after Pre-exposure+Treatment+ATP.

HMGB1

As assessed by a linear mixed effects model, supernatant HMGB1 expression was not significantly influenced by CORT pre-exposure, LPS treatment or ATP treatment conditions overall ($p>0.05$) (Figure 5A, B). Pairwise comparisons did not reveal any significant group differences ($p>0.05$).

NLRP3

Supernatant NLRP3 expression (Figure 5C) was not significantly influenced by Pre-exposure, LPS treatment or ATP treatment conditions overall ($p>0.05$). Post hoc pairwise comparisons showed a significant increase in NLRP3 expression measured from the supernatant of *50 nM CORT+LPS+2.5 mM ATP* (mean difference =0.09, $p<0.05$), *500 nM CORT+LPS+1 mM ATP* (mean difference = 0.14, $p<0.01$), and *500 nM CORT+LPS+ 2.5 mM ATP* (mean difference =0.11, pM0.05) treated cells.

ASC

Supernatant AS expression (Figure 2D) was significantly decreased by 500 nM pre-exposure independent of all other conditions ($B = -0.25$, $t(16)= 2.62$, $p<0.05$). CORT pre-exposure further interacted with 500 nM pre-exposure to cause increased ASC expression ($B= 0.27$, $t(176) =3.35$, $p<0.01$). Post hoc analysis further revealed significant increases in supernatant ASC expression from *500 nM CORT+vehicle+0 mM ATP* (mean difference =0.22, $p<0.001$), and *500 nM CORT+vehicle+1 mM ATP* (mean

difference =0.19, $p<0.01$) conditions compared to corresponding vehicle pre-exposure conditions.

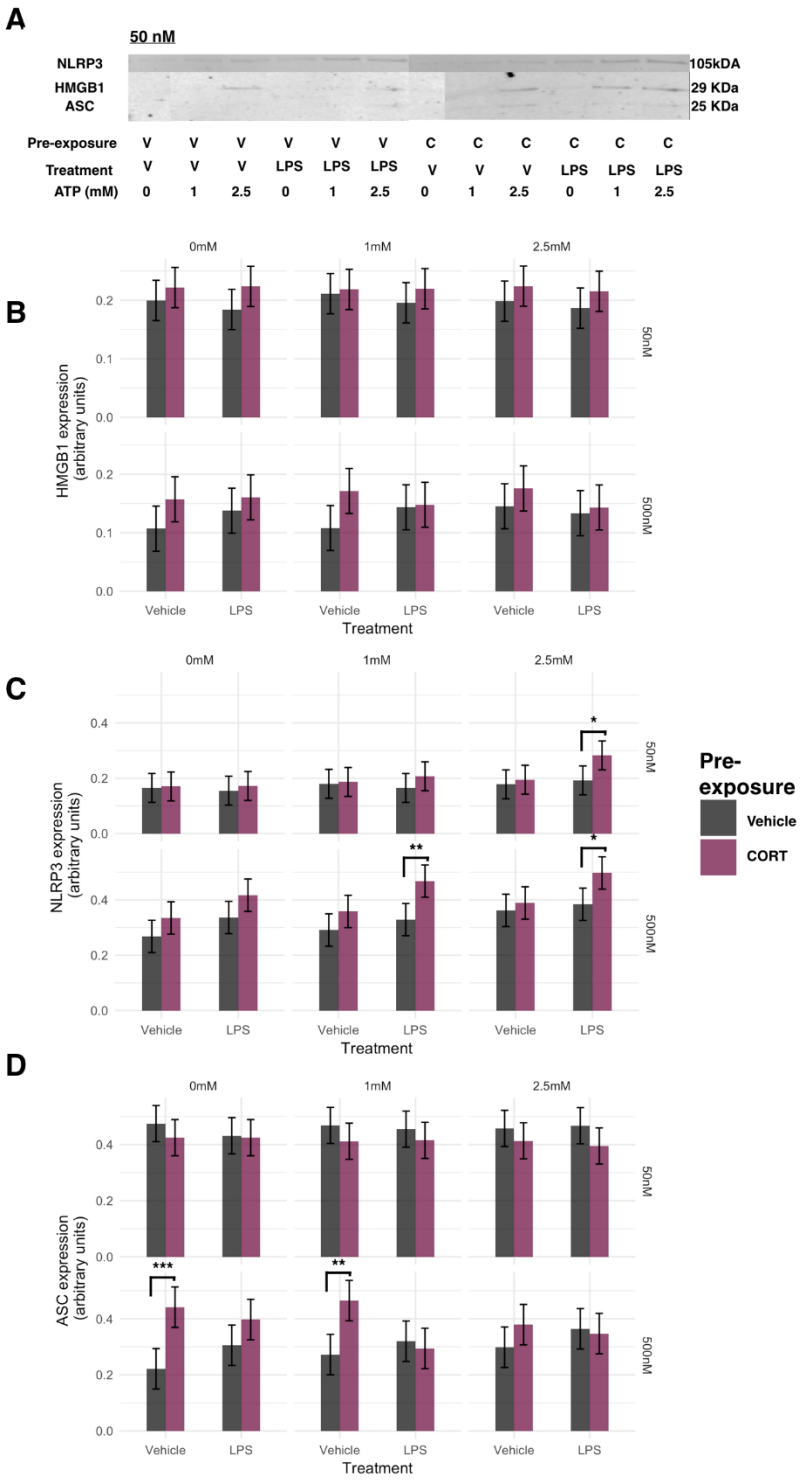

Figure 5. Extracellular NLRP3 and ASC expression is increased by CORT pre-exposure measured after Pre-exposure + Treatment + ATP conditions. A) Representative western blots showing measures of extracellular B) HMGB1, C) NLRP3, and D) ASC expression (N=12). All values represent least squares means +/- standard errors. Asterisks represent pairwise comparisons using Tukey's correction. * <0.005, **<0.01, ***<0.001, ****<0.0001.

9.3.6 CORT pre-exposure does not influence intracellular protein expression of HMGB1, ASC and NLRP3 measured after ATP.

HMGB1

Intracellular HMGB1 expression measured after *pre-exposure+treatment+ATP* conditions was not significantly influenced by each treatment ($p>0.05$) (Figure 6A).

NLRP3

Intracellular NLRP3 expression (Figure 6B) significantly increased after LPS treatment independent of all other treatments ($B=1.70$, $t(66)=4.79$, $p<0.0001$).No other treatment independently influenced NLRP3 expression ($p>0.05$). Post hoc pairwise comparisons did not find any difference between CORT pre-exposed and vehicle pre-exposed groups ($p>0.05$).

ASC

Intracellular ASC expression was not significantly modified by each treatment ($p>0.05$) (Figure 6C).

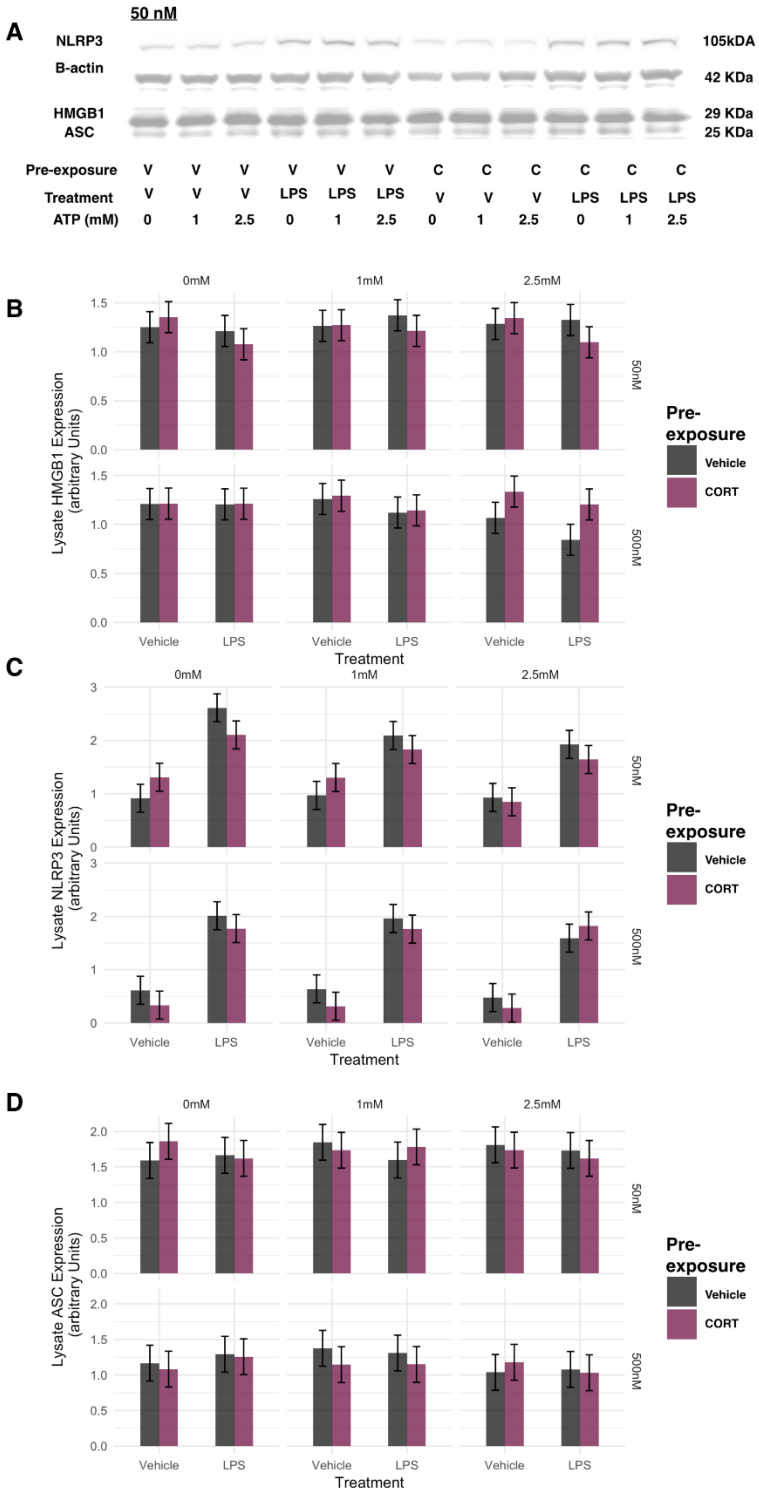

Figure 6. Intracellular protein expression is not altered by CORT pre-exposure when measured after pre-exposure+treatment+ATP. A) Representative western blots showing of cell lysate expression of B) HMGB1, C) NLRP3, and D) ASC expression (N=6). All values represent least squares means +/- standard errors. Asterisks represent pairwise comparisons using Tukey's correction. * <0.005, **<0.01, ***<0.001, ****<0.0001.

9.4 Discussion

CORT pre-exposure in BV2 cells decreased attached and detached cell viability after LPS+ 2.5 mM ATP treatment, without changes to LDH activity in the supernatant. Intracellular protein expression of HMGB1, NLRP3 and ASC were unchanged by CORT pre-exposure after Treatment + ATP conditions. Extracellular NLRP3 was increased after 1 and 2.5 mM ATP in *500 nM CORT+LPS* treatments, while extracellular ASC was increased after 0 mM and 1 mM ATP in *500 nM CORT + vehicle* treatments. Low concentration CORT pre-exposure also increased ATP-induced cell motility, while also increasing the rate of cellular 'blebbing' when exposed to ATP. GR or MR antagonists did not differentially modify CORT effects on ATP-induced cell motility. Thus, CORT pre-exposure appears to cause adaptations that last past a further 24 h LPS and 1 hr ATP treatment, changing cellular responses to these conditions overall, but the GR or MR dependency of these effects is still unclear.

Increases in cell motility and changes in cell morphology during ATP treatment was evident in this pre-exposure model. A high concentration (mM) of ATP was used in order to activate purinergic P2X7 receptors, which can cause inflammasome activation and pyroptosis via the same pathway (Pelegrin, Barroso-Gutierrez and Surprenant, 2008). Exogenous ATP can also cause the release of the inflammasome component Caspase-1 in extracellular space after LPS+ATP treatment (Qu *et al.*, 2009). Here, we found that 500 nM CORT pre-exposure decreased cell viability after pre-exposure+treatment+2.5mM ATP. Extracellular NLRP3 was increased after 1 and 2.5mM ATP in 500nM CORT+LPS treatments, while extracellular ASC was increased after 0mM and 1mM ATP in 500nM CORT + vehicle treatments. These results are

consistent with previous reports showing CORT-induced priming of primary microglia through upregulation of the inflammasome pathway (Frank *et al.*, 2014; Alcocer-Gómez *et al.*, 2015; Sobesky *et al.*, 2016).

9.4.1 CORT followed by LPS exposure causes an increase in BV2 cell motility and rate of morphological change in response to ATP

Previous studies have demonstrated ATP-induced microvesicle formation and exosome release in MG6 microglia-like cells (Takenouchi *et al.*, 2015), which resemble the membrane 'blebbing' seen here in BV2 cells. The current results further show that BV2 cells pre-exposed to CORT developed 'blebbing' morphology more rapidly. Cellular 'blebbing' is associated with increased cell motility and early-stage apoptosis (see review Charras, 2008). Given that no significant changes in cytotoxicity was found after 50 nM CORT pre-exposure, together with the increase in cell motility during 1 mM ATP treatment, this increased rate of morphological change may be more related to CORT-induced increase in cell motility. However, the application of GR and MR antagonists revealed no clear indication of whether this effect is due to MR or GR signalling. The actions of GR or MR antagonists appear to both influence motility dependent on LPS or vehicle treatment here. This is seen from the both antagonists attenuating cell motility increase only in [CORT + antagonist] + vehicle treated cells rather than [CORT + antagonist] + LPS conditions. Furthermore, there are no differential actions of either antagonists, indicating that the actions of CORT may not be via either receptor. More experiments are required to verify this result, and the mechanism underlying these findings.

9.4.2 CORT pre-exposure primes 2.5 mM ATP-induced loss of cell viability

Given the significant loss of viability in both detached and attached cell viability after 2.5 mM ATP, 500 nM CORT pre-exposure appears to have increased cell death in these conditions. Although exact mechanisms were not investigated here, it is likely due to ATP-induced pyroptosis (Pelegrin, Barroso-Gutierrez and Surprenant, 2008). ATP has previously been shown to cause cell death via P2X7 receptor activation in microglia-like and primary microglia cells between 30-90 min of 2-5 mM concentrations (Brough *et al.*, 2002; Qu *et al.*, 2009; Bartlett, Yerbury and Sluyter, 2013). The decreased cell viability here at 2.5 mM may thus indicate increased vulnerability in CORT pre-exposed cells. This result is unsurprising, since high concentrations of glucocorticoids induce immune cell death (Wu *et al.*, 2013). However, an important consideration here is the lack of LDH increase in the supernatant harvested from these cells, which indicate that the loss in cell viability may not be directly related to cytotoxicity.

9.4.3 Persistent CORT pre-exposure priming of NLRP3, but not HMGB1 release

The changes to extracellular protein measures after pre-exposure + treatment + ATP take on a different pattern to measures after pre-exposure and pre-exposure + treatment seen in Chapter 8. Firstly, CORT increased extracellular HMGB1 expression after 24 h exposure, sustaining through an additional 24 h of treatment. After ATP treatment, however, the CORT effect on extracellular HMGB1 was lost. Moreover, CORT pre-exposure increased ASC after vehicle + 0 or 1 mM ATP, not seen in measures after prior treatments. Extracellular NLRP3 expression remained increased after 1 mM and 2.5 mM ATP treatments here, suggesting that CORT pre-exposure has a long-lasting impact on the NLRP3 release. Interestingly, these extracellular protein

expression increases took place without corresponding change in intracellular protein expression, suggesting that CORT pre-exposure only alters release mechanisms (including cell death), rather than total protein expression.

9.4.4 Limitations

Since the experiments in this chapter were performed entirely using BV2 cells, it is still unconfirmed if microglia will exhibit the same CORT pre-exposure effects. Previous studies have found purinergic induction of microglial motility (Ohsawa and Kohsaka, 2011), and cell death (Brough *et al.*, 2002), but ATP-induced DAMP protein release has yet to be shown. Furthermore, the added effects of CORT pre-exposure have not been explored in these effects on microglia. Thus, a primary cell model is required in order to confirm these identified CORT pre-exposure effects on ATP actions in microglia. Importantly, ATP was not identified as a common immune-stimulatory compound in BV2 and primary microglia, as indicated by the systematic review in Chapter 3. The CORT pre-exposure effects on ATP-induced loss of cell viability, NLRP3 release and increase in cell motility therefore cannot be generalised to microglia. Nevertheless, the CORT-induced apoptosis (Molitoris *et al.*, 2011) and cell motility (Schweingruber *et al.*, 2014) have been well characterised in immunocompetent cells, and our results here support those findings. Moreover, GR and MR independent effects of CORT in priming BV2 cell motility found here provide an interesting avenue for further exploration.

Chapter 8 showed that CORT effects are strongest directly after the 24 h exposure. In contrast, the results after 1 h of ATP may not be enough time for the accumulation of extracellular protein. This is evident by the lower signal seen in this chapter, when

compared to extracellular protein measurements in Chapter 8. Furthermore, the experiments in this chapter all included a second 24 h LPS or vehicle before ATP administration. The delayed addition of ATP in this model may therefore be testing a different system indirect from CORT actions, thus potentially explaining the lack of GR and MR dependency of the effects measured here. Administration of ATP directly after, or during CORT exposure may therefore reveal additional and more direct effects. The additional use of DEX and Aldosterone, as specific GR and MR agonists respectively, can also further test GR and MR effects on ATP-induced cell motility, cell viability and protein release.

9.5 Conclusion

The current chapter thus found increased extracellular release of inflammasome-related proteins alongside decreased cell viability in response to high concentrations of ATP in BV2 cells pre-exposed to CORT. Given that extracellular NLRP3 inflammasome has demonstrated pro-inflammatory signalling properties (Baroja-Mazo *et al.*, 2014), future investigations may include the functional significance of these released proteins after pre-exposure to CORT. Furthermore, the exact mechanisms connecting cell death and protein release needs clarification. In vivo investigations of microglia motility following stress or CORT treatments may also provide insight towards the functional significance of the BV2 results gathered here.

References

Alcocer-Gómez, E., Ulecia-Morón, C., Marín-Aguilar, F., Rybkina, T., Casas-Barquero, N., Ruiz-Cabello, J., Ryffel, B., Apetoh, L., Ghiringhelli, F., Bullón, P., Sánchez-Alcazar, J. A., Carrión, A. M. and Cordero, M. D. (2015) 'Stress-Induced Depressive Behaviors Require a Functional NLRP3 Inflammasome', *Molecular Neurobiology*, pp. 1–9. doi: 10.1007/s12035-015-9408-7.

Baroja-Mazo, A., Martín-Sánchez, F., Gomez, A. I., Martínez, C. M., Amores-Iniesta, J., Compan, V., Barberà-Cremades, M., Yagüe, J., Ruiz-Ortiz, E., Antón, J., Buján, S., Couillin, I., Brough, D., Arostegui, J. I. and Pelegrín, P. (2014) 'The NLRP3 inflammasome is released as a particulate danger signal that amplifies the inflammatory response.', *Nature immunology*, (5 mM), pp. 1–5. doi: 10.1038/ni.2919.

Bartlett, R., Yerbury, J. J. and Sluyter, R. (2013) 'P2X7 Receptor Activation Induces Reactive Oxygen Species Formation and Cell Death in Murine EOC13 Microglia', 2013.

Besedovsky, L., Born, J. and Lange, T. (2014) 'Endogenous glucocorticoid receptor signaling drives rhythmic changes in human T-cell subset numbers and the expression of the chemokine receptor CXCR4.', *FASEB journal : official publication of the Federation of American Societies for Experimental Biology*, 28(1), pp. 67–75. doi: 10.1096/fj.13-237958.

Brough, D., Le Feuvre, R. A., Iwakura, Y. and Rothwell, N. J. (2002) 'Purinergic (P2X7) Receptor Activation of Microglia Induces Cell Death via an Interleukin-1-Independent Mechanism', *Molecular and Cellular Neuroscience*, 19(2), pp. 272–

280. doi: 10.1006/mcne.2001.1054.

Charras, G. T. (2008) 'A short history of blebbing', *Journal of Microscopy*, 231(3), pp. 466–478. doi: 10.1111/j.1365-2818.2008.02059.x.

Choi, M. S., Cho, K. S., Shin, S. M., Ko, H. M., Kwon, K. J., Shin, C. Y. and Ko, K. H. (2010) 'ATP induced microglial cell migration through non-transcriptional activation of matrix metalloproteinase-9', *Archives of Pharmacal Research*, 33(2), pp. 257–265. doi: 10.1007/s12272-010-0211-8.

Dhabhar, F. S., Malarkey, W. B., Neri, E. and McEwen, B. S. (2012) 'Stress-induced redistribution of immune cells—From barracks to boulevards to battlefields: A tale of three hormones – Curt Richter Award Winner', *Psychoneuroendocrinology*, 37(9), pp. 1345–1368. doi: 10.1016/j.psyneuen.2012.05.008.

Dou, Y., Wu, H., Li, H., Qin, S., Wang, Y., Li, J., Lou, H., Chen, Z., Li, X., Luo, Q. and Duan, S. (2012) 'Microglial migration mediated by ATP-induced ATP release from lysosomes', *Cell Research*. Nature Publishing Group, 22(6), pp. 1022–1033. doi: 10.1038/cr.2012.10.

Elftman, M. D., Norbury, C. C., Bonneau, R. H. and Truckenmiller, M. E. (2007) 'Corticosterone impairs dendritic cell maturation and function', *Immunology*, 122(2), pp. 279–290. doi: 10.1111/j.1365-2567.2007.02637.x.

Fink, S. L. and Cookson, B. T. (2006) 'Caspase-1-dependent pore formation during pyroptosis leads to osmotic lysis of infected host macrophages', *Cellular Microbiology*, 8(11), pp. 1812–1825. doi: 10.1111/j.1462-5822.2006.00751.x.

Frank, M. G., Hershman, S. A., Weber, M. D., Watkins, L. R. and Maier, S. F. (2014) 'Chronic exposure to exogenous glucocorticoids primes microglia to pro-inflammatory stimuli and induces NLRP3 mRNA in the hippocampus', *Psychoneuroendocrinology*. Elsevier Ltd, 40, pp. 191–200. doi: 10.1016/j.psyneuen.2013.11.006.

Koizumi, S., Ohsawa, K., Inoue, K. and Kohsaka, S. (2013) 'Purinergic receptors in microglia: Functional modal shifts of microglia mediated by P2 and P1 receptors', *Glia*, 61(1), pp. 47–54. doi: 10.1002/glia.22358.

Liu, Y., Cousin, J. M., Hughes, J., Van, J., Seckl, J. R., Haslett, C., Savill, J., Rossi, A. G., Damme, J. Van, Van Damme, J. and Dransfield, I. (1999) 'Glucocorticoids Promote Nonphlogistic Phagocytosis of Apoptotic Leukocytes', *Journal of Immunology*, 162(6), pp. 3639–46. Available at: http://www.ncbi.nlm.nih.gov/pubmed/10092825.

Molitoris, J. K., McColl, K. S., Swerdlow, S., Matsuyama, M., Lam, M., Finkel, T. H., Matsuyama, S. and Distelhorst, C. W. (2011) 'Glucocorticoid elevation of dexamethasone-induced gene 2 (Dig2/RTP801/REDD1) protein mediates autophagy in lymphocytes', *Journal of Biological Chemistry*, 286(34), pp. 30181–30189. doi: 10.1074/jbc.M111.245423.

Ohsawa, K. and Kohsaka, S. (2011) 'Dynamic motility of microglia: Purinergic modulation of microglial movement in the normal and pathological brain', *Glia*, 59(12), pp. 1793–1799. doi: 10.1002/glia.21238.

Okutsu, M., Ishii, K., Niu, K. J. and Nagatomi, R. (2005) 'Cortisol-induced CXCR4 augmentation mobilizes T lymphocytes after acute physical stress.', *American*

journal of physiology. Regulatory, integrative and comparative physiology, 288(3), pp. R591-9. doi: 10.1152/ajpregu.00438.2004.

Pelegrin, P., Barroso-Gutierrez, C. and Surprenant, a. (2008) 'P2X7 Receptor Differentially Couples to Distinct Release Pathways for IL-1 in Mouse Macrophage', *The Journal of Immunology*, 180(11), pp. 7147–7157. doi: 10.4049/jimmunol.180.11.7147.

Piccinini, F., Kiss, A. and Horvath, P. (2016) 'CellTracker (not only) for dummies', *Bioinformatics*, 32(6), pp. 955–957. doi: 10.1093/bioinformatics/btv686.

Prinz, M. and Priller, J. (2014) 'Microglia and brain macrophages in the molecular age: from origin to neuropsychiatric disease', *Nature Reviews Neuroscience*. Nature Publishing Group, 15(5), pp. 300–312. doi: 10.1038/nrn3722.

Qu, Y., Ramachandra, L., Mohr, S., Franchi, L., Harding, C. V, Nunez, G. and Dubyak, G. R. (2009) 'P2X7 receptor-stimulated secretion of MHC class II-containing exosomes requires the ASC/NLRP3 inflammasome but is independent of caspase-1.', *Journal of immunology (Baltimore, Md. : 1950)*, 182(8), pp. 5052–62. doi: 10.4049/jimmunol.0802968.

R Core Team (2016) 'R: A language and environment for statistical computing', *R Foundation for Statistical Computing*. Vienna, Austria.

Russo, H. M., Rathkey, J., Boyd-tressler, A., Katsnelson, M. A., Abbott, D. W., George, R., Abbott, D. W. and Dubyak, G. R. (2016) 'Active Caspase-1 Induces Plasma Membrane Pores That Precede Pyroptotic Lysis and Are Blocked by Lanthanides'. doi: 10.4049/jimmunol.1600699.

Sawicki, C. M. M., McKim, D. B. B., Wohleb, E. S. S., Jarrett, B. L. L., Reader, B. F. F., Norden, D. M. M., Godbout, J. P. P. and Sheridan, J. F. F. (2015) 'Social defeat promotes a reactive endothelium in a brain region-dependent manner with increased expression of key adhesion molecules, selectins and chemokines associated with the recruitment of myeloid cells to the brain', *Neuroscience*. IBRO, 302, pp. 151–164. doi: 10.1016/j.neuroscience.2014.10.004.

Schweingruber, N., Fischer, H. J., Fischer, L., van den Brandt, J., Karabinskaya, A., Labi, V., Villunger, A., Kretzschmar, B., Huppke, P., Simons, M., Tuckermann, J. P., Flügel, A., Lühder, F. and Reichardt, H. M. (2014) 'Chemokine-mediated redirection of T cells constitutes a critical mechanism of glucocorticoid therapy in autoimmune CNS responses.', *Acta neuropathologica*, 127(5), pp. 713–29. doi: 10.1007/s00401-014-1248-4.

Sobesky, J. L., D'Angelo, H. M., Weber, M. D., Anderson, N. D., Frank, M. G., Watkins, L. R., Maier, S. F. and Barrientos, R. M. (2016) 'Glucocorticoids Mediate Short-Term High-Fat Diet Induction of Neuroinflammatory Priming, the NLRP3 Inflammasome, and the Danger Signal HMGB1', *eNeuro*, 3(4), pp. 1–17. doi: 10.1523/ENEURO.0113-16.2016.

Takenouchi, T., Tsukimoto, M., Iwamaru, Y. and Sugama, S. (2015) 'Extracellular ATP induces unconventional release of glyceraldehyde-3-phosphate dehydrogenase from microglial cells', *Immunology Letters*. Elsevier B.V., 167(2), pp. 116–124. doi: 10.1016/j.imlet.2015.08.002.

Willingham, S. B., Allen, I. C., Bergstralh, D. T., Brickey, W. J., Huang, M. T.-H., Taxman, D. J., Duncan, J. A. and Ting, J. P.-Y. (2009) 'NLRP3 (NALP3, Cryopyrin) facilitates

in vivo caspase-1 activation, necrosis, and HMGB1 release via inflammasome-dependent and -independent pathways.', *Journal of immunology (Baltimore, Md. : 1950)*, 183(3), pp. 2008–15. doi: 10.4049/jimmunol.0900138.

Wu, I., Shin, S. C., Cao, Y., Bender, I. K., Jafari, N., Feng, G., Lin, S., Cidlowski, J. A., Schleimer, R. P. and Lu, N. Z. (2013) 'Selective glucocorticoid receptor translational isoforms reveal glucocorticoid-induced apoptotic transcriptomes', *Cell Death and Disease*, 4(1), p. e453. doi: 10.1038/cddis.2012.193.

Yeager, M. P., Pioli, P. A., Collins, J., Barr, F., Metzler, S., Sites, B. D. and Guyre, P. M. (2016) 'Glucocorticoids enhance the in vivo migratory response of human monocytes', *Brain, Behavior, and Immunity*. Elsevier Inc., 54, pp. 86–94. doi: 10.1016/j.bbi.2016.01.004.

Zhou, J.-Y., Zhong, H.-J., Yang, C., Yan, J., Wang, H.-Y. and Jiang, J.-X. (2010) 'Corticosterone exerts immunostimulatory effects on macrophages via endoplasmic reticulum stress', *British Journal of Surgery*, 97(2), pp. 281–293. doi: 10.1002/bjs.6820.

Chapter 10: The bidirectional interface between innate immunity and the HPA axis – Implications and future directions

Stress has been implicated in the exacerbation of inflammatory conditions and have multiple interactions with innate immune functioning in health and disease (Kemeny and Schedlowski, 2007). Although the neuroendocrine stress response is the best studied physiological link between stress and innate immunity, the mechanistic extent of these interactions is still unclear. Exploring the bidirectional interface between innate immunity and the neuroendocrine system in the context of stress, the work in this thesis can be broadly categorised into 3 main studies. The first study (Chapters 2-3) focused on the role of the TLR4-MyD88 innate immune signalling pathway on the stress response system. This was assessed via corticosterone responses to forced swim stress, tail suspension stress and administration of ACTH to adrenals *ex vivo.* Behavioural immobility during tail suspension and forced swim stressors was also observed (Table 1). This study established that the deletion of *Tlr4* or *Myd88* in mice can have a profound influence on baseline stress behaviour and HPA responses following these stimuli. These differences were not recapitulated in acute pharmacological inhibition of TLR4 and IL-1R1, thus showing that TLR4 and IL-1R1 signalling at the time of acute stress does not influence stress responses. Additionally, chronic or developmental changes resulting from lacking *Tlr4* or *Myd88* may underlie the differences in the transgenic mice.

Study 2 (Chapters 4-7) examined the other side of the bidirectional relationship between neuroendocrine and innate immunity by measuring TLR4-NF-κB signalling

changes after pre-treatment of corticosterone *in vitro.* Here, further investigation of the presence and concentration of corticosterone pre-treatment during immune stimulation of BV2 microglia-like cells was conducted. Corticosterone pre-exposure primed the innate immune response to LPS and TNF-α administration, causing increased NF-κB translocation and IL-1β release from BV2 cells (Table 2). These effects were only seen in low concentration pre-exposure of CORT, and were reversed by a MR antagonist, therefore indicating that MR mediates the TLR4-NF-κB priming effects of low concentration CORT. Partial replication of the results obtained from BV2 cells was further achieved with adult primary microglia. Due to low total signal of IL-1β release from primary microglia, priming of IL-1β responses were not measured. However, similar to BV2 cells, low concentration CORT pre-exposure primed LPS-induced NF-κB translocation and TNF-α release in adult primary microglia. These results thus provide support for the TLR4-NF-κB priming effect of low concentration CORT pre-exposure in microglia.

Study 3 (Chapters 8-9) further expanded on the *in vitro* model developed in study 2, examining the effect of CORT on cell viability, cytotoxicity and DAMP-related protein release. In this study, primary microglia exposed to CORT exhibited significant HMGB1 cytoplasmic translocation, a measure associated with increased releasable HMGB1. Furthermore, BV2 cells exhibited GR dependent increase in extracellular HMGB1 protein and increased cell death after 24 h exposure to high concentration CORT (Table 3). Most CORT-induced effects did not persist after a second 24 h treatment of LPS and a further 1h ATP administration. Collectively, the studies in this thesis have shown: 1) intrinsic relationship between glucocorticoid and TLR4-MyD88 signalling; 2)

the pervasive effects of this relationship on behaviour, systemic neuroendocrine responses, and immune signalling performance.

10.1 The Impact of TLR4-MyD88 signalling on stress responses

Previous research on immune effects on stress mainly use immunogenic stressors, like LPS, to elicit behavioural change (Chapter 1 Figure 4). Long-term effects of prenatal and neonatal exposures to immune challenges are especially interesting, as these effects usually persist into adulthood, inducing increased anxiety behaviours in rodents (Walker et al., 2009; Sominsky et al., 2013). Although the authors introduce the idea that immune factors can fundamentally influence the stress response, how this intrinsic immune-neuroendocrine connection influences non-immune related stress is unclear. Uncovering the effects of baseline signalling on non-immunogenic stressors may thus uncover inherent connections between the two systems on a genetic level, which has potential implications to individual differences in stress responses.

Thus, Study 1 examined the effect of immune signalling on baseline immobility behaviours during forced swim stress and tail suspension stress, and the corticosterone responses following stressors in $Tlr4^{-/-}$ and $Myd88^{-/-}$ mice. Interestingly, this finding was not replicated using acute innate immune antagonists IL-1RA and (+)-Naltrexone. Due to the changes in behavioural and CORT responses, further investigation on the positive and negative feedback mechanisms was conducted. Differential adaptations in both positive and negative feedback systems were observed in transgenic mice, characterised by increased adrenal sensitivity to ACTH, and hypothalamic CBG and GR protein expressions. These adaptations may underlie the

neuroendocrine changes seen. Thus, stress behaviour, neuroendocrine and TLR4-MyD88 signalling are fundamentally linked in baseline stress responses, interacting through feedforward and feedback pathways, but in a more complex manner than initially anticipated.

The manifestation of stress-modulatory functions in long-term innate immune signalling deficits raises research questions about developmental factors which may underlie these changes, as well as whether this work has an impact on long-term immune changes seen in chronic illness. The observed within-strain difference between immobility performances in forced swim and tail suspension stressors were surprising given the assumption that immobility during both stressors indicates depressive-like behaviour (Steru et al., 1985). Interpretation of behaviour during the stress response is thus more complex than initially anticipated, and these differences may be illustrative of individual differences in stress behaviours. For example, fear conditioning to the same stimulus is not uniform in humans (Gershman and Hartley, 2015; McLaughlin et al., 2016). Individual variation has been accepted in behavioural research, and multiple explanations for these individual differences, from biological variables such as age, sex genetic polymorphisms, neuroendocrine and neural activity to environmentally influenced factors such as mood, personality, time of day, sleep, levels of stress and life adversity (see review Lonsdorf et al., 2017).

Critically, individual variation within each mouse strain is also evident in animal studies. As a result, some studies utilised stratified division of subgroups distinguishing between “responders” and “non-responders” to stressful stimuli from the same rodent strain (Wellman et al.; Carreira et al., 2017), even in established stress protocols such

as restraint stress (Hetzel and Rosenkranz, 2014). Given this diversity to stress response, the nature of stress resilience and vulnerability has become a topic of focus within stress research (Füchsl et al., 2014; Gerber et al., 2017; Santarelli et al., 2017). The results in Study 1 suggest that genetic deletions of *Myd88* and *Tlr4* may be involved in different presentations of immobility behaviours towards stressful stimuli, but how this relates to stress resilience requires further study of other behavioural performances to a battery of behavioural tests.

Since strain differences were observed in behavioural immobility and changes to circulatory CORT concentrations resulting from forced swim and tail suspension stress, a relationship between the two measures was expected. Yet, data collected on behavioural performance and corticosterone concentration did not show any significant linear relationship, suggesting that although genetic alterations to TLR4-MyD88 signalling has an impact on both behaviour and neuroendocrine responses, they neither vary in the same way, nor in a straightforward manner. This finding demonstrated the complexity of the connection between innate immune signalling, neuroendocrine responses and behaviour. Given the initial hypothesis that bidirectional immune and neuroendocrine interactions were integral towards the stress response, Studies 2 and 3 shifted the focus on how glucocorticoids, as part of the neuroendocrine stress response, influenced innate immune function.

10.2 Actions of the stress hormone, corticosterone on innate immune signalling: Immunosuppression and immune priming

10.2.1 MR dependent pro-inflammatory priming

CORT has shown paradoxical immunosuppressive (Sapolsky et al., 2000) and immune priming (Sawicki et al., 2015; Sobesky et al., 2016) properties in the literature, but these different actions remain unresolved. Studies 2 and 3 thus investigated the conditions required for immunosuppressive and immune priming actions on a microglia-like cell line, and further verified key findings in adult primary microglia. Through manipulating concentrations and models of pre-treatment, Studies 2 and 3 demonstrated both actions, which generally occurred under different conditions. The findings were therefore able to unify some of these disparate actions in the context of an *in vitro* environment. Illustrating this, Study 2 found immunosuppression of IL-6 responses while immune priming of IL-1β responses following LPS treatment in the same cells. Additionally, the IL-1β priming effect only occurred after CORT pre-exposure was removed prior to addition of LPS or TNF-α.

Furthermore, Study 2 verified that IL-1β protein production and release can be potentiated by low concentrations of corticosterone pre-exposure prior to LPS treatment in BV2 microglia-like cells. This finding is consistent with biphasic concentration dependency previously seen in glucocorticoids, where low concentrations elevated, but high concentrations suppressed the immune response (Yeager et al., 2011). Applying this treatment model to isolated adult primary microglia, Study 2 further confirmed microglial priming with the same low concentration CORT pre-exposure on microglial TNF-α release.

Interestingly, through use of pharmacological antagonists, CORT actions were found to be mediated by MR rather than GR binding. This result is consistent with the binding properties of GR vs MR, where low concentrations would preferentially bind the high-affinity and non-abundant MR (Lu et al., 2006; Harris et al., 2013). Furthermore, in support of these findings, MR activation in BV2 cells has previously demonstrated immune stimulatory effects, resulting in increased NF-κB translocation and IL-6 production (Chantong et al., 2012). The potential role of MR in innate immune priming may therefore extend the stress response system to other agonists of MR, such as aldosterone, which recruits the renin-angiotensin-aldosterone system (RAAS) in the systemic innate immune responses. In cardiomyocytes, aldosterone aids the formation of TLR4/CD14 complexes, thus indicating that MR activation can directly enhance TLR4 signalling (Mannic et al., 2015). The effects of MR signalling on neuroimmune activity is still unclear, and we demonstrate here that there is an avenue for further investigation *in vivo*. The implications of MR involvement in stress induced priming could therefore introduce systemic osmotic homeostasis in consideration of innate immune priming.

In addition, CORT pre-exposure primed IL-1β release in TNF-α treated BV2 cells, showing the potential NF-κB dependency of this result. Study 2 further confirmed that NF-κB translocation was increased in CORT pre-exposed BV2 cells and primary microglia. Together, these findings suggest that CORT may have effects early in the TLR4 signalling pathway. Critically, the effects of Study 2 are unlikely to be via cell death mechanisms, since it takes a high concentration of CORT to cause significant cell damage, and GR rather than MR, seen in Study 3, mediates this process. This result, however, does not exclude the possibility that single cell differences may mediate

these changes. Given common pathways between inflammasome activation and pyroptotic cell death (Fink and Cookson, 2006), high inflammasome and IL-1β expressing cells may become more likely to be damaged, and thus elevate supernatant IL-1β disproportionately. Furthermore, since supernatant levels were measured via ELISA due to low detection levels on western blots, we are unable to conclude if the measured IL-1β was the active mature form. Additionally, it is unknown if the elevation in IL-1β has any further functional downstream signalling properties. Thus, high-throughput single cell analysis with the ability to discern pro- and mature- IL-1β forms is required to verify this.

10.2.2 GR dependent cytotoxicity and DAMP-related protein release

With emerging evidence that DAMP release mediates stress-induced priming (Frank et al., 2015), Study 3 focused on DAMP related protein release. Non-cytokine endpoints for CORT pre-exposure actions were also assessed, through cell motility changes, cell viability and cytotoxicity. Moreover, immunocompetent cells have far more functions than pro-inflammatory signalling through cytokine production such as cell migration towards areas of injury, antigen presentation, and phagocytosis. Thus, an appreciation of how CORT influences some of these functions would provide a more holistic view of how stress may influence innate immunity.

Study 3 supported the immunosuppressive properties of high concentration CORT pre-exposure found in Study 2, demonstrated by the increased cytotoxicity and decreased cell viability. Cell death is one of the primary functions of CORT induced immunosuppression (Keshwani et al., 2015), and this process can also mediate

cytokine (Edwan et al., 2015) and DAMP (Willingham et al., 2009) release via inflammasome involvement. In support of this hypothesis, HMGB1 protein expression is increased extracellularly after 24h exposure to CORT. Unlike Study 2, however, this effect was observed after exposure to high concentrations of CORT, and involved GR instead of MR activity. This result was shown in 2 separate treatment conditions 1) using Dexamethasone, a specific GR agonist, and 2) CORT in combination with Mifepristone and Spironolactone, specific GR and MR antagonists respectively. Additionally, partial support for increased HMGB1 was found in primary microglia, in which CORT treatments induced cytoplasmic translocation of HMGB1. After LPS treatment, high concentration CORT pre-exposed cells also exhibited increased extracellular NLRP3 expression suggesting that CORT can cause increased DAMP signalling. The paracrine or endocrine signalling properties of these extracellular DAMPs are still unexplored, and would be interesting to see if it can cause pro-inflammatory responses in other cells.

10.2.3 Low-concentration CORT increases cell motility and morphological change

In both BV2 cells and primary microglia, low concentration CORT pre-exposure resulted in a more ramified morphology during LPS exposure in Study 2. Low concentration CORT pre-exposure also caused increased cell motility and rate of cellular 'blebbing' following ATP administration in BV2 cells. These results demonstrate the effects of CORT on other innate immune actions beyond pro-inflammatory signalling, therefore indicating that CORT pre-exposure results in a unique state which causes long-term change to immune function. The increased cell motility in Study 3 is

consistent with research showing elevated peripheral immune cell migration in stress (Sawicki et al., 2015) and CORT-treated participants (Yeager et al., 2016).

Together with the primed IL-1β responses seen in Study 2, this elevation in cell motility could potentially mediate some of the glucocorticoid-related pro-inflammatory actions. Thus, when BV2 microglia-like cells are pre-exposed to low concentrations of CORT, NF-κB translocation is increased, and cells become primed towards IL-1β release in response to further LPS treatment, as well as more responsive towards ATP-induced cell motility. These actions suggest that CORT pre-exposed cells more likely to become pro-inflammatory, and that these actions are more likely to influence a wider area due to the increased cellular movement. The actual physiological impact of this scenario is however still unclear, since inflammatory signalling can be protective, through the resolution of pathogenic infections in normal physiology, or deleterious, in cases of cytokine induced prolonged maladaptive behavioural changes (Walker et al., 2009).

10.2.4 High concentration CORT is not necessarily immunosuppressive

In the case of the stress-like high concentration pre-exposure, CORT can be immunosuppressive via increased cell toxicity and reduced cell viability, but may potentially prime other cells in a paracrine manner through increased DAMP protein release. Since HMGB1 antibody administration can prevent the development of priming in hippocampal microglia (Weber et al., 2015), stress-induced DAMPs can initiate priming. The increased extracellular expression of HMGB1 resulting from stress levels of CORT applied to BV2 cells, and further attenuation using GR antagonist Mifepristone found in Study 3 further suggest that CORT, via GR signalling may initiate

this stress-related priming in the whole animal. Mifepristone use *in vivo* has also shown GR dependency of this stress-induced priming (Frank et al., 2012; Sobesky et al., 2016), thus further supporting this result. Taken together, both low concentration and high concentration CORT across results from Studies 2 and 3 show glucocorticoid involvement in the priming of innate immune responses via different mechanisms in low and high concentrations.

CORT has a robust impact on innate immune function, influencing almost all measures across Studies 2 and 3, thus showing potent immunomodulatory functions. Furthermore, the findings across studies show that CORT can mediate both immune priming and immunosuppressive responses in an immunocompetent cell line and in primary microglia. CORT actions seen here are therefore diverse, but not contradictory, generally requiring different conditions to elicit each action. Physiological changes seen *in vivo* are also supported by the results seen from direct actions of glucocorticoids on BV2 cells observed in this study. We have therefore identified specific candidate mechanisms, both via MR and GR, which can contribute towards the explanations of priming and immunosuppression seen in stress research.

10.3 Exploration of data analysis techniques

Ongoing debates in the scientific community about the over-dependence on p-values (Gale et al., 2016), and statistical pipeline (Leek and Peng, 2015), have led towards the exploration of other alternatives to presenting experimental findings in this thesis. For example, Study 1 used some linear regression analysis on individual animal data, illustrating the disconnect between behavioural and neuroendocrine performances in

animals. On the surface, measuring an increase in forced swim immobility and increased overall corticosterone responses after this stressor in Myd88$^{-/-}$ animals may indicate that these two systems may be connected. When accounting for individual animals, however, there was little relationship between the two measures, in that high immobility animals not necessarily exhibited high circulating corticosterone concentrations measured after the stressor. The lack of a clear linear relationship suggests that the systems connecting stress behaviour and corticosterone production is more complex than anticipated, and may potentially originate from separate pathways during stress. Examining co-varying continuous measures within studies thus provides further perspectives towards the measures within a study.

10.3.1 Linear mixed models for repeated measures

Linear mixed effects regression was applied to measures of intracellular gene expression and pro-IL-1β protein expression measures and concurrent extracellular IL-1β responses in Study 2. This statistical method was applied to test the hypothesis that CORT pre-exposure may change the release mechanisms of IL-1β in this study. In the absence of targeted experimental manipulation, natural variability as a result of CORT pre-exposure or co-treatment was analysed. Mixed-effects modelling was used to control for differences across biological replicates throughout this thesis, thus treating each measurement within a passage or animal as repeated measures. As a result, assumption of a shared variation within each biological replicate was applied, and thus each biological replicate required all measures present. This has implications for experimental design, as each passage of cells required the same number of conditions applied, and internal controls to verify the findings. The findings of this analysis

suggested that some part of the IL-1β release mechanism was altered, although the exact location within the pathway was not identified.

10.3.2 Classification as means of determining effects of treatment conditions

Studies 2 and 3 also introduced the use of support vector machines (SVM) classification in the analysis of treatment differences and receptor signalling differences respectively. Experimental research generally aims to determine if treatment conditions applied result in differences in measured outcomes. Thus, Frequentist parametric tests assess how well the data fit the assumption that no effect is present, or the null hypothesis (Anderson et al., 2000). Conversely, statistical classifiers assess how well the conditions or treatment groups fit the data, therefore approximating the underlying relationship (Hastie et al., 2009). In this context, classification becomes an optimisation problem, where accuracy of fit can be adjusted based on sensitivity or specificity, instead of a predefined type-1 error rate using Frequentist statistical methods. Additionally, SVM can be non-linear, and can account for multi-dimensional datasets (as seen in Chapter 7), thus providing a way to identify patterns across multiple measures.

10.3.3 Multi-dimensional approaches to analysis

Multi-dimensional approaches become more informative of systemic or pathway differences. This approach is most evident in genomics, transcriptomics and proteomics research, where datasets are extremely large. Studies 2 and 3 explored the use of multi-dimensional analysis in relatively controlled *in vitro* settings. Although sample sizes were not ideal, the results were consistent with the patterns already

assessed via frequentist methods. Interpretability, however, suffers with increasing numbers of measures for each study. Thus, principal components analysis (PCA) was used in study 3 for dimensionality reduction. This method is useful for presentation of data on 2 axes, as long as enough variability is captured by the PCA components.

Another problem with multi-dimensional datasets is the need for larger N numbers, and redundancy of measures. For example, measuring two closely related genes does not include any additional information into the model, and can sometimes obfuscate relationships within the model. Thus, parameter selection is paramount for streamlining the analysis. Regularisation techniques are frequently employed in genetics studies to circumvent the problem of redundancy (Wu et al., 2009). LASSO regression, a type of L1 regularisation, was applied to gene transcription data predicting IL-1β responses in Study 2. LASSO regularisation takes a wide dataset (a dataset with many variables), and progressively penalizes the coefficients of the model during each iteration, thus removing each independent variable from the regression model when coefficient values reach '0' (Friedman et al., 2010). The degree of penalization (λ) thus determines how many independent variables are selected. The optimum value of λ is selected by choosing the largest λ value within 1SE of the minimum mean squared error of k-fold cross validation analysis (Waldmann et al., 2013). Using this analysis implemented using the glmnet package in R (Friedman et al., 2010), the candidate gene expressions best explaining the variation in IL-1β in CORT and vehicle pre-exposed cells were assessed in Study 2.

Collectively, the analysis techniques explored in the studies here hope to provide some considerations to future experimental design. Similar to genetics research, there is an emerging need to have multiple concurrent measures from each sample, for example intracellular and extracellular measures, in order to perform multi-dimensional analysis. This would thus enable a better systematic understanding to biological phenomena investigated.

10.4 Limitations and further considerations

Study 1 took an observational approach of characterising baseline differences in the transgenic animals to show intrinsic connections between TLR4-MyD88 signalling and the baseline stress responses. We were unable to replicate these findings using acute pharmacological antagonists, which limits the mechanistic interpretations of these transgenic differences. Furthermore, given that adaptations were evident in both the hypothalamus and adrenals, it becomes difficult to pinpoint the exact location in which TLR4-MyD88 acts to cause changes to HPA reactivity. To circumvent this, additional studies with tissue-level manipulation of TLR4 and MyD88 are required. Use of conditional knockouts may be an option towards further experimentation to that end.

10.4.1 Considerations of gut-brain communication in the immune and neuroendocrine interface

Other systemic considerations that have an impact on both immune and neuroendocrine responses to stress, such as the role of the gut-brain axis, have not been investigated in this work. Emerging evidence show that behaviour, immune and HPA activity can be influenced by gut microbiota (Rea et al., 2016). For example, germ

free rats have elevated hypothalamic CRF mRNA CORT responses following open-field test, and accompanying increased anxiety-like behaviour during the behavioural test (Crumeyrolle-Arias et al., 2014). Host microbiome is also critical towards microglial function, since temporal eradication of microbiota increased total microglia and ramification of microglial morphology in multiple brain regions (Erny et al., 2015). This study also showed impaired cytokine transcription from primary microglia isolated from germ free mice following 6 h LPS stimulation.

Taken together, there is strong evidence that the microbiome can influence both stress behaviour, neuroendocrine, and neuroimmune responses. However, the role of TLR4 signalling and HPA adaptations in these microglia changes are still unclear and may be an avenue for more exploration. Indeed, microbiome dysbiosis due to high fat diet has been associated with elevated TLR4 signalling, and increased neuropathy and impaired gut motility (Reichardt et al., 2016). Interestingly, Reichardt et al. (2016) showed that mice lacking TLR4 did not develop motility changes and neuronal loss, thus indicating that TLR4 may mediate some changes arising from microbiome dysbiosis. These systems may also contribute towards the immune and endocrine backdrop, which can ultimately modulate systemic responses. Thus, further explorations of these differences in the whole animal are encouraged. For example, use of adoptive transfer of microbiome between *Tlr4*$^{-/-}$, *Myd88*$^{-/-}$ and wild type mice may be a way to further test if the neuroendocrine or behavioural changes seen in these transgenic mice may be related to the microbiome dysbiosis.

10.4.2 Use of immortalized cell line for mechanistic investigations

The predominant use of BV2 microglia-like cell line in Studies 2 and 3 is another limitation, since these immortalized cells have exhibited impaired IRF-related gene transcriptions compared to primary microglia in previous RNAseq studies (Das et al., 2015, 2016). Thus, a brief systematic review on the similarities and differences between BV2 cells and primary microglia was conducted in Chapter 3, which suggested that NF-κB dependent actions were conserved in BV2 cells. The experiments conducted in Study 2 therefore mainly tested NF-κB actions. Furthermore, a subset of experiments was repeated on adult primary microglia to verify key findings. Logically, the next steps would include verifying these results in a more physiological setting such as organotypic cultures, to preserve the interactions between the different CNS cell types. Moreover, other meaningful areas of study, such as the investigation of these glucocorticoid actions across different age groups and sex can be further investigated.

10.4.3 Potential role of age-related adaptations in neuroendocrine and immune dysregulations

It is accepted that age-related adaptations can have a profound impact on both neuroendocrine and immune activity from the critical stress-sensitive periods in development (Sominsky et al., 2013) to marked dysregulation of HPA activity (see systematic review Belvederi Murri et al., 2014), and increased microglial alterations during aging (Galatro et al., 2017). Moreover, a higher level of pro-inflammatory signalling and increased depressive-like behaviour is evident in aged rats (Huang et al., 2008), suggesting that there may be some differences in stress responses. However, whether this relates to the physiological neuroendocrine changes is still unclear. Sex

differences are also evident in innate immune responses (Wegner et al., 2017), and HPA activity in humans (Carpenter et al., 2017). Therefore, an investigation of glucocorticoid priming in these populations could contribute toward understanding the heterogeneity of stress responses.

10.4.4 Potential role of TLR4 and MyD88 in glucocorticoid-induced priming of innate immune responses

Characterising glucocorticoid priming responses in *Tlr4*$^{-/-}$ and *Myd88*$^{-/-}$ transgenic mice used in Study 1 could be used to evaluate the importance of TLR4-MyD88 signalling in priming innate immune responses. This experiment could be performed using both stress and *ex vivo* administration of glucocorticoids. A consideration here is the avoidance of LPS as the immune stimulant, as it would directly conflict with the genetic manipulations of the system. Instead, TNF-α used successfully in Study 2 could be administered as the immune stimulant instead.

10.4.5 Constant concentration over 24 h in cell experiments

Another notable consideration here is that 24 h or 48 h drug treatments will be difficult to maintain in *ex vivo* cultures due to a high rate of cell death. As an example, IBA-1 staining in *ex vivo* slices attempted here to compare 1 h and 25 h drug treatments exhibit tissue and cellular degradation (Appendix A). Furthermore, as demonstrated in Chapter 6 and 8, isolated primary microglia appear to suffer from significant cell loss in experiments. Thus, long-term organotypic cultures which require careful culturing over the course of 3 weeks prior to drug treatments may be a be a

better model, since it has been previously demonstrated that microglia survive and retain responsiveness to LPS after 3 weeks of organotypic culture (Ajmone‑Cat et al., 2013). A benefit of this approach is the increased feedback from neurons and astrocytes, which increases the translatability of the model. However, this long duration spent outside of a physiological system can alter microglia responses, causing increased activation and inhibiting hippocampal neurogenesis (Gerlach et al., 2016). This increased activity may therefore influence further inflammatory and anti-inflammatory responses. Furthermore, corticosterone response in this model also remains unknown, and would likely require careful optimisation.

A large portion of the *in vitro* work here only used a single pre-exposure across a 24 h period without changes to CORT concentrations over time. This limits the translatability of these findings to in vivo physiology, since CORT is dynamically regulated by various systems. Demonstrating this regulation, Study 1 showed that acute stress triggers both feedforward and feedback mechanisms tightly regulating CORT, while levels return close to baseline within one hour after the acute stress. Furthermore, the actual half-life of CORT is 8-12 hours (Chrousos et al., 2000). Thus, this 24hr consistent elevation is unlikely representative of physiological conditions, and requires further verification.

As an example, use of an *in vitro* microfluidics system which dynamically controls CORT concentrations over time may be used further provide validity to the priming effects of CORT. Additionally, instead of a full 24 h pre-exposure, a shorter exposure with a

recovery period prior to LPS treatment may be a viable option. This was previously implemented in RAW264.7 cells, showing that acute elevations in glucocorticoids can cause prolonged priming of pro-inflammatory responses (Smyth et al., 2004). In this study, a 1 h 100 nM pre-exposure to CORT primed the LPS-induced IL-6, Nitrate and TNF-α release, and CD14 expression, 12 and 24 h after discontinuation of the pre-exposure. Using this model of glucocorticoid pre-exposure, the priming effect was found to be more potent after the cells are given a recovery period. Furthermore, the transient increase in CORT applied here may mimic the acute stress response better. This pre-exposure model has yet to be used in microglia, and further exploration may yield more physiologically relevant results. Nevertheless, the current *in vitro* model is useful in providing a mechanistic direction, via identifying pathways in which glucocorticoids can act (GR vs MR for example), as well as potential overlaps with NF-κB signalling pathway in situations of innate immune stimulation. Further *in vivo* or *in vitro* studies can therefore use these results and methods of analysis for further interrogation into mechanistic links between stress neuroendocrine and innate immunity.

10.4.5 Functional significance of HMGB1 elevation

Although an elevation of HMGB1 expression was found, the functional significance of this extracellular HMGB1 is largely unknown. HMGB1 has previously been found from the supernatants of primed microglia isolated from rats previously exposed to inescapable shock (Weber et al., 2015). In this study, the authors showed that a HMGB1 neutralising antibody administered prior to stress was also used successfully to inhibit the priming of microglia. Thus, extracellular HMGB1 appears to play a

significant role in the priming of microglia during stress. Despite finding increased HMGB1 in the cell supernatants after 24 h CORT exposure in Study 3, the paracrine or autocrine properties of this release was not directly measured. Furthermore, the redox state of this released HMGB1 is also unknown. The redox state is important for the function of HMGB1, in which the partially reduced and fully reduced forms have cytokine and chemokine-like properties respectively (Venereau et al., 2012). Furthermore, artificial oxidation using H_2O_2 has been shown to attenuate the immune stimulatory actions of reduced HMGB1 during ischemia reperfusion injury (Liu et al., 2012). Thus, redox state of HMGB1 determines the actions of the released protein, and is a reversible process determined by environmental factors.

Given that CORT pre-exposure demonstrated both immune priming of IL-1β release and increased cell motility in BV2 cells, it is unclear if these actions of CORT may be mediated by the increased HMGB1 release. One possible mechanism could be the triggering of pro-inflammatory pathways through binding of disulfide-HMGB1 to known innate immune receptors, TLR4 and RAGE (Aini *et al.*, 2013, Yang *et al.*, 2015). Measurement of redox state and modulation of HMGB1 activity through pharmacological inhibition could therefore serve as a direct measure of this protein in the cellular responses to immune stimulation. Additionally, the paracrine signalling capacity of this protein could be indirectly tested through exposure of cells to media conditioned by cells previously exposed to CORT.

10.4.6 Unknown release mechanisms

Although Studies 2 and 3 showed that CORT exposure caused increased HMGB1 and primed the release of IL-1β, the exact release mechanisms were not captured with the methods used here. Previous studies demonstrated exosomal and microvesicle transport of IL-1β (Qu et al., 2009; Piccioli and Rubartelli, 2013) and HMGB1 (Vande Walle et al., 2011) after inflammasome activation. Differentiation of these mechanisms of release would advance understanding of the underlying mechanisms in DAMP signalling in the brain, with potential applications to drug design. Additionally, P2X7 activation causes the formation of pores in the cell membrane, which allows extracellular molecules to enter the cell, and can lead to pyroptosis (Fink and Cookson, 2006). This process is implicated in the release of IL-1β from microglia (Monif et al., 2016). Examining formation of microvesicles, exosomes, or pores in the cell membrane during the various treatment models seen here may therefore provide a mechanistic understanding of protein release resulting from corticosterone exposure. A live-cell examination of these cell membrane disturbances is now possible through use of phase holographic microscopy, with nm precision in the z-dimension (El-Schich et al., 2017). This technology has been used on macrophages, and is able to determine morphological changes following viral infections (Mendoza Rodriguez et al., 2017). Use of high-resolution 4-dimensional microscopy can also help explain the potential functions of the cellular “blebbing” seen during high concentration ATP treatment in Study 3.

10.5 Future research directions

10.5.1 Given the roles of GR and MR shown here, what does this mean for stress research?

Previous studies have shown that stress can influence the distribution of GR and MR in the hippocampus. For example, early life stress induced by increased maternal separation is associated with lower MR and GR mRNA expression in CA2 and CA1 regions of the hippocampus in marmosets (Arabadzisz et al., 2010). MR antagonism also reduced development of forced swim immobility behaviours resulting from CORT treatment (Wu et al., 2013), demonstrating that MR receptor signalling can influence behaviours in rodent studies. Both GR and MR inhibition attenuated glucocorticoid resistance in monocytes, measured by the lack of glucocorticoid suppression of TNF-α production (Cheng et al., 2016). The authors also showed a reversal of this inverse relationship between glucocorticoid resistance and depressive mood in patients after clinical administration of GR and MR antagonists. Taken together, there is evidence for expression, and some functional differences of GR and MR in stress and depression research, however the direction of these changes is unclear. Given the findings of GR and MR -related innate immune priming seen here, differences in either the ratio of, or absolute expression of GR and MR in immunocompetent cells could therefore cause differential CORT signalling, and impact on immune priming. The behavioural relevance of this work is still unclear, and would require an in vivo investigation in GR and MR signalling relating to behaviours in the context of immune priming. Consideration of MR agonist aldosterone levels in stress-related studies can also build understanding of systemic interactions between these neuroendocrine systems and innate immune functioning.

10.5.2 High throughput experiments to characterise glucocorticoid pre-exposure effects

The findings in vitro have identified the NF-κB pathway as a potential mechanism for CORT induced priming via MR. Due to inconsistent results from downstream protein expression, seen in NLRP3 expression and IL-6 release, some other modulator of transcription or translation of these proteins may be influenced in this CORT pre-exposure model. Thus, higher throughput studies with more in-depth measures such as full RNA sequencing or proteomics would help identify the mechanisms seen here. Given the increased extracellular HMGB1, B Actin and NLRP3 protein seen in high concentration CORT pre-exposure, proteomics analysis on the extracellular environment using mass spectrometry following CORT would help to identify other DAMPs potentially present in the extracellular space. Relatedly, characterising the cell metabolic state may be more informative towards the general cell physiology during the pre-exposure + treatment models. High throughput experiments would increase dataset size, both in the number of dimensions and sample size, thus more machine learning approaches would be applicable to these datasets to gleam additional information about these systems. Moreover, the functional signalling properties of these extracellular changes have yet to be determined. Experiments using conditioned supernatants harvested in the pre-exposure model developed in Studies 2 and 3 as treatments on other cells may thus contain information regarding the functional significance of these changes here.

10.6 Implications of glucocorticoid-induced priming in health and disease

10.6.1 The role of immune dysregulation in the development of stress disorders

The findings in this thesis show the intrinsic and intertwined relationship between innate immunity and glucocorticoids through the stress response in vivo, and immune responses in vitro. In a broader context, the results here may have implications towards understanding individual differences in stress and glucocorticoid responses. For example, the factors that contribute towards the propensity to develop stress disorders could be investigated by investigating behavioural, neuroendocrine and immune factors. Retrospective characterisation studies have established the association between the neuroendocrine and immune system dysregulation in bipolar (Teixeira and Souza, 2015), depression (Lichtblau et al., 2013; Vogelzangs et al., 2014), schizophrenia (Domenici et al., 2010), and PTSD (Breen et al., 2015). Study 1 suggests that baseline differences in immune signalling can change the behavioural and neuroendocrine responses. Breen et al. (2015) showed that individuals that developed PTSD after deployment also had an association with increased interferon and innate immune gene expression in blood leukocytes. Together with the finding that innate immune signalling can fundamentally change neuroendocrine and behavioural responses to stress (Chapter 2), individual differences in immune signalling may account for some of the variability in the development of stress-related disorders. Moreover, previous studies have investigated glucocorticoid resistance as an explanation to increased pro-inflammatory signalling in monocytes isolated from chronically stressed non-professional patient caregivers (Miller et al., 2014). However,

the researchers did not consider MR expression as a mechanism by which these differences could be mediated.

Studies 2 and 3 suggest that the presence of the dysregulation of the immune and neuroendocrine systems and subsequent vulnerability to inflammatory disorders may arise from direct glucocorticoid actions originating from stressful events. Under the assumption that the development of psychiatric disorder or the comorbid inflammatory conditions are related to over-responsiveness to immune challenges, individual differences in glucocorticoid-induced priming response may thus confer differential propensity towards the development of these conditions. However, the long-term consequence of this stress and glucocorticoid-induced priming of immune responses is still not established.

10.6.2 The effect of glucocorticoid-induced microglial priming on neurodegenerative disease states

Microglia play an integral role in the development and persistence of neurodegenerative diseases. Microglia can function adaptively through phagocytosis of Amyloid β plaques in Alzheimer's disease, or maladaptively via persistent pro-inflammatory signalling, resulting in neuronal damage (see review Heneka et al., 2015). In part mirroring the elevated levels of pro-inflammatory signalling present in neurodegenerative diseases, Chapter 4 demonstrated that glucocorticoids can prime the over-secretion of IL-1β and increase in NF-κB translocation. Conversely, increased cell motility towards exogenous ATP, a danger signal, suggests that these cells may be primed towards a quicker resolution of injury. However, the phagocytic function of

glucocorticoid-primed cells is still unknown, and will require testing. Previous studies have performed *ex vivo* and *in vitro* measurements of Amyloid β phagocytosis (Halle et al., 2008; Fricker et al., 2012), and this would be an interesting application of stress and glucocorticoid-primed microglia.

Excitotoxicity, which involves elevated glutamate signalling and increased microglial activity, has been proposed as a common mechanism of neurodegenerative diseases, and psychiatric conditions (Rao et al., 2010; Mehta et al., 2013). Stress and exogenous corticosterone have been shown to increase microglial proliferation in vivo, via NMDA receptor activation in mice (Nair and Bonneau, 2006). In this study, both GR antagonist and NMDA receptor antagonist abolished restraint-stress induced microgliosis, which occurred 4 days after administration of stress. The involvement of NMDA receptor activation, the predicate for excitotoxicity, suggests that excitotoxicity may mediate some stress-related microglial actions.

Glucocorticoid-induced exacerbation of hippocampal neurotoxicity involves neuronal GR activity, which increases CX3CL1 chemokine release and decrease in neuronal growth factor BDNF (Sorrells et al., 2013). In this study, prior exposure to exogenous glucocorticoids also induced increased NF-κB and IL-1β expression following exposure to kainic acid model of excitotoxicity. The dynamic nature of this response was further demonstrated by the decrease in IL-1β and IBA-1 expression due to endogenous glucocorticoids resulting from the injury alone, but when animals were pre-exposed to exogenous glucocorticoids, an over-response in these measures was observed. Thus, pre-exposure to glucocorticoids can cause increased damage in excitotoxic injury

model, and this is related to microglia actions. Interestingly, the increase in IL-1β and NF-κB signalling in the Sorrells et al. (2013) study is consistent with the findings in Chapter 4 and 5, suggesting that the BV2 cell model and primary microglia may have some applications towards excitotoxicity research.

Given that neurodegenerative diseases largely occur later in life, age-related adaptations may have added implications towards microglial function and priming in these disease states. For example, is stress-induced microglia priming an adaptive response which becomes maladaptive due to age? Relatedly, does age predispose dysregulation of microglial function in response to stress, or does lifetime stress cumulatively cause this dysregulation? Lastly, if alterations to this priming response is evident in aged or in the diseased CNS, can it be reset pharmacologically? For example, GR and MR antagonists may be used to 'tune' microglia sensitivity to a desired level, and this may therefore serve as a mechanism for treatment. To answer these multi-factorial questions, carefully controlled experiments with age, stress and priming will be required in neurodegenerative models *in vitro* and *ex vivo*. Development of new assays to fully characterise microglia functions that encapsulate these multi-faceted experimental manipulations will also be necessary. Multi-dimensional arrays and single-cell analysis are therefore most suited towards the analysis of such function.

10.6.3 The role of glucocorticoid-related immune dysregulation in resilience towards of stress disorders

On the other end of the spectrum, stress resilient individuals also exhibit related differences in immune responses, and it is still unclear where stress-induced immune

priming sits on this spectrum. In one study, immunisation with mycobacterium vaccae conferred protection against anxiety and submissive behaviour, increased pro-active behaviour during a chronic social stressor resulted in histological damage to chemically induced colitis (Reber et al., 2016). In this study, colitis was used as the inflammatory challenge, while changing the immune responsiveness through immunisation was sufficient to change behavioural and immune responses to further insult. This resilience towards stress and insult was associated with a markedly decreased IL-6/IL-10 cytokine ratio, and these changes were further reversed when T-cells were depleted following the immunisation. Thus, involvement of the cell-mediated adaptive immune response has been implicated in the development of behavioural stress resilience in rats, but the role of glucocorticoid priming of immune responses has not been investigated in this context.

Conversely, as seen in Study 1, transgenic animals lacking *Myd88* and *Tlr4* did not necessarily exhibit resilience towards acute stress. These transgenic animals displayed increased duration of CORT secretion concurrent with behavioural adaptations characterised by increased or decreased behavioural immobility depending on forced swim or tail suspension stress. Stress resilience therefore likely involves a balance between immune and neuroendocrine activity, but the exact requirements for developing stress-resilience is still unclear. Further studies investigating the optimum levels of immune and neuroendocrine activity are therefore needed.

10.6.4 Does stress-induced priming exacerbate or resolve disease and injury?

Related to stress resilience and vulnerability, the adaptive or maladaptive role of glucocorticoid-induced priming is another important consideration in this research. Conceptually, these glucocorticoid-induced immunosuppressive and immune priming responses appear sensible in the context of the dynamic stress response. The classical immunosuppression during stress, as evidenced by increased immune cell damage (Chapter 8) and decreased pro-inflammatory signalling following immune stimulation (Chapter 4), can confer increased vulnerability towards pathogenic infections (Webster Marketon and Glaser, 2008). Thus, a primed immune response following the resolution of glucocorticoid signalling may be adaptive towards restoration of homeostasis. Indeed, stress induced priming of immune responses has been hypothesised as "parainflammation", which is in-between homeostatic and inflammatory states, which aims to restore homeostasis (Wohleb, 2016). Thus, the immune priming following stress may be a physiological response to immunosuppression during the stressor, and restore homeostasis via accelerating the resolution of insult.

Furthermore, elevations in cytokines, including IL-1β alone are not indicative of increased inflammation, and can lead to adaptive responses in some instances. For example, IL-1β pre-treatment alleviated neurotoxicity in vitro, and this effect was reversed by addition of an IL-1β antibody (Strijbos et al., 1995). Other cytokines such as IL-6 also possess pro- and anti-inflammatory actions, through facilitating the fever response to infections while also triggering the release of IL-1RA and IL-10 anti-inflammatory cytokines (Tilg et al., 1994). Both these actions are contextually adaptive towards quicker resolution of pathogenic infections while constraining over-

responsiveness of immune signalling respectively. Additionally, morphological changes, peripheral immune cell infiltration, and increased phagocytosis do not necessarily cause damage or detrimental outcomes (see review Estes and McAllister, 2014). For example, transgenic knockout mouse models of *Tlr4* (Tahara et al., 2006) and *Myd88* (Michaud and Richard, 2012) present with aggravated amyloid build-up. Furthermore, increasing phagocytic potential of microglia through novel TLR4 agonists can also cause a reduction of Amyloid β peptides (Michaud et al., 2013), suggesting that pro-inflammatory responses in the brain are essential towards normal physiology. Nevertheless, the investigation of the long-term consequence of the stress-related priming is thus required for understanding the adaptive or maladaptive outcomes of this primed state.

Together with the complex adaptations to behavioural and neuroendocrine stress responses to acute stress seen in Study 1, innate immune signalling appears to have an important role in the set points of HPA responses, but the adaptive or maladaptive levels of this relationship is still not established. More study of the complex inter-relations between immune and HPA systems is therefore imperative towards understanding and characterising adaptive and maladaptive phenotypes going forward.

10.7 Conclusion

This thesis contains a collection of findings that expand and unify concepts in the field regarding the intrinsic connections between neuroendocrine and immune signalling in stress research. The first study focused broadly on whether the relationship between TLR4-MyD88 signalling had an impact on baseline non-immunogenic acute stress responses. At the other end of the spectrum, Studies 2 and 3 tested existing ideas about how stress can interact with innate immune function through glucocorticoid signalling *in vitro*. In doing so, both immune priming and immunosuppressive actions of glucocorticoids were found under different conditions, and thus presented some evidence to unify the disparate and paradoxical actions of glucocorticoids on innate immune function through various conditions and measures. These studies have uncovered complex relationships between the innate immune system and the HPA axis, where both systems interact in multiple ways across different cell types. Furthermore, subtle changes to CORT treatments on immunocompetent cells can elicit profound differences ranging from immunosuppression to immune priming, mediated through different receptors. The work included in this thesis thus has implications toward the understanding of how stress interacts with immune system through the HPA axis and innate immune signalling, highlighting some mechanisms that are involved. Cumulatively, these considerations may have further applications to dysregulations in both systems seen in chronic stress disorders, neurodegenerative disease and may have implications towards understanding stress resilience.

References

Aini, Z., Armour, C. L., Phipps, S. and Sukkar, M. B. (2013) 'RAGE and TLRs : Relatives , friends or neighbours ?', *Molecular Immunology*. Elsevier Ltd, 56(4), pp. 739–744. doi: 10.1016/j.molimm.2013.07.008.

Ajmone‐Cat MA, Mancini M, Simone R. 2013. Microglial polarization and plasticity: Evidence from organotypic hippocampal slice cultures. Glia 61:1698–1711.

Anderson D, Burnham K, Thompson W. 2000. Null Hypothesis Testing : Problems , Prevalence , and an Alternative Author (s): David R . Anderson , Kenneth P . Burnham and William L . Thompson Published by : Wiley on behalf of the Wildlife Society. J Wildl Manage 64:912–923.

Belvederi M, Pariante C, Mondelli V, Masotti M, Rita A, Mellacqua Z, Antonioli M, Ghio L, Menchetti M, Zanetidou S, Innamorati M, Amore M. 2014. ScienceDirect REVIEW HPA axis and aging in depression : Systematic review and meta-analysis. Psychoneuroendocrinology 41:46–62.

Breen MS, Maihofer AX, Glatt SJ, Tylee DS, Chandler SD, Tsuang MT, Risbrough VB, Baker DG, O'Connor DT, Nievergelt CM, Woelk CH. 2015. Gene networks specific for innate immunity define post-traumatic stress disorder. Mol Psychiatry 20:1538–1545.

Carpenter T, Grecian SM, Reynolds RM. 2017. Sex differences in early-life programming of the hypothalamic – pituitary – adrenal axis in humans suggest increased vulnerability in females : a systematic review. 8:244–255.

Carreira MB, Cossio R, Britton GB. 2017. Individual and sex differences in high and low

responder phenotypes. Behav Processes 136:20–27.

Chantong B, Kratschmar D V, Nashev LG, Balazs Z, Odermatt A. 2012. Mineralocorticoid and glucocorticoid receptors differentially regulate NF-kappaB activity and pro-inflammatory cytokine production in murine BV-2 microglial cells. J Neuroinflammation 9:1.

Chrousos G, Pavlaki AN, Magiakou MA. 2000. Glucocorticoid Therapy and Adrenal Suppression. Endotext:1–27.

Crumeyrolle-Arias M, Jaglin M, Bruneau A, Vancassel S, Cardona A, Daugé V, Naudon L, Rabot S. 2014. Absence of the gut microbiota enhances anxiety-like behavior and neuroendocrine response to acute stress in rats. Psychoneuroendocrinology 42:207–217.

Das A, Chai JC, Kim SH, Lee YS, Park KS, Jung KH, Chai YG. 2015. Transcriptome sequencing of microglial cells stimulated with TLR3 and TLR4 ligands. BMC Genomics 16:517.

Das A, Kim SH, Arifuzzaman S, Yoon T, Chai JC, Lee YS, Park KS, Jung KH, Chai YG. 2016. Transcriptome sequencing reveals that LPS-triggered transcriptional responses in established microglia BV2 cell lines are poorly representative of primary microglia. J Neuroinflammation:1–18.

Domenici E, Willé DR, Tozzi F, Prokopenko I, Miller S, McKeown A, Brittain C, Rujescu D, Giegling I, Turck CW, Holsboer F, Bullmore ET, Middleton L, Merlo-Pich E, Alexander RC, Muglia P. 2010. Plasma protein biomarkers for depression and schizophrenia by multi analyte profiling of case-control collections. PLoS One

5:e9166.

Edwan JH, Goldbach-Mansky R, Colbert RA. 2015. Identification of interleukin-1β-producing monocytes that are susceptible to pyronecrotic cell death in patients with neonatal-onset multisystem inflammatory disease. Arthritis Rheumatol 67:3286–3297.

El-Schich Z, Kamlund S, Janicke B, Alm K, Wingren AG. 2017. Holography: The Usefulness of Digital Holographic Microscopy for Clinical Diagnostics. In: Holographic Materials and Optical Systems. InTech.

Erny D, Hrabě de Angelis AL, Jaitin D, Wieghofer P, Staszewski O, David E, Keren-Shaul H, Mahlakoiv T, Jakobshagen K, Buch T, Schwierzeck V, Utermöhlen O, Chun E, Garrett WS, McCoy KD, Diefenbach A, Staeheli P, Stecher B, Amit I, Prinz M. 2015. Host microbiota constantly control maturation and function of microglia in the CNS. Nat Neurosci 18:965–977.

Fink SL, Cookson BT. 2006. Caspase-1-dependent pore formation during pyroptosis leads to osmotic lysis of infected host macrophages. Cell Microbiol 8:1812–1825.

Frank MG, Thompson BM, Watkins LR, Maier SF. 2012. Glucocorticoids mediate stress-induced priming of microglial pro-inflammatory responses. Brain Behav Immun 26:337–345.

Frank MG, Weber MD, Watkins LR, Maier SF. 2015. Stress sounds the alarmin: The role of the danger-associated molecular pattern HMGB1 in stress-induced neuroinflammatory priming. Brain Behav Immun:1–7.

Fricker M, Oliva-Martín MJ, Brown GC. 2012. Primary phagocytosis of viable neurons

by microglia activated with LPS or Aβ is dependent on calreticulin/LRP phagocytic signalling. J Neuroinflammation 9:196.

Friedman J, Hastie T, Tibshirani R. 2010. Regularization Paths for Generalized Linear Models via Coordinate Descent. J Stat Softw 33:1–20.

Füchsl AM, Neumann ID, Reber SO. 2014. Stress resilience: a low-anxiety genotype protects male mice from the consequences of chronic psychosocial stress. Endocrinology 155:117–26.

Galatro TF, Holtman IR, Lerario AM, Vainchtein ID, Brouwer N, Sola PR, Veras MM, Pereira TF, Leite REP, Möller T, Wes PD, Sogayar MC, Laman JD, Dunnen W Den, Pasqualucci CA, Oba-shinjo SM, Boddeke EWGM, Marie SKN, Eggen BJL. 2017. Transcriptomic analysis of purified human cortical microglia reveals age-associated changes. Nat Publ Gr.

Gale RP, Hochhaus A, M-J Z. 2016. What is the (p-) value of the P -value? Leukemia 30:1965–1967.

Gerber M, Ludyga S, Mücke M, Colledge F, Brand S. 2017. Low vigorous physical activity is associated with increased adrenocortical reactivity to psychosocial stress in students with high stress perceptions. Psychoneuroendocrinology 80:104–113.

Gerlach J, Donkels C, Münzner G, Haas CA. 2016. Persistent Gliosis Interferes with Neurogenesis in Organotypic Hippocampal Slice Cultures. 10:1–17.

Gershman SJ, Hartley CA. 2015. Individual differences in learning predict the return of fear. Learn Behav 43:243–250.

Halle A, Hornung V, Petzold GC, Stewart CR, Monks BG, Reinheckel T, Fitzgerald KA, Latz E, Moore KJ, Golenbock DT. 2008. The NALP3 inflammasome is involved in the innate immune response to amyloid-beta. Nat Immunol 9:857–865.

Harris a P, Holmes MC, de Kloet ER, Chapman KE, Seckl JR. 2013. Mineralocorticoid and glucocorticoid receptor balance in control of HPA axis and behaviour. Psychoneuroendocrinology 38:648–58.

Hastie T, Tibshirani R, Friedman J. 2009. The Elements of Statistical Learning. New York, NY: Springer New York.

Heneka MT, Carson MJ, Khoury J El, Landreth GE, Brosseron F, Feinstein DL, Jacobs AH, Wyss-Coray T, Vitorica J, Ransohoff RM, Herrup K, Frautschy SA, Finsen B, Brown GC, Verkhratsky A, Yamanaka K, Koistinaho J, Latz E, Halle A, Petzold GC, Town T, Morgan D, Shinohara ML, Perry VH, Holmes C, Bazan NG, Brooks DJ, Hunot S, Joseph B, Deigendesch N, Garaschuk O, Boddeke E, Dinarello CA, Breitner JC, Cole GM, Golenbock DT, Kummer MP. 2015. Neuroinflammation in Alzheimer's disease. Lancet Neurol 14:388–405.

Hetzel A, Rosenkranz JA. 2014. Distinct effects of repeated restraint stress on basolateral amygdala neuronal membrane properties in resilient adolescent and adult rats. Neuropsychopharmacology 39:2114–30.

Holland JM, Schatzberg AF, Hara RO, Marquett RM, Gallagher-thompson D. 2013. Pretreatment cortisol levels predict posttreatment outcomes among older adults with depression in cognitive behavioral therapy. Psychiatry Res 210:444–450.

Huang Y, Henry CJ, Dantzer R, Johnson RW, Godbout JP. 2008. Exaggerated sickness

behavior and brain proinflammatory cytokine expression in aged mice in response to intracerebroventricular lipopolysaccharide. Neurobiol Aging 29:1744–1753.

Kemeny ME, Schedlowski M. 2007. Understanding the interaction between psychosocial stress and immune-related diseases: A stepwise progression. Brain Behav Immun 21:1009–1018.

Keshwani MM, Kanter JR, Ma Y, Wilderman A, Darshi M, Insel PA, Taylor SS. 2015. Mechanisms of cyclic AMP/protein kinase A- and glucocorticoid-mediated apoptosis using S49 lymphoma cells as a model system. Proc Natl Acad Sci 112:12681–12686.

Leek JT, Peng RD. 2015. Statistics: P values are just the tip of the iceberg. Nature 520:612–612.

Lichtblau N, Schmidt FM, Schumann R, Kirkby KC, Himmerich H. 2013. Cytokines as biomarkers in depressive disorder: current standing and prospects. Int Rev Psychiatry 25:592–603.

Liu A, Fang H, Dirsch O, Jin H, Dahmen U. 2012. Oxidation of HMGB1 Causes Attenuation of Its Pro- Inflammatory Activity and Occurs during Liver Ischemia and Reperfusion. 7.

Lonsdorf TB, Menz MM, Andreatta M, Fullana MA, Golkar A, Haaker J, Heitland I, Hermann A, Kuhn M, Kruse O, Meir S, Meulders A, Nees F, Pittig A, Richter J, Römer S, Shiban Y, Schmitz A, Straube B, Vervliet B, Wendt J, Baas JMP, Merz CJ. 2017. Neuroscience and Biobehavioral Reviews Don ' t fear " fear conditioning ": Methodological considerations for the design and analysis of studies on human

fear acquisition , extinction , and return of fear. Neurosci Biobehav Rev 77:247–285.

Lu NZ, Wardell SE, Burnstein KL, Defranco D, Fuller PJ, Giguere V. 2006. The Pharmacology and Classification of the Nuclear Receptor Superfamily: Glucocorticoid, Mineralocorticoid, Progesterone, and Androgen Receptors. J Biol Chem 58:782–797.

Mannic T, Satta N, Pagano S, Python M, Virzi J, Montecucco F, Frias MA, James RW, Maturana AD, Rossier MF, Vuilleumier N. 2015. CD14 as a mediator of the mineralocorticoid receptor-dependent anti-apolipoprotein a-1 IgG chronotropic effect on cardiomyocytes. Endocrinology 156:4707–4719.

McLaughlin KA, Sheridan MA, Gold AL, Duys A, Lambert HK, Peverill M, Heleniak C, Shechner T, Wojcieszak Z, Pine DS. 2016. Maltreatment Exposure, Brain Structure, and Fear Conditioning in Children and Adolescents. Neuropsychopharmacology 41:1956–1964.

Mehta A, Prabhakar M, Kumar P, Deshmukh R, Sharma PL. 2013. Excitotoxicity: Bridge to various triggers in neurodegenerative disorders. Eur J Pharmacol 698:6–18.

Mendoza Rodriguez E, Organista-Castelblanco C, Camacho M, Monroy Ramírez F. 2017. Digital holographic microscopy as a technique to monitor macrophages infected by leishmania. In: Ferraro P, Grilli S, Ritsch-Marte M, Hitzenberger CK, editors. Vol. 10333. . p 103330P.

Miller GE, Murphy MLM, Cashman R, Ma R, Ma J, Arevalo JMG, Kobor MS, Cole SW. 2014. Greater inflammatory activity and blunted glucocorticoid signaling in

monocytes of chronically stressed caregivers. Brain Behav Immun 41:191–199.

Monif M, Reid CA, Powell KL, Drummond KJ, Brien TJO, Williams DA. 2016. Interleukin-1 β has trophic effects in microglia and its release is mediated by P2X7R pore. J Neuroinflammation:1–15.

Piccioli P, Rubartelli A. 2013. The secretion of IL-1β and options for release. Semin Immunol 25:425–429.

Qu Y, Ramachandra L, Mohr S, Franchi L, Harding C V, Nunez G, Dubyak GR. 2009. P2X7 receptor-stimulated secretion of MHC class II-containing exosomes requires the ASC/NLRP3 inflammasome but is independent of caspase-1. J Immunol 182:5052–62.

Rao JS, Harry GJ, Rapoport SI, Kim HW. 2010. Increased excitotoxicity and neuroinflammatory markers in postmortem frontal cortex from bipolar disorder patients. Mol Psychiatry 15:384–392.

Rea K, Dinan TG, Cryan JF. 2016. The microbiome: A key regulator of stress and neuroinflammation. Neurobiol Stress 4:23–33.

Reber SO, Siebler PH, Donner NC, Morton JT, Smith DG, Kopelman JM, Lowe KR, Wheeler KJ, Fox JH, Hassell JE, Greenwood BN, Jansch C, Lechner A, Schmidt D, Uschold-Schmidt N, Füchsl AM, Langgartner D, Walker FR, Hale MW, Lopez Perez G, Van Treuren W, González A, Halweg-Edwards AL, Fleshner M, Raison CL, Rook GA, Peddada SD, Knight R, Lowry CA. 2016. Immunization with a heat-killed preparation of the environmental bacterium Mycobacterium vaccae promotes stress resilience in mice. Proc Natl Acad Sci 113:E3130–E3139.

Reichardt F, Chassaing B, Nezami BG, Li G, Tabatabavakili S, Mwangi S, Uppal K, Liang B, Vijay-Kumar M, Jones D, Gewirtz AT, Srinivasan S. 2016. Western diet induces colonic nitrergic myenteric neuropathy and dysmotility in mice via saturated fatty acid- and LPS-induced TLR4 signaling. J Physiol 5:1831–1846.

Rubin RT, Miller TH, Rhodes ME, Czambel RK. 2006. Adrenal cortical responses to low- and high-dose ACTH(1-24) administration in major depressives vs. matched controls. Psychiatry Res 143:43–50.

Santarelli S, Zimmermann C, Kalideris G, Lesuis SL, Arloth J, Uribe A, Dournes C, Balsevich G, Hartmann J, Masana M, Binder EB, Spengler D, Schmidt M V. 2017. An adverse early life environment can enhance stress resilience in adulthood. Psychoneuroendocrinology 78:213–221.

Sapolsky RM, Romero LM, Munck AU. 2000. How Do Glucocorticoids Influence Stress Responses ? Integrating Permissive, Suppressive, Stimulatory and Preparative Actions *. Endocr Rev 21:55–89.

Sawicki CM, McKim DB, Wohleb ES, Jarrett BL, Reader BF, Norden DM, Godbout JP, Sheridan JF. 2015. Social defeat promotes a reactive endothelium in a brain region-dependent manner with increased expression of key adhesion molecules, selectins and chemokines associated with the recruitment of myeloid cells to the brain. Neuroscience 302:151–164.

Sobesky JL, D'Angelo HM, Weber MD, Anderson ND, Frank MG, Watkins LR, Maier SF, Barrientos RM. 2016. Glucocorticoids Mediate Short-Term High-Fat Diet Induction of Neuroinflammatory Priming, the NLRP3 Inflammasome, and the Danger Signal HMGB1. eNeuro 3:1–17.

Sominsky L, Fuller E a., Bondarenko E, Ong LK, Averell L, Nalivaiko E, Dunkley PR, Dickson PW, Hodgson DM. 2013. Functional Programming of the Autonomic Nervous System by Early Life Immune Exposure: Implications for Anxiety. PLoS One 8:e57700.

Sorrells SF, Caso JR, Munhoz CD, Hu CK, Tran K V, Miguel ZD, Chien BY, Sapolsky RM. 2013. Glucocorticoid signaling in myeloid cells worsens acute CNS injury and inflammation. J Neurosci 33:7877–89.

Steru L, Chermat R, Thierry B, Simon P. 1985. The tail suspension test: A new method for screening antidepressants in mice. Psychopharmacology (Berl) 85:367–370.

Teixeira A, Souza R. 2015. Increased plasma levels of soluble TNF receptors 1 and 2 in bipolar depression and impact of lithium treatment. Hum …:52–56.

Tilg H, Trehu E, Atkins M, Dinarello C, Mier J. 1994. Interleukin-6 (IL-6) as an anti-inflammatory cytokine: induction of circulating IL-1 receptor antagonist and soluble tumor necrosis factor receptor p55. Blood 83:113–18.

Venereau E, Casalgrandi M, Schiraldi M, Antoine DJ, Cattaneo a., De Marchis F, Liu J, Antonelli a., Preti a., Raeli L, Shams SS, Yang H, Varani L, Andersson U, Tracey KJ, Bachi a., Uguccioni M, Bianchi ME. 2012. Mutually exclusive redox forms of HMGB1 promote cell recruitment or proinflammatory cytokine release. J Gen Physiol 140:i6–i6.

Vogelzangs N, Beekman AT, van Reedt Dortland AK, Schoevers R a, Giltay EJ, de Jonge P, Penninx BW. 2014. Inflammatory and metabolic dysregulation and the 2-year course of depressive disorders in antidepressant users.

Neuropsychopharmacology 39:1624–34.

Waldmann P, Mészáros G, Gredler B, Fuerst C, Sölkner J. 2013. Evaluation of the lasso and the elastic net in genome-wide association studies. 4:1–11.

Walker AK, Nakamura T, Byrne RJ, Naicker S, Tynan RJ, Hunter M, Hodgson DM. 2009. Neonatal lipopolysaccharide and adult stress exposure predisposes rats to anxiety-like behaviour and blunted corticosterone responses: Implications for the double-hit hypothesis. Psychoneuroendocrinology 34:1515–1525.

Vande Walle L, Kanneganti T-D, Lamkanfi M. 2011. HMGB1 release by inflammasomes. Virulence 2:162–165.

Weber MD, Frank MG, Tracey KJ, Watkins LR, Maier SF. 2015. Stress Induces the Danger-Associated Molecular Pattern HMGB-1 in the Hippocampus of Male Sprague Dawley Rats: A Priming Stimulus of Microglia and the NLRP3 Inflammasome. J Neurosci 35:316–24.

Webster Marketon JI, Glaser R. 2008. Stress hormones and immune function. Cell Immunol 252:16–26.

Wegner A, Benson S, Rebernik L, Schedlowski M, Spreitzer I, Ja M, Elsenbruch S, Engler H. 2017. Sex differences in the pro-inflammatory cytokine response to endotoxin unfold in vivo but not ex vivo in healthy humans.

Wellman LL, Fitzpatrick ME, Hallum OY, Sutton AM, Williams BL, Sanford LD. Individual Differences in Animal Stress Models : Considering Resilience , Vulnerability , and the Amygdala in Mediating the Effects of Stress and Conditioned Fear on Sleep. :1293–1303.

Willingham SB, Allen IC, Bergstralh DT, Brickey WJ, Huang MT-H, Taxman DJ, Duncan JA, Ting JP-Y. 2009. NLRP3 (NALP3, Cryopyrin) facilitates in vivo caspase-1 activation, necrosis, and HMGB1 release via inflammasome-dependent and -independent pathways. J Immunol 183:2008–15.

Wu TT, Chen YF, Hastie T, Sobel E, Lange K. 2009. Genome-wide association analysis by lasso penalized logistic regression. 25:714–721.

Yang, H., Wang, H., Ju, Z., Ragab, A. a, Lundbäck, P., Long, W., Valdes-ferrer, S. I., He, M., Pribis, J. P., Li, J., Lu, B., Gero, D., Szabo, C., Antoine, D. J., Harris, H. E., Golenbock, D. T., Meng, J., Roth, J., Chavan, S. S., Andersson, U., Billiar, T. R., Tracey, K. J. and Al-abed, Y. (2015) 'MD-2 is required for disulfide HMGB1 – dependent TLR4 signaling', 212(1), pp. 0–9. doi: 10.1084/jem.20141318.

Yeager MP, Pioli PA, Collins J, Barr F, Metzler S, Sites BD, Guyre PM. 2016. Glucocorticoids enhance the in vivo migratory response of human. Brain Behav Immun 54:86–94.

Yeager MP, Pioli PA, Guyre PM. 2011. Cortisol Exerts Bi-Phasic Regulation of Inflammation in Humans. Dose-Response 9:332–347.

Stress/ endocrine stimulation	Measure	TLR4-MyD88 manipulation	Result
Forced swim stress	Behavioural immobility	Tlr4 -/- mice	No difference from control
	Behavioural immobility	Myd88 -/- mice	Increased from control
	Circulating corticosterone	Tlr4 -/- mice	No difference from control
	Circulating corticosterone	Myd88 -/- mice	Remains elevated at 45min, while other strains have returned to baseline
	Hypothalamic CBG expression	Tlr4 -/- mice	Elevated compared to MyD88-/- and Balb/c mice
	Hypothalamic CBG expression	Myd88 -/- mice	No different to Balb/c mice
	Hypothalamic GR expression	Tlr4 -/- mice	No difference from control
	Hypothalamic GR expression	Myd88 -/- mice	No difference from control
	Behavioural immobility	(+)- Naltrexone acute administration	No different to saline control
	Behavioural immobility	IL-1RA acute administration	No different to saline control
	Circulating corticosterone	(+)- Naltrexone acute administration	No different to saline control
	Circulating corticosterone	IL-1RA acute administration	No different to saline control
Tail suspension stress	Behavioural immobility	Tlr4 -/- mice	Reduced compared to Balb/c
	Behavioural immobility	Myd88 -/- mice	Reduced compared to Balb/c
	Circulating corticosterone	Tlr4 -/- mice	Remains elevated at 51 min, while other strains have returned to baseline
	Circulating corticosterone	Myd88 -/- mice	Reduction from peak at 36 min, while other strains are still elevated

	Behavioural immobility	(+)- Naltrexone acute administration	No different to saline control
	Behavioural immobility	IL-1RA acute administration	No different to saline control
	Circulating corticosterone	(+)- Naltrexone acute administration	No different to saline control
	Circulating corticosterone	IL-1RA acute administration	No different to saline control
ACTH stimulation of adrenals	Corticosterone secretion	Tlr4 -/- mice	Elevated (compared to Balb/c) at 6hr 100ng/ml
	Corticosterone secretion	Myd88 -/- mice	Elevated (compared to Balb/c) at 6hr 100ng/ml

Table 1. Summary of main results obtained in study 1 (Chapter 2)

Measure	Pre-treatment model	Pre-treatment concentration	GR / MR mediated	CORT vs Vehicle result
LPS-induced IL-1β release	Pre-exposure	50 nM, 100 nM, 150 nM	MR at 50nM	Primed
	Pre-exposure	300 nM, 500 nM, 1 uM	GR at 500nM	Suppressed
	Co-treatment	50 nM to 1 uM	GR at 50nM	Suppressed
TNF-α-induced IL-1β release	Pre-exposure	50 nM	NA	Primed
	Pre-exposure	500 nM	NA	Primed
NF-κB translocation	Pre-exposure	50nM	NA	Primed
	Pre-exposure	500 nM	NA	No difference from vehicle pre-exposure
Gene transcription	Pre-exposure	50nM	NA	Different gene expression profile from vehicle pre-exposure
LPS-induced IL-6 release	Pre-exposure	50 nM to 1 uM	GR	Suppressed
ATP-induced IL-1β release	Pre-exposure	50 nM	NA	Suppressed
LPS-induced TNF-α release (Adult primary microglia)	**Pre-exposure**	**50 nM**	**NA**	**Primed**
LPS-induced NF-κB translocation	**Pre-exposure**	**50 nM**	**NA**	**Primed**

Table 2. Summary of main results obtained in Study 2 (Chapter 4-7)

Measure	Time point	Pre-treatment conc.	GR / MR signalling	CORT vs Vehicle	DEX vs Vehicle
LDH cytotoxicity	After pre-exposure	50 nM	NA	No difference from control	Increased
	After pre-exposure	500 nM	GR	Increased	Increased
	After LPS treatment	500 nM	Neither	Increased	Increased
	After LPS+ ATP treatment	50 nM	NA	Increased at 2.5 mM ATP	NA
	After LPS+ ATP treatment	500 nM	NA	No different from control	NA
Attached cell viability	After pre-exposure	50 nM	NA	Decreased	Decreased
	After pre-exposure	500 nM	GR	Decreased	Decreased compared to control and CORT
	After LPS treatment	500 nM	GR	No difference from control	Decreased compared to control and CORT
	After LPS+ ATP treatment	50 nM	NA	No difference from control	
	After LPS+ ATP treatment	500 nM	NA	Suppressed at 2.5 mM ATP	
Detached cell viability	After pre-exposure	50 nM	NA	No difference from control	No difference from control
	After pre-exposure	500 nM	GR	No difference from control	Increased
	After LPS treatment	500 nM	MR	No difference from control	No difference from control
	After LPS+ ATP treatment	50 nM	NA	No difference from control	NA

	After LPS+ ATP treatment	500 nM	NA	Suppressed at 2.5 mM ATP	NA
Extracellular HMGB1 expression	After pre-exposure	500 nM	GR	Increased	Increased
	After LPS treatment	500 nM	Neither	Increased	No difference from control
	After LPS+ ATP treatment	50 nM	NA	No difference from control	NA
	After LPS+ ATP treatment	500 nM	NA	No difference from control	NA
Extracellular B Actin expression	After pre-exposure	500 nM	GR	Increased	Increased
	After LPS treatment	500 nM	Neither	Increased	No difference from control
	After LPS+ ATP treatment	50 nM	NA	Increased at 2.5 mM ATP	NA
	After LPS+ ATP treatment	500 nM	NA	No difference from control	NA
Extracellular NLRP3 expression	After LPS treatment	500 nM	Neither	Increased	No difference from control
	After LPS+ ATP treatment	50 nM	NA	Increased AT 2.5 mM ATP	NA
	After LPS+ ATP treatment	500 nM	NA	Increased at 1 mM and 2.5 mM ATP	NA
Extracellular ASC expression	After LPS treatment	500 nM	Neither	No difference from control	No difference

					from control
	After LPS+ ATP treatment	50 nM	NA	No difference from control	NA
	After LPS+ ATP treatment	500 nM	NA	Incrased at 1mM and 0mM ATP	NA
ATP - induced cell motility		50 nM	Neither	Increased from control	NA
		500 nM		No difference from control	NA
Rate of ATP-induced Cellular 'blebbing'		50 nM	NA	Increased from control	NA
		500 nM	NA	No difference from control	NA
Localization of HMGB1 expression (primary microglia)	**After pre-exposure**	**500 nM**	**NA**	**Increased diffusion of cytoplasmic HMGB1 expression**	**NA**
Attached cell viability (primary microglia)	**After pre-exposure**	**500 nM**	**NA**	**No difference from control**	**NA**

Table 3. Summary of main results obtained in study 3 (chapter 7-8)

Appendices:

- **Appendix A:** Methods for *ex vivo* microglia extraction and stimulation
- **Appendix B:** Method development single-cell analysis of pro-inflammatory responses
- **Appendix C:** Source code – Image analysis: Translocator (versions 0.0.1 and 0.0.2)
- **Appendix D:** Source code – Pubscraper: Pubmed scraping and natural language processing in Python
- **Appendix E:** Statistical methods using R

Appendix A: Methods for *ex vivo* microglia extraction and stimulation

Due to the predominant use of *in vitro* cell lines as immunocompetent models in this thesis, there was a pertinent need to verify the results obtained in a primary cell model. Microglia are the prime focus in this thesis, and therefore primary cell models of microglia were explored. Two main models of microglia were assessed during the course of experimentation: 1) Dissociated primary mixed culture, and 2) primary microglia isolation using Percoll gradients.
As stated in Chapter 6, adult primary microglia were most representative of existing stress research. Thus, adult Balb/c mice were used to obtain microglia from the brains if these animals. This section explores the two models of primary microglia used during the course of this thesis.

Method 1: CORT + LPS treatment induced NF-kB translocation in dissociated primary Balb/c organotypic or mixed neural culture

Protocol: Short-term organotypic culture of brain slices for LPS-induced NF-κB Immunohistochemistry imaging
Prepare buffers:
ACSF
CORT 50nM /vehicle diluted in ACSF (warm to 37 degrees)
PBS pH7.2 + 0.5% BSA (on ice)

Procedure:

1) Knock out animal with isofluorine prior to cervical dislocation
2) Working quickly, extract the brain using sterile tools
3) Rinse brain once with Ice cold ACSF, and immediately slice into 2mm sections using a scalpel and brain mould
4) Obtain about 8 slices between the prefrontal cortex and cerebellum

Brain 1: 24 h pre-exposure to 50 nM CORT or vehicle prior to LPS treatment (30 min or 2 h)

1) Transfer each slide into wells of a 12-well plate containing 2ml ACSF containing with either CORT (50 nM) or volume matched vehicle (24 h pre-exposure samples only)
2) Incubate in 5% CO_2, 37 °C for 24 h pre-exposure
3) After pre-exposure step, wash each slice briefly using fresh ACSF
4) 1 slice from each condition was immediately fixed using 4% at this step
5) For the remining 6 slices, replace media with ACSF containing either vehicle or 1 µg/ml LPS. Incubate for either 2 h or 3 min

Brain 2: No pre-exposure, naïve, LPS or vehicle treatment

1) Immediately after obtaining brain slices, fix 2 brain slices using 4% PFA
2) Treat remaining 4 slices with either vehicle or 1 µg/ml LPS diluted in ACSF. Incubate for 2 h or 30 min prior to fixation

Fixing, mounting and slicing:

1) Following all drug treatments, post-fix each sample by placing slices into individual 5 ml tubes containing 3 ml 4% PFA solution
2) After 24 h of fixative, wash slices 3 times in PBS
3) Dehydrate slices by taking them through a sucrose gradient (10% - 20% - 30%).
4) After the tissues have sunk in 30% sucrose (after 2 days of increments in sucrose %), submerge tissues in OCT using cryostat moulds
5) Leave each sample to equilibrate a room temperature before freezing by partially submerging each mould in Isopropyl cooled with liquid N_2
6) Store tissues at -80 °C overnight prior to sectioning
7) Section tissues on a cryostat (set between -14 °C and -15 °C) into 10 µm slices. A total of 3 slides containing triplicate sections obtained for each condition (9 per condition)

Staining protocol:

1) Air dry slides at room temperature for 1 h
2) Wax added to perimeter of each sample using a pap pen. Apply 1x 10 min PBS wash
3) Block samples for 2 h with 10% NDS, 0.01% Triton-x in PBS at room temperature
4) Apply primaries for 48 h at 4 °C in a humidifying chamber. (Antibodies: Rb anti NF-kB 1:100; Gt anti IBA-1 1:200 diluted in 1% NDS, 0.01% Triton-x + PBS)
5) Wash samples 3x 10min using pBS
6) Apply secondaries for 2 h at room temperature. Keep in the dark in a humidifying chamber. (Antibodies: D anti Rabbit 568nm 1:1000, D anti Goat 488nm 1:1000, DAPI 1:10,000 diluted in PBS) ‘
7) Wash 3x PBS
8) Apply coverslips. Use PST aqueous mounting solution and leave to air dry in the dark for a few hours before storage

Confocal imaging results

Laser Settings (JJ_DAPI_488_561):
405 nm– gain 794 -0.6% offset Line averaging 6 (Blue channel, DAPI)
488 nm– gain 900 -0.6% offset Line averaging 8 (Green channel, IBA-1)
561 nm -- gain 842 -0.7% offset Line averaging 8-16 (Red channel, NF-kB)
Image-capture settings:
Scan frequency 400Hz
Zoom 1x
Resolution 1024 x 1024
All stacks: full 10um captured in 6 slices (avg 8 min per stack capture)

From the imaging, a large amount of tissue degradation is evident after 24 h treatment (Figure 1 and 2) when compared to naïve brains (Figure 3). Interestingly, there appears to be increased IBA-1 staining after LPS, suggesting that microglia remain responsive towards LPS. NF-κB staining was no different from background, thus suggesting that the staining protocol may be unsuitable for NF-κB translocation analysis.

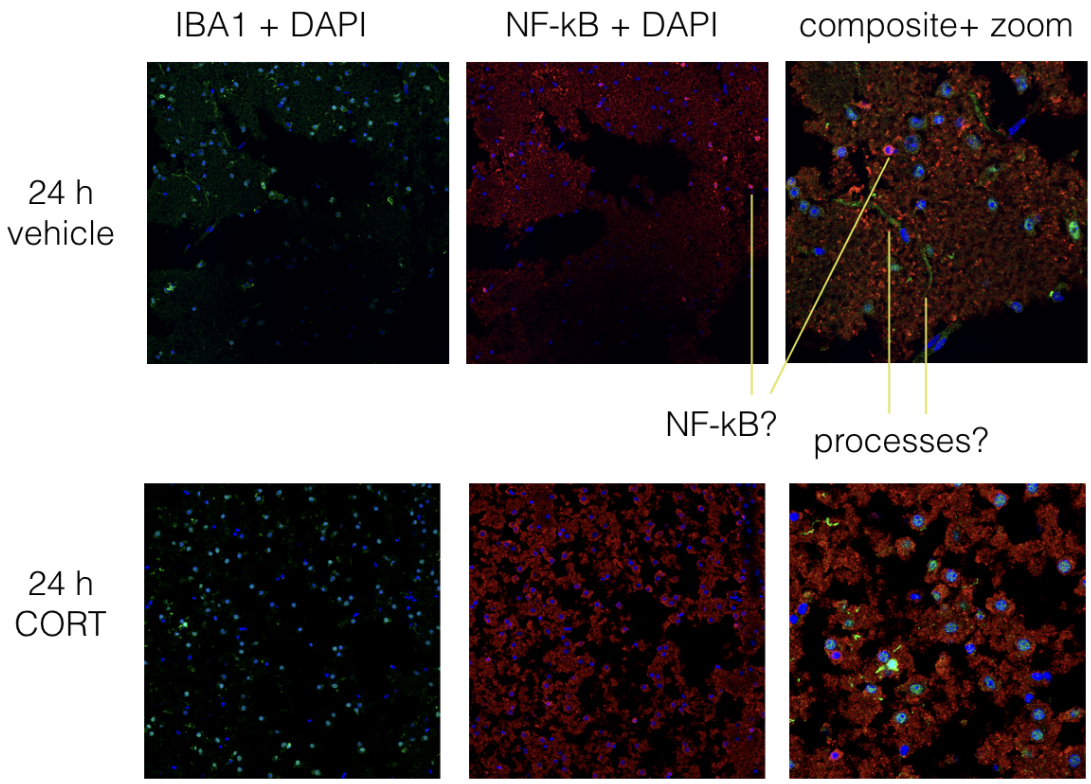

Figure 1: Confocal images IBA-1 and NF-kB immunohistochemistry in brain slices after 24 h exposure to either vehicle or CORT (50 nM)

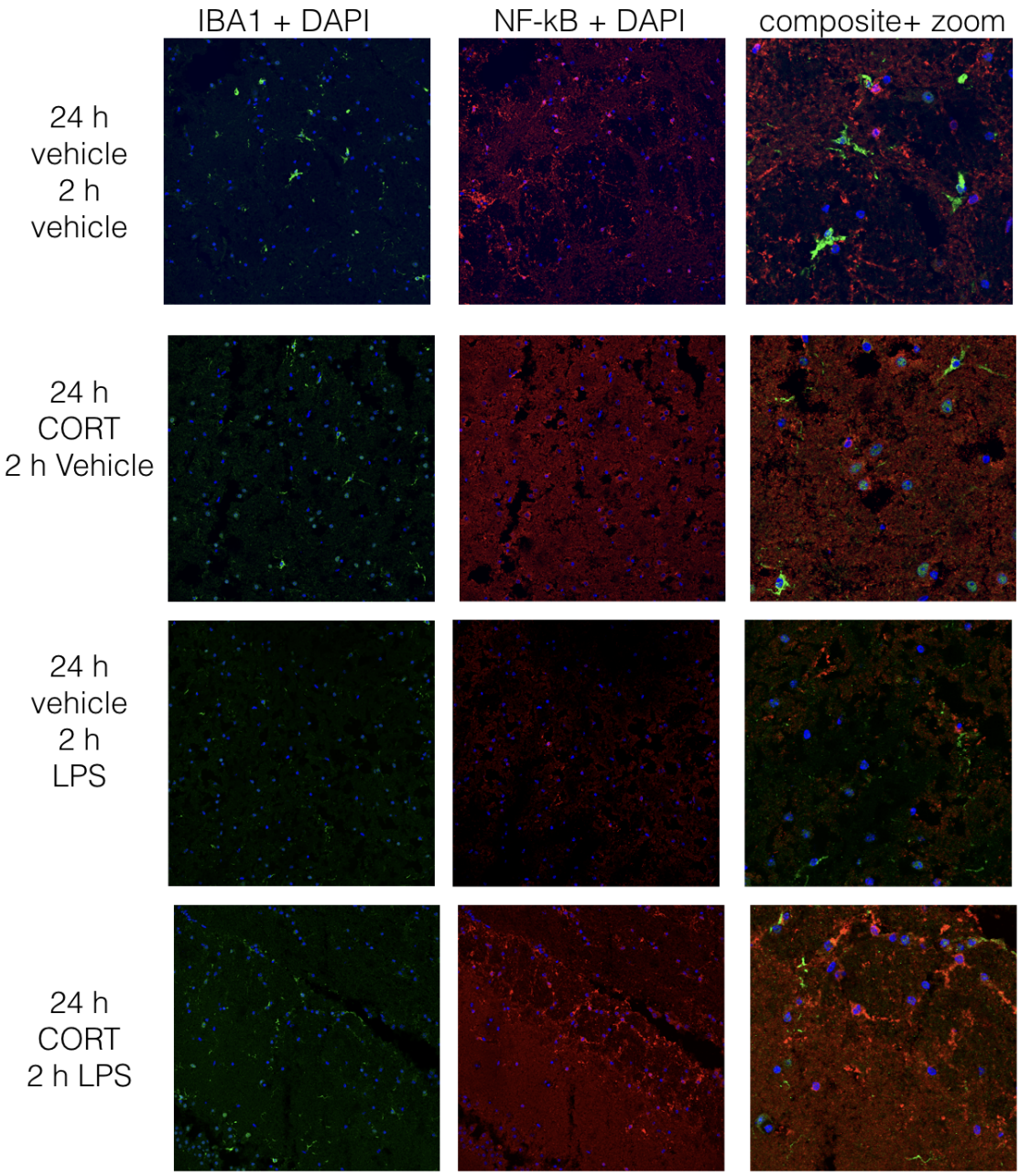

Figure 2. IBA-1 and NF-κB immunohistochemistry after 24 h pre-exposure + 2 h LPS or vehicle treatment.

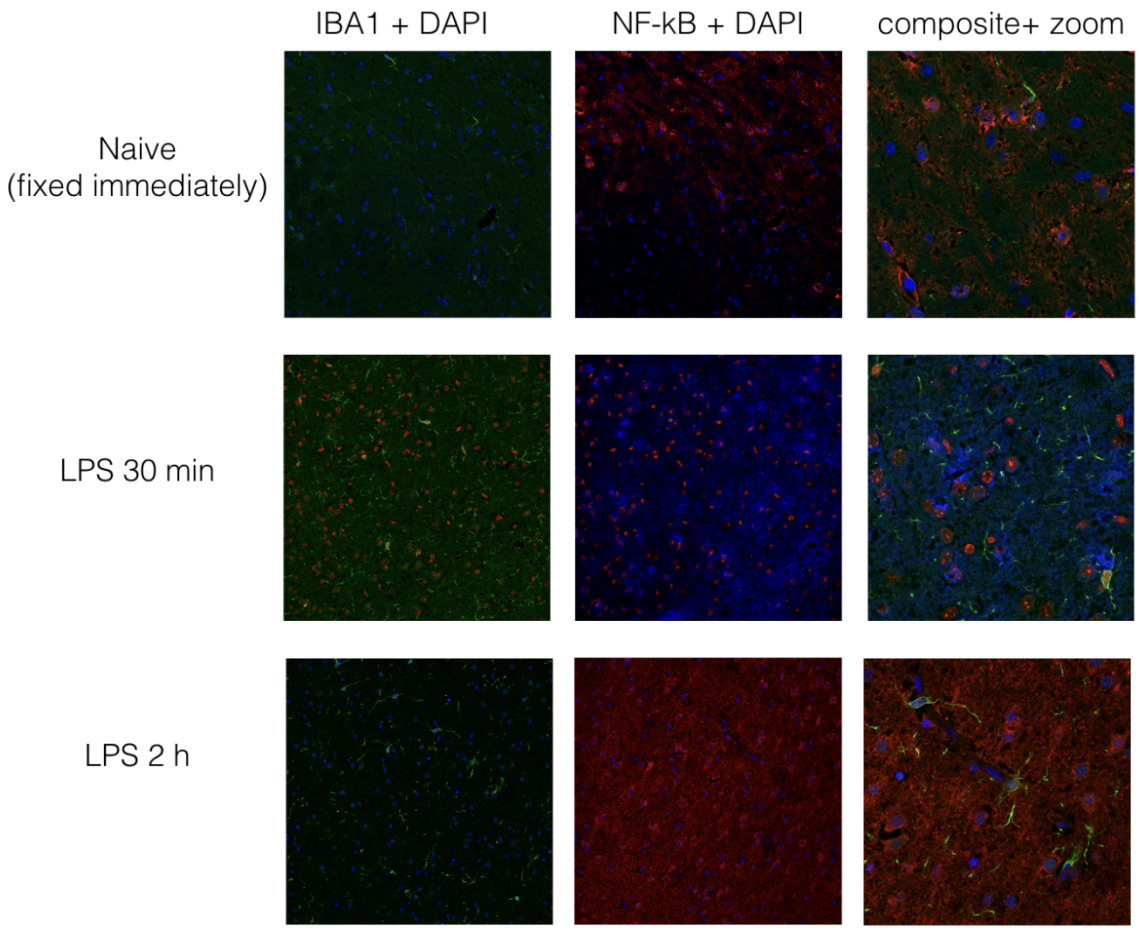

Figure 3. IBA-1 and NF-κB immunohistochemistry in naïve brain, or after 30 min or 2 h treatment with either LPS or vehicle.

Method 2: Adult primary microglia isolation using Percoll gradients
Protocol:
Solutions:
Isotonic Percoll solutions (70%, 50%, 35% and 0%) diluted in PBS pH 7.4 – prepare 3.5 ml of each density per brain
Miltenyi neural dissociation kit (P): prepare enzyme mixes A and B according to manufacturer's recommendation
PBS (Ice cold)
HBSS (Without Ca^{2+} and Mg^{2+})
Procedure:

1) Cull 5-6 week old mice via pentobarbitone overdose (60 mg/ml)
2) Perform cardiac perfusion with ice-cold PBS
3) Extract brain aseptically, and place each brain in HBSS on ice- total of 3 brains can be processed during each batch
4) Hemisect brain and remove meninges using fine forceps under a dissecting microscope
5) Chop tissue with a sterile blade to 1 mm^3 approximate size
6) Transfer tissue to a C-tube containing enzyme mix A
7) Add enzyme mix B to each tube and run gentle mac program ABDK_37 to dissociate tissue
8) After dissociation, briefly centrifuge each C-tube to collect cell suspension at tip
9) Aspirate and pass cell suspension through a pre-wet 70 µm cell strainer into a 50 ml centrifuge tube
10) Pass an additional 10 ml PBS through strainer to collect all remaining cells
11) Centrifuge each filtered cell suspension for 6 min at 600 g 10 °C
12) Aspirate supernatant leaving cell palette
13) Resuspend palette in 70% isotonic Percoll solution and transfer to a fresh 15 ml centrifuge tube (3 ml per brain)
14) Careful not to mix the layers, gently pipette 50% on top of the 70% layer (3 ml per brain)
15) Layer 3 ml 35% Percoll solution on top, followed by 2 ml 0% Percoll
16) Centrifuge each tube at 2000 g for 20 min 10 °Cwith slow acceleration and brake
17) Aspirate debris between 35% and 0% layers using a sterile Pasteur pipette - discard
18) Using a fresh Pasteur pipette, collect microglia between 70% and 50% interface, and transfer to a fresh 15 ml centrifuge tube (during this step, collect most of 50% layer)
19) Add 10 ml PBS, mix by inverting tube, and centrifuge at 600 g for 6 min 10 °C to palette cells
20) Aspirate supernatants and resuspend cells in 3 ml media (DMEM + FBS 10% + 2 m M L-glutamine + 50 ug/ml Streptomycin + 100 ug/ml Normocin
21) Perform cell counts

Characterising primary microglia purity using immunocytochemistry

Primary Antibodies: IBA-1 (1:500), CD11B (1:500), and GFAP 488 nm (1:1000)

Secondary Antibodies: Anti-Rat 647 nm (1:1000; CD11B), Anti-Gt 594 nm (1:1000; IBA-1)

DAPI counter stain (1:10,000)

Procedure:

1) Seed primary microglia (1 * 10^5 cells/well) onto 8-well Ibidi glass-bottom slides
2) Incubate cells overnight at 37 °C 5% $_{CO2}$ to allow microglia to attach to the well surfaces
3) Fix cells using 4% PFA + 5% Sucrose solution for 10 min at room temperature
4) Wash 3x with PBS
5) Apply blocking solution 5% NDS + PBS Triton 0.15% for 10 min
6) Apply Primary antibodies diluted in blocking solution overnight at 4 °C. Keep samples in the dark
7) Wash 3x with PBS
8) Apply Secondary antibodies for 2 h, at room temperature. Keep samples in the dark

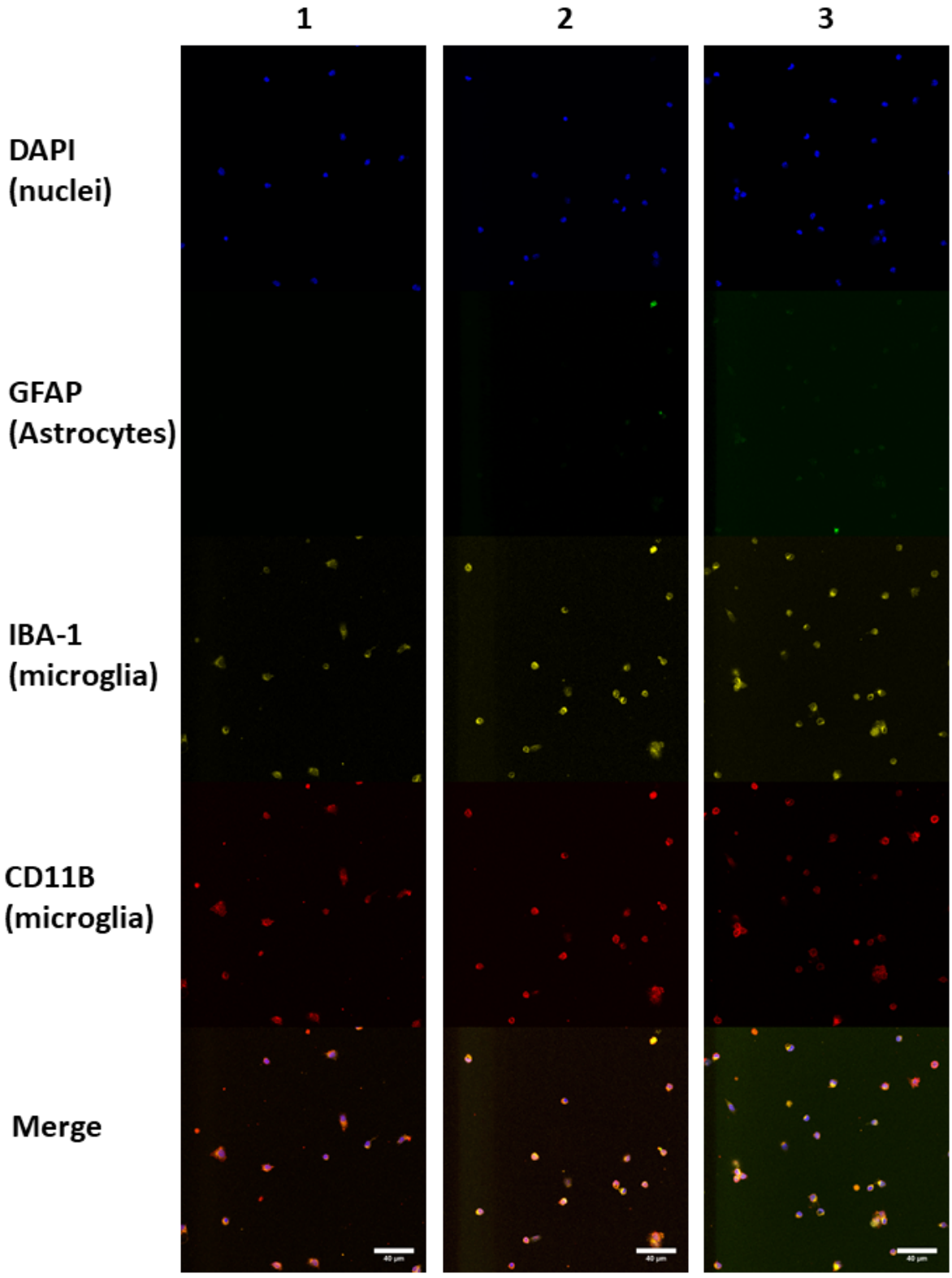

Figure 4. Immunocytochemistry characterisation of Percoll microglia isolation. Panels display representative individual channels and merged image (from top to bottom), from 3 separate isolations (left to right).

Appendix B: Method development for single-cell analysis of pro-inflammatory responses

Introduction

Although most measures are made as an aggregate of cellular responses in vitro, it assumes homogenous responses within a cell population. Thus, little is known about single cell contribution to population responses. For example, aggregate responses may be attributable towards a select few high-responders within a cell population.

In assays including flow cytometry, single signals are accumulated in each analysis, capturing natural variability on a single cell level. Using this method, different sub-populations can be identified, and is frequently used to separate different cell types. Single cell analysis has also been applied at the level of RNA sequencing, with new technologies developed to characterise variation in gene expression amongst a population of T cells (Gaublomme *et al.*, 2015).

The aim of this appendix section is to outline the methods of single cell analysis undertaken here. Thus, single cell analysis of pro-inflammatory markers amongst a genetically homogenous population of cells was explored and optimised over the course of the studies in this thesis. The techniques examined here are in-cell western blots, Oncelisa and NF-kB translocation using immunocytochemistry.

Part 1: In-Cell Western blot

Introduction

The In-cell western technique used to measure protein expression from fixed cells following experimental manipulations, commonly drug treatments, in an in-vitro setting (Egorina, Sovershaev and Østerud, 2006). It uses antibodies that are suitable for immunofluorescence while applying secondary antibodies conjugated to fluophores conjugated to the infrared range, and measured via imaging using infrared scanners such as the Odyssey scanner (Licor, USA).

Although In-cell westerns have been applied to some inflammatory markers, namely CCL28 (Sun *et al.*, 2013), to our knowledge, it has not been applied on macrophage-like RAW264.7 and microglia-like BV2 cell lines. In-cell western blots have may be a high-throughput approach to protein quantification, which can be done in 96-well formats, thus potentially yielding 32 triplicate measures, as compared to 8-10 measures per western blot gel. Furthermore, due to the adaptable use of antibodies, in this assay, there is also potential for flexibility. Together, there could perhaps be use for In-cell westerns in application to screening for changes in multiple protein expression after treatment.

The aim of this section is thus to explore, optimise and apply In-cell western assays to RAW264.7 and BV2 cells, and do discern if these two cell lines differ in protein responses to LPS and glucocorticoid treatment.

Protocol:
RAW264.7 and BV2 cells were seeded onto 96-well plates at a cell density of 1.5E5 cells/ml and 7.5E4 cells/ml respectively. Cells were left to attach overnight before addition of drug treatments.

After completion of drug treatments, remove supernatant and wash twice by gently applying 200ul PBS pH 7.4, while avoiding direct water stream contact with cells to prevent cell loss. Fix cells using 4% Formaldehyde for 20 min at room temperature on the bench. Following which, wash the wells twice with PBS pH 7.4 and permeabalize the cells using 0.1% Triton + PBS four times, each shaken on a plate rocker for 5 min.

Odyssey blocking buffer was diluted 1:4 in PBS. 50ul was applied to each well for 2hr at room temperature, and placed on a rocker to shake gently. After application of blocking, buffer is removed and kept at 4 °C. Pre-diluted Odyssey blocking buffer can be re-used once within the week. Primary antibodies were diluted in 1:4 odyssey blocking buffer at the required concentration (Table 1), and was gently agitated on a rocker overnight at 4 °C.

After incubation of primary antibodies, each well was washed with 0.1% Tween + PBS four times for 5 minutes each on a rocker. Secondary antibodies diluted in Odyssey blocking buffer at the required concentration (Table 1) were then applied for 1hr at room temperature, gently shaking. Finally, all wells were washed again 4 times in 0.1% Tween + PBS for 5 minutes, shaken.

Imaging was done on the Odyssey scanner at 3.0mm focus adjustment to account for the thickness of the 96-well plates, on plate-mode, which flips the image to the right orientation when imaging. A pre-scan at 5.0 gain first is recommended to check the stain intensities. Gain settings can be further adjusted accordingly.

Primary antibodies	Concentration	Manufacturer	Product Number
Rb anti-GR	1:50	Santa Cruz	SC-1004
Rb anti- NF-kB	1:100	Santa Cruz	SC-372
Mu anti- NLRP3	1:100	Adipogen	AG-20B-0014
Rat anti- CD11b (ox-42)	1:100	ABD Serotech	MCA275R
Gt anti-CD11b	1:100	Santa Cruz	SC-6614
Mu anti- TLR4	1:100	Novus	NB100-56566
Rb anti- COX2	1:100	Cayman	600-16126
Secondary Antibodies			
D anti-Mu 700nm	1:500	Rocklands	610-750-124
D ant-Rat 800nm	1:500	Rocklands	612-732-120
D anti-Rb 800nm	1:750	Rocklands	611-731-127
D anti-Gt 800nm	1:750	Thermo Fisher	Q12086703

Table 1. Antibody information.

Method optimisation

Normalisation of signal

Due to potential differences in cell number as a result of inconsistent plating or effects of drug treatments, all results have to be normalised to cell number. Thus, a DNA stain using a combination of Sapphire700 and DRAQ5 (Biostatus, DR05500), which fluoresce under 700nm wavelength excitation was used to control for cell number differences by taking a ratio of the fluorescence of the protein of interest divided by the fluorescence of cell normalisation. This would serve as the 'loading control' often employed by ratiometric measures of biological samples.

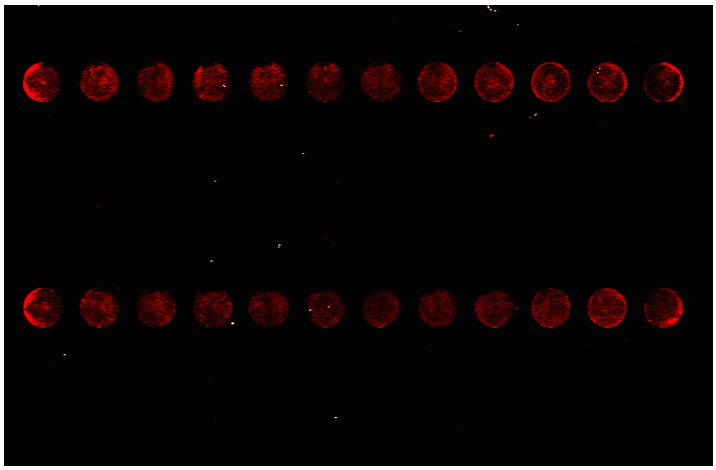

Figure 2. Sapphire700 + DRAQ5 stain as loading control for in-cell westerns measures.

Blocking solution

To reduce non-specific background signals from antibody binding, a blocking step is required to mask non-specific sites prior to application of the first antibody. We first tested Fish gelatine (2%), which was potentially an effective blocking agent, and an alternative to commercially available Licor Odyssey blocker (Licor, 829-31080). When tested however, fish gelatine performed poorly as a blocking agent, unable to mask various secondary antibody signals, as seen from high background signals (figure 3a.). Odyssey blocking buffer was thus used for all future experiments.

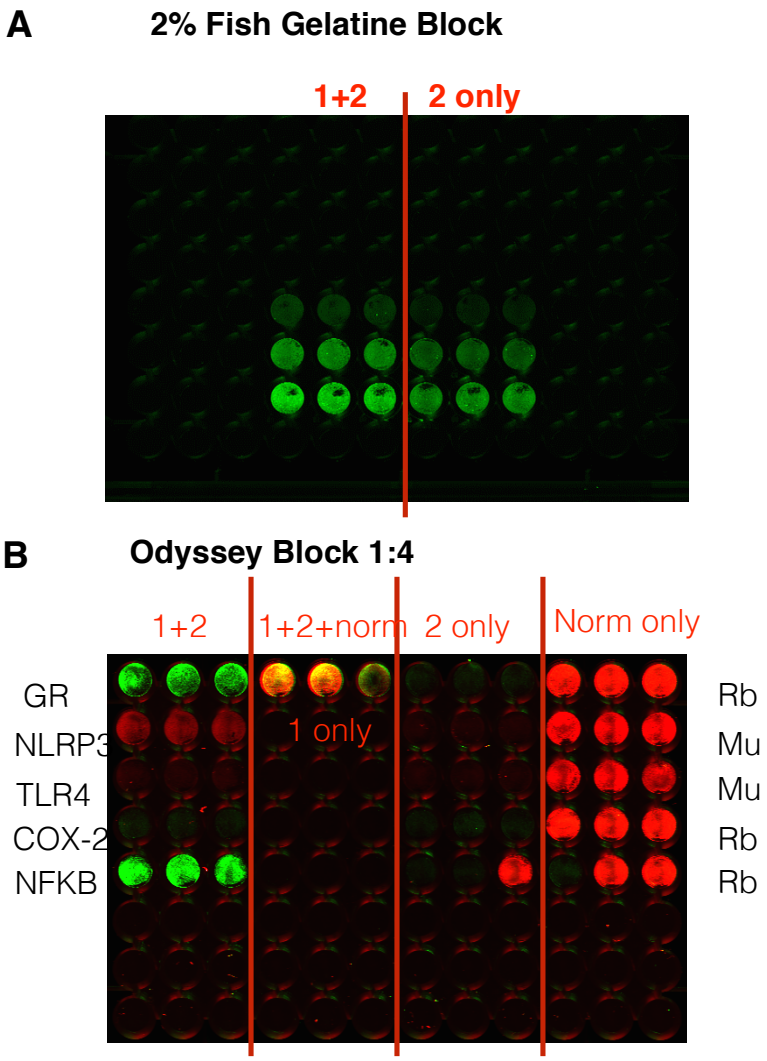

Figure3. Optimisation of blocking step. (A) Fish gelatine (2%) was unable to reduce background binding, as estimated from secondary only conditions. (B) Odyssey blocking buffer used at 1:4 dilution performed well at blocking non-specific secondary binding (see 2-only columns) across different types of primary and secondary antibodies. This was true with both 700nm (red) and 800nm (green) channels. All measures were done on naïve RAW264.7 cells.

Antibody verification

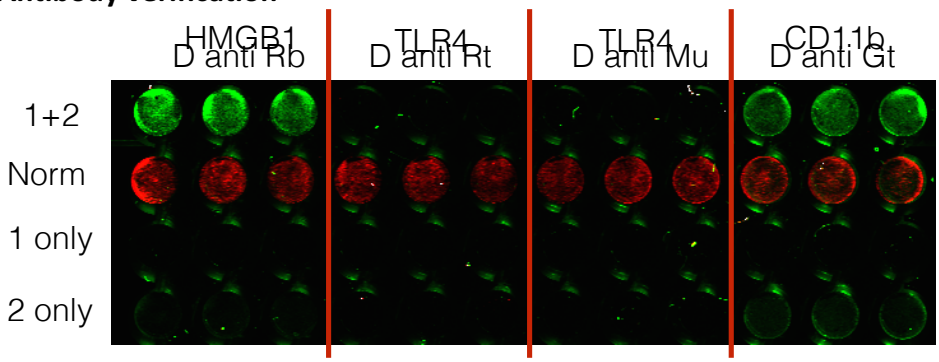

Figure 4. Testing antibody binding signal, and secondary antibody non-specificity to RAW264.7 cells.

To test antibody specificity, and potential background signals, RAW264.7 cells were stained with several available antibodies raised in different species, along with the appropriate secondary antibodies, both in isolation and in mixture (figure 3b, 4). Donkey anti-goat secondary antibody appears to yield the highest non-specific background signals, even when using the Odyssey blocking buffer, and were thus avoided. TLR4 antibodies appear to not yield detectible signals, and were also avoided. Due to lack of non- goat CD11b primary antibodies, CD11b was also excluded from future in-cell western experiments. The final list of approved antibodies were: rabbit anti-HMGB1(Abcam, ab18256), rabbit anti-GR (Santa Cruz, M-20), rabbit anti-NF-kB(Abcam ab16502) and mouse anti-NLRP3 (adipogen AG-20B-0014).

Assay sensitivity test

LPS and HMGB1 are TLR4 agonists via binding to MD2 and CD14, and therefore trigger the innate-immune proinflammatory response (Kim *et al.*, 2013; Wu *et al.*, 2015). TLR4 activation via LPS and HMGB1 has been shown to increase NFKB p65 nuclear translocation and NLRP3 expression in RAW264.7 cells (Park *et al.*, 2006; Qiao *et al.*, 2012; Kim *et al.*, 2016). NFKB and NLRP3 were therefore measured to quantify In-Cell western sensitivity to protein expression changes. GC, a glucocorticoid steroid hormone which binds to intracellular glucocorticoid receptor (GR), is also able to influence innate-immune activity (Liu, Buisman-Pijlman and Hutchinson, 2014). Thus, we measured its effects on GR, NLRP3 and NFkB expressions.

After 24 h drug stimulation, RAW264.7 cells were fixed and stained using the In-cell western protocol. In cell western was able to capture trends in drug treatments. Namely, GC and LPS both appeared to reduce GR and NFKB expression slightly after 24 hours. HMGB1 appeared to increase GR expression, however did not show any difference from vehicle treatment in NFKB and NLRP3 expressions. LPS appeared to be the only treatment that increased NLRP3 expression.

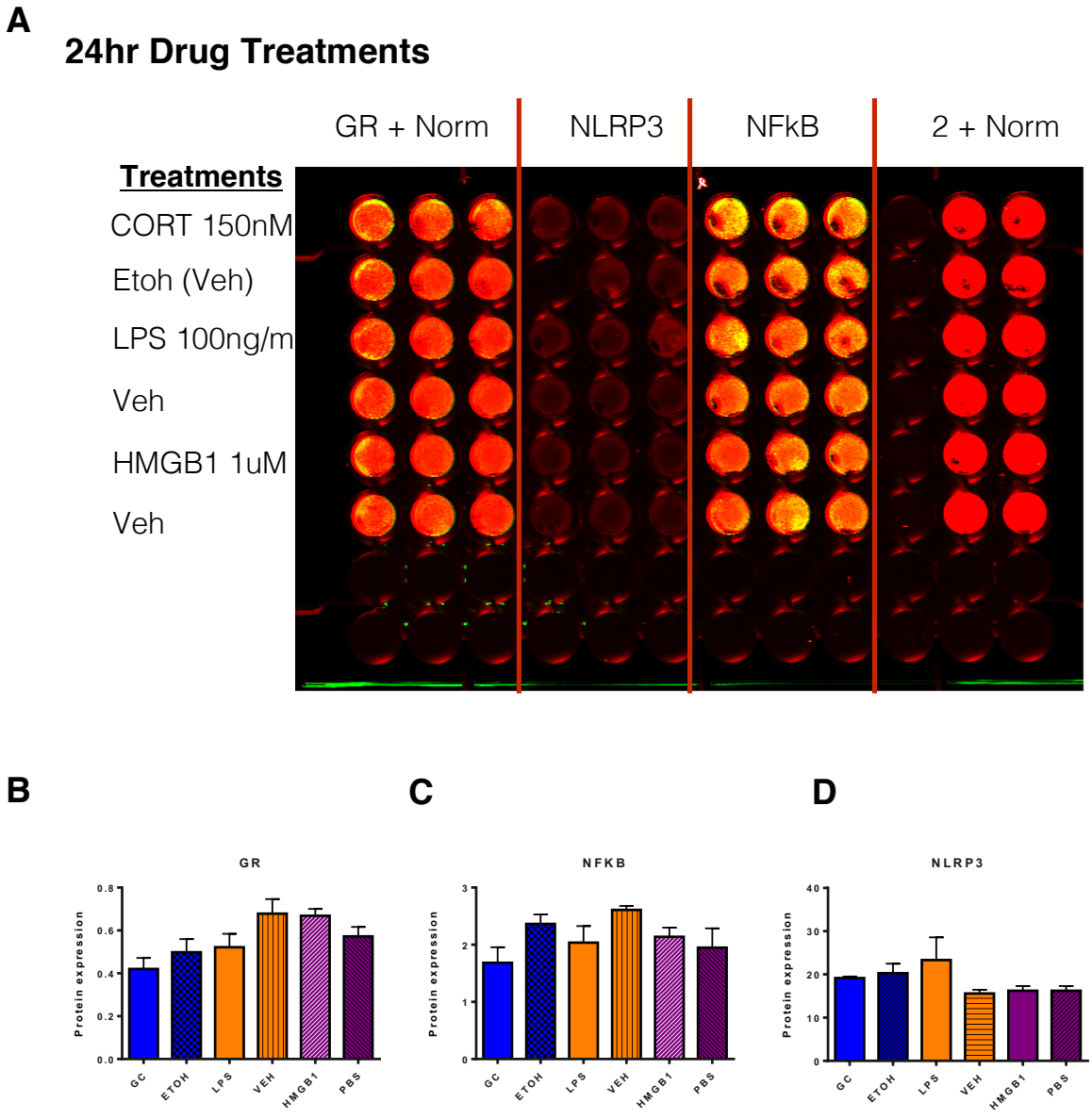

Figure 5. RAW264.7 response to 24 hour treatments of Corticosterone (GC; 150nM), ethanol (vehicle for GC), LPS (100ng/ml), media (VEH; vehicle for LPS), HMGB1 peptide (1uM), and PBS (vehicle for HMGB1). (A) Raw data image, (B-D) Quantified ratiometric values. Protein measures (arbitrary units): Glucocorticoid Receptor (GR; B), NF-kB (NFKB; C) and NACHT, LRR and PYD domains-containing protein 3 (NLRP3; D).

BV2 responses to 1ug/ml LPS

BV2 cells are microglia-like, and are commonly used in in-vitro models to investigate drug effects on the central immune system. LPS-induced protein expression changes were thus explored. P38 phosphorylation and expression has also been associated with TLR4 activation, and can be a measure of immune-cell proinflammatory activity (Hutchinson *et al.*, 2012). HMGB1 may also be produced in response to LPS stimulation, and was therefore measured.

In all proteins measured, there appears to be a slight trend towards increased NFKB expression after 3hr LPS stimulation in BV2 cells.

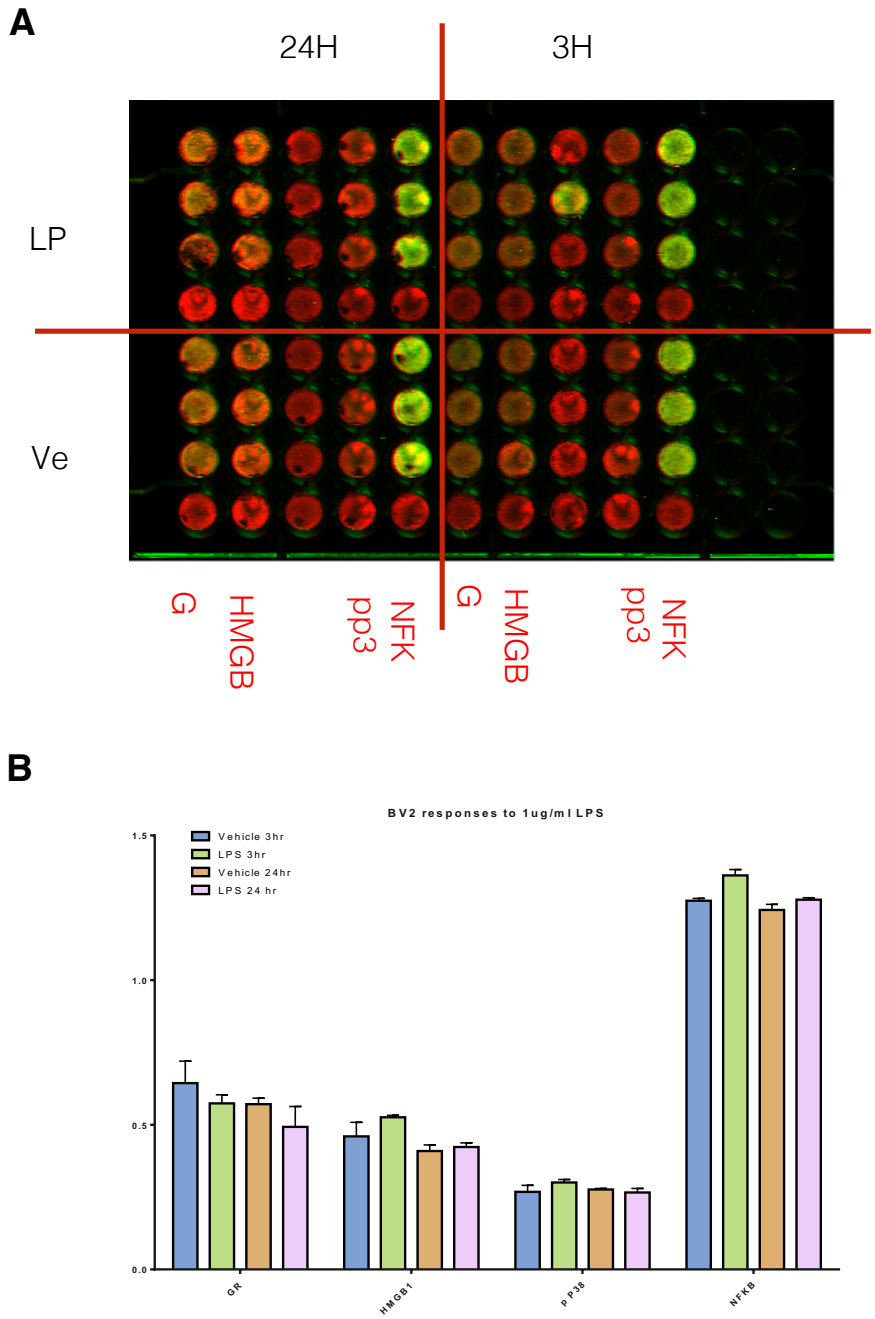

Figure 6. BV2 cell responses to 1ug/ml LPS stimulation after 3 and 24 hours. (A) Raw data and (B) bar graph of GR, HMGB1 pP38 and NFKB expression after stimulation, measured by In-cell westerns.

Protein expression comparisons between RAW264.7 and BV2 cells

From experiments in the previous section, GC application appears to influence GR and NFKB expression as compared to vehicle in RAW264.7 cells. To test further effects of GC, NFKB and further investigations into HMGB1 and p p38 were measured. HMGB1 expression has previously been shown to increase after stress, and this effect was attenuated by blocking GR (Frank *et al.*, 2015). The applicability of this technique was also extended to BV2 microglia-like cells, in order to further test the generalisability of the assay. A successful implementation in multiple cell types would thus indicate suitability towards characterising cell type differences, which would be useful in contrasting central and peripheral immune protein responses to treatments.

RAW264.7 cells appear to be more sensitive towards glucocorticoid administration, by displaying larger differences as compared to BV2 cells across all proteins investigated. Of note is the differences between ETOH vehicle and media controls, indicating that ETOH could be changing RAW264.7 protein expression even after correcting for cell numbers.

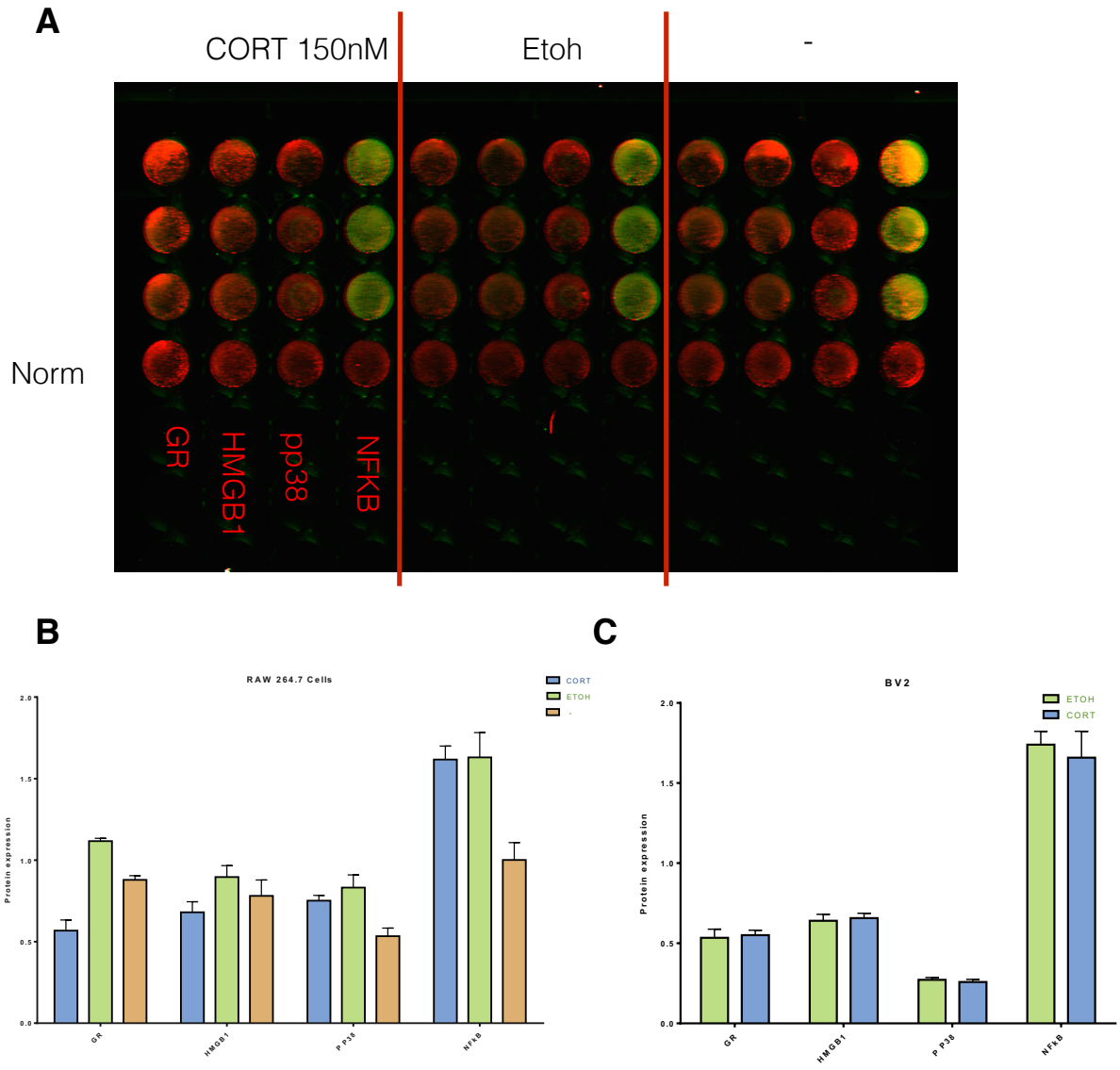

Figure 7. In-cell western of 24 hour GC (150nM), vehicle (ETOH) and media (-) treatment. (A) Raw data of In Cell western showing GR, HMGB1, phospho P38 and NFKB expression levels in macrophage-like RAW264.7 cells (N=3) (B) and BV2 microglia-like cells (N=1)(C).

Conclusions

The In-cell western technique provides a fast and simple technique to look at gross expression of protein in response to treatment. This assay can be assembled across 1 day, in 96-well format, providing a high-throughput snapshot into protein expression. Measurements are also relatively simple, since plates can be imaged using the Licor scanner, as well as select plate readers with fluorescent capabilities. I have chosen to show Licor scanning due to the imaging capabilities, which can look at cell distribution within a well, whereas plate readers would typically average out values. This allows for higher scrutiny of data quality for this approach.

In-cell western blots however, have several limitations and considerations. Even with imaging techniques using the Licor Odyssey infrared scanner, there was insufficient resolution to visualise single cells, and therefore lose information on cell morphology or compartmentalisation of protein expression. For example, NF-kB p65 translocates into the nucleus in response to TLR4 activation, and may not be reflected in total protein expression levels (Zhao *et al.*, 2014). Furthermore, due to limitations with the Licor scanner, there is a limitation to 2 channels of fluorescence, 700nm and 800nm. With the 700nm channel taken up by the sapphire700 and DRAQ5 dyes for essential cell number normalisation, it leaves one channel for antibody binding, therefore requiring more wells to investigate several proteins, and inflating the cost of the assay. These issues of multiple staining and micrometre resolution are resolved in immunocytochemistry technique. However, that requires use of microscope, which then reduces the throughput of experimentation.

Moreover, specificity of the assay may be difficult to determine without use of other techniques such as western blots. Since western blots employ the use of electrophoresis to separate proteins into different molecular weights, non-specific binding is reduced by only measuring values from the right molecular weight of the protein of interest. Although this non-specificity is reduced by using the commercially available Odyssey Blocking buffer (see figure 3.), our testing methods shown here could only investigate non-specificity of the secondary antibody, leaving potential sources of non-specificity from the primary antibodies. This would theoretically be reduced by further using monocolonal antibodies, or by first verifying that the antibodies used do not have significant noise associated by western blot analysis. In-cell westerns are therefore only useful when there is confidence in the quality of antibodies.

Lastly, due to the nature of ratiometric analyses without known protein standards, it is difficult for in-cell westerns to have the precision of quantitative measures of proteins such as mass spectrometry and ELISA. This therefore requires stringent controls, and as a result, can only quantify fold changes between treatment and controls, rather than attach a meaningful quantitative value to protein measures. Furthermore, it is difficult to quantify changes in baseline, and inter-plate variability from this technique. Thus, where possible, it is advised to utilise ELISA methods, which can both provide high-throughput and semi-quantitative measures of protein expression by use of known protein standards.

In conclusion, while In-cell westerns offer a high-throughput snapshot into protein expression differences between treatments, it also has several limitations. It could therefore be used as an initial pilot for studies, if the antibodies used in the technique have already been verified. Furthermore, although it does not provide specialised measures such as ELISA assays and immunocytochemistry in terms of quantitativeness and cell compartment resolution respectively, In-cell westerns does offer a combination approach. For example, due to the ability to image each well, into distribution of cells across the well, and can therefore be useful in some applications where drugs applied may cause cell death, leading to loss of cells.

Part 2: OnCELISA on adhered BV2 cells

Introduction

OnCELISA is a novel technique that measures cell-released proteins, such as cytokines, on a cellular level, down to pg/ml sensitivity. This novel assay was developed in the Centre for Nanoscale Biophotonics by Liu and colleagues (unpublished). OnCELISA labels released molecules from single cells, and is able to discern high responders from low responders to LPS within a cell population (unpublished). As the cells can be kept alive throughout the staining process, high responders are then able to be magnetically separate, and further cultured.

Since it was shown that low- dose CORT pre-exposure can preferentially prime IL-1β, but inhibit IL-6 (Chapters 4 and 5), OnCELISA provides an opportunity to test whether the priming and inhibitory effects of CORT, is due to additive effects on the whole cell population, or if these effects are due to a select few high or low responders. The developers of this assay, however, have only used this method on suspended BV2 cells rather than attached cell lines. Due to the importance of cell morphology in this study (Chapters 4 and 6), it is important to understand if high- and low- responders take on different cell morphologies. Moreover, inclusion of other immunocytochemistry measures, such as NF-κB translocation could potentially be informative, providing a second dimension to measure cell inflammatory responses. This section thus focuses on the optimisation and adaptation experiments that were conducted on cell-attached models of BV2 cells, and aims to investigate if high proinflammatory cytokine responders also take on more ameboid morphology, as well as increased NF-kB translocation.

Protocol

Preparing IL-6 magnetic microbeads

Fluorescent magnetic microbeads (Bangs Laboratories #MC03F) were dispersed in 100mM MES buffer pH 5.2 at 1mg/ml concentration, and mixed with 3.2mg of 1-ethyl-3-[3 dimethylaminopropyl] carbodiimide hydrochloride and 1.8g of N-hydroxysuccinimide to form covalent bonds with the covalently funtionalised microbeads. The pH was then adjusted to 8.0 using a pH strip. IL-6 antibody (R&D #MAB5061) was then added to the mixture at 10ug/ml final antibody concentration, and the solution was mixed on a tube-inverter for 2hr at room temperature. The functionalised magnetic beads were washed 3 times in 10X PBS pH 7.4, by using a magnet to palette the beads at the bottom of the tube. Lastly, beads were redispersed in 0.5ml of 1x PBS, and stored at 4degrees Celsius in the dark, before use in OnCELISA. The resultant mixture is 10ug antibody per mg of beads.

OnCELISA assay procedure

After culturing 2 T75 flasks of BV-2 cells to a confluency level of 80-90%, emdia was removed and cells were sahed with ice-cold PBS. Cells were then biotinylated using the manufacturer's specification (Thermo Fisher # PIE89881). Briefly, 10ml of ice-cold biotin solution was added to each flask, and was incubated for 30min with gentle agitation at 4 degrees Celsius. After incubation, 500ul of quenching solution was added to each flask, and the biotinylated BV2 cells were gently scraped into the solution. All biotinylated cells in the solution were transferred to a 50ml tube, and centrifuged at 200rcf for 5 min. The supernatant containing excess biotin solution was then discarded. Cells were resuspeded in 10ml TBS and centrifuged again to wash. Cell counts were conducted at this stage to monitor cell numbers.

After the wash step, the cell surfaces were functionalised by resuspension in a solution containing DMEM with 10% gelatine, biotinylated IL-6 antibody (R&D system #506-ML), and 4ug of Neutravidin (Thermo Fisher #PIE31000). Neutravidin serves as a link between the two biotinylated ends on the cell surface and antibody, to create IL-6 antibody binding sites on the cell surface. The cells were incubated with the solution for 2hr at 37 degrees Celsius.

Following surface functionalization, the cells were centrifuged at 37 degres Celsius, at 200 rcf for 6 min. The supernatant was removed nad cells were resuspended in PBS to wash. Cell counts were also done at this stage to monitor cell loss during surface functionalization. Cells were divided into tubes at a cell density of 1E6cells/ml per tube, and resuspended in either media or 100ng/ml LPS. These cells were then seeded onto coverslips in 12-well plates. After drug treatments, SPIO_Ab was added at a concentration of 20ul/ml, and incubated for 1hr at 37degrees Celsius.

Immunocytochemistry staining

Wheat germ agglutin-633nm cell membrane stain was added to each well at 1ug/ml concentration for 10 min, after SPIO_Ab was removed. After which, cells were fixed using 4% PFA containing 5% sucrose solution for 10min at room temperature. Following 3 washes of PBS, non-specific binding sites were blocked using 3% skim milk in TBS solution for 10 min. NF-kB antibodies (Abcam ab16502; 1:500 dilution) was

added to detect nuclear translocation of NF-kB, a marker of immune activity. Finally, the cells were washed 3 times using PBS, and secondary antibody donkey anti-rabbit antibody (Life technologies, R37119; 1:1000) conjugated to 594nm fluorescent tag was added, in conjunction with DAPI cell nucleus staining (1:1000). To collect images, coverslips were imaged under the confocal microscope.

Results

OnCELISA results

From observations of antibody staining using the confocal microscope, LPS successfully triggered an inflammatory response, since there was NF-kB translocation in LPS treated cells. There is however, little difference in IL-6 fluorescent magnetic bead (green) expression between LPS and vehicle conditions (Figure 1.).

Large aggregates of fluorescent bead conjugated IL-6 was also displayed by the images. Overall, due to relatively high binding within the cell membrane, the OnCELISA had high noise and low signal.

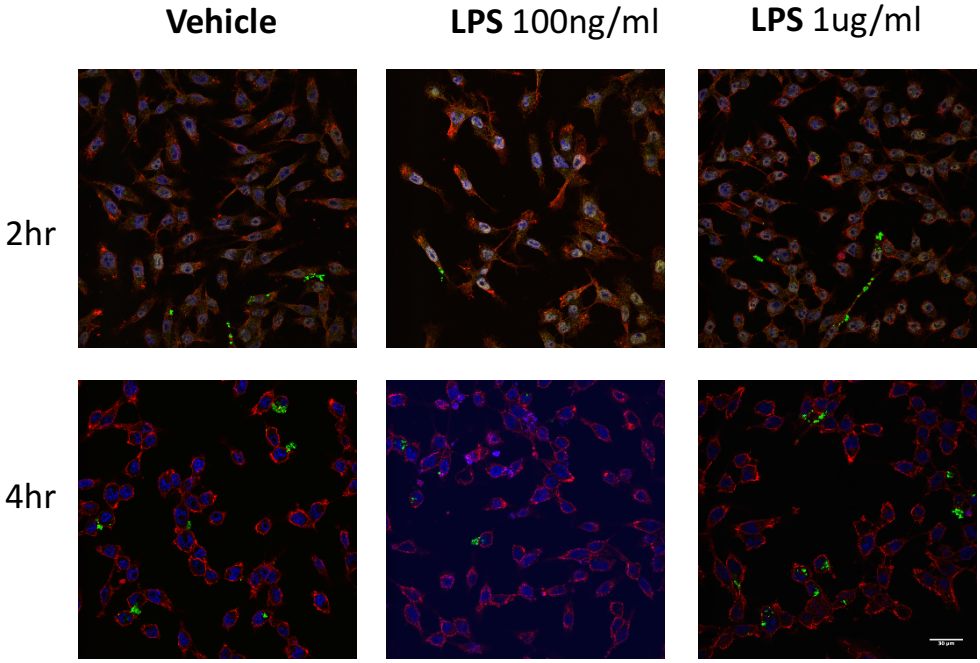

Figure 1. Attached cell model: OnCELISA confocal images. vehicle or LPS 100ng/ml, LPS 1ug/ml treatment was applied to BV2 cells for 2 or 4 hours. Red: cell membrane stain (WGA), blue: nucleus stain (DAPI), green: SPIO_ab conjugated to IL-6 (OnCELISA), yellow: NF-kB (2hr treatment only).

Experiment	Stage	Cell Counts	Cell Viability
1	post-biotinylation	1.56E+07	96%
1	post-antibody labelling	1.21E+07	82%
2	post-biotinylation		
2	post-antibody labelling		

Table 1. Cell counts and viability pre and post- surface labelling with biotinylated IL-6 antibodies.

Verification: SPIO_Ab binding specificity

Since a low IL-6 signal was observed in the OnCELISA, it could be due to low assay sensitivity. To test the sensitivity of SPIO_Ab binding, a sandwich ELISA was constructed, where known concentrations of IL-6 peptide was bound to capture antibody lining bottom of wells in a 96-well plate using a commercially available kit (BD bioscience, 555240). The detection antibody provided by the kit was substituted by SPIO_AB (1ug/ml), thus producing a fluorescent signal at 480nm. After incubation with SPIO_Ab for 1hr, excess unbound SPIO_Ab was transferred to separate wells. Fluorescent readings were measured using a plate reader (Biotek, USA).

SPIO_Ab binding did not increase with increased IL-6 peptide concentrations, showing low sensitivity of binding. Moreover, unbound antibody signal was higher than the bound portion, thus indicating that there was sufficient SPIO_Ab added to the system (Figure 2A). Furthermore, there was a weak negative relationship between the bound and unbound portion, indicating that there was some consistency in total antibody added to each well (Figure 2B). There may therefore also be problems with binding specificity that was not tested with this assay verification.

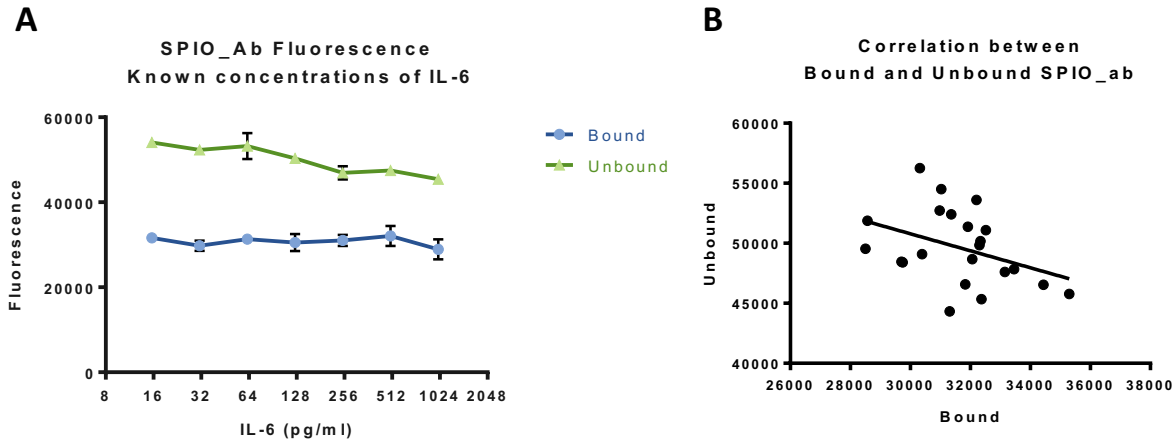

Figure 2. Binding sensitivity of the fluorescent bead- conjugated IL-6 antibody (SPIO_Ab). A) SPIO_Ab binding to known concentrations of IL-6 in a sandwich ELISA assay. B) Scatter plot of fluorescent readings from bound and unbound SPIO_Ab from the sandwich ELISA assay.

Verification 2: SPIO_Ab internalisation and phagocytosis

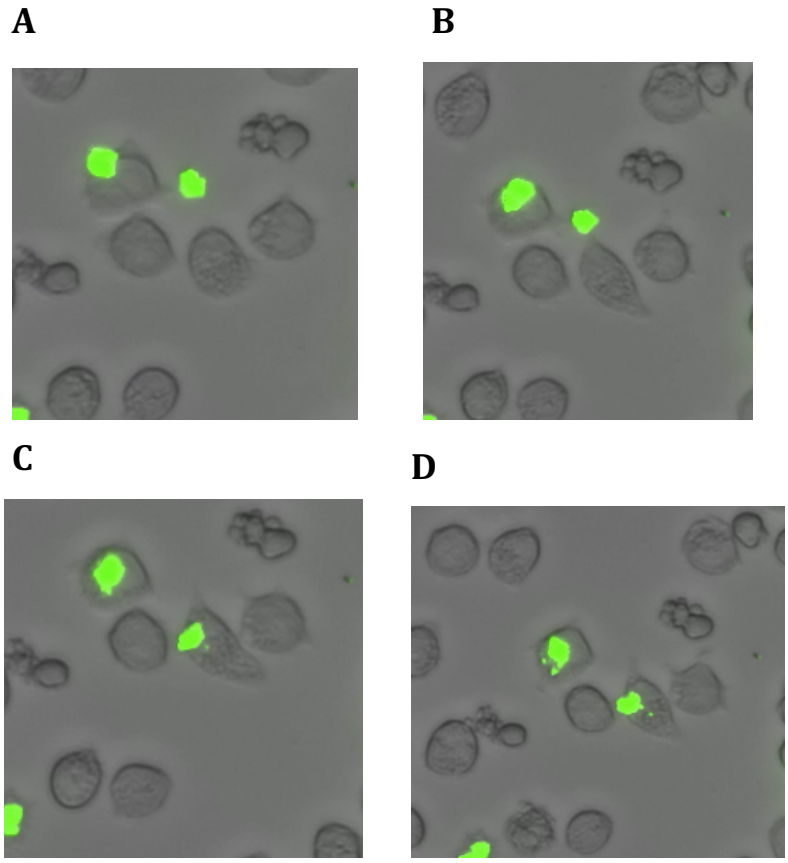

Figure 3. Time-lapse images from live-cell microscopy. Each frame is 10 minutes apart. SPIO_Ab (green) is phagocytosed by BV2 cells.

Since SPIO_Ab is added to live BV2 cells in OnCELISA, it was investigated if the aggregates seen inside BV2 cells from OnCELISA images is due to active internalisation by BV2 cells. Emulating OnCELISA conditions under live-cell microscopy at 5% CO2 and 37degrees celsius, SPIO_AB was added to biotinylated and membrane-functionalized cells. If successful, cells releasing IL-6 would be labelled with SPIO_Ab over the course of 1hr. When looking at the videos however, some cells were actively phagocytosing the SPIO_Ab (Figure 3). In addition, there was also large aggregates and uneven distribution of SPIO_Ab particles throughout the images, thus displaying failure of SPIO_Ab dispersion.

Other wells in live-cell microscopy included a test of membrane functionalization of the biotinylated cell surface with biotinylated IL-6 antibody using fluorescent conjuagated strepdavidin-480 to link the two biotin ends. There was however, no visible signal in those cells (not shown), suggesting that there may be failure in the cell surface functionalization step.

Verification 3: Biotinylated antibody binding to Cell surface

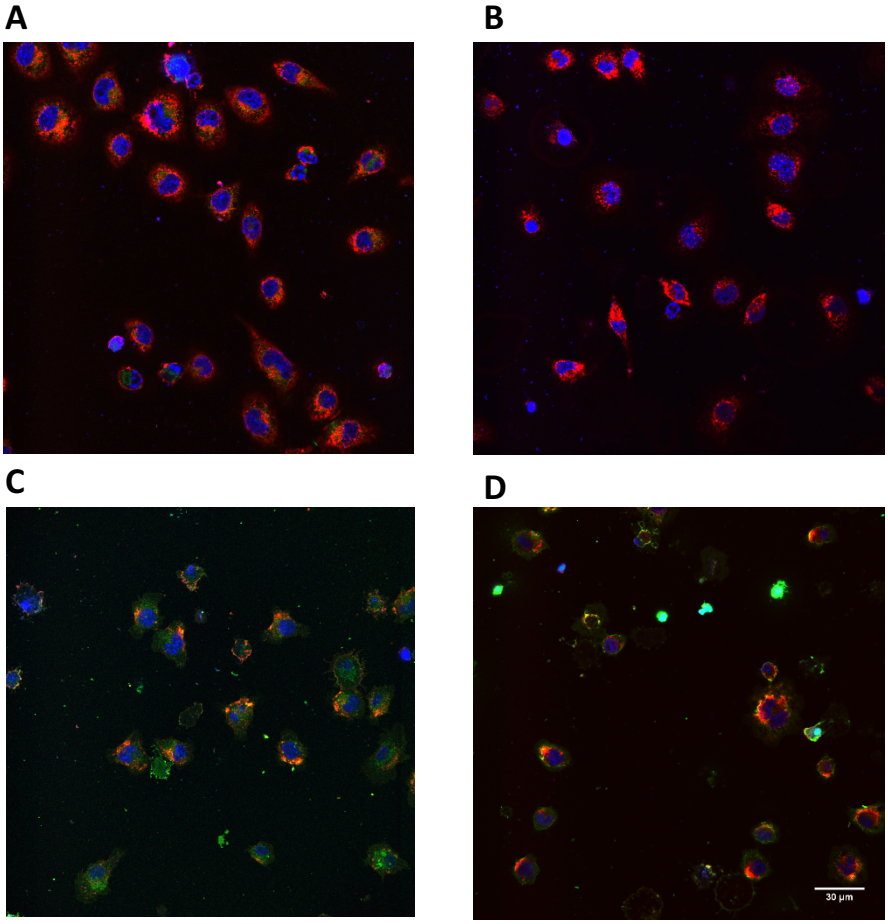

Figure 4. Biotinylated antibody binding in A) non-biotinylated BV2 cells fixed after addition of Strepdavidin-594 and biotinylated IL-6 antibody B) non-biotinylated BV2 fixed prior to addition of Strepdavidin-594 and biotinylated IL-6 antibody, C) biotinylated BV2 cells fixed after addition of Strepdavidin-594 antibody and biotinylated IL-6 antibody, and D) biotinylated BV2 cells fixed before addition of Strepdavidin-594 and biotinylated IL-6 antibody. Colours: Cell membrane stain (WGA; red), Strepdavidin-594 (green), nucleus (DAPI; blue). Images were gain-matched on all channels

To check if biotinlyated antibody functionalization of the cell surface was successful in live cells, confocal images were taken from BV2 cells that were either biotinylated or not, and either received surface functionalization before or after cells have been fixed. Surface functionalization with biotinylated IL-6 was visualised using fluorescent-strepdavidin to link the two biotin ends (figure 4).

Non-biotinylated cells had no visible strepdavidin binding regardless of order of staining. In biotinylated cells, there appears to be an effect of staining order, in which cells that have been fixed prior to addition of strepdavidin and IL-6 antibody retained a higher signal, with more of the signal localised with the cell membrane, resulting in yellow- coloured pixels (figure 4D). On the other hand, biotinylated cells that have received surface functionalization while live (prior to addition of fixative) displayed increased cytoplasmic strepdavidin signal, and lower overall signal strength. Loss of

signal in the OnCELISA could therefore be due to failure of cell surface functionalization, possibly because of active internalisation of strepdavidin and biotinylated IL-6 anitbody in live cells.

Conclusion

The novel OnCELISA assay had potentially provided a way to visualise distribution of high and low cytokine responders within a cell population. When tested on attached BV2 cells however, this assay did not provide a clear signal, due to lack of sensitivity and problems with cell phagocytosis of antibodies.

The OnCELISA has previously been shown to work on suspended BV2 cells with success in cell separation between high and low responders. We were unable to replicate these results in the cell-attached model, mainly due to low signals, and potentially high noise due to phagocytosis of the surface functionalization compounds, and labelling SPIO_Ab. As BV2 cells are microglia-like, they have been shown to actively phagocytose particulate matter in the microenvironment (Majerova *et al.*, 2014). It is also worth noting that the fluorescent microbeads used to conjugate to IL-6 antibody has been recommended for use in phagocytosis assays according to the manufacturer's guidelines. It is therefore unsurprising that live BV2 cells would phagocytose foreign particles over the course of this assay. In conclusion, this assay requires significant optimisation and change of materials used in order to be used for future analysis.

Appendix C: Source code – Image analysis: Translocator (versions 0.0.1 and 0.0.2)

Image J analysis for NF-kB translocation: Translocator (Ver 0.0.1)

Macro for Image J (Java)

Outputs .txt file onto desktop with profile plots for each RGB channel. Takes an RGB image stack.

/* Calculate specimen width in pixels using a line profile Requires:

- Single channel image stack
- Line profile drawn on image Output:
- Text file on desktop with numeric data with format: ImageJ macro - Stack profile Plot Total image slices = 56 Pixels in profile plot = 40

  Rows of Plot Intensities: 110, 126, 108, 107, ... 108, 111, 115, 105, ... 112, 103, 102, 99, ... Modified from http://imagej.nih.gov/ij/macros/StackProfilePlot.txt (http://imagej.nih.gov/ij/macros/StackProfilePlot.txt) Pariksheet Nanda */

/ Further modifications: 1) added support for multiple ROIs using roiManager 2) removed bitmap 3) output for all images in stack 4) removed all descriptive output to simplify file for post-processing in python JJliujj90@gmail.com (mailto:liujj90@gmail.com) /

```
macro "Stack profile Plot" {

Y_MIN = 0; Y_MAX = 16383;

// sanity check if (nSlices==1) exit("Stack required");

setBatchMode(true); saveSettings(); run("Profile Plot Options...", "width=400 height=400
minimum="+Y_MIN+" maximum="+Y_MAX+" fixed" );

// prepare stacks original_stack = getImageID; plot_stack = 0; total_slices = nSlices;

// save to file home = getDirectory("home"); // Returns the path to users home directory. if (home == "")
exit("No desktop directory available"); temp_file = home + "Desktop/" + getInfo("image.filename") +
"_profiles.txt"; f = File.open(temp_file);

b = roiManager("count"); for(i = 0; i < b; i++) { roiManager("Select", i);
// cycle through image leaves for (slice = 1; slice <= total_slices; slice++) {

        showProgress(slice, total_slices);

        selectImage(original_stack);
        setSlice(slice);

        // get plot data
        value = getProfile();
        positions = lengthOf(value);

        // write slice plot to file

        file_str = toString(value[0]);
        for (pixel = 1; pixel < positions; pixel++)
            file_str += ", " + value[pixel];
        print(f, file_str);

    }
    print(f);

}

setSlice(1);

setBatchMode(false);

restoreSettings(); }
```

Example workflow

1) After imaging, open .lif file in FIJI distributioon of ImageJ

2) Convert image to RGB stack (one image for each color channel)

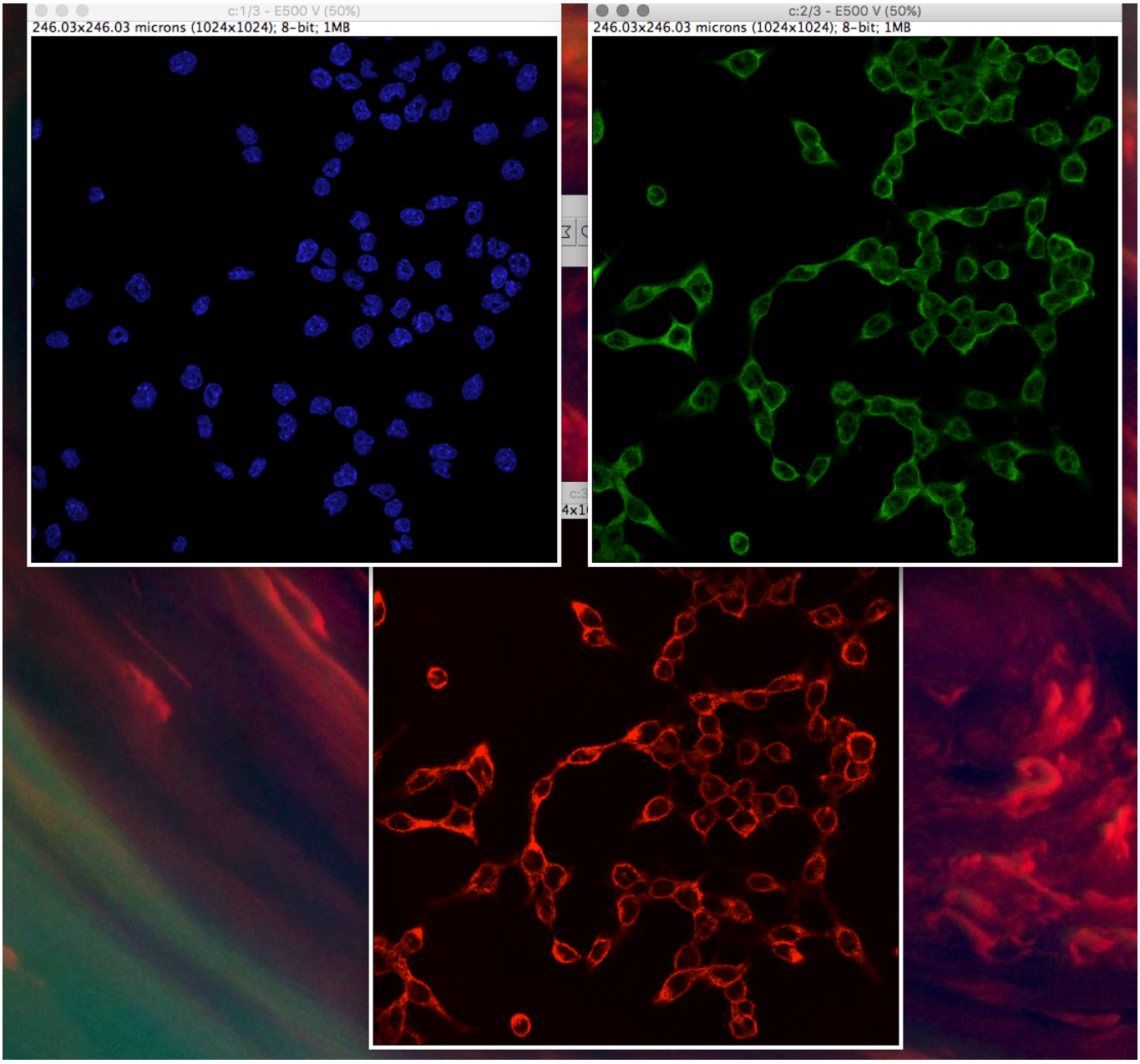

3) On WGA channel (cell membrane) pick out 15 cells in focus, drawing a line across the longest diameter of each cell

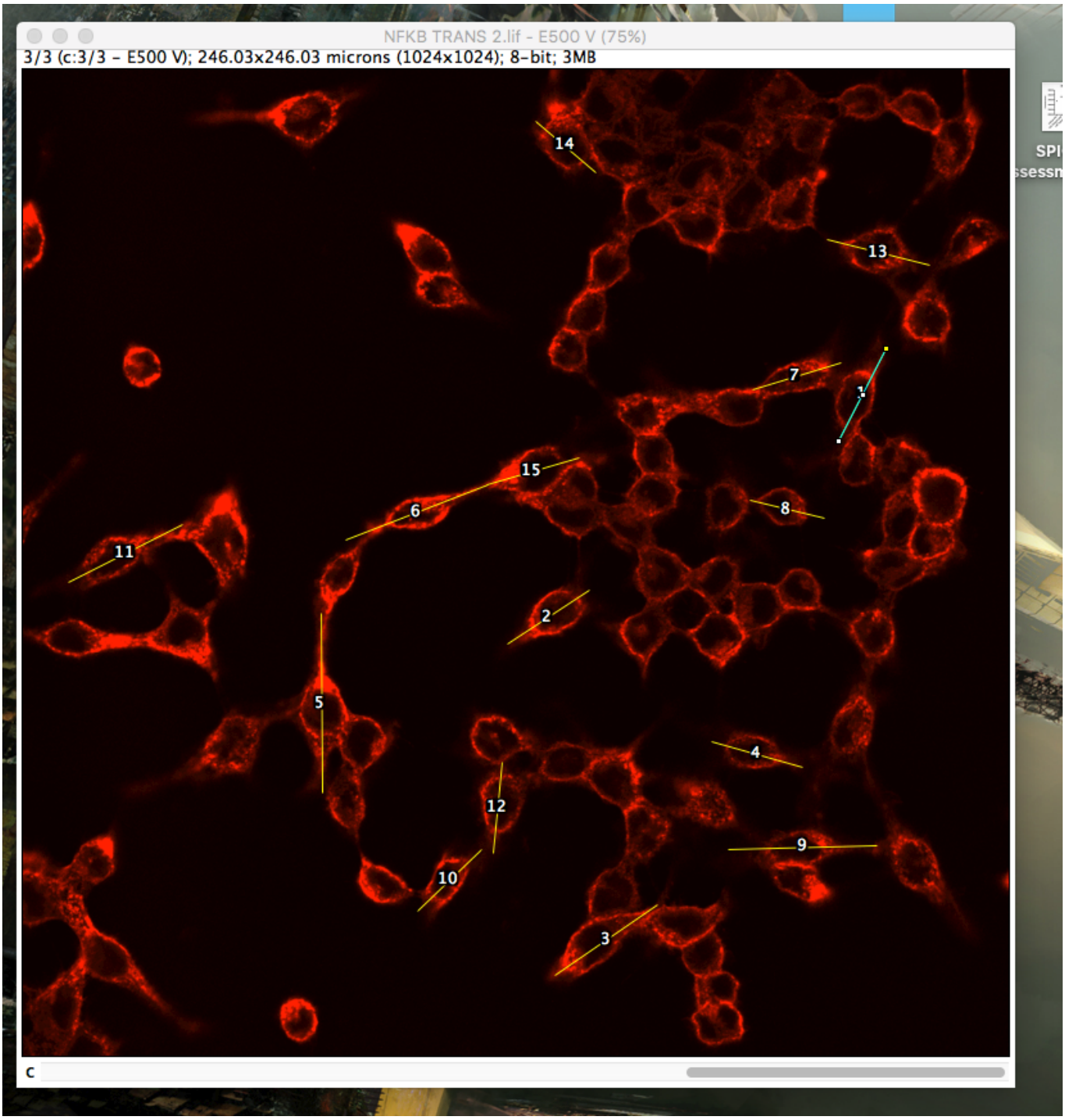

4) Run macro

5) On desktop, find exported file, open in Microsoft excel and transpose dataset (so each column represents one channel)

6) Save transposed file as .csv in working directory for R analysis

In [ ]:

In [1]:
```
library(ggplot2)
library(dplyr)
library(pracma)
library(scales)
```

```
Warning message:
“package ‘ggplot2’ was built under R version 3.3.2”
Attaching package: ‘dplyr’

The following objects are masked from ‘package:stats’:

    filter, lag

The following objects are masked from ‘package:base’:

    intersect, setdiff, setequal, union

Warning message:
“package ‘scales’ was built under R version 3.3.2”
```

In [2]:
```
# import dataframe
E50V <- read.csv('E50 V.csv', header = FALSE)
E50L2<- read.csv('E50 L2.csv', header = FALSE)
E50L30<- read.csv("E50 L.5.csv", header = FALSE)

C50V<- read.csv('C50 V.csv',header = FALSE)
C50L2<- read.csv('C50 L2.csv',header = FALSE)
C50L30<- read.csv('C50 L.5.csv',header = FALSE)

E500V <- read.csv('E500 V.csv', header = FALSE)
E500L2<- read.csv('E500 L2.csv', header = FALSE)

C500V<- read.csv('C500 V.csv',header = FALSE)
C500L2<- read.csv('C500 L2.csv',header = FALSE)
C500L30<- read.csv('C500 L.5.csv',header = FALSE)
```

Plotting RGB channel intensity x Location for individual cells

In [1]:
```
GetPlots<- function(df, R, G, B){ #df =  dataframe, order of R/G/B channels, which col ie.(3,1,2)
    for (i in 3: ncol(df)){
        if (i %% 3 == 0){ # if divisible by 3
            ndf = df[,((i-2):i)] # subset df into columns
            # Standardise column names
            colnames(ndf)[R]<- 'Red'
            colnames(ndf)[B]<- 'Blue'
            colnames(ndf)[G]<- 'Green'
            # Plot
            plot<- ggplot(data = ndf, aes(x = seq_along(Red),
                                          y = c(Red,Green,Blue)))+
                        geom_line(aes(y = Green), colour = "#66CC99")+
                        geom_line(aes(y = Blue), colour = '#00CCCC')+
                        geom_line(aes(y = Red), colour = '#CC0000')+
                        theme_bw()+
                        scale_x_continuous(breaks= pretty_breaks(n=15))+
                        labs(y = "Intensity",  x="Distance(Pixels)", title = paste("Cell number",
toString(i/3)))
            print (plot)
        }

    }

}
```

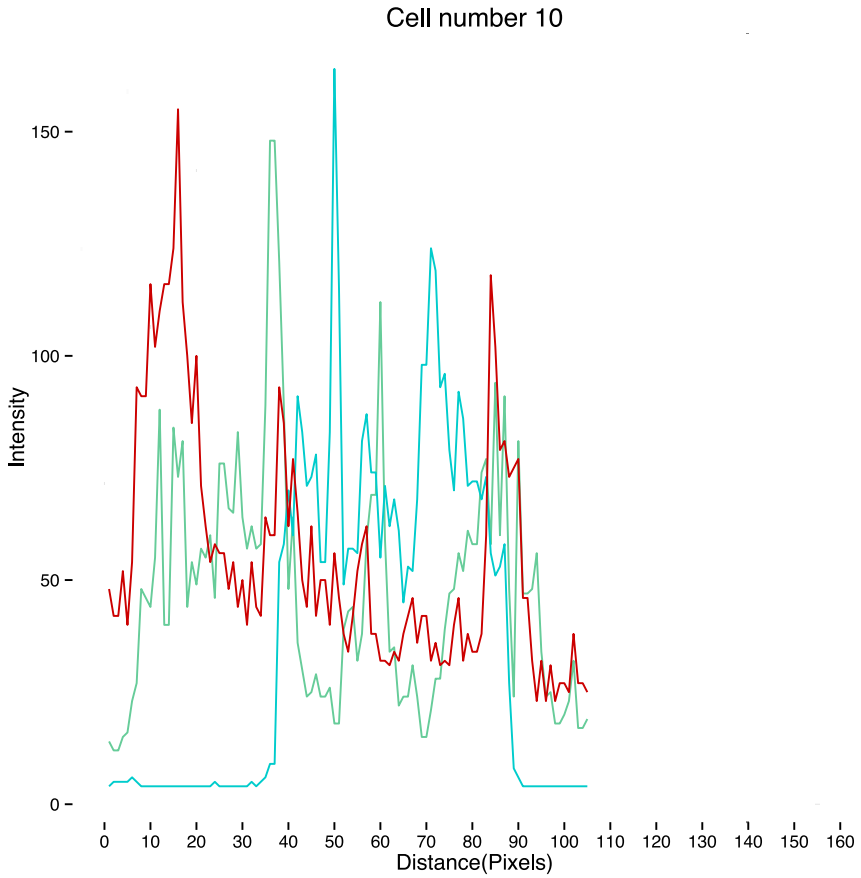

Integrate Area Under Curve: Nucleus vs Total

In [4]:
```
#intensitydata: dataframe with intensity values
#locationdata: dataframe with pixel locations of nucleus and membrane of cells
#POIChannelNumber: Channel (1st,2nd,3rd...) in which protein of interest is at (integer please)
#TotChannelNumebr: Total number of channels measured


IntegrateIntensity<- function(intensitydata, locationdata, POIChannelNumber, TotChannelNumber){
        # Create empty list/vector
    percentdata<- c()
    totalnucleus<- c()
        #for number of cells on frame
    for (cellID in 1:15){#because we only sample 15 cells / image
            # select cols in intensity data
        intensityVals<- intensitydata[,(TotChannelNumber*cellID-(TotChannelNumber-POIChannelNumber))]
        intensityVals<- data_frame(intensityVals)
            #sequence lower, upper bounds for cell, nucleus
        NucleusLower<-locationdata[cellID,"NuclearLower"]
        NucleusUpper<-locationdata[cellID,"NuclearUpper"]

        CellLower<-locationdata[cellID, "CellLower"]
        CellUpper<-locationdata[cellID,"CellUpper"]

        NucleusPosition<- seq(NucleusLower,NucleusUpper,1)
        CellPosition<- seq(CellLower, CellUpper,1)
             #slice intensity values for nucleus, cell
        NucleusIntensity<- slice(intensityVals, NucleusLower:NucleusUpper+1)
        TotalIntensity<- slice(intensityVals, CellLower:CellUpper+1)
            #integrate values
        NucleusVector<- as.vector(as.matrix(NucleusIntensity[,1]))
        NucleusIntegral<- trapz(NucleusPosition, NucleusVector)

        CellVector<- as.vector(as.matrix(TotalIntensity[,1]))
        TotalIntegral<- trapz(CellPosition, CellVector)
            #Percent nuclear expression of protein
        newpercentage<- NucleusIntegral/TotalIntegral * 100
            #Append percent to list
        percentdata<- c(percentdata, newpercentage)
        totalnucleus<- c(totalnucleus, NucleusIntegral)

    };
    return(percentdata) #returns list of percent expression of POI in Nucleus vs whole cell
};
```

Low Dose Pretreatment

In [5]:
```
# import locationdata
locE50V<- read.delim("Bounds50EV.txt", header = TRUE)
locE50L<- read.delim("Bounds50EL.txt", header = TRUE)
locE50L30<- read.delim('Bounds50EL30.txt', header= TRUE)

locC50V<- read.delim('Bounds50CV.txt', header= TRUE)
locC50L<- read.delim('Bounds50CL.txt', header= TRUE)
locC50L30<- read.delim('Bounds50CL30.txt', header= TRUE)
```

In [6]:
```
E50Vintegrated<-IntegrateIntensity(E50V, locE50V, 2, 3)
E50Lintegrated<- IntegrateIntensity(E50L2,locE50L,2,3)
E50L30integrated<- IntegrateIntensity(E50L30,locE50L30,2,3)

C50Vintegrated<- IntegrateIntensity(C50V,locC50V,2,3)
C50Lintegrated<- IntegrateIntensity(C50L2,locC50L,2,3)
C50L30integrated<- IntegrateIntensity(C50L30,locC50L30,2,3)
```

In [7]:
```
# Get percentdata for each condition: NFKB translocation
NT50data<- cbind(E50Vintegrated,E50Lintegrated,E50L30integrated, C50Vintegrated,C50Lintegrated,C50L30integrat
ed)
NT50data<- as.data.frame(NT50data)

NT50data<- rename(NT50data, E50V=E50Vintegrated, E50L_2h=E50Lintegrated , E50L_0.5h=E50L30integrated ,
                  C50V=C50Vintegrated ,C50L_2h=C50Lintegrated, C50L_.5h = C50L30integrated)
NT50data
```

Out[7]:

	E50V	E50L_2h	E50L_0.5h	C50V	C50L_2h	C50L_.5h
1	34.13515	49.41435	50.69896	52.6857	69.55108	56.63092
2	54.44368	54.63185	45.0676	43.16802	70.50127	48.79989
3	51.28242	62.72201	74.30298	37.09862	70.49858	49.29107
4	25.42096	57.92308	75.84045	42.6039	72.9443	67.25072
5	NaN	55.11539	78.57143	69.66663	85.10545	57.75503
6	44.99075	NaN	74.34151	68.41645	69.43417	NA
7	17.74545	50.8934	62.5	37.17567	63.87957	64.33641
8	32.50111	57.51936	60.20897	75.80822	66.72374	41.30956
9	42.08961	50.97701	47.33558	38.23216	46.85004	63.55719
10	47.45881	77.54641	71.64844	66.1391	NaN	NaN
11	NaN	90.25877	71.95213	51.18547	59.92876	68.88489
12	26.35149	72.00531	62.01328	49.46785	50.34602	75.89267
13	31.46447	56.13789	70.51225	71.75036	85.81928	71.23426
14	16.79651	74.24377	NA	53.30273	67.65303	56.24018
15	39.10006	65.86715	82.72312	NaN	70.41569	52.90974

In [8]:
```
summary(NT50data)
```

Out[8]:
```
      E50V          E50L_2h        E50L_0.5h          C50V
 Min.   :16.80   Min.   :49.41   Min.   :45.07   Min.   :37.10
 1st Qu.:26.35   1st Qu.:54.75   1st Qu.:60.66   1st Qu.:42.74
 Median :34.14   Median :57.72   Median :71.08   Median :51.94
 Mean   :35.68   Mean   :62.52   Mean   :66.27   Mean   :54.05
 3rd Qu.:44.99   3rd Qu.:70.47   3rd Qu.:74.33   3rd Qu.:67.85
 Max.   :54.44   Max.   :90.26   Max.   :82.72   Max.   :75.81
 NA's   :2       NA's   :1       NA's   :1       NA's   :1
    C50L_2h         C50L_.5h
 Min.   :46.85   Min.   :41.31
 1st Qu.:64.59   1st Qu.:52.91
 Median :69.49   Median :57.76
 Mean   :67.83   Mean   :59.55
 3rd Qu.:70.50   3rd Qu.:67.25
 Max.   :85.82   Max.   :75.89
 NA's   :1       NA's   :2
```

In [9]:
```
boxplot(NT50data)
```

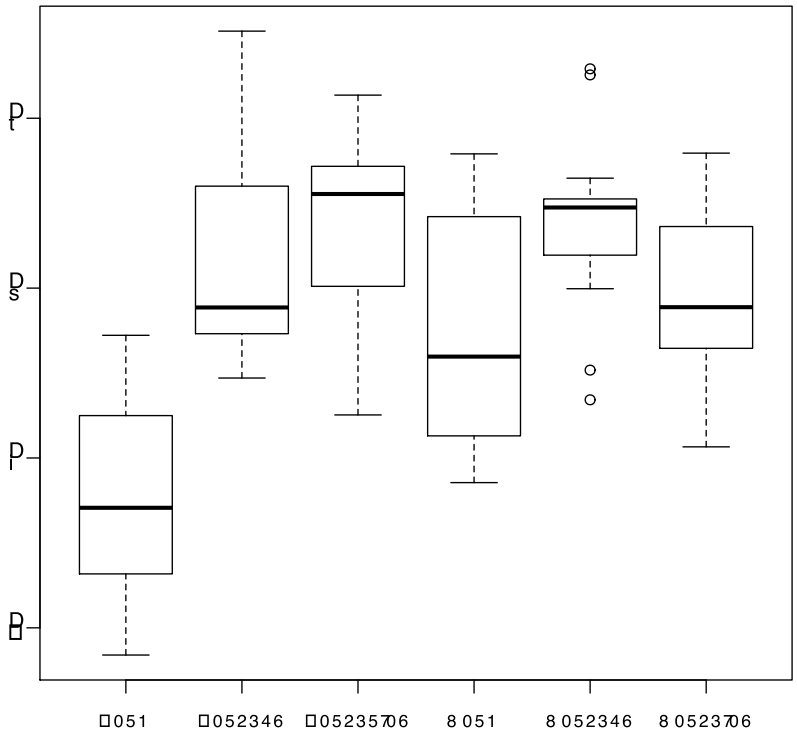

High Dose Pretreatment

In [7]:
```
# import locationdata
locE500V<- read.delim("Bounds500EV.txt", header = TRUE)
locE500L<- read.delim("Bounds500EL.txt", header = TRUE)

locC500V<- read.delim('Bounds500CV.txt', header= TRUE)
locC500L<- read.delim('Bounds500CL.txt', header= TRUE)
locC500L30<- read.delim('Bounds500CL30.txt', header= TRUE)
```

In [8]:
```
E500Vintegrated<-IntegrateIntensity(E500V, locE500V, 2, 3)
E500Lintegrated<- IntegrateIntensity(E500L2,locE500L,2,3)

C500Vintegrated<- IntegrateIntensity(C500V,locC500V,2,3)
C500Lintegrated<- IntegrateIntensity(C500L2,locC500L,2,3)
C500L30integrated<- IntegrateIntensity(C500L30,locC500L30,2,3)
```

In [13]:
```
NT500data<- cbind(E500Vintegrated,E500Lintegrated, C500Vintegrated,C500Lintegrated,C500L30integrated)
NT500data<- as.data.frame(NT500data)

NT500data<- rename(NT500data, E500V=E500Vintegrated, E500L_2h=E500Lintegrated ,
                   C500V=C500Vintegrated ,C500L_2h=C500Lintegrated, C500L_.5h = C500L30integrated)
NT500data
```

Out[13]:

	E500V	E500L_2h	C500V	C500L_2h	C500L_.5h
1	43.59248	72.76596	87.0911	47.38665	NaN
2	30.76873	86.85675	45.94637	40.5487	53.03399
3	46.60729	71.17823	35.0586	44.44255	89.26242
4	34.12591	73.75556	71.99705	NA	41.16588
5	30.04155	82.58776	NA	59.22276	33.64937
6	47.09688	68.61904	47.67692	62.48183	57.07334
7	39.67956	NA	49.73307	42.00438	39.70505
8	29.86581	78.30731	34.11911	68.35373	59.42114
9	35.84985	81.53639	NaN	62.03616	30.17051
10	56.21845	59.55434	34.35863	47.62685	38.51956
11	67.1158	69.02234	55.90644	38.38773	60.52384
12	69.0463	73.63499	53.00102	52.98691	68.07491
13	NaN	44.06502	56.52462	60.5672	53.83221
14	NA	51.39288	70.88091	54.53636	64.66905
15	54.18036	38.66232	48.19877	48.15947	62.08439

In [14]:
```
boxplot(NT500data)
```

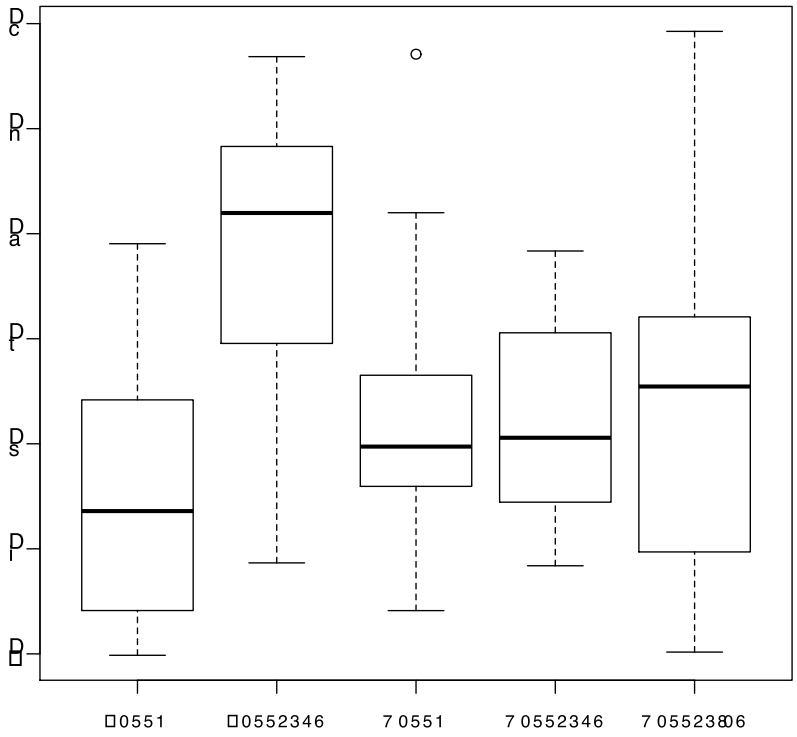

Size data

In [9]:
```
get_size_data <- function(locationData){
    Diameter<- mutate(locationData,
                cellDiameter = CellUpper - CellLower,
                nucleusDiameter = NuclearUpper - NuclearLower)

    Diameter <- mutate(Diameter, nucleusProportion = nucleusDiameter/cellDiameter *100)
    return (Diameter)
};
```

In [10]:
```
locE50V<-get_size_data(locE50V)
locE50L<-get_size_data(locE50L)
locE50L30<-get_size_data(locE50L30)

locE500V<-get_size_data(locE500V)
locE500L<-get_size_data(locE500L)

locC50V<-get_size_data(locC50V)
locC50L<-get_size_data(locC50L)
locC50L30<-get_size_data(locC50L30)

locC500V<-get_size_data(locC500V)
locC500L<-get_size_data(locC500L)
locC500L30<-get_size_data(locC500L30)
```

In [23]:
```
locE50L30
```

Out[23]:

	CellNumber	CellLower	CellUpper	NuclearLower	NuclearUpper	cellDiameter	nucleusDiameter	nucleusProportion
1	1	5	145	20	80	140	60	42.85714
2	2	5	125	65	110	120	45	37.5
3	3	0	100	30	85	100	55	55
4	4	5	95	30	80	90	50	55.55556
5	5	0	110	50	110	110	60	54.54545
6	6	0	110	35	95	110	60	54.54545
7	7	0	105	25	75	105	50	47.61905
8	8	0	125	25	85	125	60	48
9	9	0	135	45	105	135	60	44.44444
10	10	0	130	50	110	130	60	46.15385
11	11	5	100	15	70	95	55	57.89474
12	12	0	145	35	100	145	65	44.82759
13	13	0	105	15	70	105	55	52.38095
14	14	0	140	35	100	140	65	46.42857
15	15	0	100	20	80	100	60	60

In [11]:
```
nucleusDiameterData<- cbind(locE50V$nucleusDiameter,
                            locE50L$nucleusDiameter,
                           locE50L30$nucleusDiameter,
                            locE500V$nucleusDiameter,
                           locE500L$nucleusDiameter,
                            locC50V$nucleusDiameter,
                            locC50L$nucleusDiameter,
                           locC50L30$nucleusDiameter,
                            locC500V$nucleusDiameter,
                            locC500L$nucleusDiameter,
                           locC500L30$nucleusDiameter)


cellDiameterData<- cbind(locE50V$cellDiameter, locE50L$cellDiameter,
                           locE50L30$cellDiameter, locE500V$cellDiameter,
                           locE500L$cellDiameter, locC50V$cellDiameter, locC50L$cellDiameter,
                           locC50L30$cellDiameter, locC500V$cellDiameter, locC500L$cellDiameter,
                          locC500L30$cellDiameter)

nucleusProportionData<- cbind(locE50V$nucleusProportion, locE50L$nucleusProportion,
                           locE50L30$nucleusProportion, locE500V$nucleusProportion,
                           locE500L$nucleusProportion, locC50V$nucleusProportion, locC50L$nucleusProportion,
                           locC50L30$nucleusProportion, locC500V$nucleusProportion, locC500L$nucleusProportio
n,
                          locC500L30$nucleusProportion)
```

In [12]:
```
colnames(nucleusDiameterData)<- c("E50V", "E50L_2h", "E50L_30min", "E500V", "E500L_2h", "C50V", "C50L_2h",
                                  "C50L_30min", "C500V", "C500L_2h", "C500L_30min")

colnames(cellDiameterData)<- c("E50V", "E50L_2h", "E50L_30min", "E500V", "E500L_2h", "C50V", "C50L_2h",
                                  "C50L_30min", "C500V", "C500L_2h", "C500L_30min")

colnames(nucleusProportionData)<- c("E50V", "E50L_2h", "E50L_30min", "E500V", "E500L_2h", "C50V", "C50L_2h",
                                  "C50L_30min", "C500V", "C500L_2h", "C500L_30min")
```

In [19]:
```
boxplot(cellDiameterData)
```

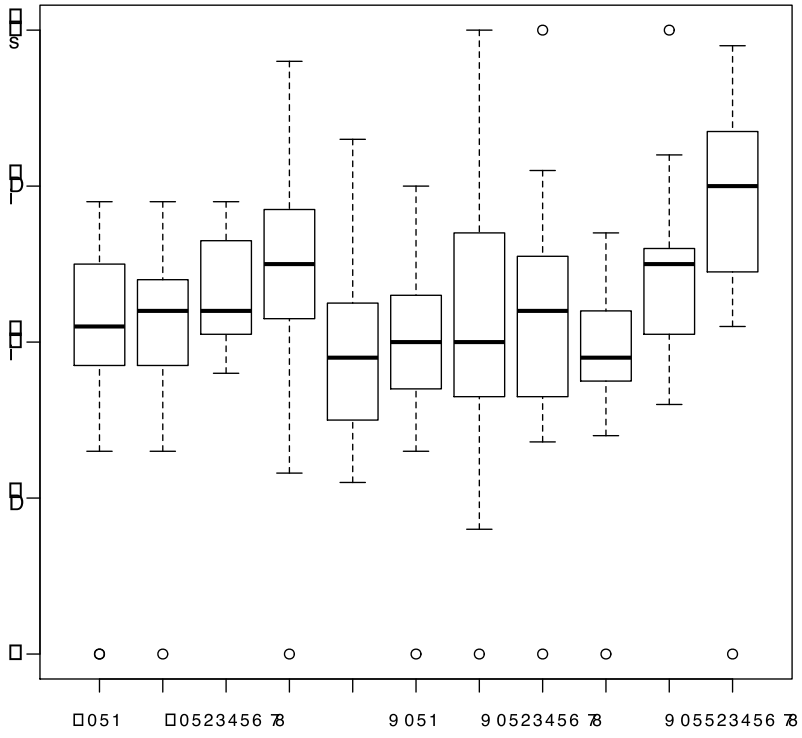

In [26]:
```
boxplot(nucleusDiameterData)
```

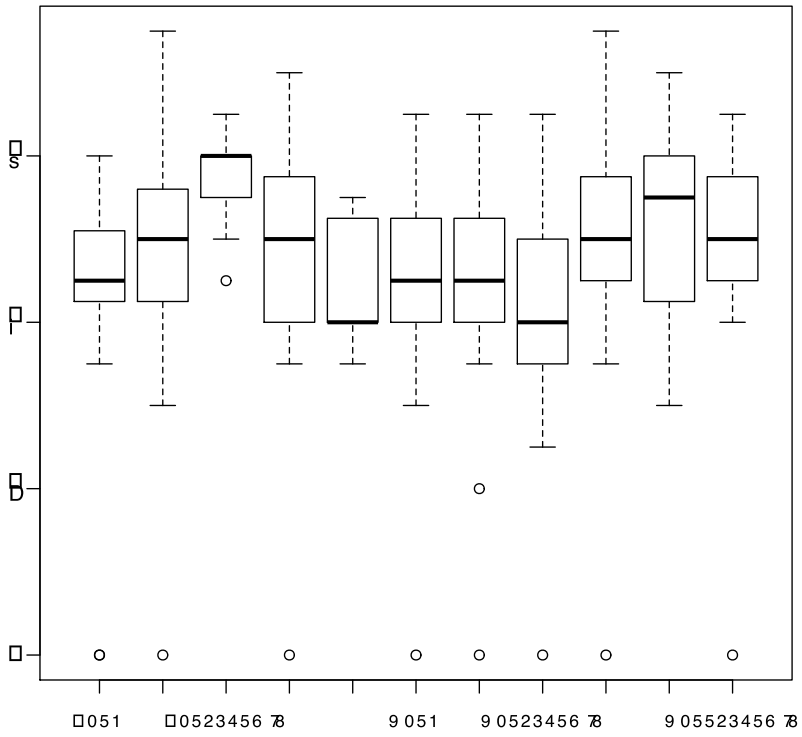

In [20]:
```
boxplot(nucleusProportionData)
```

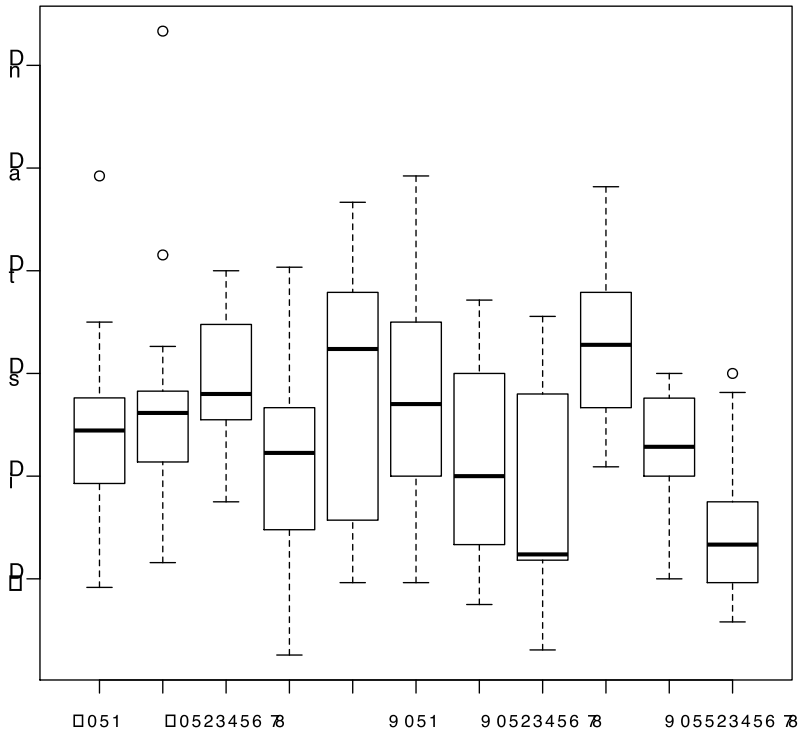

In [13]:
```
nucleusProportionData
```

Out[13]:

E50V	E50L_2h	E50L_30min	E500V	E500L_2h	C50V	C50L_2h	C50L_30min	C500V	C500L_2h	C500L_30min
52.17391	47.27273	42.85714	26.31579	53.33333	55.55556	40.00000	32.25806	68.18182	34.78261	NaN
69.23077	46.15385	37.50000	36.36364	61.53846	37.50000	52.94118	31.81818	48.14815	43.75000	33.33333
47.61905	47.61905	55.00000	41.66667	63.63636	30.00000	50.00000	41.17647	43.47826	42.85714	36.00000
34.48276	45.45455	55.55556	42.85714	66.66667	47.36842	33.33333	55.55556	57.89474	47.36842	25.80645
NaN	40.90909	54.54545	38.09524	57.89474	50.00000	50.00000	31.25000	57.14286	42.30769	27.77778
47.61905	NaN	54.54545	46.66667	38.09524	62.50000	50.00000	30.76923	57.14286	42.30769	42.85714
40.00000	31.57895	47.61905	32.00000	57.89474	29.62963	27.50000	31.81818	52.63158	30.00000	29.62963
41.66667	46.15385	48.00000	44.00000	42.10526	54.54545	37.50000	23.07692	41.66667	50.00000	30.30303
44.44444	40.00000	44.44444	46.15385	53.33333	43.33333	50.00000	32.00000	NaN	37.50000	26.47059
55.00000	61.53846	46.15385	34.78261	33.33333	55.00000	NaN	NaN	40.90909	44.44444	30.76923
NaN	83.33333	57.89474	55.55556	50.00000	40.00000	38.23529	53.33333	52.38095	40.00000	37.50000
29.16667	43.47826	44.82759	60.34483	52.38095	46.66667	33.33333	48.00000	63.15789	47.82609	50.00000
39.28571	41.37931	52.38095	NaN	29.62963	69.23077	57.14286	51.47059	52.94118	48.00000	33.33333
33.33333	52.63158	46.42857	22.58065	33.33333	40.74074	33.33333	47.61905	61.11111	48.00000	34.37500
47.36842	48.27586	60.00000	48.27586	33.33333	NaN	40.00000	32.50000	46.66667	40.00000	48.14815

Percent Nucleucs x Nucleus Proportion

Since there seems to be treatment/pretreatment- dependent shifts in cell morphology, it may be influencing the raw NF-KB proportion results. Test whether proportion of nucleus to cell diameter correlated with NF-kB expression in nucleus.

In [21]:
```
E50Vcor<- cbind(locE50V$nucleusProportion, E50Vintegrated)
E50Lcor<- cbind(locE50L$nucleusProportion, E50Lintegrated)
E50L30cor<- cbind(locE50L30$nucleusProportion, E50L30integrated)

C50Vcor<- cbind(locC50V$nucleusProportion, C50Vintegrated)
C50Lcor<- cbind(locC50L$nucleusProportion, C50Lintegrated)
C50L30cor<- cbind(locC50L30$nucleusProportion, C50L30integrated)

E500Vcor<- cbind(locE500V$nucleusProportion, E500Vintegrated)
E500Lcor<- cbind(locE500L$nucleusProportion, E500Lintegrated)

C500Vcor<- cbind(locC500V$nucleusProportion, C500Vintegrated)
C500Lcor<- cbind(locC500L$nucleusProportion, C500Lintegrated)
C500L30cor<- cbind(locC500L30$nucleusProportion, C500L30integrated)
```

In [22]:
```
# rename columns

rename_columns_proportions<- function(df){
    colnames(df)[1]<- "Percent_Nucleus"
    colnames(df)[2]<- "Percent_NFKB_Nucleus"
    return(df)
}
```

In [23]:
```
E50Vcor<- rename_columns_proportions(E50Vcor)
E50Lcor<- rename_columns_proportions(E50Lcor)
E50L30cor<- rename_columns_proportions(E50L30cor)

C50Vcor<- rename_columns_proportions(C50Vcor)
C50Lcor<- rename_columns_proportions(C50Lcor)
C50L30cor<- rename_columns_proportions(C50L30cor)

E500Vcor<- rename_columns_proportions(E500Vcor)
E500Lcor<- rename_columns_proportions(E500Lcor)

C500Vcor<- rename_columns_proportions(C500Vcor)
C500Lcor<- rename_columns_proportions(C500Lcor)
C500L30cor<- rename_columns_proportions(C500L30cor)
```

In [24]:
```
# plot Percent expression of NFKB in Nucleus x Proportion of nucleus to cell diameter
    #x axis: Porportion of nucleus to cell diameter
    #y axis: Percent expression of NFKB in Nucleus

par(mfrow = c(2,3))
plot(E50Vcor)
plot(E50Lcor)
plot(E50L30cor)
plot(C50Vcor)
plot(C50Lcor)
plot(C50L30cor)
```

50 nM plots

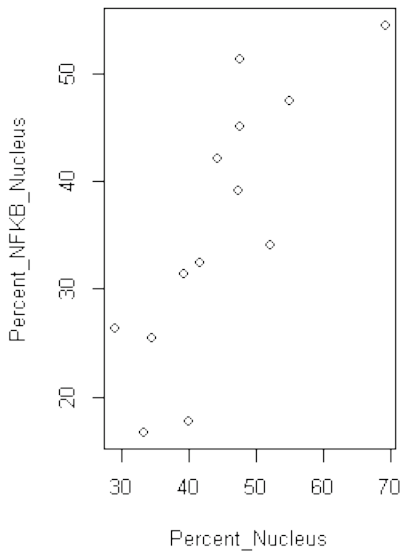
Percent_NFKB_Nucleus
Percent_Nucleus
20
30
40
50
30
40
50
60
70

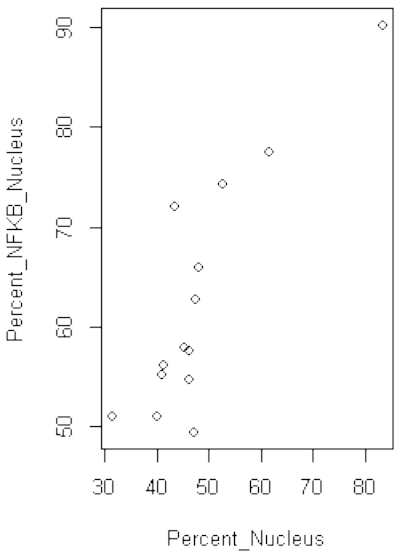
Percent_NFKB_Nucleus
Percent_Nucleus
50
60
70
80
90
30
40
50
60
70
80

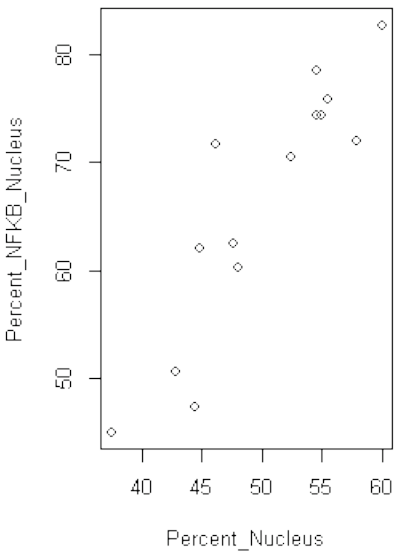
Percent_NFKB_Nucleus
Percent_Nucleus
50
60
70
80
40
45
50
55
60

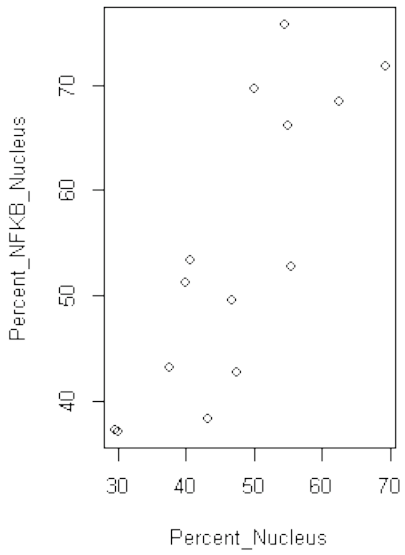
Percent_NFKB_Nucleus
Percent_Nucleus
40
50
60
70
30
40
50
60
70

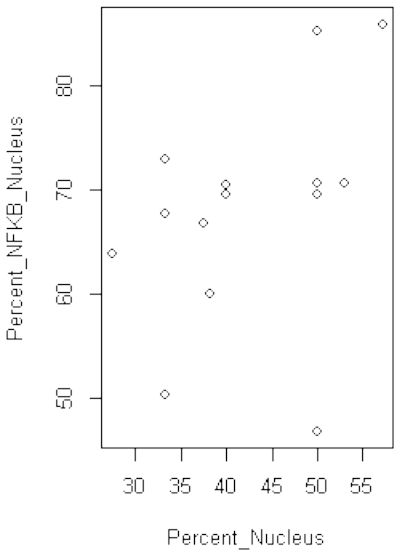
Percent_NFKB_Nucleus
Percent_Nucleus
50
60
70
80
30
35
40
45
50
55

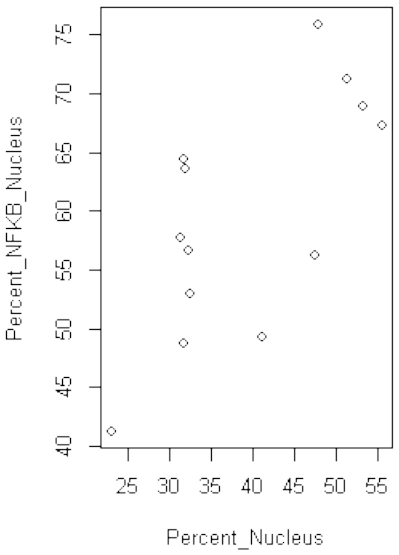
Percent_NFKB_Nucleus
Percent_Nucleus
40
45
50
55
60
65
70
75
25
30
35
40
45
50
55

500 nM plots

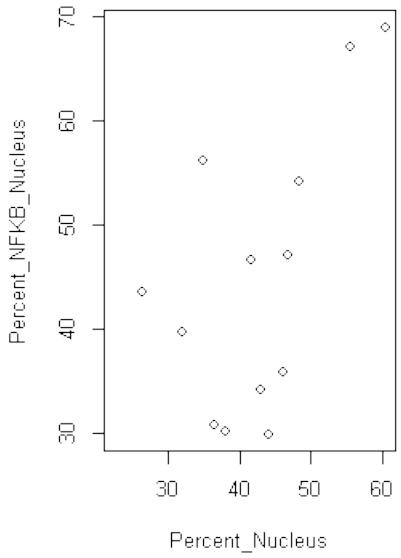
Percent_NFKB_Nucleus
Percent_Nucleus
30
40
50
60
70

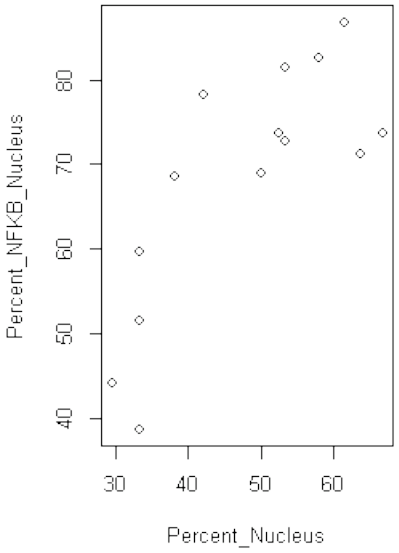
Percent_NFKB_Nucleus
Percent_Nucleus
40
50
60
70
80

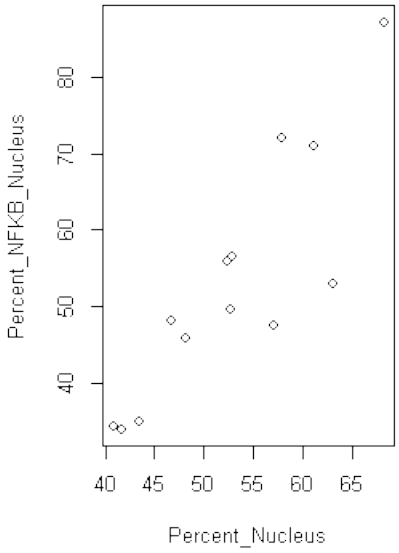
Percent_NFKB_Nucleus
Percent_Nucleus
40
50
60
70
80

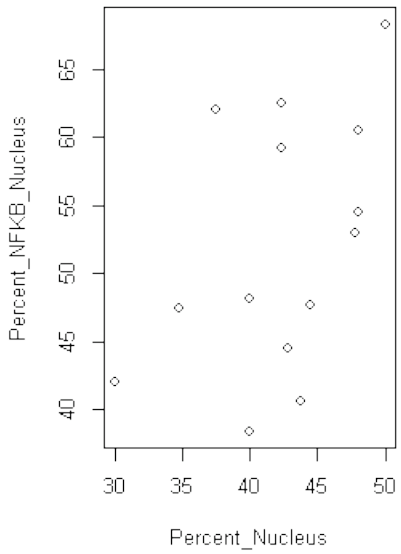
Percent_NFKB_Nucleus
Percent_Nucleus
40
45
50
55
60
65

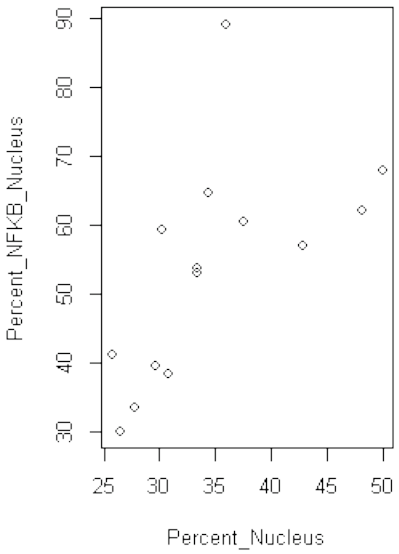
Percent_NFKB_Nucleus
Percent_Nucleus
30
40
50
60
70
80
90

In [25]:
```
par(mfrow = c(2,3))
plot(E500Vcor)
plot(E500Lcor)

plot(C500Vcor)
plot(C500Lcor)
plot(C500L30cor)
```

Appears that percent of NFKB expression in nuceus can be mostly explained by variation of cell diameter (proportion of nucleus to cell diameter)

. Ameboid cells have higher proportiono of NFKB in nucleus

. This effect is unaffacted by presence of LPS

. cell shape contributes to nucelar translocation?, or artefact of dataset?

=> normalise percentage by nucleus diameter: (NFKB proportion in nucleus) / (proportion of nucleus to cell diameter)

Get normalised values

In [26]:
```
# generate  (NFKB proportion in nucleus) / (proportion of nucleus to cell diameter) for each condition

make_ratios<- function(df){
    df<- as.data.frame(df)
    df<- mutate(df, ratio = Percent_NFKB_Nucleus/ Percent_Nucleus )
    return(df)
}
```

In [27]:
```
E50Vcor<- make_ratios(E50Vcor)
E50Lcor<- make_ratios(E50Lcor)
E50L30cor<- make_ratios(E50L30cor)

C50Vcor<- make_ratios(C50Vcor)
C50Lcor<- make_ratios(C50Lcor)
C50L30cor<- make_ratios(C50L30cor)

E500Vcor<- make_ratios(E500Vcor)
E500Lcor<- make_ratios(E500Lcor)

C500Vcor<- make_ratios(C500Vcor)
C500Lcor<- make_ratios(C500Lcor)
C500L30cor<- make_ratios(C500L30cor)
```

In [28]:
```
# Low dose ratios
Low_dose_ratios<- cbind(E50Vcor$ratio, E50Lcor$ratio,E50L30cor$ratio,C50Vcor$ratio,C50Lcor$ratio,C50L30cor$ra
tio)
colnames(Low_dose_ratios)<- c("E50V", "E50L_2h", "E50L_30min", "C50V", "C50L_2h",
                                  "C50L_30min")

# High dose ratios

High_dose_ratios<- cbind(E500Vcor$ratio, E500Lcor$ratio,C500Vcor$ratio,C500Lcor$ratio,C500L30cor$ratio)
colnames(High_dose_ratios)<- c("E500V", "E500L_2h", "C500V", "C500L_2h",
                                  "C500L_30min")
```

In [29]:
```
#Plot Before(left) and after(right) correcting for Nucleus proportion
par(mfrow = c(1,2))
boxplot(NT50data)
boxplot(Low_dose_ratios)
```

50 nM before and after normalisation

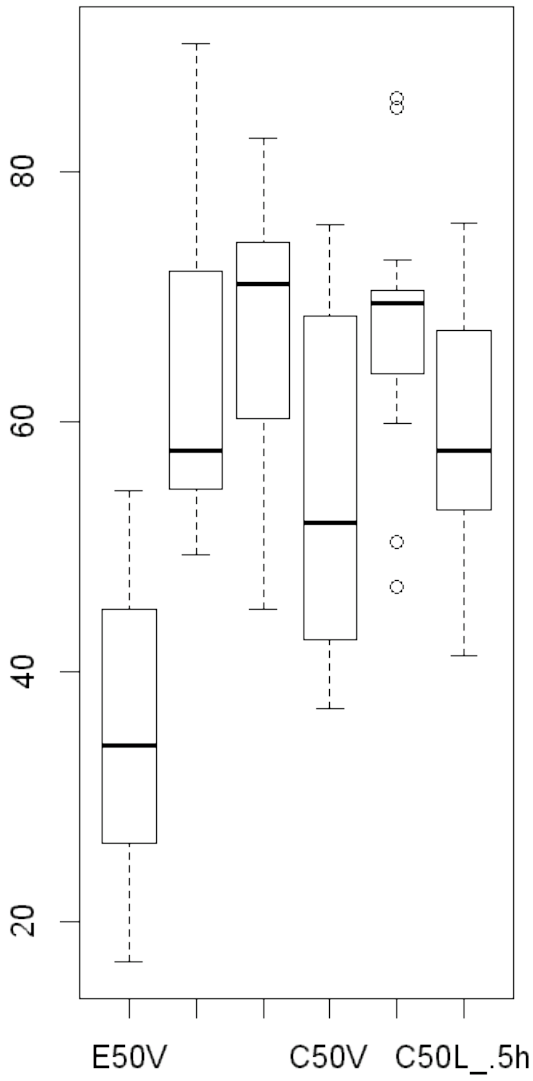

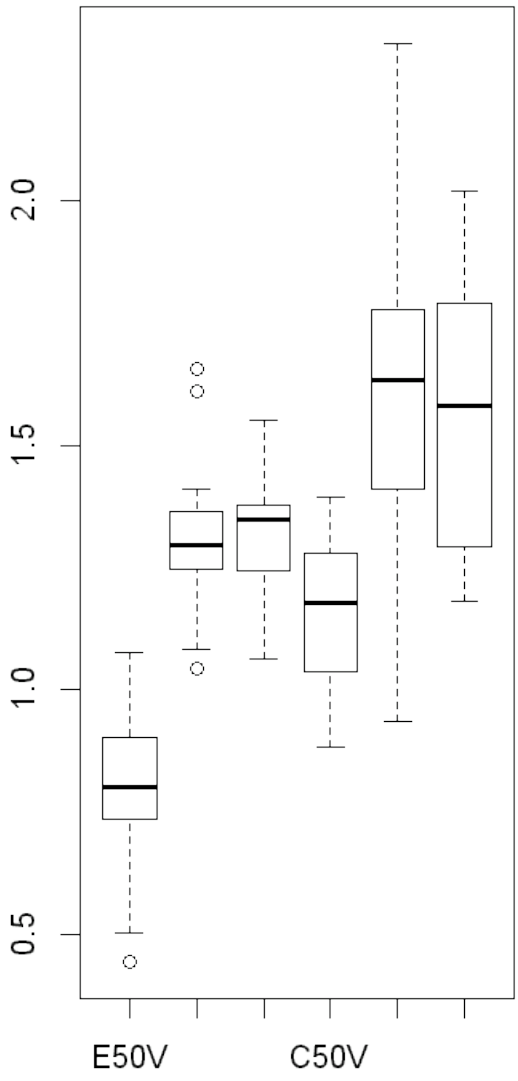

500 nM before and after normalisation

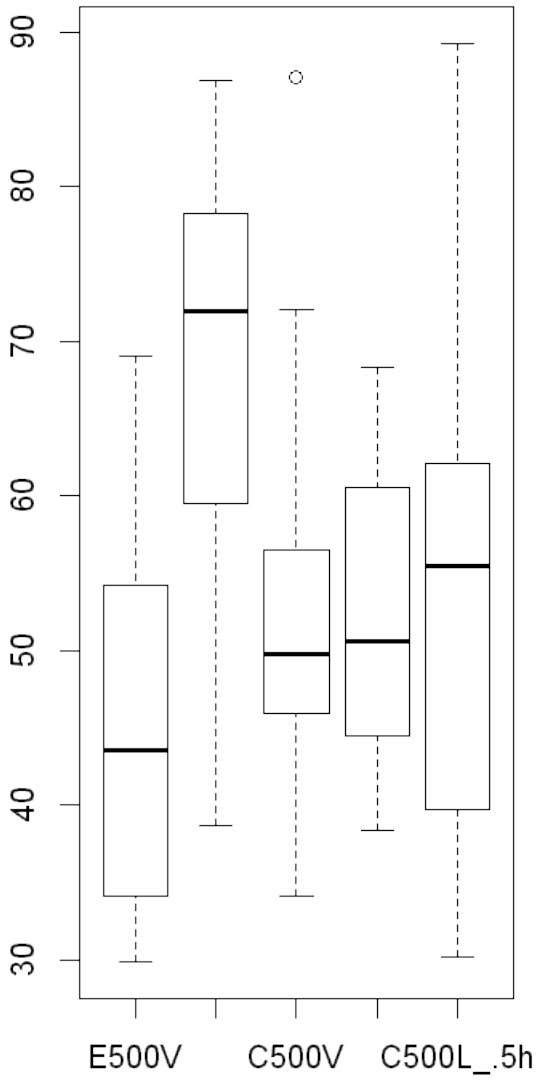

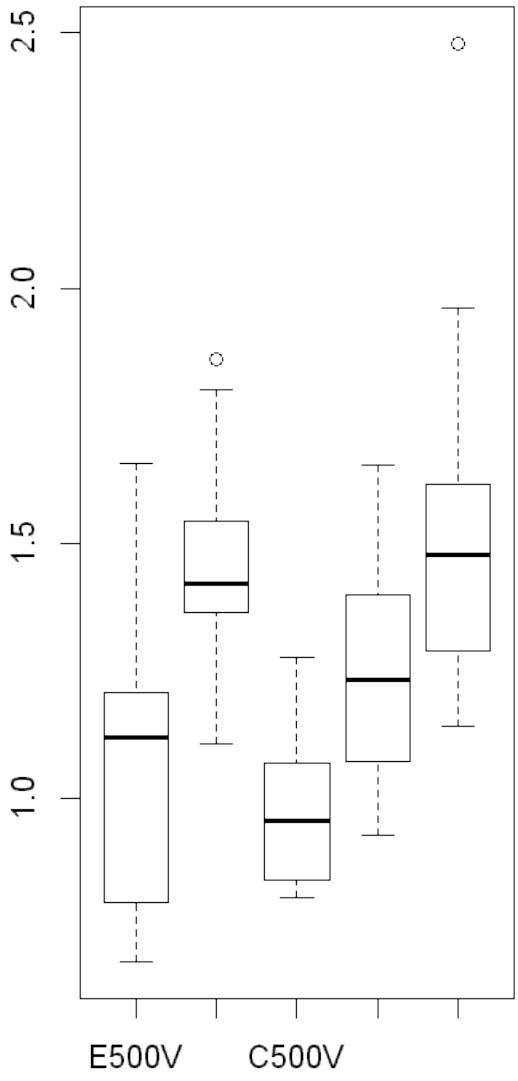

In [30]:
```
par(mfrow = c(1,2))
boxplot(NT500data)
boxplot(High_dose_ratios)
```

In [32]:
```
library(psych)

describe(Low_dose_ratios)
```

Out[32]:

	vars	n	mean	sd	median	trimmed	mad	min	max	range	skew	kurtosis
E50V	1	13	0.7897624	0.1764612	0.8009137	0.7951222	0.1520641	0.4436362	1.076931	0.6332947	-0.4795737	-0.654628
E50L_2h	2	14	1.316505	0.1694965	1.295794	1.310804	0.0959756	1.045304	1.656122	0.6108185	0.443465	-0.429241
E50L_30min	3	14	1.317115	0.1207205	1.348553	1.318514	0.09486875	1.065051	1.552383	0.4873323	-0.1999644	-0.334972
C50V	4	14	1.152659	0.1707266	1.176838	1.155134	0.1840753	0.8822807	1.393333	0.5110519	-0.1754017	-1.40277
C50L_2h	5	14	1.65488	0.3626509	1.634738	1.659036	0.2737829	0.9370009	2.322894	1.385893	0.09250099	-0.578346
C50L_30min	6	13	1.56992	0.2992004	1.581097	1.564174	0.3959489	1.181044	2.022001	0.8409576	0.05231222	-1.585078

In [ ]:

HMGB1 localisation in primary microglia (Translocator 0.0.2)

Aims:

1) Localise HMGB1 expression within the cell using confocal microscopy - main determinant of nuclear vs cytoplasmic expression

2) Expression profile within each cell (ie. is the expression predominantly in the nucleus or cytoplasm? Requires retention of pixel intensity, colocalisation algorithms therefore NOT suitable)

Challenges:

1) Due to the low microglia yields and sparse distribution on each coverslip during imaging, more images per sample required to achieve larger cell numbers

2) Due to the heterogeneity of morphology between cells (ie. some cells clump, some appear rounded, while some retain processess and remain stretched out), previous method developed for BV2 cells using cell diameter for localisation is not suitable

3) Inconsistent stain intensity and z-position of cells in each image hinders automation across all cells per image, since fluorescent signal obtained from these cells will be inaccurate in determining out-of-plane expressions. A more directed approach is therefore required.

Experimental parameters

1) After isolation, seed adult primary microglia at 1E^5 cells per well in a poly-D-lysine coated 8-well ibidi slide

2) After overnight incubation, administer either 500nM CORT or vehicle for a further 24hr

Imaging parameters

1) Take at least 3 images per sample to obtain required cell numbers (>20)

2) Use 63x water immersion objective and capture image at 1024x1024 resolution

3) Channels:

```
- DAPI Nucleus (405nm, blue) - gain  600V - 850V, pinhole between 130um -2
00um, line average 4
- HMGB1 (488nm, green) - gain between 850V - 950V, pinhole  200um - 300um,
 line average 8, frame average 2
- WGA Cell Membrane (633nm, red) gain  650V - 850V, pinhole  150um - 250 u
m, line average 8, frame average 2
```

Image analysis

Image J macro (saveParticles.ijm)

/* Particle analysis Input: Thresholded image Outputs:

```
    1) Identifies Particles above 10 um^2 area

    2) Saves ROI list (in zip), Summary results, thresholded image and particl
    es identified to desktop
```

Contact details:

JJliujj90@gmail.com (mailto:liujj90@gmail.com)

*/

```
macro "saveParticles" {

// set name vars

home = getDirectory("home"); // Returns the path to users home directory.

if (home == "")

exit("No desktop directory available");

image_name = getTitle();

names = getString("Input filename to save", image_name);

saveAs("PNG", home + "Desktop/" + names + "_threshold.png");

// Run particle analysis

run("Analyze Particles...", "size=10-Infinity show=Masks clear include summarize record add");

saveAs("PNG", home + "Desktop/" + names + "_mask.png");

run("Summarize");

saveAs("Results", home + "Desktop/" + names + "_data.csv");

roiManager("Save", home + "Desktop/" + names + "_ROI.zip");

// clear output

array1 = newArray("0");;

for (i=1; i<roiManager("count"); i++){

    array1 = Array.concat(array1,i);

    Array.print(array1);


};

roiManager("Select", array1);
```

Example workflow

1) load image from .lif file (confocal output) in an RGB stack, save image as tiff to working directory

2) Convert stack to individual image file: Image>Stack>Stack to Images

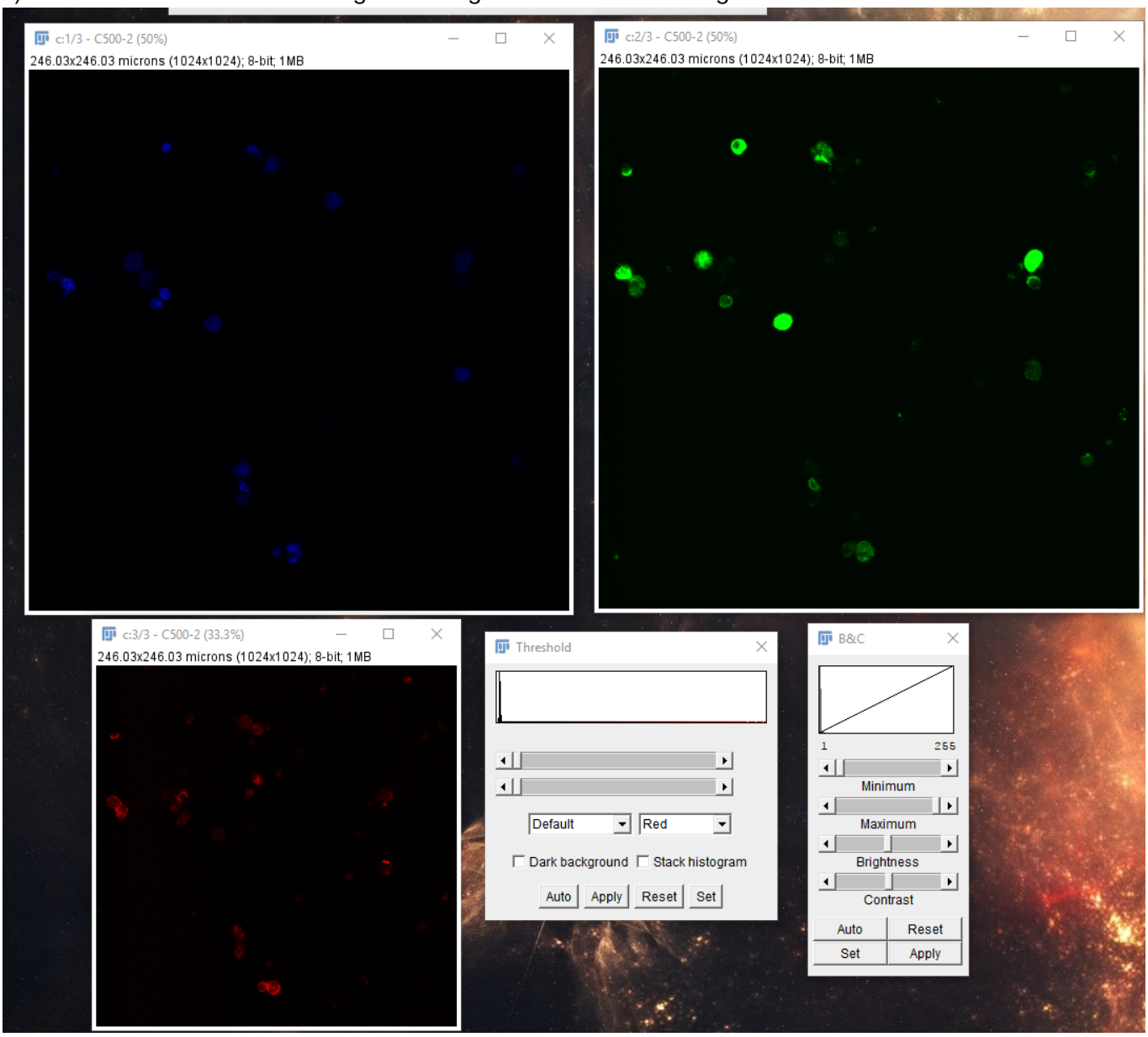

3) Run threshold to identify cells and HMGB1 signal on blue and green channels respectively

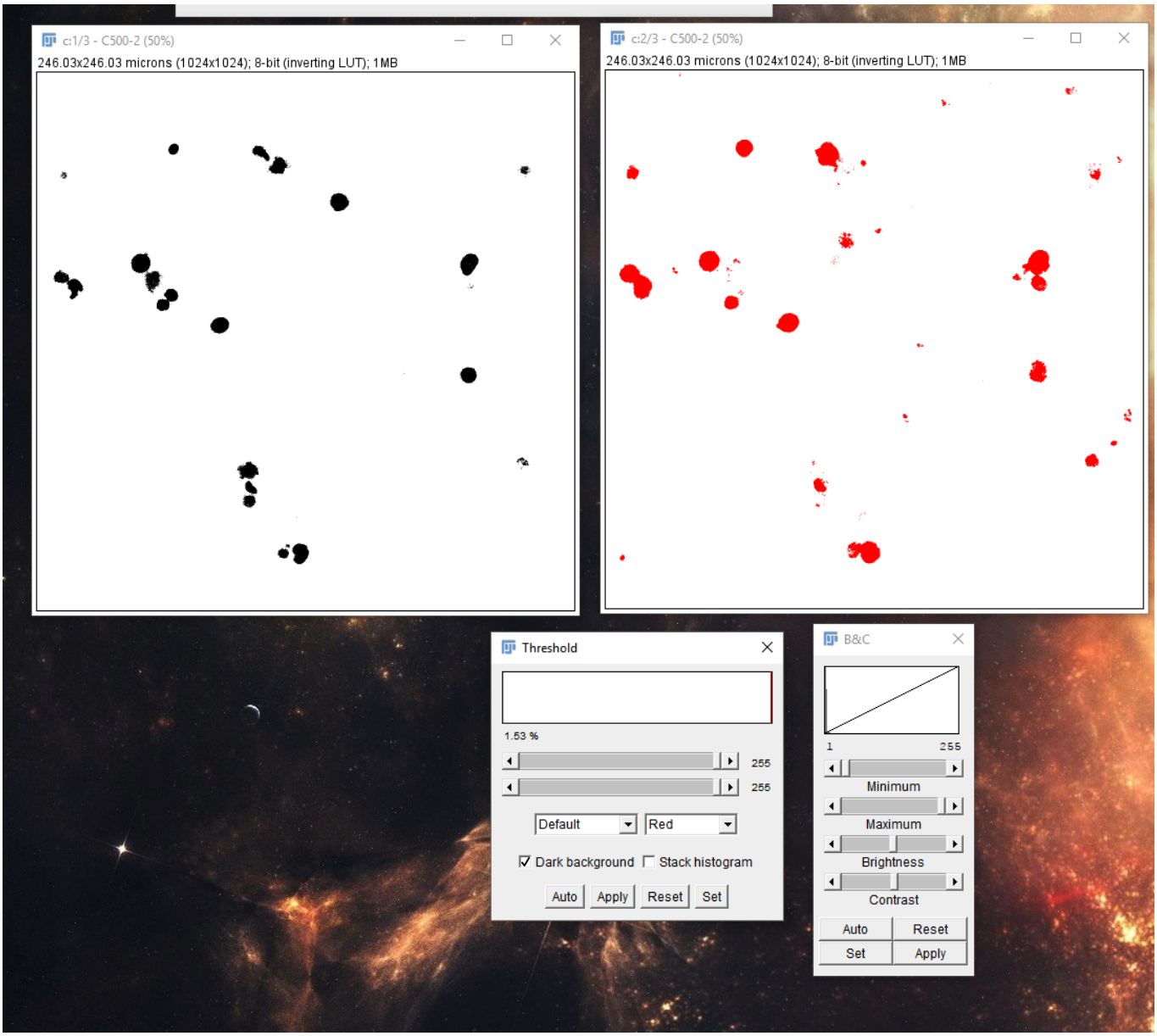

4) Run macro on both green and blue channels separately: saveParticles.ijm. A popup box will prompt for filename (files will be saved using this supplied name. Supply a different name for HMGB1 and DAPI channels). After input, 2 new windows will pop up:

```
A) An image mask identifying the particles. Scan through this image to vis
ually check if these particles represent the source image well.

B) Results window containing data for each particle identified

The mask image, summary data, ROI for each particle and thresholded image
 will all be saved onto the desktop
```

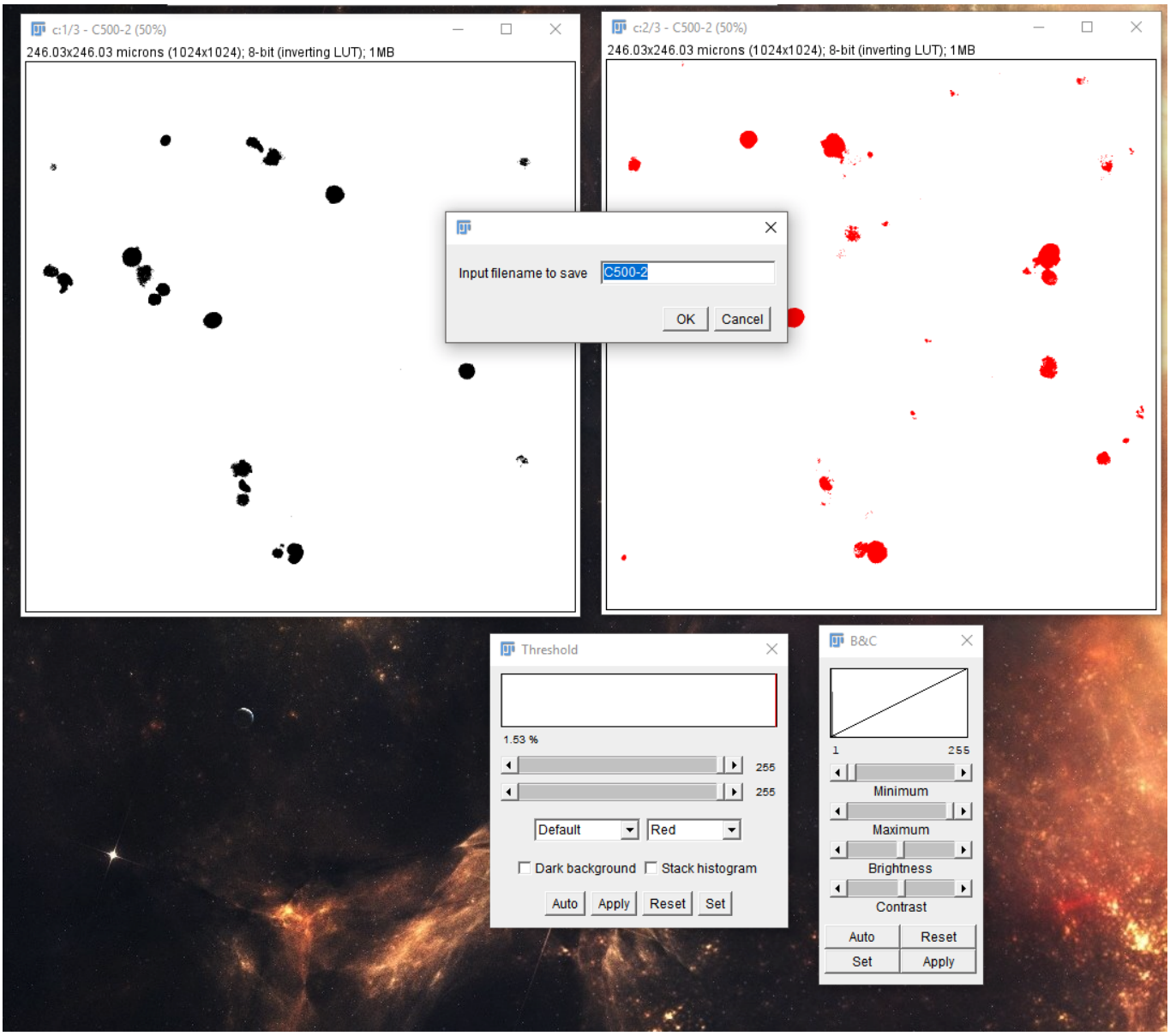
c:1/3 - C500-2 (50%)
246.03x246.03 microns (1024x1024); 8-bit (inverting LUT); 1MB
c:2/3 - C500-2 (50%)
246.03x246.03 microns (1024x1024); 8-bit (inverting LUT); 1MB
Input filename to save
C500-2
OK
Cancel
Threshold
1.53 %
255
255
Default
Red
Dark background
Stack histogram
Auto
Apply
Reset
Set
B&C
1
255
Minimum
Maximum
Brightness
Contrast
Auto
Reset
Set
Apply

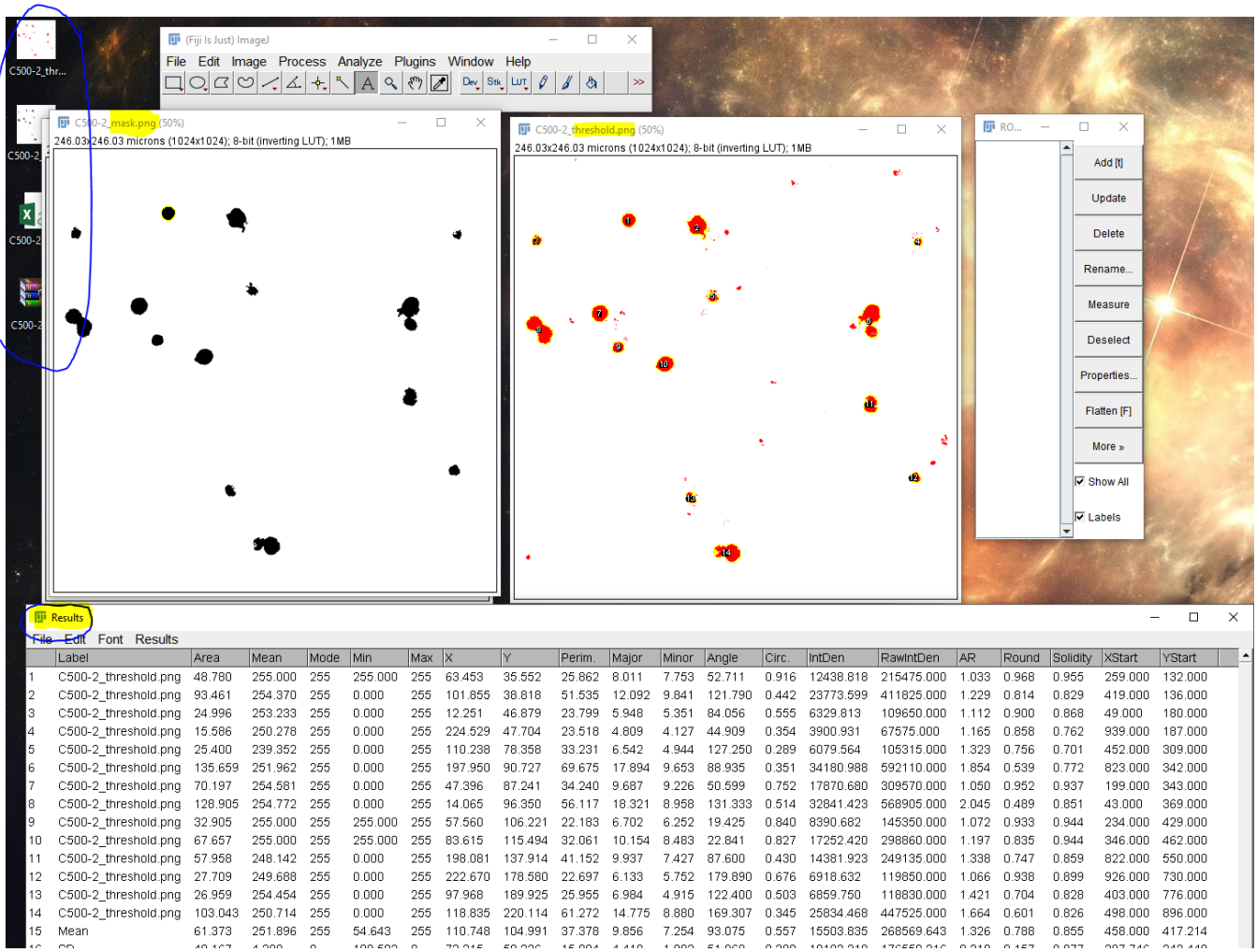

	Label	Area	Mean	Mode	Min	Max	X	Y	Perim.	Major	Minor	Angle	Circ.	IntDen	RawIntDen	AR	Round	Solidity	XStart	YStart
1	C500-2_threshold.png	48.780	255.000	255	255.000	255	63.453	35.552	25.862	8.011	7.753	52.711	0.916	12438.818	215475.000	1.033	0.968	0.955	259.000	132.000
2	C500-2_threshold.png	93.461	254.370	255	0.000	255	101.855	38.818	51.535	12.092	9.841	121.790	0.442	23773.599	411825.000	1.229	0.814	0.829	419.000	136.000
3	C500-2_threshold.png	24.996	253.233	255	0.000	255	12.251	46.879	23.799	5.948	5.351	84.056	0.555	6329.813	109650.000	1.112	0.900	0.868	49.000	180.000
4	C500-2_threshold.png	15.586	250.278	255	0.000	255	224.529	47.704	23.518	4.809	4.127	44.909	0.354	3900.931	67575.000	1.165	0.858	0.762	939.000	187.000
5	C500-2_threshold.png	25.400	239.352	255	0.000	255	110.238	78.358	33.231	6.542	4.944	127.250	0.289	6079.564	105315.000	1.323	0.756	0.701	452.000	309.000
6	C500-2_threshold.png	135.659	251.962	255	0.000	255	197.950	90.727	69.675	17.894	9.653	88.935	0.351	34180.988	592110.000	1.854	0.539	0.772	823.000	342.000
7	C500-2_threshold.png	70.197	254.581	255	0.000	255	47.396	87.241	34.240	9.687	9.226	50.599	0.752	17870.680	309570.000	1.050	0.952	0.937	199.000	343.000
8	C500-2_threshold.png	128.905	254.772	255	0.000	255	14.065	96.350	56.117	18.321	8.958	131.333	0.514	32841.423	568905.000	2.045	0.489	0.851	43.000	369.000
9	C500-2_threshold.png	32.905	255.000	255	255.000	255	57.560	106.221	22.183	6.702	6.252	19.425	0.840	8390.682	145350.000	1.072	0.933	0.944	234.000	429.000
10	C500-2_threshold.png	67.657	255.000	255	255.000	255	83.615	115.494	32.061	10.154	8.483	22.841	0.827	17252.420	298860.000	1.197	0.835	0.944	346.000	462.000
11	C500-2_threshold.png	57.958	248.142	255	0.000	255	198.081	137.914	41.152	9.937	7.427	87.600	0.430	14381.923	249135.000	1.338	0.747	0.859	822.000	550.000
12	C500-2_threshold.png	27.709	249.688	255	0.000	255	222.670	178.580	22.697	6.133	5.752	179.890	0.676	6918.632	119850.000	1.066	0.938	0.899	926.000	730.000
13	C500-2_threshold.png	26.959	254.454	255	0.000	255	97.968	189.925	25.955	6.984	4.915	122.400	0.503	6859.750	118830.000	1.421	0.704	0.828	403.000	776.000
14	C500-2_threshold.png	103.043	250.714	255	0.000	255	118.835	220.114	61.272	14.775	8.880	169.307	0.345	25834.468	447525.000	1.664	0.601	0.826	498.000	896.000
15	Mean	61.373	251.896	255	54.643	255	110.748	104.991	37.378	9.856	7.254	93.075	0.557	15503.835	268569.643	1.326	0.788	0.855	458.000	417.214

5) Save all files created to a working directory

6) From working directory, reload .tiff source fill (RGB stack)

7) On ROImanger, load nuclei ROI, select all ROI and change ROI color to red ROImanager>properties>color = red.

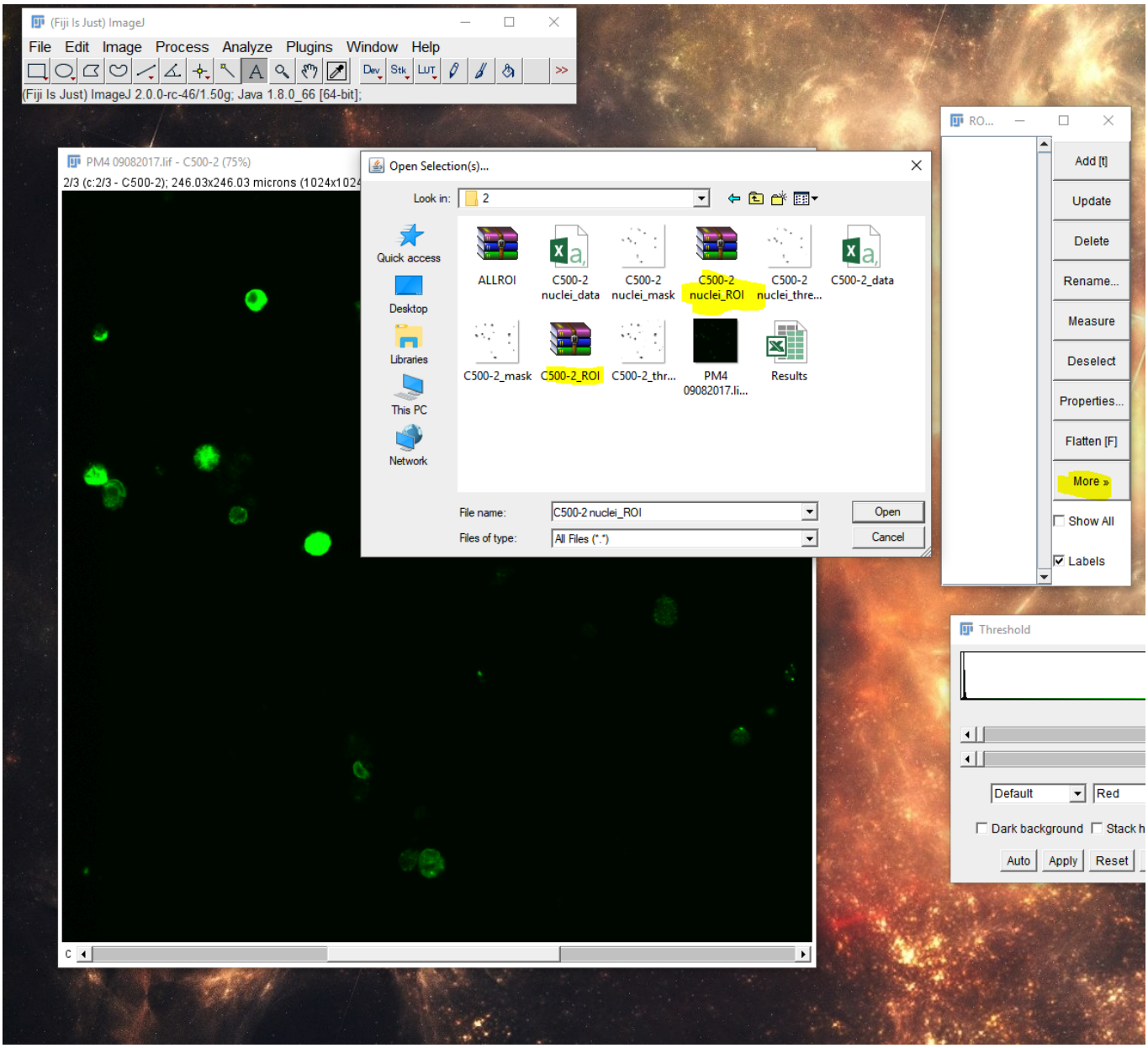

8) On the HMGB1-signal containing channel, go through each nucleus ROI and rename (select ROI>roiManager>rename) each ROI as either a HMGB1-expressing cell (recommended naming scheme: cellnumber_B), or non-HMGB1 expressing cell (NO_cellnumber)

9) on ROImanager, load HMGB1 ROI, and toggle through all ROI to make sure each HMGB1 ROI is paired with a nucleus ROI. Rename each as either a HMGB1-expression cell (cellnunber_G), or non-specific signal (NO_green_cell number)

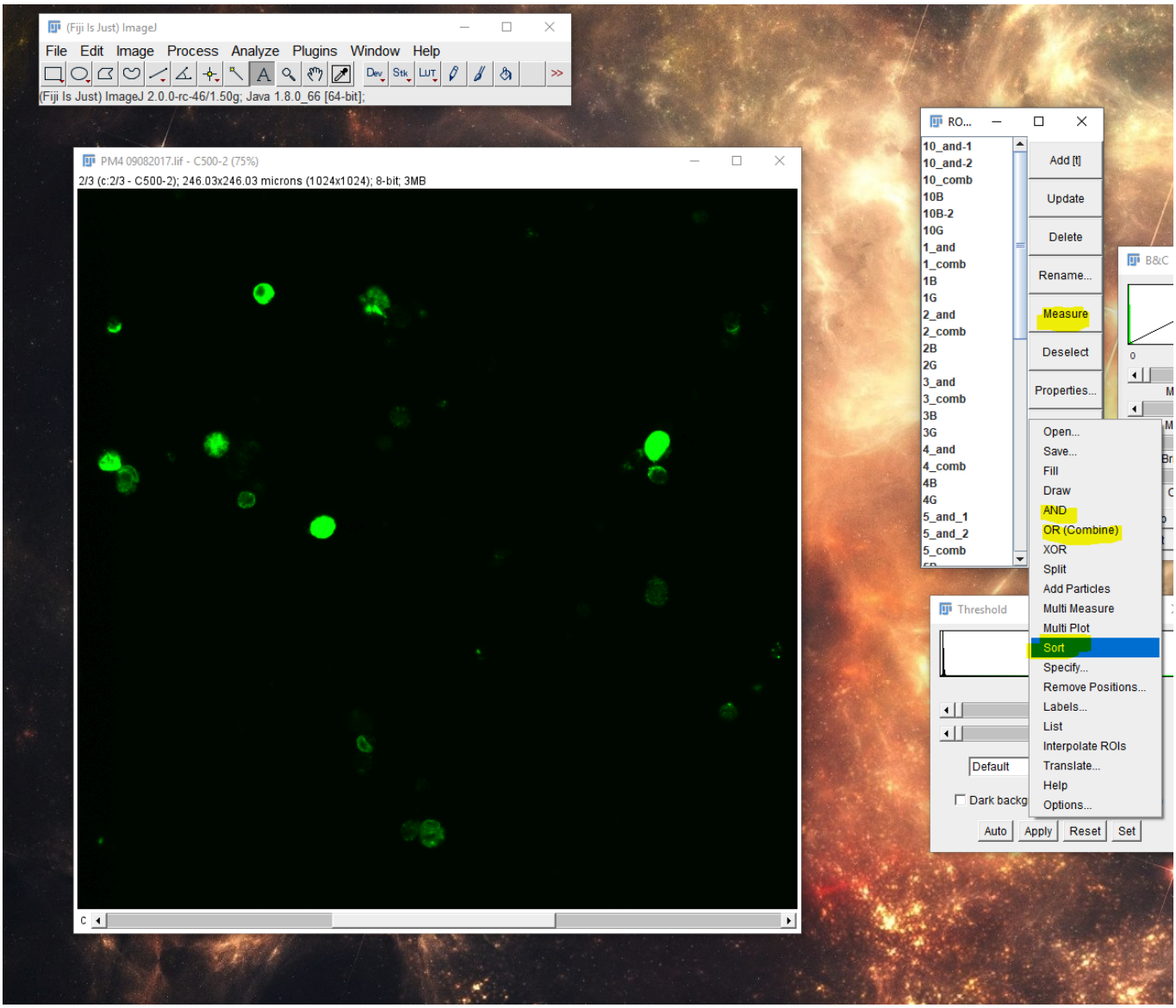

10) Once done, sort all ROI using ROImanager>more>sort

11) Create composite ROI using each paired ROI: select pair of ROI>ROImanager>more>OR(combine)>[t] for combined ROI (nucleus plus HMGB1), and ROImanager>more>AND>[t] (overlap between nucleus and HMGB1 signal)

12) Rename each composite ROI as either cellnumber_comb or cellnumber_and. Sort again

13) Select all ROI and show all to double check if everything makes sense

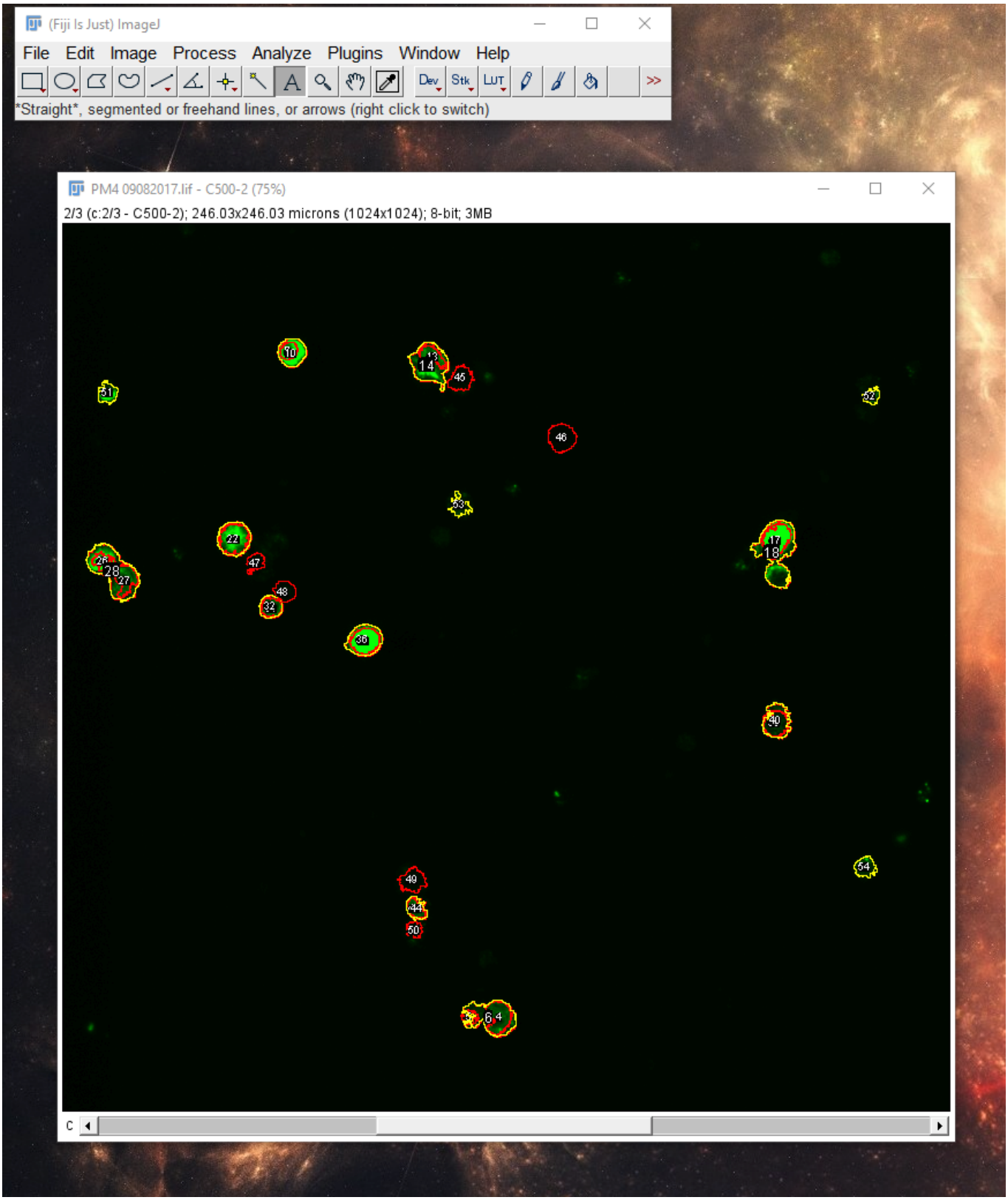

14) run measure ROImanager>measure. A window will popup containing all summry data for each ROI. Save data to file in working directory. Most important output: labels (contains the ROI names to ensure everything is matched); Area; Mean (pixel intensity); integrated density (summed pixel intensity * Area)

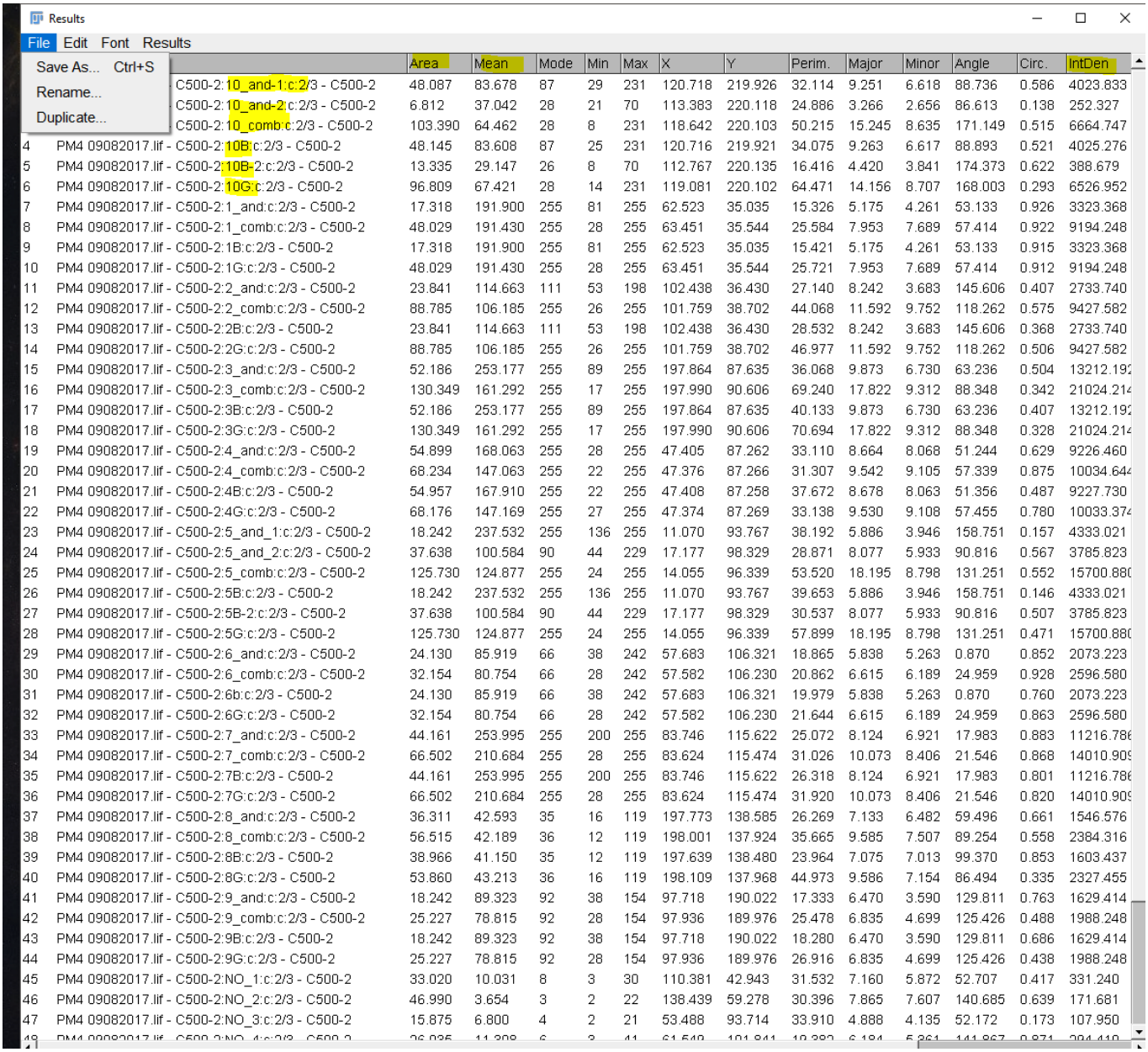

Results

File Edit Font Results

Save As... Ctrl+S
Rename...
Duplicate...

		Area	Mean	Mode	Min	Max	X	Y	Perim.	Major	Minor	Angle	Circ.	IntDen
	C500-2:10_and-1:c:2/3 - C500-2	48.087	83.678	87	29	231	120.718	219.926	32.114	9.251	6.618	88.736	0.586	4023.833
	C500-2:10_and-2:c:2/3 - C500-2	6.812	37.042	28	21	70	113.383	220.118	24.886	3.266	2.656	86.613	0.138	252.327
	C500-2:10_comb:c:2/3 - C500-2	103.390	64.462	28	8	231	118.642	220.103	50.215	15.245	8.635	171.149	0.515	6664.747
4	PM4 09082017.lif - C500-2:10B:c:2/3 - C500-2	48.145	83.608	87	25	231	120.716	219.921	34.075	9.263	6.617	88.893	0.521	4025.276
5	PM4 09082017.lif - C500-2:10B-2:c:2/3 - C500-2	13.335	29.147	26	8	70	112.767	220.135	16.416	4.420	3.841	174.373	0.622	388.679
6	PM4 09082017.lif - C500-2:10G:c:2/3 - C500-2	96.809	67.421	28	14	231	119.081	220.102	64.471	14.156	8.707	168.003	0.293	6526.952
7	PM4 09082017.lif - C500-2:1_and:c:2/3 - C500-2	17.318	191.900	255	81	255	62.523	35.035	15.326	5.175	4.261	53.133	0.926	3323.368
8	PM4 09082017.lif - C500-2:1_comb:c:2/3 - C500-2	48.029	191.430	255	28	255	63.451	35.544	25.584	7.953	7.689	57.414	0.922	9194.248
9	PM4 09082017.lif - C500-2:1B:c:2/3 - C500-2	17.318	191.900	255	81	255	62.523	35.035	15.421	5.175	4.261	53.133	0.915	3323.368
10	PM4 09082017.lif - C500-2:1G:c:2/3 - C500-2	48.029	191.430	255	28	255	63.451	35.544	25.721	7.953	7.689	57.414	0.912	9194.248
11	PM4 09082017.lif - C500-2:2_and:c:2/3 - C500-2	23.841	114.663	111	53	198	102.438	36.430	27.140	8.242	3.683	145.606	0.407	2733.740
12	PM4 09082017.lif - C500-2:2_comb:c:2/3 - C500-2	88.785	106.185	255	26	255	101.759	38.702	44.068	11.592	9.752	118.262	0.575	9427.582
13	PM4 09082017.lif - C500-2:2B:c:2/3 - C500-2	23.841	114.663	111	53	198	102.438	36.430	28.532	8.242	3.683	145.606	0.368	2733.740
14	PM4 09082017.lif - C500-2:2G:c:2/3 - C500-2	88.785	106.185	255	26	255	101.759	38.702	46.977	11.592	9.752	118.262	0.506	9427.582
15	PM4 09082017.lif - C500-2:3_and:c:2/3 - C500-2	52.186	253.177	255	89	255	197.864	87.635	36.068	9.873	6.730	63.236	0.504	13212.192
16	PM4 09082017.lif - C500-2:3_comb:c:2/3 - C500-2	130.349	161.292	255	17	255	197.990	90.606	69.240	17.822	9.312	88.348	0.342	21024.214
17	PM4 09082017.lif - C500-2:3B:c:2/3 - C500-2	52.186	253.177	255	89	255	197.864	87.635	40.133	9.873	6.730	63.236	0.407	13212.192
18	PM4 09082017.lif - C500-2:3G:c:2/3 - C500-2	130.349	161.292	255	17	255	197.990	90.606	70.694	17.822	9.312	88.348	0.328	21024.214
19	PM4 09082017.lif - C500-2:4_and:c:2/3 - C500-2	54.899	168.063	255	28	255	47.405	87.262	33.110	8.664	8.068	51.244	0.629	9226.460
20	PM4 09082017.lif - C500-2:4_comb:c:2/3 - C500-2	68.234	147.063	255	22	255	47.376	87.266	31.307	9.542	9.105	57.339	0.875	10034.644
21	PM4 09082017.lif - C500-2:4B:c:2/3 - C500-2	54.957	167.910	255	22	255	47.408	87.258	37.672	8.678	8.063	51.356	0.487	9227.730
22	PM4 09082017.lif - C500-2:4G:c:2/3 - C500-2	68.176	147.169	255	27	255	47.374	87.269	33.138	9.530	9.108	57.455	0.780	10033.374
23	PM4 09082017.lif - C500-2:5_and_1:c:2/3 - C500-2	18.242	237.532	255	136	255	11.070	93.767	38.192	5.886	3.946	158.751	0.157	4333.021
24	PM4 09082017.lif - C500-2:5_and_2:c:2/3 - C500-2	37.638	100.584	90	44	229	17.177	98.329	28.871	8.077	5.933	90.816	0.567	3785.823
25	PM4 09082017.lif - C500-2:5_comb:c:2/3 - C500-2	125.730	124.877	255	24	255	14.055	96.339	53.520	18.195	8.798	131.251	0.552	15700.880
26	PM4 09082017.lif - C500-2:5B:c:2/3 - C500-2	18.242	237.532	255	136	255	11.070	93.767	39.653	5.886	3.946	158.751	0.146	4333.021
27	PM4 09082017.lif - C500-2:5B-2:c:2/3 - C500-2	37.638	100.584	90	44	229	17.177	98.329	30.537	8.077	5.933	90.816	0.507	3785.823
28	PM4 09082017.lif - C500-2:5G:c:2/3 - C500-2	125.730	124.877	255	24	255	14.055	96.339	57.899	18.195	8.798	131.251	0.471	15700.880
29	PM4 09082017.lif - C500-2:6_and:c:2/3 - C500-2	24.130	85.919	66	38	242	57.683	106.321	18.865	5.838	5.263	0.870	0.852	2073.223
30	PM4 09082017.lif - C500-2:6_comb:c:2/3 - C500-2	32.154	80.754	66	28	242	57.582	106.230	20.862	6.615	6.189	24.959	0.928	2596.580
31	PM4 09082017.lif - C500-2:6b:c:2/3 - C500-2	24.130	85.919	66	38	242	57.683	106.321	19.979	5.838	5.263	0.870	0.760	2073.223
32	PM4 09082017.lif - C500-2:6G:c:2/3 - C500-2	32.154	80.754	66	28	242	57.582	106.230	21.644	6.615	6.189	24.959	0.863	2596.580
33	PM4 09082017.lif - C500-2:7_and:c:2/3 - C500-2	44.161	253.995	255	200	255	83.746	115.622	25.072	8.124	6.921	17.983	0.883	11216.786
34	PM4 09082017.lif - C500-2:7_comb:c:2/3 - C500-2	66.502	210.684	255	28	255	83.624	115.474	31.026	10.073	8.406	21.546	0.868	14010.909
35	PM4 09082017.lif - C500-2:7B:c:2/3 - C500-2	44.161	253.995	255	200	255	83.746	115.622	26.318	8.124	6.921	17.983	0.801	11216.786
36	PM4 09082017.lif - C500-2:7G:c:2/3 - C500-2	66.502	210.684	255	28	255	83.624	115.474	31.920	10.073	8.406	21.546	0.820	14010.909
37	PM4 09082017.lif - C500-2:8_and:c:2/3 - C500-2	36.311	42.593	35	16	119	197.773	138.585	26.269	7.133	6.482	59.496	0.661	1546.576
38	PM4 09082017.lif - C500-2:8_comb:c:2/3 - C500-2	56.515	42.189	36	12	119	198.001	137.924	35.665	9.585	7.507	89.254	0.558	2384.316
39	PM4 09082017.lif - C500-2:8B:c:2/3 - C500-2	38.966	41.150	35	12	119	197.639	138.480	23.964	7.075	7.013	99.370	0.853	1603.437
40	PM4 09082017.lif - C500-2:8G:c:2/3 - C500-2	53.860	43.213	36	16	119	198.109	137.968	44.973	9.586	7.154	86.494	0.335	2327.455
41	PM4 09082017.lif - C500-2:9_and:c:2/3 - C500-2	18.242	89.323	92	38	154	97.718	190.022	17.333	6.470	3.590	129.811	0.763	1629.414
42	PM4 09082017.lif - C500-2:9_comb:c:2/3 - C500-2	25.227	78.815	92	28	154	97.936	189.976	25.478	6.835	4.699	125.426	0.488	1988.248
43	PM4 09082017.lif - C500-2:9B:c:2/3 - C500-2	18.242	89.323	92	38	154	97.718	190.022	18.280	6.470	3.590	129.811	0.686	1629.414
44	PM4 09082017.lif - C500-2:9G:c:2/3 - C500-2	25.227	78.815	92	28	154	97.936	189.976	26.916	6.835	4.699	125.426	0.438	1988.248
45	PM4 09082017.lif - C500-2:NO_1:c:2/3 - C500-2	33.020	10.031	8	3	30	110.381	42.943	31.532	7.160	5.872	52.707	0.417	331.240
46	PM4 09082017.lif - C500-2:NO_2:c:2/3 - C500-2	46.990	3.654	3	2	22	138.439	59.278	30.396	7.865	7.607	140.685	0.639	171.681
47	PM4 09082017.lif - C500-2:NO_3:c:2/3 - C500-2	15.875	6.800	4	2	21	53.488	93.714	33.910	4.888	4.135	52.172	0.173	107.950

Data wrangling using python scripts

In [2]:

```
## Adding gouping variable to each labelL: addLabels.py

from sys import argv
import pandas as pd

script, filename = argv
df = pd.read_csv(filename, index_col = 0)
#split label into channel info, condiditon type, ROI
labels = df['Label'].str.split('-', expand = True)
if len(labels.columns)< 3:
    labels['4'] = None
labels.columns = ['Condition', 'ROI','Multinucleated_cells']

# split into Image number and cellnumber_ROItype
label_2 = labels['ROI'].str.split(':', expand = True)
label_2.columns = ['ImageNumber', 'CellNumber_ROIType']

#join all labels
all_labels = labels.join(label_2)

# Create conditional ROI types as column
all_labels['Conditional_ROI']= all_labels['CellNumber_ROIType'].apply(lambda x:
{'AND': 'AND', 'OR':'OR'}.get(x.upper().split('_')[-1]), None)

# join back to df
new_df = all_labels.join(df)

#save
new_df.to_csv('image_results%s.csv' %all_labels.iloc[0][3], index = False)

'''
To run in command line:
$ cd to dir
$ python addLabels.py, '<filename.csv>'
'''
```

Next steps

At end of workflow, individual datasets with all grouping variables will be obtained for each image. Each CSV can be joined and statistically analysed.

Appendix D: Source code- Pubscraper: Pubmed scraping and natural language processing in Python

Scraping Pubmed (NCBI database) for abstract data

Using Biopython library via Python 3 to generate a data frame (.csv) from available medline data of a pre-defined search string

In [15]:
```
# import libraries
import Bio
import matplotlib
import pandas
from Bio import Entrez
import matplotlib.pyplot as plt
%matplotlib inline
import seaborn as sb
import pandas as pd

# Check version
print('Pandas version: %s' %pd.__version__)
print('Biopython version: %s' %Bio.__version__)
print('Matplotlib version: %s' %matplotlib.__version__)
```

```
Pandas version: 0.20.3
Biopython version: 1.66
Matplotlib version: 1.5.1+1795.g515ba4b
```

Total number of Pubmed entries

In [52]:
```
Entrez.email = "jiajun.liu@adelaide.edu.au"
handle = Entrez.egquery(term="glucocor* AND immune")
record = Entrez.read(handle)

# number of entries
for row in record["eGQueryResult"]:
    numberentries = 0
    if row["DbName"]=="pubmed":
        print(row["Count"])
        numberentries = row["Count"]

numberentries
```

```
8502
```

Out[52]:
```
0
```

Get list of PubMed IDs

In [17]:
```
#esearch to generate list of PMID
handle= Entrez.esearch(db="pubmed",term="glucocor* AND immune", usehistory = 'y', retmax = 8494 )
searchrecord= Entrez.read(handle)

idlist= searchrecord["IdList"]
count = len(idlist)
print("Found %i results" % count)
#print(idlist)

#Store Session cookie and QueryKey
webenv= searchrecord["WebEnv"]
query_key = searchrecord["QueryKey"]


print (query_key)
print (webenv)
```

```
Found 10 results
1
NCID_1_151528049_130.14.18.34_9001_1501575572_617495126_0MetA0_S_MegaStore_F_1
```

```
/Library/Python/2.7/site-packages/biopython-1.66-py2.7-macosx-10.11-intel.egg/Bio/Entrez/__init__.py:502: Us
erWarning:
Email address is not specified.

To make use of NCBI's E-utilities, NCBI requires you to specify your
email address with each request.  As an example, if your email address
is A.N.Other@example.com, you can specify it as follows:
   from Bio import Entrez
   Entrez.email = 'A.N.Other@example.com'
In case of excessive usage of the E-utilities, NCBI will attempt to contact
a user at the email address provided before blocking access to the
E-utilities.
  E-utilities.""", UserWarning)
```

In [4]:
```
## WRITE ID LIST TO FILE

IDLIST = list(idlist)
#IDLIST = pd.Series(IDLIST)
#IDLIST.to_csv('IDLIST.csv')
```

Get Medline file of searched PMIDs

In [18]:
```
## Import Medline

import time

output = open("data.txt", "w")
# Determine Batch
batch_size = 10
# Fetch data in batches


for start in range(0, count, batch_size):
    end = min(count, start+batch_size)
    print("going to download record %i to %i" % (start+1, end));
    fetch_handle = Entrez.efetch(db = "pubmed", rettype = "medline", retmode = "text",
                                 retstart= start, retmax = end, webenv=webenv, query_key=query_key, post = Tr
ue)
    data = fetch_handle.read()
    output.write(data)
    time.sleep(3) # make sure to sleep between each batch
output.close()
```

```
going to download record 1 to 10
```

In [ ]:
```
## DEPLOY ONLY IF USE HISTORY FAILS
#import time
#output = open("data.txt", "w")
# Determine Batch
#batch_size = 10
## Fetch data in batches

"""
for start in range(0, count, batch_size):
    end = min(count, start+batch_size)
    print("going to download record %i to %i" % (start+1, end))
    fetch_handle = Entrez.efetch(db = "pubmed", rettype = "medline", retmode = "text",
                                 id = idlist, retstart= start, retmax = end, post = True)
    data = fetch_handle.read()
    output.write(data)
    time.sleep(3) # make sure to sleep between each batch
output.close()
"""
```

Generate DataFrame

In [80]:
```
from Bio import Medline
dataset = open("data.txt", "r")

# Parse medline data
data = Medline.parse(dataset)
```

In [81]:
```
medlinefile = list(data)

#reader = pd.read_csv('alldata.csv', error_bad_lines = False, nrows = 1000000, low_memory=False) ## Debug: Me
mory issue
```

In [82]:
```
# set up dataframe
d = pd.DataFrame(medlinefile)
```

In [ ]:
```
# d['PMID'].value_counts() # Check How many duplicates there are
# d.loc[d.PMID.isin(['%s'])] %TOP_DUPLICATE_VALUE # Look at duplicate rows- check if they make sense
```

In [76]:
```
#drop duplicates
x= d.drop_duplicates(subset = ['PMID'])
```

Out[76]:
```
19404519    128
19418731    128
19404521    128
19424046    128
19426224    128
19419738    128
19409827    128
21425972    128
19432889    128
19399500    128
19384873    127
19387765    127
19376397    127
19387032    127
19373457    127
19440116    127
19398001    127
19467321    127
19435796    127
19433626    127
19464360    127
19494313    127
19398916    127
19386083    127
19371813    127
19489103    127
19435479    127
25384870    127
21426128    127
19390148    127
            ...
26767526      1
26799851      1
11054347      1
26749950      1
11024552      1
26801639      1
11061532      1
26756637      1
11007144      1
26762089      1
11016271      1
26745276      1
26748887      1
26746234      1
11054981      1
11056663      1
26801103      1
11024533      1
26810223      1
11067955      1
11060520      1
11019530      1
26790188      1
26807874      1
11060527      1
26812334      1
26745435      1
11042469      1
26778776      1
11044214      1
dtype: int64
```

In [96]:
```
# Write dataframe to csv, LOAD THIS FILE FOR ANALYSIS INSTEAD
x.to_csv('dataframe.csv', header = True, index = False)
```

Exploratory data analysis on medline data using Python 3

In [1]:
```
#import libraries
import matplotlib
import pandas as pd
import matplotlib.pyplot as plt
%matplotlib inline
print('Pandas version %s' %pd.__version__)
print('Matplotlib version %s' %matplotlib.__version__)
```

```
Pandas version 0.20.2
Matplotlib version 2.0.2
```

In [3]:
```
# Set plotting style
plt.style.use('fivethirtyeight')
```

Prepare dataframe

In [134]:
```
# df1 (original) and df2 (updated June 2017)
df1 = pd.read_csv('combined_df.csv', low_memory =  False)
df2 = pd.read_csv('dataframe_5.csv', low_memory = False)

#Join datasets
df = pd.concat([df1,df2])
```

Out[134]:

	AB	AD	AID	AU	AUID	BTI	CDAT	CI	CIN	CN	...	SI	
0	Dysregulation of the hypothalamic-pituitary-ad...	Department of Psychiatry, University of Califo...	['S0306-4530(16)30007-5 [pii]', '10.1016/j.psy...	['Cheng T', 'Dimitrov S', 'Pruitt C', 'Hong S']	NaN	NaN	NaN	['Published by Elsevier Ltd.']	NaN	NaN	...	NaN	Psych 2016
1	The article contains the description of a clin...	NaN	NaN	['Gavrilina NS', 'Sedova GA', 'Kosyura SD', 'F...	NaN	NaN	NaN	NaN	NaN	NaN	...	NaN	Eksp 2015;(
2	The objective of this experiment was to determ...	NaN	['10.2527/jas.2015-9407 [doi]']	['Foote AP', 'Hales KE', 'Tait RG', 'Berry ED'...	NaN	NaN	NaN	NaN	NaN	NaN	...	NaN	J Anin Jan;94 10.252
3	PTPN22 gene variation associates with multiple...	Joslin Diabetes Center, Harvard Medical School...	['jimmunol.1501877 [pii]', '10.4049/jimmunol.1...	['Nowakowska DJ', 'Kissler S']	NaN	NaN	NaN	['Copyright (c) 2016 by The American Associati...	NaN	NaN	...	NaN	J Imm pii: 15
4	Melanocortins are a highly conserved family of...	a Autoimmune and Rare Diseases , Mallinckrodt ...	['10.3109/09273948.2015.1092560 [doi]']	['Clemson CM', 'Yost J', 'Taylor AW']	NaN	NaN	NaN	NaN	NaN	NaN	...	NaN	Ocul I 2016

5 rows × 75 columns

In [135]:
```
#save DF to csv
df.to_csv('combined_df.csv', header = True, index = False)
```

In [2]:
```
df = pd.read_csv('combined_df.csv', low_memory = False)
```

Example 1: Query DataFrame

In [136]:
```
len(df)
```

Out[136]: 10510

In [137]:
```
#df[1:3]['AB'].tolist() # example of how to retrieve Abstract from row number

## Example: retreiving all Titles from Journal == 'J immunol'
jimmu= df.loc[df.TA.isin(['J Immunol'])] # search Journal ==  J Immunol
jimmuTi = jimmu['TI'].tolist() # Return list of Titles
```

In [138]:
```
len(jimmuTi)
```

Out[138]: 220

Example 2: Incidence of MesH Keywords

- MesH keywords are storerd as list variable within dataframe, so the first step is to extract data as a list
- Transform list back to dataframe in order to plot

In [5]:
```
# Turn MESH into list
from ast import literal_eval

def multientry_to_list(dataframe, MedlineKeyword, columnName):
    # Subset out column of interest, trim df to exclude NA
    columnName = dataframe[[MedlineKeyword,"PMID"]].dropna(subset=[MedlineKeyword]).reset_index().drop("inde
x", axis=1)
    count = 0
    #Create nestedlist
    newnestedlist = [[] for _ in range(len(columnName))]
    # Append each value to list
    for i in columnName[MedlineKeyword]:
        newnestedlist[count].append(literal_eval(i))
        count += 1
    #global new_list
    new_list= [columnName, pd.DataFrame(newnestedlist)]
    return new_list
# Call function on MESH
mesh= multientry_to_list(df, "MH", 'MESHKEYWORDS')
```

In [6]:
```
def list_to_dataframe(fromlist, MedlineKeyword, column):
    newdf=pd.concat(fromlist, axis=1).drop(MedlineKeyword, axis= 1)
    newdf.columns = ['PMID', column]
    # Use list comprehension to make DataFrame
    rows = []
    _ = newdf.apply(lambda row: [rows.append([row['PMID'], nn])
                                 for nn in row[column]], axis=1)
    #global df_new
    df_new = pd.DataFrame(rows, columns=newdf.columns).set_index('PMID')
    return df_new
MeshData = list_to_dataframe(mesh, 'MH', 'MESHKEYWORDS')
#save output to variable - to be used later
MeshData = pd.DataFrame(MeshData)
```

In [141]:
```
# count number of unique values
frequency=pd.value_counts(MeshData['MESHKEYWORDS'].values)
# only take Top 500 entires
frequency2 = frequency[0:50]
```

In [144]:
```
# MesH Keyword incidence Plot
#set plot size
plt.figure(figsize = (20,25))
#Plot incidence of keywords
incidenceplot= frequency2.plot(kind = 'barh', colormap = 'Accent', fontsize = 22)
plt.savefig('MesHterms.png', dpi= 300, bbox_inches ='tight')
```

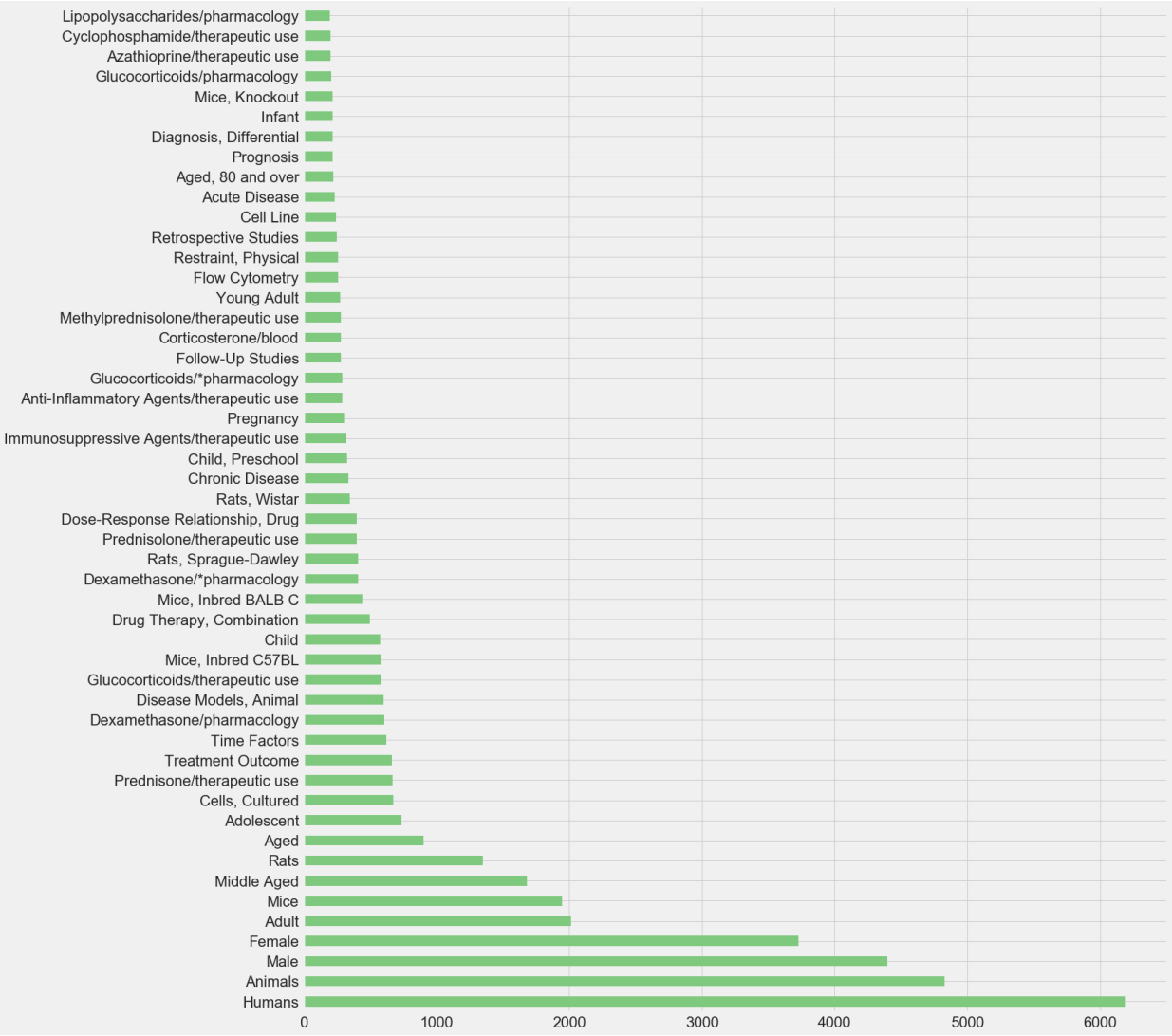

Example 3: Incidence of [keyword] per year

In [7]:
```
# Hierarchical index for Keywords

# Join MesH keywords with date of publication
dates = df[['PMID', 'DA']]
dates = dates.set_index('PMID')

# Join dates with keywords
datespluskeywords = MeshData.join(dates)
```

In [146]:
```
# Search MesH DF for Keyword
keywordGlu = datespluskeywords.loc[datespluskeywords.MESHKEYWORDS.isin(['Glucocorticoids/pharmacology',
                                                                         'Glucocorticoids/*pharmacology',
                                                                         'Dexamethasone/pharmacology',
                                                                         'Dexamethasone/*pharmacology'])]

# check how many ebtrues listed
len(keywordGlu.index)
```

Out[146]: 1513

In [147]:
```
# Count unique dates for glucocorticoids
datesforglu = keywordGlu['DA'].value_counts()
# Set dataframe to plot
datesforglu = pd.DataFrame(datesforglu)
datesforglu = datesforglu.reset_index()
datesforglu.columns = ['Date', 'Count']

# Set date column to date dtype

datesforglu.Date = datesforglu['Date'].apply(lambda x:
                                             pd.to_datetime(str(x), format = '%Y%m%d'))
# Get only Year and Month
datesforglu['Year'] = datesforglu['Date'].dt.year
```

In [148]:
```
len(datesforglu.index)
```

Out[148]: 1145

In [172]:
```
#plt.figure(figsize=(20,100))
yearlygluoccurance = datesforglu.groupby(['Year']).sum()
dateplot= yearlygluoccurance.plot(kind = 'bar', figsize = (25,10), fontsize = 24, colormap= 'Accent')
dateplot
```

Out[172]: <matplotlib.axes._subplots.AxesSubplot at 0x1f9a68f5fd0>

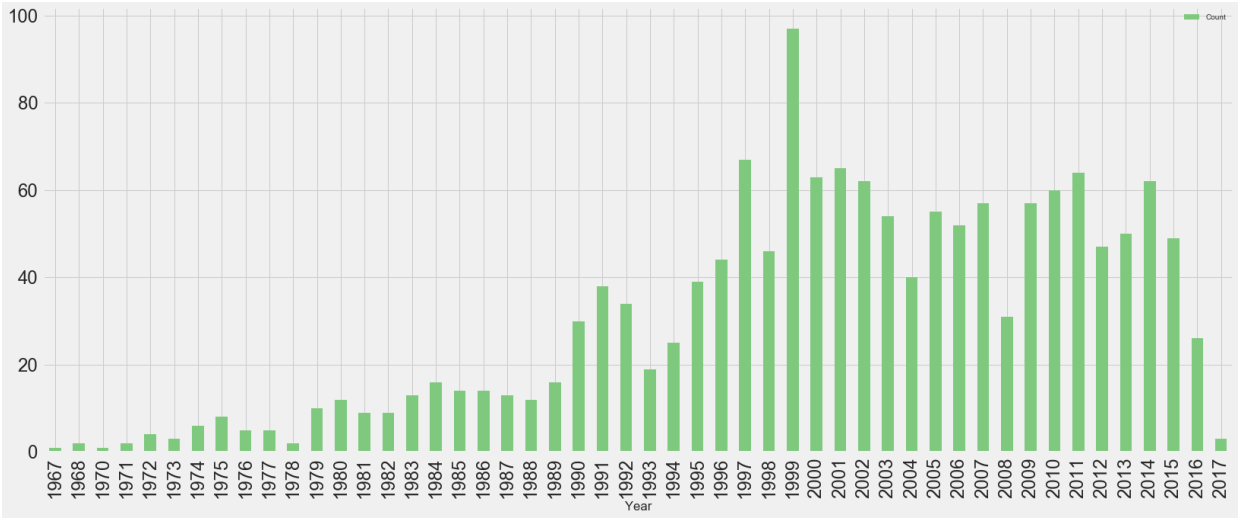

Example 4: Analysing author data

In [8]:
```
authorData= multientry_to_list(df,'AU', 'Author')
authorData = list_to_dataframe(authorData, 'AU', 'Author')
#save as new var
authorData = pd.DataFrame(authorData)
```

In [9]:
```
authorfrequency=pd.value_counts(authorData['Author'].values)
top150authors = authorfrequency[0:50]
```

In [152]:
```
authorPlot = top150authors.plot(kind = "barh", colormap= 'Accent', fontsize= , figsize= (20,20))
plt.savefig('auth_plot.png', dpi = 300, bbox_inches = 'tight')
```

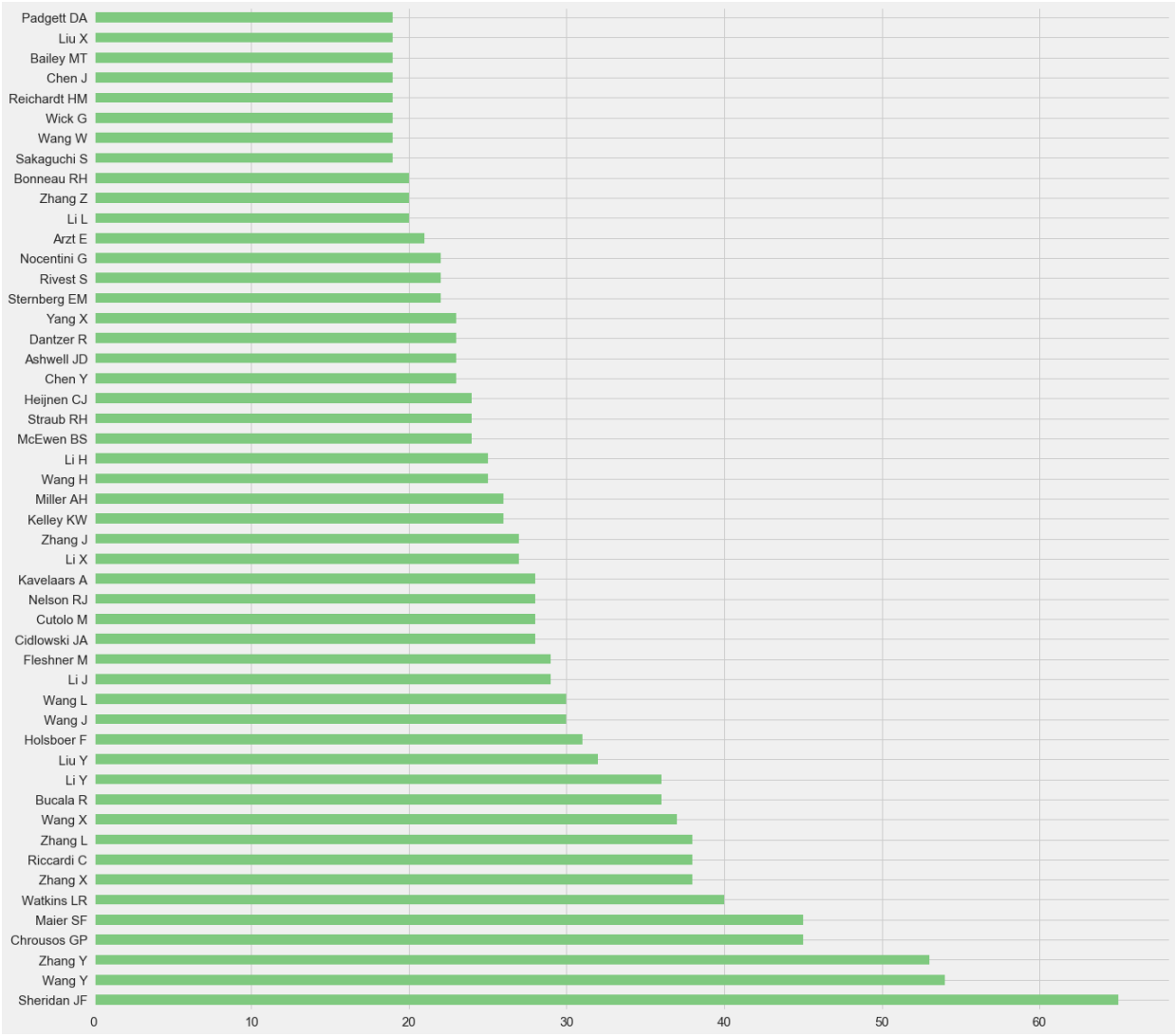

In [10]:
```
#join dataframe

authorMesh= authorData.join(MeshData)
```

In [11]:
```
keywordGluAu = authorMesh.loc[authorMesh.MESHKEYWORDS.isin(['Glucocorticoids/pharmacology',
                                                            'Glucocorticoids/*pharmacology',
                                                            'Dexamethasone/pharmacology',
                                                            'Dexamethasone/*pharmacology'])]
```

In [12]:
```
GluAu = keywordGluAu['Author'].value_counts()
GluAu = pd.DataFrame(GluAu)
GluAu = GluAu.reset_index()
GluAu.columns = ['Author', 'Count']
top50GluAu = GluAu[0:50]
top50GluAu = top50GluAu.set_index('Author')
```

In [13]:
```
topGluAuPlot = top50GluAu.plot(kind = 'barh', figsize= (20,15), colormap= 'Accent')
```

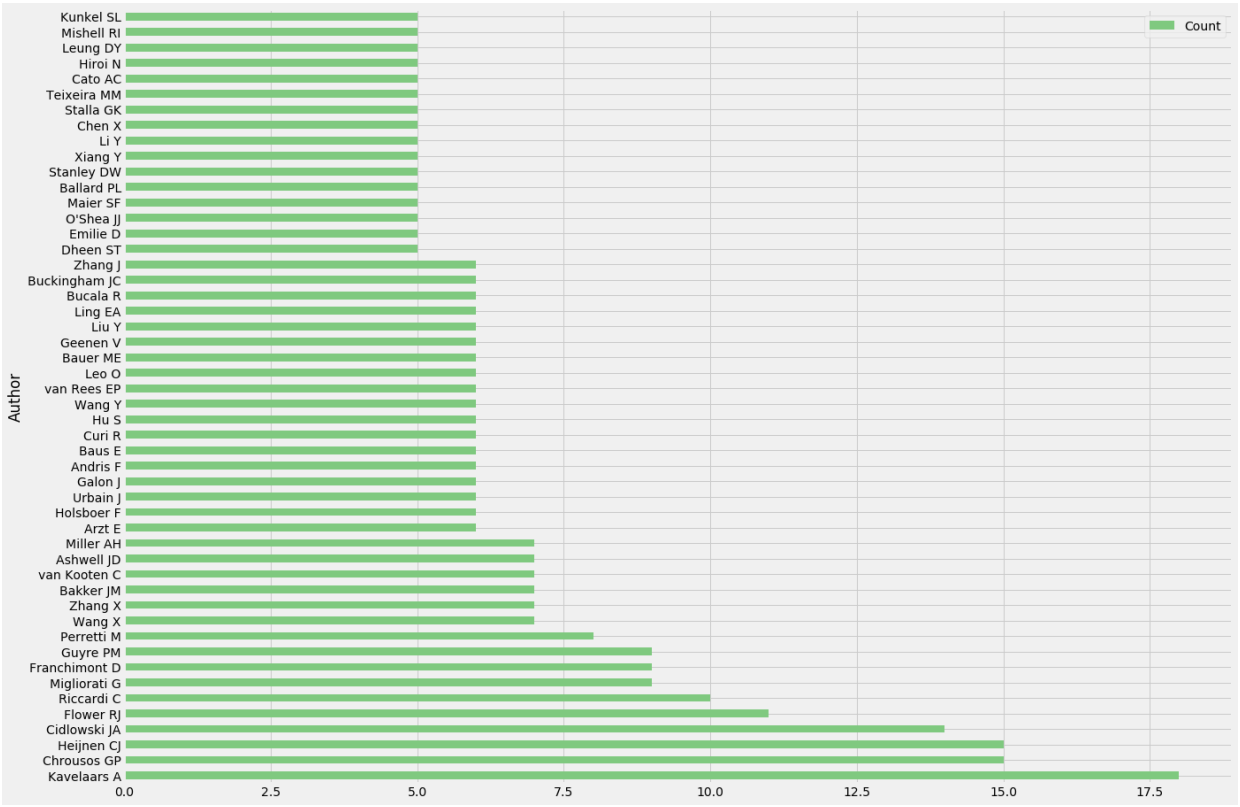

Example 5: Combining Keywords, authors, MesH and titles

In [18]:
```
# Prepare List variables: Authors, Mesh, Keywords

aulist = multientry_to_list(df, "AU", "Author")
meshlist = multientry_to_list(df, "MH", "Mesh")
keylist = multientry_to_list(df, "OT", "Keywords")

# Prepare Dataframe
authordata = list_to_dataframe(aulist, "AU", "Author")
authordata = pd.DataFrame(authordata)
meshdata  = list_to_dataframe(meshlist, "MH", "Mesh")
meshdata = pd.DataFrame(meshdata)
keydata = list_to_dataframe(keylist, "OT", "Keywords")
keydata = pd.DataFrame(keydata)
```

In [19]:
```
# title data
titledata = df[['PMID', 'TI']]
titledata = titledata.set_index('PMID')
titledata.head()
```

Out[19]:

	TI
PMID	
26829709	Glucocorticoid mediated regulation of inflamma...
26817126	[SCLEROUSIS CHOLANGITIS AT THE AUTOIMMUNE PANC...
26812334	Relationship of glucocorticoids and hematologi...
26810223	Ptpn22 Modifies Regulatory T Cell Homeostasis ...
26807874	The Role of Alpha-MSH as a Modulator of Ocular...

In [20]:
```
# join datafrmaes

KMNTdata = titledata.join(authordata).join(dates).join(meshdata).join(keydata)
KMNTdata.to_csv('KMNT.csv',  header = True, index = True)
```

In [22]:
```
KMNTdata.head()
```

Out[22]:

	TI	Author	DA	Mesh	Keywords
PMID					
777	[Prolonged treatment with prednisone and azath...	Runcan V	19760219	Adolescent	NaN
777	[Prolonged treatment with prednisone and azath...	Runcan V	19760219	Adult	NaN
777	[Prolonged treatment with prednisone and azath...	Runcan V	19760219	Anabolic Agents/therapeutic use	NaN
777	[Prolonged treatment with prednisone and azath...	Runcan V	19760219	Azathioprine/*therapeutic use	NaN
777	[Prolonged treatment with prednisone and azath...	Runcan V	19760219	Dietary Proteins/therapeutic use	NaN

In [26]:
```
# find all rows containing where MESH contains (corti | cytokine)

searchedKMNT_1= pd.DataFrame(KMNTdata[KMNTdata['Mesh'].str.contains("Cytokine|Interleukin", na = False)])
glutKMNT=  pd.DataFrame(KMNTdata[KMNTdata['Mesh'].str.contains("Glucocorticoids|Dexamethasone", na = False)])
```

In [32]:
```
searchedKMNT_1= searchedKMNT_1.drop_duplicates('TI')
glutKMNT= glutKMNT.drop_duplicates('TI')
```

In [38]:
```
searchedKMNT = pd.concat([searchedKMNT_1,glutKMNT], axis =0)
searchedKMNT.to_csv('searchedKMNT.csv', header= True, index = True)
len(searchedKMNT.index)
```

Out[38]:
```
5819
```

In [39]:
```
searchedKMNT.DA = searchedKMNT['DA'].apply(lambda x:
                                           pd.to_datetime(str(x), format = '%Y%m%d'))
# Get only Year and Month
searchedKMNT['Year'] = searchedKMNT['DA'].dt.year
```

In [40]:
```
searchedKMNT['TI'].head()
```

Out[40]:
```
PMID
1333539                Growth control of cultured microglia.
1333964    Metabolic and neuroendocrine effects of pro-in...
1356919    Effects of PMA, cytokines and dexamethasone on...
1370208    Glucocorticoids downregulate gene expression o...
1379841    Cyclosporin A, FK506, rapamycin: the use of a ...
Name: TI, dtype: object
```

In [211]:
```
# groupby first
intermediatedates = searchedKMNT.groupby(['TI']).first()

datesfrequency=pd.value_counts(intermediatedates['Year'].values, sort= False)
```

In [213]:
```
datesfrequency.head()
```

Out[213]:
```
1982    2
1983    5
1984    5
1985    3
1986    5
dtype: int64
```

In [214]:
```
newdates = pd.concat([yearlygluoccurance,datesfrequency], axis = 1)
newdates.columns = ['Glucocorticoid', 'Cytokine']
```

In [215]:
```
#plt.figure(figsize=(25,12))
dateplot2= newdates.plot.bar(figsize = (25,10), colormap='Accent', fontsize = 25)
fig = dateplot2.get_figure()
#fig.savefig('cortCytokine_Trends.png', pad_inches = 1, dpi=300 , bbox_inches = 'tight')
```

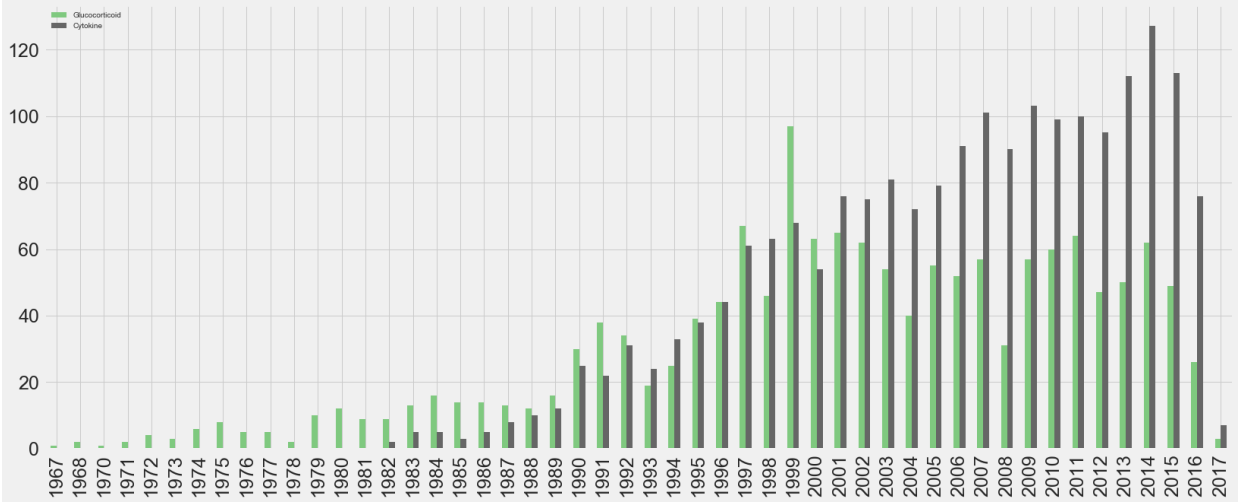

In [153]:
```
# First author
firstauthorfreq = pd.value_counts(intermediatedates['Author'].values)
plt.style.use('fivethirtyeight')
plt.figure(figsize = (20,25))
authplot = firstauthorfreq[0:100].plot(kind = 'barh')
authplot
```

Out[153]: <matplotlib.axes._subplots.AxesSubplot at 0x21eb08d3470>

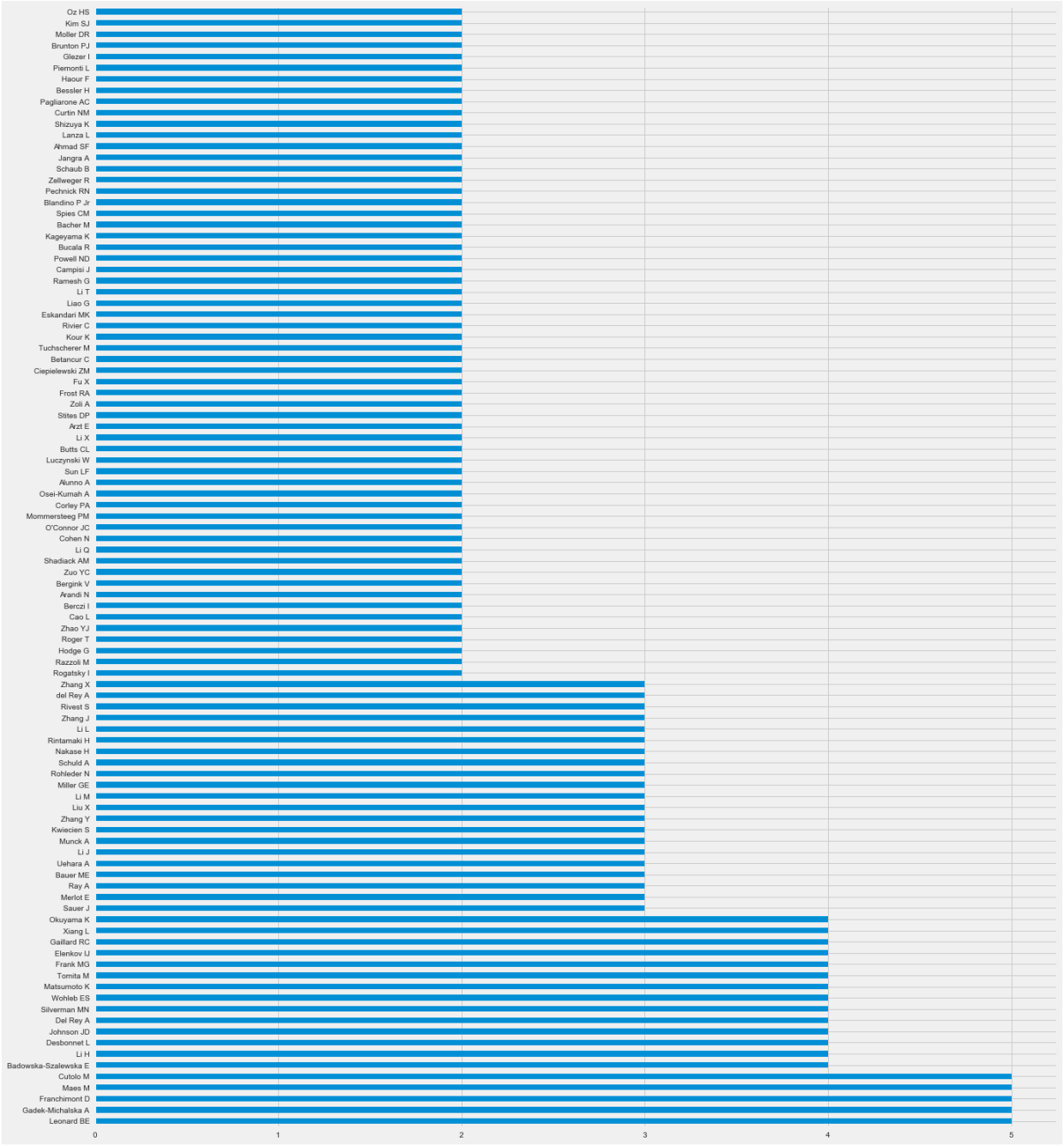

In [154]:
```
# groupby last author
intermediatelast = searchedKMNT.groupby(['TI']).last()

lastauthfreq=pd.value_counts(intermediatelast['Author'].values)
plt.style.use('fivethirtyeight')
plt.figure(figsize=(20,25))
authplot2= lastauthfreq[0:100].plot(kind = 'barh')
authplot2
```

Out[154]:
```
<matplotlib.axes._subplots.AxesSubplot at 0x21eb05d16d8>
```

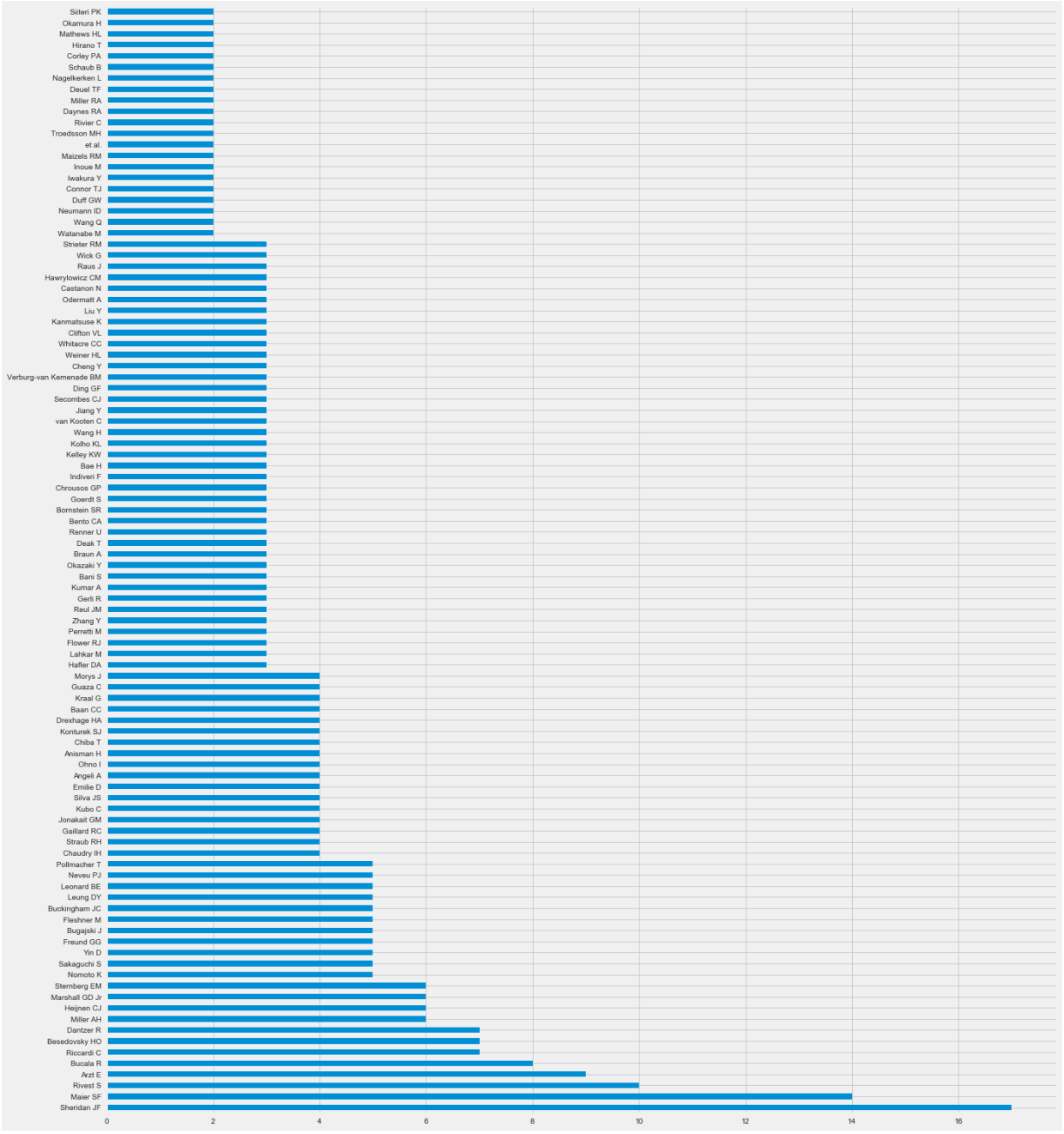

In [155]:
```
len(intermediatelast.index)
```

Out[155]:
```
1893
```

Example 6: Journal names

In [170]:
```
Jname= df['JT']
```

In [171]:
```
Journals = pd.value_counts(Jname)
plt.style.use('fivethirtyeight')
plt.figure(figsize = (20,25))
jplot = Journals[0:50].plot(kind = 'barh', colormap = 'Accent', fontsize = 22)
plt.savefig('Journals.png', dpi = 300, bbox_inches = 'tight')
```

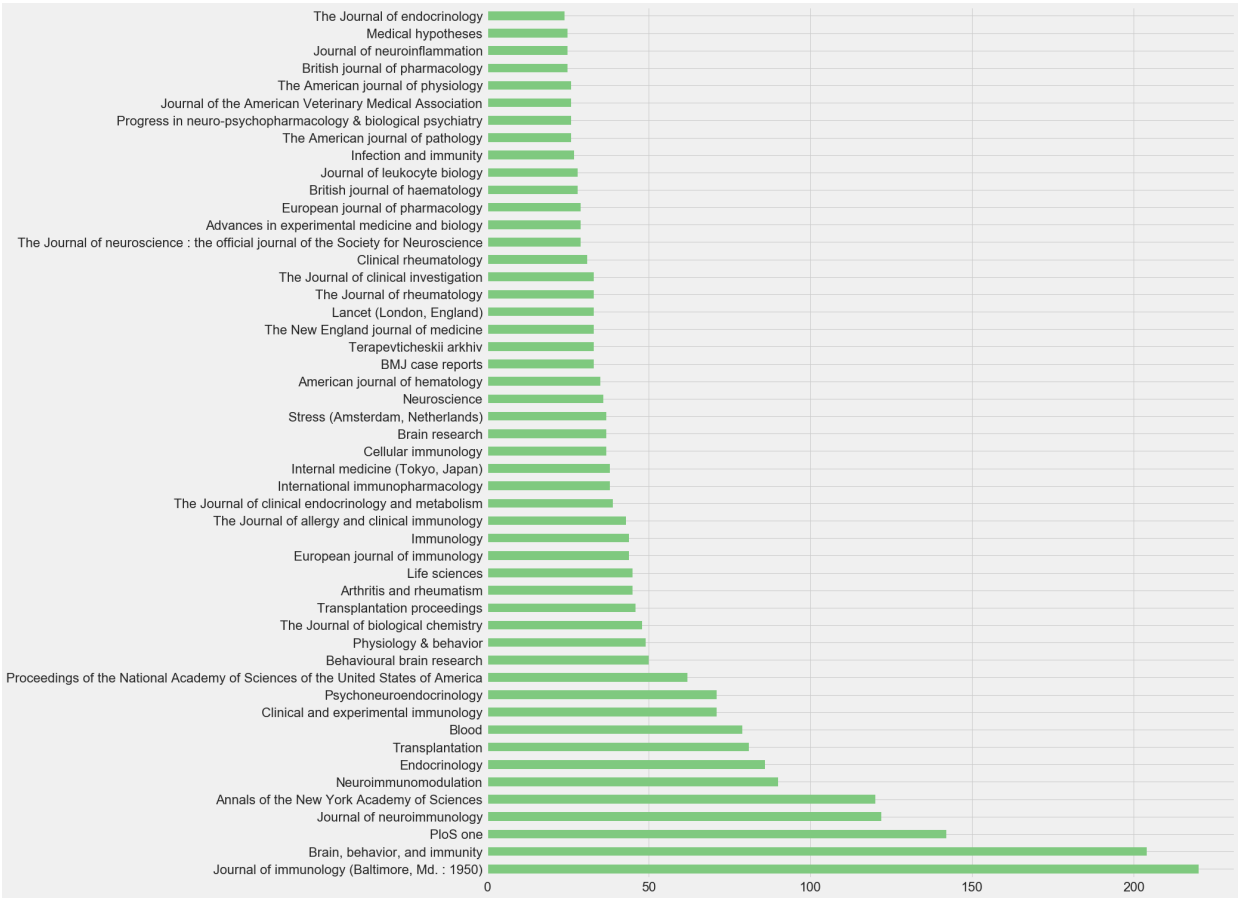

Example 7: Article types

In [71]:
```
x = df['PT'].str.split("'")
jtype = pd.DataFrame(x.apply(pd.Series))[1]
jtype = jtype.apply(lambda x: x.lower())
```

In [101]:
```
year = df['DA'].apply(lambda x:pd.to_datetime(str(x), format = '%Y%m%d'))
pubtype = pd.concat([year.dt.year, jtype], axis = 1)
pubtype.columns = ['Year', 'Article Type']
```

In [102]:
```
pubtype.head()
```

Out[102]:

	Year	Article Type
0	2016	journal article
1	2016	english abstract
2	2016	journal article
3	2016	journal article
4	2016	journal article

In [109]:
```
Pubs = pubtype.groupby(['Year', 'Article Type']).size()
```

In [113]:
```
pubtype.groupby(['Article Type']).size()
```

Out[113]:
```
Article Type
addresses                                1
book chapter                             3
case reports                          1436
clinical conference                      1
clinical study                           3
clinical trial                         298
clinical trial, phase i                  8
clinical trial, phase ii                10
clinical trial, phase iii                7
clinical trial, phase iv                 2
comment                                 43
comparative study                      619
congresses                               3
consensus development conference         2
controlled clinical trial               14
corrected and republished article        2
duplicate publication                    3
editorial                                8
english abstract                       493
evaluation studies                      25
guideline                                2
historical article                      10
introductory journal article             1
journal article                       7228
lectures                                 2
letter                                  21
news                                     1
newspaper article                        1
published erratum                        1
review                                  18
dtype: int64
```

Natural Language Processing on abstracts obtained via medline data

Using NLTK library in Python 3

In [1]:
```
%matplotlib inline
import pandas as pd
import matplotlib.pyplot as plt
plt.style.use('fivethirtyeight')
import pylab
import numpy as np
import nltk
from nltk.tokenize import word_tokenize
from nltk.corpus import stopwords
from nltk.stem import *
import matplotlib.colors as cm

print('NLTK version:%s'%nltk.__version__)
```

```
NLTK version:3.2.4
```

In [2]:
```
# load dataframe
data = pd.read_csv('combined_df.csv', low_memory= False)
pmiddf = pd.DataFrame(data['PMID'])
data = pd.DataFrame(data.set_index('PMID'))
data.head()
```

Out[2]:

	AB	AD	AID	AU	AUID	BTI	CDAT	CI	CIN	CN	...	SI
PMID												
26829709	Dysregulation of the hypothalamic-pituitary-ad...	Department of Psychiatry, University of Califo...	['S0306-4530(16)30007-5 [pii]', '10.1016/j.psy...	['Cheng T', 'Dimitrov S', 'Pruitt C', 'Hong S']	NaN	NaN	NaN	['Published by Elsevier Ltd.']	NaN	NaN	...	Na
26817126	The article contains the description of a clin...	NaN	NaN	['Gavrilina NS', 'Sedova GA', 'Kosyura SD', 'F...	NaN	NaN	NaN	NaN	NaN	NaN	...	Na
26812334	The objective of this experiment was to determ...	NaN	['10.2527/jas.2015-9407 [doi]']	['Foote AP', 'Hales KE', 'Tait RG', 'Berry ED'...	NaN	NaN	NaN	NaN	NaN	NaN	...	Na
26810223	PTPN22 gene variation associates with multiple...	Joslin Diabetes Center, Harvard Medical School...	['jimmunol.1501877 [pii]', '10.4049/jimmunol.1...	['Nowakowska DJ', 'Kissler S']	NaN	NaN	NaN	['Copyright (c) 2016 by The American Associati...	NaN	NaN	...	Na
26807874	Melanocortins are a highly conserved family of...	a Autoimmune and Rare Diseases , Mallinckrodt ...	['10.3109/09273948.2015.1092560 [doi]']	['Clemson CM', 'Yost J', 'Taylor AW']	NaN	NaN	NaN	NaN	NaN	NaN	...	Na

5 rows × 74 columns

In [56]:
```
len(data.index)
```

Out[56]: 10510

In [3]:
```
### Define Preprocessing:
'''
Input: pd series of abstracts
Output: list of abstracts- lowercase, tokanized, stopwords removed
'''
def preprocess_abstracts(abstract_series):
    stopWords = stopwords.words('english')+['.', '(', ')', '=', ',', '-', '%', ':', 'in']
    tostring = abstract_series.to_string()
    lowercaseData= abstract_series.str.lower()
    splitdata = lowercaseData.apply(word_tokenize)
    stopped = splitdata.apply(lambda x: [item for item in x if item not in stopWords])
    return stopped
```

In [4]:
```
processeddata = preprocess_abstracts(data['AB'].apply(str))
```

In [62]:
```
processeddata.head()
```

Out[62]:
```
PMID
26829709    [dysregulation, hypothalamic-pituitary-adrenal...
26817126    [article, contains, description, clinical, cas...
26812334    [objective, experiment, determine, association...
26810223    [ptpn22, gene, variation, associates, multiple...
26807874    [melanocortins, highly, conserved, family, pep...
Name: AB, dtype: object
```

In [63]:
```
# to join all abstracts

allabstracts = [x for x in data['AB'].apply(str).str.lower()]
joinedText = '\n'.join(allabstracts)
```

Word Frequency in Abstracts

In [64]:
```
def abstract_word_frequency(preprocessed_data):
    wordFrequency = preprocessed_data.apply(nltk.FreqDist)
    return wordFrequency

def stemming_words(preprocessed_data):
    st= LancasterStemmer()
    stemmedWords= preprocessed_data.apply(lambda x:[st.stem(item) for item in x])
    return stemmedWords
```

In [65]:
```
import nltk
# word frequency

wordFrequency = pd.DataFrame(processeddata.apply(nltk.FreqDist))
```

In [66]:
```
newdata = pd.DataFrame(d for idx, d in wordFrequency['AB'].items())
```

In [67]:
```
freqCounts = newdata.sum(axis = 0)
```

In [68]:
```
freqCounts = freqCounts.sort_values(ascending = False)
```

In [74]:
```
plt.figure(figsize = (15,10))
freqCounts[:50].plot(kind = 'barh', figsize = (20,20), colormap= 'Accent', fontsize =22)
plt.savefig('abstractwordFreq.png', dpi=300, bbox_inches = 'tight')
```

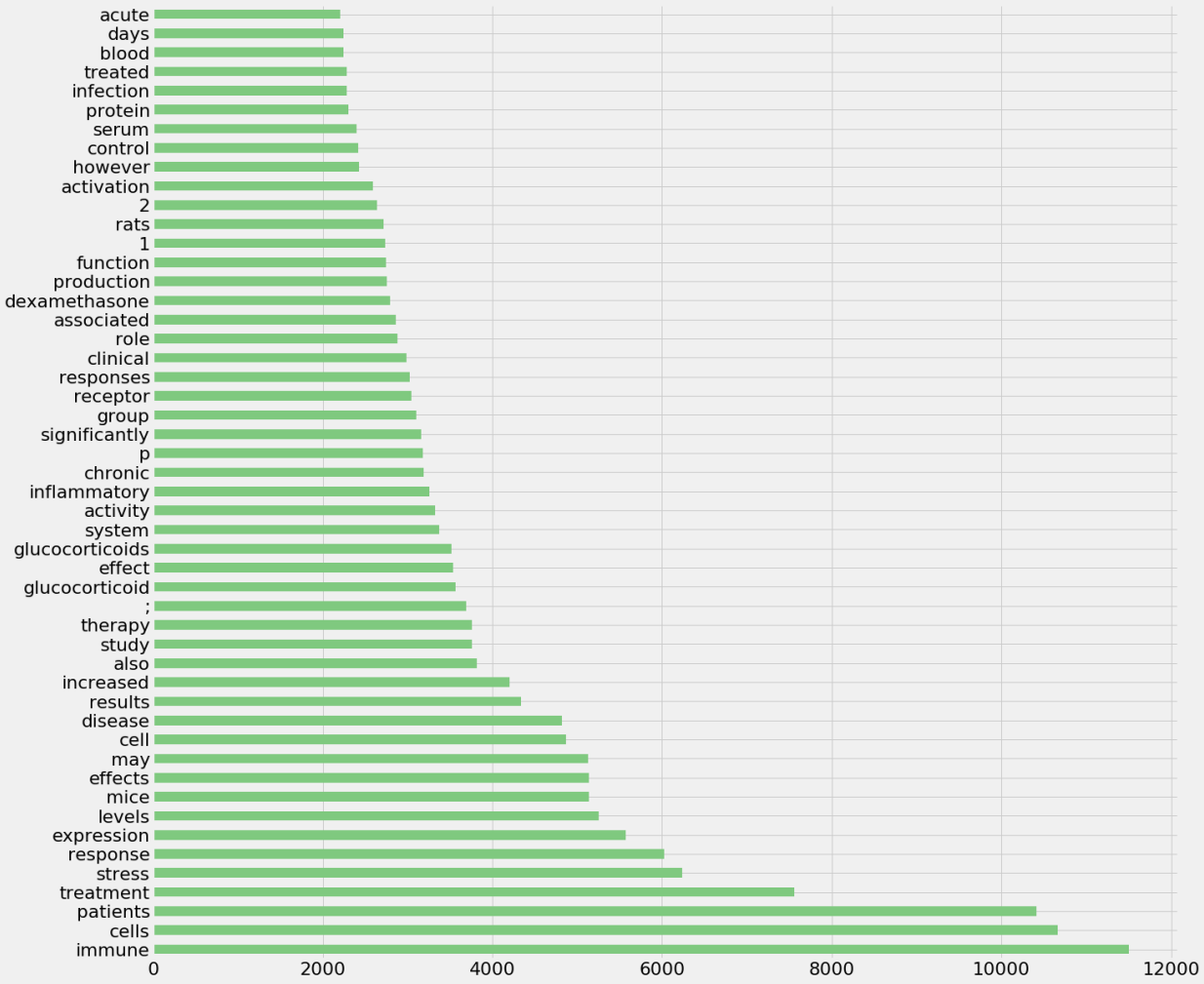

Stemming vs Lemmatization - FreqDist

In [75]:
```
stemmedDF= stemming_words(processeddata)
stemmedDF.head()
```

Out[75]:
```
PMID
26829709    [dysreg, hypothalamic-pituitary-adrenal, hpa, ...
26817126    [artic, contain, describ, clin, cas, paty, p.,...
26812334    [object, expery, determin, assocy, glucocortic...
26810223    [ptpn22, gen, vary, assocy, multipl, autoimmun...
26807874    [melanocortin, high, conserv, famy, peptid, re...
Name: AB, dtype: object
```

In [76]:
```
from nltk.stem import WordNetLemmatizer

lemmatizer = WordNetLemmatizer()
lemmatizedAB = processeddata.apply(lambda x: [lemmatizer.lemmatize(word) for word in x])
```

In [78]:
```
lemmatizedWF = pd.DataFrame(lemmatizedAB.apply(nltk.FreqDist))
unpacked_lemmatizedWF =pd.DataFrame(d for idx, d in lemmatizedWF['AB'].items())
```

In [80]:
```
lemmatizedFreqCounts = unpacked_lemmatizedWF.sum(axis = 0)
lemmatizedFreqCounts=lemmatizedFreqCounts.sort_values(ascending= False)
plt.figure(figsize = (15,10))
lemmatizedFreqCounts[:50].plot(kind = 'barh', figsize = (20,20), colormap= 'Accent', fontsize =22)
plt.savefig('lemmatizedFreqDist.png', dpi=300, bbox_inches = 'tight')
```

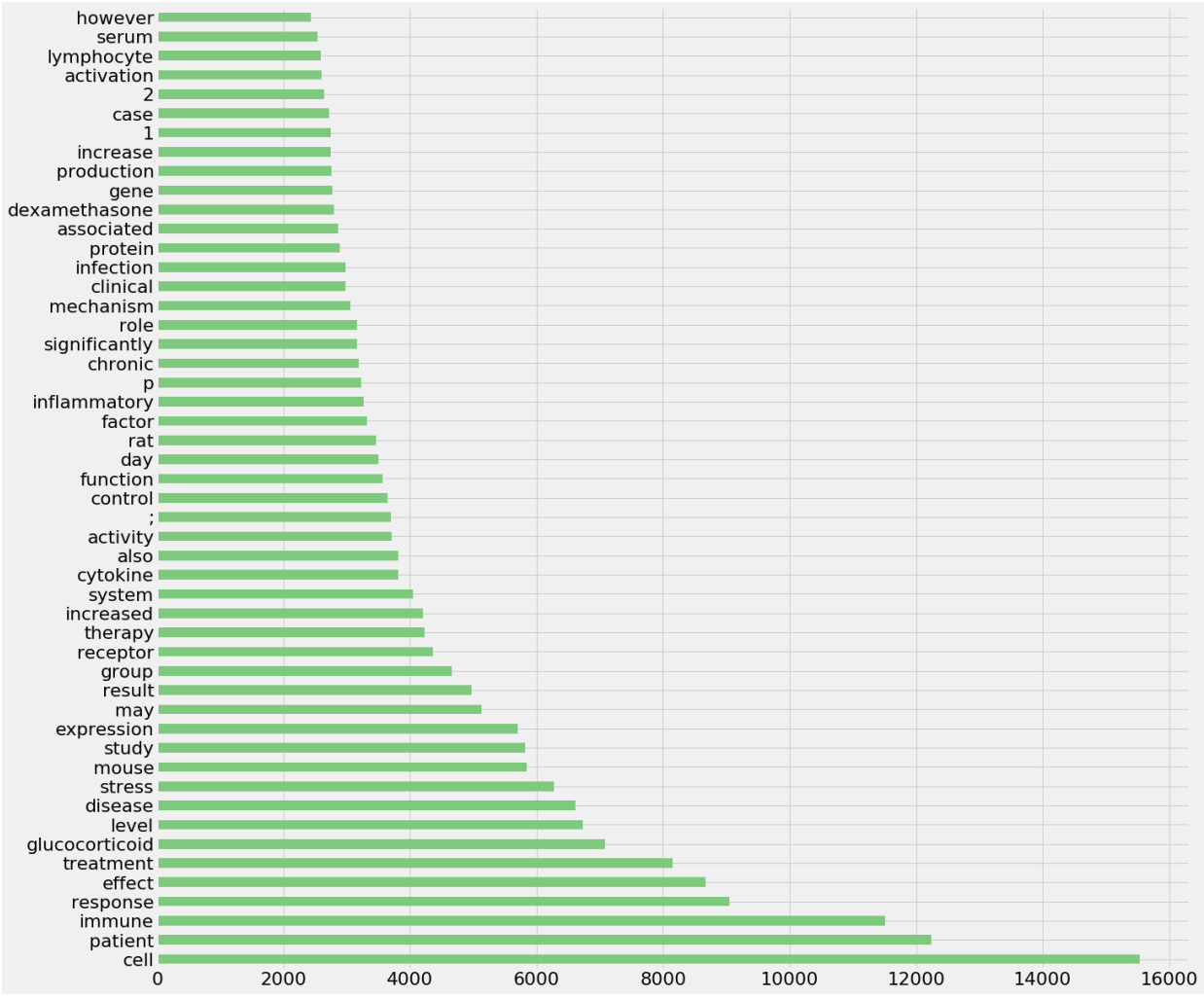

In [82]:
```
from nltk.stem import *
st = LancasterStemmer()

stemmedAB = processeddata.apply(lambda x: [st.stem(word) for word in x])
stemmedWF = pd.DataFrame(stemmedAB.apply(nltk.FreqDist))
unpacked_stemmedWF = pd.DataFrame(d for idx, d in stemmedWF['AB'].items())
```

In [83]:
```
stemmedFreqCounts = unpacked_stemmedWF.sum(axis = 0)
stemmedFreqCounts = stemmedFreqCounts.sort_values(ascending= False)
plt.figure(figsize = (15,10))
stemmedFreqCounts[:50].plot(kind = 'barh',figsize = (20,20), colormap= 'Accent', fontsize =22)
plt.savefig('stemmedFreqDist.png', dpi= 300, bbox_inches = 'tight')
```

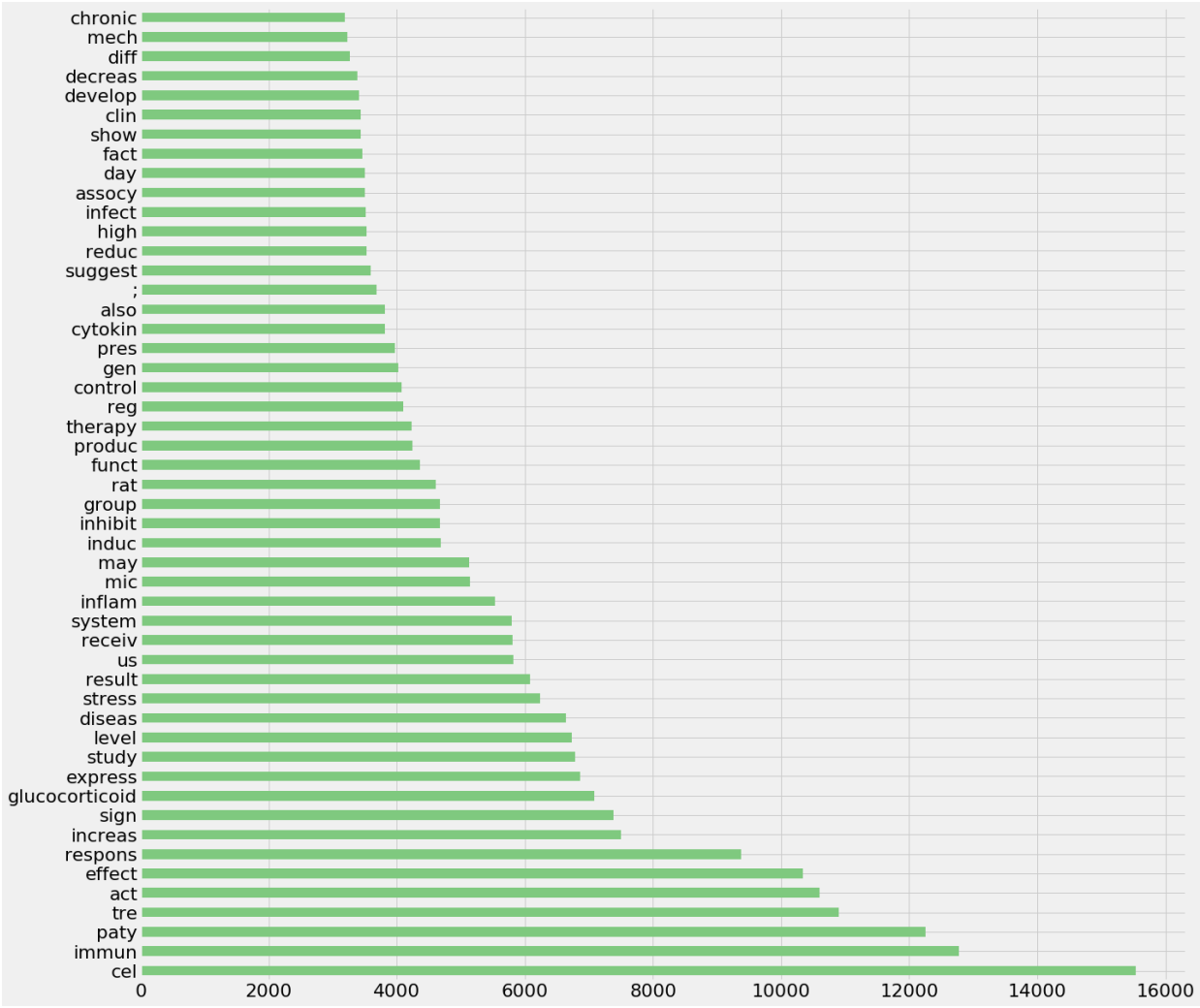

Most common Nouns

In [84]:
```
def findtags(tag_prefix, tagged_text):
    cfd = nltk.ConditionalFreqDist((tag, word) for (word, tag) in tagged_text
                                   if tag.startswith(tag_prefix))
    return dict((tag, cfd[tag].most_common(5)) for tag in cfd.conditions())
```

In [85]:
```
#findNN = pd.DataFrame(tagged.apply(lambda x: findtags('NN', x)))

def unpackseries(words):
    for tag in sorted(words):
        return(tag, words[tag])

#new = findNN['AB'].apply(lambda x: unpackseries(x))
#findNN['AB'].apply(lambda x: x.get('NNS'))
```

In [86]:
```
{'NNS': [('factors', 3), ('compounds', 2), ('treatments', 2), ('designs', 1), ('aspects', 1)],
 'NN': [('ms', 5), ('treatment', 3), ('development', 2), ('disease', 2), ('chain', 1)]}
```

Out[86]:
```
{'NN': [('ms', 5),
  ('treatment', 3),
  ('development', 2),
  ('disease', 2),
  ('chain', 1)],
 'NNS': [('factors', 3),
  ('compounds', 2),
  ('treatments', 2),
  ('designs', 1),
  ('aspects', 1)]}
```

In [87]:
```
## soup data
tokenedsoup = [word_tokenize(x) for x in allabstracts]
taggedsoup = [nltk.pos_tag(x) for x in tokenedsoup]
```

In [88]:
```
NNtaggedsoup = [findtags('NN', x) for x in taggedsoup]
```

In [89]:
```
from collections import Counter
NNtaggedsoupdf = pd.DataFrame(NNtaggedsoup)
NNonly = NNtaggedsoupdf['NN'].tolist()
NNPonly = NNtaggedsoupdf['NNP'].tolist()
NNPSonly = NNtaggedsoupdf['NNPS'].tolist()
NNSonly = NNtaggedsoupdf['NNS'].tolist()

nounsonly = NNSonly + NNPSonly + NNSonly  + NNPonly
```

In [90]:
```
NNonlydict = [dict(x) for x in NNonly]
count = Counter()
for d in NNonlydict:
    count+= Counter(d)
nouncounts = pd.Series(count)
```

In [91]:
```
NNonlydict[:5]
```

Out[91]:
```
[{'bmi': 5, 'comir': 8, 'depression': 5, 'mood': 4, 'obesity': 7},
 {'aip': 3, 'case': 2, 'g/l': 3, 'pancreas': 3, 'pancreatitis': 2},
 {'adg': 6, 'analysis': 4, 'corticosterone': 7, 'cortisol': 5, 'dmi': 9},
 {'cell': 8, 'gitr': 5, 'increase': 3, 'ptpn22': 4, 'treg': 10},
 {'family': 1,
  'homeostasis': 1,
  'inflammation': 2,
  'melanocortin': 3,
  'role': 2}]
```

In [92]:
```
nouncounts= nouncounts.sort_values(ascending = False)
plt.figure(figsize=(15,10))
nouncounts[:50].plot(kind = 'barh')
#pylab.savefig('nounOnlyfreqdist.png')
```

Out[92]:
```
<matplotlib.axes._subplots.AxesSubplot at 0x19236daf8d0>
```

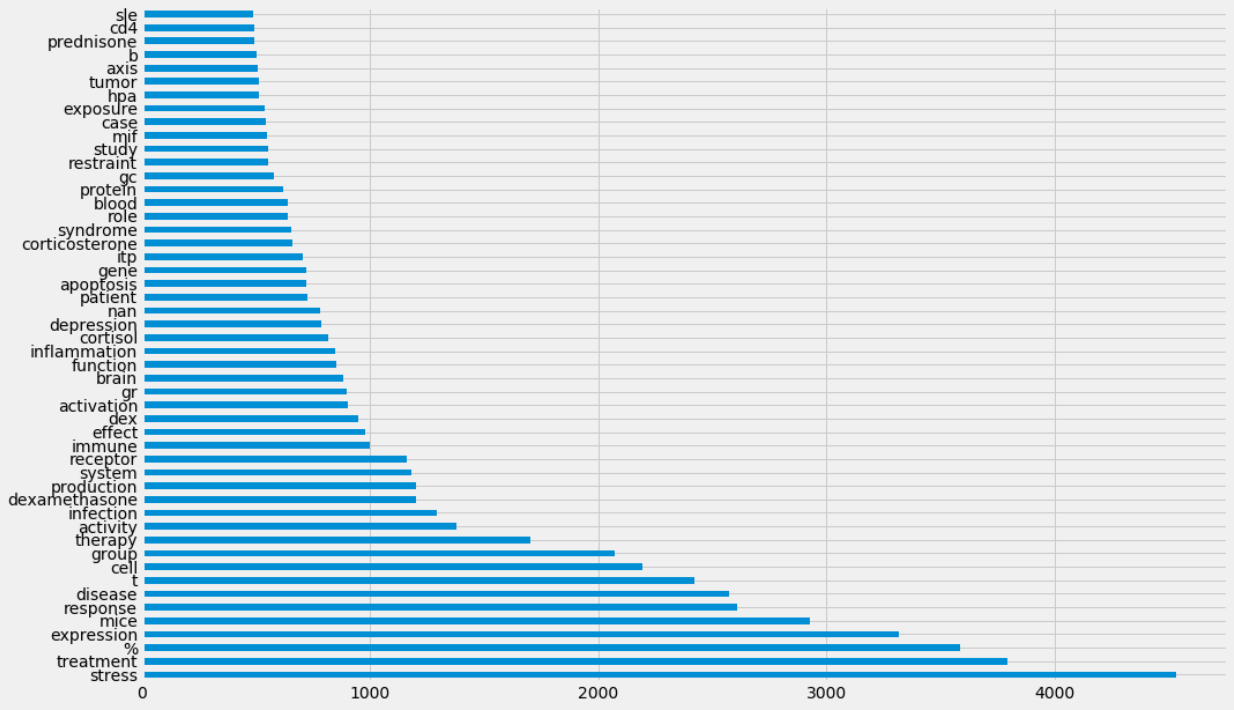

Noun Trends

In [93]:
```
NNtaggedsoupdf  =  pd.DataFrame(NNtaggedsoup)
#join PMID to Nouns
nounsDF = pmiddf.join(NNtaggedsoupdf).set_index('PMID')
nounsDF.head()
```

Out[93]:

	NN	NNP	NNPS	NNS
PMID				
26829709	[(comir, 8), (obesity, 7), (depression, 5), (b...	[(<, 2)]	NaN	[(conditions, 2), (analyses, 2), (findings, 2)...
26817126	[(aip, 3), (g/l, 3), (pancreas, 3), (case, 2),...	NaN	NaN	[(times, 2), (years, 1), (hospitals, 1), (orga...
26812334	[(dmi, 9), (corticosterone, 7), (adg, 6), (cor...	[(<, 3), (>, 1)]	NaN	[(heifers, 8), (steers, 5), (samples, 2), (tra...
26810223	[(treg, 10), (cell, 8), (gitr, 5), (ptpn22, 4)...	NaN	NaN	[(cells, 5), (associates, 1), (diseases, 1), (...
26807874	[(melanocortin, 3), (role, 2), (inflammation, ...	NaN	NaN	[(melanocortins, 4), (peptides, 2), (receptors...

In [94]:
```
#import fulldataset
fulldata = pd.read_csv('combined_df.csv', low_memory =  False).set_index('PMID')

#Get dates
datedata = fulldata['DA'].apply(lambda x: pd.to_datetime(str(x), format = '%Y%m%d'))
#set dates to YYYYmm
datedata = pd.DataFrame(datedata.apply(lambda x: int(100*x.year + x.month)))
datedata = pd.DataFrame(datedata['DA'].apply(lambda x: pd.to_datetime(str(x), format = '%Y%m')))
#join dates to DF
#datesplusnouns = datedata.join(nounsDF)
```

In [95]:
```
def convert_to_dict(item):
    if type(item) is not float:
        return dict(item)
    else:
        return({'NA': 0})
def count_my_words(entry):
    c = Counter()
    for word in entry:
        c += Counter(word)
        return c

#temp =temp['NNP'].apply(lambda x: convert_to_dict(x))
#datesplusnouns['NNPS'].apply(lambda x: convert_to_dict(x))
#datesplusnouns['NNS'].apply(lambda x: convert_to_dict(x))
```

In [96]:
```
datesplusnouns = pd.DataFrame(nounsDF['NN'].apply(lambda x: convert_to_dict(x)))
datesplusnouns = datesplusnouns.join(datedata)
datesplusnouns = datesplusnouns.reset_index()
datesplusnouns.head()
```

Out[96]:

	PMID	NN	DA
0	777	{'nan': 1}	1976-02-01
1	1639	{'panarteritis': 3, 'autopsy': 2, 'year': 2, '...	1976-04-01
2	17412	{'pneumocystis': 4, 'pneumonia': 2, 'tissue': ...	1977-07-01
3	26522	{'process': 2, 'vasculitis': 1, 'syndrome': 1,...	1978-08-01
4	38306	{'exudation': 6, 'blood': 4, 'flow': 4, 'react...	1979-10-01

In [97]:
```
allunpacked = pd.concat([pd.DataFrame(d for idx, d in datesplusnouns['NN'].items()), datesplusnouns['DA']], a
xis =1 )
```

In [219]:
```
## select top 8 and control (p)

top5words = allunpacked[['p', 'stress', 'corticosterone', 'dexamethasone', 'cytokine','inflammasome' ,'DA']]
```

In [322]:
```
top5words = allunpacked[['restraint', 'behavior', 'lps', 'shock', 'defeat', 'cms', 'cus', 'swim','DA']]
```

In [328]:
```
top5summ
```

Out[328]:
```
Forced Swim                     14.0
Chronic Unpredictable Stress    91.0
Chronic Mild Stress            121.0
Social Defeat                  137.0
Inescapable Shock              142.0
lps                            379.0
Behavior                       407.0
Restraint Stress               571.0
dtype: float64
```

In [108]:
```
trending5 = top5words.groupby('DA').agg(np.sum)
plt.figure(figsize = (25,10))
plt.plot(trending5, 'o')
#trending5.plot(kind = 'area',subplots= True, figsize =(25,30), sharey=True)
#plt.title('Trending words')
plt.legend(trending5.columns, loc ='best')
#pylab.savefig('trends.png',bbox_inches='tight' )
```

Out[108]:
```
<matplotlib.legend.Legend at 0x19238cfb2b0>
```

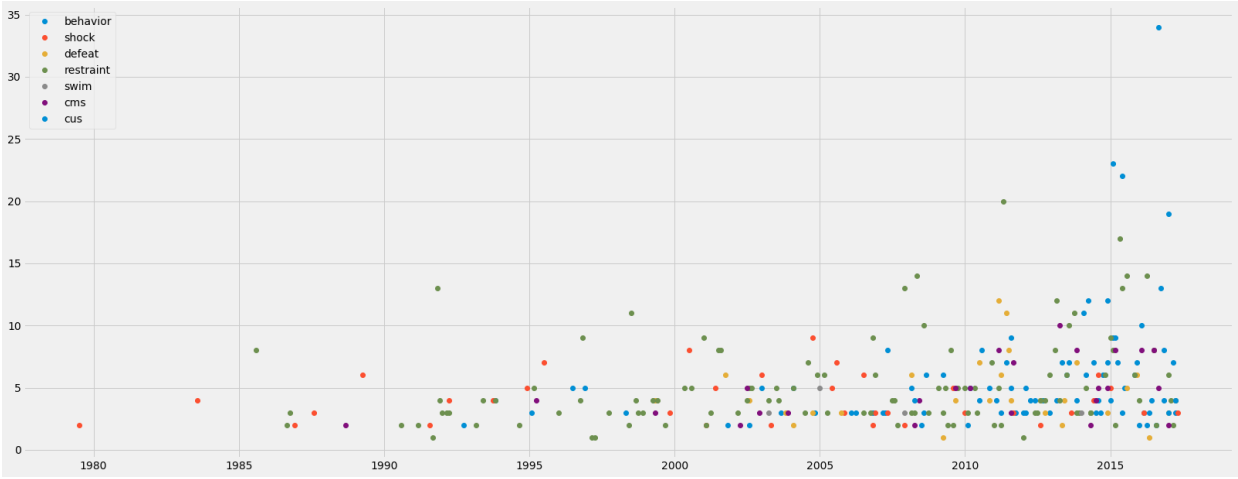

Commonly co-occurring words

In [113]:
```
def get_all_phases_containing_tar_wrd(target_word, tar_passage, left_margin = 10, right_margin = 10):
    """
        Function to get all the phases that contain the target word in a text/passage tar_passage.
        Workaround to save the output given by nltk Concordance function

        str target_word, str tar_passage int left_margin int right_margin --> list of str
        left_margin and right_margin allocate the number of words/pununciation before and after target word
        Left margin will take note of the beginning of the text
    """
    # Source: https://simplypython.wordpress.com/2014/03/14/saving-output-of-nltk-text-concordance/
    ## Create list of tokens using nltk function
    tokens = nltk.word_tokenize(tar_passage)

    ## Create the text of tokens
    text = nltk.Text(tokens)

    ## Collect all the index or offset position of the target word
    c = nltk.ConcordanceIndex(text.tokens, key = lambda s: s.lower())

    ## Collect the range of the words that is within the target word by using text.tokens[start;end].
    ## The map function is use so that when the offset position - the target range < 0, it will be default to
 zero
    concordance_txt = ([text.tokens[list(map(lambda x: x-5 if (x-left_margin)>0 else 0, [offset]))
[0]:offset+right_margin]
                        for offset in c.offsets(target_word)])
    ## join the sentences for each of the target phrase and return it
    return [''.join([x+' ' for x in con_sub]) for con_sub in concordance_txt]
```

In [114]:
```
import csv

def csv_writer(writelist,filename):
    newseries = pd.Series(writelist)
    newseries.to_csv(filename)
```

In [115]:
```
concord2 = get_all_phases_containing_tar_wrd('increase', joinedText)
```

In [127]:
```
concord2[:10]
```

Out[127]:
```
['of abdominal organs showed diffusion increase pancreas with a peripheral hypointensive rim , local stenosi
s ',
 'but the mechanism driving this increase is unknown . in this study , we show ',
 'of ptpn22 caused a concomitant increase in the proportion of cd44hicd62llo effector treg cells , ',
 'central treg cells . the increase in treg cell numbers , but not their differentiation ',
 'immune challenge exhibited a relative increase from the first to the second round of indoor ',
 'adrenalectomised asthmatic rats attenuated the increase in rl and eosinophil count in both asthmatic model
s ',
 'alarin restored the ucms-induced an increase in the levels of the pro-inflammatory cytokines interleukin (
',
 'in the following way : increase in th inos expression -- > increase in the ',
 'th inos expression -- > increase in the no production -- > increase in the ',
 'the no production -- > increase in the sgc activity -- > increase in intracellular ']
```

In [117]:
```
csv_writer(concord2, 'phasescontaining-increasing.csv')
```

In [119]:
```
concord_decrease = get_all_phases_containing_tar_wrd('decrease', joinedText)
```

In [120]:
```
csv_writer(concord_decrease, 'phasescontaining-decrease.csv')
```

In [121]:
```
# for associate|associated |association
concord_associate = get_all_phases_containing_tar_wrd('associate', joinedText)
concord_associated = get_all_phases_containing_tar_wrd('associated', joinedText)
concord_association = get_all_phases_containing_tar_wrd('association', joinedText)

concord_total_associat = concord_associate + concord_associated + concord_association
```

In [122]:
```
csv_writer(concord_total_associat, 'phasescontaining-associate.csv')
```

n-grams

In [123]:
```
from nltk.collocations import *
bigram_measures = nltk.collocations.BigramAssocMeasures()
trigram_measures = nltk.collocations.TrigramAssocMeasures()
finder = processeddata.apply(lambda x: BigramCollocationFinder.from_words(x))
```

In [124]:
```
# Naive bi-grams
bigram = finder.apply(lambda df: df.nbest(bigram_measures.pmi, 20))
# Naive tri-grams
Trifinder = processeddata.apply(lambda x: TrigramCollocationFinder.from_words(x))
trigram = Trifinder.apply(lambda df: df.nbest(trigram_measures.pmi, 20))
```

In [126]:
```
# token all soup
stopWords = stopwords.words('english')+['.', '(', ')', '=', ',', '-', '%', ':', 'in']
tokendata = word_tokenize(joinedText)
stoppeddata = [x for x in joinedText if x not in stopWords]
```

In [127]:
```
#stem text
st= LancasterStemmer()
stemmedWords= [st.stem(item) for item in stoppeddata]
```

In [129]:
```
# increase N-grams
tokenincrease = [word_tokenize(x) for x in concord2]
stopincrase= []
for item in tokenincrease:
    for word in item:
        if word not in stopWords:
            stopincrase.append(word)
```

In [130]:
```
#trigram increase
increaseTrigram = [TrigramCollocationFinder.from_words(stopincrase)]
increaseTrigramcounts =  [x.nbest(trigram_measures.raw_freq, 30) for x in increaseTrigram]
```

In [131]:
```
increaseTrigramcounts
```

Out[131]:
```
[[('increase', 'platelet', 'count'),
  ('p', '<', '0.05'),
  ('increase', 'plasma', 'corticosterone'),
  ('increase', 'serum', 'corticosterone'),
  ('caused', 'significant', 'increase'),
  ('increase', 'corticosterone', 'levels'),
  ('showed', 'significant', 'increase'),
  ('associated', 'significant', 'increase'),
  ('resulted', 'significant', 'increase'),
  ('increase', 'p', '<'),
  ('induced', 'significant', 'increase'),
  ('produced', 'significant', 'increase'),
  ('increase', 'lipid', 'peroxidation'),
  ('accompanied', 'significant', 'increase'),
  ('increase', 'plasma', 'levels'),
  ('p', '<', '0.001'),
  ('plasma', 'corticosterone', 'levels'),
  ('significant', 'increase', 'serum'),
  ('--', '>', 'increase'),
  ('[', 'ca2+', ']'),
  ('increase', 'vascular', 'permeability'),
  ('led', 'significant', 'increase'),
  ('marked', 'increase', 'plasma'),
  ('may', 'increase', 'risk'),
  ('significant', 'increase', 'number'),
  ('stress', 'induced', 'increase'),
  ('caused', 'marked', 'increase'),
  ('cd4', '+', 'cd25'),
  ('immune', 'function', 'increase'),
  ('increase', 'cd4', '+')]]
```

In [132]:
```
# decrease N-grams
tokenasso = [word_tokenize(x) for x in concord_total_associat]
stopasso= []
for item in tokenasso:
    for word in item:
        if word not in stopWords:
            stopasso.append(word)
```

In [133]:
```
#trigram assoc
assoTrigram = [TrigramCollocationFinder.from_words(stopasso)]
assoTrigramcounts =  [x.nbest(trigram_measures.raw_freq, 30) for x in assoTrigram]
assoTrigramcounts
```

Out[133]:
```
[[('associated', 'increased', 'risk'),
  ('chronic', 'stress', 'associated'),
  ('immune', 'response', 'associated'),
  ('psychological', 'stress', 'associated'),
  ('side', 'effects', 'associated'),
  ('systemic', 'lupus', 'erythematosus'),
  ('associated', 'significant', 'increase'),
  ('crohn', "'s", 'disease'),
  ('lupus', 'erythematosus', 'sle'),
  ('associated', 'autoimmune', 'diseases'),
  ('associated', 'increased', 'levels'),
  ('gene', 'expression', 'associated'),
  ('associated', 'increased', 'incidence'),
  ('associated', 'significantly', 'increased'),
  ('defect', 'serotonergic', 'function'),
  ('genome-wide', 'association', 'studies'),
  ('immune', 'function', 'associated'),
  ('stress', 'associated', 'increased'),
  ("'s", 'disease', 'associated'),
  ('adverse', 'effects', 'associated'),
  ('also', 'associated', 'increased'),
  ('associated', 'high', 'mortality'),
  ('associated', 'immune', 'system'),
  ('associated', 'impaired', 'immune'),
  ('associated', 'systemic', 'lupus'),
  ('cushing', "'s", 'syndrome'),
  ('disease', 'associated', 'increased'),
  ('erythematosus', 'sle', 'associated'),
  ('human', 'immunodeficiency', 'virus'),
  ('hypothalamic-pituitary-adrenal', 'hpa', 'axis')]]
```

In [134]:
```
# asssociation N-grams
tokendecrease = [word_tokenize(x) for x in concord_decrease]
stopdecrease= []
for item in tokendecrease:
    for word in item:
        if word not in stopWords:
            stopdecrease.append(word)
```

In [135]:
```
#trigram decrease
decraseTrigram = [TrigramCollocationFinder.from_words(stopdecrease)]
decreaseTrigramcounts =  [x.nbest(trigram_measures.raw_freq, 30) for x in decraseTrigram]
decreaseTrigramcounts
```

Out[135]:
```
[[('resulted', 'significant', 'decrease'),
  ('showed', 'significant', 'decrease'),
  ('p', '<', '0.05'),
  ('caused', 'significant', 'decrease'),
  ('decrease', 'immune', 'response'),
  ('significant', 'decrease', 'number'),
  ('decrease', 'body', 'weight'),
  ('decrease', 'cd4', '+'),
  ('induced', 'significant', 'decrease'),
  ('nk', 'cell', 'activity'),
  ('<', '0.05', 'decrease'),
  ('accompanied', 'significant', 'decrease'),
  ('circulating', 'immune', 'complexes'),
  ('decrease', 'nk', 'cell'),
  ('led', 'significant', 'decrease'),
  ('significant', 'decrease', 'plasma'),
  ('significant', 'decrease', 'proteinuria'),
  ('also', 'found', 'decrease'),
  ('characterized', 'significant', 'decrease'),
  ('crf', 'r2beta', 'mrna'),
  ('decrease', 'cell', 'proliferation'),
  ('decrease', 'crf', 'r2beta'),
  ('decrease', 'cytokine', 'production'),
  ('decrease', 'expression', 'levels'),
  ('decrease', 'food', 'intake'),
  ('decrease', 'ia', 'expression'),
  ('decrease', 'number', 'function'),
  ('decrease', 'p', '<'),
  ('decrease', 'proliferative', 'response'),
  ('decrease', 'serum', 'igg')]]
```

Bag of words approach: Term vectorising

- counts per word per document, turns abstracts into sparse matrix (loses the ability to contextualise)

- good for building a dictionary of terms used

In [136]:
```
from sklearn.feature_extraction.text import CountVectorizer
from sklearn.feature_extraction.text import TfidfTransformer
```

In [159]:
```
#stemmeddata= stemming_words(processeddata)
listabstracts= lemmatizedAB.apply(lambda x:' '.join(x)).tolist()
```

In [160]:
```
vectorizer = CountVectorizer(analyzer= 'word',
                             tokenizer = None,
                             stop_words= None
                             )
datafeatures = vectorizer.fit_transform(listabstracts)
datafeaturesarray = datafeatures.toarray()
datafeatures[:2]
```

Out[160]:
```
<2x34861 sparse matrix of type '<class 'numpy.int64'>'
        with 291 stored elements in Compressed Sparse Row format>
```

In [161]:
```
tfVec = TfidfTransformer()
data_tfidf = tfVec.fit_transform(datafeatures)
data_tfidf= data_tfidf.toarray()
data_tfidf[:2]
```

Out[161]:
```
array([[ 0.,  0.,  0., ...,  0.,  0.,  0.],
       [ 0.,  0.,  0., ...,  0.,  0.,  0.]])
```

In [162]:
```
vocab = vectorizer.get_feature_names()
vecdist= np.sum(datafeaturesarray, axis = 0)
tfidfdist= np.sum(data_tfidf, axis = 0)
```

In [163]:
```
vecdata= pd.DataFrame(datafeaturesarray)
vecdata.columns= vocab
vecdata.head()
```

Out[163]:

	00	000	0000	00001	00002297	00003	000035	00005	00009	0001	...	zucker	zuckerman	zusanli	zvad	zygomycetes	zygomycosi
0	0	0	0	0	0	0	0	0	0	0	...	0	0	0	0	0	0
1	0	0	0	0	0	0	0	0	0	0	...	0	0	0	0	0	0
2	0	0	0	0	0	0	0	0	0	0	...	0	0	0	0	0	0
3	0	0	0	0	0	0	0	0	0	0	...	0	0	0	0	0	0
4	0	0	0	0	0	0	0	0	0	0	...	0	0	0	0	0	0

5 rows × 34861 columns

TFIDF: Term Freqency - Inverse Document Frequency

- Corrects term frequency by document frequency -- higher weights to terms repeatedly mentioned across documents rather than within documents ie. mentioning a condition several times per abstract

- Controls for terms which are mainly mentioned many times within a subset of articles

In [200]:
```
len(tfidf_data)
```

Out[200]: 10510

In [166]:
```
tfidf_data = pd.DataFrame(data_tfidf)
tfidf_data.columns= vocab
summed_tfidf= tfidf_data.sum(axis = 0)
summed_tfidf= summed_tfidf.sort_values(ascending= False)
```

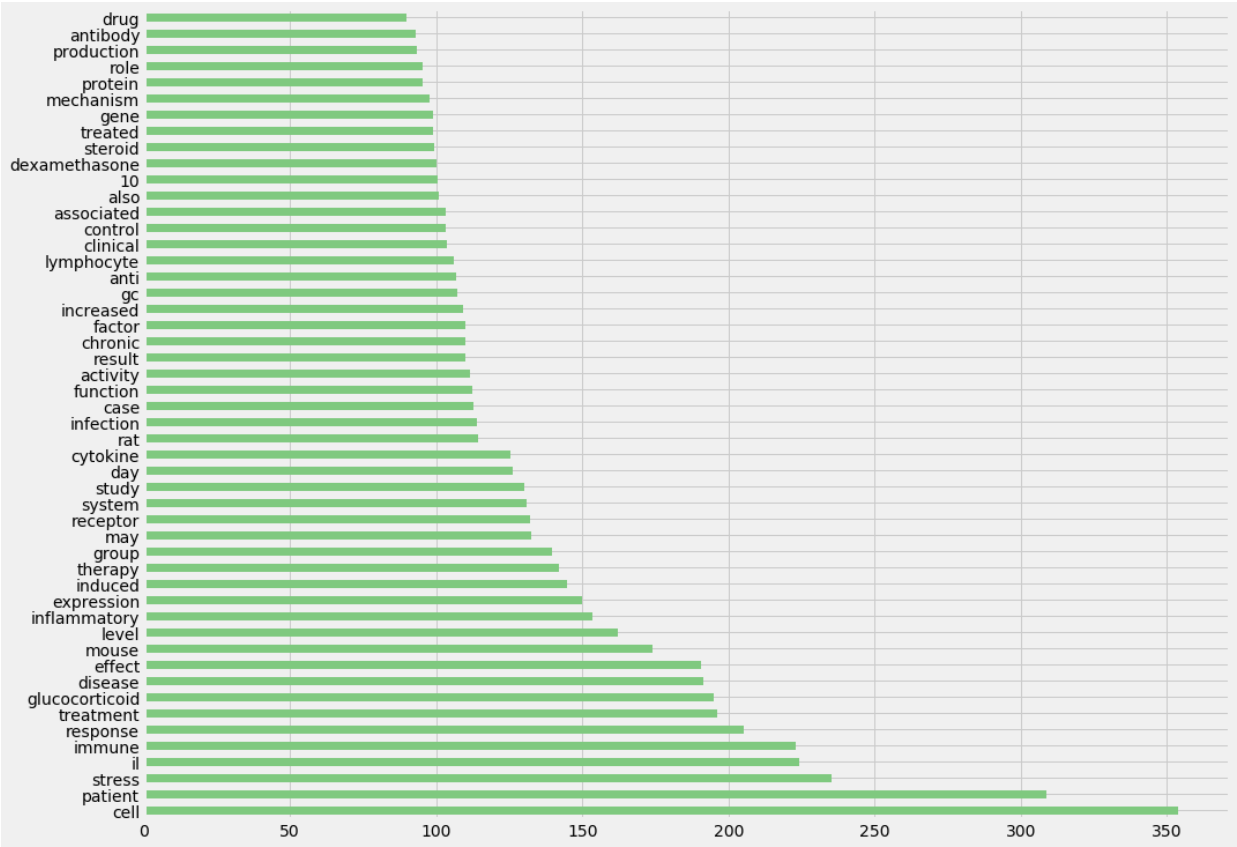

In [190]:
```
tfidfplot = summed_tfidf[1:51].plot(kind='barh',  figsize = (15,12), colormap = 'Accent')
tfidfplot.set_xlabel('Tfidf transformed frequency')
plt.savefig('tfidfBOW.png', dpi =300, bbox_inches = 'tight')
```

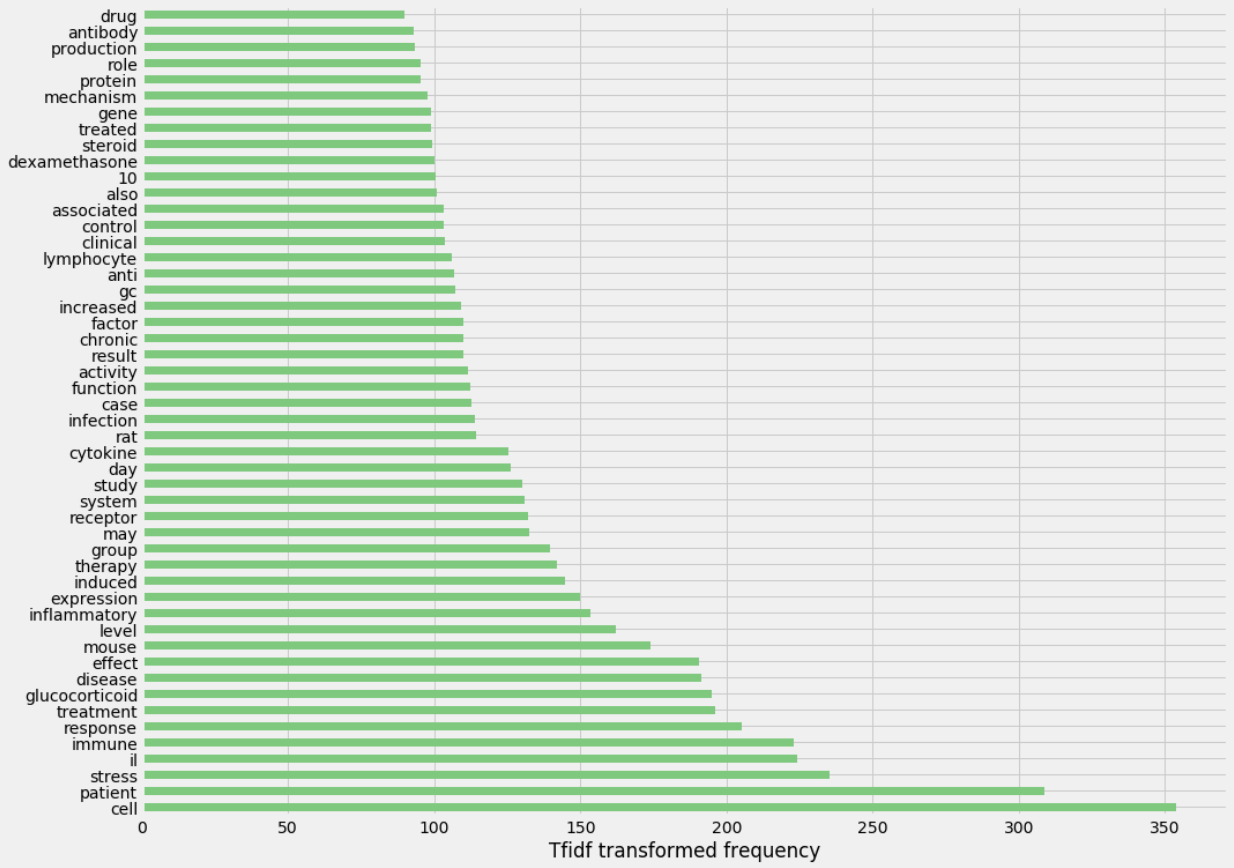

In [ ]:
```
```

Appendix E: Statistical methods using R

Data Analysis Workflow

Exploratory data analysis

Parametric tests using Linear mixed effects model

Example data from study 3

In [4]:
```
#libraries
library(ggplot2)
library(dplyr)

#colourscheme
prePal<- c('#111111', '#65737e', '#a7adba')
```

```
Warning message:
“package ‘ggplot2’ was built under R version 3.3.2”
Attaching package: ‘dplyr’

The following objects are masked from ‘package:stats’:

    filter, lag

The following objects are masked from ‘package:base’:

    intersect, setdiff, setequal, union
```

In [5]:
```
#load dataset
df<- read.csv('viability.csv', header= T)
df$N<- as.factor(df$N)
df$Pre.ExposureDose<- as.factor(df$Pre.ExposureDose)

df$Antagonist<- factor(df$Antagonist, levels = c('Vehicle', 'Spironolactone', 'Mifepristone','none'))
df$Pre.Exposure<- factor(df$Pre.Exposure, levels = c('Vehicle', 'CORT', 'Dexamethasone'))
df$Treatment <- factor(df$Treatment, levels = c('Vehicle', 'LPS', 'none'))
summary(df)

noAntagonist<- filter(df, Antagonist == 'none')
Ant<- filter(df, Antagonist!='none')
beforeLPS<- filter(df, Treatment == 'none')
afterLPS<- filter(df, Treatment != 'none')
```

```
 N        Condition            Antagonist        Pre.Exposure Pre.ExposureDose
 1:36   SCV    : 12   Vehicle       :48   Vehicle      :96    50 : 54
 2:36   C 50   :  6   Spironolactone:48   CORT         :96    500:162
 3:36   C 500  :  6   Mifepristone  :48   Dexamethasone:24
 4:36   CL     :  6   none          :72
 5:36   CV     :  6
 6:36   D 50   :  6
        (Other):174
   Treatment        LDH         CellViability    SupernatantViability
 Vehicle: 54   Min.   :0.0755   Min.   :0.2925   Min.   :0.0810
 LPS    : 54   1st Qu.:0.1633   1st Qu.:0.4860   1st Qu.:0.1179
 none   :108   Median :0.3967   Median :0.5875   Median :0.1540
               Mean   :0.3454   Mean   :0.5760   Mean   :0.2806
               3rd Qu.:0.4730   3rd Qu.:0.6716   3rd Qu.:0.3638
               Max.   :0.6960   Max.   :0.8565   Max.   :1.3930

 ViabilityChange
 Min.   :0.3993
 1st Qu.:0.8280
 Median :0.9412
 Mean   :0.9136
 3rd Qu.:1.0141
 Max.   :1.3814
 NA's   :96
```

Exploratory data analysis

In [116]:
```
ggplot(data =df, aes(y = LDH, x = Antagonist, group = Pre.Exposure))+
  facet_grid(Treatment~Pre.ExposureDose)+
  geom_point(aes(colour = Pre.Exposure), position = position_dodge(0.5))+
 # geom_text(aes(label = N), hjust = 2, vjust = 0)+
  theme_bw()+
    theme(axis.text.x= element_text(angle = 45, hjust=1))+
  scale_color_manual(values = prePal)

ggplot(data =df, aes(y = CellViability, x = Antagonist, group = Pre.Exposure))+
  facet_grid(Treatment~Pre.ExposureDose)+
  geom_point(aes(colour = Pre.Exposure), position = position_dodge(0.5))+
  # geom_text(aes(label = N), hjust = 2, vjust = 0)+
  theme_bw()+
    theme(axis.text.x= element_text(angle = 45, hjust=1))+

  scale_color_manual(values = prePal)

ggplot(data =df, aes(y = SupernatantViability, x = Antagonist, group = Pre.Exposure))+
  facet_grid(Treatment~Pre.ExposureDose)+
  geom_point(aes(colour = Pre.Exposure), position = position_dodge(0.5))+
  # geom_text(aes(label = N), hjust = 2, vjust = 0)+
  theme_bw()+
    theme(axis.text.x= element_text(angle = 45, hjust=1))+
  scale_color_manual(values = prePal)
```

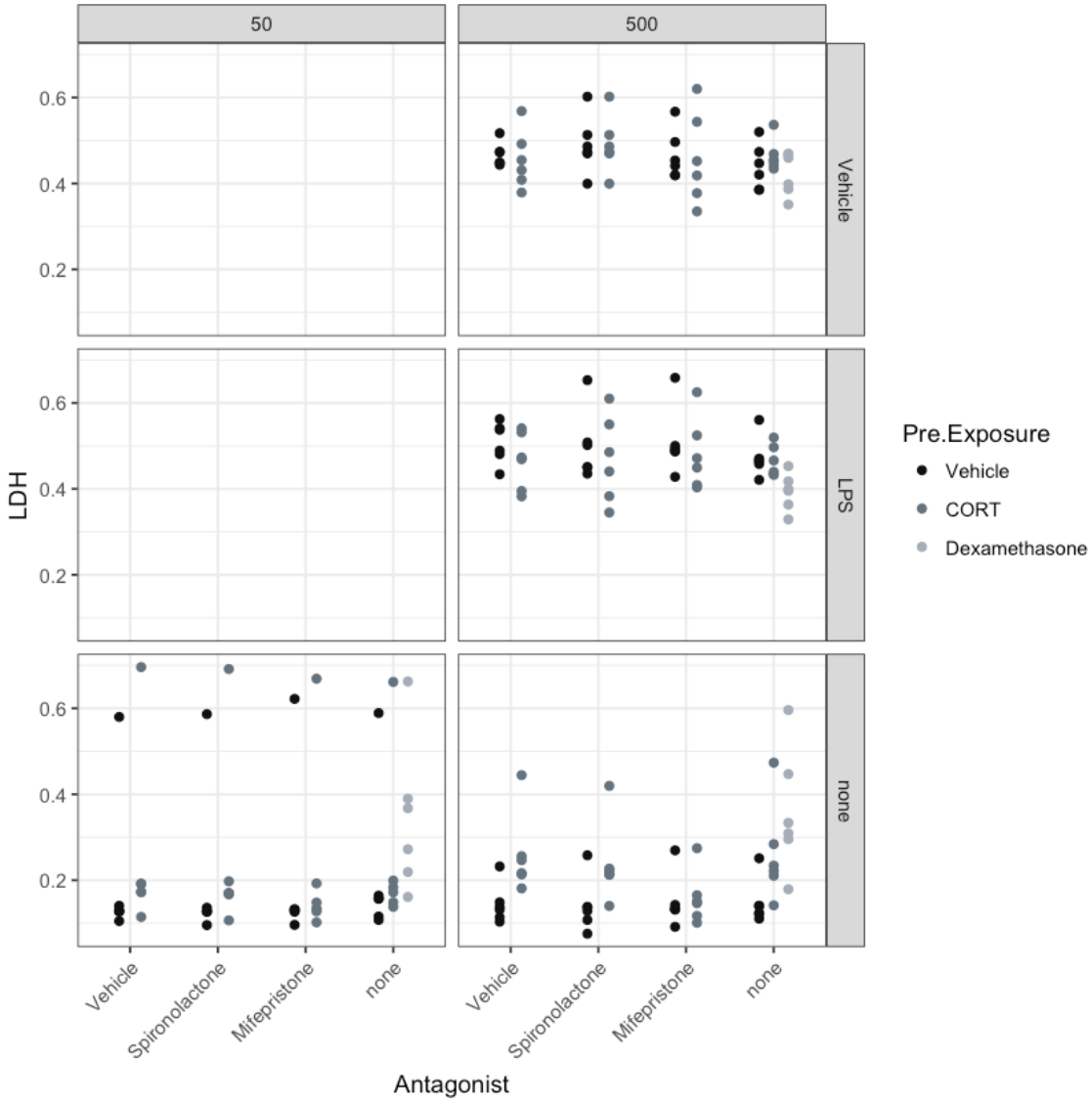
50
500
Vehicle
LPS
none
LDH
0.6
0.4
0.2
Vehicle
Spironolactone
Mifepristone
none
Antagonist
Pre.Exposure
Vehicle
CORT
Dexamethasone

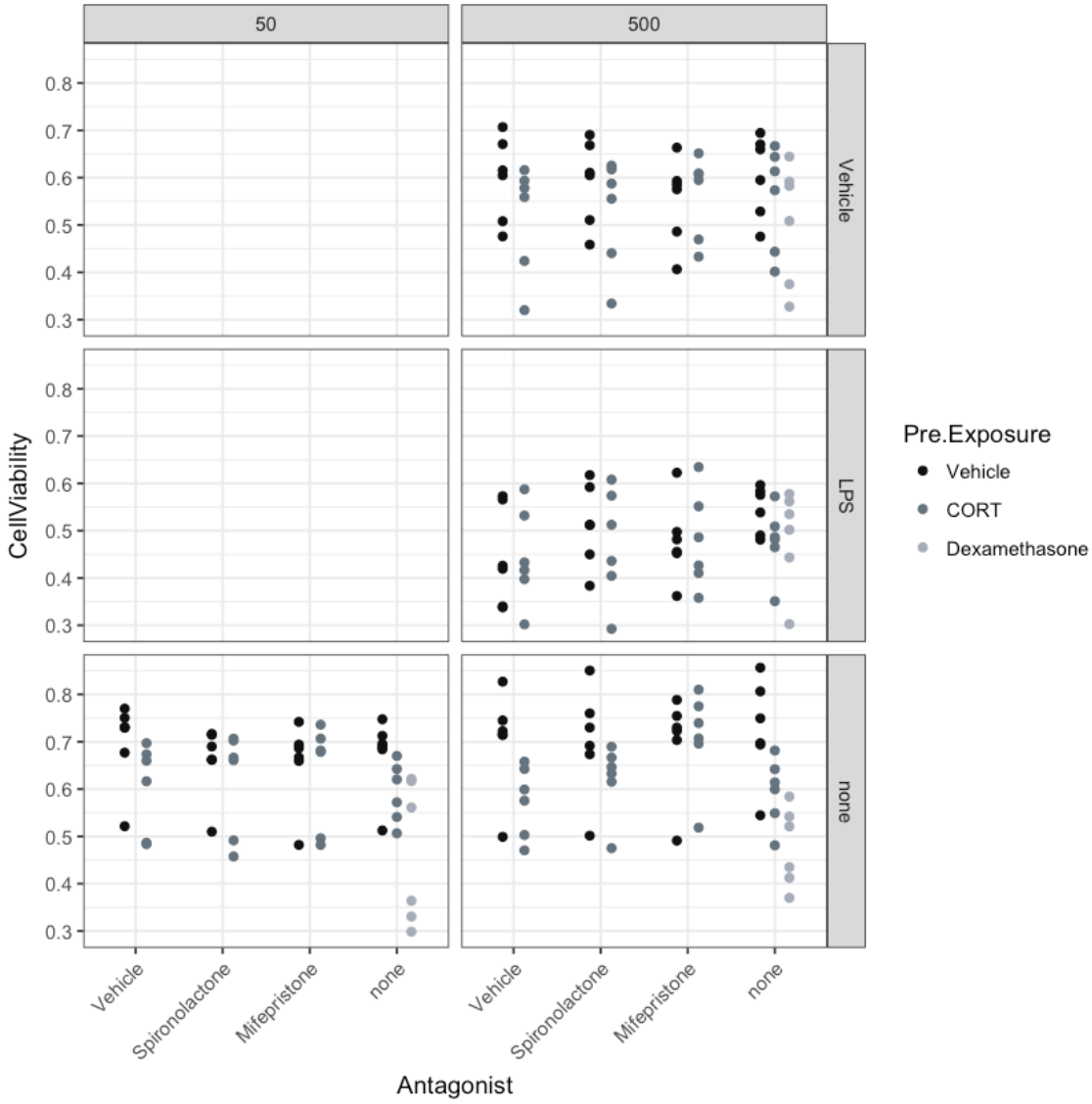
50
500
Vehicle
LPS
none
CellViability
0.8
0.7
0.6
0.5
0.4
0.3
Vehicle
Spironolactone
Mifepristone
none
Antagonist
Pre.Exposure
Vehicle
CORT
Dexamethasone

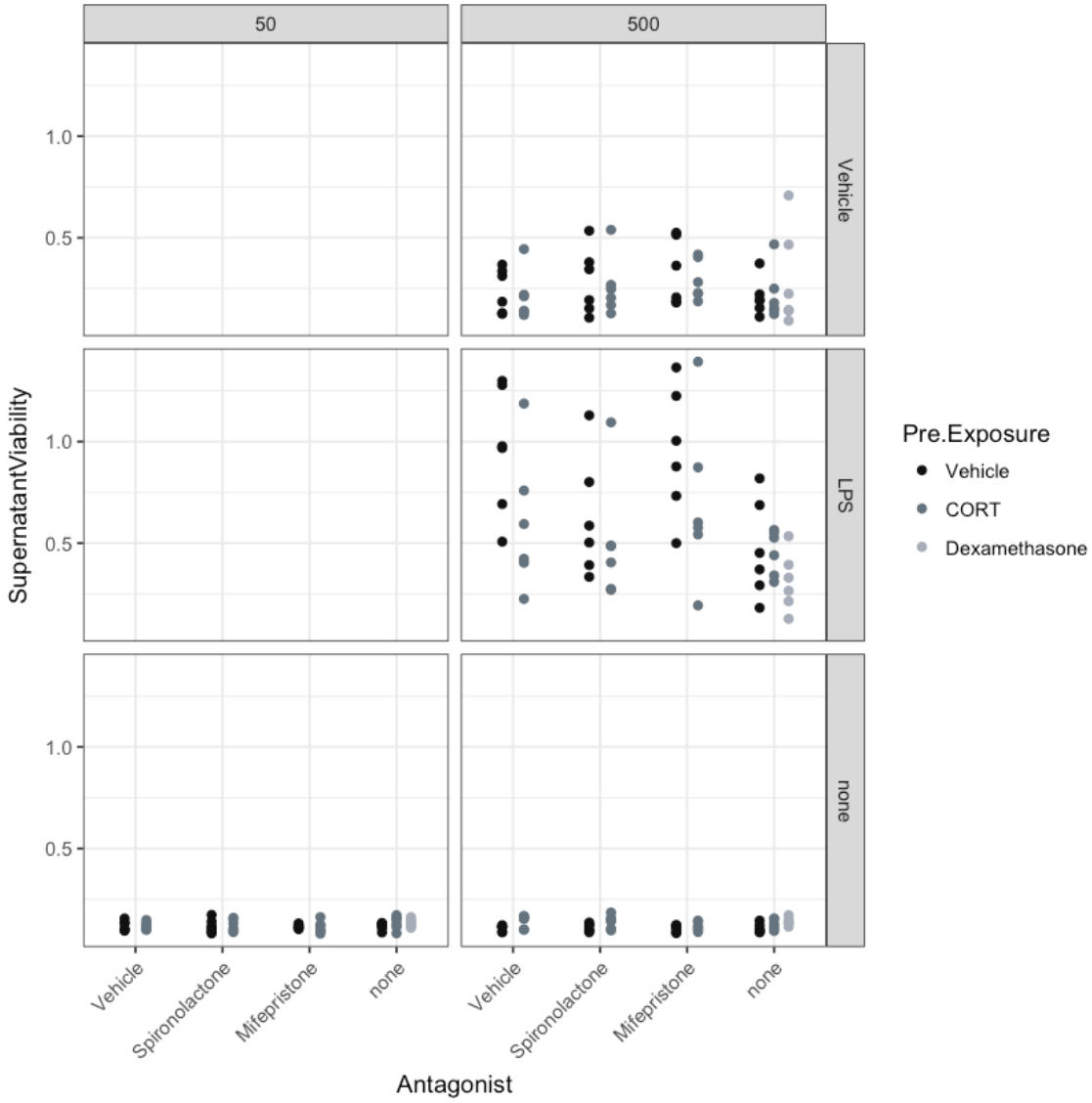
50
500
Vehicle
LPS
none
SupernatantViability
1.0
0.5
Vehicle
Spironolactone
Mifepristone
none
Antagonist
Pre.Exposure
Vehicle
CORT
Dexamethasone

In [119]:
```
# relationship between cellViability and LDH
ggplot(data = filter(df, Pre.ExposureDose == '500'), aes(x = CellViability, y = LDH, group = Pre.Exposure))+
  facet_grid(Treatment ~ Antagonist)+
  geom_point(aes(colour = Pre.Exposure, shape = Antagonist),size = 2)+
  stat_density2d(aes(fill = Pre.Exposure), geom = 'polygon', alpha = 0.1)+
  #scale_y_log10()+
  theme_bw()+
  theme(aspect.ratio = 1)+
  scale_color_manual(values = prePal)+
  scale_fill_manual(values = prePal)
```

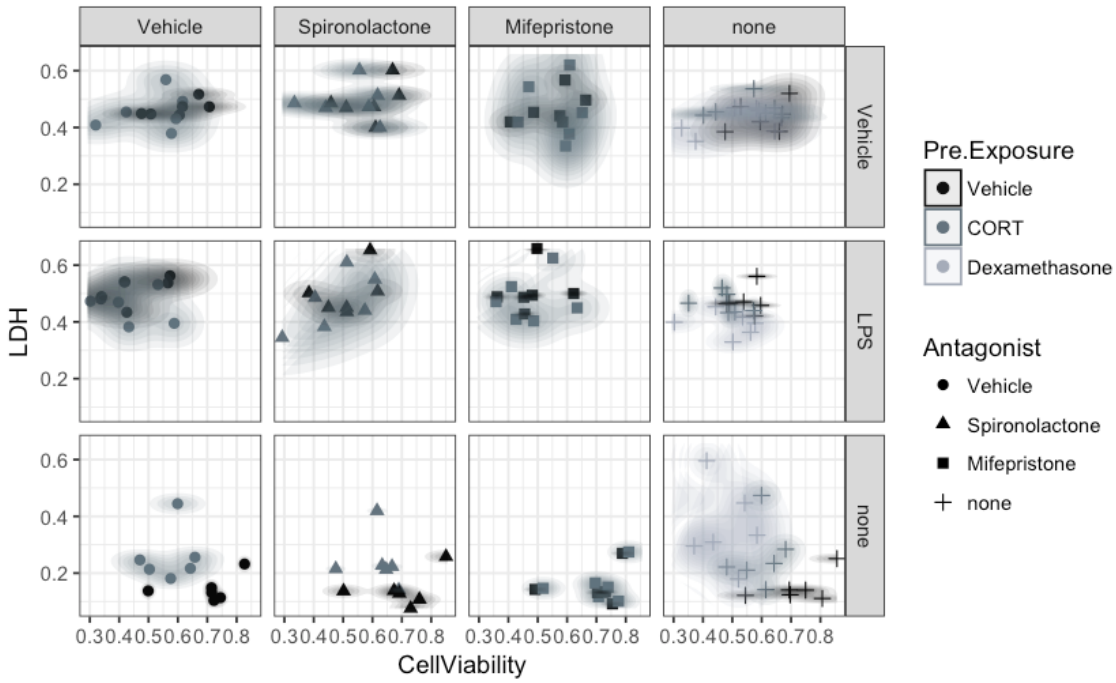

Linear mixed effects models for categorical independent variables

Example using LDH measure

In [120]:
```
library(nlme)
library(lsmeans)
```

In [121]:
```
#lm for LDH
## Before LPS
### Antagonist effect
lme1data<- filter(beforeLPS,Pre.Exposure != 'Dexamethasone', Antagonist !='none')
#lme1data$Pre.ExposureDose<-factor(lme1data$Pre.ExposureDose, levels = c('500', '50'))
lme1<- lme(LDH ~ Antagonist * Pre.Exposure * Pre.ExposureDose, random = (~1|N), data = lme1data)
summary(lme1)
lme1ls<- summary(lsmeans(lme1, pairwise~ Pre.Exposure | (Pre.ExposureDose+Antagonist)))
lme1ls
lme1means<- as.data.frame(lme1ls$lsmeans)
lme1comp<- as.data.frame(lme1ls$contrasts)
plot7<- ggplot(data = lme1means, aes(y = lsmean, x = Antagonist, group = Pre.Exposure))+
  facet_grid(.~ Pre.ExposureDose)+
  geom_bar(stat = 'identity', aes(fill = Pre.Exposure), width = 0.5, position = position_dodge(.5), alpha =
0.7 )+
  geom_errorbar(aes(ymax = lsmean + SE, ymin = lsmean -SE), width = 0.2, position = position_dodge(.5))+
  theme_minimal(base_size = 15)+
  theme(aspect.ratio = 1, axis.text.x = element_blank())+
  labs(y = "LDH activity (arbitrary units)", x = '')+
  scale_fill_manual(values = prePal)

plot7
```

```
Linear mixed-effects model fit by REML
 Data: lme1data
       AIC       BIC  logLik
  -72.6268 -43.30597 50.3134

Random effects:
 Formula: ~1 | N
        (Intercept)   Residual
StdDev:   0.1347793 0.07501231

Fixed effects: LDH ~ Antagonist * Pre.Exposure * Pre.ExposureDose
                                                                      Value
(Intercept)                                                        0.20150000
AntagonistSpironolactone                                          -0.00150000
AntagonistMifepristone                                             0.00483333
Pre.ExposureCORT                                                   0.05500000
Pre.ExposureDose500                                               -0.05708333
AntagonistSpironolactone:Pre.ExposureCORT                         -0.00458333
AntagonistMifepristone:Pre.ExposureCORT                           -0.03241667
AntagonistSpironolactone:Pre.ExposureDose500                      -0.00225000
AntagonistMifepristone:Pre.ExposureDose500                         0.00100000
Pre.ExposureCORT:Pre.ExposureDose500                               0.06025000
AntagonistSpironolactone:Pre.ExposureCORT:Pre.ExposureDose500      0.01183333
AntagonistMifepristone:Pre.ExposureCORT:Pre.ExposureDose500       -0.07400000
                                                                   Std.Error DF
(Intercept)                                                        0.06297132 55
AntagonistSpironolactone                                           0.04330838 55
AntagonistMifepristone                                             0.04330838 55
Pre.ExposureCORT                                                   0.04330838 55
Pre.ExposureDose500                                                0.04330838 55
AntagonistSpironolactone:Pre.ExposureCORT                          0.06124730 55
AntagonistMifepristone:Pre.ExposureCORT                            0.06124730 55
AntagonistSpironolactone:Pre.ExposureDose500                       0.06124730 55
AntagonistMifepristone:Pre.ExposureDose500                         0.06124730 55
Pre.ExposureCORT:Pre.ExposureDose500                               0.06124730 55
AntagonistSpironolactone:Pre.ExposureCORT:Pre.ExposureDose500      0.08661676 55
AntagonistMifepristone:Pre.ExposureCORT:Pre.ExposureDose500        0.08661676 55
                                                                     t-value p-value
(Intercept)                                                        3.199870  0.0023
AntagonistSpironolactone                                          -0.034635  0.9725
AntagonistMifepristone                                             0.111603  0.9115
Pre.ExposureCORT                                                   1.269962  0.2094
Pre.ExposureDose500                                               -1.318067  0.1929
AntagonistSpironolactone:Pre.ExposureCORT                         -0.074833  0.9406
AntagonistMifepristone:Pre.ExposureCORT                           -0.529275  0.5987
AntagonistSpironolactone:Pre.ExposureDose500                      -0.036736  0.9708
AntagonistMifepristone:Pre.ExposureDose500                         0.016327  0.9870
Pre.ExposureCORT:Pre.ExposureDose500                               0.983717  0.3296
AntagonistSpironolactone:Pre.ExposureCORT:Pre.ExposureDose500      -0.136617  0.8918
AntagonistMifepristone:Pre.ExposureCORT:Pre.ExposureDose500        -0.854338  0.3966
 Correlation:
                                                                   (Intr) AntgnS
AntagonistSpironolactone                                           -0.344
AntagonistMifepristone                                             -0.344  0.500
Pre.ExposureCORT                                                   -0.344  0.500
Pre.ExposureDose500                                                -0.344  0.500
AntagonistSpironolactone:Pre.ExposureCORT                           0.243 -0.707
AntagonistMifepristone:Pre.ExposureCORT                             0.243 -0.354
AntagonistSpironolactone:Pre.ExposureDose500                        0.243 -0.707
AntagonistMifepristone:Pre.ExposureDose500                          0.243 -0.354
Pre.ExposureCORT:Pre.ExposureDose500                                0.243 -0.354
AntagonistSpironolactone:Pre.ExposureCORT:Pre.ExposureDose500       -0.172  0.500
AntagonistMifepristone:Pre.ExposureCORT:Pre.ExposureDose500         -0.172  0.250
                                                                   AntgnM Pr.ECORT
AntagonistSpironolactone
AntagonistMifepristone
Pre.ExposureCORT                                                    0.500
Pre.ExposureDose500                                                 0.500  0.500
AntagonistSpironolactone:Pre.ExposureCORT                          -0.354 -0.707
AntagonistMifepristone:Pre.ExposureCORT                            -0.707 -0.707
AntagonistSpironolactone:Pre.ExposureDose500                       -0.354 -0.354
AntagonistMifepristone:Pre.ExposureDose500                         -0.707 -0.354
Pre.ExposureCORT:Pre.ExposureDose500                               -0.354 -0.707
AntagonistSpironolactone:Pre.ExposureCORT:Pre.ExposureDose500        0.250  0.500
AntagonistMifepristone:Pre.ExposureCORT:Pre.ExposureDose500          0.500  0.500
                                                                   P.ED50
AntagonistSpironolactone
AntagonistMifepristone
Pre.ExposureCORT
Pre.ExposureDose500
AntagonistSpironolactone:Pre.ExposureCORT                          -0.354
AntagonistMifepristone:Pre.ExposureCORT                            -0.354
AntagonistSpironolactone:Pre.ExposureDose500                       -0.707
AntagonistMifepristone:Pre.ExposureDose500                         -0.707
Pre.ExposureCORT:Pre.ExposureDose500                               -0.707
AntagonistSpironolactone:Pre.ExposureCORT:Pre.ExposureDose500        0.500
AntagonistMifepristone:Pre.ExposureCORT:Pre.ExposureDose500          0.500
                                                                   AnS:P.ECORT
```

```
AntagonistSpironolactone
AntagonistMifepristone
Pre.ExposureCORT
Pre.ExposureDose500
AntagonistSpironolactone:Pre.ExposureCORT
AntagonistMifepristone:Pre.ExposureCORT                          0.500
AntagonistSpironolactone:Pre.ExposureDose500                     0.500
AntagonistMifepristone:Pre.ExposureDose500                       0.250
Pre.ExposureCORT:Pre.ExposureDose500                             0.500
AntagonistSpironolactone:Pre.ExposureCORT:Pre.ExposureDose500 -0.707
AntagonistMifepristone:Pre.ExposureCORT:Pre.ExposureDose500   -0.354
                                                              AnM:P.ECORT
AntagonistSpironolactone
AntagonistMifepristone
Pre.ExposureCORT
Pre.ExposureDose500
AntagonistSpironolactone:Pre.ExposureCORT
AntagonistMifepristone:Pre.ExposureCORT
AntagonistSpironolactone:Pre.ExposureDose500                     0.250
AntagonistMifepristone:Pre.ExposureDose500                       0.500
Pre.ExposureCORT:Pre.ExposureDose500                             0.500
AntagonistSpironolactone:Pre.ExposureCORT:Pre.ExposureDose500 -0.354
AntagonistMifepristone:Pre.ExposureCORT:Pre.ExposureDose500   -0.707
                                                              AS:P.ED AM:P.ED
AntagonistSpironolactone
AntagonistMifepristone
Pre.ExposureCORT
Pre.ExposureDose500
AntagonistSpironolactone:Pre.ExposureCORT
AntagonistMifepristone:Pre.ExposureCORT
AntagonistSpironolactone:Pre.ExposureDose500
AntagonistMifepristone:Pre.ExposureDose500                       0.500
Pre.ExposureCORT:Pre.ExposureDose500                             0.500   0.500
AntagonistSpironolactone:Pre.ExposureCORT:Pre.ExposureDose500 -0.707  -0.354
AntagonistMifepristone:Pre.ExposureCORT:Pre.ExposureDose500   -0.354  -0.707
                                                              P.ECORT:
AntagonistSpironolactone
AntagonistMifepristone
Pre.ExposureCORT
Pre.ExposureDose500
AntagonistSpironolactone:Pre.ExposureCORT
AntagonistMifepristone:Pre.ExposureCORT
AntagonistSpironolactone:Pre.ExposureDose500
AntagonistMifepristone:Pre.ExposureDose500
Pre.ExposureCORT:Pre.ExposureDose500
AntagonistSpironolactone:Pre.ExposureCORT:Pre.ExposureDose500 -0.707
AntagonistMifepristone:Pre.ExposureCORT:Pre.ExposureDose500   -0.707
                                                              AS:P.ECORT:
AntagonistSpironolactone
AntagonistMifepristone
Pre.ExposureCORT
Pre.ExposureDose500
AntagonistSpironolactone:Pre.ExposureCORT
AntagonistMifepristone:Pre.ExposureCORT
AntagonistSpironolactone:Pre.ExposureDose500
AntagonistMifepristone:Pre.ExposureDose500
Pre.ExposureCORT:Pre.ExposureDose500
AntagonistSpironolactone:Pre.ExposureCORT:Pre.ExposureDose500
AntagonistMifepristone:Pre.ExposureCORT:Pre.ExposureDose500    0.500

Standardized Within-Group Residuals:
        Min          Q1         Med          Q3         Max
-2.41245521 -0.44239931 -0.04124594  0.38800771  2.30010443

Number of Observations: 72
Number of Groups: 6
```

$lsmeans

Pre.Exposure	Pre.ExposureDose	Antagonist	lsmean	SE	df	lower.CL	upper.CL
Vehicle	50	Vehicle	0.2015000	0.06297132	5	0.039627078	0.3633729
CORT	50	Vehicle	0.2565000	0.06297132	5	0.094627078	0.4183729
Vehicle	500	Vehicle	0.1444167	0.06297132	5	-0.017456255	0.3062896
CORT	500	Vehicle	0.2596667	0.06297132	5	0.097793745	0.4215396
Vehicle	50	Spironolactone	0.2000000	0.06297132	5	0.038127078	0.3618729
CORT	50	Spironolactone	0.2504167	0.06297132	5	0.088543745	0.4122896
Vehicle	500	Spironolactone	0.1406667	0.06297132	5	-0.021206255	0.3025396
CORT	500	Spironolactone	0.2395000	0.06297132	5	0.077627078	0.4013729
Vehicle	50	Mifepristone	0.2063333	0.06297132	5	0.044460411	0.3682063
CORT	50	Mifepristone	0.2289167	0.06297132	5	0.067043745	0.3907896
Vehicle	500	Mifepristone	0.1502500	0.06297132	5	-0.011622922	0.3121229
CORT	500	Mifepristone	0.1590833	0.06297132	5	-0.002789589	0.3209563

$contrasts

contrast	Pre.ExposureDose	Antagonist	estimate	SE	df	t.ratio	p.value
Vehicle - CORT	50	Vehicle	-0.055000000	0.04330838	55	-1.2699621	0.20944486
Vehicle - CORT	500	Vehicle	-0.115250000	0.04330838	55	-2.6611478	0.01018740
Vehicle - CORT	50	Spironolactone	-0.050416667	0.04330838	55	-1.1641319	0.24939562
Vehicle - CORT	500	Spironolactone	-0.098833333	0.04330838	55	-2.2820834	0.02637617
Vehicle - CORT	50	Mifepristone	-0.022583333	0.04330838	55	-0.5214541	0.60414399
Vehicle - CORT	500	Mifepristone	-0.008833333	0.04330838	55	-0.2039636	0.83913477

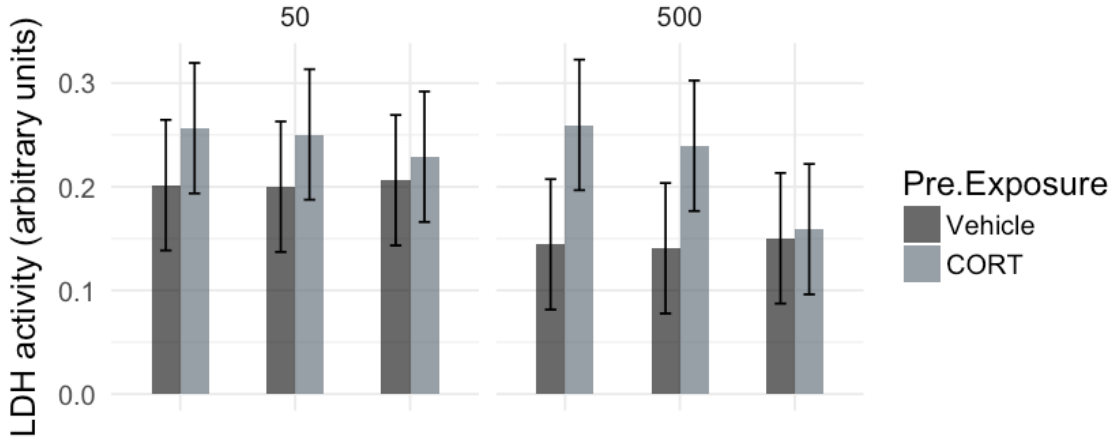

In [122]:
```
### DEX effect
lme2<- lme(LDH ~ Pre.Exposure * Pre.ExposureDose, random = (~1|N), data = filter(beforeLPS, Antagonist =='non
e'))
summary(lme2)
lme2ls<-summary(lsmeans(lme2, pairwise~ Pre.Exposure | Pre.ExposureDose))
lme2means<- as.data.frame(lme2ls$lsmeans)
lme2comp<- as.data.frame(lme2ls$contrasts)
lme2ls
plot1<- ggplot(data = lme2means, aes(y = lsmean, x = Pre.ExposureDose, group = Pre.Exposure))+
  geom_bar(stat = 'identity', aes(fill = Pre.Exposure),width = 0.5, position = position_dodge(0.5), alpha =
0.7)+
  geom_errorbar(aes(ymax = lsmean+SE, ymin = lsmean -SE), width = 0.2, position= position_dodge(0.5), size =
0.8)+
  theme_minimal(base_size = 20)+
  theme(aspect.ratio =1 , axis.text.x = element_text(angle = 45, hjust = 1))+
  labs(y= 'LDH activity (arbitrary units)', x = 'Pre-Exposure Concentration (nM)')+
  scale_fill_manual(values = prePal)
plot1
```

```
Linear mixed-effects model fit by REML
 Data: filter(beforeLPS, Antagonist == "none")
        AIC       BIC   logLik
  -29.36183 -18.15225 22.68092

Random effects:
 Formula: ~1 | N
        (Intercept)  Residual
StdDev:   0.1358567 0.0735574

Fixed effects: LDH ~ Pre.Exposure * Pre.ExposureDose
                                                 Value  Std.Error DF
(Intercept)                                  0.21500000 0.06307102 25
Pre.ExposureCORT                             0.03541667 0.04246838 25
Pre.ExposureDexamethasone                    0.13025000 0.04246838 25
Pre.ExposureDose500                         -0.06716667 0.04246838 25
Pre.ExposureCORT:Pre.ExposureDose500          0.07758333 0.06005937 25
Pre.ExposureDexamethasone:Pre.ExposureDose500  0.08191667 0.06005937 25
                                              t-value p-value
(Intercept)                                  3.408855  0.0022
Pre.ExposureCORT                             0.833954  0.4122
Pre.ExposureDexamethasone                    3.066987  0.0051
Pre.ExposureDose500                         -1.581569  0.1263
Pre.ExposureCORT:Pre.ExposureDose500          1.291777  0.2082
Pre.ExposureDexamethasone:Pre.ExposureDose500  1.363928  0.1847
 Correlation:
                                            (Intr) Pr.ECORT Pr.ExD P.ED50
Pre.ExposureCORT                            -0.337
Pre.ExposureDexamethasone                   -0.337  0.500
Pre.ExposureDose500                         -0.337  0.500    0.500
Pre.ExposureCORT:Pre.ExposureDose500          0.238 -0.707   -0.354 -0.707
Pre.ExposureDexamethasone:Pre.ExposureDose500  0.238 -0.354   -0.707 -0.707
                                            P.ECORT:
Pre.ExposureCORT
Pre.ExposureDexamethasone
Pre.ExposureDose500
Pre.ExposureCORT:Pre.ExposureDose500
Pre.ExposureDexamethasone:Pre.ExposureDose500  0.500

Standardized Within-Group Residuals:
        Min          Q1         Med          Q3         Max
-2.17089299 -0.57613608 -0.06309135  0.38172784  2.01518029

Number of Observations: 36
Number of Groups: 6
```

$lsmeans

Pre.Exposure	Pre.ExposureDose	lsmean	SE	df	lower.CL	upper.CL
Vehicle	50	0.2150000	0.06307102	5	0.05287077	0.3771292
CORT	50	0.2504167	0.06307102	5	0.08828744	0.4125459
Dexamethasone	50	0.3452500	0.06307102	5	0.18312077	0.5073792
Vehicle	500	0.1478333	0.06307102	5	-0.01429590	0.3099626
CORT	500	0.2608333	0.06307102	5	0.09870410	0.4229626
Dexamethasone	500	0.3600000	0.06307102	5	0.19787077	0.5221292

$contrasts

contrast	Pre.ExposureDose	estimate	SE	df	t.ratio	p.value
Vehicle - CORT	50	-0.03541667	0.04246838	25	-0.8339537	0.6858428851
Vehicle - Dexamethasone	50	-0.13025000	0.04246838	25	-3.0669874	0.0137376868
CORT - Dexamethasone	50	-0.09483333	0.04246838	25	-2.2330337	0.0849965919
Vehicle - CORT	500	-0.11300000	0.04246838	25	-2.6608029	0.0346278108
Vehicle - Dexamethasone	500	-0.21216667	0.04246838	25	-4.9958732	0.0001083724
CORT - Dexamethasone	500	-0.09916667	0.04246838	25	-2.3350704	0.0691797530

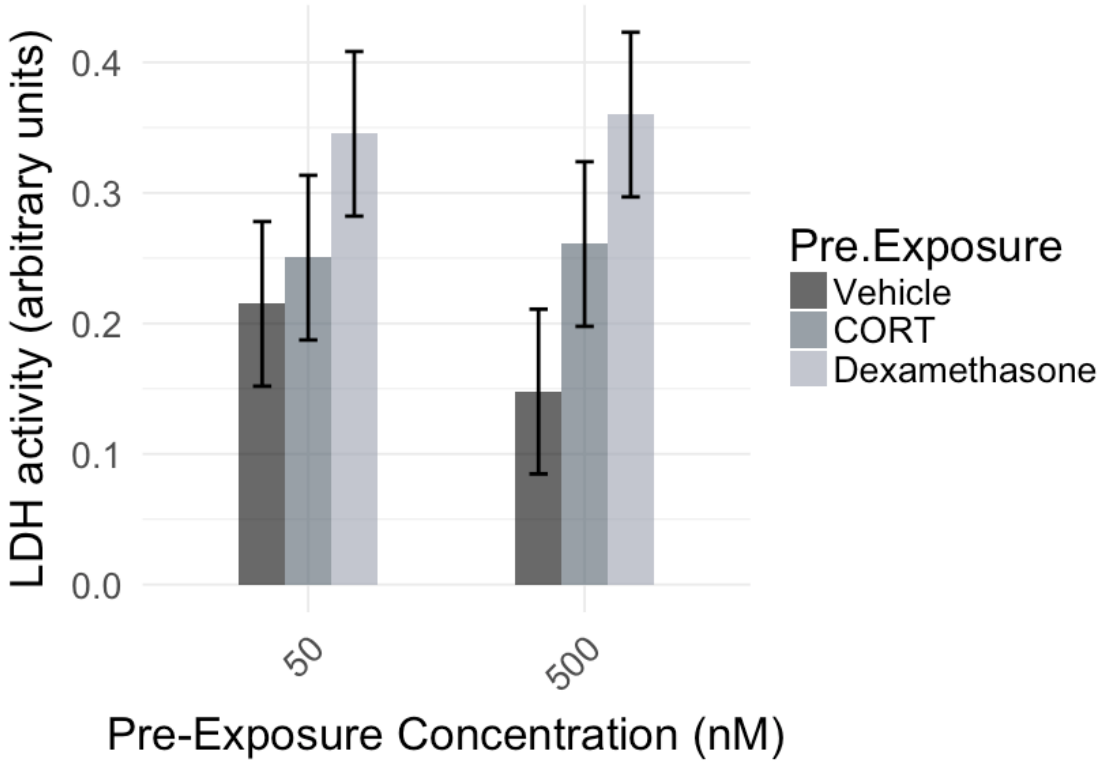
LDH activity (arbitrary units)
0.4
0.3
0.2
0.1
0.0
50
500
Pre-Exposure Concentration (nM)
Pre.Exposure
Vehicle
CORT
Dexamethasone

PCA and SVM analysis

In [42]:
```
library(factoextra)
library(ggplot2)
library(dplyr)
library(caret)
```

In [43]:
```
# load dataset
df<- read.csv('TOTALDF.csv', header = T)
df<- df %>%
mutate(GR_Activity = ifelse(PreExposure == 'Vehicle', 0,
                            ifelse(PreExposure == 'DEX', 1,
                                   ifelse(PreExposure == 'CORT' &
                                          (Antagonist =='Vehicle'| Antagonist == 'Spironolactone'| Antagonist =
= 'None'),
                                          1, 0)))) %>%
mutate(MR_Activity = ifelse(PreExposure == 'Vehicle', 0,
                            ifelse(PreExposure == 'DEX', 0,
                                   ifelse(PreExposure == 'CORT' &
                                          (Antagonist =='Vehicle'| Antagonist == 'Mifepristone'| Antagonist ==
'None'),
                                          1, 0)))) %>%
mutate(Receptor_activity = ifelse(GR_Activity == 0 & MR_Activity == 0, 'None',
                                  ifelse(GR_Activity == 1 & MR_Activity == 0, 'GR only',
                                         ifelse(GR_Activity == 0 & MR_Activity == 1, 'MR only',
                                                'GR + MR'))))

df<- select(df, -BetaActin)
df$Receptor_activity<- as.factor(df$Receptor_activity)
df$Receptor_activity<- factor(df$Receptor_activity, levels = c('None', 'GR + MR', 'GR only', 'MR only'))
```

PCA for visualising multiple measures

In [44]:
```
summary(df)
```

```
       N         PreExposure          Antagonist   Treatment      HMGB1       
 Min.   :1.0   CORT   :72   Mifepristone  :36   LPS    :54   Min.   :0.00000  
 1st Qu.:2.0   DEX    :18   None          :54   None   :54   1st Qu.:0.07994  
 Median :3.5   Vehicle:72   Spironolactone:36   Vehicle:54   Median :0.22012  
 Mean   :3.5                Vehicle       :36                Mean   :0.24488  
 3rd Qu.:5.0                                                 3rd Qu.:0.39337  
 Max.   :6.0                                                 Max.   :0.73529  
      ASC               NLRP3              LDH          CellViability     
 Min.   :0.00000   Min.   :0.0000   Min.   :0.0755   Min.   :0.2925  
 1st Qu.:0.07877   1st Qu.:0.0140   1st Qu.:0.2522   1st Qu.:0.4756  
 Median :0.34982   Median :0.0623   Median :0.4343   Median :0.5747  
 Mean   :0.38104   Mean   :0.1006   Mean   :0.3807   Mean   :0.5610  
 3rd Qu.:0.62671   3rd Qu.:0.1341   3rd Qu.:0.4735   3rd Qu.:0.6444  
 Max.   :1.53425   Max.   :0.6142   Max.   :0.6585   Max.   :0.8565  
 SupernatantViability  GR_Activity      MR_Activity     Receptor_activity
 Min.   :0.0840       Min.   :0.0000   Min.   :0.0000   None   :72       
 1st Qu.:0.1280       1st Qu.:0.0000   1st Qu.:0.0000   GR + MR:36       
 Median :0.1940       Median :0.0000   Median :0.0000   GR only:36       
 Mean   :0.3334       Mean   :0.4444   Mean   :0.3333   MR only:18       
 3rd Qu.:0.4500       3rd Qu.:1.0000   3rd Qu.:1.0000                    
 Max.   :1.3930       Max.   :1.0000   Max.   :1.0000                    
```

In [45]:
```
pc <- prcomp(df[5:10], scale = T)
eig<- pc$sdev^2
variance <- eig*100/sum(eig)
cumvar <- cumsum(variance)
eiganvals<-data.frame(eig = eig, variance =variance, cumvar=cumvar)
eiganvals
```

eig	variance	cumvar
2.0105216	33.508694	33.50869
1.5927288	26.545481	60.05417
0.9260070	15.433451	75.48763
0.5654853	9.424755	84.91238
0.4749016	7.915026	92.82741
0.4303556	7.172593	100.00000

In [46]:
```
pc$rotation #identify the transformation parameter for each variable according to PC dimensions
```

	PC1	PC2	PC3	PC4	PC5	PC6
HMGB1	0.1498836	-0.63369395	0.21235976	-0.541743461	0.34697549	-0.3420413
ASC	0.2717559	-0.54699886	0.40474669	0.347420594	-0.41435660	0.4131932
NLRP3	-0.1614402	0.37460074	0.85835523	0.008329851	-0.05944999	-0.3053424
LDH	0.4800656	0.34993098	0.06268232	-0.656890901	-0.25441586	0.3833056
CellViability	-0.5830819	-0.06172465	0.18201906	-0.198205257	0.37469059	0.6658801
SupernatantViability	0.5542321	0.18065681	0.13133826	0.339046585	0.70658463	0.1694867

In [47]:
```
summary(pc)
screeplot(pc) # visulaises varibility captured
```

```
Importance of components:
                          PC1    PC2    PC3     PC4     PC5     PC6
Standard deviation     1.4179 1.2620 0.9623 0.75199 0.68913 0.65601
Proportion of Variance 0.3351 0.2655 0.1543 0.09425 0.07915 0.07173
Cumulative Proportion  0.3351 0.6005 0.7549 0.84912 0.92827 1.00000
```

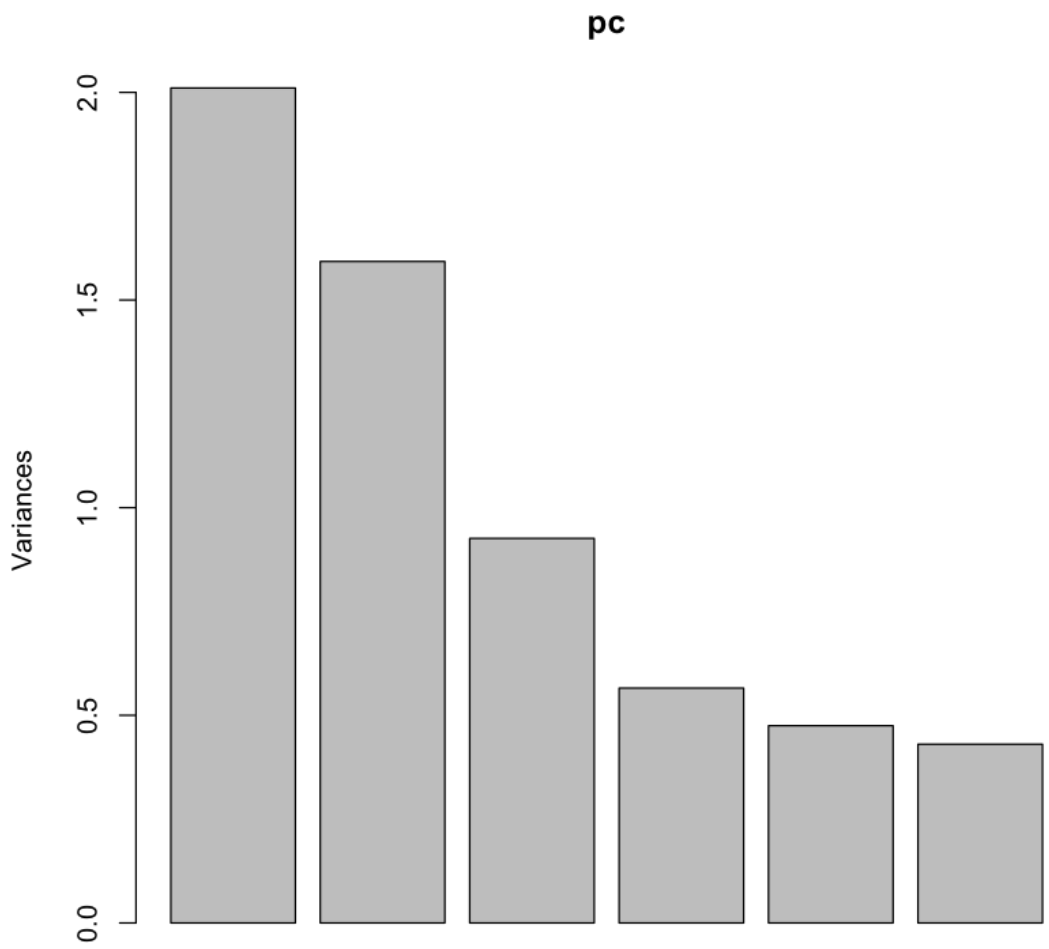

In [48]:
```
fviz_pca_var(pc) # principal component directions and weights
fviz_pca_ind(pc, col.ind='contrib')+
      scale_color_gradient2(low="black", mid="blue",
      high="red")
```

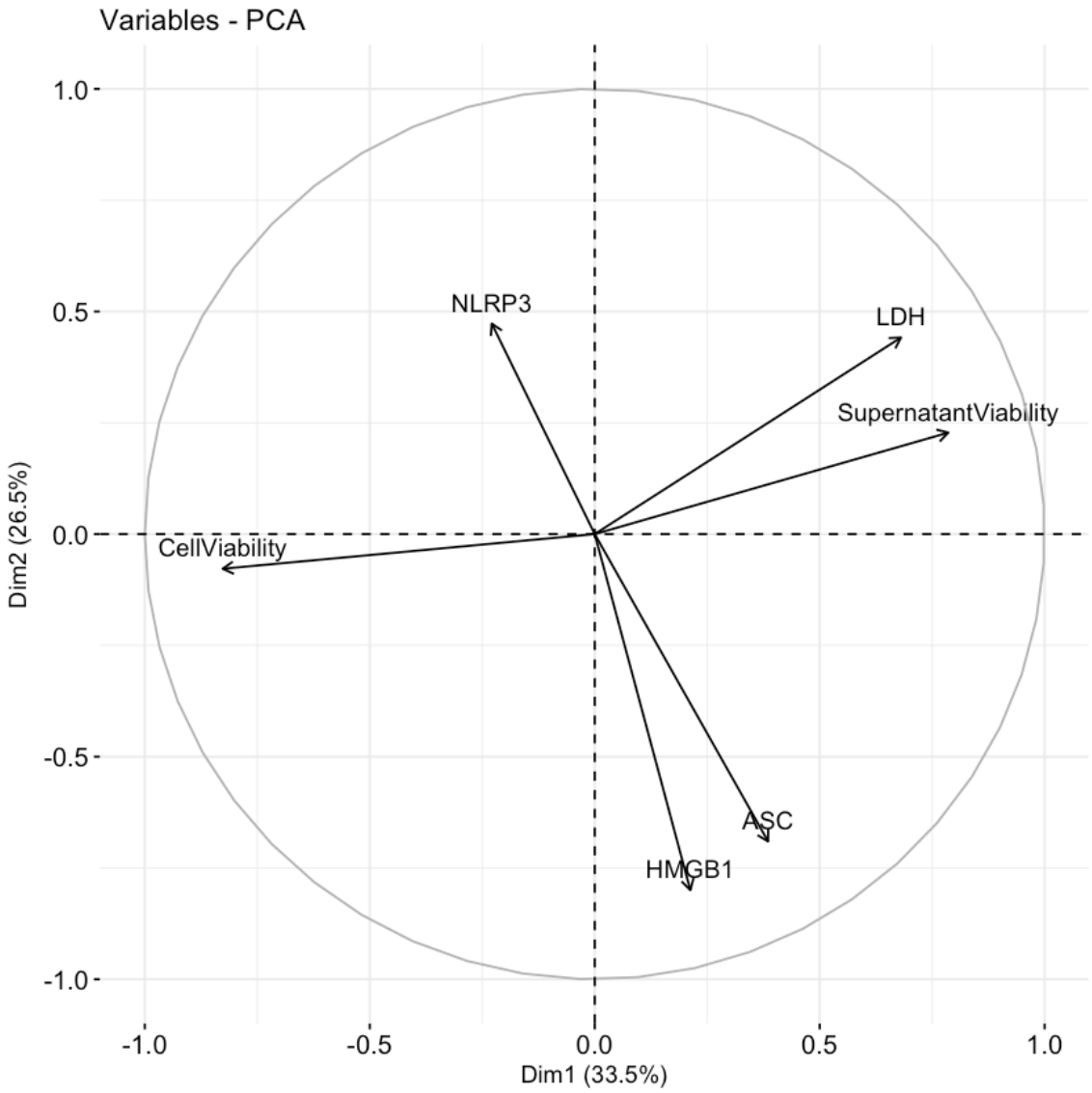
Variables - PCA
1.0
0.5
0.0
-0.5
-1.0
Dim2 (26.5%)
NLRP3
LDH
SupernatantViability
CellViability
ASC
HMGB1
-1.0
-0.5
0.0
0.5
1.0
Dim1 (33.5%)

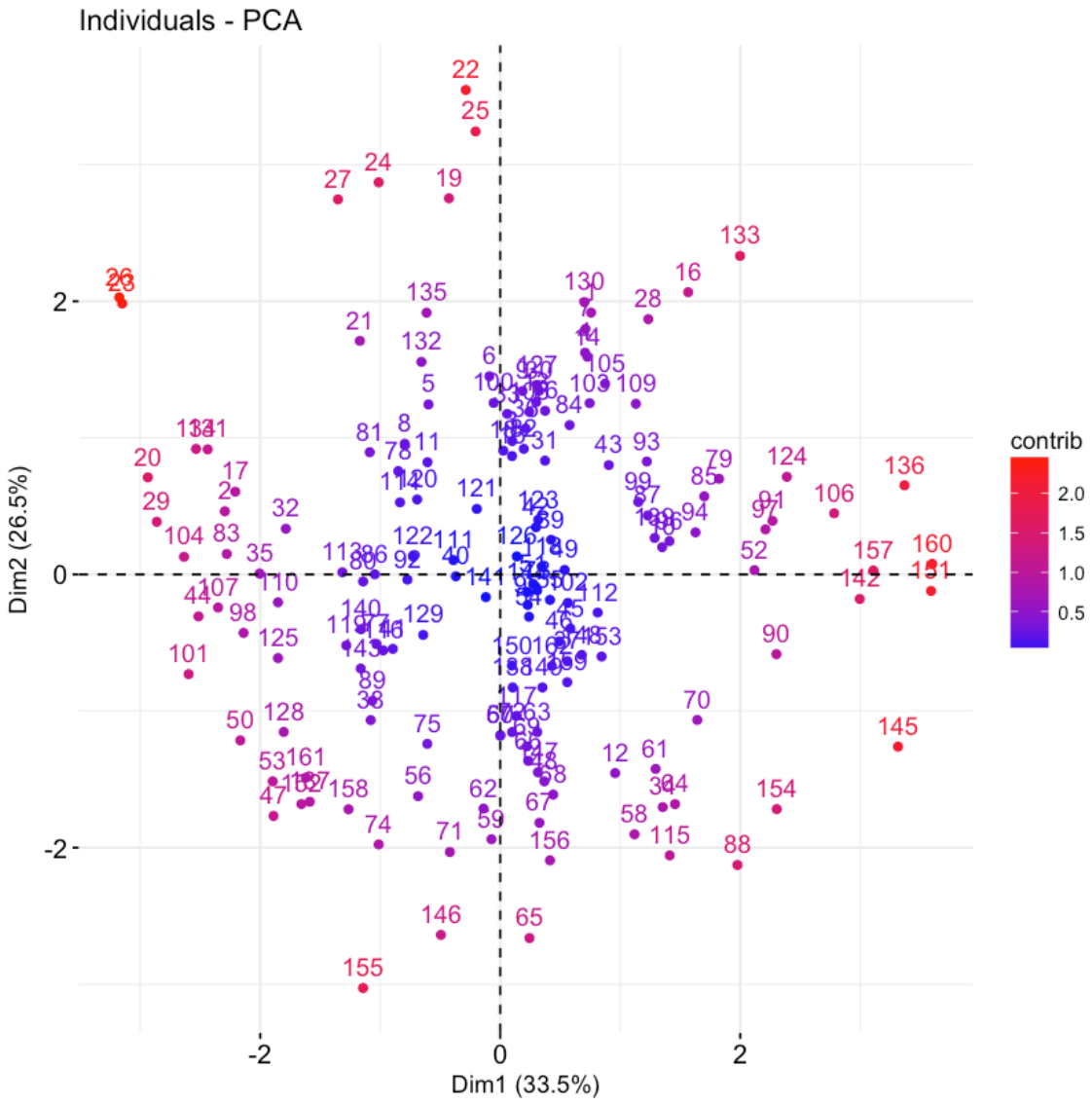

In [49]:
```
groups <- cbind(df[1:4], df[11:13])
rotateddf<- data.frame(groups, pc$x) #use rotation from PCA transformation on original data points
newvar<-get_pca_var(pc)
newvar
coordinates<- data.frame(varnames= rownames(newvar$coord), newvar$coord) #variable data
coordinates #variable coordinates according to
```

```
Principal Component Analysis Results for variables
 ===================================================
  Name       Description
1 "$coord"   "Coordinates for the variables"
2 "$cor"     "Correlations between variables and dimensions"
3 "$cos2"    "Cos2 for the variables"
4 "$contrib" "contributions of the variables"
```

	varnames	Dim.1	Dim.2	Dim.3	Dim.4	Dim.5	Dim.6
HMGB1	HMGB1	0.2125243	-0.79974306	0.20435223	-0.407384351	0.23911158	-0.2243842
ASC	ASC	0.3853305	-0.69033095	0.38948475	0.261255969	-0.28554600	0.2710609
NLRP3	NLRP3	-0.2289107	0.47275873	0.82598888	0.006263945	-0.04096884	-0.2003091
LDH	LDH	0.6806988	0.44162466	0.06031874	-0.493973794	-0.17532587	0.2514542
CellViability	CellViability	-0.8267685	-0.07789859	0.17515559	-0.149047890	0.25821091	0.4368273
SupernatantViability	SupernatantViability	0.7858616	0.22799497	0.12638583	0.254958819	0.48692940	0.1111858

In [50]:
```
# preparing data frame for plotting
rotateddf$Treatment<- factor(rotateddf$Treatment, levels = c('None', 'Vehicle', 'LPS'))
rotateddf$Antagonist<- factor(rotateddf$Antagonist, levels = c('None', 'Vehicle', 'Mifepristone', 'Spironolac
tone'))
rotateddf$Receptor_activity <- factor(rotateddf$Receptor_activity, levels = c('None', 'GR + MR','GR only','MR
 only'))

none_only<- rotateddf %>%
filter(Receptor_activity =='None')
```

In [51]:
```
#Plot all datapoints on PC1 and PC2
plot16<- ggplot(data = rotateddf, aes(x = PC1, y = PC2))+
geom_point(size = 2, alpha = 0.2)+
geom_segment(data = coordinates, aes(x = 0, y = 0, xend = Dim.1*2, yend = Dim.2*2),
             arrow = arrow(length = unit(0.3, 'cm')), alpha = 0.75, color = 'black')+
geom_text(data=coordinates, aes(x=Dim.1*2.7, y=Dim.2*2.7, label=varnames), size = 5, color="black", alpha =
0.75)+
theme_minimal(base_size = 18)+
labs(y = 'Principal component 1', x = 'Principal componant 2')+
theme(aspect.ratio = 1, legend.position = 'none')

plot16
```

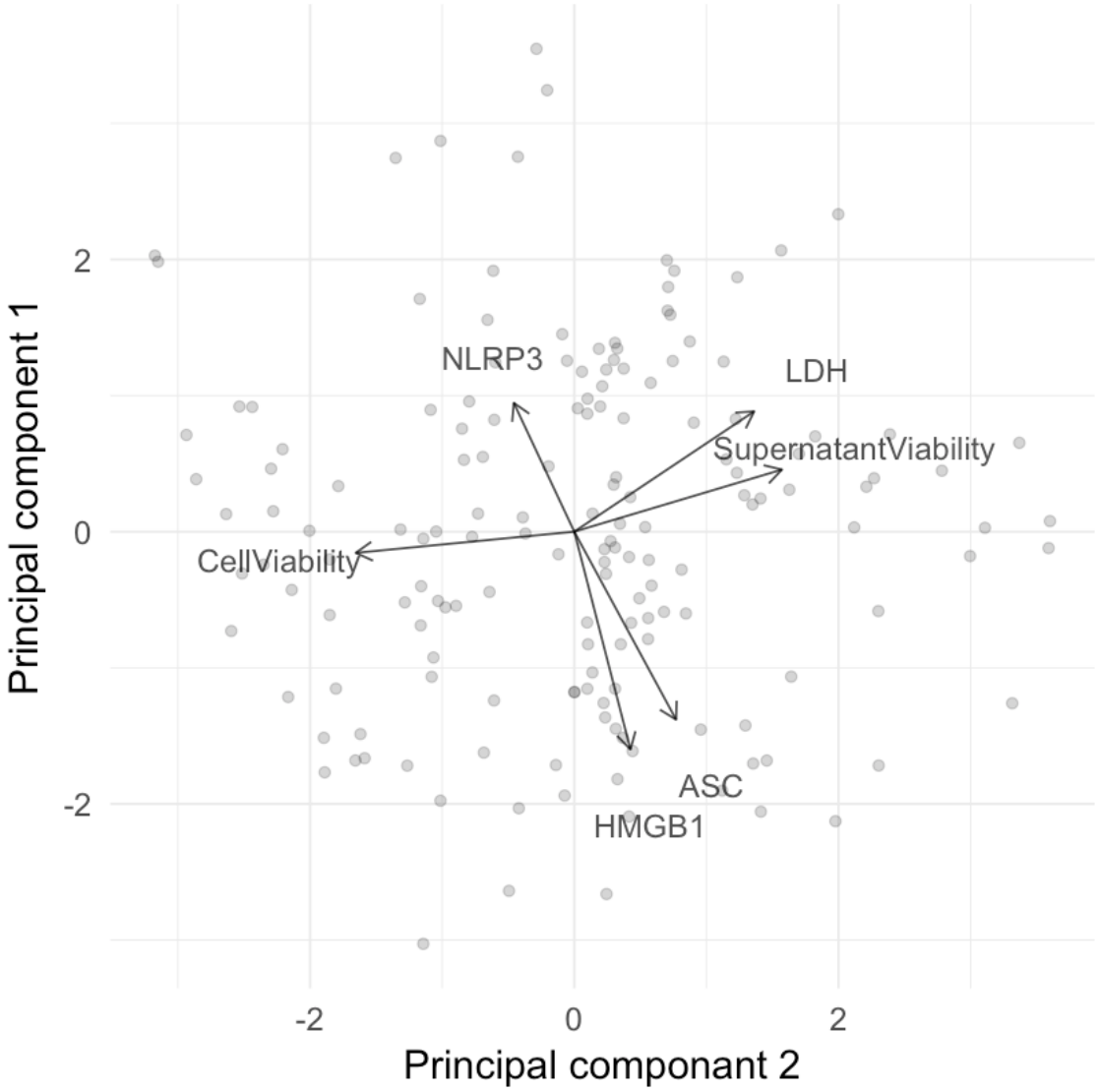

In [52]:
```
ggsave(plot17, filename = 'pcaplot_palette_nobeta.png')
```

```
Saving 7 x 7 in image
```

In [53]:
```
# split plots intop different subgroups according to receptor activity and treatments
plot17<- ggplot(data = filter(rotateddf, Receptor_activity != 'None'), aes(x = PC1, y = PC2))+
facet_grid(Receptor_activity~Treatment)+
geom_point(aes(colour = Receptor_activity), size = 2)+
geom_segment(data = coordinates, aes(x = 0, y = 0, xend = Dim.1*2, yend = Dim.2*2),
             arrow = arrow(length = unit(0.1, 'cm')), alpha = 0.75, color = 'black')+
geom_text(data=coordinates, aes(x=Dim.1*1.5, y=Dim.2*2.5, label=varnames), size = 2.5, color="black", alpha =
 0.75)+
geom_point(data = none_only[, c('Treatment','PC1', 'PC2')], aes(y = PC2, x = PC1), colour = 'grey', alpha =
0.75)+
stat_density2d(geom = 'polygon', aes(fill = Receptor_activity), alpha = 0.05)+
theme_minimal(base_size = 13)+
labs(y = 'Principal component 1', x = 'Principal componant 2')+
theme(aspect.ratio = 1, legend.position = 'bottom')+
scale_color_manual(values = palette)+
scale_fill_manual(values = palette)

plot17
```

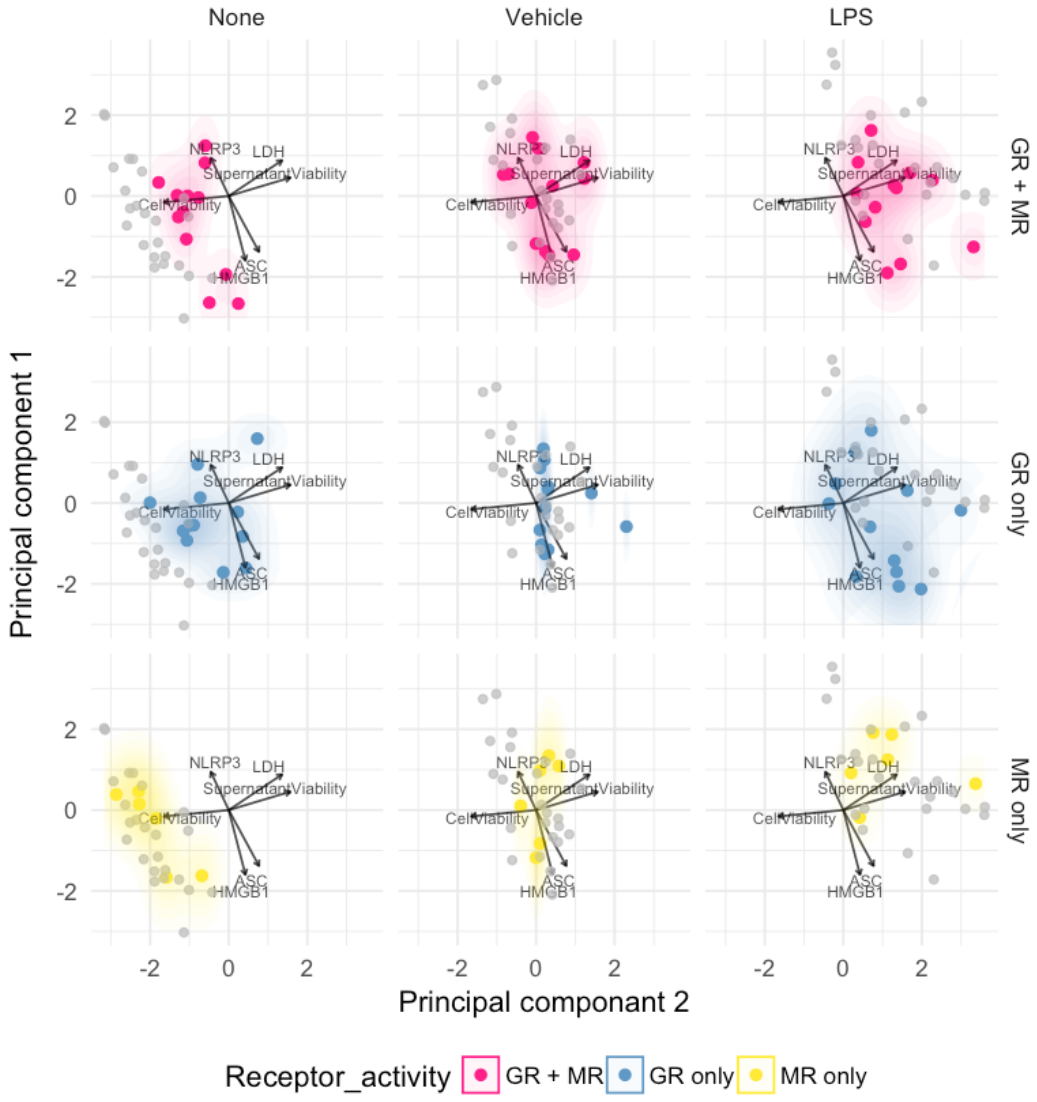

PCA with feature scaling on dataset separated by GR / MR receptor activity:

- Grey dots represent no GR or MR activity (vehicle pre-exposure)
- Supporting Linear model findings, most differences in receptor activity appear to be beforer addition of a furt her 24h treatment of either vehicle or LPS
- MR only (GR antagonist) appears to be least different from no receptor activity
- GR only (MR antagonist, DEX treatment) and GR + MR activity (CORT with no antagonist) seem to separate from no receptor activity.

Multinomial logistic regression

- Predicting Receptor activity from available measures using logistic regression

In [54]:
```
library(nnet)
```

In [55]:
```
model<-  multinom(Receptor_activity ~ PC1 + PC2 + Treatment , data = rotateddf)
summary(model)
```

```
# weights:  24 (15 variable)
initial  value 224.579687
iter  10 value 198.903834
iter  20 value 198.547652
iter  20 value 198.547652
iter  20 value 198.547652
final  value 198.547652
converged
```

```
Call:
multinom(formula = Receptor_activity ~ PC1 + PC2 + Treatment,
    data = rotateddf)

Coefficients:
         (Intercept)        PC1         PC2 TreatmentVehicle TreatmentLPS
GR + MR -0.116268504 0.49582125 -0.21284447       -0.6305544   -1.1187076
GR only  0.006841524 0.62334720 -0.23329448       -0.7951191   -1.4465792
MR only -1.246574623 0.07202778  0.08808535       -0.1725186   -0.2666905

Std. Errors:
        (Intercept)       PC1       PC2 TreatmentVehicle TreatmentLPS
GR + MR   0.5232064 0.2509225 0.1877826        0.6656713    0.8802319
GR only   0.5169661 0.2517700 0.1900994        0.6637461    0.8862440
MR only   0.7216790 0.3305842 0.2377315        0.8910884    1.1578426

Residual Deviance: 397.0953
AIC: 427.0953
```

In [56]:
```
cm<-  table(predict(model), rotateddf$Receptor_activity)
confusionMatrix(cm)
```

```
Confusion Matrix and Statistics


          None GR + MR GR only MR only
  None      65      31      27      17
  GR + MR    0       0       0       0
  GR only    7       5       9       1
  MR only    0       0       0       0

Overall Statistics

               Accuracy : 0.4568
                 95% CI : (0.3784, 0.5368)
    No Information Rate : 0.4444
    P-Value [Acc > NIR] : 0.4052

                  Kappa : 0.0726
 Mcnemar's Test P-Value : NA

Statistics by Class:

                     Class: None Class: GR + MR Class: GR only Class: MR only
Sensitivity               0.9028         0.0000        0.25000         0.0000
Specificity               0.1667         1.0000        0.89683         1.0000
Pos Pred Value            0.4643            NaN        0.40909            NaN
Neg Pred Value            0.6818         0.7778        0.80714         0.8889
Prevalence                0.4444         0.2222        0.22222         0.1111
Detection Rate            0.4012         0.0000        0.05556         0.0000
Detection Prevalence      0.8642         0.0000        0.13580         0.0000
Balanced Accuracy         0.5347         0.5000        0.57341         0.5000
```

SVM only on treatment == 'None'

- Since most antagonist differences are only seen prior to further 24h treatment with Vehicle / LPS, can better classification be achieved if we just look at prior treatments?

In [57]:
```
library(e1071) # for svm() function
```

In [58]:
```
df3<- filter(df, Treatment == 'None')
df2<- as.matrix( df3 %>%  select(HMGB1, CellViability, SupernatantViability, LDH) %>%
                mutate_each(funs(scale)))
df2<- data.frame(Receptor_activity = df3$Receptor_activity, df2)
```

In [59]:
```
summary(df2)
```

```
 Receptor_activity     HMGB1          CellViability      SupernatantViability
 None   :24        Min.   :-1.1889   Min.   :-2.3165   Min.   :-1.47137
 GR + MR:12        1st Qu.:-0.8032   1st Qu.:-0.8362   1st Qu.:-0.81134
 GR only:12        Median :-0.2723   Median : 0.2122   Median :-0.06459
 MR only: 6        Mean   : 0.0000   Mean   : 0.0000   Mean   : 0.00000
                   3rd Qu.: 0.5966   3rd Qu.: 0.7032   3rd Qu.: 0.77369
                   Max.   : 2.4437   Max.   : 1.7842   Max.   : 2.44062
      LDH
 Min.   :-1.2127
 1st Qu.:-0.6810
 Median :-0.3222
 Mean   : 0.0000
 3rd Qu.: 0.3964
 Max.   : 3.5905
```

In [60]:
```
svm1<- svm(Receptor_activity ~ HMGB1+ CellViability+ SupernatantViability+LDH, data =df2, kernel = 'radial')
summary(svm1)
```

```
Call:
svm(formula = Receptor_activity ~ HMGB1 + CellViability + SupernatantViability +
    LDH, data = df2, kernel = "radial")


Parameters:
   SVM-Type:  C-classification
 SVM-Kernel:  radial
       cost:  1
      gamma:  0.25

Number of Support Vectors:  47

 ( 6 12 12 17 )


Number of Classes:  4

Levels:
 None GR + MR GR only MR only
```

In [61]:
```
cm<-table(predicted = predict(svm1), actual = df2$Receptor_activity) # confusion matrix
confusionMatrix(cm)
```

```
Confusion Matrix and Statistics

          actual
predicted None GR + MR GR only MR only
  None      24       2       1       6
  GR + MR    0       9       5       0
  GR only    0       1       6       0
  MR only    0       0       0       0

Overall Statistics

               Accuracy : 0.7222
                 95% CI : (0.5836, 0.8354)
    No Information Rate : 0.4444
    P-Value [Acc > NIR] : 3.323e-05

                  Kappa : 0.5673
 Mcnemar's Test P-Value : NA

Statistics by Class:

                     Class: None Class: GR + MR Class: GR only Class: MR only
Sensitivity               1.0000         0.7500         0.5000         0.0000
Specificity               0.7000         0.8810         0.9762         1.0000
Pos Pred Value            0.7273         0.6429         0.8571            NaN
Neg Pred Value            1.0000         0.9250         0.8723         0.8889
Prevalence                0.4444         0.2222         0.2222         0.1111
Detection Rate            0.4444         0.1667         0.1111         0.0000
Detection Prevalence      0.6111         0.2593         0.1296         0.0000
Balanced Accuracy         0.8500         0.8155         0.7381         0.5000
```

PCA for visualising SVM analysis

In [62]:
```
pca1<- prcomp(df2[2:5])
pca1$rotation
```

	PC1	PC2	PC3	PC4
HMGB1	0.2418926	-0.72371419	-0.60287006	-0.2329666
CellViability	0.3412489	0.67365615	-0.51506366	-0.4055195
SupernatantViability	-0.6192584	0.14140974	-0.60415779	0.4811608
LDH	-0.6644970	-0.04927923	0.07905994	-0.7414613

In [63]:
```
screeplot(pca1)
```

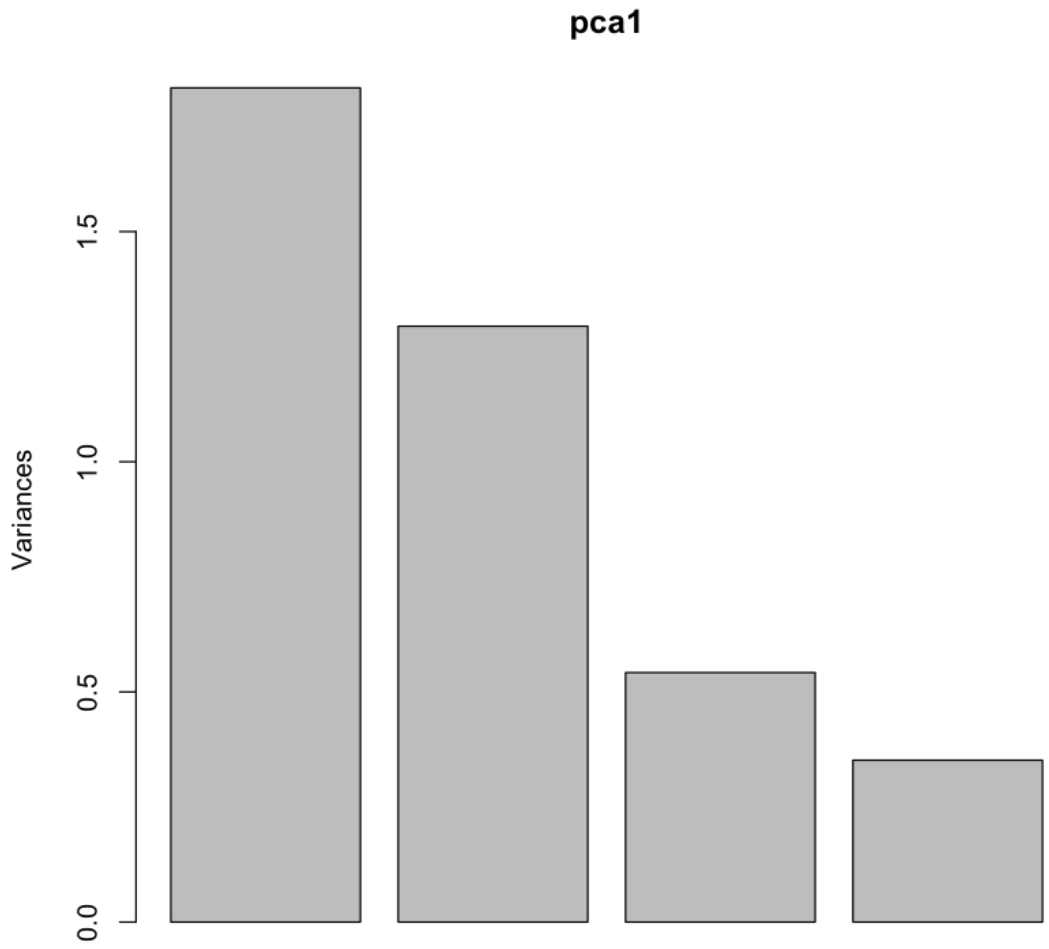

In [64]:
```
# To show cassification boundaries, project classification predictions using a regular grid of values
# Note: Computationally expensive depending on grid size of each variable
# Test data is just a grid of values to predict
testData<- expand.grid(HMGB1= seq(min(df2[,2]-.5), max(df2[,2]+.5), by = 0.35),
                       CellViability   = seq(min(df2[,3]-.5), max(df2[,3]+.5), by = 0.35),
                    SupernatantViability= seq(min(df2[,4]-.5), max(df2[,4]+.5), by =0.35),
                   LDH = seq(min(df2[,5]-.5), max(df2[,5]+.5), by =0.35))
```

In [65]:
```
predicted <- predict(svm1, testData) # Predict classification using testData
```

In [66]:
```
testData<- data.frame(predicted, testData) #format into data frame
```

In [67]:
```
traindata<-data.frame(pca1$x, df3[,2:4], df3[13]) # rotate predicted values using same PCA transformation
```

In [68]:
```
summary(testData)
```

```
   predicted         HMGB1          CellViability     SupernatantViability
 None    :24299   Min.   :-1.6889   Min.   :-2.8165   Min.   :-1.9714
 GR + MR:17906   1st Qu.:-0.6389   1st Qu.:-1.7665   1st Qu.:-0.9214
 GR only:11345   Median : 0.5861   Median :-0.3665   Median : 0.4786
 MR only:    0   Mean   : 0.5861   Mean   :-0.3665   Mean   : 0.4786
                 3rd Qu.: 1.8111   3rd Qu.: 1.0335   3rd Qu.: 1.8786
                 Max.   : 2.8611   Max.   : 2.0835   Max.   : 2.9286
      LDH
 Min.   :-1.7127
 1st Qu.:-0.3127
 Median : 1.0873
 Mean   : 1.0873
 3rd Qu.: 2.4873
 Max.   : 3.8873
```

In [69]:
```
rotatedpred<- scale(testData[2:5], pca1$center, pca1$scale) %*% pca1$rotation
```

In [70]:
```
rotatedpred<- data.frame(predicted, rotatedpred)
```

In [71]:
```
summary(rotatedpred)
```

```
   predicted          PC1               PC2               PC3
 None    :24299   Min.   :-5.7663   Min.   :-4.4383   Min.   :-4.7027
 GR + MR:17906   1st Qu.:-2.1426   1st Qu.:-1.7028   1st Qu.:-1.4117
 GR only:11345   Median :-1.0022   Median :-0.6569   Median :-0.3678
 MR only:    0   Mean   :-1.0022   Mean   :-0.6569   Mean   :-0.3678
                 3rd Qu.: 0.1382   3rd Qu.: 0.3889   3rd Qu.: 0.6762
                 Max.   : 3.7620   Max.   : 3.1244   Max.   : 3.9672
      PC4
 Min.   :-5.3422
 1st Qu.:-1.7475
 Median :-0.5638
 Mean   :-0.5638
 3rd Qu.: 0.6200
 Max.   : 4.2147
```

In [72]:
```
newvar<-get_pca_var(pca1)
newvar
coordinates<- data.frame(varnames= rownames(newvar$coord), newvar$coord) #variable data
coordinates #variable coordinates
```

```
Principal Component Analysis Results for variables
 ===================================================
  Name       Description
1 "$coord"   "Coordinates for the variables"
2 "$cor"     "Correlations between variables and dimensions"
3 "$cos2"    "Cos2 for the variables"
4 "$contrib" "contributions of the variables"
```

	varnames	Dim.1	Dim.2	Dim.3	Dim.4
HMGB1	HMGB1	0.3256217	-0.82336385	-0.4437984	-0.1381501
CellViability	CellViability	0.4593692	0.76641322	-0.3791604	-0.2404747
SupernatantViability	SupernatantViability	-0.8336094	0.16088073	-0.4447464	0.2853303
LDH	LDH	-0.8945069	-0.05606459	0.0581994	-0.4396896

In [73]:
```
palette <- c('#ff008d', '#619bc7', '#ffe700', '#545454')
```

In [74]:
```
#Plot training and predicted data
svmPCAplot<-ggplot(data = as.data.frame(rotatedpred), aes(y= PC1, x = PC2, colour = predicted))+ #predicted
 data
geom_point(size = 0.1, alpha = 0.3)+
geom_point(data = traindata, aes(y = PC1, x = PC2, colour = Receptor_activity), size = 3)+ # training data
geom_segment(data = coordinates, aes(x = 0, y = 0, xend = Dim.1*2, yend = Dim.2*2),
             arrow = arrow(length = unit(0.2, 'cm')), alpha = 0.75, color = 'black', size = 1)+
geom_text(data=coordinates, aes(x=Dim.1*3, y=Dim.2*2.5, label=varnames), size = 5, color="black")+
theme_minimal(base_size = 15)+
labs(y = 'Principal component 1', x = 'Principal componant 2')+
theme(aspect.ratio= 1.5, legend.position = 'bottom', panel.grid.major = element_blank(), panel.grid.minor = e
lement_blank(),
     panel.background = element_blank(), panel.border = element_rect(fill =NA, colour = 'grey'))+
scale_color_manual(values = palette)

svmPCAplot
```

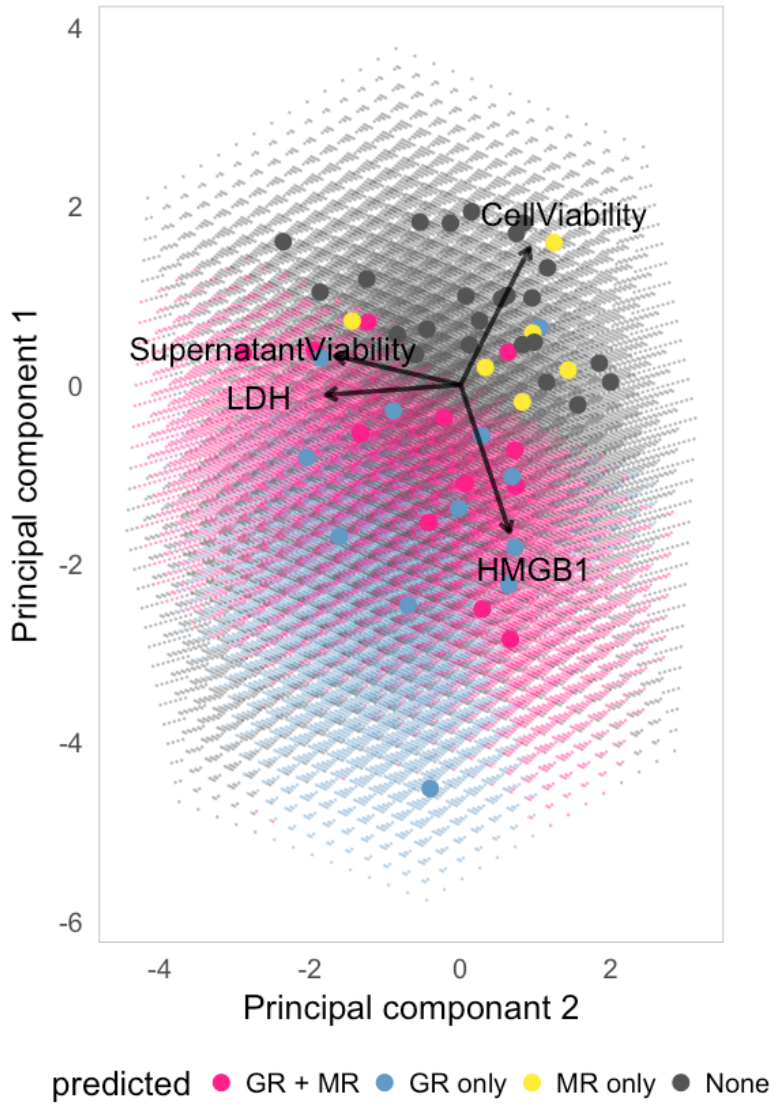

In [75]:
```
ggsave(svmPCAplot, filename = 'svmpcaplot_no beta.png')
```

```
Saving 7 x 7 in image
```

Verifying results

Double checking results using random (shuffled) data is a good way to check if model is informative

In [76]:
```
# what happens when you shuffle the dataset? Better than chance?

randomised<- rotateddf %>%
filter(Treatment =='None') %>%
mutate(Receptor_activity = sample(Receptor_activity))

head(randomised)
table(Predicted = predict(model_svm), Random = randomised$Receptor_activity)
```

N	PreExposure	Antagonist	Treatment	GR_Activity	MR_Activity	Receptor_activity	PC1	PC2	PC3	PC4
1	CORT	Mifepristone	None	0	1	GR only	-2.2946353	0.4623768	-0.9588067	-0.1270812
1	CORT	None	None	1	1	GR only	-0.5975874	1.2445676	-1.3634736	-0.4080886
1	CORT	Spironolactone	None	1	0	GR + MR	-0.7954919	0.9566342	-0.5375007	-0.0675687
1	CORT	Vehicle	None	1	1	None	-0.6055690	0.8215507	-1.2823332	-0.5706274
1	DEX	None	None	1	0	None	0.7271522	1.5935499	-1.6061561	-0.6645309
1	Vehicle	Mifepristone	None	0	0	None	-2.2079600	0.6057800	-0.8859029	0.13139408

```
Error in predict(model_svm): object 'model_svm' not found
Traceback:

1. table(Predicted = predict(model_svm), Random = randomised$Receptor_activity)
2. predict(model_svm)
```

In [ ]:
```
#Actual
confusionMatrix(table(Predicted = predict(model_svm), actual = filter(rotateddf, Treatment == 'None')$Recepto
r_activity))
#Shuffled
confusionMatrix(table(Predicted = predict(model_svm), Random = randomised$Receptor_activity))
```

Summary:

- Overall accuracy is better than before (57%)
- Some discrimination between GR + MR and GR only class (low sensitivity but high-ish specificity)
- balanced accuracy is also improved
- Could this be over-fitting?

In [ ]: